ICTIMES - 2017

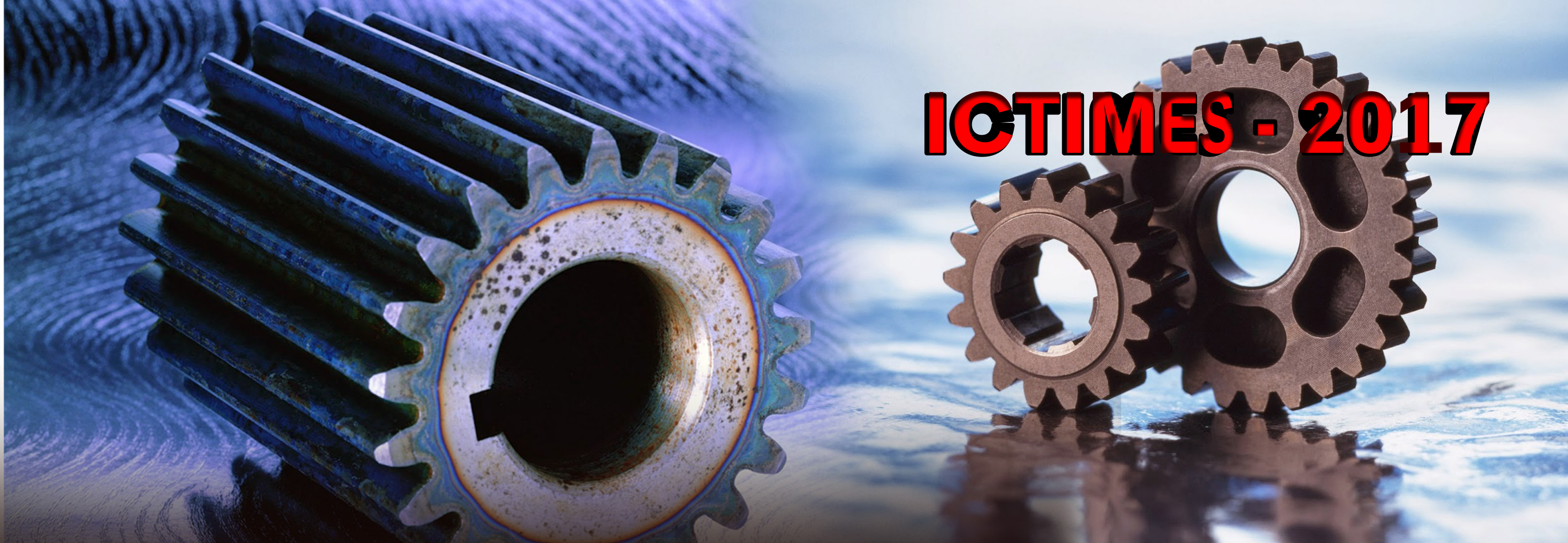

Proceedings of

International Conference on Advances in Future Technologies in Mechanical Engineering (ICFTME)

ISBN No: 978-93-85100-09-3

Under the Auspices of International Conference on trends in Information,Management, Engineering and Sciences (ICTIMES)

MALLA REDDY COLLEGE OF ENGINEERING (MRCE)

Permanently Affiliated to JNTUH, Approved by AICTE(New Delhi),Accredited by NBA
An ISO 9001:2015 Certified Institution.
Maisammaguda, Hyderabad - 500 100.
www.mrce.in

Convenor
Dr. Vel Murgan
Prof. - MECH Dept.

Editor
Dr. S.S Gowda
HOD - MECH Dept.

Editor in Chief
Dr. P. John Paul
Principal

ICTIMES - 2017

ISBN No: 978-93-85100-09-3

Proceedings of International Conference on Advances in Future Technologies in Mechanical Engineering (ICFTME)

Chief Patron:

Sri Ch. Malla Reddy, Founder Chairman, MRGI
(Member of Parliament, Govt., INDIA)

Patrons:

Mr. Ch. Mahender Reddy, Secretary MRGI
Dr. Ch. Bhadra Reddy, Treasurer MRGI

International Advisory Committee:

Col. G. Ram Reddy, Director (Admin), MRGI
Mr. N Sudhir Reddy, Director, Administration, MRCE
Dr. S. R. C. Murthy, University of Sydney, Australia
Dr. A.V. Vidya Sagar, BELL, USA
Dr. K.V.S. S. Narayana Rao, NITIE, Bombay
Dr. K. Vijay Kumar, CEO, First ESCO India, Vizag
Dr. Ch. A.V. Prasad, Senior Consultant, TCS
Dr. A. Govardhan, Principal, JNTUH
Dr. B. Sudeer Prem Kumar, Chairman, BOS, JNTUH
Dr. K. Venkateswar Rao, JNTUH
Dr. P. Dasharathan, JNTUH
Dr. B.N. Bhandari, Director DAP, JNTUH
Dr. M. Manzoor Hussain, Director Administrations, JNTUH
Dr. M. Madhavi Latha, Former Director, I-Tech, JNTUH
Dr. V.C.V. Prathap Reddy, RIT Rochester, USA
Dr. S. Venkateswara Rao, Head- Physics, JNTUH
Mr. N. Shyam Kumar, Group Manager, Tech Mahindra
Mr. S. Goutam, Manager, TCS
Dr. Hussain Reddy, SKU, A.P.
Dr. Seow Ta Wee, University Tun Hussein Onn Malaysia.
Ir. Dr. Goh Hui Hwang, Malaysia

Chief Guest:

Dr. T.G Thomas, Dean-Admissions (Campus Wide) - BITS Pilani, Dubai Campus,Academic City,Dubai,UAE.

Guest of Honor:

Dr. Balajied Lang Nongrum, Biola University USA.

Keynote Speakers:

Dr. T.G Thomas,BITS Pilani,Dubai UAE
Dr. Balajied Lang Nongrum, Biola University USA
Dr. C. Krishna Mohan, IIT Hyderabad
Dr. R.Thundil Karuppa Raj, VIT University
Dr. K. Ramulu, Central University, Hyderabad

Conference General Chair:

Dr. P John Paul, Principal, MRCE

KNOWLEDGE IS DIVINE

MALLA REDDY COLLEGE OF ENGINEERING (MRCE)

Permanently Affiliated to JNTUH, Approved by AICTE (New Delhi),Accredited by NBA, An ISO 9001:2015 Certified Institution.
Maisammaguda, Hyderabad,India - 500 100.
www.mrce.in

ICTIMES - 2017
ISBN No: 978-93-85100-09-3
Proceedings of International Conference on Advances in Future Technologies in Mechanical Engineering (ICFTME)

Organizing Committee:

Dr. M. Thamarai, Dean Academics (Chair)
Dr. V. Bhoopathy, Dean R&D - CSE
Dr. P.Velmurgan, Dean R&D - MECH
Dr. Nikhil Raj, Dean R&D - ECE
Dr. Ch. Shankar , Dean Academics - MBA
Dr. J. Gladson, Dean Student Affairs - CSE

Co– ordination Committee:

Prof. Rajesh Durgam
Prof. M. Shiva kumar
Prof. Ch. Vijaya Kumari
Prof. C. Shashi Kanth
Prof. J. Shashi Kumar

Program Committee

Dr. T. V. Reddy, Vice Principal (Chair)
Dr. T. Sunil , Dean Academics - CSE
Dr. S.S Gowda, Dean Academics - MECH
Dr. G. Sridhar , Dean Student Affairs - ECE
Dr. A. Karthikeyan, Dean Student Affairs – MECH

Information Contact:

Dr. P John Paul
Principal, MRCE
+91-9348161222, 9346162620
E-mail: principal@mrce.in

MALLA REDDY COLLEGE OF ENGINEERING (MRCE)

Permanently Affiliated to JNTUH, Approved by AICTE (New Delhi),Accredited by NBA, An ISO 9001:2015 Certified Institution.
Maisammaguda, Hyderabad,India - 500 100.
www.mrce.in

Malla Reddy College of Engineering

Permanently Affiliated to JNTUH, Approved by AICTE(New Delhi),Accredited by NBA
An ISO 9001:2015 Certified Institution.
Maisammaguda, Hyderabad - 500 100.
www.mrce.in

Sri. Ch. Malla Reddy
Founder Chairman,MRGI
Member of Parliment

Best Wishes:

I Congrtulate Mechanical Department on Conducting International Conference on " Emerging Technologies in Mechanical Engineering" (ICFTME)

Malla Reddy College of Engineering

Permanently Affiliated to JNTUH, Approved by AICTE(New Delhi),Accredited by NBA
An ISO 9001:2015 Certified Institution.
Maisammaguda, Hyderabad - 500 100.
www.mrce.in

Sri. Ch. Mahender Reddy
Secretary, MRGI

Sri. Ch. Bhadra Reddy
Treasurer, MRGI

Best Wishes:

We Congrtulate Mechanical Department on Conducting International Conference on “ Emerging Technologies in Mechanical Engineering” (ICFTME)

Malla Reddy College of Engineering

Permanently Affiliated to JNTUH, Approved by AICTE(New Delhi),Accredited by NBA
An ISO 9001:2015 Certified Institution.
Maisammaguda, Hyderabad - 500 100.
www.mrce.in

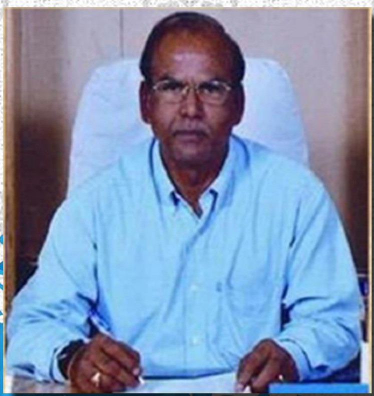

Col. G. Ram Reddy
Director/Administrations, MRGI

Sri. N. Sudhir Reddy
Director, MRCE

Best Wishes:

We Congrtulate Mechanical Department on Conducting International Conference on " Emerging Technologies in Mechanical Engineering" (ICFTME)

Dr. P. John Paul
Principal,MRCE
Editor in Chief

Best Wishes:

My wishes to Mechanical Department on Conducting International Conference on " Emerging Technologies in Mechanical Engineering" (ICFTME)

Malla Reddy College of Engineering

Permanently Affiliated to JNTUH, Approved by AICTE(New Delhi),Accredited by NBA
An ISO 9001:2015 Certified Institution.
Maisammaguda, Hyderabad - 500 100.
www.mrce.in

Dr. T.G Thomas
Dean Admissions (Campus Wide) BITS Pilani,
Dubai Campus, Academic city, Dubai, UAE.

Best Wishes:

My warmest congratulations to you, MRCE and all staff on conducting International Conference on " Emerging Technologies in Mechanical Engineering" (ICFTME)

Malla Reddy College of Engineering

Permanently Affiliated to JNTUH, Approved by AICTE(New Delhi),Accredited by NBA
An ISO 9001:2015 Certified Institution.
Maisammaguda, Hyderabad - 500 100.
www.mrce.in

Dr. Balajied Lang Nongrum

Biola University, USA.

Best Wishes:

My warmest congratulations to you, MRCE and all staff on conducting International Conference on " Emerging Technologies in Mechanical Engineering " (ICETME)

Malla Reddy College of Engineering

Permanently Affiliated to JNTUH, Approved by AICTE(New Delhi),Accredited by NBA
An ISO 9001:2015 Certified Institution.
Maisammaguda, Hyderabad - 500 100.
www.mrce.in

Dr. R. Thundil Karuppa Raj
VIT University

Best Wishes:

My warmest congratulations to you, MRCE and all staff on conducting International Conference on " Emerging Technologies in Mechanical Engineering" (ICFTME)

Malla Reddy College of Engineering

Permanently Affiliated to JNTUH, Approved by AICTE(New Delhi),Accredited by NBA
An ISO 9001:2015 Certified Institution.
Maisammaguda, Hyderabad - 500 100.
www.mrce.in

Dr. S.S Gowda
HOD - MECH Dept. , MRCE

Dr. Velmurgan
Prof. - MECH Dept, MRCE

Best Wishes:

We Congrtulate Mechanical Department on Conducting International Conference on " Emerging Technologies in Mechanical Engineering" (ICFTME)

Wear studies on AL6061/Graphite & AL6061/Graphite/Albite AMC's

Dr.J.N.Prakash[1], Dr.Shiva Shankare Gowda A.S [2], Dr.A.Ramesha[3]

[1] Professor, Noble College of Engineering and Technology, Rangareddy (District), Telangana, India.
email: prakash69jnp09ace@gmail.com
[2] Professor and Dean Academics, Department of Mechanical Engineering,
Mallareddy College of Engineering, Hyderabad, Telangana, India.
email: ssgowda105@gmail.com
[3] Professor, BITS , Hindupur, Andhra Pradesh , India.
email: prof_ramesh_epcet@yahoo.com

Abstract- This paper describes the abrasive wear rate of AI (6061) alloy reinforced with graphite composites and AL6061/Graphite composites reinforced with Albite particulates. The present investigation is on the wear behavior of AL6061/Graphite composites and AL6061/Graphite/Albite composites. The 'vortex method' of production was employed in which the particulates were dispersed in to the vortex created by stirring the molten metal by means of a mechanical agitator. The Albite and Graphite were coated to enhance interface bonding so as to improve wear properties. The sliding distances and percentage of reinforcements of the composites were varied. Addition of Albite particulates had a considerable influence on the wear rate compared to AL6061/Graphite composite and matrix alloy. Dry sliding wear behavior of AL6061 based composites has been investigated using a pin-on-disc wear-testing machine. Amongst the investigated composite wear samples , a comparative analysis was carried out. The composites containing both Albite and Graphite exhibited a transition from mild to severe wear depending on sliding distance and applied load. Two modes of wear have been identified to be operative based on the detail examination of wear surface, wear debris and analysis of the wear data. The transition from mild wear to severe wear was influenced by the applied load, sliding distance, hardness and strength of the composite material.

Key words: *Aluminum, Composites, Albite, Graphite, wear*

I INTRODUCTION

New materials for high performance tribiological applications have been one of the major incentives for the development of aluminium-based metal matrix composites (MMCs). MMC's have received attention because of their improved specific strength, good wear resistance, higher thermal conductivity, than ceramics, lower coefficient of thermal expansion (CTE)**[1-4].** The incorporation of ceramic materials in an Al-alloy increases its load bearing capacity, and hence the load and sliding speed range within which dry sliding wear is mild**[5,6]**. This has been investigated in detail by many researchers and opens new opportunities for the employment of Al-based metal matrix composites (MMC) in applications where sliding resistance of concern. The investigation of the wear behaviour of Al-based MMC against friction materials is receiving particular attention because of the possibility of using these materials for disc brakes in automotive application. In comparison to conventional cast iron disc, Al MMC discs offer promising advantages such as, lower density and higher thermal conductivity. Investigators have also reported that friction and wear behaviour of Al MMCs against, organic as well as semi-metallic friction materials. Each of these alloys acting as matrix of composite materials will provide it with diverse properties determined by its state, the reinforcement's percentage[7] and the nature of matrix particles interface[8].There is no doubt that the nature of matrix hardener phase will influence decisively the latter and this will do so upon wear resistance.

The incorporation of Albite and Graphite reinforcements in an AL-alloy increases, its load bearing capacity and hence the load and sliding speed range within which dry sliding wear is mild. This has been investigated in detail by many researchers and opens new opportunities for the employment of Al-based metal matrix composites in applications where sliding resistance is of concern. The investigation of the wear behavior of Al-MMCs against friction materials has received particular attention because of the possibility of using these materials for disc brakes in an automotive application. With respect to the conventional cast iron Al-MMCs discs offers promising advantages such as lower density and higher thermal conductivity. Howell and Ball investigated the friction and wear behavior or aluminum matrix composites against organic as well as semi-metallic friction materials.

The aim of this paper is to examine the effect of graphite particulate on the abrasive wear resistance of Aluminium alloy(AL6061) and influence of hard ceramic Albite particulates when reinforced in Graphite/ Al(6061) composites, which are candidate materials for aerospace and automotive components which require fabrication processing and relate changes in the wear properties to the microstructural changes in the Al alloy matrices. The weight fraction of albite particulates and graphite 1 to 4 % and were used for making MMCs. Keeping this in this study, dry sliding wear tests were conducted on ascast hybrid composites using pin on disc machine with different sliding velocities 4.5 m/sec, 5.34 m/sec and 6.23m/sec at 4 N load and a sliding distance of 3Km. In addition to this a systematic evaluation of the wear rate characteristics and a systematic worn out surface examination was carried out using scanning electron microscope.

II EXPERIMENTAL PROCEDURES

A. Materials

Chemical composition of Aluminium 6061 alloy		
Mg	**Si**	**Fe**
0.92	0.76	0.28
Cu	**Ti**	**Cr**
0.22	0.10	0.07
Zn	**Mn**	**Be**
0.06	0.04	0.003
V	**Al**	
0.01	Bal	

Table 1: Chemical composition of AL6061 by weight percentage

Chemical composition of reinforcement Albite	
Silica(6SiO_2)	**Alumina**
68.7	19.5
Soda	
11.8	

Table 2: Chemical composition of Albite by weight percentage

The matrix material used for the MMCs in this study is AL6061 alloy. This alloy is best suited for mass production of lightweight metal castings. Table1 shows the chemical composition of Al6061 and Table 2 the chemical composition of the albite. The albite and graphite 50μm were reinforced in the matrix material. Liquid metallurgy technique was used to fabricate the composite materials in which the reinforcing materials were introduced into the molten metal pool through a vortex created in the melt by the use of an alumina coated stainless steel stirrer. The coating of an alumina to the blades of the stirrer is essential to prevent the migration of ferrous ions from the stirrer into the molten metal. The stirrer was rotated at 500 rpm and the depth of immersion of the stirrer was maintained about two-thirds the depth of the molten metal. Reinforcing materials preheated at 300°C were added one after the other into the vortex of the liquid melt which was degassed using pure nitrogen for about 3 min - 4 min prior to the addition of the reinforcements. The resulting mixture was tilt poured into the preheated permanent metallic molds.

After casting the AL6061/Graphite and Al6061 based hybrid composites, wear test specimens were prepared by machining from the cylindrical bar castings. Each specimen was 6 mm in diameter and 25 mm length in its dimensions. The specimen surfaces were polished with 1μm diamond paste. The results presented are an average taken from four samples of each coinposites[2,5].

B. Wear Tests

Sample code	Matrix	Reinforcement
AL_GR_1	AL6061	1%wt of Graphite
AL_GR_2	AL6061	2%wt of Graphite
AL_GR_3	AL6061	3%wt of Graphite
AL_GR_4	AL6061	4%wt of Graphite

Table 3: Details of AL6061/Graphite composites

Sample code	Matrix	Reinforcement
AL_ALB_GR_1	AL6061	1%wt of Albite, Graphite
AL_ALB_GR_2	AL6061	2%wt of Albite, Graphite
AL_ALB_GR_3	AL6061	3%wt of Albite, Graphite
AL_ALB_GR_4	AL6061	4%wt of Albite, Graphite

Table 4: Details of Hybrid composite

Wear tests were carried out using a pin -on -disc machine. The tests were carried out by rubbing a hybrid composite specimen against a rotating disc of steel (200mm diameter and 58 ± 0.5 HRC) under dry conditions. Aluminum alloy reinforced with graphite particulates composite samples are designated as AL_GR_1,2,3&4 ref: Table3.The hybrid composites were designated as AL_ALB_GR_1,2,3&4 refer Table 4 for different percentages .Before testing, the surfaces of both the pin and disc wear samples were polished with 400, 600, 800 and 1000 grit emery paper. The surface roughness of both specimens were about 0.3 µm .

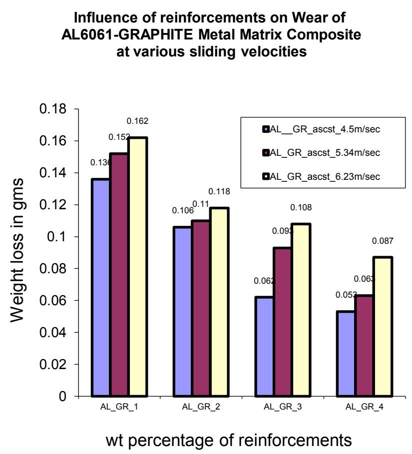

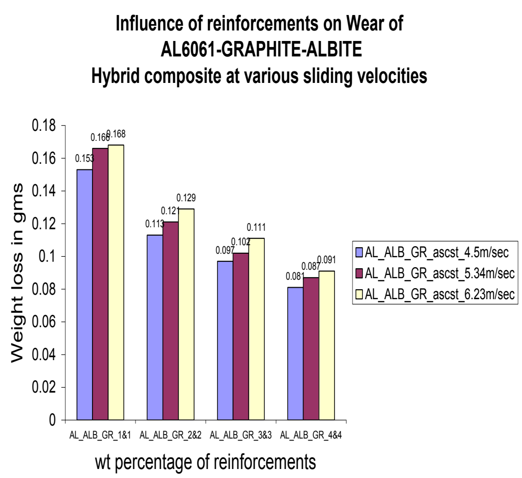

Fig 2 : The Bar chart shows the influence of Albite and Graphite on wear properties

The test environment was kept at a room temperature· and a relative humidity of 30% (measured using dry and wet bulb thermometer). Sliding velocities was varied from 4.5 m/sec to 6.2 m/sec for a sliding distance of 3 Km and a load of 4 N. Before and after testing the weight of the pin was measured to an accuracy 10^{-4} g using a digital balance to determine mass loss and each hybrid composites were tested four times. Refer **Table 2 & 3** for sample details. Lastly, wear surface-were studied with SEM to determine the wear mechanism undergone by the material.

A typical Pin on Disc wear testing set up

III RESULTS AND DISCUSSIONS

A. Wear tests

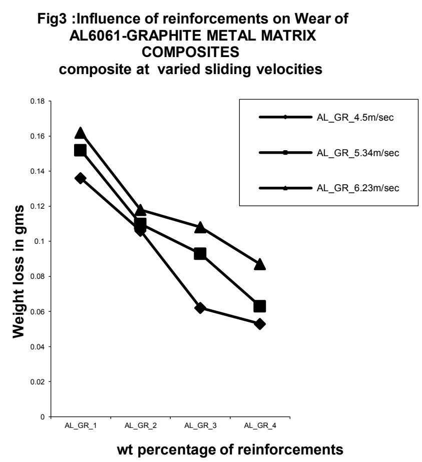

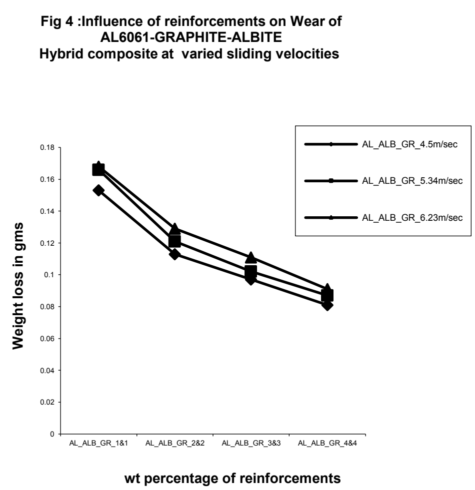

The wear tests carried out on the as-cast hybrid and as-cast AL6061/Graphite composite material by means of a pin-on-disc technique. Changes quantum of reinforcements experiences a change of its wear resistance in relation to the base AL6061 alloy. The wear rates were plotted against sliding velocity(Refer figures 3,4 &5,6. At lower velocity, (4.5 m/s) the reinforced hybrid composite were in a steady state but there was an increase in wear rate with increasing sliding velocity. At velocity of 5.34m/s was found to attain flash temperatures that can cause oxidation. The flash temperature depends strongly on the sliding velocity but hardly on the load. The metallic oxide formed was hard and acts as a thermal insulator, thereby providing good resistance to wear.

Fig 5 : AL6061-GRAPHITE reinforced metal matrix composites

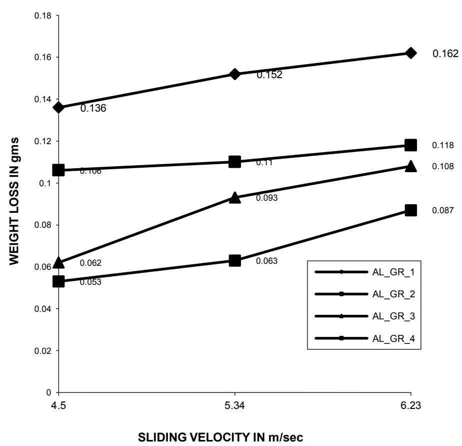

At medium sliding velocity (below 5.34 ms^{-1}) reinforced hybrid composite shows steady state wear rate that was lower when compared with matrix alloy. At higher sliding velocities due to increase in temperature of the reinforced composite, oxidation occurs. The aluminum oxide film partly acts as an insulator and its temperature rises to the point of plastic deformation. The deformation zones penetrate deeper and the volume loss is higher. Aluminum hybrid composite (4%) was found to be more wear resistant, when compared to reinforced alloys of 1,2& 3 %'s, however reveals that in the higher wear regime an increasing trend might be discern. The composite having a lower amount of graphite reinforcement content appears to produce generally higher amount of frictional traction than the one with larger amount of graphite. A closer examination of the data suggests that the extra graphite particulates did provide some additional lubricating effect during tests.

Fig 6 : AL6061-ALBITE-GRAPHITE reinforced hybrid composites

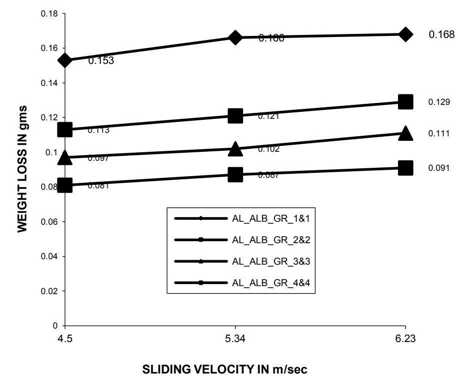

SEM examinations of worn surfaces, suggest that the substantial presence of wear debris gave rise to abrasive wear. The lubricating effect contributed by the graphite particulates is overshadowed by this increase, giving rise to an increase in total frictional traction in these composites when tested.

B. Worn surfaces

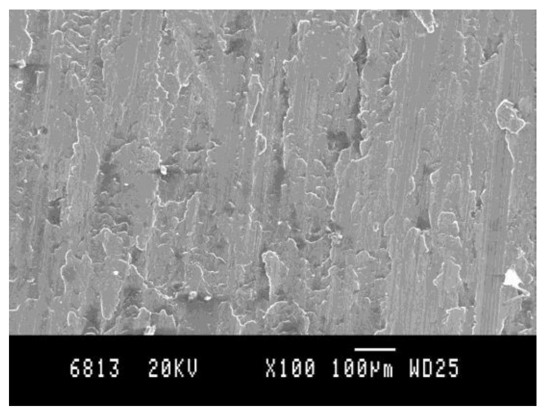

Figure 7 : SEM of Graphite/AL6061 composite subjected 3Km sliding distance

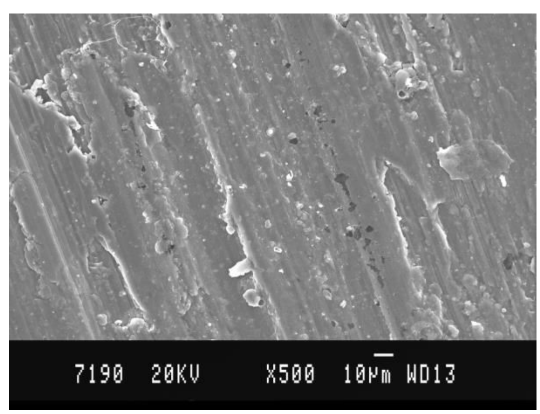

Figure 8 : SEM of AL6061 Hybrid composite subjected 3Km sliding distance

SEM of the worn surface of the as-cast hybrid composite specimens (at a load of 4 N) are shown in Figure 8. The SEM reveals wear tracks have made it possible to deduce that the path is not homogeneous, but a non-uniform wear was noticeable instead, showing wear outstanding zones and areas with grooves along the sliding direction and plastic deformation after a sliding distance of 3Km., Grooves have been formed by the reinforcing materials. On this surface, areas a fractured surface like appearance can be observed. It can be seen that the layer of material has been removed as debris from the surface and that the debris is in the form of thin sheets. In reference to SEM studies of worn-out surfaces, it could be observed that wear damage was caused by plastic flow of the matrix. With accumulation of material within valleys. Apart from extensive surface flow, long ploughing lines could be seen especially in the worn surface of the composite. Such a feature suggests the operation of abrasive wear during sliding. This supports our earlier observation that a sizable amount of small fragments of matrix material were produced as a byproduct of graphite de-bonding process. The debonding induced debris would then be work hardened by the sliding process, becoming hard abrasive particles which would lead to an increase in the frictional traction during sliding.

IV CONCLUSIONS

The introduction of reinforcing materials in AL6061 matrix reduces the wear rate. Addition of hard Albite particulates in to AL6061/Graphite composites marginally increased the wear rate the presence of the feldspar class of reinforcement increased hardness of the composite and reduced ductility when compared to AL6061/Graphite composites. The wettablity of the reinforcements with the base alloy also seems to have been affected, thereby increasing the wear loss when compared to AL alloy reinforced with graphite. The role of graphite as solid lubricant is again proved to be an effective in enhancing the wear resistance of base alloy. Thus, for wear resistance applications, metal matrix hybrid composites based on Al appear to be an attractive alternative. The wear tests carried out to determines the influence of albite and graphite reinforcements on the wear resistance of the hybrid composite material. It has been determined that the erosive performance of the steel disc increases the oxidation rate on the surface of the material tested at medium sliding velocities. The wear rate of the AI-based hybrid composites depended on type of primary and secondary reinforcements which in this case Graphite and Albite, but wear rate of the hybrid composites increases with increasing the weight percentage of reinforcing materials. Weight loss has increased linearly with increasing sliding velocities Graphite not only reduces the hardness of the composite but also provides the requisite lubrication necessary to curtail the wear of the hybrid composite.

REFERENCES

[1] T.W. Clyne, (1993), “An Introduction to Metal Matrix Composites”, Cambridge University Press, Cambridge, 1993, pp. 65-72.

[2] A. Needleman, (1993), “Fundamentals of Metal Matrix Composites, Butterworths”, Boston, pp. 83-90.

[3] F.L. Matthews and R.D. Rawlings, (1985), Composite materials: Engineering and Science, Woodhead publishing Ltd., 3 Edition, pp. 24-30.

[4] Rohatgi, P. K., Ray, S. and Lin, Y. “Tribological properties of metal matrix graphite particle composites. International Materials Review”, 1992, Vol 37, No.3, pp 129-135.

[5] McCoy, J. M., Prones, C. and Warner, “Wear properties of metal matrix graphite particle composites” F. E. 1. Materials Science., 1988, Vol 1, pp 37.

[6] Pillai, U. T. S. and Pandey, R. K, “Studies on mechanical behaviour of cast and forged aluminium graphite particle composites”, Journal of Composite Materials, 1989, Vol 23, February, pp 108

[7] K.H.W Seah ., S.C.Sharma., B.M.Girish , “Mechanical properties of cast ZA-27/graphite particulate composites” , Materials and Design, 1995, Vol 16, pp 271- 275

[8] Hoskings, F. M., Portillo, F. F., Wunderlin, R. and Mehrabian, R. “Composites of Al-alloys: fabrication and wear behavior”. Journal Materials Science , 1982, Vol 17,pp 477-498.

Two Body Abrasive Wear behavior of Polyurethane & Polyester composites reinforced with E-Glass Fibres

Dr.J.N.Prakash[1], **Dr. A.Ramesh**[2], **Dr.Shiva Shankare Gowda** A.S[3]

[1] Professor, Noble College of Engineering and Technology Rangareddy (District) Telangana, India
email: prakash69jnp09ace@gmail.com
[2] Professor, BITS , Hindupur, Andhra Pradesh , India.
email: prof_ramesh_epect@yahoo.com
[3] Professor & Dean, Mechanical Engineering, Mallareddy College of Engineering,
Hyderabad, Telangana, India
email: shankar105@gmail.com

Abstract-Experimental investigations have been undertaken on chopped strand mat and woven matt glass fiber reinforced polymer composites (FRPC) composites to study its tribological performance. Friction and wear tests were carried out using pin-on-disc configuration under dry sliding contact conditions. In the present work, tribological characteristics of FRPC composites were analysed. Polyester and Vacuum grade two component Polyurethane resin systems have been used as the matrix resin systems. These thermoset resin systems have been used to prepare the FRPC's. The effect of various experimental test parameters such as applied loads, sliding distances, and sliding speeds was studied. Detailed studies on worn surfaces have been made to categorize the wear failure mechanisms. Friction and wear results are presented as a function of normal loads, sliding velocities, and sliding distances. The results of friction and wear, in general, are strongly influenced by all the test parameters. Although the sliding took place against smooth stainless steel counterface, the micrographs of the worn surfaces reveal various mechanisms of abrasive wear nature, i.e. fiber fracture, fragmentation, and peeling off, and micro crack initiation in the matrix and debris formation has been reported in this paper.

Key words: *Polyurethane; Polyester; composites; E-glass fibres; wear*

I INTRODUCTION

In recent times, there has been a remarkable growth in the large-scale production of fiber reinforced polymer matrix composites. Because of their high strength-to-weight and stiffness-to-weight ratios, they are extensively used for a wide variety of structural applications as in aerospace, automotive and chemical industries [1] On account of their good combination of properties, fiber reinforced polymer composites (FRPC's) are used for producing a number of mechanical components such as gears, cams, wheels, brakes, clutches, bearings and seals. Most of these are subjected to tribological loading conditions. The FRPC's exhibit relatively low densities and they can also be tailored for our design requirements by altering the stacking sequences to provide high strength and stiffness in the direction of high loading [2]. A number of material-processing strategies have been used to improve the wear performance of polymers. Glass fiber reinforced polymeric composites traditionally show poor wear resistance and high friction due to the brittle nature of the reinforcing fibers. This has prompted many researchers to cast the polymers with fibers/fillers. Considerable efforts are being made to extend the range of applications. Such use would provide economical and functional benefits to both manufacturers and consumers. Various researchers have studied the tribological behaviour of FRPCs. Studies have been conducted with various shapes, sizes, types and compositions of fibers in a number of matrices [3-8]. In general these materials exhibit lower wear and friction when compared to pure polymers. An understanding of the friction and wear mechanisms of FRPC's would aid in the development of a new class of materials so as to counter the challenges faced by researchers. Reviews of such works found in articles have shown that the friction and wear behaviour of FRPCs exhibits anisotropic characteristics. Use of glass fibres as glass fibre reinforcement in polymeric composites is increasing. The reinforcements not only reduce the cost of the composites, but also meet performance requirements. Solid lubricants such as graphite and MoS [8-9] when added to polymers proved to be effective in reducing the coefficient of friction and wear rate of composites. The use of graphite as a particulate filler has been reported to improve tribological behavior in metal matrix composites (MMCs) [10].

Most of the above findings are based on either randomly oriented or unidirectional oriented fiber composites. Chopped strand and Woven fabric reinforced composites are gaining popularity because of their balanced properties in the fabric plane as well as their ease of handling during fabrication. Mody et al. have shown that the simultaneous existence of parallel and anti parallel oriented carbon fibers in a woven configuration leads to a synergistic effect on the enhancement of the wear resistance of the composite.

The objective of this work is to investigate the friction and wear properties of glass fibre reinforced Polyurethane composites hence referred to as FRPu's and Glass fibre reinforced unsaturated polyester resin hence referred to as FRPY's sliding against a hardened steel counter face. Filler materials have been used in composites reinforced with woven mat fabric. This work is believed to be helpful for understanding the function of different variants of glass fibre reinforcement ranging from chopped strand mat to woven mat in G- Pu composites and G-PY composites and also the effective role played by graphite particulates as filler materials in woven glass fabric reinforced polyurethanes and Polyester resins.

II EXPERIMENTAL

A. Materials

Two component vacuum grade polyurethane system

Property	**Ureol 5236-VG-Isocynate**	**Ureol 5236-1VG-Polyol**
Appearance	Translucent yellow liquid	White Opaque liquid
Specific gravity	1.1	1.0
Viscosity at 25^0C	40-60 mPas	280-230mPas

Table 1 : Typical PU-product data

Property	Polyurethane
Density	1.1gm/cm^3
Shore D hardness	78
Flexural strength	66-70 MPa
Flexural Modulus	1800 MPa
Impact strength (Charpy)	25 KJ/m^2
Compressive strength	60N/mm^2
E modulus(compressive)	1400 MPa
Tensile strength	40MPa
Tensile modulus	1700MPa
Elongation at break	4%

Table 2: Typical Properties of Polyurethane Resin

Property	**Dester Dup-6001 Isophthalic acid based Unsaturated Polyester Resin**
Appearance	Light pale yellow clear liquid
Specific gravity	1.2 +/- 0.015
Viscosity at 25^0C	500+/-CPS

Table 3 : Typical Polyester Resin Product Data

Property	Unfilled Cured Rein
Specific Gravity	1.18
Flexural strength	115 MPa
Impact strength (Charpy)	12 KJ/m^2
Compressive strength	60N/mm^2
Tensile strength	70Mpa
Elongation at break	2-2.5%

Table 4: Typical Properties Of Polyester Resin

Chopped strand mat of 350 GSM and Woven glass fabrics made of 360 GSM containing E-glass fibers of diameter 5-10 µm has been employed. The matrix system used is a medium viscosity two-component vacuum grade polyurethane system used for rapid prototyping was procured from Ciba specialty Chemicals, Bombay India. Refer Tables 1&2.Graphite particulates of size ranging from 50µm have been used as filler material in woven fabric reinforced FRPu's.

B. Unsaturated Polyester Resin

DUP-6001 is a Isophthalic acid based Unsaturated Polyester Resin supplied by Dujodwala Paper Chemicals Ltd. Refer tables (3&4) Having good chemical and mechanical properties. It is a medium viscosity Polyester Resin which wet the surface in the form to cloth, chopped strand mat (CSM) etc. to produce FRP laminate and moldings. It Is suitable for making chemical process equipments like reaction vessels, storage tanks, scrubbers, pipes, ducts etc. In corrosive environment due to acid and weak alkaline conditions, also it may also be used for making boats and for other marine applications.

The catalyst (MEKP) and accelerator 3% of cobalt be thoroughly dispersed in the Resin. The accelerator should be blended in the resin first thoroughly and correct quantity of catalyst should be added shortly before use. The atmospheric conditions play a great part in deciding the percentage of catalyst and accelerator. Generally in winter and rainy season the percentage of catalyst should be added more than 1% and varying the percentage of accelerator controls gel time. Under no circumstances the catalyst used should be less than 1%.

C. Apparatus used for processing polyurethanes.

Property	Ureol 5236-1VG-Polyol
Pot life : 500g at 25^{0}C	20mns
Demoulding time (mould at 40-70^{0}C)	1.5-2hrs
Mixed viscosity at 25^{0}C	160-180mPas
Maximum wall thickness	12mm

Table 5: Processing properties

The fluid cylinders which houses the two components of the vacuum grades polyurethane rein system is activated by a pneumatic circuit comprising of a two stage compressor, FLR (Fluid, lubricator, regulator) unit, and DCV valves. Predetermined quantities of the processing variables are injected in to the fluid cylinders, which in turn pressurize the component fluids and mixing takes places in the mixing chamber. The processed polyurethane is then used for fabricating the FRPu laminates. **Fig 1** represents a scaled modal of the system.

D. Fabrication

All laminates used in this study were manufactured by dry hand lay up technique. E-glass plain weaves roving fabric and chopped strand mat, which is compatible to polyurethane resin, is used as the reinforcement. The Polyol and isocynate components are mixed in specially designed pneumatically actuated resin handling system 100:100 by weight. The stacking procedure consists of placing the fabric one above the other with the resin mix well spread between the fabrics. A porous teflon film is placed on the completed stack. To ensure uniform thickness of the sample a spacer of size 4 mm is used. The mold plates have a release agent smeared on it. The whole assembly is pressed in a hydraulic press (0.5 MPa) and allowed to cure for a day at room temperature.

After demolding, post curing was done at 120°C for 2 h using an electrical oven. The laminate so prepared has a size 250 mm X 250 mm X 4 mm. To prepare the filled G-Pu composites, filler (Graphite) is mixed with a known amount of polyurethane resin. The test samples are cut to size 5 mm x 5 mm x 3 mm with the help of a diamond tipped cutter.

Figure 1: Resin handling support system for handling 2 component Vacuum grade polyurethanes

The unsaturated polyester resin also has been reinforced with the same percentage of reinforcement E-Glass fibre of chopped strand type and woven mat. The fabrication technique adopted for preparation of FRPy laminates is same as that adopted for FRPu's. Graphite powder (50μm to 100μm) has been added to both FRPu and FRPy laminates as filler material (ie., samples PUWMGR & PYWMGR) . Details of samples is as shown in **Table 6 &7**

Sample code	Matrix	Reinforcement	Filler	Wt %
PUCM	Polyurethane	Chopped strand matt	------	
PUWM	Polyurethane	Woven matt	-------	
PUWMGR	Polyurethane	Woven matt	Graphite	5

Table 6 Details of FRPU samples prepared

Sample code	Matrix	Reinforcement	Filler	Wt %
PYCM	Polyester	Chopped strand matt	------	
PYWM	Polyester	Woven matt	-------	
PYWMGR	Polyester	Woven matt	Graphite	5

Table 7: Details of FRPY samples prepared

E. Test procedure

A pin-on-disc test setup was used for slide wear experiments. The surface of the sample (5 mm X 5 mm) glued to a pin of dimensions 6 mm diameter and 22 mm length comes in contact with a hardened disc of hardness 62 HRC. The counter surface disc was made of En 32 steel having dimensions of 165 mm diameter, 8 mm thick and surface roughness (Ra) of 84 µm. The test was conducted on a track of 115 mm diameter for a specified test duration, load and velocity [11]. Prior to testing, the test samples were rubbed against a 600-grade SiC paper. The surfaces of both the sample and the disc were cleaned with a soft paper soaked in acetone before the test. The pin assembly was initially weighed using a digital electronic balance (0.1 mg accuracy). The test was carried out by applying normal load (30 N to 70 N) and run for a constant sliding distance (3000 m) at different sliding velocities (4, 5 and 6 m/s). At the end of the test, the pin assembly was again weighed in the same balance. The difference between the initial and final weights was a measure of slide wear loss. A minimum of three trials was conducted to ensure repeatability of test data. The friction force at the sliding interface of the specimen was measured at an interval of 5 minutes using a frictional load cell. The coefficient of friction was obtained by dividing the frictional force by the applied normal force. Selected samples were coated with a thin layer of gold on the worn surface and subjected to microscopic examination using Scanning Electron Microscope.

III RESULTS AND DISCUSSIONS

Experimental data on the slide wear loss of Chopped strand matt (PUCM) and woven fabric (PUWM & PUWMGR) reinforced G-Pu composite samples are shown in Figs. 2,4 & 6. Polyester based FRPy composite samples ie., PYCM,PYWM & PYWMGR are shown in Figs.3,5 & 7 for different applied Normal loads (30 to 70 N) and sliding velocities (4 to 6 m/s). Table 8 & 9 shows the results pertaining to the coefficient of friction of chopped strand mat reinforced FRPu & FRPy and woven fabric reinforced FRPu &FRPy composite systems. It is observed from the figures and Tables 8 & 9 that there is a strong inter-dependence between the friction coefficients and wear loss irrespective of the loads and sliding velocities employed. The SEM's of select combinations of strand matt (PUCM & PYCM), woven matt fabric (PUWM & PYWM) and filler based (PUWMGR & PYWMGR) samples subjected to slide wear are shown in Figs 6 to 11 respectively.

A. Coefficient of friction

Coefficient of friction			
Load in N	Sliding velocity 4m/s		
	PUCM	**PUWM**	**PUWMGR**
30	0.20	0.28	0.27
50	0.23	0.32	0.30
70	0.25	0.41	0.40
Coefficient of friction			
Load in N	**Sliding velocity 5m/s**		
	PUCM	**PUWM**	**PUWMGR**
30	0.23	0.31	0.28
50	0.28	0.37	0.35
70	0.37	0.44	0.42
Coefficient of friction			
Load in N	**Sliding velocity 6m/s**		
	PUCM	**PUWM**	**PUWMGR**
30	0.21	0.26	0.30
50	0.29	0.32	0.41
70	0.35	0.39	0.45

Table 8: Coefficient of friction of samples tested

The variation in coefficient of friction with varying sliding velocities/loads of PUCM and PUWM composites is shown in Table 8 and that of PYCM and PYWM composites in Table 9. For the graphite woven fabric reinforced PUWMGR & PYWMGR composites, an increasing trend in the coefficient of friction is seen, with increase in sliding velocity/load.

Coefficient of friction			
Load in N	Sliding velocity 4m/s		
	PYCM	**PYWM**	**PYWMGR**
30	0.42	0.47	0.45
50	0.45	0.53	0.50
70	0.47	0.63	0.51
Coefficient of friction			
Load in N	**Sliding velocity 5m/s**		
	PYCM	**PYWM**	**PYWMGR**
30	0.43	0.51	0.48
50	0.48	0.57	0.55
70	0.57	0.64	0.62
Coefficient of friction			
Load in N	**Sliding velocity 6m/s**		
	PYCM	**PYWM**	**PYWMGR**
30	0.44	0.45	0.38
50	0.48	0.51	0.47
70	0.57	0.63	0.55

Table 9 Coefficient of friction of FRPY samples tested

But comparatively less when compared to woven fabric reinforced composites (ie., PUWM and PYWM). Results reveal that the coefficient of friction of PUWMGR samples is less. The reduction in coefficient of friction is attributed to the presence of graphite particulates acting as a solid lubricant. The same has been observed in

PYWMGR Samples. PUCM samples exhibited excellent wear resistance when compared PUWM samples, PUCM samples have the least coefficient of friction and the Fig 8 confirms the same, the dense nature of the reinforcement coupled with good adhesion and excellent binding to the reinforcement enhances the wear resistance of the FRPu sample.

For the unfilled PUWM samples, an increase in sliding velocity/load results in increase in the coefficient of friction. The increase in coefficient of friction is due to the fact that easy detachment of reinforcing fibres and subsequent breakage and on further increase sliding velocity / load, wear resistant property of the matrix material comes to the fore which is main predominant reason for the drop in coefficient of friction and associated weight loss.

B. Slide wear data

It is seen from Figs. 6 and 7 that the filler ie Graphite particulates in PUWMGR ad PYWMGR composites appears to influence the friction and wear behaviour. The wear losses of the composites decreases with filler addition and show the maximum wear resistance (least wear loss) . For PUWM sample, the fibers reoriented parallel to the sliding surface and also to the sliding direction. In this position the can be easily detached from the matrix; hence it is observed that the increase in wear loss is much greater than that observed in filled PUWMGR composite samples. Further, increased exposure of the reinforcement of fibers to the counter surface results in increased fiber fracture due to the frictional thrust.

Graphite filled PYWM samples showed a marked improvement in wear resistance when compared to unfilled PYWM samples. Comparative analysis of FRPU and FRPy samples Figure 8 indicate the FRPU samples exhibit excellent wear resistance . Researchers have reported the same when other variants of Polyurethane resins were reinforced with glass fibres. The data also confirms that chopped matt reinforced Pu resin systems and Polyester resin exhibit excellent wear resistance when compared that with woven mat

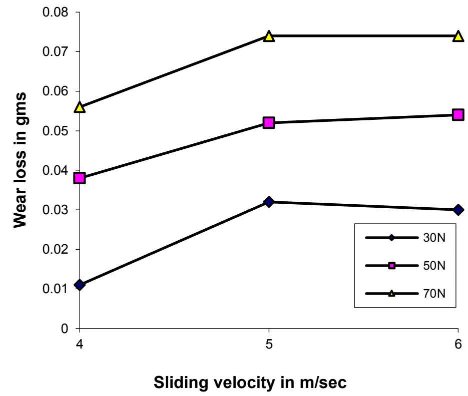

Figure 2 Wear loss V/s Sliding velocity of PUCM sample

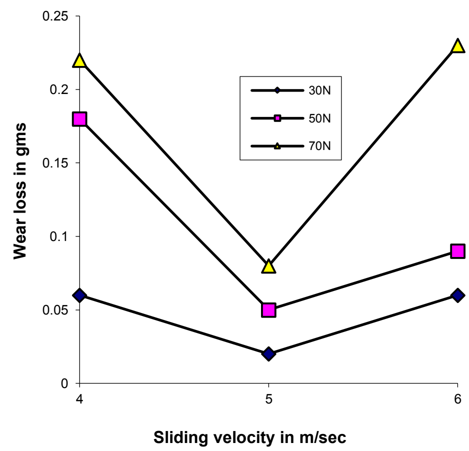

Figure 3 Wear loss V/s Sliding velocity of PYCM sample

C. Scanning Electron Micrography

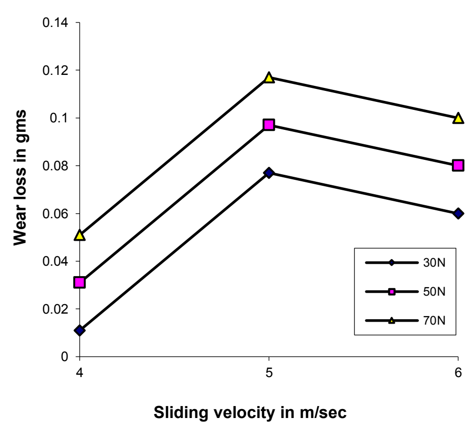

Figure 4 Wear loss V/s Sliding velocity of PUWM sample

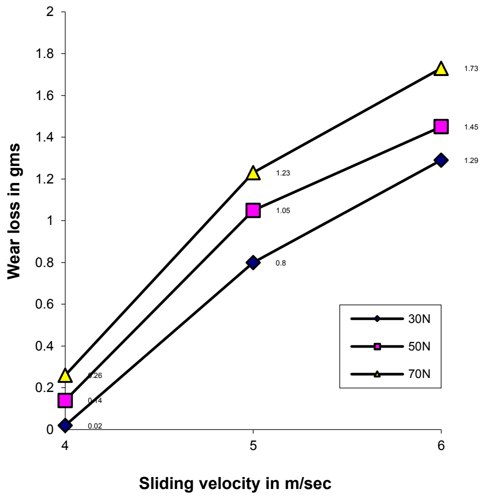

Figure 5 Wear loss V/s Sliding velocity of PYWM sample

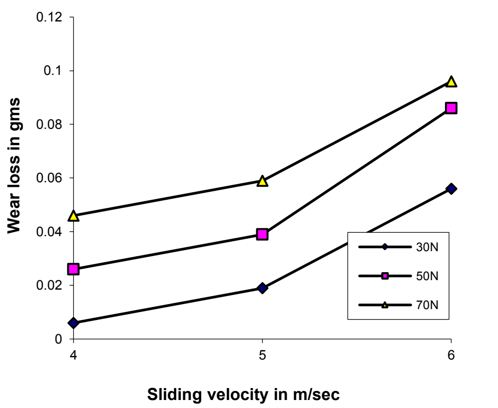

Figure 6 Wear loss V/s Sliding velocity of PUWMGR sample

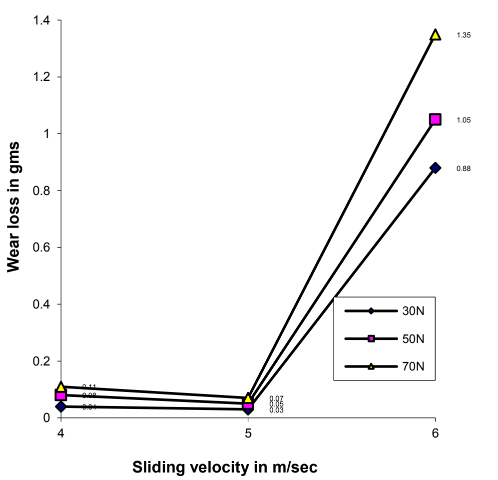

Figure 7: Wear loss V/s Sliding velocity of PYWMGR sample

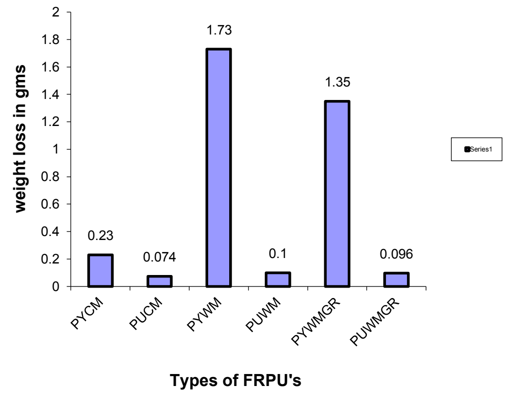

Figure 8 Comparative Wear loss of various FRPu and FRPy samples at Sliding velocity of 6 m/s ,sliding distance of 3km and applied Normal load of 70N

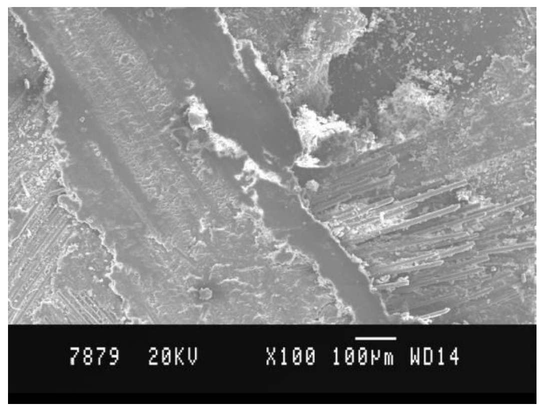

Figure 6 SEM of PUCM sample at 30N/5m/s

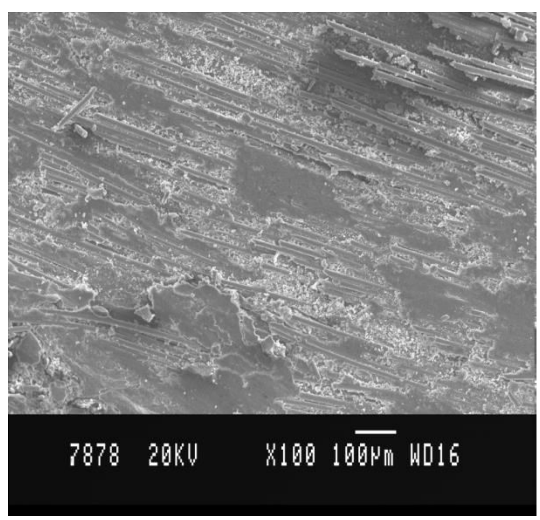

Figure 7 SEM of PUWM sample at 30N/5m/s

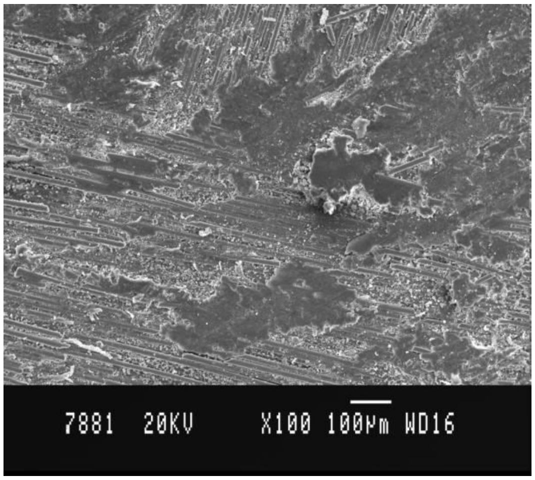

Figure 8 SEM of PUWMGR sample at 30N 5m/s

The slide wear data in respect of select samples are discussed based on the SEM features. The Fig 6 sample PUCM shown pertaining to the test conditions of 30 N, 5 m/s is considered for interpretation. Fig. 6 shows higher degree of fiber breakage, mostly cleavage type of smaller size and smearing of debris on the fibers. The observations corroborate the wear data reported in Fig. 2. Fig 6 records increased breakage of fibers with cleavage type of fracture, interface separation between the fibers and matrix and debris formation concentrated at specific locations. Further, few fibers along the sliding direction are found to be disoriented. There is one to one correspondence between the micrographs observations and wear test results.
Fig 9 exhibits the wear of FRPY samples (ie., PYCM) higher wear when compared PUCM samples.

PUWM sample subjected to a load of 30 N and sliding velocity5 m/sec is shown in Fig. 7. The spread of the matrix and fewer wear debris formation are noticed. Both delamination and debonding increased with increasing sliding velocity (5 mIs), which resulted in exposure of reinforced fibers along the sliding direction. In Fig. 7, it is noticed that the debris begins to cluster around the fibers. It is obvious that with application of higher load and no change in sliding velocity there has been observed increase of more breakage of fibers and further the broken fibers show inclined type of fracture.

The same has been observed in fig 10 of PYWM sample but more wear loss has been observed when compared to PUWM.

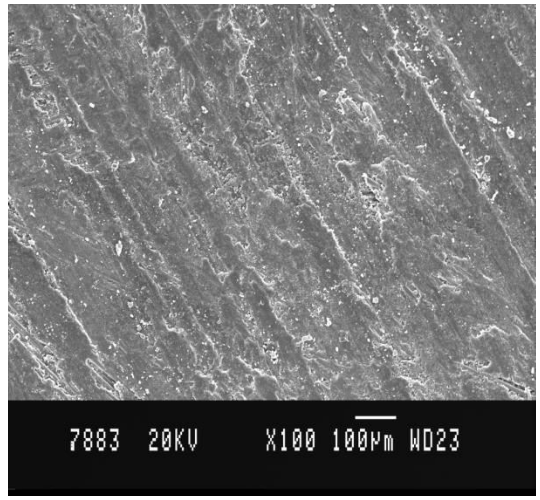

Figure 9 SEM of PYCM sample at 30N/5m/s

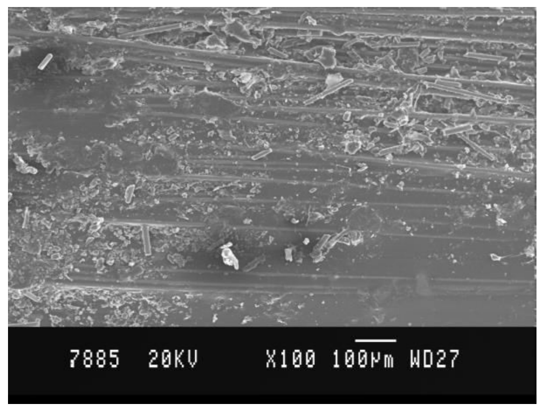

Figure 10 SEM of PUWM sample at 30N/5m/s

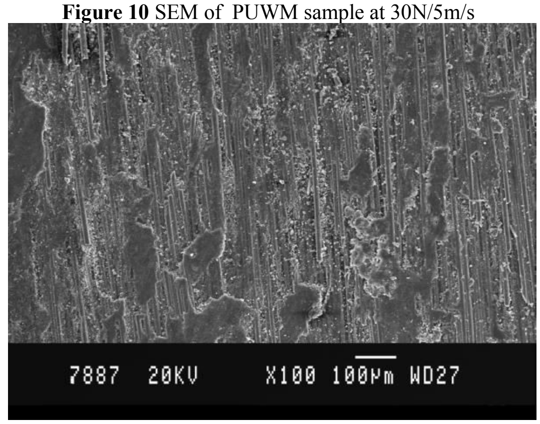

Figure 11 SEM of PUWMGR sample at 30N 5m/s

The SEM of PUWMGR type samples (Graphite filled PUWM composite) .Fig. 8 and PYWMGR type sample as shown in Fig 11 shows the sample subjected to 30 N load and a sliding velocity of 5 m/sec. It is observed that the matrix wear is more and fiber exposure is less. These features support the wear behaviour as seen in SEM (Fig 8 & 11). which reveals that the matrix debris is well spread, yielding more number of glass fiber breakages but comparatively less when compared to the PUWM sample Increasing the sliding velocity to 5 m/s for the same sample (Fig. 8)) results in higher matrix debris formation and heavy breakage of glass fibers (cleavage type) in large numbers compared to. Also, the wear debris is getting totally distributed. These SEMS corroborate the wear data shown in figures pertaining to the wear loss Vs sliding velocity

IV CONCLUSIONS

The following inferences are drawn from the above study.

- Inclusion of chopped strand matt as reinforcement contributed significantly in reducing friction and exhibited better wear resistant properties.
- Chopped strand matt reinforced Polyurethane composites are more wear resistant when compared to Woven fabric Pu- composites
- Graphite filled woven fabric reinforced Pu-composites and FRPy shows higher resistance to slide wear compared to unfilled fabric Pu and Polyester composites.
- FRPu composites showed significant improvement in wear resistance over FRPy composites

REFERENCES

[1] ASM Hand book, 1992, Materials Park, Ohio, USA, ASM International, Volume 18.

[2] Pascoe, M.W., 1973, "Plain and filled plastics materials in bearing: a review." *Tribology,* Vol. 6 No. 5, pp. 184-190.

[3] Sung, N.H., and Suh, N.P., 1979, "Effect of Fiber orientation on friction and wear of fiber reinforced polymeric composites." *Wear, Vol.* 53, pp. 129-141.

[4] Chang, H.W., 1983, "Wear characteristics of composite: effect of fiber orientation." *Wear, Vol*. 85, No. 1, pp. 8 1-91.

[5] Suresha, B., Chandramohan, G., Samapthkumaran, P., Seetharamu, S., and Vynatheya, S., 2006, "Friction and wear characteristics of carbon-epoxy and glass-epoxy woven roving fiber composites." *Journal of Reinforced Polymers and composites,* Vol. 25, pp. 771-782.

[6] Bijwe, J., Tewari, U.S., and Vasudevan, P., 1989 "Friction and wear studies of short glass fiber reinforced polythermide composite." *Wear, Vol.* 132, pp. 247-264.

[7] Viswanth, B., Verma, A.P., and Rao, C.V.S.K., 1991, "Effect of fiber geometry on friction and wear of glass fiber-reinforced composites." *Wear, Vol.* 145, pp. 3 15-327.

[8] Tripaty, B.S., Furey, M.J., 1993, "Tribological behaviour unidirectional graphite-epoxy and carbon -PEEK composites. *Wear, Vol.* 162-164, pp. 3 85-396.

[9] Wang, J., Gu, M., Songhao, Ge, S., 2003, "The role of the influence of MoS on the tribological properties of carbon fiber reinforced Nylon 1010 composites." *Wear, Vol.* 255, pp. 774-779.

[10] Basavarajappa, S., Chandramohan, G. C., 2005, "Wear studies on metal matrix composites:A Taguchi Approach." *J. of Materials Sci. and Tech.,* Vol. 21, No. 6, pp. 348-350.

[11] *Annual hand book of ASTM standards,* Section3,03,02. ASTM G-99[1995], Philidelphia, USA

Effect of Fiber Length and NaOH Treatment on the Flexural Behavior of Coir Fiber Reinforced Epoxy Composite

Ayyavoo Karthikeyan[1*] **Anbarasu Kalpana[2]**
[1]Professor [2]Assistant Professor
[1]Departmentof Mechanical Engineering, Malla Reddy College of Engineering, Secunderabad, India – 500100.
karthirajme@gmail.com
[2]Department of Chemistry, Sri Saradha College for Women, Salem, India – 636 016
kalpanaanbarasu@gmail.com
*** - Corresponding Author**

***Abstract* - This paper presents the study on the effect of fiber length and fiber surface modification on flexural properties of coir fiber reinforced epoxy composites. The composite sample was fabricated with three different fiber lengths namely 10, 20, and 30 mm. The fiber treatment was carried out using sodium hydroxide (NaOH) solution at five different concentrations such as 2, 4, 6, 8 & 10%. The fabrication was made by hand lay-up techniques. Mechanical interlocking between fiber and matrix was observed from the SEM (scanning electron microscope) micrographs. The study reveals that increases NaOH concentration in the fiber treatment was found to increase the flexural strength up to 4% and further increase in NaOH concentration reduce the flexural strength and also the strength increase with increasing fiber length.**

Key words - Coir fiber, epoxy matrix, fiber length, sodium hydroxide, flexural strength

I. INTRODUCTION

Natural fiber composites have become a popular new materials because of their high strength and stiffness, natural availability and environmental ‘friendly’ [1-2]. Additionally they are also recyclable, renewable and have a very low raw material cost [3]. The advantage of natural lignocellulosic fibers over traditional reinforcing materials such as glass fibers, talc and mica are acceptable specific strength properties, low cost, low density, non-abrasive, good thermal properties, enhanced energy recovery and bio-degradability. The main bottle necks in the broad use of these natural fibers in various polymer matrixes are poor compatibility between fiber and the matrix and the inherent high moisture abortion, which brings about dimensional changes in the lignocellulosic based fibers [4]. The efficiency of a fiber reinforced composite depends on the fiber/matrix interface and the ability to transfer stress from the matrix to fiber. This stress transfer efficiency plays a dominant role in determining the mechanical properties of the composite. Coir is an important lignocellulosic fiber obtained from coconut tree which grow extensively in tropical countries. Because of its hard wearing quality, durability and other advantages. It is used for making a wide variety of floor furnishing materials, yarns, rope etc [5]. However these traditional coir products consume only a small percentage of the potential total world production of coconut husk. Hence research and development efforts have been underway to find new use areas for coir including utilization of coir as reinforcement in polymer composite [6-11]. The alkali treatment of coir fiber for coir polyester composites. The experimental results proved that flexural strength, modulus and impact strength of treated fiber composites were 40% higher than those containing the same volume fraction of untreated fibers [12]. Rout et al. [13] have studied the influence of fiber treatment on the performance of coir fiber polyester composites. The investigation proved that the 2% alkali treated coir fiber polyester composites showed better tensile strength (26.80Mpa) whereas 5% alkali treated composites showed better flexural (60.4Mpa) and impact strength (634.6 J/m). Karthikeyan et al. [14] have studied the coconut fiber reinforced epoxy composite with alkali treatment. The results proved that treated fiber composites have better impact strength (27kJ/m2) and also impact strength was greatly influenced by the fiber lengths. Therefore, in this research the coir fibre is chosen to be the sources of fiber for producing reinforced composites and investigate the effects of fiber length and surface modification by NaOH treatment on flexural properties of epoxy resin composites.

II. MATERIALS AND METHODS

In this work, the main studies were carried out to investigate how fiber length of coir fiber reinforced epoxy composite affects flexural strength with and without NaOH treatment. The coir fibers were collected from the rural area of Erode, Tamil Nadu. Coir fibers were carefully extracted from the coconut husk. A diameter of coir fiber was in the range of 0.2743mm. After that the coir fibers were immersed in the NaOH solution (2, 4, 6, 8, & 10% concentration) for 10days. Thereafter, fibers were rinsed with water to remove the excess of NaOH sticking in the fiber. The fibers were then dried at room temperature for 5 days. After that, composites containing 30% by weight of fiber were prepared using fiber of length in the range 10, 20, and 30 mm. A matrix was created by mixing epoxy resin with its hardener in the ratio 10:1 by weight percentage. The mixture was poured into the metal mould of size 300x300x3mm. The fabrication of the composite material was carried out through the hand lay- up technique. The top & bottom surface of the mold and the walls were coated with remover & allowed to dry. The chopped fibers with epoxy resin were mixed manually. Epoxy resin properly mixed with coir fiber was transfer to the mold and the mold close, and then it is pressed in the compression testing machine and left for 24hr for curing. After the curing process, the samples were cut into the required size prescribed in the ASTM D790 standards. The microstructure of composites sample was investigated by scanning electron microscope (SEM).

III. EXPERIMENTAL SETUP

Flexural strength is defined as a material's ability to resist deformation under load. The short beam shear tests are performed on the composite samples to evaluate the value of inter-laminar shear strength. It was a 3-point bend test, which generally promotes failure by inter-laminar shear. This test was conducted as per ASTM standard D790 using UTM. The loading arrangement is shown in Figure 1. The dimension of the specimen was (137x13x3) mm.

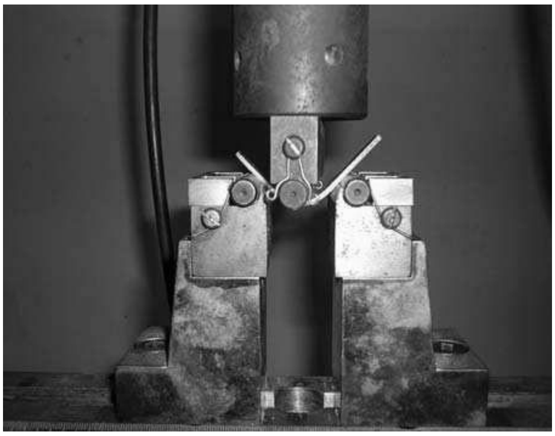

Figure 1 Loading arrangement for flexural test

IV. RESULTS AND DISCUSSION

The average diameter of untreated coir fiber rounded off to two decimals is observed to be 0.27mm. The average tensile strength of the coir fiber is found to be 617.6 mPa. SEM image of untreated coir fiber is shown in Figure 2.

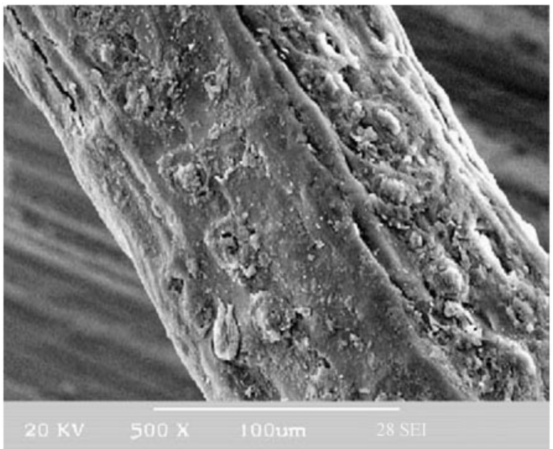

Figures 2 SEM image of untreated coir fiber

The surface of the coir fiber is covered with a layer of substances, which may include pectin, lignin and other impurities. The surface is rough with nodes and irregular stripes. Figure 3 shows similar improvements in the flexural strength of coir fiber reinforced epoxy composite.

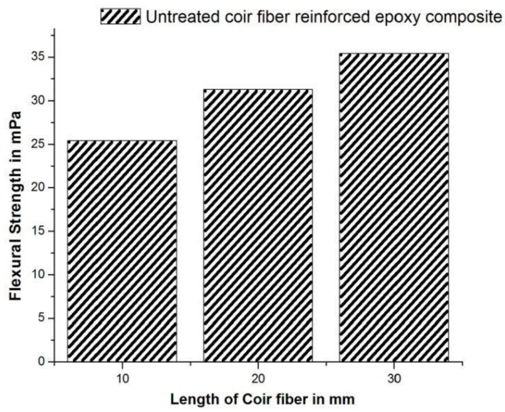

Figure 3 Flexural strength of untreated coir fiber composite

SEM picture (Figure 4) of failed coir epoxy composite under flexural loading also shows evidence for poor interfacial bonding. This gives a clue that the tensile and flexural strengths of coir fiber reinforced epoxy composite could be improved by increasing the length of the fiber and also by improving interfacial bonding.

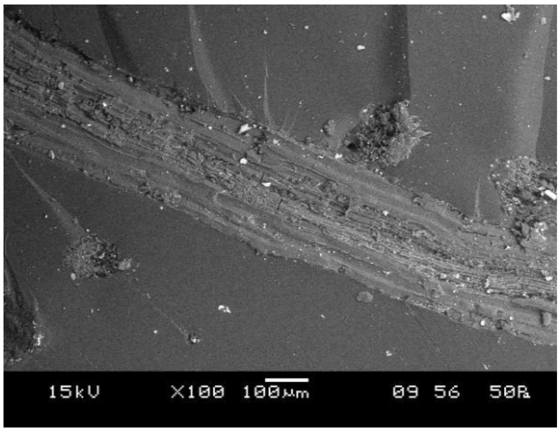

Figure 4 SEM image of failed 10mm long coir composite surface after flexural test

A. Alkaline treated coir fibre

In the composite load is shared between the matrix and fiber. The fiber offers resistance to load in two different ways. One is through its tensile strength and the other is through the interlocking of the fiber surface with the matrix. If the load carrying capacity of the fiber through their tensile strength is poorer than the resistance through the mechanical interlocking of the fiber, it will fail by tensile failure. If it is the other way, it will fail by slipping or pull out of fibers. The tensile resistance offered will be dependent on the net cross-section of the fiber. The mechanical interlocking of the fiber depends on three factors.

1. Co-efficient of sliding friction between the fiber and matrix.
2. Surface properties of the fiber (surface roughness) measured along the axis.
3. Total surface area of fiber.

The NaOH treatment results in changing all the above three parameters simultaneously. The nature of variation of the co-efficient of friction of the fiber is to be investigated. It may improve or deteriorate the frictional resistance offered. The tensile strength of NaOH treated coir fiber is presented in Figure 5.

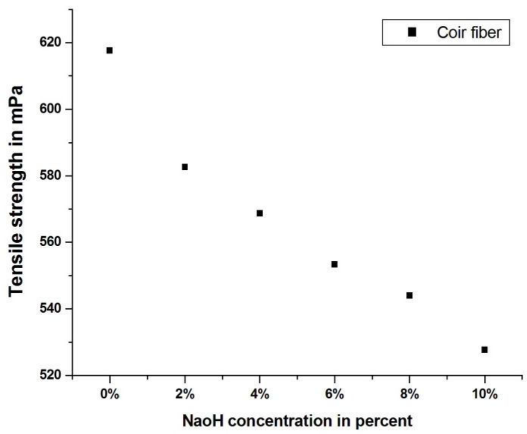

Figure 5 Tensile strength of NaOH treated coir fiber

A decreased trend in the tensile strength of the fiber is seen with increased NaOH concentration. Denser NaOH solution provides more Na+ and OH- ions to react with the substance on the fiber, causing greater amount of lignin, pectin to leach out. It seems that lignin, pectin are stronger than the core of the fiber and hence their removal results in loss of strength. The diameter of NaOH treated coir fiber is presented in Figure 6.

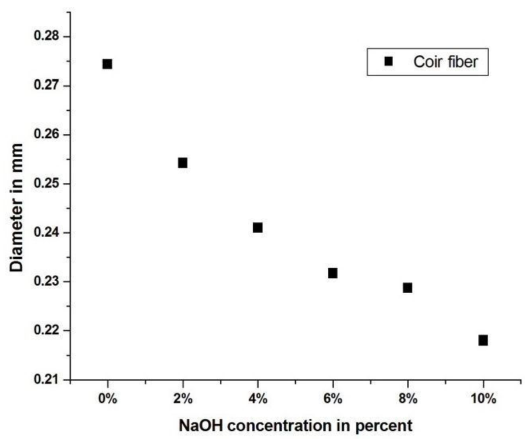

Figure 6 Influence of NaOH treatment on coir fiber diameter

Figure 6 shows how the variation in NaOH concentration affects the fiber diameter. Stronger NaOH solutions remove more and more lignin, pectin and other impurities from the surface of the coir fiber there by reducing the diameter.

B. SEM image of NAOH treated coir fiber

The effect of NaOH treatment on fiber surface morphology was analyzed by scanning electron microscope. The NaOH treatment seems to modify the surface of the coir fiber. Removal of pectin, lignin and other impurities has resulted in increase in the surface roughness. Figure 7 show the surface modification of coir fiber treated with 2% NaOH concentration. 2% NaOH solution has reacted with the nodes and strips on the fiber surface turning the fiber surface a bit smother than the untreated fiber surface.

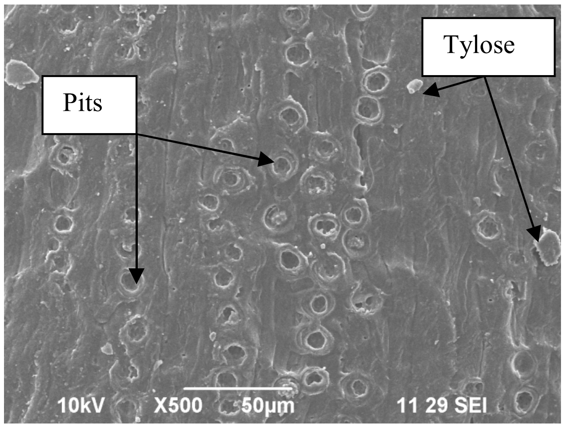

Figure 7 SEM image of 2% NaOH treated coir fiber

The SEM image also shows a number of pits which are evidence of such reactions. As a result of these reactions fatty deposits called tyloses are found to be dislodged and spread over the surface. As a result of increasing the NaOH concentration up to 4%, the surface roughness is increased as evidenced from more number of rows of pits on the surfaces. The globular protrusions called tyloses shown in Figure 7 are appearing on the fiber surface. Pits are seen to have spread along the entire cell wall outside of the parenchyma cells of NaOH treated fibers. The presences of pits after chemical treatment are important for increasing the effective surface area and the surface roughness, consequently improving the mechanical interlocking with the polymeric matrix. An increase in NaOH concentration up to 6% the surface roughness increases. Most of the fatty deposits have been removed from the fiber surface. Only shallow pits less in number are seen, on the fiber surface as compared to that of 4% concentration. Absence of ridges and valleys on the fiber surface may lead to less resistance to relative sliding between fiber and matrix. Increase in NaOH concentration up to 8%, has led to aggressive reaction leaving behind more number of ridges and valleys. There is also evidence for diameter having reduced. A further increase in NaOH concentration up to 10% leads to further increase in surface roughness. The fiber diameter is also seen to have further reduced. Increased surface roughness in the case NaOH treated coir fibers with 8% and 10% concentration may improve the interlocking between the fiber and matrix but at the same time the reduction in fiber diameter may weaken its load carrying capacity.

C. Flexural strength of NaOH treated coir epoxy composite

From Figure 8 it is seen that the flexural strength increases with increase in fiber length. The flexural strength of the composite increases with NaOH concentration up to 4% and reduces thereafter.

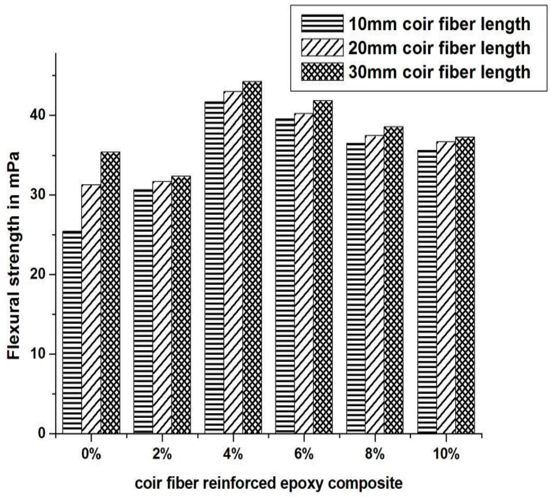

Figure 8 Flexural strength of untreated coir/epoxy composite and NaOH treated coir/epoxy composite

The flexural strength of the NaOH treated coir fiber reinforced epoxy composite has improved when compared to that of untreated coir fiber reinforced epoxy composite. SEM pictures of failed surfaces of NaOH treated 10mm fiber reinforced epoxy composite show evidence for fiber pullouts. Even though SEM pictures of NaOH treated 20mm fiber reinforced epoxy composites show similar pulled out fibers across the failed surface, they are less concentrated when compared to that of 10mm NaOH treated fiber reinforced epoxy composites (Figure 9). As for as the flexural strength is concerned reinforcing with 10mm NaOH treated fibers introduced a maximum of 63.99% increase when treated with 4% NaOH solution, whereas 20mm and 30mm NaOH treated fibers introduced only about 33.34% and 24.92% increase in the flexural strength.

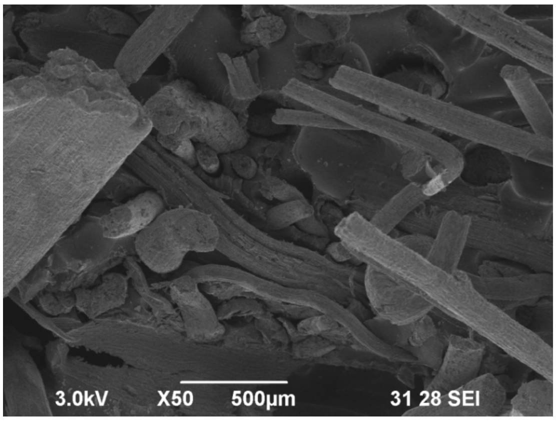

Figure 9 SEM image of 4% NaOH treated 10mm long coir/epoxy composite after flexural failure

Even though the fiber treated with higher concentrations of NaOH leads to improved surface properties as evidenced from reduced pull outs (Figures 10), the fiber diameter is also reduced as a result of which the flexural strength of the composite reduces. Hence 10mm fiber treated with 4% NaOH solution is found to be preferable to increase the flexural strength of the composites.

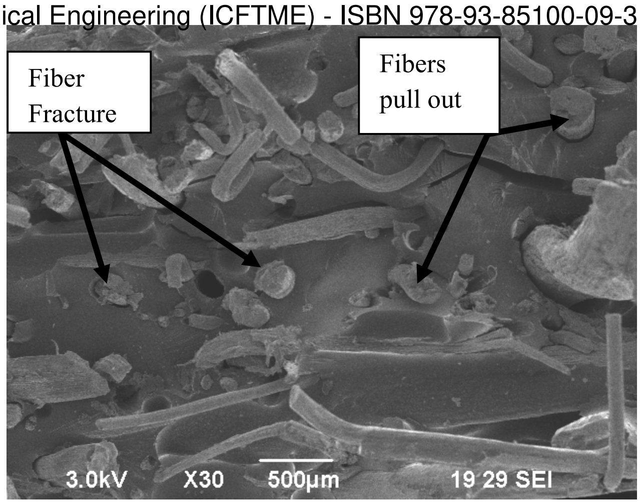

Figure 10 SEM image of 4% NaOH treated 20mm long coir/epoxy composite after flexural failure

V. CONCLUSION

1. This work shows that successful fabrication of a coir fiber reinforced epoxy composites with different fiber lengths is possible by simple hand layup techniques.
2. The surface of untreated coir fiber is covered with a layer of substance, which may include pectin, lignin and other impurities. The coir fiber surface is rough with nodes and irregular stripes.
3. For the untreated coir fiber of length 10mm, the mechanical interlocking between fiber and matrix is weak and the frictional resistance is small the fiber slips, thereby letting the fiber to take only limited tensile load.
4. Increasing the length of untreated fiber (20, 30mm) increases the surface area in the interface between fiber and matrix, increasing the frictional load carrying capacity.
5. When the fiber is treated with NaOH solution, a decreased trend in the tensile strength is seen with increased NaOH concentration. The NaOH solution reacts with the substance on the fiber, causing greater amount of lignin, pectin to leach out. Their removal results in loss of strength, due to reduced diameter and an increase in the surface roughness, thereby increasing the mechanical interlocking between fiber and matrix.
6. 10mm NaOH treated coir fiber reinforced epoxy composite introduced a maximum of 63.99% increase in flexural strength when treated with 4% NaOH solution, whereas 20mm and 30mm NaOH treated fibers introduced only about 37.34% and 24.92% increase as compared to that of untreated coir fiber reinforced epoxy composite.

VI. REFERENCE

[1] S.M. Sapuan, A. Leenie, M. Harimi, Y.K. Beng, *Mater. & Design.,* 27, 689-93 (2006).

[2] S. Mukhopadyay, S. Srikanta, *Poly. Degrad Stability.,* 93, 2048-51 (2008).

[3] N.G. Justiz Smith, G. Junior Uirgo, V.E. Buchanan, *Mater. Charact.,* 59, 1273-8 (2008).

[4] N. Chand, P.K. Rohatgi, K.G. Satyanarayana, *In Lac Stuard M. editor. Inter. Encyclopedia of compo. VCH publishers, Germany.,* 4, 9 (1991).
[5] K.G. Satyanarayana, A.G. Kulkarni, P.K. Rohatgi, *J Scient. Ind. Res.,* 40, 222 (1981).
[6] O. Owolabi, T. Czuikovszky, I. Kovacs, *J Appl. Polym. Sci.,* 30, 1827 (1985).
[7] D.S. Varma, M. Varma, I.K. Varma, *J Reinf. Plast. Compos*., 4, 419 (1985).
[8] Varma DS, Varma M, Varma IK. *Ind. Eng. Chem. Prod. Res. Dev.* 1986, 25, 282.
[9] V.G. Geethamma, K. Thomas Mathew, R. Lakshminarayan, S. Thomas, *Polym.,* 39, 1483 (1988).
[10] A. Paul, S. Thomas, *J Appl. Polym. Sci.,* 63(2), 247 (1997).
[11] H.P.S. Abdul Khalil, H.D. Rozman, M.N. Ahmad, H. Ismail, *Polym. Plast. Techno.l Eng.,* 39(4), 757 (2000).
[12] S.V. Prasad, C. Pavithran, P.K. Rohatgi, *J Mater. Sci*., 18, 1443 (1987).
[13] J. Rout, M. Misra, S.S. Tripathy, S.K. Nayak, A.K. Mohanty, *Compos. Sci.,* 61, 1310 "(2001).
[14] A. Karthiieyan, K. Balamurugan, *J Sci. Ind. Res.,* 71, 627-631 (2012).

First. Author was born in Salem city, Tamil Nadu, India, in 1981. He received the B.E. Mechanical Engineering from Periyar University, salem in 2003 and M.E. Engineering Design degrees from Anna University, Chennai, in 2005 and the Ph.D. degree in mechanical engineering from Anna University, Chennai, in 2014. From 2006 to 2017, he was an Assistant professor and Associate Professor in the department of Mechanical Engineering, K.S.R. College of Engineering, Tiruchengode, Namakkal, Tamil Nadu. Now he is working as a Professor in the department of Mechanical Engineering, Malla Reddy College of Engineering, Secunderabad, India. He has published 07 research papers in international journals with good impact factor and 01 paper in international conference and 02 paper in national conference. He filed 05 patent among that 02 was completed registered. He was act as a reviewer of few journals and conferences. His research interest includes composites and anthropomorphic hand/Brain computer interfece. He is guiding three Ph.D., research scholars.

Second. Author was born in Salem city, Tamil Nadu, India, in 1977. She received the B.Sc. Chemistry from Periyar University, Salem in 1997 and M.Sc. Chemistry degrees from Periyar University, Chennai, in 2005 and now submitted her Ph.D. thesis in 2017. From 2008 to 2017, she was an Assistant professor in the department of Chemistry, Sri Saradha College for Women, Salem, India – 636 016. She has published 08 research papers in reputed journals like Elsver international journals with good impact factor and 01 paper in international conference and 02 paper in national conference.

5

EFFECT OF CONSTRUCTIONAL CHANGE IN I.C ENGINE PISTON BY PARTIALLY CERAMIC COATING

M.PONMURUGAN
ASST.PROFESSOR /MECH,
BANNARI AMMAN INSITUTE OF TECHNOLOGY,
SATHYAMANGALAM-638401
ERODE DISTRICT- TAMILNADU
ponstms@yahoo.co.in

A.SUNDARAMAHALINGAM
ASST.PROFESSOR /MECH,
BANNARI AMMAN INSITUTE OF TECHNOLOGY,
SATHYAMANGALAM-638401
ERODE DISTRICT- TAMILNADU
sundaramahalingama@bitsathy.ac.in

Dr.M. RAVIKUMAR
HOD /MECH,
BANNARI AMMAN INSITUTE OF TECHNOLOGY,
SATHYAMANGALAM-638401
ERODE DISTRICT- TAMILNADU
RAVIKUMARM@bitsathy.ac.in

ABSTRACT

To modify the construction of the piston in S.I. engine is the main goal of this project. Modifying the construction improves the engine operating parameters.As a consequence, the durability of the piston gets reduced. In order to increase the durability of the piston, “Partially ceramic coating” is given on the piston.

Thermal analysis are to be investigated on a conventional(uncoated) SI engine piston, made of AlSi alloy and steel. Secondly, thermal analysis are to be performed on piston, coated with MgO-ZrO2 material by means of using a commercial code, namely ANSYS. Finally, the results of different pistons will be compared. The effect of coatings on the thermal behaviour of the piston are to be investigated and improved.

INTRODUCTION

In general, the efficiency of any petrol engines is around 55% i.e. only 55% of the heat input obtained by burning the fuel is utilized for useful work and the remaining 45% is wasted in the form of heat losses. An effort has been made to maintain high temperature inside the cylinder by reducing the heat transfer through the coolant and exhaust gases, for complete combustion and to increase the efficiency.

The demand for higher specific output diesel engines and increasingly radical bowl geometries used to meet legislated emission regulations has focused on the need for improvements in aluminium alloy pistons. At high engine outputs, steel- crowned articulate pistons have been substituted for aluminium pistons with great success because of the increased strength of steel at higher temperatures. However, articulate steel piston usage results in increased cost, increased reciprocating weight. Therefore, some geometrical compromises, for e.g..an offset piston bowl are not practical.

Given that the application of a thermal barrier coating and constructional change to the aluminium piston crown results in a reduction in the substrate temperature, it may be possible to return the aluminium piston to historic durability levels at the higher engine output levels.

The intent of this investigation is to determine whether a finite element analysis can be used to provide accurate estimates of temperatures and stresses occurring within the constructional change thermal barrier coating applied to an aluminium alloy piston crown for various coating thicknesses.

1.PETROL ENGINE

The Otto cycle is the ideal cycle for SI engines. The CI engine, first proposed by A.N. Otto, it is very similar to the SI engines, the air-fuel mixture is compressed to a temperature that is below the self ignition temperature of the fuel. The combustion process is initiated by firing a spark plug. In CI engines, air alone is compressed to a temperature that is above the auto ignition temperature of the fuel and the combustion starts as the fuel is injected into this hot air. Therefore, the spark plug and carburetor in petrol engines are replaced by a fuel injector in diesel engines. The compression ratio of an SI engine is between 6 and 10 and that for a CI engine is from 16 to 20.

2.THERMAL BARRIER COATING

Thermal barrier coating usually consist of two layers (duplex structure). The first layer, a metallic one, is the so-called bond coat, whose function is, on the one side, protects the basic material against oxidation and corrosion and, on the other side, to provide with good adhesion o he thermal insulating ceramic layer. The second layer containing the thermal barrier, a ceramic coating is mostly made of yttria partially stabilized zerconia (YSZ), since this material has turned out particularly stabilized during the last decades. Recently, nevertheless, new developments are coming up but are still in research stage.

In industries there are two different processes for the manufacturing of thermal barrier coatings: the electron beam – physical vapor deposition (EB-PVD) and the plasma sparing (PS). Whilst EB-PVD process is usually used to applies vacuum plasma – sprayed bond coats, which are mostly made of MCrAIYs (M=Ni, Co). Recently, the high velocity oxy-fuel technology (HVOF) is also increasingly used for this task. The ceramic layer is usually deposited by means of the atmospheric plasma spraying (APS).

3.STUDY OF EXISTING SYSTEM

The existing system is an experimental low speed petrol engine used for power generation. It has an open type combustion chamber, clearly indicating that it is a low speed engine. An old worn out piston of this engine is used for modeling the piston (as it needed the sectioning of the model).

The analysis needed a clear definition of the material properties, selection of element, boundary conditions and initial conditions. For which the certain data are calculated using the petrol engine cycle and some are taken from the literatures. All the data assumed in the analysis are theoretical values and hence the analysis is purely theoretical.

4.ENGINE SPECIFICATION

Make	Mahel
No. of cylinder	One
Type of cooling	Oil
Ignition	Spark Ignition
Bore	95 mm
Stroke	110 mm
Compression ratio	8.8:1
Speed	1500 rpm
Fuel oil	Petrol
Brake power	3.9kW
SFC	0.251 kg/kW hr

5.MATERIAL PROPERTIES

The piston is made of cast aluminium alloy (AlSi). Its material property is presented in Table. 3.3.1. It has good strength and hardness at elevated temperatures with good wear resistance.

Material property	Al Alloy
Thermal conductivity, k (W/mK)	155
Density, ρ (kg/m^3)	2700
Specific heat, C (J/kg K)	965
Coefficient of thermal expansion (1/k)	19.5×10^3
Young's modulus, E (Mpa)	90×10^3
Yield strength (Mpa)	410
Poisson's ratio	0.3

properties of cast aluminium alloy

6.FINITE ELEMENT MODELING AND MESHING

The piston is modeled in PRO-E WILDFIRE-3, which is one of the most effective modeling packages. PRO-E is very-friendly and comprehensive. IGES (Initial Graphics Exchange Specification) is the ANSI standard that defines a natural format for the exchange of information between CAD/CAM systems, with an IGES translator; you can translate a PRO-E modeling into a format that can be read CATIA or other CAD systems. IGES format reduces the number of translators required to move the information among multiple CAD/CAM formats.

7.STRUCTURAL BOUNDARY CONDITION

There are two boundary conditions and various constraints are applied to this model. Basically there are two constraints that are applied in this model. One on the piston rings region and the other at the gudgeon pin.

The first boundary condition is the pressure applies at the piston head as shown in the fig indicated by red arrows the applied pressure is around 15.25 bar as calculated at the end of the compression of the theoretical constant pressure cycle.

Pressure at the end of the compression,

$$P_2 = P_1 \times \left(\frac{T_2}{T_1}\right)^{\gamma/(\gamma-1)}$$

P_2 = 15.25 bar

Where, P_1 – Absolute Pressure

T_1 – Ambient Temperature

T_2 – Temperature at the end of compression

γ - Isentropic index, 1.4 (for air)

The second boundary condition on the gudgeon pin, there the resultant force of 821.45 N is applied along the Y-direction. The resultant force is obtained through the theoretical calculation of petrol cycle.

The actual engine power,

$$P = F \times r \times \frac{2\pi N}{60}$$

F= 451.8 N

The force obtained is an actual force calculated with respect to the output but the calculation is based on the theoretical cycle. The efficiency of the engine is only 30%, hence, the theoretical reaction force ($F_{theoretical}$) acting on the gudgeon pin is calculated.

$F_{theoretical}$ = 821.45 N

Where, N – Engine Speed in rpm

r – Half of stroke length in m

F – Reaction force in N

8. DESIGN CALCULATION OF EXISTING PISTON

- Calculations of total volume of the cylinder any reduction of compression rings, oil ring, cylinder inner cut portion and Gudgeon pin portions,

Volume of the solid cylinder,

$V_{solid} = \pi r^2 h$

Were, r = 26.50 mm

h = 41.06 mm

$= \pi\times(26.50)^2 \times 41.06$

V_{solid}= 90539.968 mm^3

- Calculations of the compression rings,

Volume of the compression ring= $\pi\times(26.50)^2 \times 1$

Were, r = 26.50 mm

h = 1 mm

= 2205.06 mm^3 ------------------ 1

Were, r = 24.50 mm

h = 1 mm

$= \pi\times(24.50)^2 \times 1$

= 1884.785 mm^3--------------- 2

Subtract equation number from 1 to 2

$V_{comp.ring1}$ = 2205.06 - 1884.785

= 320.28 mm^3

Both the compression rings are same dimensions so,

Volume of the compression ring,

$V_{comp.ring2}$ = 320.28 mm^3

Volume of the compression rings,

$V_{comp.\ rings} = V_{comp.ring1} + V_{comp.ring2}$

= 320.28 + 320.28

= 640.56 mm^3

- Calculations of the oil ring,

Were, r = 26.50 mm

h = 1.21 mm

$=\pi\times(26.50)^2\times1.21$

= 2668.128 mm^3 ----------------- 3

Were, r = 24.50 mm

h = 1.21 mm

$= \pi\times(24.50)^2 \times 1.21$

= 2280.589 mm^3 ----- 4

Subtract equation number from 3 to 4 =2668.128-2280.589 $V_{oil\ ring}$ = 387.539 mm^3

- Calculations of the Gudgeon pin portions V_g,

There are two Gudgeon pin portions are there

Were, r= 7 mm

h = 3.7 mm

$= \pi\times(7)^2 \times 3.7$

Volume of the portion V_{g1} = 569.282 mm^3

Both the Gudgeon pin portions are same dimensions so,

Volume of the portion V_{g2} = 569.282 mm^3

Volume of the both the Gudgeon pin portions,$V_g=V_{g1}+V_{g2}$ =569.282+569.282

V_g = 1138.564 mm^3

- Calculations of the cylinder inner cut portion,

There are two inner cut portions are there

Were, r = 19.62 mm

h = 10.47 mm

Volume of the cylinder inner cut portion,

$V_{inner\ cut\ 1} = \pi\times(19.62)^2 \times 10.47$ = 12655.355 mm

Were, r = 22.8 mm

h = 20.59 mm

Volume of the cylinder inner cut portion,

$V_{inner\ cut\ 2} = \pi*(22.8)^2 *20.59$

= 33609.007 mm^3

Total volume of the piston,

$V = V_{solid} - V_{comp.\ rings} - V_{oil\ ring} - V_g - V_{inner\ cut\ 1} - V_{inner\ cut\ 2}$

= 90539.968 - 640.56 - 387.539 - 1138.564 - 12655.355 - 33609.007

V = 42108.943 mm^3

Mass, m $= \rho V$

$= 2700 \times 42108.943\times10^{-9}$

= 113.69 gm

9. EXISTING PISTON

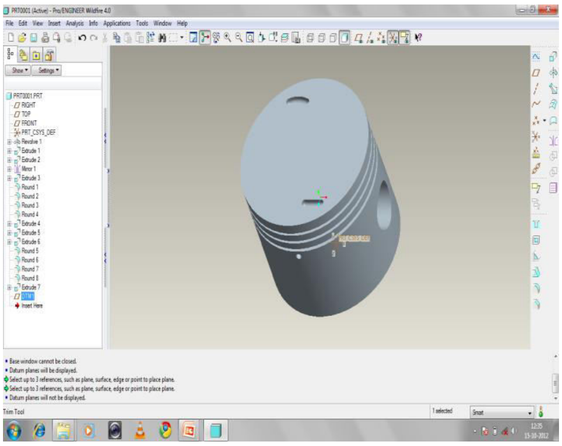

Modified Piston Without Ceramic Coating

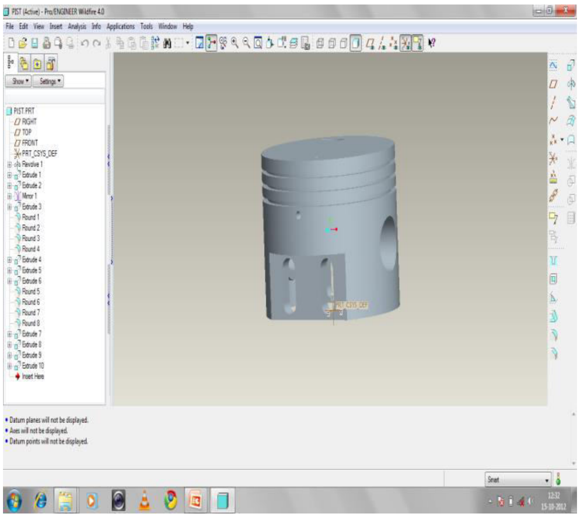

Meshed View Of Existing Piston

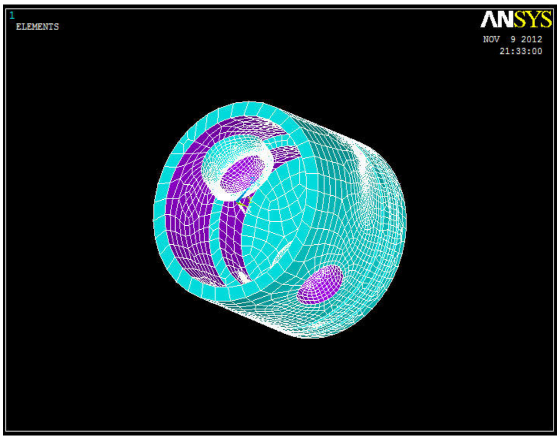

POST PROCESSING

Once the boundary conditions are applied, the problem is solved using the Ansys 11.0 solver. The results obtained are temperature distribution, heat flux, deflection and total stress.

10. TEMPERATURE DISTRIBUTION

The fig. shown above gives the temperature distribution over the volume of the piston at steady state after and application of thermal loads. The maximum temperature occurs at the top of the piston. Even though the working medium is at the higher temperatures, the surface temperature at the combustion temperature is comparatively low (Around 790.52K).

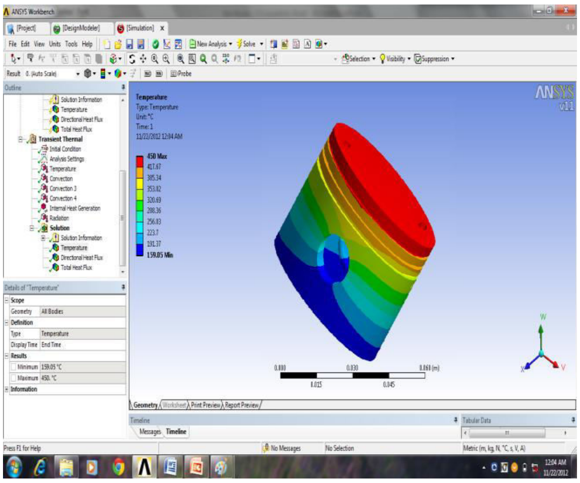

Temperature distribution

11. HEAT FLUX

The fig.shown above gives the thermal flux distribution over the volume of the piston at steady state after the application of thermal loads.

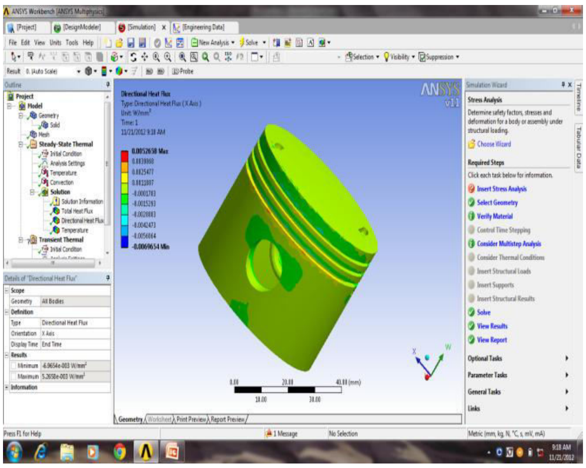

Directional Heat flux

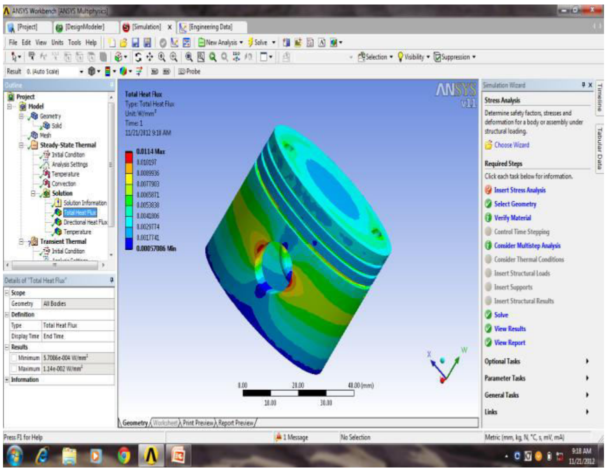

Total heat flux

FUTURE WORK

The existing piston is designed using Pro-E software and analyses by ansys software. The coating of ceramic (magnesium oxide (MgO) and zirconium oxide (ZiO)) over existing aluminium alloy piston will be done and behavior will be analyzed to improve the performance of the given engine.

REFERENCES

1. Bhaumik Patel, AshwinBhabhorDESIGN AND PREDICTION OF TEMPERATURE DISTRIBUTION OF PISTON OF RECIPROCATING AIR COMPRESSOR, International journal of Advanced Engineering.IJAERS/Vol. I/ Issue III/April-June, 2012/172-174
2. P. Gustof, A. HornikThe influence of the engine load on value and temperature distribution in the piston of the turbocharged Diesel engine.
3. EkremBuyukkaya , MuhammetCerit "Thermal analysis of a ceramic coating diesel engine piston using 3-D finite element method" Surface and coatings technology, june 2007.
4. MuhammetCerit "Thermo mechanical analysis of a partially ceramic coated piston used in an SI engine" ,Surface & coatings Technology, december 2010.
5. M.M.Ragman, A.K.Arifin,N.Jamaludin"Fatique life prediction of two stroke free piston engine mounting using frequency response approach" European journal of scientific research, Vol 22 No.4, 2008.
6. Mirowslawkarczewski,Krzysztofkolinskijercywalentynowcisz "Optical analysis of combustion engine elements" journal of KONES Powertrain and transport , Vol 18, No.1, 2011.
7. Jing Yang, Yi Wang, "Heat load analysis of piston based on the ANSYS", Advanced materials research, Vol 199-200, 2011.
8. EkremBuyukkaya, MuhammetCerit, Theoretical analysis of ceramic coated petrol engine piston using finite element method, Sakarya University, Engineering Faculty, Department of Mechanical Engineering, Esentepe Campus, Sakarya 54187, Turkey (2007).
9. ImdatTaymaz, The effect of thermal barrier coatings on Petrol engine performance, Faculty of Engineering, University of Sakarya, EsentepeKampusu, 54178, Adapazan, Turkey (1993).

Performance study for 49 cm^2 multi pass flow channel of PEMFC

Dr.V.Lakshminarayanan
Department of Mechanical Engineering, B V Raju Institute of Technology, Narsapur,
Telangana, India – 502313
lux32engineer@yahoo.co.in

Dr.P.Velmurugan
Department of Mechanical Engineering, Malla Reddy College of Engineering, Hyderabad-500014

Jobin.C. Varghese
Department of Mechanical Engineering, B V Raju Institute of Technology, Narsapur,
Telangana, India – 502313
jobinvarghese20@gmail.com\

ABSTRACT

The Polymer Electrolyte Membrane Fuel Cell (PEMFC) performance depends on the design and operatingparameters. In this paper, optimization of operating parameters such as pressure, temperature, stoichiometric ratio of inlet reactant mass flow rate and design parameters like various landing to channel width (L:C) 1:1, 1:2, 2:1 and 2:2 on 49 cm^2 effective area multi pass serpentine flow channel of the PEMFC was studied. The analysis was carried out on the various parameters by Ansys Fluent CFD (Computational Fluid Dynamics) and optimization was done by Taguchi method using Minitab 17 software. Based on the optimization study, the L: C-1:2 havegiven 0.223 W/cm^2 maximum power density on PEMFC performance and square of response factor (R^2) was achieved as 99.69 %.

Keywords- Optimization; Design parameters; PEMFC; CFD; Square of response factor ; Multi pass serpentine flow channel.

I. INTRODUCTION

Fuel cells are converting chemical energy of fuels (hydrogen and oxygen) directly into electricity without any intermediate stage like classical combustion of two and four stroke engine. It has become an integral part of alternative energy sources with high energy efficiency without affecting the environment. Among all types of fuel cells, the proton exchange membrane fuel cell has reached important stage, particularly for mobile and portable applications. Besides their high-power producing capability, PEMFCs work at low temperatures, produce only water and heat as byproduct, and can be compactly assembled, making it as one of the leading candidates for the next generation power generator [1]. The PEMFC consists of polymer solid electrolyte membrane sandwiched between an anode and cathode. However, water and heat is the by-product of electrochemical reaction. The water management of PEMFC has become an important task, whereas too much of water accumulation causes “flooding” or too little water causes dryness of membrane can adversely impact the performance and lifetime of PEMFCs. Water accumulation leads the fuel cell performance unpredictable and unreliable under the nominally identical operating conditions. In order to enhance the performance and reliability of PEMFC, it is important to know more about the mechanism which causes performance loss, such as current density distributions, high ionic resistance due to dry membrane and flooding on the cathode [2-4].Dehydration is drying the membrane due to deficiency of water in the anode side which indicates to higher ohmic and ionic losses, which leads to a significant drop of potential and power in the PEMFC [5-6].

The numerical analysis were carried out with six different cross-sections of the channel (square, triangle, parallelogram 14^o, parallelogram 26^o, trapezium and inverted trapezium) with a constant cross sectional area of single pass PEMFC [7]. It was concluded that, square flow channel of single pass PEMFC having a peak power density of 1.133 W/cm^2 @ 2.834 A/cm^2& 0.4 V. The performance enhancement of the combined effect of design and operating parameters of serpentine and interdigitated flow channel with 25 cm^2 active area of PEMFC with four different parameters using optimization technique and CFD [8]. The results revealed that the peak power density of interdigitated flow channel with landing to channel width (L:C) 1:2 showed better than the serpentine flow channel with L: C- 1:2.optimization of operating and design parameters such as pressure, temperature, stoichiometricratio of inlet reactant mass flow rate and various landing to channel width on serpentine flow channel of 16 cm^2 active area of the PEMFC was studied by Lakshminarayanan et al [9]. The results were concluded that, the L: C- 1:2 has maximum power density of 0.422 W/cm^{2}and square of response factor (R^2) was achieved by Taguchi method as 97.90 %.The effect of the various parameters and various landing to channel width of (L: C) 1:1, 1:2 and 2:2 Multipass serpentine flow channel PEMFC with 36 cm^2 (6cm x 6cm) effective area was analyzed numerically by Lakshminarayanan et al [10].He concluded that the maximum power density of 0.658W/cm^2 was obtained in the L: C of 1:1. However, operating parameters like pressure, temperature and inlet mass flow rate of reactants influenced the performance of PEMFC significantly. The critical issue for PEMFCs can be resolved through appropriate design of flow channels and finding the proper operating parameters for effective removal of water built on the flow field plates. Hence the immediate attention required towards optimizing the simultaneous influence of operating and design parameters for the performance of the PEMFC using CFD Fluent and MINITAB software packages. Hence this paper has a detailed study about the optimization of operating pressure, temperature, stoichiometric ratio of inlet reactant mass flow rate and various landing to channel width (L:C)-1:1,1:2,2:1&2:2 of 49 cm^2 active area on multi pass serpentine flow channel of PEMFC are studied and influence their performance were compared.

II. MODEL DEVELOPMENT

The modeling was done by creating individual parts of the PEMFC and the dimensions of individual parts such as the anode and cathode GDL, solid polymer electrolyte membrane, the anode and cathode catalyst layers as shown in the Table 1.The assignments of zones for various parts were done by Workbench 14.5. The various geometrical models (L: C-1:1, 1:2, 2:1 and 2:2) of serpentine multi pass flow channel were meshed by using ICEM 14.5 (a module of Ansys 14.5). Three dimensional (3-D) PEMFC model with serpentine flow channel of various landing to channel width configurations were created by Creo Parametric 2.0 as shown in Fig.1.

Table 1.Dimensions and Zone type, ssigning of fuel cell

<table>
<tr><th>S.No</th><th>Part Name</th><th>Width (mm)</th><th>Length (mm)</th><th>Thickness (mm)</th><th>Zone type</th></tr>
<tr><td>1</td><td>Anode & Cathode Flow channel</td><td rowspan="4">40</td><td rowspan="4">40</td><td>10</td><td>Solid</td></tr>
<tr><td>2</td><td>Anode & Cathode catalyst</td><td>0.08</td><td>Fluid</td></tr>
<tr><td>3</td><td>Membrane</td><td>0.127</td><td>Fluid</td></tr>
<tr><td>4</td><td>GDL anode & cathode</td><td>0.3</td><td>Fluid</td></tr>
</table>

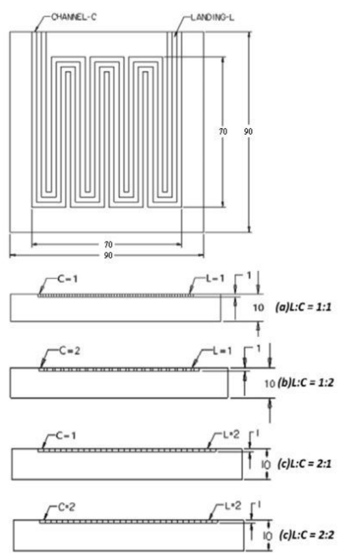

Fig.1.Various landing to channel width (L: C) (a)1:1 (b)1:2 (c)2:1 and (d)2:2 of multi pass serpentine flow channel of 49 cm^2 active area of PEMFC.

a. Boundary conditions

Anode gas channel and Cathode gas channel is set as inlet (mass flow inlet) and outlet zones(pressure outlet)

Surfaces that represent anode and cathode terminals

Optional boundary zones that could be defined include any voltage jump surfaces, interior flow surfaces or non-conformal interfaces that are required.

B .Continuum Zone

Flow Channels for anode and cathode-sides

Anode and cathode current collectors

Anode and cathode gas diffusion layers

Anode and cathode catalyst layers

Electrolyte membrane

The anode is grounded (V = 0) and the cathode terminal is at a fixed potential which is less than the open-circuit potential. Both the terminals should be assigned the ‘wall’ boundary type.

A. Meshing on PEMFC

After geometry building, the next step was discretization done by ANSYS 14.5 ICEM software. The meshing method was used as Cartesian grid, which helps in the formation of hexahedral mesh to get accurate results. Hence the entire cell was divided into finite number of discrete volume elements or computational cells to solve the equations associated with the fuel cell simulation. Split block method used for blocking and meshing was done with Cartesian method. Body fitted mesh was used and projection factor was set to 1. The projection factor determines how closely the edges of the mesh match up with the grid.

B. Governing Equations

The simulation was solved by simultaneous equations like conservation of mass, momentum, energy, species concentration, butler–Volmer equation, Joule heating reaction and the Nernst equation to obtain reaction kinetics of the PEMFC. The model used to consider the system as 3-D, steady state and inlet gases as ideal condition, system as an isothermal and flow as laminar, fluid as incompressible, thermo physical properties as constant and the porous GDL, two catalyst layers and the membrane as an isotropic.

C. Solver

A control volume approach based on commercial solver FLUENT 14.5 was used to solve the various governing equations. Three-dimensional, double precision and serial processing were used for this model.

The species concentration on anode side of H_2, O_2, and H_2O were 0.8, 0, and 0.2 respectively. Similarly, on the cathode side were 0, 0.2 and 0.1 respectively. The porosity at anode and cathode side was 0.5. Open circuit voltage was set at 0.95 V on the cathode and the anode was grounded. The cathode voltage has been varied from 0.05 V to 0.95 V used for solving kinetics reaction in order to get the current flux density, H_2, O_2, and H_2O fractions along with the flow field design. Multi grid settings were modified as F-Cycle for all the equations and entered termination restriction value was set as 0.001 for H_2, O_2, H_2O and water saturation. The electric and proton potential values were set at 0.0001. Stabilization method BCGSTAB was selected for H_2, O_2, H_2O, water saturation, electric and proton potential. The Anode and Cathode reference current density was set to be10000A/cm^{2}and 20 A/cm^2 respectively 0.1 kmol/m^3 was set to anode and cathode reference concentration,Anode and cathode exchange coefficient was set to be 2.The Reference diffusivity of H_2,O_2 and H_2O was set to as 3E-5.

III. **TAGUCHI METHOD**

Taguchi method can be used to find out the most optimum combination among the input parameters (Design and Operating) which will result in getting the maximum possible output which cause the performance enhancement of PEMFC. In Taguchi method L16 standard orthogonal array with 4-level and 4 factors was used and the parameters were considered as low, high and medium range values. When this orthogonal array was used, significance of factors and optimum combination can be found in 16 runs itself. The factors considered for the analysis were landing to channel ratios on serpentine multi pass flow field design (L: C-1:1, 1:2, 2:1 and 2:2), pressure (1, 1.5, 2 and 2.5 bar), temperature (313, 323, 333 and 343 K), anode and cathode reactants as stoichiometric ratios (S/F) of 3, 3.5, 4 and 4.5. The theoretical value of hydrogen in the anode side was 4.33E-07 kg/s and cathode side was 3.33E-06 kg/s.

IV. **RESULTS AND DISCUSSION**

As per L16 orthogonal array, the inputs were given to the analysis software and having all other parameters constant. The power density from polarization curve was found by numerical study using CFD Fluent 14.5 software package for all 16 runs and the corresponding Signal/Noise (S/N) ratios were found from MINITAB 17 software and were shown in Table 2.

The landing to channel width ratio of 1:2 for serpentine multi pass flow field has shown maximum and minimum power density of 0.214 W/cm^2 and 0.151 W/cm^2 respectively. Similarly for L:C of 1:2 and 2:1 having maximum power density of 0.223 W/cm^2 and 0.133 W/cm^2 respectively. The minimum power densities for the same L:C ratios having 0.126 W/cm^2 and 0.104 W/cm^2 respectively. For the landing to channel width ratio of 2:2 has shown maximum power density of 0.178 W/cm^2 and minimum power density of 0.095 W/cm^2. The optimization was performed for "Larger the Better" type of Taguchi method since power output of PEMFC must be maximized. The S/N ratio plot for the same were obtained using MINITAB 17 software and the corresponding maximum S/N ratio gives better performance as analyzed based on larger the better as shown in the Fig.2.

Table 2. Factors, levels, power density and S/N ratio for 16 runs of optimization

Run	L:C	Pressure	Temperature	Stoi.Ratio	Power Density (W/cm^2)	S/N Ratio
1	1x1	1	313	3	0.151	-16.40
2		1.5	323	3.5	0.193	-14.28
3		2	333	4	0.214	-13.39
4		2.5	343	4.5	0.173	-15.24
5	1x2	1	323	4	0.126	-17.98
6		1.5	313	4.5	0.193	-14.27
7		2	343	3	0.219	-13.19
8		2.5	333	3.5	0.223	-13.04
9	2x1	1	333	4.5	0.125	-18.07

10		1.5	343	4	0.133	-17.53
11		2	313	3.5	0.114	-18.83
12		2.5	323	3	0.104	-19.62
13	2x2	1	343	3.5	0.095	-20.48
14		1.5	333	3	0.119	-18.49
15		2	323	4.5	0.163	-15.77
16		2.5	313	4	0.178	-15.00
					Average S/N Ratio	-16.35

It was concluded that the design parameter such as, landing to channel ratio of serpentine multi pass flow channel having - 1:2 as A2, and the operating parameters like pressure - 3 bar as B3, temperature - 333 K as C3, Stoichiometric ratio of inlet mass flow rate - 4.5 as D4 were the optimum parameters to show the better PEMFC performance.

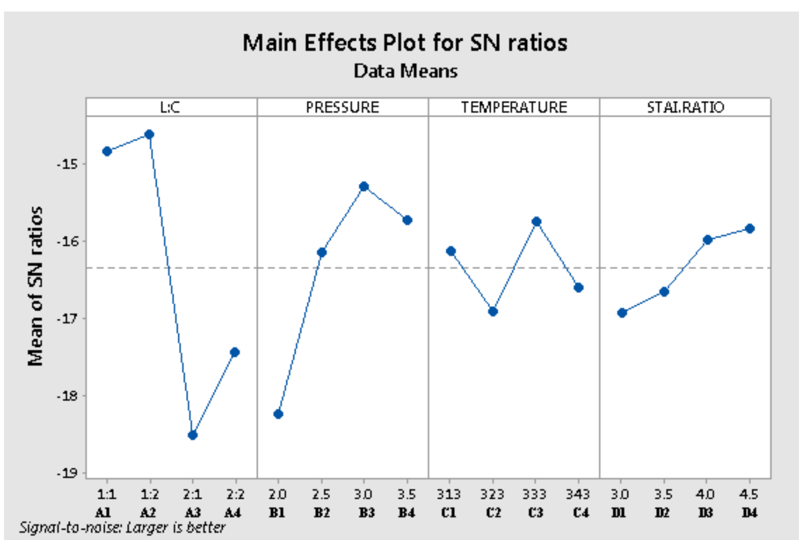

Fig .2. Mean S/N ratio plot for L:C (A1-A4),Pressure (B1-B4),Temperature (C1-C4), Stoi.Ratio (D1-D4).

The optimization results of various parameters were based on S/N ratios and the significance of each factor by ranking them according to their performance. Delta value of each factor available on the MINITAB 17 software itself was shown in Table 3. The factor with highest delta value indicates higher significance.

Table 3. Mean S/N ratios, Delta and Rank for each level of factors

Factors	Level 1	Level 2	Level 3	Level 4	Delta	Rank
Landing to Channel width (L:C)	-14.83	-14.62	-18.52	-17.43	3.9	1
Pressure (bar)	-18.23	-16.14	-15.3	-15.73	2.94	2
Temperature (K)	-16.13	-16.91	-15.75	-16.61	1.17	3
Stoi.Ratio	-16.93	-16.66	-15.97	-15.84	1.09	4

It was found that landing to channel width (L:C) of 49 cm^2serpentine multi pass flow channel was the predominant factor affecting the performance of PEMFC. The other parameters were also influencing the performance of PEMFC to a considerable extent such as, operating pressure, operating temperature, stoichiometric ratio of inlet mass flow rate respectively. The percentage contribution of individual parameters, P-test and F-test on the serpentine multi pass flow fields for the performance of PEMFC has been shown in the Table 4.It has been observed thatthe operating pressure has been shown to be 34.3 % contribution on peak power performance of the PEMFC for the serpentine multi pass flow field. Similarly for the L:C, operating temperature and stoichiometric ratio of the reactants has contributed 28.9 %, 6.3 % and 1.9 % respectively of the PEMFC performance. Also the combined effect of combination of pressure with temperature and pressure with L:Chas shown 9.8 % and 16.6 % respectively contributing to peak power performance of the PEMFC.

Table 4.The percentage contribution of individual parameters of serpentine multi pass flow channel

Factors	DOF	Sum of squares	Variance	F-test	P-Test	Contribution (%)
Pressure	2	0.006615	0.00331	157.44	0.031	34.3
Temperature	2	0.001287	0.00064	2.08	1.021	6.3
Stoi.ratio	2	0.000447	0.00022	10.65	0.299	1.9
L:C	3	0.008395	0.00280	66.61	0.015	28.9
Pressure & Temperature	1	0.000891	0.00089	21.2	0.044	9.8
Pressure & L:C	3	0.004882	0.00163	38.73	0.025	16.6
Error	2	0.000084	0.00004			2.2
Total	15	0.027311	0.009533	296.71	1.435	100.00

CONCLUSION

The combined effect of all the parameters exhibited a different response compared to their individual effects. The maximum power density of optimizing the four different parameters on serpentine multi passmulti flow channel of 49cm^2 active area of PEMFC using Minitab 17 provides 0.223 W/cm^2 and R^2 value was arrived 99.69 %. The optimum power density 0.404 W/cm^2 was obtained from L:C-1:2 with 3bar operating pressure, 333 K temperature and 4.5 stoichiometric ratio of inlet reactant gases of 49 cm^2 active area of the CFD PEMFC model. Theeffect of operating and design parameters was affecting the performance of PEMFC more significantly.

REFERENCES

[1] Yun Wang, SumanBasu, Chao-Yang Wang. Modeling two-phase flow in PEM fuel cell

channels, Journal of Power Sources. , 2008, 179 ; 603–617.

[2] Owejan, J.P.; Trabold, T.A.; Jacobson, D.L.; Arif, M.; Kandlikar, S.G. (2007). Effects of flow field and diffusion layer properties on water accumulation in a PEM fuel cell, International Journal of Hydrogen Energy, 32, 4489 – 4502.

[3]NattawutJaruwasupanta.; YottanaKhunatorna.(2011). Effects of difference flow channel designs on Proton Exchange Membrane Fuel Cell using 3-D Model, Energy Procedia, 9, 326 – 337.

[4] Xianguo Li, Imran Sabir, Jaewan Park, "A flow channel design procedure for PEM fuel cells with effective water removal," Journal of Power Sources, vol.163(2), pp.933-942, 2007.

[5] Y. Sone, P. Ekdunge, D. Simonsson, "Proton Conductivity of Nafion 117 as Measured by a Four-Electrode AC Impedance Method," J. Electrochem.Soc,vol. 143, pp. 1254-1259, 1996.

[6] T. V. Nguyen, R.E. White, "A Water and Heat management Model for Proton-Exchange-Membrane Fuel Cells," J. Electrochem. Soc. Vol.140, pp. 2178–2186,1993.

[7] Lakshminarayanan V, Karthikeyan P, Muthukumar M, Senthilkumar A P, Kavin B, Kavyaraj A, 'Numerical investigation of performance studies on single pass PEM fuel cell with various flow channel design', Applied Mechanics and Materials, Vols. 592-594 , pp 1672-1676, 2014.

[8] Lakshminarayanan V &Karthikeyan P. "Optimization of Flow Channel Design and Operating Parameters on Proton Exchange Membrane Fuel Cell Using Mat lab", PeriodicaPolytechnica Chemical Engineering. Budapest Univ Technology Economics, 60, 3; 173-180, 2016.

[9]. Lakshminarayanan V, BalaKarthick KS. Optimisation of 16cm^2 Single Pass Serpentine Flow Channel of PEMFC Using Taguchi Method', International Journal of Theoretical and Applied Mechanics, 2017, 12, 523-532.

[10] Lakshminarayanan V, Karthikeyan P, Kiran Kumar D S and Dhilip Kumar S M K, 'Numerical analysis on 36cm^2 PEM fuel cell for performance enhancement', ARPN Journal of Engineering and Applied Sciences, Vol. 11, no. 2, 2016. ISSN 1819-6608.

DESIGN AND CHARACTERIZATION OF E-GLASS FIBER REINFORCED COMPOSITE MATERIAL WITH USE OF SISAL FIBER

B.Sandhya Rani[1], Dr.A.Ramesh [2], Dr.B.Durga Prasad [3], Dr Shiva Shankare Gowda A S[4]

1:Ph.D.Research Scholor, JNTUA, Ananathapuramu. sandhyarani25@gmail.com
2:PrincipalBITS,Hindupur,A.P.
3:Profesor& HOD, Dept. of Mechanical Engineering, JNTUA, Ananthapur, A.P.
4:Prof and Dean Academics, Dept of Mech Engg, M R C E, HYDERABAD

ABSTRACT

The present work describes the development and mechanical characterization of new polymer composites consisting of E-glass fiber[1] reinforcement, Epoxy resin, and hardener, natural fiber (Sisal fiber).The newly developed composites are characterized by their mechanical properties. Experiments like Hardness test, tensile test, Compression test, Impact test were conducted to find the significant influence of natural fiber (sisal) on mechanical characteristics of Glass fiber Reinforcement composites.

Composites are an important class of materials available to mankind. Studies of these composites play a very important role in material science, metallurgy, chemistry, solid mechanics and engineering applications. The E-glass fiber[1] reinforced polymer composite is more widely used in the automotive industry and other industrial applications, due to their advantages, like low cost, noise control, low weight and ease of processing.

Natural fibers1 are cheap and environment-friendly materials. Glass Fiber[2] composites are considered to have potential use as a reinforcing material in epoxy polymer-based composites because of their good strength, stiffness etc., in the present study, mechanical properties[3] for glass fiber composites were evaluated.

The present work describes the mechanical characterization of new polymer composites consisting of glass fiber reinforcement, epoxy resin, and sisal fiber. The newly developed composites are characterized for their mechanical properties[3]. Experiments like the tensile test, compression test, hardness test and impact test were conducted to find the significant influence of sisal fiber on mechanical characteristics of GFRP3 (Glass Fiber Reinforced Polymer) composites.

Keywords: Epoxy hybrid composites, E-glass fiber, sisal fiber

1. INTRODUCTION

1.1 INTRODUCTION TO COMPOSITE MATERIAL

This is a new generation of reinforcements and supplements for polymer[2] based materials. Fibers from plants such as cotton, hemp, jute, sisal, pineapple, ramie, bamboo, banana, etc., used as the reinforcement in polymer matrix composites[4]. Their availability, low density, and price as well as satisfactory mechanical properties, make them attractive alternative reinforcements to glass, carbon and other manmade fibers.

A composite material can be defined as a combination of two or more materials that results in better properties than those of the individual components used alone. In contrast to metallic alloys are separate chemical, physical and mechanical properties[3]. The reinforcing phase of the composites [4] provides the strength and stiffness, to make them harder, stronger and stiffer than the matrix. The reinforcement is usually in the form of a fiber or a particulate.

The length-to-diameter ratio is known as the aspect ratio and can vary greatly for fibers[5] because the length of the fiber is much greater than its diameter. Continuous fibers1 have high aspect ratios, while discontinuous fibers have low aspect ratios, and the orientation of continuous fiber composites normally is perfect, while discontinuous fibers generally have a random orientation.

Continuous fiber composites are often made into laminates by stacking single sheets of fibers in different orientations to obtain the desired strength and stiffness properties [15] with fiber volume as high as 60 to 70%. In general, the smaller the diameter of the fiber, the higher its strength [5], but the cost increases when the diameter becomes smaller.

In addition, smaller diameter fibers have greater flexibility, and are more amenable to fabrication processes such as weaving or forming, across the radius.

The continuous phase is the matrix, which is a polymer[2], metal or ceramic. Polymers [12] have low strength and stiffness, metals have intermediate strength and stiffness but high ductility, and ceramics have high strength and stiffness but are brittle. Discontinuous fiber composites are normally random in alignment which drastically reduces their strength and modulus. However, these composites are generally much less costly than continuous fiber composites. Therefore, continuous fiber composites are used where higher strength and stiffness are required even at a higher cost, and discontinuous fiber composites16 are used where cost is the main driver and strength and stiffness are less important.

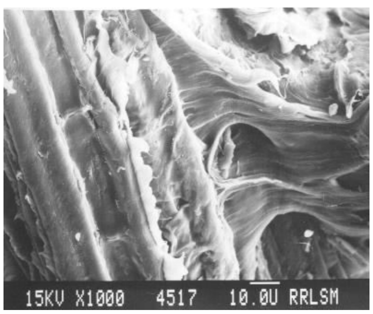

Figure 1: Scanning Electron Micrograph of NaoH treated sisal fiber-epoxy composites showing better fiber-matrix adhesion

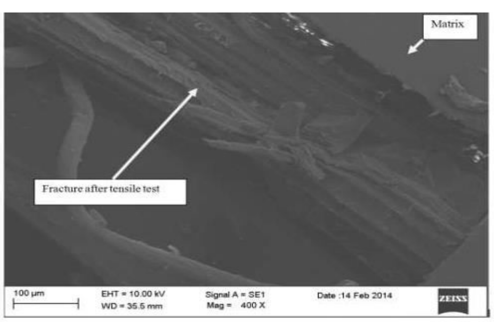

Figure 2:SEM image of tensile tested hybrid glass/sisal reinforced epoxy composites

1.1.1 CLASSIFICATION OF COMPOSITE MATERIALS

Composite materials are broadly classified into three categories as given Composites

Metal matrix composites (MMCs)

Ceramic matrix composites (CMCs)

Polymer matrix composites (PMCs)

1.2 INTRODUCTION TO GLASS FIBER

Glass fiber10 also called fiberglass. It is a material made from extremely fine fibers of glass Fiberglass is a lightweight, extremely strong, and robust material. Although strength properties are somewhat lower than carbon fiber and it is less stiff, the material is typically far less brittle, and the raw materials are much less expensive. Its bulk strength and weight properties are favorable when compared to metals, and it can be easily formed using molding processes. Glass is the oldest, and most familiar, performance fiber13. Fibers have been manufactured from glass since the 1930s.

Figure 3: Glass Fiber

1.2TYPES OF GLASS FIBERS

1. A type glass fiber
2. AR type glass fiber
3. C type glass fiber
4. D type glass fiber
5. E type glass fiber
6. ECR type glass fiber
7. R type glass fiber
8. S type glass fiber

1. A Type glass fiber

Alkali glass made with soda lime silicate. Used where an electrical resistivity of E-glass is not needed. A-glass or soda lime glass is the predominate glass used for containers and windowpane.

- Properties of A-type glass fiber

Density	-	2.44 g/cm3
Tensile strength	-	3300MPa
Young’s modulus	-	72 GPa
% of elongation	-	4.8

2. AR- type glass fiber

Alkali Resistant glass made with zirconium silicates. Used in Portland cement substrates.

- Properties of AR-type glass fiber

Density	-	2.7 g/cm3
Tensile strength	-	1700MPa
Young's modulus	-	72 GPa
% of elongation	-	2.3

3. C – type glass fiber

Corrosive resistant glass made with calcium borosilicate. Used in acid corrosive environments.

- Properties of C- type glass fiber

Density	-	2.56g/cm3
Tensile strength	-	3300MPa
Young's modulus	-	69 GPa
% of elongation	-	4.8

4. D – type glass fiber

Low dielectric constant glass made with borosilicate. Used in electrical applications.

- Properties of D –type glass fiber

Density	-	2.11 g/cm3
Tensile strength	-	2500MPa
Young's modulus	-	55 GPa
% of elongation	-	4.5

5. E- type glass fiber

Alkali-free, highly electrically resistive glass[10] made with alumina-calcium borosilicate. E-glass is known in the industry as a general-purpose fiber for its strength and electrical resistance. It is the most commonly used fiber in the fiber reinforced polymer composite industry.

- Properties of E –type glass fiber

Density	-	2.54g/cm3
Tensile strength	-	3400MPa
Young's modulus	-	72 GPa
% of elongation	-	4.7

Physical properties

- Low cost.
- High production rates.
- High strength.
- High stiffness.
- Relatively low density.
- Non-flammable.
- Resistant to heat.
- Good chemical resistance.
- Relatively insensitive to moisture.
- Able to maintain strength properties over a wide range of conditions.
- Good electrical insulation.

Composition

SiO2	-	54%
Al2O3	-	14%
Cao + Mgo	-	22%
B2O3	-	10%

6. ECR –type glass fiber

An E-glass with higher acid corrosion resistance made with calcium aluminosilicates. Used where strength, electrical conductivity, and acid corrosion resistance is needed.

- Properties of ECR –type glass fiber

Density	-	2.72g/cm3
Tensile strength	-	3400MPa
Young's modulus	-	80 GPa
% of elongation	-	4.3

7. R – Type glass fiber

A reinforcement glass made with calcium13 aluminosilicates used where higher strength and acid corrosion resistance is needed.

- Properties of R –type glass fiber

Density	-	2.52g/cm3
Tensile strength	-	4400MPa
Young's modulus	-	86 GPa
% of elongation	-	5.1

Composition

SiO2	-	58-60%
Al2O3	-	23.5-25.5%
Cao + MgO	-	14-17%

8. S –Type glass fiber

High strength[13] glass made with magnesium aluminosilicates. Used where high strength, high stiffness, extreme temperature resistance, and corrosive resistance is needed.

- Properties of S–type glass fiber

Density	-	2.523/cm3
Tensile strength	-	4600MPa

Young's modulus - 89 GPa
% of elongation - 5.3

- Physical properties

- High production rates.
- Improved mechanical properties10 compared to E-glass.
- High strength.
- High stiffness.
- Relatively low density.
- Non-flammable.
- Resistant to heat.
- Good chemical resistance.
- Relatively insensitive to moisture.
- Able to maintain strength properties over a wide range of conditions.

Composition

Sio2 - 65%
Al2O3 - 25%
Mgo - 10%

1.3 INTRODUCTION TO E-GLASS FIBER

Fiberglass has a white color and is available as a dry fiber fabric as shown in Fig.1. Four major types of Glass Fiber used for composites: E-glass: have good strength & electrical resistivity. S-glass: have 40% higher strength, better retention of properties[10] at elevated temperatures. C-glass have corrosion resistant. Quartz: have low dielectric properties, good for antennae. There are two different types of form we put glass fiber.

- Unidirectional

Unidirectional tapes have been the standard within the aerospace industry for many years, and the fibre[10] is typically impregnated with thermosetting resins. Tape products have high strength in the fiber direction. The fibers are mixed with the resin.

- Bi-directional

Most fabric constructions offer more flexibility for the layup of complex shapes than straight unidirectional tapes offer. Fabrics offer the option for resin mixed either by hot melt or the solution process. Generally, fabrics used for structural applications use like fibers[13] or strands of the same weight or yield in both the warp (longitudinal) and fill (transverse) directions. For aerospace structures, tightly woven fabrics are usually to save weight, minimizing size, and maintaining during the fabrication process.

Figure 4:E-Glass Fiber Matt.

Figure 5: Epoxy resin and Hardener

In this research work, materials tested consist of E-glass fiber[10] reinforced composites with Epoxy resin as matrix reinforced composites. The E-glass fiber matt is used, supplied by GO GREEN PRODUCTS, CHENNAI

1.4 INTRODUCTION TO EPOXY RESIN

The resin is a generic term used to designate the polymer. The resin, its chemical composition, and physical properties[16] fundamentally affect the processing, material. Thermosetting resins are the most diverse and widely used of all man-made materials. They are easily poured or formed into any shape, are compatible with most other materials, and cure readily (by heat or catalyst) into an insoluble solid. Thermosetting resins are also excellent adhesives and bonding agents. Epoxy resin[6] is mostly used.

Epoxy resins are much more expensive than polyester resins [7] because of the high cost of the precursor chemicals most notably epichlorohydrin. However, the increased complexity of the 'epoxy' polymer chain and the potential for a greater degree of control of the cross-linking process gives a much-improved matrix in terms of strength and ductility. Most epoxies require the hardener and resin to be mixed in equal proportions.epoxies are used for full strength.It requires heating to complete the curing process. This can be advantageous as the resin can be applied directly to the fibres[5] and curing need only take place at the time of manufacture. And known as pre or pre-impregnated fiber.

Epoxy polymers [6] are made by reacting epichlorohydrin with bisphenol-A in an alkaline solution which absorbs the HCl released during the condensation polymerization reaction. Each chain has a molecular weight between 900 and 3000 with an epoxide grouping at each end of the chain but none within the polymer chain.

The epoxy is adding by a hardener in equal amounts and it is heated to about 120°C. The hardeners are usually short chain diamines such as ethylene diamine. Heat is usually required since the cross-linking involves the condensation of water which must be removed in the vapor phase.

Hardener

A substance or mixture added to the plastic composition to promote or control the curing action by taking part in it. Also, a substance added to control the degree of hardness of the cured film.

1.5 INTRODUCTION TO NATURAL FIBER (SISAL FIBER)

In the last ten years, there has been an increase in the use of natural fiber composites.There is tremendous potential for future growth in this area both in terms of their research aspects and industrial applications. The reason for this is mainly to resist deforestation, and there is the demand for new materials due to the growth in the world's population. The natural fiber composites are environment-friendly and biodegradable materials[7] (somehow these composites are called Green Composites‘“‘).Recent studies in natural fiber composites offer significant improvement in materials from renewable sources, with enhanced support for global sustainability.

Natural fibers[5] are renewable, cheap, completely or partially recyclable, biodegradable, and environment-friendly materials. This is a new generation of reinforcements and supplements for polymer-based materials. Fibers develop from plants such as ramie, bamboo, banana, cotton, hemp, jute, sisal, pineapple, etc.Wood and seeds of flax are used as the reinforcement in polymer matrix composites.

Their availability, low density, and price as well as satisfactory mechanical properties7, make them attractive alternative reinforcements to glass, carbon and other manmade fibers.

Natural fibers are alike hair material that is continuous filaments[5]. It is similar to pieces of the thread and it can be converted into filaments. Natural fibers are grouped into different categories, based on their origin, derivations of plant, animal and mineral types, and are presented. These sustainable and eco-efficient fibers have been applied as substitutions for glass and other synthetic fibers in diverse engineering applications. With the consideration of environmental consciousness, natural fibers are biodegradable and hence, they can alleviate the problem of massive solid wastes, and relieve the pressure on landfills, if they are used for replacing other non-degradable materials for product development. Besides, according to their inherent properties, natural fibers are flexible for processing, due to their being less susceptible to machine tool damage and health hazards during manufacture.

The natural fibers are the potential replacements for synthetic fibers in the material selection process1 due to the ecological risks. Restricting the emission of greenhouse effect causing gases such as CO2 into the atmosphere, and an increasing awareness of the finiteness of fossil energy resources, lead to the development of new materials that are entirely based on renewable resources. Factors like poor wet ability, poor bonding and degradation at the fiber/matrix interface, and damage of the fiber during the manufacturing process, are the main causes for the reduction of the composite's strength.

1.5.1 SISAL FIBER

Sisal fiber is obtained from the leaves of the plant Agave Sisalana, which is grouped under the broad heading of "hard fibers", among which sisal[7] is placed second to Manila in durability and strength. In ancient days, these fibers were prepared by hand and used for making ropes, carpets, and clothing. It is one of the most extensively cultivated hard fibers in the world and accounts for half the total production of textile fibers. The reason for this is the ease of real improvement of sisal plants, which have short times and are fairly easy to grow in all kinds of environments. A good sisal plant yields about 200 leaves11 and each leaf contains around 1000 fibers. The seasonal sisal plants are presented in below

Figure 6: Sisal Fiber Plants

Figure 7: Extraction of sisal from sisal plants

Figure 8: Dried Sisal fiber

Physically, each fiber cell is made up of the secondary and primary cell wall. The cell wall consists of several layers of febrile, and the primary wall has a reticulated fibrillate structure. In the outer secondary wall, which is located inside the primary wall, the fibrillate are arranged in spirals with a spiral angle of 40° in relation to the longitudinal axis of the cell. The fibrillate[7] in the inner secondary wall of the sisal fibers have a sharper slope of 18 to 25°. The thin, innermost, tertiary wall has a parallel fibrillate structure and encloses the lumen.

The sisal leaf contains three types of fibers, such as mechanical fibers, ribbon fibers, and xylem fibers. The mechanical fibers are extracted mostly from the periphery of the leaf.

They are the most commercially useful sisal fiber. Ribbon fibers occur in association with the conducting tissues in the median line of the leaf.The ribbon fibers are the longest fibers when compared to the mechanical fibers they can be easily split longitudinally during processing. Xylem fibers have an irregular shape and occur opposite to the ribbon fibers. The SEM micrographs of the sisal fibers are presented in which shows the surface features of the sisal fiber. In the case of micro fibrillated sisal fibers, the surface micro fibrils[7] and aggregates were well developed, providing a larger contact area and introducing micro or Nano-sized reinforcement to the fiber surface as shown.

1.6 SCOPE OF THE PRESENT STUDY

Natural fibers are mostly available in many countries. It can be using locally available manpower and technology. The latest development in the use of composites is to protect man against fire, impact and a tendency to a more environment-friendly design, leading to the introduction of natural fibers[5] in composite technology. These include the process of extraction of fibers from the respective plants, then, the extracted fibers could be added alone with resin or in the hybrid composites by substituting industrial fibers.

1.7 NEED FOR THE PRESENT STUDY

Now-a-days, natural fiber reinforced composite materials5 are replacing the conventional, synthetic and manmade fiber reinforced composites, due to their easy availability, biodegradability, Eco-friendliness, in-homogeneity, non-ductility, renewable nature and user-friendly characteristics. Glass fiber reinforced composites have excellent mechanical properties[13], but the process of disposal is very difficult due to severe environmental concerns, and the process of recycling these composites has been a serious problem. Though glass and other synthetic fiber reinforced composites[10] possess high strength, the field of their application is restricted, because of their higher cost of production and low biodegradability. The usage of natural fiber based composite materials is growing during recent years, due to their specific properties, positive environmental impact, economical production and processing, and their safe handling and working conditions.

To take advantage of sisal fiber added with glass fiber conjointly to the matrix, so that an optimal, superior but economical composite can be obtained.

1.8 PROPERTIES OF SISAL FIBER

Each leaf of a sisal plant has a composition of 4% fiber, 0.75% cuticle, 8% other dry matter and 87.5% of moisture

A normal leaf weighing about 600g yields about 3% by weight of fiber16.

It has high tensile strength when compared to the other natural fibers.

It has low specific weight resulting in a higher specific strength and stiffness.

1.9 Advantages of Sisal Fiber

- It is a renewable source, the production requires little energy and CO2 is consumed and O2 is given back to the atmosphere.
- It has good thermal and acoustic insulating properties7.
- The thickness of the fiber is high when compared to the other natural fibers.
- It is a short natural fiber when compared to jute, and this confers
- Very good impact strength.

1.10 Applications of Sisal Fiber

- Manufacturing of post-boxes, grain storage silos, bio-gas containers, etc.
- Manufacturing of chairs, tables, showers, bath units, etc.
- Making of electric devices, electrical appliances, pipes, etc.

- Used in everyday applications, such as lampshades, suitcases, helmets, etc.
- Used for making automobile interiors and panels.

1.11 Sisal fiber Properties

Tensile Strength (Mpa)	:	350 to 680
Elongation of Break (%)	:	6.8
Diameter (mm)	:	0.8 to 1.2mm
Density (g/cm3)	:	1.58
Young’s Modulus (Gpa)	:	19.8

2. BASIC DESIGN PROCEDURE

The following are the materials used to prepare e glass fiber composite material specimen with addition of natural fiber (sisal fiber)

2.1 MATERIALS USED

- E-Glass fiber
- Sisal fiber (Natural fiber)
- Epoxy and hardener

2.2 PREPARATION OF SPECIMEN:

The following Specimen consists of three layers in which E-glass fiber mat is placed top and bottom of the specimen. A middle layer is filled with sisal fiber. The layers of fibers are fabricated by adding required amount of Epoxy resin. Initially, sisal fiber is soaked in alkaline solution NaoH for two hours and dried in hot oven for three hours to remove moisture. Epoxy6 and hardener are mixed in the ratio of 10:1.After mixing the epoxy resin is used to prepare a specimen. Before going to the making of specimen the glass fiber matt is cut into required dimensions. The following are the dimensions of glass fiber and sisal to prepare a required specimen.

2.2.1 SPECIMEN -1

DIMENSIONS: Width=200mm
Length=300mm

Chopped sisal fiber length=300mm

Fabrication details: Glass fiber to natural fiber = 1:1

E-glass fiber	= 40gms
Sisal fiber	= 40gms
Epoxy and hardener	= 220gms

Cut the glass fiber into required size. Initially, E-glass fiber is placed on an Aluminum foil and resin is coated on E-glass fiber using roller brush.

Chopped sisal fiber is placed on a glass fiber and resin is coated on sisal fiber. Another glass fiber layer is placed on the sisal fiber. After these three layers, aluminum foil is placed on the specimen. Weight is placed on the specimen and allowed to cure for three hours for the purpose of uniform shape.

- After fabrication the final weight of the specimen was almost 200gms

Figure 9: E-glass Fiber composite specimen-1

Figure 10: E-glass Fiber composite Specimen-2(For Tensile Test)

2.2.2 SPECIMEN-2:

Dimensions:

Width=50mm
Length=300mm

Fabrication details:

Glass fiber to natural fiber	= 1:1
E-glass fiber	= 17gms
Sisal fiber	= 17gms
Epoxy and hardener	= 55gms

Cut the glass fiber into required size. First E-glass fiber is placed on an Aluminum foil and resin is coated on E-glass fiber using roller brush. Chopped sisal fiber is placed on a glass fiber and resin is coated on sisal fiber. Another glass fiber layer is placed on the sisal fiber. After these three layers, aluminum foil is placed on the specimen. Weight is placed on the specimen and allowed to cure for 3 hours for the purpose of uniform shape.

•Final weight of the specimen=55 grams

2.2.3 SPECIMEN-3

OVAL SHAPE

Fabrication details:

Glass fiber to natural fiber	= 1:1
E-glass fiber	= 20gms
Sisal fiber	= 20gms
Epoxy and resin	= 220 gms

First, prepare the oval-shaped mold. Cut the glass fiber into an oval shape. Apply grease in the mould. After applying grease place aluminum foil in the mould .Place glass fiber on aluminum foil epoxy resin is coated on glass fiber using a brush. Sisal fiber is placed on glass fiber and epoxy resin coated on sisal fiber. Another glass fiber is placed on sisal fiber. After these three layers, aluminum foil is placed on the specimen. A weight is kept on specimen allowed to cure for few hours.

•Final weight of the specimen=75 gms

Figure 11: Pattern making for Oval shape E-glass fiber composite specimen

2.2.4 SPECIMEN-4

Square plate

Dimensions:

Width = 300mm

Length = 300mm

Fabrication details:

Glass fiber to natural fiber	= 1:1
Glass fiber	= 70gms
Sisal fiber	= 70gms
Epoxy and hardener	= 220gms

Cut the glass fiber into required size. First E-glass fiber is placed on an Aluminum foil and resin is coated on E-glass fiber using roller brush. Chopped sisal fiber is placed on a glass fiber and resin is coated on sisal fiber. Another glass fiber layer is placed on the sisal fiber. After these three layers, aluminum foil is placed on the specimen. Weight is placed on the specimen and allowed to cure for 3 hours.

•Final weight of the specimen =260gms

Figure 12: E-glass fiber composite Specimen-4 (For Hardness Test)

3. RESULTS AND DISCUSSION

After fabrication of composite specimens, the specimens are being subjected to following tests to know the mechanical characterization.

3.1 TESTS CONDUCTED

- Tensile test
- Compression test
- Rockwell hardness test
- Impact test

3.1.1 TENSILE TEST

MEANING OF TENSILE:

Tensile strength is the capacity of material or structure to withstand loads tending to elongate, as opposed to compressive strength, which withstands loads tending to reduce size.Tensile strength resists tension.

Tensile strength is the measurement of the force required to pull something such as rope, wire, or a structural beam to the point where it breaks.

The specimen-2 is tested in the universal testing machine (UTM) and the samples are left to break till the ultimate tensile strength occurs. The stress-strain curve is plotted for the determination of ultimate tensile strength and elastic modulus. Graph generated directly from the machine for the tensile test with respect to load and displacement for Glass Fiber /sisal Reinforced Composite material.

Figure 13: Glass fiber/sisal Rectangular specimen 300x50 mm before testing (Tensile)

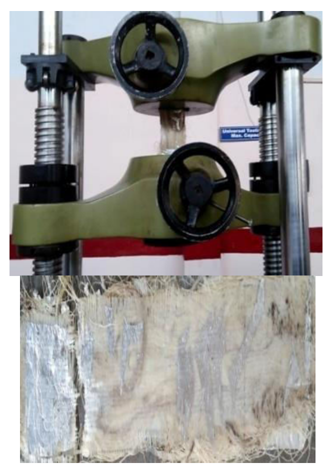

Figure 14: Composite Specimen under universal testing machine Fig.14: Specimen after tensile test

The testing process involves the test specimen in the testing machine and it is slowly extending it until it fractures. During this process, the elongation of the gauge section is recorded against the applied force. The data is manipulated. The elongation measurement is used to calculate the relations between stress and strain, stress and displacement and load and displacement.

The machine does these calculations as the force increases so that the data points can be graphed into a stress-strain curve, load-displacement curve and stress-displacement curve.

The following above figure represents the specimen obtained after testing. The following are the curves obtained by the universal testing machine as shown below.

- STRESS VS DISPLACEMENT
- LOAD VS DISPLACEMENT
- STRESS VS STRAIN

The sisal/glass fiber hybrid composites resembled to ductile material during testing as the sisal fibers are flexible. T The composites have exhibited 110% in breaking strength. The strength of these composites depend on loading geometry and strain rate.

The following graph shows the relationship between stress and displacement when the load on the specimen increases.

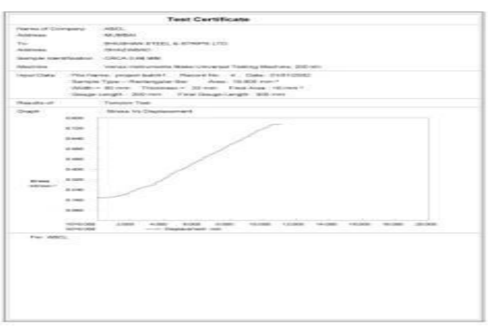

Figure 15:Tensile Test Graph for Rectangular specimen (Stress vs Displacement)

The following graph shows the relationship between load applied and displacement obtained on the specimen.

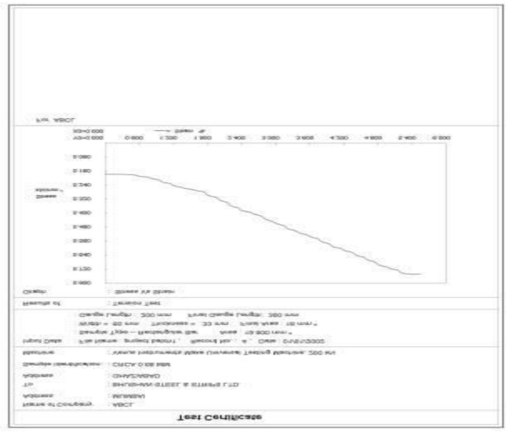

Figure 16: Tensile Test for Rectangular Specimen (Load vs Displacement)

The following graph shows the relation between stress and strain on the specimen.

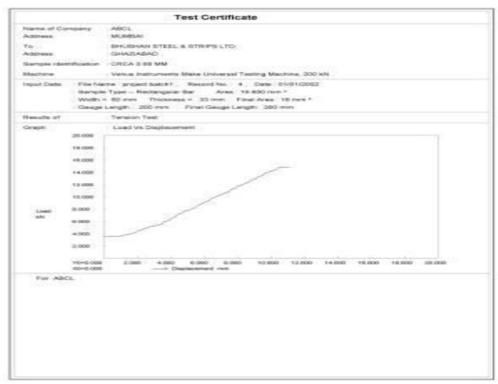

Figure 17: Tensile Test for Rectangular Specimen (Stress vs Strain)

3.1.1.1. Results from Tensile Test for rectangular specimen:

Sample Area: 19.8 mm^2
Final Area : 18 mm^2
Gauge length: 200 mm
Final gauge length: 300 mm

S. No	Stage	Stress $_{vs}$ Displacement		Load $_{vs}$ Displacement		Stress $_{vs}$ Strain	
		Stress KN/mm^2	Displacement mm	Load KN	Displacement mm	Stress KN/mm^2	Strain
1.	Initial	0.18	0	3.5	0	0.19	0.75
2.	Final	0.75	11	15	11	0	5.4

TABLE:1 Tensile test results for Rectangular speciman

3.1.2 COMPRESSION TEST

Compressive strength is the capacity of a material to withstand loads tending to reduce the size, as opposed to tensile strength, which withstands loads tending to elongate.Compressive strength resists compression whereas tensile strength resists tension.

Some materials fracture at their compressive strength limit.So a given amount of deformation may be considered as the limit for the compressive load. Compressive strength is a key value for a design of structures. Compressive strength is often measured on a universal testing machine

The specimen size for compression test is 300*300*3 mm cube. Compression test is conducted in the universal testing machine. Graphs are developed from the machine for compression test with respect to displacement and load for Glass fiber reinforced the composite material.

Figure 18: Specimen 200x300 mm before compression

Figure 19: Compression test in universal testing machine

After testing of compression test in universal testing machine, the following are the graphs obtained as the load increases. The graphs are followed as shown below.

- STRESS VS DISPLACEMENT
- LOAD VS DISPLACEMENT
- STRESS VS STRAIN

The following graph shows the relation between stress and displacement when the load on the specimen increases.

Fig.20: Compression Test for Rectangular specimen (Stress vs Displacement)

The following graph shows the relationship between load applied and displacement obtained on the specimen.

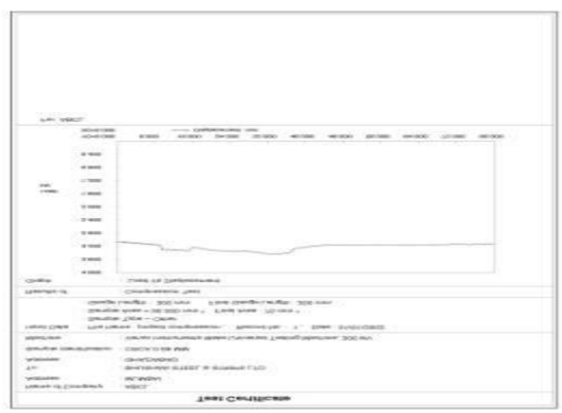

Figure 20: Compression Test for Rectangular specimen (Load vs Displacement)

The following graph shows the relation between stress and strain on the specimen.

Figure 21: Compression Test for Rectangular specimen (Stress vs Strain)

3.1.2.1. Results from Compression Test for Rectangular specimen:

Sample Area: 90 mm^2
Final Area : 75 mm^2
Gauge length: 300 mm
Final gauge length: 250 mm

S. No	Stage	Stress vs Displacement		Load vs Displacement		Stress vs Strain	
		Stress KN/mm^2	Displacement mm	Load KN	Displacement mm	Stress KN/mm^2	Strain
1.	Initial	0.035	0	3.10	0	0.035	0
2.	Final	0.03	80	3	80	0.03	29

TABLE:2 Compression test for Rectangular speciman

3.1.3 HARDNESS TEST

Hardness is a measure of how resistant solid matter. and is to various kinds of permanent shape change when a compressive force is applied. Some materials are harder than plastics. Macroscopic hardness is generally characterized by strong intermolecular bonds.

The measurements of hardness are classified into 3 types those are scratch hardness, indentation hardness, and rebound hardness. Hardness is dependent on ductility, strength, toughness, viscoelasticity, elastic stiffness, plasticity, strain, and viscosity.

The examples of hard matter are ceramics, certain metals, concrete and super hard materials. which can be contrasted with the soft matter.

The hardness measurements are classified into 3 types.Those are scratch, indentation, and rebound. These classes of measurement are individual measurement scales. These are used for practical reasons, conversion tables and those are used to convert between one scale and another.

Scratch Hardness

Scratch hardness is used for a measure of how resistant a sample is to fracture or deformation due to friction from a sharp object. The principle is that an object made of a harder material will scratch an object and it made of a softer material. The testing coatings and scratch hardness refer to the force necessary to cut through the film to the substrate. The most common test is Mohs scale.It is used in mineralogy.

Rebound hardness

Rebound hardness, also known as dynamic hardness.It measures the height of the "bounce" of a diamond-tipped hammer dropped from a fixed height onto a material. This type of hardness is related to elasticity. The device used to take this measurement and it is known as a sclera scope.

Indentation hardness

Indentation hardness measures the resistance of a sample to material deformation due to a constant compression load from a sharp object. They are primarily used in engineering and metallurgy fields. The hardness tests process depends on the measuring the dimensions. Common indentation hardness scales are Vickers, Shore, Rockwell, and Brinell. The Rockwell hardness test carried out for the Glass fiber reinforced the composite material and obtained the result is applied 60kg for 1/4inch penetrator the B scale reading for all specimens.

These are the following results for hardness obtained by Rockwell hardness testing machine.

3.1.3.1 Results from Hardness Test for Rectangular 1 & 2, oval and square specimens:

SI.NO	POINT	SPECIMEN 1 HARDNESS	SPECIMEN 2 HARDNESS	SPECIMEN 3 HARDNESS	SPECIMEN 4 HARDNESS
1	1	B20	B45	B34	B45
2	2	B24	B33	B31	B32
3	3	B32	B28	B31.5	B30
4	4	B34	B32	B33	B26

TABLE:3 Hardness for Diffarent specimans

Figure 22: Rockwell hardness testing machine

Figure 23: Impact Testing Machine

3.1.4. IMPACT TEST

An impact is a high force over a short time period when two or more bodies collide. Such a force or acceleration usually has a greater effect than a lower force applied over a proportionally longer period. The effect depends on the relative velocity of the bodies to one another.

At normal speeds, during a perfectly inelastic collision, an object struck by a projectile will deform, and this deformation will absorb most or all of the force of the collision. The conservation of energy is changed into perspective, the kinetic energy of the projectile is changed into heat and sound energy, as a result of the deformations and vibrations induced in the struck object. Impact resistance decreases with an increase in the modulus of elasticity, which means that stiffer materials will have less impact resistance.

Resilient materials will have better impact resistance. The impact test is conducted on two specimens for one specimen Charpy impact test and for another specimen Izod impact test. The result indicated that maximum Charpy impact strength obtained is 516 Joules. Specimen size for the Charpy impact strength is 75x8x3 mm.

For Izod impact, test result indicates that maximum Izod impact strength obtained is 228 Joules. Specimen size for the Izod impact strength is 75x8x3 mm.

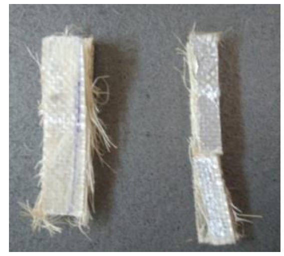

Figure 24: Specimens after impact test

3.1.4.1. Results from Impact Test for specimen.

SI.NO	READINGS	CHARPY IMPACT TEST (div)	IZOD IMPACT TEST (div)
1	Initial reading	300	168
2	Final reading	42	54
3	Final impact	258	114
4	In joules	258*2 =516	114*2=228

NOTE: 1div=2joules

CONCLUSION

In this project the design and fabrication of e glass fiber reinforced composite material performed with addition of sisal fiber and it is concluded that, the E-glass fiber reinforced composite material with adding of sisal fiber is more advantageous for aerospace and automobile applications. The following conclusions were made as follows:

- The Hardness, tensile, compression, impact characteristics of E-Glass fiber reinforced sisal composite material gives better results compare than Ordinary E-Glass fiber composite material.
- By conducting different types of mechanical tests we obtain better results compared than normal E-Glass fiber matrix composite material.
- The hardness, tension and compression values are better than normal E Glass fiber matrix material by adding natural fiber (Sisal fiber).

REFERNCES

1) Li X, Tabil LG &Panigrahi S, *J Polym Environ*, 15 (2007) 25.
2) Gupta M K & Srivastava R K, *Int J Fibre Text Res*, 5 (2015) 30.
3) Prasad AV R, Rao K M &Nagasrinivasulu, *Indian J Fibre Text Res*, 34 (2009) 162.
4) Mukhopadhyay S, Pal R, Narula V &Mayank M, *Indian JFibre Text Res*, 38 (2013) 87.
5) Bajpai PK, Singh I &Madaan J, *Wear*, 297 (2013) 829.
6) Gupta A, Kumar A, Patnaik A & Biswas S, *Int J PolymSci,*(2011) 10 .
7) Kaewkuk S, Sutapun W &Jarukumjorn K, *Compos Part B*,45 (2013) 544.
8) Mohanty S, Verma S K &Nayak S K, *Compos Sci Technol*,66 (2006) 538.
9) Cheng S, Lau K, Liu T, Zhao Y, Lam P & Yin Y, *Compos Part B,* 40 (2009) 650.
10) Bader MG, Collins JF. The effect of fibre-interface and processing variables on the mechanical properties of glass-fibre filled nylon 6. FibreSciTechnol 1983;18:217–31.
11) Venkateshwaran N, ElyayaPerumal A, Alavudeen A &Thiruchitrambalam M, *Mater Des*, 32.
12) Gupta M K & Srivastava R K, *Am J PolymSci Engg,*3(2015) 1.
13) Bijsterbosch H, Gaymans RJ. Polyamide 6-long glass fiber injection moldings. Polym Compos 1995;16:363–9.
14) Prasad V R, Rao K M M, Rao K M & Kumar M A, *Indian J Fibre Text Res*, 31 (2006) 335.
15) Wang W, Sain M & Cooper PA, *Compos SciTechnol,* 66(2006) 379.
16) Gupta M K & Srivastava R K, *Am J PolymSci Engg,*3(2015) 208.

A comparative study of Mechanical Properties Al/4.5%Cu-WC and Al2024-WC MMC's

Dr.J.N.Prakash[1], K. Punith Gowda [2], Dr.Shiva Shankare Gowda[3]

[1] Professor, Noble College of Engineering and Technology, Rangareddy (District), Telangana, India
email: prakash69jnp09ace@gmail.com
[2] Assistant Professor, Department of Mechanical Engineering, East West College of Engineering and Technology, Bangalore, Karnataka, India
email:pgpunith@gmail.com
[3] Prof and Dean Academics, Department of Mechanical Engineering, Mallareddy College of Engineering, Hyderabad, Telangana, India, email: ssgowda105@gmail.com.

Abstract - The present work reveals the comparative of study of mechanical properties of Al/4.5%Cu alloy and commercially available Al2024 alloy reinforced with tungsten carbide (WC) particulates as primary reinforcement. The reinforcing particulates in AL/Cu and Al2024 alloy were varied from 1% to 5% by weight. The vortex method of cast production was employed to fabricate the MMCs, in which the reinforcement was poured into the vortex created by stirring the molten metal by means of a mechanical agitator. The composite so produced was subjected to a series of mechanical tests. The results of this study revealed that as the tungsten carbide particle content was increased, there were significant increases in the ultimate tensile strength, hardness and young's modulus, compressive strength, accompanied by a reduction in its ductility. It has been observed there is a limit for the percentage of addition of reinforcement. An attempt is made in the paper to provide explanations for these phenomena.

Key words : AL2024 ; WC; Composites; Mechanical Properties ; Al-Cu alloy

I INTRODUCTION

Metal matrix composites (MMCs) are becoming more and more attractive materials for industrial and aerospace applications since their properties can be tailored through the addition of selected reinforcements [1-2]. MMCs have their own essence for the specific applications because of their specific strength and modulus at elevated and room temperatures [3]. It is understood that the elastic properties of MMCs are strongly influenced by micro structural parameters of the reinforcement such as shape, size, orientation, distribution and volume fraction [4]. AMCs have proved themselves to be a best choice as engineering materials in recent decades. The introduction of a ceramic reinforcement into a metal matrix produces a composite material that yields an attractive combination of physical and mechanical properties which cannot be obtained with monolithic alloys. Owing to the wider commercial applications, there is an ever increasing demand to know about the processing techniques and mechanical behaviour of particulate MMCs. The ease of availability and low cost manufacturing process adopted have gained the attention of researchers to work in the area of particulate composites. Aluminium alloy-based particulate-reinforced composites have a large potential for a number of engineering applications. Aiming of reinforcing Al alloy based matrices with ceramic particles is mainly due to the low weight to volume ratio, low coefficient of thermal expansion and high strength and modulus of the reinforcements and also due to their availability. Among the various useful aluminium alloys, aluminium alloy 2024 is typically characterized by properties such as fluidity, cast ability, corrosion resistance and high strength-weight ratio. This alloy has been commonly used as a base metal for MMCs reinforced with a variety of fibres, particles and whiskers [5-7]. Past studies revealed, if the particle size of reinforcement were in the range (50µm to 100µm) the composite provided optimum results with respect to mechanical properties and tribological properties [8]. The most common reinforcements are alumina, SiC, B_4C, TiC, graphite and WC to explore better mechanical properties. Awerbuch et al. [9] has worked on aluminium 6061 and showed that the compressive deformation can be enhanced more than 50 percent with a specimen length to diameter ratio equal to unity, which in turn improves compressive strength. Hence, in the present study of investigation, priority is also given to the compressive properties along with tensile properties like ductility, young's modulus, UTS and hardness.

Aluminium 2024 is widely used in aircraft structures, rivet hardware, truck wheels, screw machine products, and other miscellaneous structural applications [10]. In the present investigation, aluminium alloy 2024 was used as the matrix material. Al2024alloy [11] has the higher specific strength and ductility of the aluminium alloys with excellent machinability and good bearing and wear properties, similar to Al6061 alloy [12]. Most of the particulate reinforced metal matrix composites are produced by liquid metallurgy, sometimes known as the 'vortex method' [13], although many different processes for fabricating these cast composites are also available which have been reported by various researchers. In the present work, the 'vortex method' of producing AMC's , in which Tungsten carbide has been used as the candidate reinforcements of particulate sizes ranging from 60 to 90 μm and added to the vortex formed in the Al-Cu melt above its liquidus temperature. Since the hardness, ultimate tensile strength (UTS), compressive strength, young's modulus and ductility of the composite material are all vital properties of a structural material, the present investigation aims at studying these properties in the Al-Cu alloy-particulate composites, a similar procedure has been adopted to prepare AL2024 commercially available alloy. The composites types so prepared have been compared for their mechanical properties.

II EXPERIMENTAL DETAILS

The properties of materials adopted and methods followed for the fabrication and testing of MMCs in the present studies are presented in the following sections.

A. Matrix and Reinforcement Materials Details

The matrix for the present studies selected was Al2024 alloy and were procured from Fenfee Metallurgical, Bangalore, in the form of ingots. The chemical composition of Al2024 alloy was supplied commercially with the chemical composition (in weight percent) of 4.850% Cu, 1.310% Mg, 0.667% Mn, 0.254% Fe, 0.110% Si, 0.079% Zn, 0.033% Cr, 0.008% Ti and balance Al. The reinforcing materials selected were tungsten carbide (WC) of 60 μm particle size and the properties of the matrix and reinforcement materials used are presented in the Table 1.

Table 1. Properties of matrix and reinforcement materials.

Material	Elastic Modulus(GPa)	Density (g/cc)	Hardness(BHN)	Tensile Strength(MPa)
Al2024	76	2.78	82	112.62
WC	627	14.9	1630*	5000

* Kg/mm^2

B. Preparation of Composites

The Al/4.5%Cu-WCand Al2024-WC composites were prepared by the vortex method [8]. The tungsten carbide contents used for the preparation of the composites were 0%, 1%, 2%, 3%, 4% and 5%.Addition of Tungsten Carbide into the molten aluminium alloy melt above its liquidus temperature of 500 °C was carried out by creating a vortex in the melt using a mechanical stainless steel stirrer coated with aluminite to prevent migration of ferrous ions from the stirrer material into the aluminium alloy melt. The melt was rotated at a speed of 500 rpm over a period of eight minutes in order to create the necessary vortex. The WC particles were preheated to 400 °C and added to the melt through the vortex. The melt was subsequently degassed by passing hexa-chloro-ethane (C_2Cl_6) tablets. The molten metal was then poured into permanent moulds for casting. The cast specimen of size 25 X 300 mm^2 MMCs were obtained.

C. Testing of Specimens

Carefully polished and mirror finished specimens were examined under Scanning Electron Microscope(SEM) to obtain microphotographs. Tensile tests were conducted at room temperature using a Universal Testing Machine (UTM) in accordance with ASTM Standard E 8-82. The tensile specimens of diameter 12.5 mm and gauge length 62.5 mm were machined from the cast composites with the gauge length of the specimens parallel to the longitudinal axis of the castings. For each composite, four tensile test specimens were tested and the average values of the UTS, Young's modulus and ductility were measured.

The hardness tests were conducted in accordance with ASTM Standard E 10 using a Brinell hardness tester with a ball indenter of 5 mm diameter and a load of 250 kg. The load was applied for 30 sec. eight hardness readings were taken for each specimen at different locations to circumvent the possible effects of particle segregation. Compression tests were conducted on a UTM in accordance with ASTM Standard E 9 at room temperature. In this test the compression loads were gradually increased and the corresponding strain was measured until the specimen failed. Each result is an average of four readings.

III RESULTS AND DISCUSSIONS

A. Microstructure Studies

Micrographs of Al2024 alloy and Al2024–WC composites are observed from Figures 1(a) & (b) The soundness of prepared casted composites in terms of increased density, reduced porosity with uniform distribution of WC particulates in the matrix alloy was noticed with the help of SEM analysis [14]. SEM structures also revealed good bonding among matrix and reinforcement particles which yields better load transfer from matrix to reinforcement material Figures 1(c) to (f).

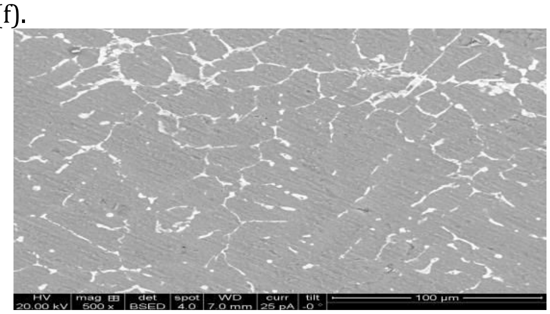

a) Al -4.5%Cu -3%WC composite

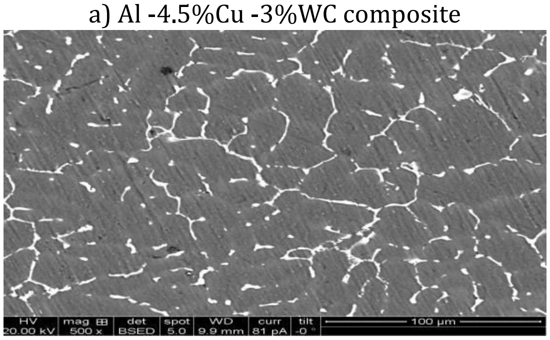

b) Al 2024 alloy-3% WC

Figure 1. SEM structures of Al-4.5Cu-WC and Al2024-WC MMCs at 500X magnification for 50μm.

B. Hardness

The effect of WC reinforcement on the hardness of casted Al-4.55/WC and Al2024-WC particulate composites is observed from Figure 2. Hardness test helps in understanding material resistance to surface penetration and maximum stress required to cause specific surface deformation. The hardness value of each test specimen is an average of six test measurements. It is observed from the test results that increase in the tungsten carbide content made increase in hardness value monotonously. In fact, as the WC content is increased from 0% to 3% the hardness increases by about 9%. In metals, there is a relation between Ultimate Tensile Strength (UTS) and hardness, increase in UTS yields increase in hardness; same would be seen in processed composites [15]. The reason for improved hardness is due to hard WC dispersoid contributing positively to the hardness of composites. The hardness value increased to about 9% for 3wt. % of WC reinforcement, compared to as cast Al2024 alloy without reinforcement. There after a decrease in hardness was observed for 4wt. % of WC reinforcement, probably due to the voids which nucleate during the plastic straining of the reinforcement.

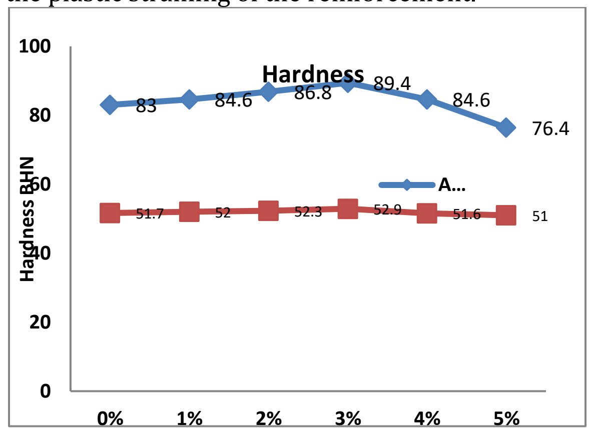

Figure 2. Effect of the WC content on hardness AL-4.5%Cu -WC and Al2024-WC composites

C. Ultimate Tensile Strength

Figure 3 shows the graph of effect of reinforcement content on ultimate tensile strength (UTS) of processed composites. Each value of UTS is an average of six measurements. From the graphs is noticed that improvement of tensile strength was achieved up to 3 wt. % WC, however it decreased beyond 4 wt. % WC. Better tensile strength was found at 3 wt % WC. As the WC content is increased from 0% to 3%, the UTS increased by about 57.5%.The decrease in tensile strength of the composites beyond 3 wt. % WC is attributed to improper bonding between the matrix and reinforcement materials. Finer the grain size better is the hardness and strength of composites. The increase in UTS can be attributed to the presence of hard WC particulates that impart strength to the matrix alloy, thereby providing enhanced resistance to tensile stresses.

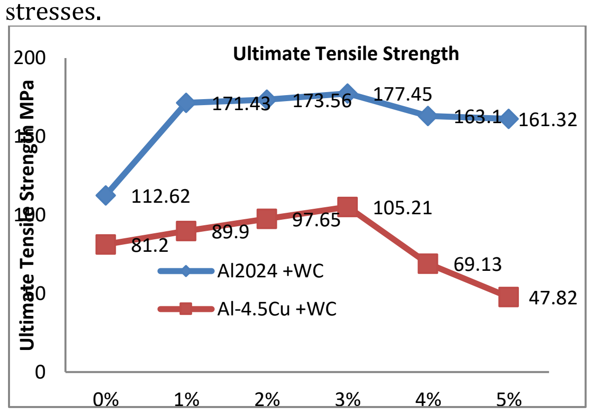

Figure 3. Effect of the WC on Ultimate Tensile Strength AL-4.5%Cu -WC and Al2024-WC composites

Addition of WC particulates results in decreasing the interspatial distance between Al 2024 and also helps in pile up of dislocations. This in turn causes restriction in plastic flow due to uniform distribution of particulates in Al 2024 alloy thereby improving tensile strength of the processed composite. Similar observations were made by Ghosh and Ray [16], who fabricated Al_2O_3 particulate reinforced aluminium alloy composites using the compo-casting method and by McCoy et al. [17] who produced TiB_2-particulate-reinforced aluminium alloy composites with particulate contents ranging from 10 to 25 vol %.

D. Youngs Modulus

From Figure 4, the percentage variation in Young's modulus provides a comparative insight in to the actual experimental results recorded for the Al2024-WC particulate reinforced composites. It is observed from the result that addition of WC content in to the Al2024 matrix improved young's modulus of prepared composite monotonously by significant amount. In fact, as the WC content is increased from 0% to 3%, the Young's modulus increases by about 47.6% and when increased from 3% to 4% the Young's modulus decreases monotonically. The increase in young's modulus is closely attributed to the prediction of rule of mixture. McDanels [18] had reported similar results for particle reinforced Aluminium composites.

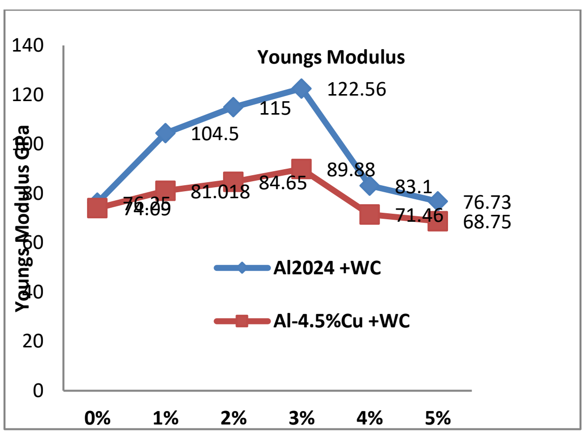

Figure 4. Effect of the WC content on Young's Modulus AL-4.5%Cu -WC and Al2024-WC composites

E. Ductility

Figure 5 shows the effect of the reinforcement content on the ductility of cast Al2024-WC particulate composites measured in terms of percentage elongation. The ductility of the composite material is less compared to as cast Al 2024 alloy. The brittleness also increased with increasing reinforcement content, since the matrix material suffered with ductility due to reinforcement. As the WC content increased from 0 to 5%, the ductility dropped by about 100%. similar results were reported by Beitz W. and Kuttner K. H.[19] &Zhu H. X. and Liu S. K[20]. The reduction in ductility is due to the hard ceramic phase due to localized crack initiation and embrittlement owing to local stress concentration sites at the particle reinforcement interface. The reinforcing particles resist the passage of dislocations by creating stress fields. Past studies have also revealed, loss of ductility due to the voids nucleating during plastic straining of the reinforcement.

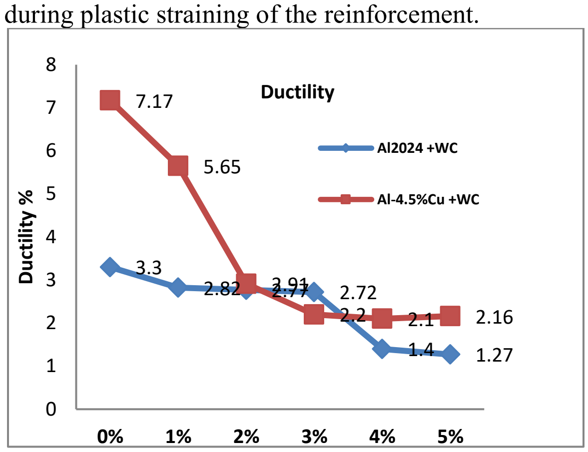

Figure 5. Effect of the WC content on Ductility in AL-4.5%Cu -WC and Al2024-WC composites

F. Compressive Strength

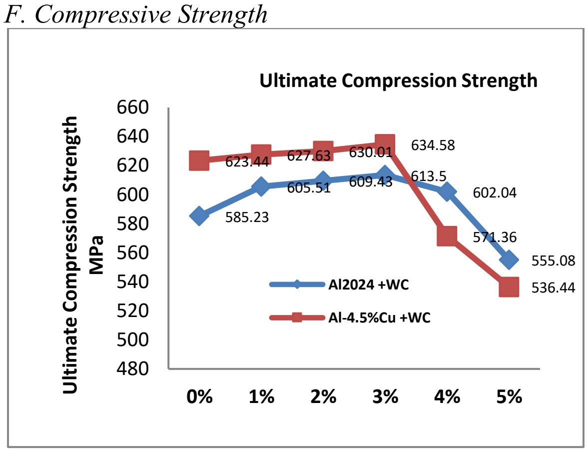

Figure 6. Effect of the WC content on Ultimate Compressive Strength AL-4.5%Cu -WC and Al2024-WC composites

It is observed from Figure 6, that the compressive strength of the composites is higher than that of the base alloy due to the presence of hard WC particles. The WC particles have higher compressive strength than the matrix. Hence an increase in compressive strength is observed with increasing wt % of reinforcement. The compressive strength however decreased with 4 wt. % of WC. Webster [21] and Towle et al [22] also reported about the increase in compressive strength while working on whisker reinforced composites. The increase in compressive strength can also be attributed to decrease in inter particle spacing between WC particles, since WC is much harder than the matrix. The hard ceramic WC particles resist deformation stress whilst increasing composite strength of the composite. Nevertheless, the addition of hard ceramic particulates has caused the MMCs to behave as brittle rather than ductile materials, as is evident from the above results.

IV CONCLUSIONS

The significant conclusions of the studies on AL-4.5%Cu and Al2024-WC metal matrix composites are as follows.

1. AL-4.5%Cu and Al2024-WC composites was prepared successfully using liquid metallurgy techniques by incorporating the reinforcing particulates.
2. It was found that increasing the carbide content within the aluminium-copper matrix results in significant increase in the ductility, UTS, compressive strength and young's modulus, however hardness values decreased with increasing reinforcing content.
3. The properties of the as cast AL-4.5%Cu and Al2024-WC composites significantly improved by varying the amount of WC. It was found that increasing the WC content within the matrix material, resulted in significant improvement in mechanical properties like hardness, tensile strength, and compressive strength at the cost of reduced ductility.
4. Highest values of mechanical properties like hardness, tensile strength and compressive strength were found at 3 wt% WC.

REFERENCES

[1]. Everett R.K and Arsenault R.J. “Metal Matrix Composites: Mechanisms and Properties”, 1991 (Academic Press, San Diego).

[2]. Kocjak M.J., Kahtri S.C., Allison J.E and Jones J.W., “Fundamentals of Metal Matrix Composites” (Ed S.Suresh, A.Mortensen and A.Needleman, 1993 (Butterworth-Heinemann, Boston)).

[3]. Lloyd D.J. and Brotzen F.R., “Particle reinforced aluminium and Mg matrix composites” Int. Mater. Rev; 1994, 39,1-39.

[4]. Lei M. and Ledbetter H., “Communications: elastic constants of SiCp/Al: measurements and modeling”, Metall. Mater. Trans., 1994, 25A, 2832-2835.

[5]. Vogelsang M., Arsenault R. J. and Fisher R. M., “In-situ HVEM study of dislocation generation at Al/SiC interfaces”, Metall. Trans. A, 1986, 17, 379.

[6]. Pai B. C., Ray S., Prabhakar, K. V. and Rohatgi P. K., “Fabrication of aluminium alumina (magnesia) particulate composites in foundries using magnesium additions to the melts”, Mater. Sci. Engng, 1976,24,31.

[7]. Sato A. and Mehrabian R., “Aluminium matrix composites: fabrication and properties”, Metall. Trans. B, 1976, 7, 443.

[8]. Pai B. C., Pillai R.M. and Sathyanarayana K.G, “Prospects for graphite aluminium composites in engineering industries” Indian Journal of Engineering and Materials Science 1994, 1, October, 279.

[9]. Awerbuch J., Goering J. and Busking K., “In Mini Mechanics Analysis and Testing of Short Fibre Composites: Experimental Methods and Results”, Vol. 121, 1988. pp964 (American Society for Testing and Materials, Philadelphia. Pennsylvania).

[10]. W. H. Cubberly, "Properties and Selection: Non-Ferrous Alloys and Pure Metals", Metals Handbook, 9th *Ed.,* ASM, Metals Park, OH, (1979).

[11]. Inampudi Narasimha Murthy, Nallabelli Arun Babu, Jinugu Babu Rao,“Comparative Studies on Microstructure and Mechanical Properties of Granulated Blast Furnace Slag and Fly Ash Reinforced AA 2024 Composites” Journal of Minerals & Materials Characterization & Engineering, 2014, 2, 319-333.

[12]. Smith W. F, “Structure and Properties of Engineering Alloys”, 2nd edn, McGraw-Hill, New York, 1993, p. 566.

[13]. Badia F. A., McDonald D. F. and Pearson J. R. Trans. AFS 1971, 79, 269.

[14]. C.S. Ramesh, R. Keshavamurthy, B.H. Channabasappa, Abrar Ahmed, “Microstructure and mechanical properties of Ni–P coated Si3N4 reinforced Al6061 composites” Materials Science and Engineering A 502 (2008) 99–106.

[15]. A. Ramesh, J. N. Prakash, A. S. Shiva Shankare Gowda and Sonnappa Appaiah “Comparison of the Mechanical Properties of AL6061/Albite and AL6061/Graphite Metal Matrix Composites” Journal of Minerals & Materials Characterization & Engineering, Vol. 8, No.2, pp 93-106, 2009.

[16]. Ghosh P. K. and Ray S. J. Mater. Sci., 1986, 21, 1167.

[17]. McCoy J. M., Prones C. and Warner F. E. 1. Mater. Sci., 1988, 1, 37.

[18]. McDanels D. L., “Analysis of stress-strain, fracture and ductility behaviour of aluminium matrix composites containing discontinuous SiC reinforcement”, Metall. Trans. A, 1985, 16, 1105-1115.

[19]. Beitz W. and Kuttner K. H. (Eds) Dubbel Handbook of Mechanical Engineering, 1994, p. D8 (Springer-Verlag, London).

[20]. Zhu H. X. and Liu S. K, “Mechanical properties of squeeze cast zinc alloy matrix composites containing alpha-alumina fibers” Composites, 1993, 24(6), 437.

[21]. Webster D. Metall. Trans. A, 1982, 13A, 511.

[22]. Towle D. J. and Fried C. M, “Comparison and compressive and tensile properties of Mg based MMCs”, J. Mater. Sci. Technol., January 1993, 9, 35-41.

DESIGN OF AIR COOLING FINS -I.C.ENGINE USING FEA ANALYSIS

Dr.P. Rathna kumar
Professor,
Department of Mechanical Engineering,
Navodaya Institute of Technology,
Raichur-584103
rathnakumar1972@gmail.com

J. Ramesh
Asst.Professor,
Department of Mechanical Engineering,
Navodaya Institute of Technology,
Raichur -584103

Dr. P. Velmurgan
Professor,
Department of Mechanical Engineering,
MallaReddy College of Engineering,
Hyderabad-500014

Dr.M.V.Malliarjuna
Professor,
Department of Mechanical Engineering,
Navodaya Institute of Technology,
Raichur-584103

ABSTRACT

Fins are basically mechanical structures which are used to cool various structures by the process of conduction and convection.It is important for an air-cooled engine to utilize fins for effective engine cooling to maintain uniform temperature in the cylinder periphery.

An attempt is made in this paper Design of IC Engine Air Cooling Fins with varying the fin pitch 10 mm and 20mm by modeling in Pro/E (creoparametric1.0) by taking the outer diameter of cylinder is 78 mm, inner diameter of cylinder is 62 mm, length of the cylinder is 120 mm and cylinder material as Aluminum, Fin material as copper.By using modeling procedure Assembly of cylinder & fins with surrounding airis done.

By using ANSYS software, the thermal analyses of IC engine air cooling fins is carried-out by discretization of numbers nodes are 21223. Shape of the element is Tetrahedral. By taking Ethylene Glycol Temperature Maximum of 120°C and heat release rate through the fins can be obtained by varying the Fin pitch .The heat release from Internal Combustion engine cylinder air cooling fins with six numbers of fin pitch 10 mm and 20 mm are obtained as the 21.02 W and 31.04 W. then the results are validated by comparing the Experimental and Ansys results and are with in the limits. Hence the work can be extended to Increase Rate of heat transfer by varying fin pitch. Changes like tapered fins, providing slits and holes in fins geometry can be made and the optimization of fins can be done with the help of ANSYS results.By keeping fins at an angle, changing the materials heat transfer can be improved.

1.0 INTRODUCTION

Extended fins are well known for enhancing the heat transfer in IC engines. However, liquid-cooling system enhances better heat transfer than air-cooling system, the construction of aircooling system is very simpler. Therefore it is important for an air-cooled engine to utilize the fins effectively to obtain uniform temperature in the cylinder periphery. There have been a number of studies on air-cooling of aircooled engine fins. Some researchers tested at air velocity from 7.2 to 72 km/h to enable the fin design of motorcycle engines but did not investigate temperature distribution in the fin circumference in detail.In many engineering applications the heat conducted through solids ,walls or surroundings has to be continuously dissipated to the surroundings or environment to maintain the system in a steady state condition and large quantities of heat have to be dissipated from small areas Heat transfer by convection between a surface and the fluid surroundings it can be increased by attaching to the surface thin strips of metals called FINS .The fins are also referred to as extended surfaces .The fins increase the effective area of the surface there by increasing the heat transfer by convection.

2.0 LITERATURE REVIEW

Pulkit Agarwal et al (3) (2011) has stated the that heat transfer rate depends upon the velocity of the vehicle, fin geometry and the ambient temperature. The heat transfer surface of the engine is modeled in GAMBIT and analysis in FLUENT software. An expression of average fin surface heat transfer coefficient in terms of wind velocity is obtained. It is observed that when the ambient temperature reduces to a very low value, it results in overcooling and poor efficiency of the engine**Dr. Subha Kumpaty et al (4) (2012)**has stated that fin’s temperature becomes excessive or insufficient it might lose functionality or cause other parts to heat or cool inadequately. By conducting heat transfer analysis, it is possible that such disasters can be avoided. Though previous studies have tested the performance of heat fins with thermocouples, none offer thermal images and intuitive understanding of how heat travels in fins. The infrared camera is used to document the thermal energy being emitted by the heated fins. **Mishra A.K et al(6) (2012)** has been carried out finned metal cylinder using CFD and is validated against the experiments.nc Alloy. In the present paper an effort is made to study the effect of fin parameters on fin array performance which includes variation in pitch and fin material. And concluded that for a given thermal load, the fin material and fin array parameters could be optimized in a better way by numerical simulation methods **U.Magarajan et al (7) (2012)** Experiment works are carried-out with the single cylinder air cooled engines was assumed to be a set of annular fins mounted on a cylinder. Numerical simulations were carried out to determine the heat transfer characteristics of different fin parameters namely, number of fins, fin thickness at varying air velocities by using CFD. The results validated with close accuracy with the experimental results. Cylinders with fins of 4 mm and 6 mm thickness were simulated for 1, 3, 4 &6 fin configurations. And they concluded that difference of heat transfer between 4mm and 6mm fins are negligible same at zero velocity. **Thundilkaruppa Raj R et al (8) (2012)** has stated that heat release of an IC engine cylinder cooling fins with six numbers of fins having pitch of 10 mm and 20 mm are calculated numerically using commercially available CFD tool. The IC engine is initially at 150°C and the heat release from the cylinder is analyzed at a wind velocity of 0 km/h. The heat release from the cylinder which is calculated numerically is validated with the experimental results**. Vignesh Shanbhag et al (9) (2012)** has been carried out to develop a finite element methodology to estimate the temperature distribution for steady-state heat transfer and thermal stresses induced by temperature difference in a silicon carbide (SiC) ceramic finned-tube of the heat transfer equipment.

2.1 OBJECTIVE OF PAPER:

An attempt is made in this paper deals with design of IC engine air cooling fins with varying the fin pitch 10mm and 20mm with Pro/E (creoparametric1.0) by taking the Outer Diameter of cylinder is 78 mm, Inner Diameter of cylinder is 62 mm and length of the cylinder is 120 mm, by considering the cylinder material is Aluminum and Fin material as copper and analysis by using ANSYS software

3.0 MODELING

This paper deals with Design of IC Engine air cooling fins with varying the fin pitch 10mm and 20mm with Pro/E (creoparametric 1.0) by taking the Outer diameter of cylinder is 78 mm, Inner diameter of cylinder is 62 mm, length of the cylinder is120 mm. cylinder material as Aluminum ,fin material as copper. By using

ANSYS software Grid formation of Assembly of cylinder & fins with surrounding air. Number of nodes are 21223.shape of the grid is Tetrahedral Because of better heat transfer. Hence project deals with heat release of an IC engine cylinder cooling fins with six numbers of fins having pitch of 10 mm and 20 mmwith available ANSYS WORKBENCH. By taking Ethylene Glycol Temperature Maximum 120^{0}C heat release rate through the fins can be obtained by varying the Fin pitch. Figure 1 and 2 shows the modeled in pro/E software, which was created cylinder with six numbers of fins. The actual dimensions of cylinder and fins are taken fromthe reference 7,8. The outer diameter of the fin is Ø148 mm, inner diameter Ø78 mm and the thickness of 6 mm. The outer and inner diameters of the cylinder are Ø78 mm and Ø62 mm. The cylinder is of a length of 120 mm. The hollow cylinder, six fins along with the outer air domain is created separately in Pro/E(creoparametric 1.0) and is then assembled. The output assembly design is created in parasolid format file for grid generation in ANSYS meshing tool.

3.1 GRID GENERATION

The 3-D model is then discretized in ANSYS meshing tool. In order to capture both the thermal and velocity boundary layers the entire model is discretized using tetrahedral mesh elements which are accurate and involve less computation effort. The entire geometry is divided into fourdomains FLUID_ETHYLENE_GLYCOL, FLUID_AIR_SOLID_FINS SORROUNDING, and SOLID_CYLINDER.Once the meshes are checked for free of errors and minimum required quality it is exported to ANSYS WORKBENCH. Figure 3 shows the mesh of air domain, fins, aluminium cylinder, ethylene glycol and assembly.

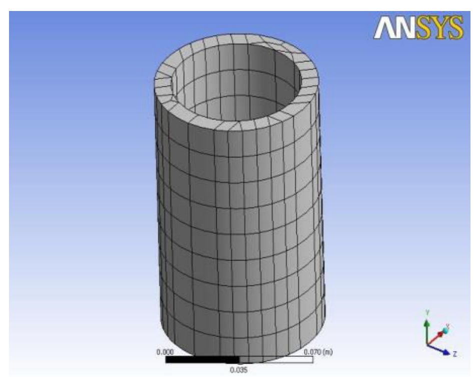

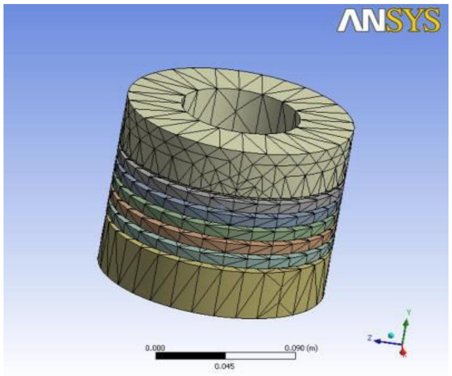

Fig:1 Grid formation of aluminum cylinder & air domain

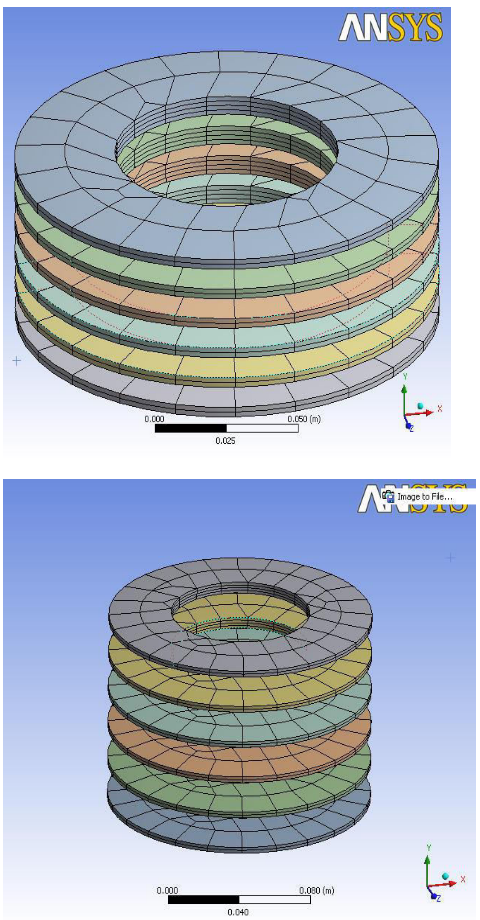

Fig:2 Grid formation of copper fins (6 no's) of 10mm & 20mm pitch

3.2 BOUNDARY CONDITIONS

Both the fluids ethylene glycol and air are assumed to be incompressible fluids. Ambient temperature and pressure are assumed as 303K and 101325 Pa respectively. The values of the boundary conditions like operating temperature, velocity of air are taken from the experimental work. Other boundary conditions like density, specific heat, thermal conductivity and other material properties are considered as constants throughout the analysis. The mesh is imported to ANSYS WORKBENCH and then the domains are initialized.The boundary conditions and the interface cylinder, fins, ethylene glycol and air are set in it. The top and bottom of the cylinder surface are assumed to be adiabatic as it is insulated as per the experiment. The heat transfer takes place due to natural convection and EthyleneGlycol temperatureas 393 K so that the fins and cylinder can be initialized with some higher temperature value than ambient temperature. After the

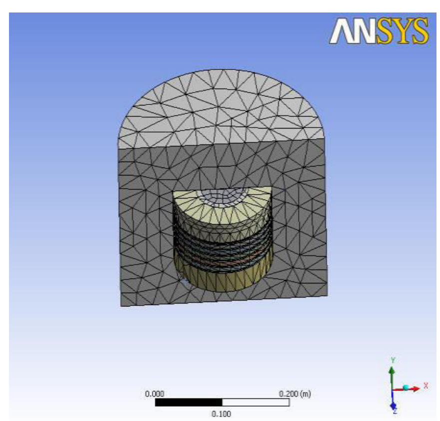

temperature reaches 393K air at inlet velocity of 0 km/h is passed over the cylinder and fins. The heat release from ethylene glycol from 393K after a time period of ten minutes is calculated.

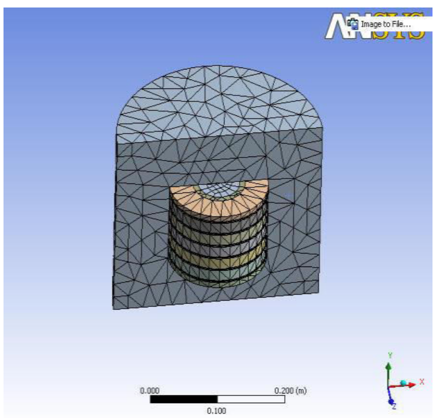

Fig:3 Grid formation of cylinder & fins with surrounding air for 10mm & 20mm pitch.

The boundary conditions here are

- All faces of air domains are have convective boundary layers with Film coefficient $3.81\mathrm{W}/m^{2}$ ^{0}C and ambient temperature as 30 ^{0}C
- All faces of ethylene glycol are kept at 120 ^{0}C

Insert thermal result in order to find the flow of Temperature and Heat Flux for

- Temperature for All bodies.
- Temperature for Ethylene glycol.
- Heat Flux for All bodies.
- Heat Flux for Ethylene glycol.

4.0 ANALYSIS

4.1 MATHEMATICAL ANALYSISOF FIN:

The knowledge of temperature distribution along the fin is necessary for the proper design of fins. The mathematical analysis for finding out the temperature distribution and heat floe from fins explained below.

Rate of heat flow Rate of heat flow Rate of heat flow

By conduction into + conduction out of = convection from surface

Element at x element at x + dx between x and x + dx

$$Q_{k,x} = Qk_{x+dx} + d\,Q_c$$

$$-kA\frac{dT}{dx}\Big|_{x} = -kA\frac{dT}{dx}\Big|_{x+dx} + h\,Pdx\,[\,T(x) - T(\infty)]$$ --------- (1)

Where P is the perimeter of the pin and Pdx is the pin surface area between x and x+dx. If k and h_c are uniform, Eq. (1) simplifies to the form

$\frac{d^2T(x)}{dx^2}$ - $\frac{hP}{kA}[T(x) - T(\infty)]$ ---------- (2)

It will be convenient define an excess temperature of the fin above the environment, $\varnothing_{(x)}$= [T(x) - T(∞)], and transform Eq. (2) into the form

$\frac{d^2\varnothing}{dx^2}$ - $m^2\varnothing = 0$ Where m^2 = h P/kA.----------- (3)

Equation (3) is a linear, homogeneous, second-order differential equation whose general solution is of the form $\varnothing(x) = C_1e^{mx} + C_2e^{-mx}$

---------- (4)

The other boundary condition dependence on the physical condition at the end of the fin. We will treat the following four cases.

Fin is very long and the temperature $\varnothing = 0$ at $x \to \infty$

The end of the fin is insulated :d$\varnothing$ = 0 at x = L

The temperature at the end of the fin is fixed : $\varnothing = \varnothing_L$ at x = L

The tip loses heat by convection :$\left.\frac{d\varnothing}{dx}\right| = h_{.L}\varnothing_L$

Evaluating $C_1 = \theta_s/1+e^{2mL}$ $C_2 = \theta_s/1+e^{-2mL}$

Substituting the above relations for C_1 and C_2 into Eq. (4) gives the temperature distribution.

$\theta= \theta_s\left[\frac{e^{mx}}{1+e^{2mL}}+\frac{e^{mx}}{1+e^{-2mL}}\right] = \theta_s\frac{\cosh\ m(L-x)}{\cosh\ (mL)}$

-------- (5)

$Q_{fin} = \sqrt{hPKA}\theta_s\tanh(mL)$

--------- (6)

ANSYS is general-purpose finite element analysis (FEA) software package. Finite Element Analysis is a numerical method of deconstructing a complex system into very small pieces (of user designed size) called elements. The software implements equations that govern the behavior these elements and solves them all; creating a comprehensive explanation of how the system acts as a whole. These results can be presented in tabulated or graphical forms. This type of analysis is typically used for the design and optimization of a system for too complex to analyze by hand. Systems that may fit into this category are too complex due to their geometry, scale, or governing equations.

4.2 General formula for calculating heat transfer:

The heat release from the cylinder was obtained by multiplying the heat capacity of the heat storage liquid by the difference between 120°C and the temperature after 10 minutes.

Heat release, $Q = mC_P\Delta T$

Where, m = mass of the heat storage liquid, in Kg,C_P= specific heat capacity of ethylene glycol, in J/kg/K, ΔT = change in temperature after 10 minutes, in K.

From the above data the Ethylene Glycol temperature reduced from maximum temperature 120°C to minimum temperature 78°C for 10mm Fin pitch and the 69°C for 20mm Fin pitch. Hence heat release rate can be calculated from the Equation

For Ethylene glycolDensity =1018 kg/m³,

C_P= 2.368 kJ/Kgk,m =0.36kg

For 10mm pitch:

After 600 sec from the ANSYS Workbench repot it is seen that For Ethylene Glycol

Heat release, Q = m C_P ΔT =0.36x2.368x (393-361.31)=27.02 W

For 20mm pitch: Heat release, Q = mC_PΔT = 0.36x2.368x (393-356.16)=31.4W

4.3 FINITE ELEMENT ANALYSIS

FEA has become an essential step in the design or modeling of a physical phenomenon in various engineering disciplines. A physical phenomenon usually occurs in a continuum of matter involving several field variables. The field variables vary from point to point, thus possessing an infinite number of solutions in the domain. It can be used to calculate deflection, stress, vibration, buckling behavior and many other phenomena.. Finite Elements packages may include pre-processors that can be used to create the geometry of the structure, or to import it from CAD files generated by other software. The FEA software includes modules to create the element mesh, to analyze the defined problem, and to review the results of the analysis

A transient thermal analysis determines the temperature distribution and other thermal quantities under conditions that vary over a period of time.To specify time-dependent loads, you can either use the function tool to define an equation or function describing the curve and the apply the function as a boundary condition, or you can divide the load-versus-time curve hence the thermal properties should be given to all the materials.

5.0 RESULTS AND DISCUSSION

5.1 ANSYS RESULTS:

i) Heat transfer analysis of 10mm&20 mm pitch fins after 600 sec

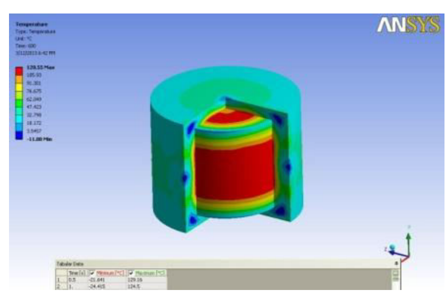

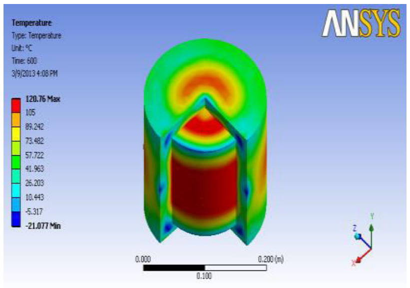

Figure: 6Temperature distribution of the sectional view of whole assembly (Pitch=10 mm&20mm) simulated by ANSYS

From the figure 6 it is taken that average temperature is as 88.31°C which is considered as final temperature for 10mm & 20mm fin pitch.

Initial temperature

= 120 °C &120°C

Final temperature

= 88.31 °C &83.16°C

Thus the ANSYS results is calculated and the heat release from ethylene glycol is found to be 27.02 W for a fin pitch of 10 mm and 31.4 W for a fin pitch of 20 mm. It is seen that by increase in fin pitch there is an increase in heat release. The temperature distribution profile of whole assembly in the sectional front view is shown in figure 6. From the figure 6 ,it is seen that the maximum temperature of the ethylene glycol is reduced from 423 K to 415 K after 600 seconds and the average temperature of ethylene glycol is 369.7236 K which is simulated from the ANSYS Workbench result. The temperature of air, cylinder and fins which are at ambient temperature is also increased from 298 K to 328 K.Heat transfer analysis of 10mm pitch fins after 600 sec. Temperature reduced from maximum temperature 120°C to minimum temperature78°C.And the average temperature is 88.31°C.Heat transfer rate is 27.02w. It is observed from the ANSYS Workbench result shown the heat transfer analysis of 20mm pitch fins after 600 sec temperature reduced from maximum temperature 120°C to minimum temperature 69°C .And the average temperature is 83.16°C.Heat transfer rate is 31.4wANSYS &Experimental results is made.

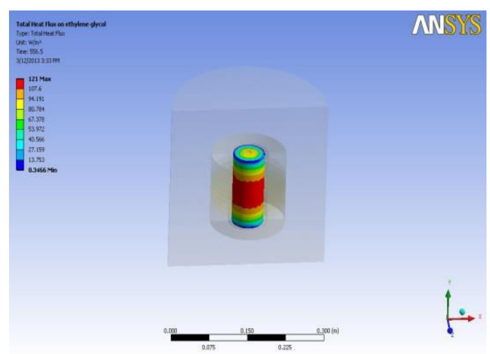

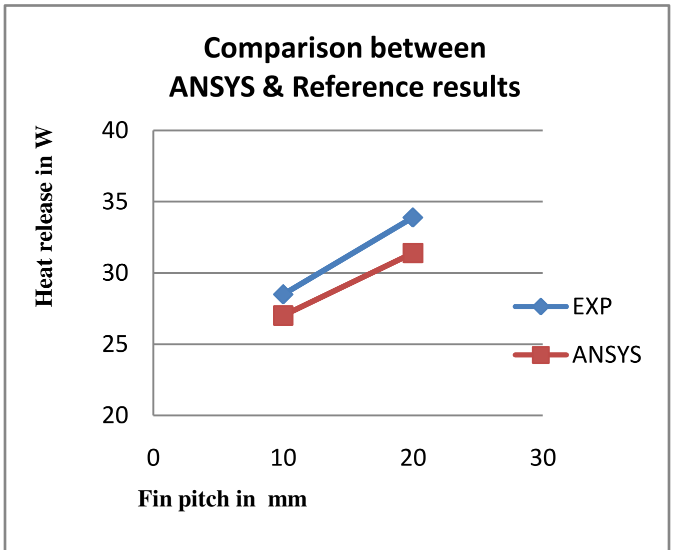

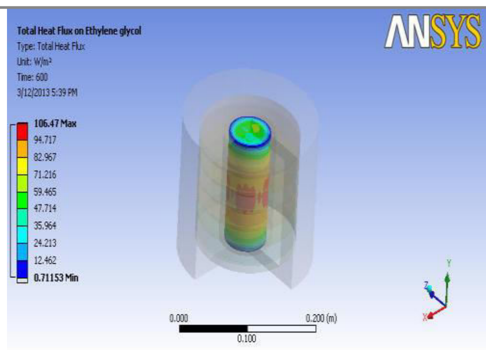

Fig: 7 Total Heat Flux on Ethylene glycol analysis of 10mm &20 mm pitch fins after 600 sec

GRAPH: Graph is drawn between Fin pitch in mm and Heat release in W.

Graph: Comparison between ANSYS &Reference result

Reference results has taken from the reference (7, 8) paper and it is compared with the ANSYS results

Pitch	REFERENCERESULTS	ANSYS RESULTS
10mm	28.50 W	27.02 W
20mm	33.90 W	31.40 W

Table: 1 Comparison between ANSYS &Experimental (Reference7, 8) results

6.0 CONCLUSION

1. A model for an air cooled motorcycle engine is developed and effects fluid and air temperature are observed..
2. An analysis of heat transfer under different surrounding temperatures has also been carried out to reduce the over cooling of engines .For a given thermal load, the fin material and fin array parameters could be optimized in a better way simulation methods.
3. ANSYS could be used to determine optimal values of fin parameters before actual design. To increase the cylinder cooling, the cylinder should have a greater number of fins.However, the cylinder cooling may decrease with an increased number of fins and too narrow a fin pitch. This is because the air could not flow well between the fins, thus the

overlapping of thermal boundary layers occurs at the upper and lower fin surfaces.

4. The heat release by both experimental and ANSYS work is approximately the same nearly 90% and should be modify the fin geometry and predict those results.
5. Therefore, in this project work, the heat transfer characteristics of the heat storage liquid by aluminum cylinder with six numbers of fins having a pitch of 10 mm and 20 mm are found.

6.1 FUTURE WORK

1. Rate of heat transfer can be improved by varying fin pitch.
2. Changes like tapered fins, providing slits and holes in fins geometry can be made and the optimization of fins can be done with the help of ANSYS results.
3. By keeping fins at an angle heat transfer can be improved.
4. By changing the temperature of ethylene glycol rate of heat transfer can be improved.
5. By changing the materials of fins heat transfer rate can be improved.

REFERENCES

1. S. A. Nada and M. Mowad Free convection from a vertical and inclined semicircularcylinder at different orientations Alexandria Engineering Journal, Vol. 42, No. 3, May 2003.

2. Gulshansachdeva ,computation of heat transfer augmentation in a plate-fin heat exchanger using rectangular / delta wing ,march, 2010.

3. Pulkit Agarwal, MayurShrikhande and P. Srinivasan Heat Transfer Simulation by CFD from Fins of an Air Cooled Motorcycle Engine under Varying Climatic Conditions, Proceedings of the World Congress on Engineering 2011 Vol III WCE(2011), London.

4. Dr.subhakumpaty , MayurShrikhande and P. Srinivasan Heat Transfer Simulation by CFD from Fins of an Air Cooled Motorcycle Engine under Varying Climatic Conditions, Proceedings of the World Congress on Engineering,2011.

5. Ashish Giriand S.A.K.JilaniEvaluation of the Performance of Annular Composite Fin using ANSYS International Journal of Computer Applications (0975 – 8887) Volume 44– No15, April 2012 .

6. Mishra A K,Elango T &ThundilKaruppa Raj R Numerical Study on Heat Transfer of Internal Combustion Engine Cooling by Extended Fins, Research Journal of Engineering Sciences Vol. 1(2), 32-40, May 2012.

7. Magarajan U, Thundilkaruppa Raj R and Elango T School of Mechanical and Building Sciences, VIT University, Research Journal of Recent Sciences Vol. 1(6), 32-37, June 2012.

8. ThundilKaruppa Raj R. ,Mishra A.K., AND Nawal S. School of Mechanical and Building Sciences, VIT University, Research Journal of Engineering Sciences Vol. 1(2), 32-40, August 2012.

9. G.Vigneshshanbagh &Mayur Shrikhande performance of rectangular fins on a vertical base in free convection heat transfer research journal of recent sciences vol. 1(6), 32-37,october 2012.

ERECTION /INSTALLATION OF MECHANICAL DEVICES &COMPARATIVE STUDY OF ELECTRO STATIC PRICIPITATOR IN SUPER THERMAL POWER PLANT

Siddappa Nyamagoud,
Assistant Professor
Mechanical dept.
Malla Reddy College of Engineering ,
Hyderabad, India
siddappanyamagoud@gmail.com

Nalla.Sneha,
Assistant Professor
Mechanical dept.
Malla Reddy College of Engineering
Hyderabad, India
snehadvr@gmail.com

***Abstract*—The growth of any country is measured by the electrical power consummation for capita. In the developed countries like USA, Japan there electrical power 2400 W per capita where as in India the power consummation per capita is around 800 W In this regard the National Thermal Power Corporation (NTPC) Ltd has entered in program of power generation to the country.**

The National Thermal Power Corporation (NTPC) Ltd was set up and accelerates power development in India since in 1975. National Thermal Power Corporation (NTPC) Ltd Kudgi to build the best 800 MW units of global standards promoting inclusive growth.

As an inspection of the receiving and storing of material at site to build the auxiliaries (Fenced lockable open yards and Covered lockable area in sheds inspection.) Inspection of the plant component and to control the inventory in a site. Study the plane and procedure of installation of plant components.

The plant design parameters like collection efficiency, Specific Collection Area, Aspect Ratio etc. are determine and comparing of above parameters between the NTPC Kudgi and National Thermal Power Corporation (NTPC) Ltd Ramgundam is under taken.

Test the Electro Statics Precipitators (ESP) components in a ground level testing methods, Kerosene test method, spirit and water level method, Gauge method and Alignment method etc.

The solid waste from power plant is used in making of bricks.

Keywords—ESP;super thermal power plan;NTPC;sulphuri acid plant;

I. INTRODUCTION

Coal & Hydro have been the main source of generation of electricity in power plant. A steam power plant continuously converts the energy stored in fossil fuels like coal, oil, etc. or fissile fuels like uranium, thorium etc into shaft work and ultimately into electricity.

The steam power plant work under principle of Rankine cycle. In an operation first energy release from burning of stem is transferred to water in the Generator (Boiler) to generate steam at a high pressure and high temperature, the steam leaving the turbine is condensed into water in the condenser, where cooling water from river circulates carrying away the heat released during condensation. The condensate (H2O) is then fed back to the Boiler (Generator) by use the pumps, and cycle goes on repeating itself. The water as the working medium and coal is fossil fuels to convert the bulk energy to electrical energy.

The power plant small proportion of CO2 is produced from the world's fossil fired in power plant by used Electro Static Precipitator (ESP) CO2 emission can reduced.

ESPs have been carefully designed to collect more than 99.5% of particles in the flue gas from many industries. ESPs efficiently collect particles of various sizes: large particles of 3 to 10 µm in diameter, and smaller particles of less than 1 µm in diameter.

An ESP is designed for a particular industrial application. Building an ESP is a costly endeavor, so a great deal of time and effort is expended during the design stage. Manufacturers use various methods to design ESPs. They also consider a variety of operating parameters that affect collection efficiency including resistivity, specific collection area, aspect ratio, gas flow distribution, and corona power. This lesson focuses on these methods and operating parameters.

In Kudgi plant steam is generated from a once through boiler at a pressure above the critical point. If the plant incorporates reheat and several stage of feed heating, there is about 2% gain in thermal efficiency compared with corresponding subcritical cycle.

II. LITERATURE REVIEW

In 1905 Dr.F.G Cottrell are being commercially used Electrostatic Precipitator (ESP) and demonstrated to its (capture acid mist suspended in exhaust of a sulphuri acid plant). ESP then was used in a variety of applications capture of solid particles suspended in flue gas stream of coal power plant, smelting plants of copper, zinc and lead to recover metal oxide from fumes, and in cement plants to clean the exhaust. Since then ESP technology and application has grown tremendously, and so is the problems associated with efficient operation of ESP. The following are major areas of investigation on flow in an ESP.

Theoretical models on ESP efficiency
Aspect Ratio
Particle migration velocity
Specific Collection Area
Size of collectors and size of particles

III. METHODALOGY

LIST OF ESP CONSTRUCTION ACTIVITIES

MECHANICAL ACTIVITIES

Unloading and storage of materials Shifting of materials from storage yards to site(manual and/or with material handling equipment)Electrical connection for erection and ground assembly work Checking of civil foundation w.r.t plant layout Checking of individual footing Erection and alignment of ESP support structure columns with bracings Checking of support structure top plate like, its spirit level, its water level and axial & diagonals distance.

Erection and alignment of support bearings Ground assembly, alignment of casing columns and welding of casing columns with panels and its leak testing by kerosene Ground assembly of inlet nozzles and leak testing by kerosene Ground assembly of outlet nozzles and leak testing by kerosene Erection of assembled casing panel with columns, top/bottom girders and its alignment/welding. Erection and alignment of collecting plate floating channel arrangement Arrangement of collecting plate assembly jig and plate straightness checking arrangement Arrangement of collecting plate lifting frame. Ground assembly of collecting plates with top and bottom tadpole after checking the plate straightness Erection of collecting plate panels. Depending on height of ESP Alignment of collecting plate panels and then erection of bottom guides/keeper bars/alignment rack

On levelled platform Ground assembly of top HV frame. Erection/Positioning of top HV frame on temporary supports Erection/Alignment/Welding of roof plates Erection, fitting and welding of pent house Erection of support insulators and its allied parts Fixing of rigitrode rapper rod and its alignment of support insulators Loading of HV frame and its alignment w.r.t collecting plates Temporary/loose locking of top HV frame with casing/girder Erection of rigitrodes & its straightness checking Fixing of rigitrode bottom guide frame Ground assembly and erection of hopper with its welding/leak test. Alignment of rigitrode w.r.t collecting plates(corona gap)Installation of items below hopper like RAV / slide gate , if applicable

Erection of TR sets with its ducting
Erection of inlet nozzle with its GD screen
Erection of outlet nozzle with its GD screen
Installation of collecting plate rapping system
Installation of rigitrode rapping system
Erection of inlet GD screen rapping system
Erection of staircase and platforms
Erection of access door level platform

Erection and welding of access doors for casing/nozzles and inside landing platform. Welding of sampling parts of ESP inlet and outlet with approach platform & ladder Air leak test and ESP thermal insulation application ELECTRICAL ACTIVITIE Laying of cable tray, as per drawing Earthing of all electrical items Cable laying Individual TR panels to respective TR sets Rapper panel to Rapper coils Support insulator heater feeder to heater JB and then to respective heaters Hopper heater feeder to heater JB and then to respective heaters Purge Air Blower feeder to Purge Air Blower Hopper level controller feeder to level controllers Making the provision of earhting point for connecting grounding hooks at casing and roof access doors Fixing of all grounding cables for all access doors, rapper coils

Fixing of hopper heating pads
Fixing of hopper level sensors
Fixing of support insulator heaters
Fixing of thermostats for insulators and hopper heaters
Installation of Rappers on ESP top
Installation of TR control panels in control room
Installation of rapper panel in control room
Cable termination of all cable as per drawing

IV. RESULTS AND DISCUSION

Calculation and Comparison of ESP Overall Collecting Efficiency η = Mass of all particles retained by collector (ESP)/Mass of all particles entering collector Deutsch Anderson equation and Matts-Ohnfeldt equation are used to find collecting efficiency.

Table 1. ESP BASES

S L.NO.	Characteristic Parameter	NTPC Kudgi	NTPC Ramgundam
1	GENERAL: Power Generation Capacity, MW	3*800 -1ststage 2*800 – 2ndstage	3* 500MW
2	Manufacturer	Larsen &Toubro Ltd.	FlaktItaliana S.P.A
3	Number of electrical field in series in direction of flow	9	4
4	Average bus voltage (KV)	60-95	70
5	Pressure drop across the precipitator(mm wc)	20	15
6	Specific collecting plate Area(Sq. m/m3/sec)	264	147.68
7	Overall collecting efficiency,% Guaranteed collection efficiency,% One of field out off service,%	99.93 99.96 99.91	98.99 99.91 98.16

8	Gas temperature across precipitator	(at guarantee point flow)	10
1	COLLECTINGELECTRODES: Size of Electrodes Width(mm) Height(mm) Thickness(mm)	2782 15240 1.2	905 13500 1.5
2	No. Of Electrode: Per gas stream	720	312
3	Total active collection area m2	357068	29322(24.340 m2projected)
4	Type of Suspension	Through special bolts	Hook
	Discharge Electrodes:		
1	No. Of Electrodes per gas stream	4212	2700
2	Length of electrode	15960	15147
3	Diameter of pipe	50NB Pipe	2.7(dia)
	Rapping Mechanism for Collecting Electrode:		
	Type	Electrical Single Impulse.	Tumbling Hammers
	Rapping Mechanism for Discharge Electrode:		
	Type	Electrical Single Impulse.	Tumbling Hammers
	Transformer – Rectifier Unit		
	GENERAL:		
1	Type	Silicon oil filled sealed type construction	AEG-TELEFUNKEN
2	Rating(KVA)	91.23 (Approx)	68
3	Method of Cooling	ONON Silicon oil	Insulating oil

NTPC KUDGI

As per Deutsch Anderson equation

As per Guarantee point

η =1- exp (-AVmo/Q)

= 1- exp (-42.3977* 250/1354)

= 99.96%

As per Design point

η =1- exp (-AVmo/Q)

η = 1-exp (-42.3977*250/1465)

=99.93% (Design Point)

NTPC RAMGUNDAM

As per Deutsch Anderson equation

η =1- exp (-AVmo/Q)

η = 1- exp (-24.3*138/730)

= 98.99%

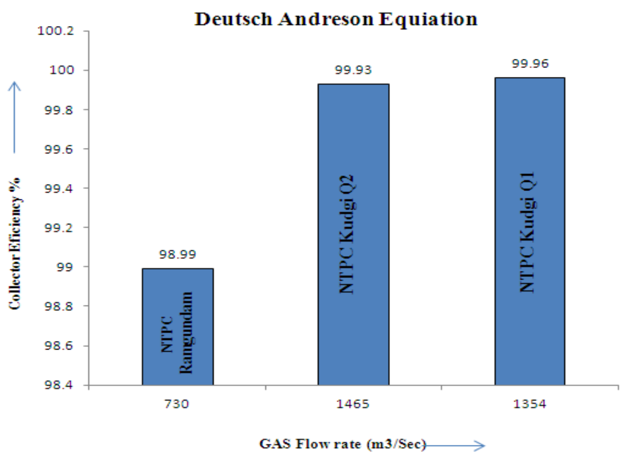

NTPC KUDGI

As per Matts-Ohnfeldt equation k=0.4

As per Guarantee point

η = 1 – exp [-wk (A /Q)] k

=1 – exp [-250(42.3977/1354)] 0.4

=89.74%

As per Design point

η = 1 – exp [-wk (A /Q)] k

= 1 – exp [-250(42.3977/1465)] 0.4

= 88.99%

NTPC RAMGUNDAM

Matts-Ohnfeldt equation k=0.4

η = 1 – exp [-wk (A /Q)] k

= 1 – exp [-138(24.3/730)] 0.4

=84.12%

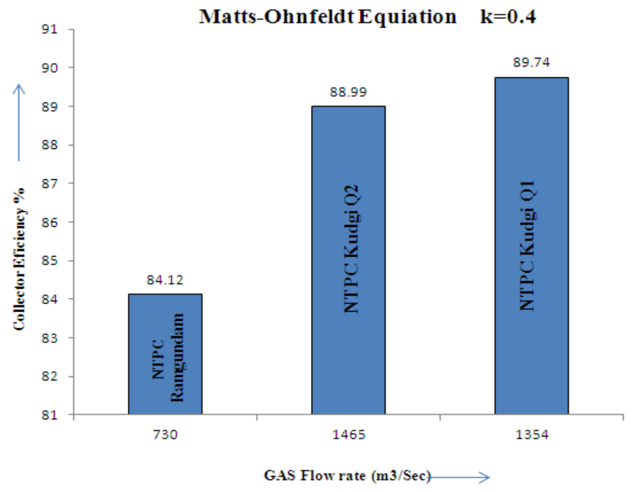

NTPC KUDGI
Matts-Ohnfeldt equation

As per Guarantee point
η = 1 – exp [-wk (A /Q)] k
=1 – exp [-250(42.3977/1354)] 0.5
=93.90%

As per Design point
η = 1 – exp [-wk (A /Q)] k
= 1 – exp [-250(42.3977/1465)] 0.5
=93.21%

NTPC RAMGUNDAM
Matts-Ohnfeldt equation

η = 1 – exp [-wk (A /Q)] k
= 1 – exp [-138(24.3/730)] 0.5
= 88.28%

Table 2. Collection Efficiency Estimation using the Deutsch Anderson equation andMatts-Ohnfeldt equation.

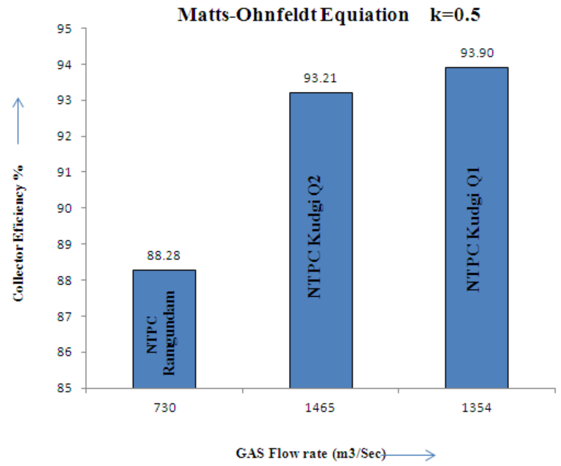

NTPC KUDGI
Matts-Ohnfeldt equation

As per Guarantee point
η = 1 – exp [-wk (A /Q)] k
= 1 – exp [-250(42.3977/1354)] 0.6
= 96.78%
As per Design point

η = 1 – exp [-wk (A /Q)] k
= 1 – exp [-250(42.3977/1465)] 0.6
=96.23%
NTPC RAMGUNDAM
Matts-Ohnfeldt equation

η = 1 – exp [-wk (A /Q)] k
= 1 – exp [-138(24.3/730)] 0.6
=91.76%

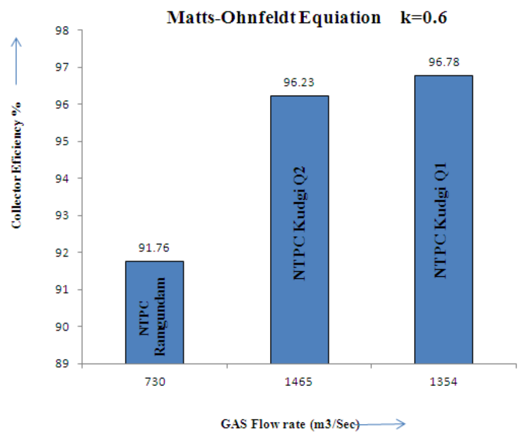

Specific Collection Area (SCA)

SL.NO	NTPC Kudgi				
		Deutsch Anderson Equation	Matts-Ohnfeldt Equation.		
			k=0.4	k=0 .5	k=0 .6
1	Guar antee point	99.96 %	89.74%	93.90%	96.78%
2	Desi gn point	99.93%	88.99%	93.21%	96.23%
		NTPC Ramgundam			
3	--------	98.99%	84.12%	88.28%	91.76%

NTPC KUDGI

SCA = Total collection surface / Gas flow rate in ESP

= A/Q m2/1000m3/hr

= 42.3977/1354

= 37.58 m2/1000m3/hr (Guarantee Point)

SCA = A/Q m2/1000m3/hr

=42.3977/1465

= 34.73 m2/1000m3/hr (Design Point)

NTPC Ramgundam

SCA = A/Q m2/1000m3/hr

=24.3/730

=33.288 m2/1000m3/hr

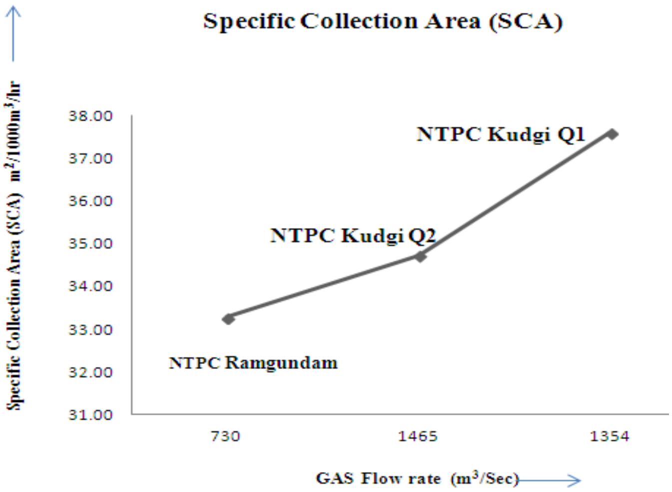

Aspect Ratio (AR)

NTPC KUDGI

AR = effective length of collector surface / effective height of collector surface

= l/h

=2782+2782+2782+2782+2782+2782+2782+2782+2782/15240 (9 no of field)

=1.64

NTPC Ramgundam

AR = l/h

=905+905+905+905/13500 (4 no of field)

=0.3

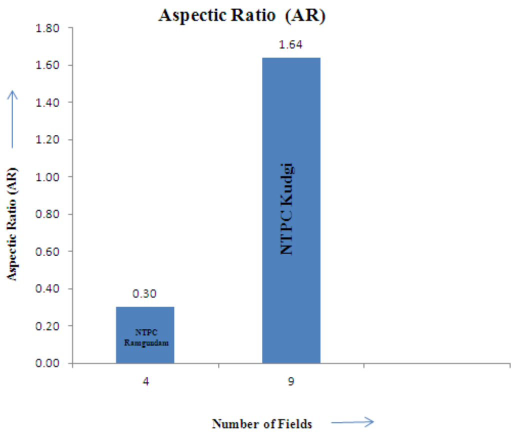

V. CONCLUSION

My project being an integral part of engineering syllabus provides not only easier understanding but also helps inform an individual with technologies.Fromtheoretical models, which differ considerably, it makes visible an individual to practical aspect of all things. The practical exposure received here will pay rich dividends to me. I gained a lot of practical knowledge which otherwise could have been exclusive to me.

During my project work altogether a good experience, since work culture and mutual co-operation were excellent in at NTPC Kudgi.Moreover, fruitful support of quality control and cognizance of safety by employees were fare which is much evident in Kudgi plant.

The change in collecting plates' size varies the overall collecting efficiency of the ESP (e.g. NTPC Kudgi 99.97% and NTPC Ramgundam 98.99%).Increase in the SCA of an ESP design will in most cases increase the collection efficiency of the ESP AR range 0.3 to 2for high-Efficiency ESP (those having collection efficiency of greater than 99%). The AR should be greater than 1 (average 1 to 1.5) and (e.g. NTPC Kudgi 1.64 and NTPC Ramgundam 0.3).

SCOPE FOR FUTURE WORK

The performance of other auxiliaries of thermal power plant can be studied thourghly and there is scope for improvement in the efficiencies of varies auxiliaries of power plants.

VI. REFERENCES

1. www.scribd.com-Erection-Manual-Tl-Design-Esp.
2. "National Thermal Power Corporation Limited | Hydroelectricity Power Distribution Company". NTPC.co.in. 2015-03-23. Retrieved 2015-03-28.
3. "Toshiba JSW to supply steam turbine for NTPC's Kudgi power project | Business Standard News". Business-standard.com. 2012-02-21. Retrieved 2015-03-28.
4. Firoz Rozindar (2015-02-03). "Kudgi NTPC thermal plant prepares for crucial hydrotest". Thehindu.com. Retrieved2015-03-28.
5. Kudgi.Stpp (2012) et.al 3*800 MW (Stage-1) Kudgi Super Thermal Power Plant at Village Kudgi, Vijayapur Dist- reg environment clearance.
6. Larsen & Toubro Limited Vadodara (2014) et.al installation instruction manual of electrostatic precipitator- innovation and advanced Technology solution for green power plant operations.
7. Maria Jędrusik and Arkadiusz Świerczok (2012). Design Efficiency of ESP, Air Pollution - Monitoring, Modelling, Health and Control, Dr. Mukesh Khare (Ed.), ISBN: 978-953-51-0381-3
8. Universidad Nacional de Catamarca Secretaría de Ciencia y Tecnología – Editorial Científica Universitaria ISBN: 978-987-661-043-837
9. Deutsch, W. Bewegung und Ladung der Elektricitatstrager im Zylinder Kondensator, Annalen der Physik 68, 335 (1922).
10. Matts, S. and Ohnfeldt, P. *Efficient Gas Cleaning with SF ESPs*; AB Svenska Flaktfabriken; Stockholm, Sweden; 1963-1964.
11. Smith, W.B., and McDonald, J.R. De*velopment of Theory for the Charging of Particles byUnipolar Ions*; J. Aerosol Sci.; Vol. 7, pp 151–166, 1976.
12. GALLIMBERTI: "Recent advancements in the physical modelling of electrostatic precipitators", Journal of Electrostatics 43 (1998) 219-247.

REDUCTION OF HUB DIAMETER VARIATION BY USING SQC TECHNIQUE

SHASHIKUMAR S
Assistant professor
Dept. of Mechanical
Malla Reddy College of Engineering ,
Hyderabad, India.
Email ID: shashikumarsolur@gmail.com

SUDHAPALLAVI JONNALAGADDA
Assistant professor
Dept. of Mechanical
Malla Reddy College of Engineering ,
Hyderabad, India.
Email ID: *Sudhapallavi24@gmail.com*

Abstract— In this paper, the concern parameters for grinding manner are improved for reduction in hub diameter variation interim keeping up quality standards in high pressure pump's cylinder head hub diameter manufacturing company. The Statistical quality control technique which is a powerful tool to study optimization for quality is used to find the optimal control parameters. The present paper deals with one of the quality issues resolved by using Statistical quality control (SQC) tools and methodology.

Keywords—statistical quality control; CNC Grinding machine;Diameter; Cause and effect diagram; gage R&R;

I. INTRODUCTION

Parts that require fine surface finishes and extremely close tolerance are candidates for precision grinding; precision grinding is becoming increasingly important for automotive industries. High pressure pumps have to produce 1600-1800bar pressure by eliminating all losses, these can to achieve by its components which are used. Cylinder head is the one of the important part in the high pressure pump, It's hub diameter play a very important role, if diameter is higher cannot do assemble, if less then fuel leakage will happen and it's diameter tolerance is 36µm. Hub diameter is grind by using CNC machine these can be grind by skilled operator. The CNC grinding machine is unstable process. Bahmuller CNC grinding machine Module have diameter variation, it can't to predictable nature for this reason operator can't maintain diameter within specification, by this critical condition 3% of parts rejection found. In this project reduce rejection rate to 0% by using effective steps by using SQC tools and techniques.

II. PROBLEM IDENTIFICATION AND FORMULATION

The important defects that occur during the production of cylinder head are Patch on hub diameter, Patch on internal diameter, patch on face, internal diameter, Hub diameter low and Hub diameter high etc. when the percentage of defects for various defects. Were drawn shown in the figure1. Hub diameter high and low was found to be of major concern and was contributing 80% of the defects.

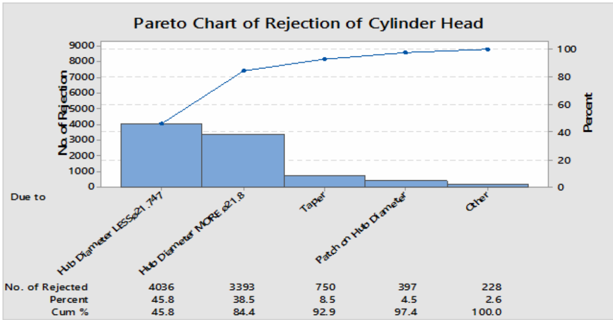

Figure 1 Pareto diagram of part rejection

Pareto analysis shows that Hub diameter variation which constitutes 20% of the type of defects are hub diameter is less than the 21.747mm and more than the 21.78mm are creating more than 80% the total defectives. If we concentrate on Pareto causes then the rejection can be brought down by more than half, which is actually the aim of the project then there will be a considerable decrease in the overall rejection.

The focus of project in the business point of perspective will be about 2.72% section created will be dismisses because of hub diameter less than 21.747mm and hub diameter more 21.78mm, it has found during 100% inspection of hub diameter. In the figure 2 shows monthly Rejection of Cylinder Head due to hub dia. more and less.

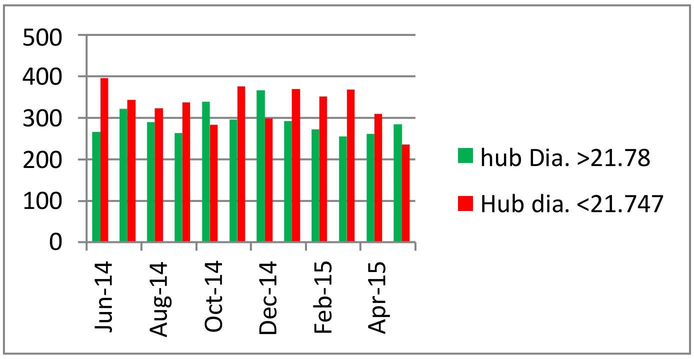

Figure 2 :Bar chart for Monthly wise Rejection of Cylinder Head due to hub dia. more and less.

III PROBLEM DISCRIPTION

In CP1H High pressure pump, the cylinder head and its hub diameter play a vital role. Its hub diameter grinding operation is carried out in CNC Bahmuller grinding machine.

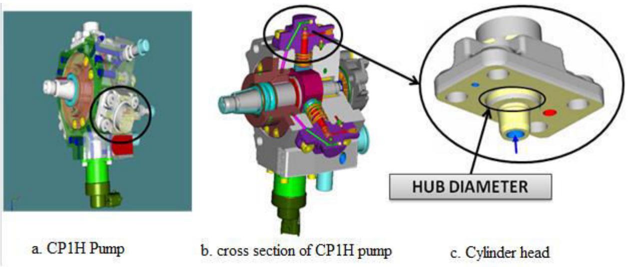

Figure 3 CP1H cylinder head

Above figure shows the CP1H pump Cylinder head with Hub diameter, its spec. 2.8 mm with tolerance -0.020 and -0.053. More than specification limit, that part can be rework by grinding process. Less than the specification limit, that part can't be reworked, it leads to oil leakage problem in the pump and these parts are rejected. The percentage rejection found in CP1H pump cylinder head part was 3% due to hub diameter out of the specification. The variation of the Hub diameter treated as cause X.

The object of the project work is to reduce the variation of the hub diameter in the hub pump cylinder head.

IV EXPERIMENTAL DETAILS

4.1. Cause-Effect Diagram for Dimensional variation Brainstorming:

Through brainstorming listed various causes (X) that contribute to problem (Y) Hub diameter variation are skill of operator, hardness in material, gauge variation, master gauge, defective grinding wheel, spindle oil, chuck run out, alignment, CNC program, wheel wear out, process capability, improper dressing, wrong correction and coolant nozzle setting. All listed causes are consolidated to Fishbone diagram shown in the figure 4.

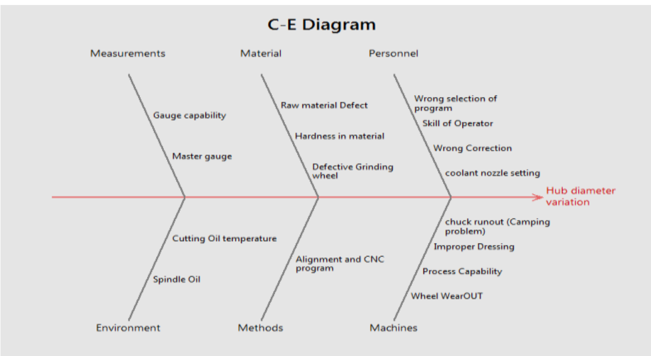

Figure 4 Cause effect Diagram

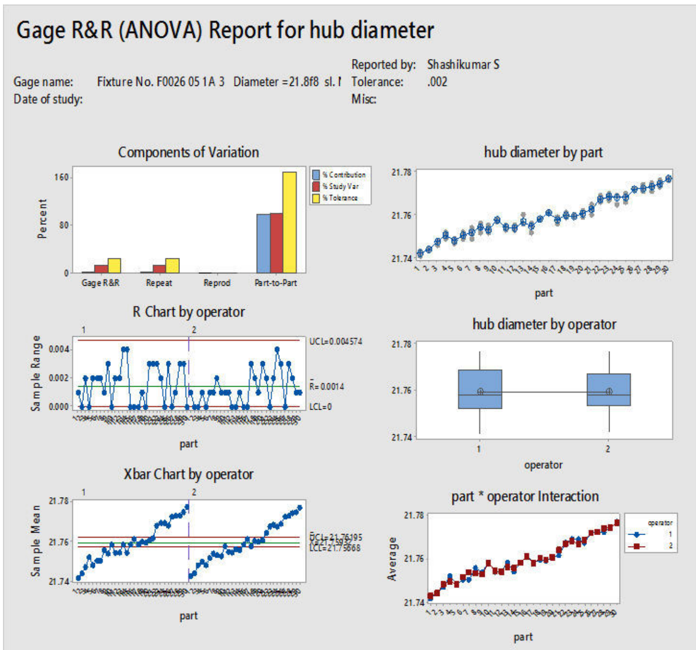

Figure:5 G R & R ANOVA report

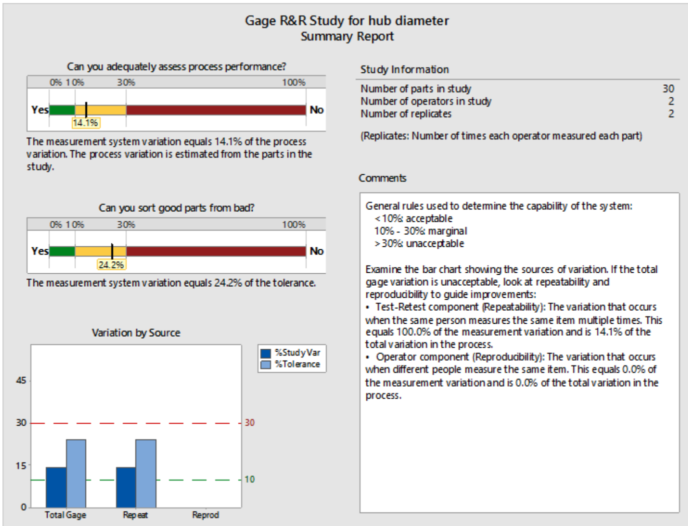

Figure 6 G R& R report

Analyzed all the factors mentioned in the cause and effect diagram , in that material, personal, environment, methods are analyzed by Visual inspection, Measurement instrument are analyzed by calculating gauge R&R , After every thirtieth part dresses the grinding wheel, parts between dressing the grinding wheel as one grinding cycle that 30parts are chosen for measurement. Two operators measure same parts twice at different periods. Gauge R&R study Analyzed using ANOVA method. The value of total G R & R found 14.11%, within the acceptable limit of 30% and hence the measurement system is acceptable. Fit for calibration. In machine parameter Chuck has been replaced, Part Dia. run out fixed. Parts produce with random variation found after dressing cycle and C_p = 1.07 and C_{pk}=0.80, this factor are suspect for produce diameter variation.

Process capability analysis:

To analyze process capability 400 parts are feed to machine for grinding process in that last five parts before dressing and next five parts after dressing process and consider as subgroup size 10. We calculated C_p and C_{pk} values for this data and was found to be 1.07, 0.80 respectively. The defect rate was 2.08%, which estimates the percentage of parts from the process that are outside the spec limits.

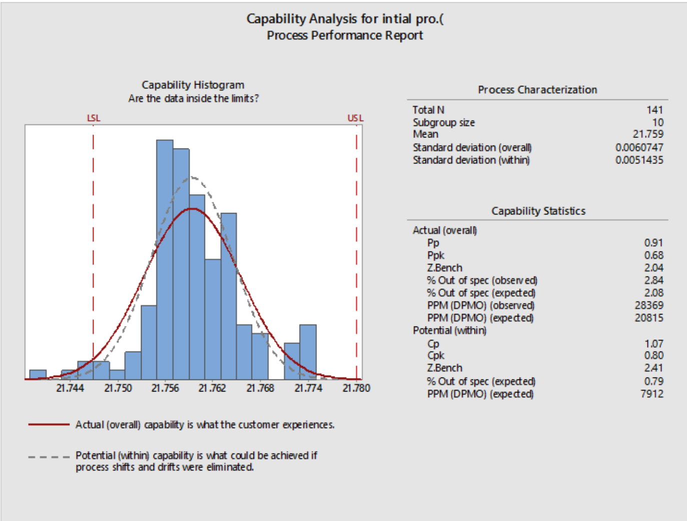

Figure 7 process capability report

Parts are numbered according to robot pickup the part and feed to machine, grind the part without influence of operator, measured five parts before dressing and five parts after dressing and plotted graph.

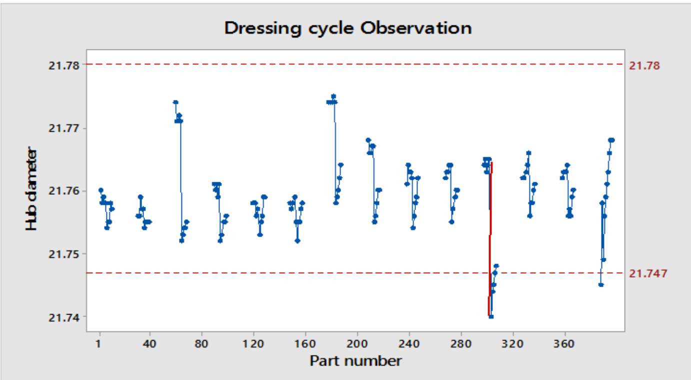

Figure 8 Dressing cycle observation

Figure 8 shows that dressing cycle observation, grinding cycle to grinding cycle in a same batch had found that higher contrast of maximum variation 23µm, by considering difference of before dressing part and after dressing part, maximum variation found in same batch with different grinding cycle.

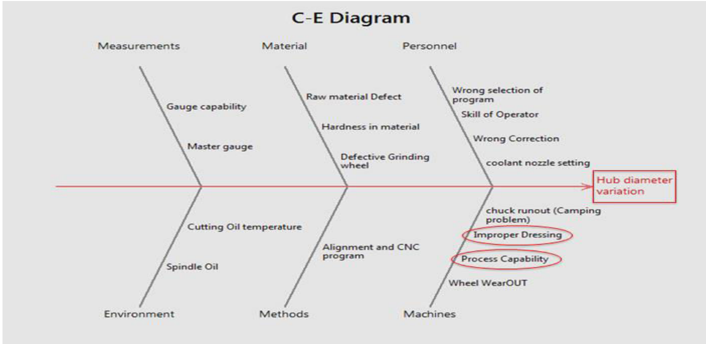

Figure 9 C-E Diagram

In cause and effect diagram shows that issues with machine, process capability was less than 1.33, after each dressing unexpected variation observed in time series plot.

V. EXPERIMENTAL DETAILS

The part of Cp1H high pressure pump cylinder head import to plant having hub diameter of 21.79mm to 21.799 mm. Initially checked relation between before grinding and after grinding process, around 0.010 mm to 0.030 mm stack will be removed during grinding process in the Bahmuller machine.

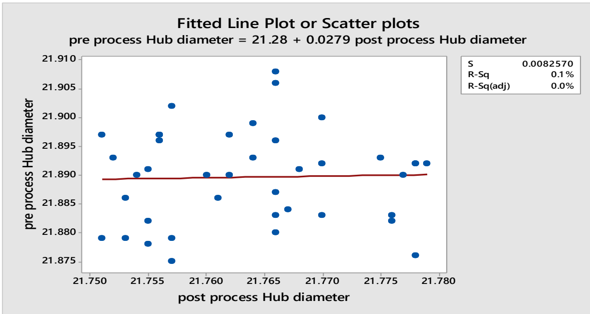

Figure 9 scatter plot

Figure 9 shows the scatter plot, in the pre and post grinding process hub diameter found zero percent contribution for regression, leading to a conclusion that there is no relationship between pre and post grind diameter. It indicates that machine grinding process takes place as per program feed in the control system. And axis of the grinding will actuate as mentioned in the program.

We observed most of the hub diameter at the final 100%inspection time, standard variation was found up to 0.0088. In this CNC grinding machine dressing will take place after every 30 parts. At each dressing cycle hub diameter pattern shows random nature in the graph so we mainly concentrate on dressing operation. We change the existing feed rate during dressing from 500mm/min to 250 mm/min, after measured output of grinding process we got standard deviation of 0.00685 and our next observation with changed dressing depth of cut from existing 0.020 mm to 0.030mm we achieved a standard deviation of 0.00322. After our experiments, with the original setting of .020mm depth of cut during dressing, the trials were conducted and standard deviation as 0.0065 was observed.

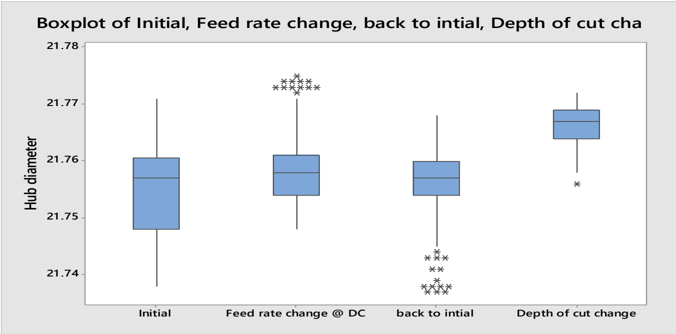

Figure 10 Box Plot

In figure 10 shows that the changes in depth of cut value in the dressing cycle are minimized the process variation than the other.

VI. Test

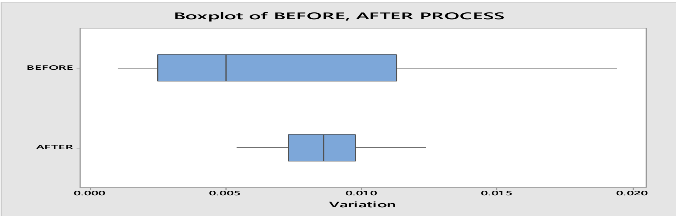

Figure 11 Box Plot

In figure 11, the box plot has drawn considering difference of average of five parts after dressing (that is 1st part to 5th part) and average of five parts before dressing (that is 26th to 30th) in the same grinding cycle.

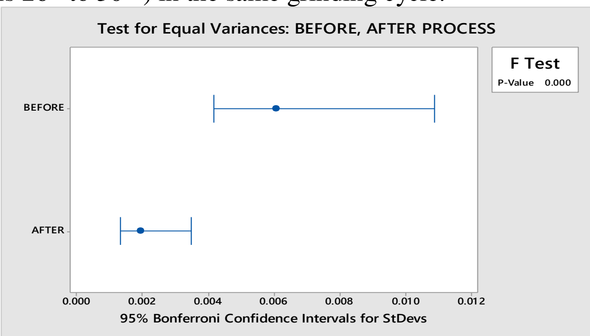

Figure 12 Test for variances

The hub diameter variation is minimized by change setting in the dressing cycle depth of cut (After) then the existing grinding process (Before) validated by using F – test.

Considering, Null hypothesis Ho: $\sigma^2_{\text{before}} = \sigma^2_{\text{after}}$

Alternative Hypothesis H1: $\sigma^2_{\text{before}} \neq \sigma^2_{\text{after}}$

The test is performed at Significance level $\alpha = 0.05$. F test as shown in the figure 5.2.4., we obtained P valve lesser than 0.05 that is 0.0. Therefore Null hypothesis H_0 is rejected. Hence, we can conclude from figure 12 that there is a significant reduction in variability after the experiment.

Comparison of process capability before and after the study was performed. The details are provided in figure 13. The comparison of C_p and C_{pk} values before and after the study is provided in table 1

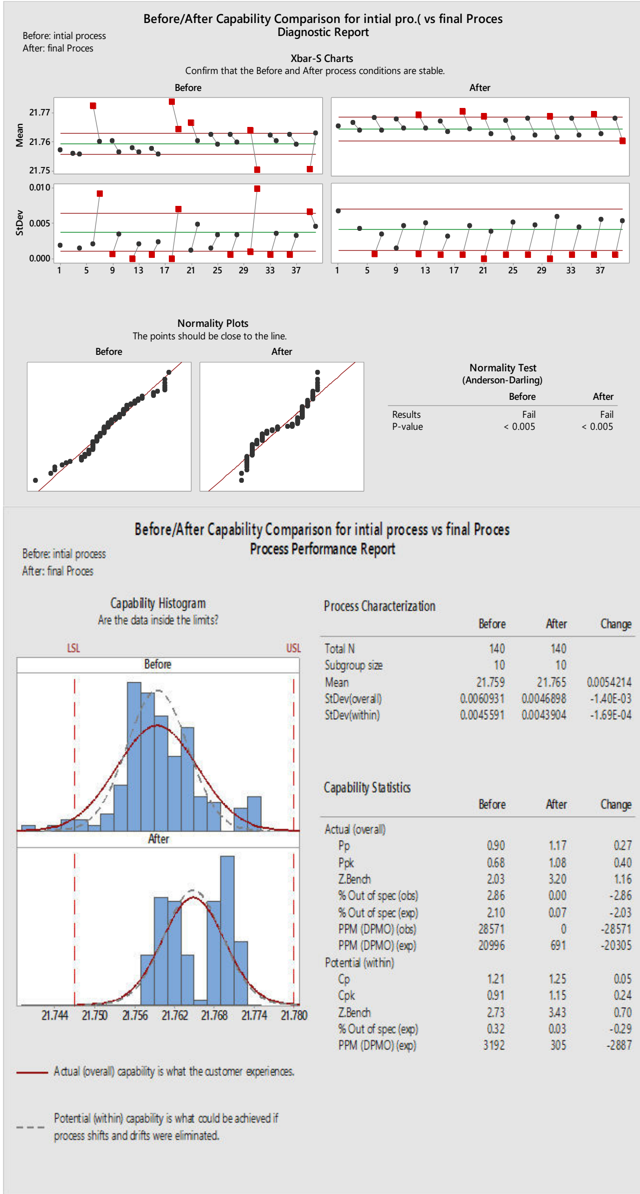

Figure 13 Capability comparison report

	Before	After
C_p	1.21	1.25
C_{pk}	0.91	1.15

Table: 1 : C_p and C_{pk} values before and after the study

VII. LEVERAGE

After understanding the root causes of the problem, so as to eliminate the hub diameter variation problems, following suggestions were made and the same were implemented.

Changing the dressing depth of cut from 0.020to 0.030 mm has resulted in minimise rejection of cylinder head due to hub diameter variation.However, the study has focused only on the root causes in the cylinder head hub diameter variation problem. Other probable sources of variation in the process of cylinder head hub grinding have to be evaluated to completely leverage the problem. The other sources of variation that could occur in the process of grinding hub diameter of cylinder head are to be identified.

Care has to be taken to avoid hub diameter variation occurring due to interruption. Effective utilization of all 6 slots buffer storage slots, at exiting state only 4 slots are used to avoid warm up cycles in the Bahmuller grinding machine during Kadia honing machine break down, increased buffer storage size from 4 to 6 slots at the feeder section.

CONCLUSION

Based on the experimentations and analysis carried out following conclusions and suggestions are derived to leverage the CP1H pump cylinder head hub diameter variation problem.The root cause was found to be improper dressing of grinding wheel used to grind cylinder head hub diameter.Rejection of Cylinder head part successfully Reduced from 3% to 0.2%.

REFERENCE

[1] Sunil sharma and anuradha r chetiya, Simplifying the six sigma toolbox through
application of shainin® doe techniques,vikalpa,vol. 34/01, jan-mar 2009, 13-19

[2] Application of six sigma methodology to reduce defects of a grinding process by E. V. Gijo, johny scaria and jiju antony. (wileyonlinelibrary.com) doi: 10.1002/qre.1212

[3] Reduction of Hub Diameter Variation In High Pressure Pump Cylinder Head by using Shainin Problem Solving Technique by Shashikumar s, IJRMEE, ISSN: 2349-7947 Volume: 2 Issue: 6,43-47

Heat Transfer Enhancement and Thermal Performance of Extended Fins

Sunil S, Assistant Professor
Mechanical Department
Malla Reddy College of Engineering
Maisammaguda, Telangana, India
Sunilmth14@gmail.com

Sudheer Hiroolikar, Assistant Professor
Mechanical Department
Malla Reddy College of Engineering
Maisammaguda, Telangana, India
Sudhirhirolikar@gmail.com

Abstract— **A fin is an extended surface which is used to increase the rate of heat transfer by connecting to the heating surface. The heat transfer rate can be increased by convection process and also by increasing surface area by means of extended surfaces.**

In the present analysis effect of increase in total surface area to improve the rate of heat transfer is studied. Thermal Analysis is performed for various perforated fin extensions with varied diameter. The analysis is carried out using commercially available finite element analysis software. Analysis called steady state thermal has been used to find out the temperature variations and heat flux of the fins.

Keywords—Modeling, meshing, boundry conditions, thermal analysis.

1. INTRODUCTION

In this chapter we have discussed basic heat transfer, modes of heat transfer, importantly natural convection has been discussed and heat transfer through extended surfaces or fins and various methods of increasing heat transfer are discussed.

Extended Surface (Fin) are used to enhance convective heat transfer in a wide range of engineering applications and offer a practical means for achieving a large total heat transfer surface area without the use of an excessive amount of primary surface area. Fins are commonly applied for heat management in electrical appliances, such as computer power supplies or substation transformers and other applications include IC engine cooling, Fins in Automobile radiator. Extensions on the finned surfaces is used to increases the surface area of the fin. When the surface area increase the more fluid contact to increase the rate of heat transfers from the base surface as compare to fin without the extensions provided to it. The concept of heat transfer through

perforated in fin array also one of the method to improve the heat transfer character. The efficiency and rate of heat transfer in perforated fin is compared to the fin with extension. The various types of extension provided on fin array such as (a) Rectangular fin with 20mm*5 perforation, (b) Rectangular fin with 20mm*7 perforation, (c) Rectangular fin with 3mm cutout, and (d) Rectangular fin with 20mm perforation and 3mm cutout.

A. Heat transfer and thermodynamics

Transfer of energy, mass, momentum etc has been included in the study of transfer phenomenon and these are all recognized as a single discipline of fundamental importance on the basis of thermodynamic forces and fluxes. Hence the transfer of such unified phenomena occurs due to a force of concentration gradient, temperature gradient, velocity gradient etc.

B. Heat transfer by extended surfaces or fins

The rate of heat transfer is given by

$q= hA(T_{surface}-T_{ambient})$

where q = coefficient of convective heat transfer.

h = convective coefficient.

A = Surface area.

T_s= Surface temperature.

T_a = ambient temperature.

To increase the convective heat transfer the following methods are used

- Increase the temperature difference (T_s-T_a)
- By increasing the coefficient of heat transfer (h).
- Increase the surface area (A).

Increasing h may require the installation of pump or fan or replacement is need for existing one with larger one. Hence alternative method for increasing the rate of heat transfer is increasing the surface area by giving extensions or perforations to the fins.

2. LITERATURE REVIEW

Nitish Kumar Jha, et. Al. (2015) Had investigated the heat transfer through extended surfaces. Fin with various extensions like fin with rectangular cavity, fin with triangular cavity, fin with trapezoidal cavity, and fin with semicircular cavity are considered for the analysis and the results are compared with the fin without cavity. About 2% to 21% of heat transfer enhancement has been recorded for fin with cavity. Fin with rectangular cavity provides more heat transfer as compared to fin without cavity. In thermal analysis the temperature variations of all the fin without cavity and fin with cavity has been analysed and the heattransfer has been calculated and percentage of variation in heat transfer has been recorded. Effectiveness of fin with rectangular cavity is more compared to fin without cavity.

V. Karthikeyan, et. al. (2015) had studied the rate of heat transfer for various extended surfaces. Fin with various extensions and different perforations are designed and analysed the results are compared with fin without extensions.

As a result heat transfer through fin with rectangular extension is higher compared to other type of extension. Fin with rectangular extensions provide 13% to 21% more enhancement of heat transfer. Fin with rectangular extension has more effectiveness compared to fin with various extensions.

Shital B. Salunkhe, et.al. (2015) In this paper the heat transfer has been analysed on the outer surface of the longitudinal finned tubes of different material such as copper, Aluminium with silver coating and Aluminium with nickel coating. Experiment is based on flow velocity. It is observed from the experimental results that the coefficient of convective heat transfer is enhanced with increase in air velocity and surface area. After comparing they concluded that coating affects heat transfer rate and heat transfer coefficient and copper is having high heat transfer coefficient as compared to other material specimen.

Pardeep Singh, et. al (2014) They had studied the design and analysis for heat transfer through fin with various extensions. The heat transfer through fin having same geometry but various extensions provide 5% to 13% increase in rate of heattransfer when compared to fin without extensions. Rate of heat transfer through fin with rectangular extensions is higher than other type of extensions. Temperature is minimum at the end of fin with rectangular extensions as compared to fin with other types of extensions.

MukeshDidwania,et. al.(2013) In this paper they have analysed the pressure loss and heat transfer for different shape of fins with rectangular duct. Rectangular fin, cylindrical fin are used for analysis. The purpose of this study is to find out the optimum dimensions and shapes for rectangular longitudinal fins, cylindrical pin fins by including transverse heat conduction. As a result after analysis they have concluded that heat transfer rate is maximum for circular fin and minimum for rectangular fin. Pressure loss is minimum for circular fin and maximum for rectangular fin in the duct. Air gets maximum temperature in case of circular fin.

A. Conclusions from literature review

- According to the literature review mentioned above rateof heat transfer can be increased by increasing the surface area.
- In one of the above papers fin with rectangular extension enhance more heat transfer.
- The temperature at the fin end is less for fin with rectangular extension.
- Hence in this project the various perforation and cutout is given to increase the heat transfer.

3. METHODOLOGY

In this chapter we are going to introduce the basic features of mechanical. The rectangular fin with various extensions and perforations are considered for analysing the heat transfer characteristics. This is done by using the steady state thermal analysis where temperature variations and total heat flux are analysed and the solutions are compared with existing model and validated for better results. So following steps shows the methodology used for analysing the results using thermal analysis.

A steady state thermal analysis can be described in the context of 4 main steps i.e.

1) Preliminary decisions
- What type of analysis has to be done
- What type of model it is.
- Selection of elements.

2) Pre-processing
- Importing model in IGS file.
- Defining and assigning material properties to the model.
- Meshing the geometry
- Applying boundary conditions
- Analyzing results

3) Solving
- Solve the model

4) Post processing
- Review the results
- Checking and Validation of result.

4. DESIGN OF MODEL

Figure shows the front view and side view 2D image of base line model which has been considered as a reference model for the analysis.

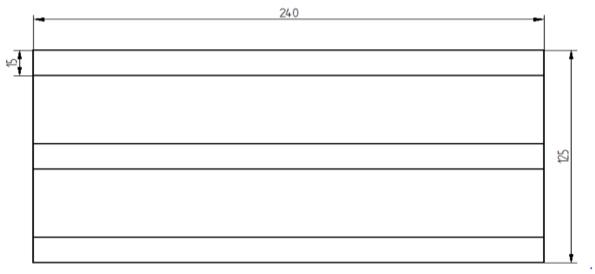

Fig 1: Front view

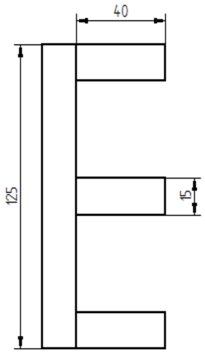

Fig 2: Side view

A. Designing of fin arrays with solid works

In this section solid model of various type of fins with perforations and cutout has been shown like existing model, rectangular fin with 20mm*5 perforation,20mm*7 perforation, 3mm cutout, 3mm cutout and 20mm perforation.

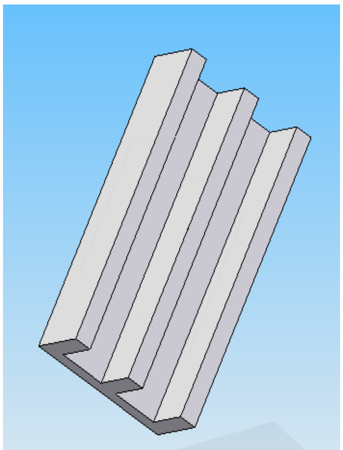

Fig 3:Base line model

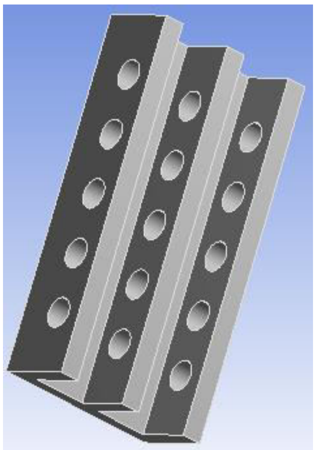

Fig 4:Rectangular fin with 20mm*5 perforation

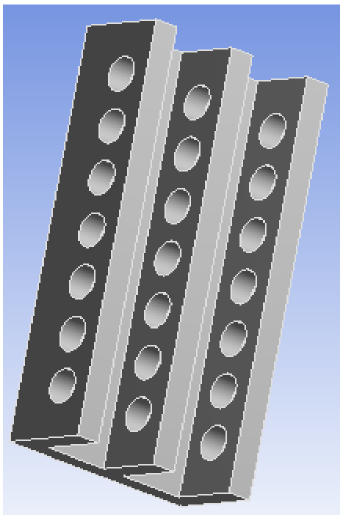

Fig 5: Rectangular fin with 20mm*7 perforation

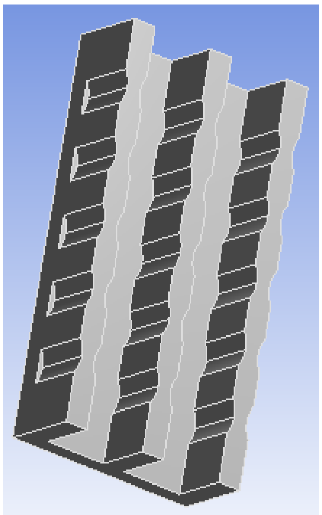

Fig 6: Rectangular fin with 3mm cutout

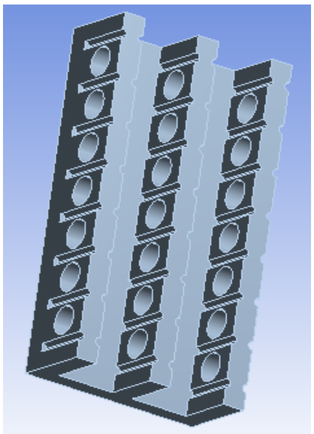

Fig 7: Rectangular fin with 20mm perforation and 3mm cutout

B. Import the geometry

Before importing the model geometry we have to check and set the unit systems to metric (m, kg, N, s, V, A) then the model geometry should be imported, the model should be in IGS format.

C. Mesh generation

In this section the meshed models are shown for fin with different diameter of perforation and cutout. Meshing is carried out by using mechanical physics preference along with fine relevance centre.

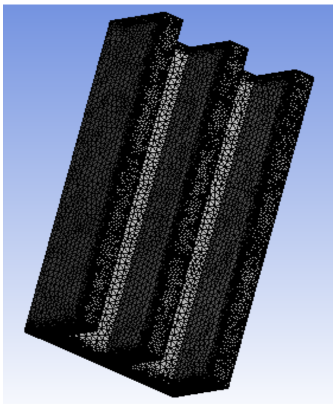

Fig 8: Model 1

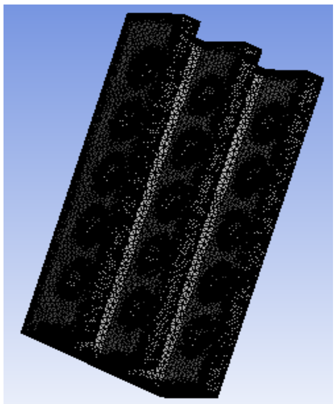

Fig 9: Model 2

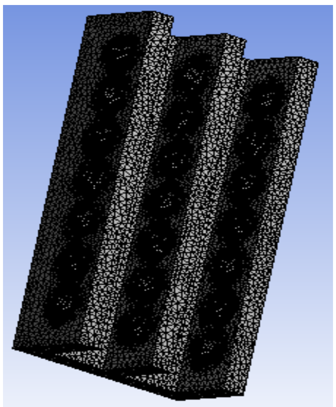

Fig 10: Model 3

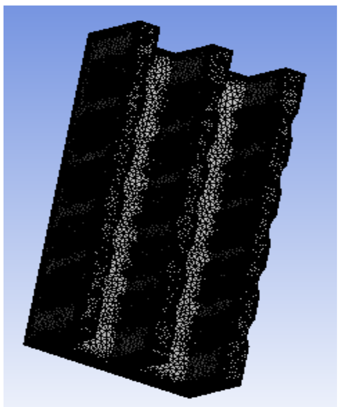

Fig 11: Model 4

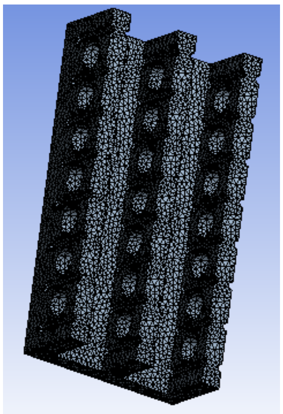

Fig 12: Model 5

D. Applying boundary conditions and assigning material properties

Aluminium has been selected for the analysis as a material which is economically good and also there is high rate of heat transfer and dissipation in this material.

Thermal conductivity, k=167 W/m^{0}c.

Thermal instantaneous coefficient expansion = 23.1*10^{-6} /k.

Base plate temperature = 55 ^{0}c.

Heat transfer coefficient = 83 W/m^2 ^{0}c

Ambient temperature = 30^{0}c.

Density = 2.70 g/cm^3

Young's modulus = 70000 Mpa

Poisson ratio = 0.35

5. ANALYSIS AND RESULTS

In this chapter first we have the material properties and boundary conditions. Then we have the temperature and heat flux analysis, graphs for temperature distribution, heat flux, rate of heat transfer.

A. Analysis

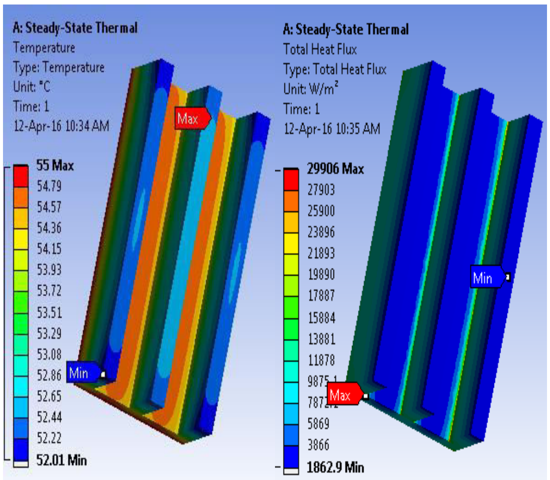

Fig 13: Temperature contour and heat flux for Model 1

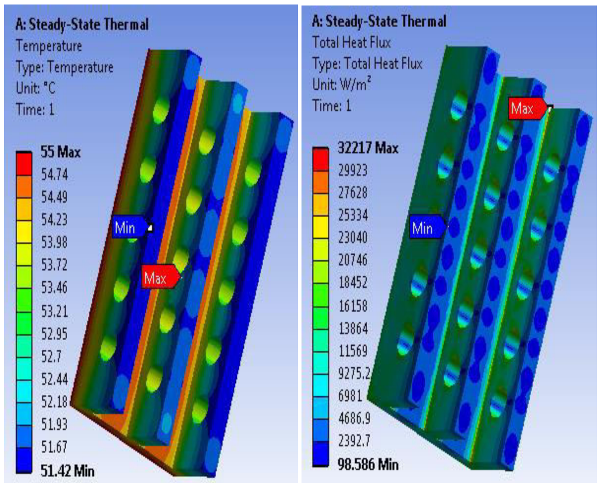

Fig 14: Temperature contour and heat flux for Model 2

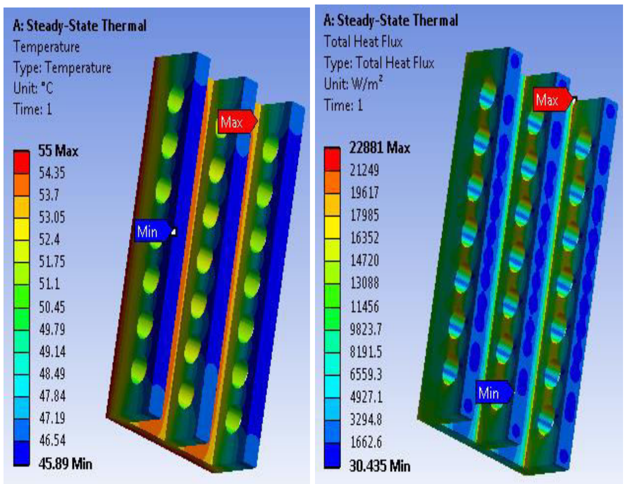

Fig 15: Temperature contour and heat flux for Model 3

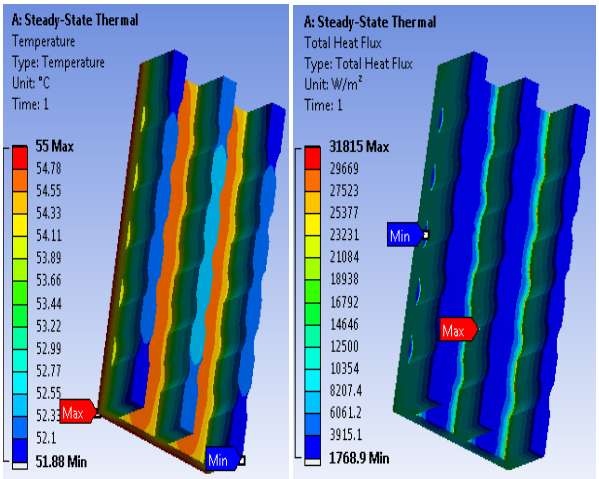

Fig 16: Temperature contour and heat flux for Model 4

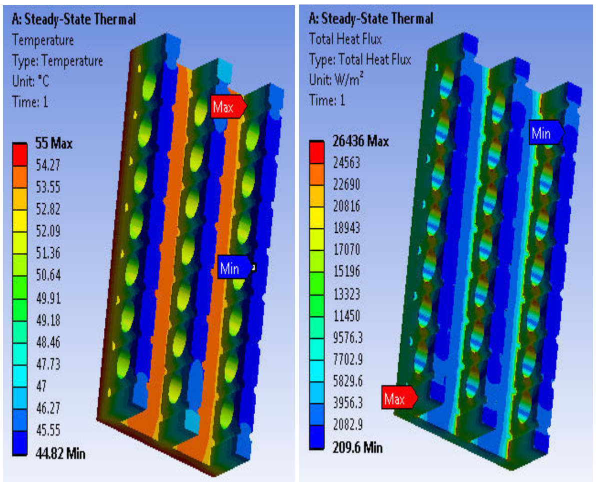

Fig 17: Temperature contour and heat flux for Model 3

Following table shows the temperature contour, maximum heat flux, minimum heat flux and rate of heat transfer for each model compared with base line model.

Table 1: Temperature variation and heat flux

S . N	Rectangular fin profiles	Temperature variations	Maximum heat flux	Minimum heat flux
1	Model 1	52.01	29906	1862.9
2	Model 2	51.42	32217	98.586
3	Model 3	45.89	22881	30.435
4	Model 4	51.88	31815	1768.9
5	Model 5	44.82	26436	209.6

Table 2: Rate of heat transfer for all models

S . N	Rectangular fin with profiles	HT w	Increase in HT W	percentage increase in HT %
1	Model 1	194.53	-	-
2	Model 2	204.3	9.77	5.02
3	Model 3	225.89	31.36	16.12
4	Model 4	234.77	40.24	20.68
5	Model 5	260.28	65.75	33.79

B. Results and discussions

The temperature distribution, maximum and minimum heat flux are recorded by analysis for fins with various perforations.

By using the heat transfer governing differential equation the rate of heat transfer is calculated for fin of finite length. The enhancement of heat transfer for fin without extension and perforation is recorded.Increase in heat transfer for fins with various perforations are compared with Base line model. The graphs are plotted for temperature distribution, max and min heat flux and rate of heat transfer for all models.

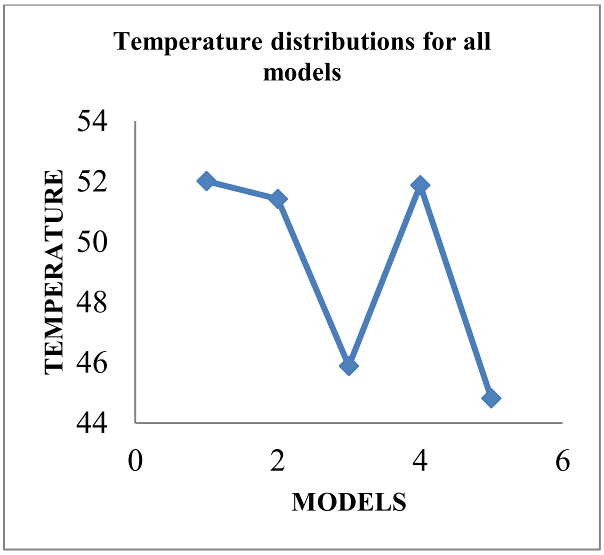

Graph 1: Temperature distributions for all models

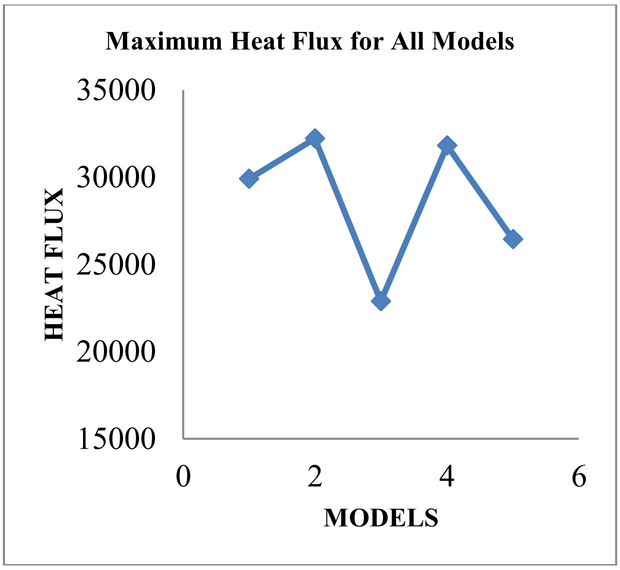

Graph 2: Maximum heat flux for all models

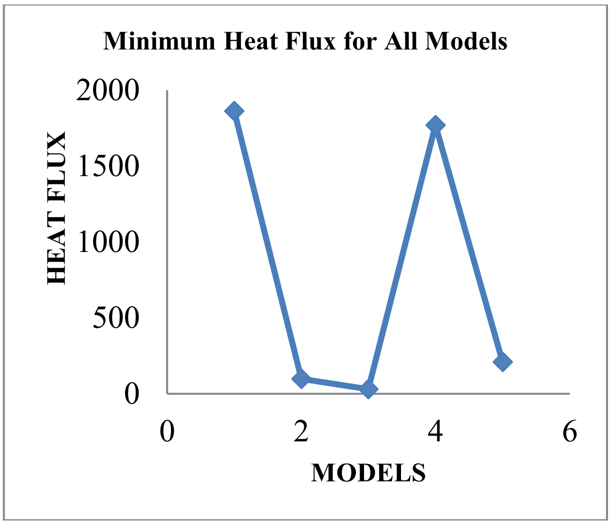

Graph 3: Minimum heat flux for all models

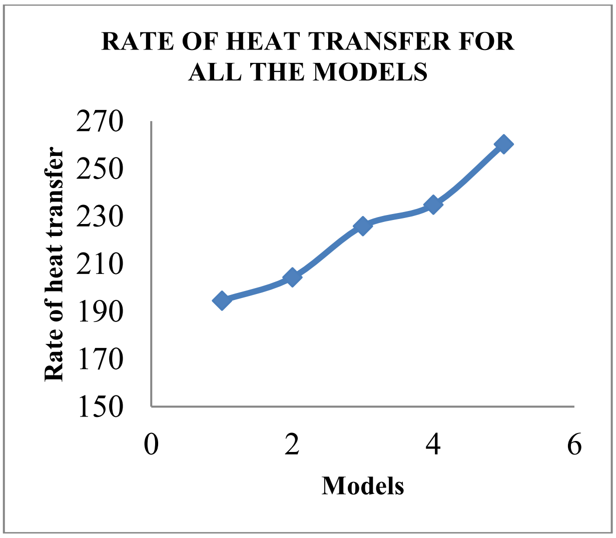

Graph 4: Rate of heat transfer for all models

6. CONCLUSIONS

- Heat transfer through Rectangular fin with 20mm perforation and 3mm cutout is higher than other type of fins when results are compared.
- Temperature at the end of rectangular fin with 20mm perforation and 3mm cutout is minimum compared to other type of fins.
- The maximum heat flux is observed for Model 2.
- The minimum heat flux is observed for Model 3.
- Rectangular fin with 3mm cutout and 20mm perforation provide 33.79% of heat transfer enhancement compared to other models.

A. Scope of future work

- Further analysis can be carried out for forced convection.
- The results may vary for forced convection heat transfer.

REFERENCES

[1] Nitish Kumar Jha, Kailash B A, 'Heat Transfer Enhancement and Thermal Performance of Extended Surfaces with Cavity'. International journal of innovative research in science,engineering and technology, volume 4, issue 10, October 2015.

[2] V. Karthikeyan, R. Suresh Babu, G. Vignesh Kumar. 'Design and Analysis of Natural Convective Heat Transfer Coefficient Comparison between Rectangular Fin Arrays with Perforated and Fin Arrays with Extension'. International journal of science, engineering and technology research (IJSETR), Volume 4, Issue 2, February 2015.

[3] Shital B. Salunkhe, Dr.RachayyaR.Arakerimath. 'CFD and Experimental Analysis of Various Extended Surfaces for Heat transfer Enhancement'. International journal of engineering technology, management and applied sciences, volume 3, issue 1, January 2015.

[4] Pardeepsingh, Harvinderlal, Baljithsinghubhi, 'Design and Analysis for Heat Transfer through Fin with Extensions'. International journal of innovative research in science, volume 3, issue 5, may 2015.

[5] MukeshDidwania, Gopal Krishnan, Ravikant, 'Study and Analysis of Heat Transfer through Two Different Shape Fins using CFD Tool'. International journal of IT, engineering and applied sciences research, volume 2, issue 4, April 2013.

I.

DESIGN, MODELING AND OPTIMIZATION OF PISTON

CHANDRASEKAR
Assistance professor
Dept. of Mechanical
Malla Reddy College of Engineering ,
Hyderabad, India.
Email ID: *chandu1439@gmail.com*
9550012358

SHASHIKANTH
Assistance professor
Dept. of Mechanical
Malla Reddy College of Engineering ,
Hyderabad, India.
Email ID: *csk262000@gmail.com*
9908618065

Abstract— In this study, A piston is a disc which reciprocates within a cylinder. It is either moved by the fluid or it moves the fluid which enters the cylinder.The piston is used in reciprocating engines, pumps and gas compressors. we have taken piston in a high pressure air compressor. piston is designed by using material Cast Iron. Piston is modeled using SOLIDWORKS software.Structural and Thermal Analysis are done on the model using two materials Cast Iron and Aluminium Alloy A360 by using COSMOSWORKS.The thickness of the barrel and thickness of the piston rings is reduced to decrease the weight of the piston.Structural and Thermal Analysis are again done on the modified model.The comparison is done for the results to decide the best material for piston.

Keywords— SOLIDWORKS;PISTON; PRO E;FEA

I. INTRODUCTION

In every engine, piston plays an important role in working and producing results. Piston forms a guide and bearing for the small end of connecting rod and also transmits the force of explosion in the cylinder, to the crank shaft through connecting rod.The piston is the single, most active and very critical component of the automotive engine. The Piston is one of the most crucial, but very much behind-the-stage parts of the engine which does the critical work of passing on the energy derived from the combustion within the combustion chamber to the crankshaft. Simply said, it carries the force of explosion of the combustion process to the crankshaft.Apart from the critical job that it does above, there are certain other functions that a piston invariably does -- It forms a sort of a seal between the combustion chambers formed within the cylinders and the crankcase. The pistons do not let the high pressure mixture from the combustion chambers over to the crankcase.

II. MATERIALS FOR MANUFACTURING PISTONS:

Aluminum alloys give light pistons and for better heat dissipation, aluminum alloys are the ideal materials due to their very high thermal conductivity. Aluminum is 3 times lighter than cast iron. Its strength is good at low temperatures but is looses about 50% of its strength at temperatures above about 320 c .Its expansion is about 2 ½ times that of cast iron and the resistance to abrasion is low at height temperatures. However these disadvantageous properties of aluminum have now been ever come by alloying it with other materials and by developing advanced designs of pistons.

The split skirt, T- sotted as well as cam ground, oval sectioned pistons made from aluminum alloys are mostly used which can be tightly fitted into the cylinder born to eliminate "piston slap". A coating of aluminum oxide or tin on aluminum alloys pistons has been found to be protective against "scuffing" or "partial seizure" during running in after overhaul.

For a cast iron piston the temperature at the centre of the piston head (Tc) is about 425c to 450c under full load conditions and the temperatures at the edges of the piston head (Tb) is about 200c to 225c.For aluminum alloy piston, Tc is about 260c to 290c and Te is about 185c to 215c.Since the aluminum alloys are aboutthree times lighter than cast iron, Therefore its mechanical strength is good at low temperatures, but they lose their strength(about 50%) at temperatures above 325c.

III. RESULTS OF FINITE ELEMENT ANALYSIS

FEA has become a solution to the task of predicting failure due to unknown stresses by showing problem areas in a material and allowing designers to see all of the theoretical stresses within. This method of product design and testing is far superior to the manufacturing costs which would accrue if each sample was actually built and tested

1.COUPLED FIELD ANALYSIS USING CAST IRON

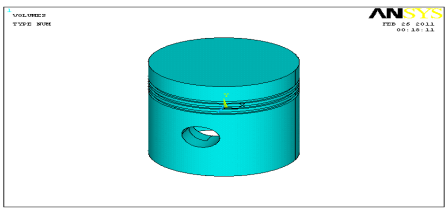

Fig. 1 IMPORTED MODEL FROM PRO/ENGINEER(CAST IRON)

THERMAL PROPERTIES

- Element Type: Solid 20 node 90
- Material Properties: Thermal Conductivity – 50w/mmk
- Specific Heat – 540J/kg k
- Density - 0.0000071kg/mm^3

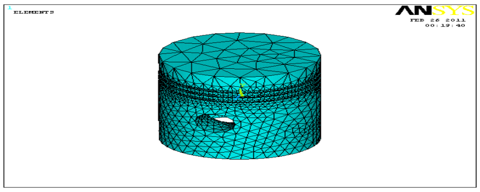

Fig 2 MESHED MODEL OF PISTON (CAST IRON)

TEMPERATURE LOADS

- Temperature – 723k
- Heat flow – 2kj/sec

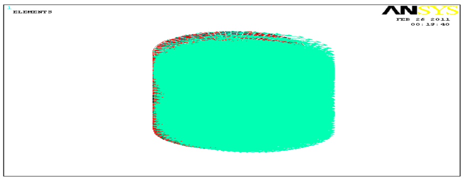

FIG 3 THERMAL LOAD APPLY ON THE PISTON HEAD

- Bulk Temperature – 570K
- Film Coefficient – 222W/mmK

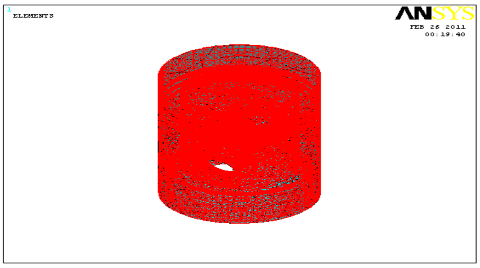

FIG. 4 BULK TEMPERATURE AND FILM CO-EFFICIENT APPLIED

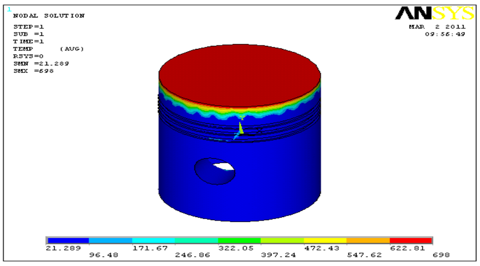

Fig 5 TEMPERATURE DISTRIBUTION

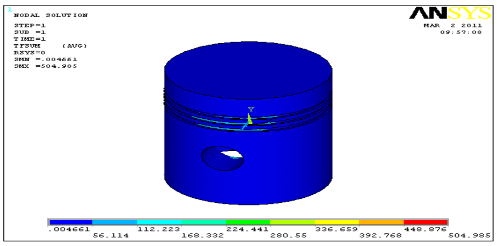

FIG : 6 NODAL SOLUTION OF THERMALFLUX

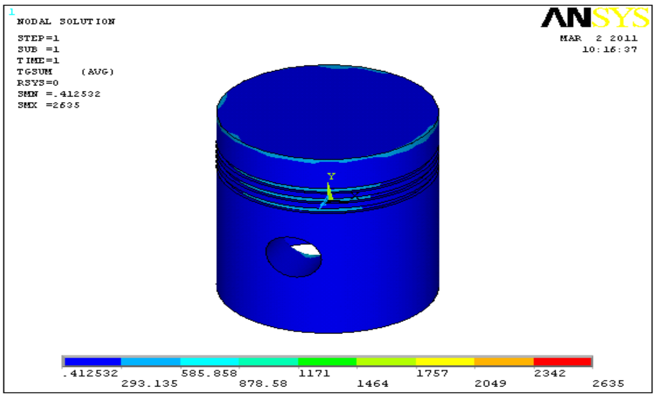

FIG 7 NODAL SOLUTION OF THERMAL GRADIENT (THERMAL STRESS)

<u>NEW ANALYSIS</u>
Structural Properties
Element Type: Solid 20 node 95
Material Properties: Density – 0.0000071kg/mm^3
Young's Modulus – 103000Mpa
Poisson's ratio - 0.211
Pressure – 15.454N/mm^2

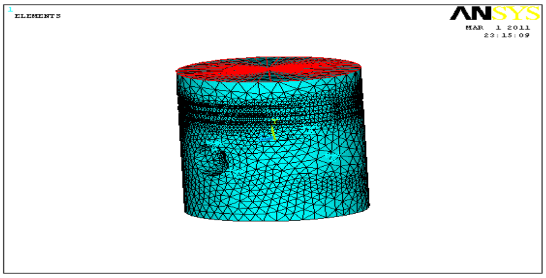

FIG 8 MATERIAL PROPOERTIES APPLIED

Post Processor

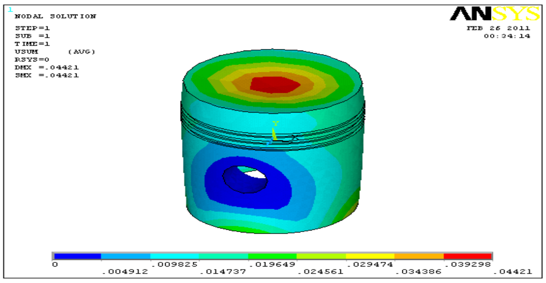

FIG 9 DISPLACEMENT ANALYSIS

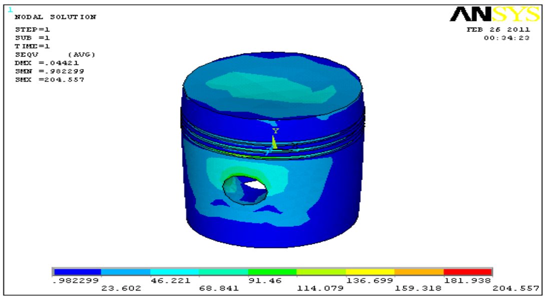

FIG 10 VON MISES STRESS DIAGRAM

2.COUPLED FIELD ANALYSIS USING ALUMINUM ALLOY A360

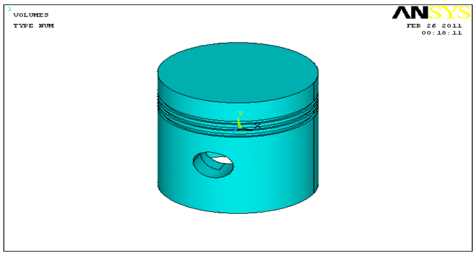

FIG 11 IMPORTED MODEL FROM PRO/ENGINEER

THERMAL PROPERTIES

Element Type: Solid 20 node 90
Material Properties: Thermal Conductivity – 113w/mmk
Specific Heat – 963J/kg k
Density - 0.0000026kg/mm^3

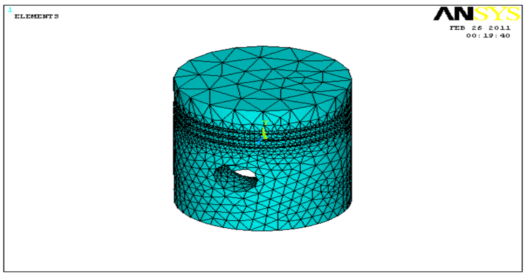

FIG 12 MESHED MODEL OF PISTON (ALUMINIUM ALLOY 360)

TEMPERATURE LOADS

Temperature – 723k
Heat flow – 2kj/sec

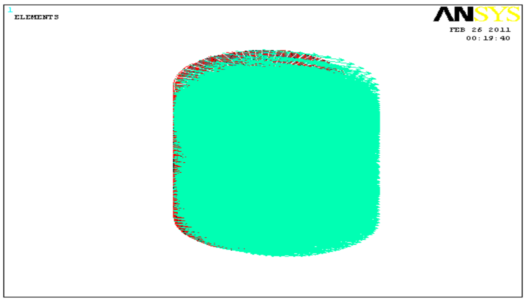

FIG 13 THERMAL LOADS APPLIED ALUMINUM ALLOY 360

Loads – define Loads – Apply – Thermal – Convection – on areas
Bulk Temperature – 570K
Film Coefficient – 222W/mmK

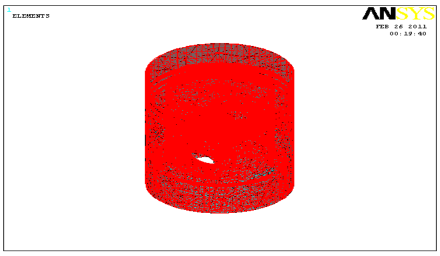

FIG 8.14 THERMAL LOADS APPLIED (BULK TEMEPERATURE FILM COEFFICENT)

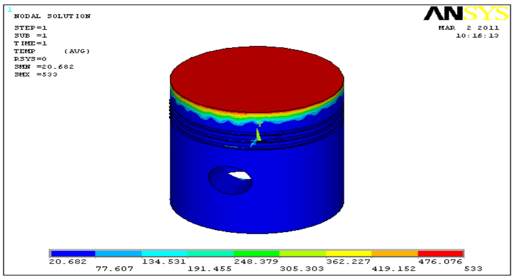

FIG 15 NODAL SOLUTION FOR NODAL TEMPERATURE FOR ALUMINUM ALLOY A360

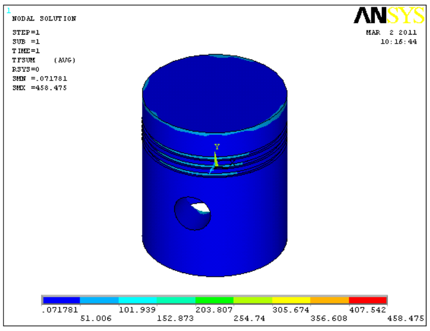

FIG 16 THERMAL FLUX DIAGRAM ALUMINUM ALLOY 360

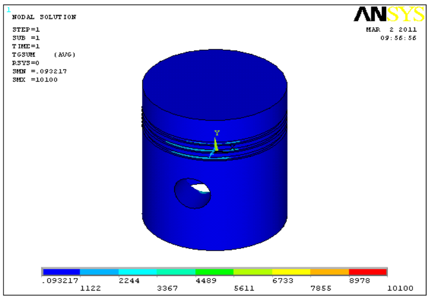

FIG 17 THERMAL GRADIENT FOR ALUMINIUM ALLOY 360

NEW ANALYSIS

Structural Properties
Element Type: Solid 20 node 95
Material Properties: Density – 0.0000026kg/mm^3
Young's Modulus – 80000Mpa
Poisson's ratio - 0.33
Pressure – 15.454N/mm^2.

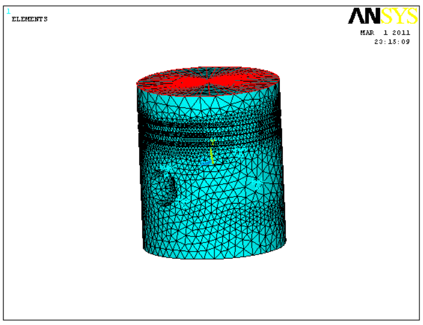

FIG 18 MATERIAL PROPERTIES APPLIED FOR ALUMINIUM ALLOY 360

POST PROCESSOR

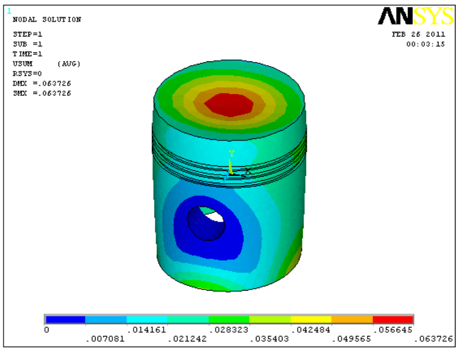

FIG 19 DISPLACEMENT DIAGRAM FOR ALUMINIUM ALLOY 360

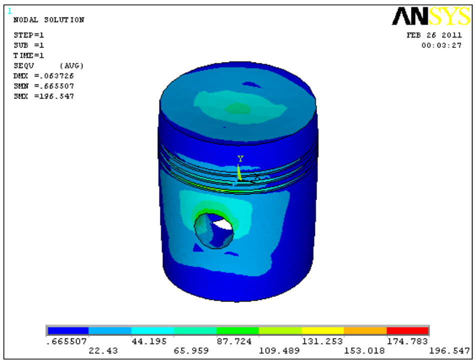

FIG 20 VON MISES STRESS DIAGRAM FOR ALUMINIUM ALLOY 360

3.COUPLED FIELD ANALYSIS USING PHOSPHOR BRONZE

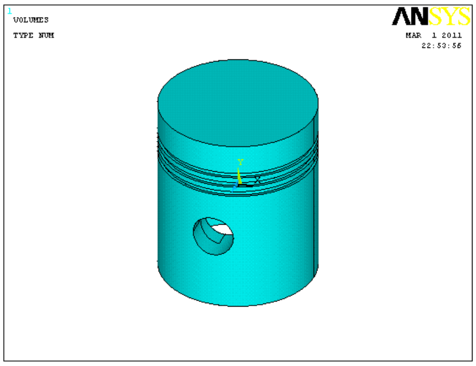

FIG 21 IMPORTED MODEL FROM PRO/ENGINEER
Thermal Properties
Element Type: Solid 20 node 90
Material Properties: Thermal Conductivity – 0.208w/mmk
Specific Heat – 45J/kg k
Density - 0.0000095kg/mm³

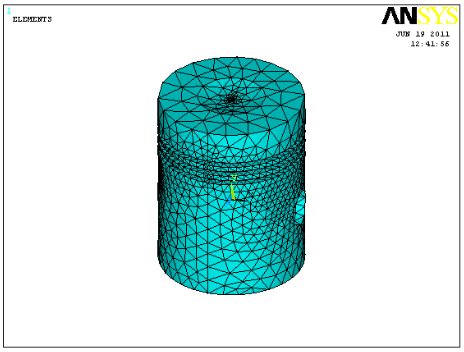

FIG 22 MESTED MODEL PHOSPHOR BRONZE
Temperature Loads
Temperature – 328k
Heat flow – 2kj/sec
Loads – define Loads – Apply – Thermal – Convection – on areas
Bulk Temperature – 1373K
Film Coefficient – 222W/mmK

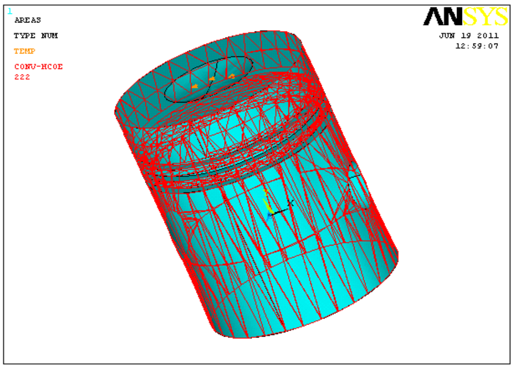

FIG 23 TEMPERATURE LOADS APPLIED ON PHOSPHOR BRONZE

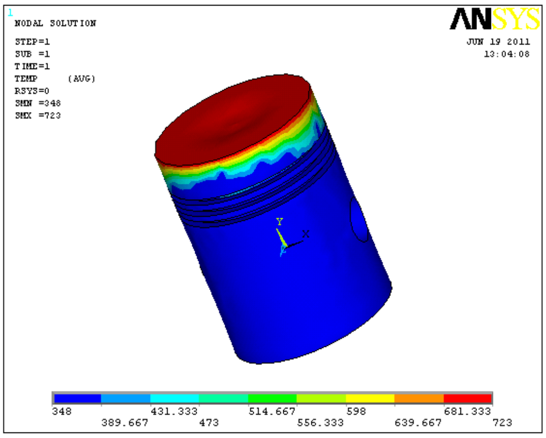

FIG 24 NODAL TEMPERATURE SOLUTION FOR PHOSPHOR BRONZE

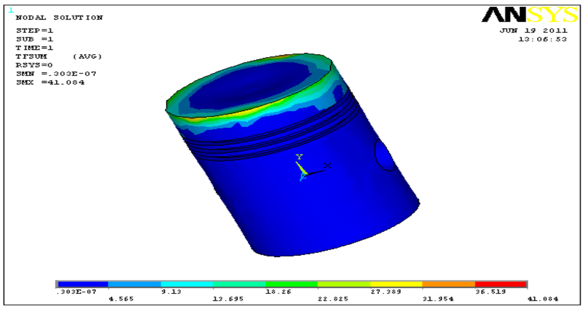

FIG 25 THERMAL FLUX SOLUTION FOR PHOSPHOR BRONZE

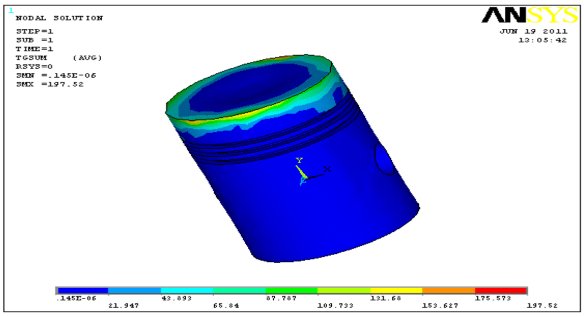

FIG 26 THERMAL GRADIENT SOLUTION FOR PHORSPHORUS BRONZE

NEW ANALYSIS

Structural Properties
Element Type: Solid 20 node 95
Material Properties: Density – 0.0000095kg/mm^3
Young's Modulus – 137000Mpa
Poisson's ratio - 0.34
Pressure – 15.454N/mm^2

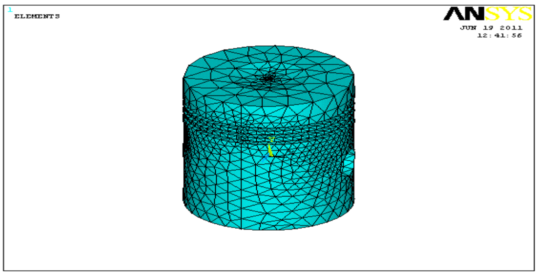

FIG 8.27 MATERIALS APPIED FOR PHORSPHORUS BRONZE

Post Processor

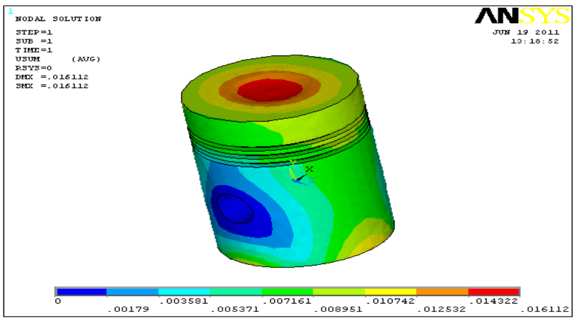

FIG 28 DISPLACEMENT DIAGRAM FOR PHOSPHOR BRONZE

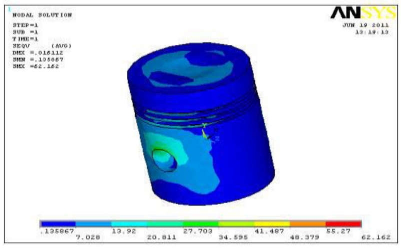

FIG 29 VON MISES STRESS FOR PHOSPHOR BRONZE

RESULTS

As per the analysis images

	Displacement (mm)	**Von Mises Stress (N/mm^2)**	**Permissible Stress (N/mm^2)**	**Nodal Temperature (K)**	**Thermal Gradient (K/mm)**	**Thermal Flux (W/mm^2)**
Cast iron	0.4421	204.557	520	698	2635	504.985
Aluminum Alloy A360	0.063726	196.547	165	533	10100	458.475
Phosphor Bronze	0.016122	62.162	793	344.605	197.52	41.084

IV. CONCLUSION

- In our project we have designed a piston 150cc petrol engine using theoretical calculations for material Aluminum Alloy A360. A 2D drawing is drafted and 3D modeling of piston is done in Pro/Engineer.
- We have done coupled field analysis (i.e) structural + thermal on piston to validate the strength of our designed model. Analysis is done using three different materials Cast Iron, Aluminum Alloy A360 and Phosphor Bronze.
- By observing the analysis result, the obtained stress values are less than their respective permissible stress values. So we can say that our design is safe under working conditions.
- When comparing the stress values for all the three materials, it is less for Aluminum Alloy A360 and Phosphor Bronze.
- When comparing the thermal property thermal gradient for all the materials, it is more for Aluminum Alloy A360 (i.e) rate of change of temperature is more.
- So from the above data, we conclude that for our designed piston Aluminum Alloy A360 is best.

V. REFERENCES

1. A.Atish Gawale, A. Shaikh and Vinay Patil, "Nonlinear Static Finite Element Analysis and Optimization of connecting rod World Journal of Science and Technology, Vol. 2(4), pp .01-04, 2012.
2. A. R. Bhagat, Y. M. Jibhakate, Thermal Analysis and Optimization of I.C. Engine Piston Using Finite Element Method, International Journal of Modern Engineering Research (IJMER), Vol.2, Issue.4, pp.2919-2921, 2012.
3. R.S.Khurmi,J.K.Gupta, A Text Book of Machine Design, S.Chand & Co., pp. 1132- 1144, 2004.
4. P. Carvalheira1, and P. Gonçalves, FEA of Two Engine Pistons Made of Aluminium Cast Alloy A390 and Ductile Iron 65-45-12 Under Service Conditions, 5th International Conference on Mechanics and Materials in Design Porto-Portugal, 24- 26, pp .1-21, 2006.
5. Gudimetal P. Gopinath C.V. Finite Element Analysis of Reverse Engineered Internal Combustion Engine Piston, King Mongkut's University of Technology North Bangkok Press, Bangkok, Thailand AIJSTPME, Vol. 2(4), pp 85-92, 2009.
6. Mirosáaw Wendeker, Paweá Magryta Adam Majczak, Michaá Biaáy, "Modeling The Thermal Loads in the Subaru EJ25 Engine" Journal of KONES Powertrain and Transport, Vol. 18, No. 1, pp. 683-688, 2011.
7. D.Janko , Jovanovi," Finite Element Evaluation and Optimization of Geometry with DOE", International Journal for Quality research UDK- 005. Vol.5, No. 1, pp. 39-45, 2011.

ESTIMATION OF SOME BIOMASS SPECIES AND THIER PROPERTIES FOR POWER GENERATION POTENTIALS

B. S. Sai Deepika
Assistant professor
Department of Mechanical Engineering
Email ID: suryabogaram14@gmail.com

M. Suresh Babu
Assistant professor
Department of Mechanical Engineering
Email ID: suresh4you247@gmail.com

ABSTRACT

India is an energy needing country. India has most of the energy resources but limited. Now a days, energy demand leads to use of conventional energy resources (i.e. fossil fuels, such as hard coal, lignite, oil and natural gas) which cause critical environmental problems like global warming due to increase in greenhouse gases which can bring drastic change in environment. Renewable energy sources release less pollution to atmosphere. So If the country wants to meet its energy demand and to be less dependent on importing energy and to minimize greenhouse gas effect and to keep environment safe then it should use renewable energy sources. Rapidly increase in energy demand and world pollution due to use of conventional fuel, scientists looked for alternatives as renewable energy sources. Among all the renewable energy sources, biomass considered as an important source of power production due to its wide availability, lower ash content and low Cox, SOx and NOx emission to the atmosphere. In this article, five different portion(leaf, new branch, main branch, bark and root) were taken from residues of two different woody biomass species and three fruit husk/peel of which don't have any commercial use. These species are Vachellia nilotica(local name- Babool), Azadirachta indica(local name- Neem), Musa acuminata(local name- Banana), Cocos nucifera (local name- coconut) and Arachis hypogaea(local name- Groundnut). Proximate analyses and gross calorific values (GCV) of all the biomass sample were determined. Among all the biomass species studied, the fixed carbon content (FC) in Coconut husk was found to be the highest (i.e. 25wt.%) while Neem leaf has the lowest value(i.e. 11wt%), the volatile matter content (VM) in main branches of Neem is the highest(i.e. 74wt.%) While Groundnut husk has the lowest (i.e. 57wt.%) among all studied biomass samples. The ash content (A) in Neem root is the highest (i.e. 17wt.%) while Babool main branch has the lowest ash content (i.e. 1wt.%). Among all thirteen biomass species studied, husk of Coconut and bark and new branches of Neem are found to be high in moisture content (i.e. 11wt.%) while bark of Babool is found to be the lowest (i.e. 7wt.%).

Similarly, the Babool leaf is the most favorable one with the highest calorific value followed by its root. Next in the order, the bark of Neem and Babool were also found to have considerably high amount of energy contents suitable for power generation. In addition, bulk densities of all the biomass species have been determined. Leaves of Neem and Babool biomass species have been found to have lower bulk densities while bark has higher bulk densities as compared to their other components. It is worthy to note that among all the studied biomass species, bark of babool has highest (i.e. 443 Kg/m3) bulk density followed by banana

peel (i.e. 422 Kg/m3) while husk of Coconut has lowest bulk density(i.e. 163 Kg/m3) followed by husk of Groundnut(i.e. 262 Kg/m3). Ash fusion temperature plays a vital role in Ash related problems such

as slagging and fouling in different kinds of combustion,corrosion problems, in bed-agglomeration and potential problems they may cause in a boiler when the fuel is fired. Further, the ash fusion temperatures of some selected biomass (Neem root, babool leaf and coconut husk) have been measured as these temperatures are the influential factors for the determination of bed agglomeration and other boiler fouling related problems.

It has been found that Initial Deformation Temperature (IDT) varies from 995 to 1178℃, softening temperature (ST) varies from 1132 ℃ to 1218 ℃ and hemispherical temperature (HT) varies from 1161 ℃ to 1253 ℃ which is suitable for safe boiler operation. The ultimate analysis has also been carried out on some selected biomass samples of Neem bark, Babool leaf and Husk of coconut. It has been found that Carbon and Hydrogen present in babool leaf and neem bark are higher compared to husk of coconut and have higher calorific value as compared to other selected samples. It is observed that around 80.868 and 154.236 hectares of land area are required for energy plantation considering Neem and Babool biomass species and respectively. It is also found that the husk of Groundnut, Coconut, and Banana peel are needed approximately 58.795, 100.95 and 407.23 hectares of land to generate that much of electricity per year. Approximately 7234.532, 6811.524, 7349.375, 7228.739, and 6732.355 tonnes of Neem, Babool, Groundnut Husk, Banana peel and Coconut husk biomass respectively was calculated to provide same amount of energy per year.

Key words: Volatile matter; Ash content; Calorific value; Ash fusion temperature; Bulk density; decentralized power generation.

INTRODUCTION

Currently Increase in energy demand is a big problem. Fossil fuels can meet the energy demand, but these are limited in reserve and costly. Fossil fuels emit a higher quantity of pollutants to the environment which leads to increase in greenhouse gasses and considered as the main cause of drastic change in climatic condition. The continuous decrease in reserve of world fossil fuel has given a challenge to the scientists for the invention of a promising energy source that can take the place of conventional fuel. Renewable energies became the most attractive options for power generations because of theses are capable of meeting the world energy demand and environment-friendly. Biomass becomes effective as it is cheap and widely available, carbon neutral and emits very less amount of pollutant to the environment.

Over last few decades the Indian economy has shown continuous growth. Today, India is the ninth largest economy in the world, driven by a real GDP growth of 8.7% in the last five years (7.5% over the past ten years).In 2010, India placed at 5th position in world GDP (gross domestic product) growth. As of March 2012, the per capita total consumption in India was estimated to be 879 kWh. As per the 2011 Census, 55.3% rural households had access to electricity. However, NSS results show that in the year 1993-94, 62% households in rural India were using kerosene as the primary source of energy for lighting. After the US, China, and Russia the fourth largest user of natural gas is India. [1].As conventional fuels are limited and emit maximum amount of greenhouse gasses to the atmosphere, it should be minimized or replaced by other energy sources for minimization of pollution. In India, more than 65% of the electricity is produced from coal-fired power plants. With limited availability of coal, the future energy demand may suffer. So for the security of future energy supply, the alternate power source is essential.

Biomass became a most attractive option for energy demand due to its advantages. It is widely available and carbon neutral and releases very less pollutants. Fossil fuels release more amounts of Cox, SOx and NOx to the atmosphere which is the main cause of global warming lead to drastic climate change. Application in biomass in generating energy can solve the problems related climatic condition, energy emergency and waste land development. Biomass can be the most promising energy source due to its wide availability. The geographical area of 21.23% of the country covered by forest. Around three crore hectares of waste land can be utilized by forestation in India which is a big advantage [2]. As per the 2011 Census, almost 85% of rural households were dependent on traditional biomass fuels for their cooking energy requirements. As on 31.03.2013 and 30.03.2014 the total biomass power generated in India were 3601.03MW and 4013.55MW. The total energy production from conventional sources decreased from 13409.47 Peta joules during 2012-13 to 13400.15 Peta joules during 2013-14 [3].

Currently, biomass playing an important role to meet the world energy demand. Continuous increase in energy demand and world pollution and limited status of conventional fuel has shown a symbol of interest within scientists for research on biomass species. Different biomass species have different properties which properties can be considered for the design of the power plant and also influence its efficiency.

For getting maximum benefits at low cost, it is important to know the different properties of the chemical composition, energy values, bulk densities, ash fusion temperatures, combustion reactivity, etc. The present thesis describes the studies on some selected biomass species. The study includes proximate analysis, ultimate analysis, and evaluation of calorific values, bulk densities, and ash fusion temperatures of different residual components of some biomass samples. These species are Vachellia nilotica(local name- Babool), Azadirachtaindica(local name- Neem), Musa acuminata(local name- banana), Cocosnucifera (local name- coconut) and Arachishypogaea(local name- groundnut). Some experiments were conducted on these biomass samples and their effect on power generation is discussed.

EXPERIMENTAL WORK

Materials Selection

For the present project work, five different components (leaf, new branch, main branch, bark, and root) were taken from residues of two separate woody plant species and fruit husk/peel of three biomass were taken from local areas which have no commercial use. These plant species are Vachellia nilotica(local name- Babool), Azadirachta indica(local name- Neem), Musa acuminata(local name- banana), Cocos nucifera (local name- coconut) and Arachis hypogaea(local name- groundnut). Considering all the components of selected biomass samples total of thirteen numbers of samples were taken for proximate analysis and calorific value determination. By keeping these samples in a cross-ventilated room for 20-30 days, the equilibrium in moisture contents of these components was attained. Before experimental work air, dried samples were grinded into powder. Three selected woody biomass samples namely

Neem bark, Babool Leaf and Coconut husk were considered for ultimate analysis.

Proximate Analysis of Studied Biomass Samples

Proximate analysis is deemed for characterizing biomass and coal samples. The quantitative analysis of the distribution of constituent products obtained when the sample is heated under designated conditions is called proximate analysis. As per ASTM D121 [51], proximate analysis separates the constituents into four categories: a) Moisture, b) Ash, c) volatile matter and d) fixed carbon.

Moisture Content Determination

The quantity of water present in the sample expressed in weight percentage (Wt.%) of the sample is moisture content of fuel. This is expressed regarding dry basis or wet basis. In the case of dry basis, only ash and ash free matter is considered, but the aggregate water, ash, and ash free matter content are considered in wet basis. It is crucial to mention the basis on which moisture is determined because moisture plays a vital role in differentiating biomass fuel.

The selected biomass sample was grinded into powder and by using a –72 mesh sieve, required –72 mesh size biomass materials were collected. A –72 mesh size sieve describes 72 holes per square inch, and the negative sign indicates passing of biomass powder particles through the holes. As per BIS 1350 [53], one gram of –72 mesh size air dried biomass sample powders were taken in borosil glass discs and heated for one hour in the furnace at a temperature of 100 ℃. After the designated time, the borosil glass discs were taken out of the oven, and the samples were weighed by electronic balance. By using the expression given below, the percentage losses in weights were calculated.

Percentage moisture content (%) = (Weight of residue obtained × 100) / Initial wt. Of sample

Ash Content Determination

Ash is the inorganic residue left after the complete burning of the biomass. It is a vital constituent present in biomass which largely affects ash fusion characteristics. Ash contains calcium, ferrous carbonate, magnesium and phosphorus, sand with clay, etc. which influence the boiler properties at a high temperature of combustion and gasification. Ash content affect the design of boiler. If the fuel comprises greater quantity of ash, then it can cause severe problems like Slagging, fouling and clogged ash removal problem associated with boilers.

Fig. 3.1: Muffle Furnace

One gram of each –72 mesh size samples was air dried and then were taken in shallow silica disc and put in a muffle furnace which is shown in Fig. 3.1. The temperature inside muffle furnace was maintained at 775- 800 ºC. The muffle furnace used for this experiment have a measuring range of temperature 0-1000 ºC with a resolution of 1 ºC and accuracy of ±5 ºC . The biomass samples were kept in maintained temperature in the muffle furnace and heated till their complete combustion usually half an hour. Then the residues obtained were measured with the help of electronic balance for each sample and expressed in a percentage similar to moisture content .

Volatile Matter Determination

The portion of the fuel that will volatilize rapidly when it is burnt at a high temperature under a particular condition is called volatile matter. When the fuel has low volatile matter by heating char formation occurs, but fuels have high volatile mass produce volatile gasses by heating. Biomass has high volatile matter content that may up to 80%, unlike coal which has very low percentage of volatile matter below 20%. Volatile matter consists of methane, hydrogen, carbon monoxide, ammonia, tar, etc. excluding moisture as residual moisture has not taken into account .

Cylindrical silica crucibles covered with the close-fitting silica lid were pre-weighted and each biomass sample of one gram of –72 mesh size powder was taken in the crucible. Then the crucibles were heated in a muffle furnace at temperature 925±10 ºC for exactly seven minutes. Then the crucibles were taken out from the furnace and air cooled. Then the weight of samples was measured with the help of electronic balance as soon as possible, and the percentage of weight loss was determined [53]. The following formula is used for calculating the weight percentage of volatile matter in dry basis.

Volatile Matter (wt.%) = % loss in weight(wt.%) – moisture content (wt.%)

Calculation of Fixed Carbon Content

The value of fixed carbon content can be calculated by subtracting the aggregate percentages of moisture, volatile matter and ash from 100. Fixed carbon content is the quantity of solid carbon residue that remains after the combustion of the sample with the removal of volatile matter. The value of fixed carbon content helps for evaluating the productivity of biomass fuel. At lower combustion temperature it improves the reactivity of fuel [53].

Fixed Carbon Content (wt.%, dry basis) =100 – {Moisture + Volatile matter + Ash} (wt %, drybasis)

Calorific Value Determination

Calorific value or energy value of any fuel may be the quantity of heat energy obtained by complete combustion of a specified quantity of fuel in the presence of oxygen. It is an important property of any fuel and influences design and controlling of the power plant which is expressed in terms of kcal/kg or MJ/kg. It is evaluated by the help of a calorimeter. Based on the effect of water vapour on energy value, calorific value is classified into two types.

a) Gross calorific value (GCV) or Higher heating value (HHV)

b) Net calorific value (NCV) or Lower heating value (LHV)

The GCV considers the latent heat of vaporization of water which is the quantity of heat generated by combustion when the water vapour produced during combustion is allowed to return to the liquid state under standard condition of temperature and pressure. When the water vapour produced during combustion remains gaseous and doesn't return to liquid state, the quantity of heat generated is called Net calorific value (NCV). Here, the condensation of water is not taken into account. Calculation of energy value is calculated using an adiabatic calorimeter.

In the present project, the gross calorific value or higher heating values of some biomass species were determined with the help of Oxygen Bomb Calorimeter, which is capable of calculating the GCV of any solid fuel [53]. This oxygen bomb calorimeter used in the present have a temperature scale resolution of 0.01 ºC and an accuracy of ±0.02 ºC. The measuring range is 0-10 ºC. First, briquetting device is used to produce briquettes of each biomass samples, and briquettes were taken in a nichrome crucible. A cotton thread of 10-15 cm long was positioned over the sample in the crucible for facilitating ignition. A fuse wire is connected between two electrodes of the crucible, and the cotton wire is suspended by using the fuse wire as shown in the Fig. 3.2. Before conducting the experiment Oxygen gas was poured into the oxygen bomb calorimeter up to a pressure 25 to 30 atm and the bucket of calorimeter were filled with two liters of water and were stirred continuously by the help of a motor and stirring mechanism maintain a uniform temperature. Then after switching on the current, the ignition of the sample was started, and the temperature of the water was recorded by thermometer attached to it. Then from the reading, the rise in temperature was calculated. With the help of rising in temperature (ΔT), water equivalent of apparatus (W.E) in cal/ºC, initial weight of the sample (w) in gram, the GCV can be calculated by the following empirical formula.

Gross calorific value = {(W.E. × ΔT) / (w) – (heat released by cotton thread +heat released by fusedwire)}

Bulk Density Determination

The bulk density of fuel gives an idea about the weight of that fuel to be provided sufficiently in a given volume of the boiler. It influences the transportation and storage costs largely. The combustion devices also largely influenced by bulk density. Higher, the bulk density lesser, will be the transportation cost. It is expressed as the weight per unit volume of material, expressed in kg/cubic meter.

The bulk densities of the biomass samples were calculated according to the ASTM E873-82 standard [57]. Each biomass sample of -72 mesh size powder was taken in a cubic container of dimension 65mm × 65 mm × 65 mm made of mild steel. Each sample was fully packed in the container and leveled at the top surface. The weight of the samples filled in the container was measured with the help of electronic balance of sensitivity 0.01gm. Then bulk density was calculated by the weight obtained from electronic balance and initially measured dimension of the container.

Bulk Density = Wt. of the sample packed in container (kg)/Volume of the container (cubic

Ash Fusion Temperature Determination

Ash fusion temperature plays a significant role in selection of fuel because at high-temperature fuel ash creates slag better known as clinker. That can pose a mechanical problem in combustion process associated with the boiler which largely influences boiler design and efficiency. Deposition of ash at high-temperature region causes slagging and fouling problems in the boiler. Hence, ash fusion temperature determination plays a crucial role in the selection of fuel which includes i) initial deformation temperature (IDT), ii) softening temperature (ST), iii) hemispherical temperature (HT) and iv) fluid temperature (FT). IDT is the temperature, at which first change in shape occurs and the temperature at which the sample starts shrinking and the corners of the sample melt is called ST and the temperature at which the cubical sample becomes hemispherical in shape is called HT and the temperature at which the sample melts and lays flat is called FT.

The ash fusion temperatures of biomass ashes were calculated according to DIN: 51730 [58]. Ashes of some selected biomass samples were taken and crushed and by mixing one drop of distil water 3mm sizes of cubic shaped sample are prepared for ash fusion test. Then the sample was put inside Leitz heating microscope which is shown in Fig.3.3. The rise in temperature was maintained at 8ºC/min, and the current was maintained at 25Amp and heated up to a maximum temperature of 1450 ºC with an accuracy of ±5 ºC and resolution of 1ºC. The external shape of the cubes was observed, and the temperatures were noted during the deformation, shrinkage of cubic samples.

3.6 Ultimate Analysis: Determination of Chemical Composition

Ultimate analysis gives complete results as compared to proximate analysis. It is capable of calculating some valuable ash free organic components like carbon, oxygen, hydrogen, nitrogen, etc. and is carried out by an elemental analyzer. In general practice, 200 mg of each sample were heated at 900 ºC in the presence of oxygen. Carbon has transformed into CO_2, hydrogen into H_2O, sulphur into SO_2 and nitrogen into N_2 during the experiment. By using an infra red detector the quantity of Carbon, hydrogen and sulphur were calculated and by using a thermal conductivity detector quantity of N_2 is determined [55]. In the present work, CHN analysis was carried out for some of the selected biomass samples at Sophisticated Analytical Instrumentation Facility, Punjab University, Chandigarh, India.

RESULTS AND DISCUSSION

Fig 4.1 shows the moisture content, ash content, volatile matter and fixed carbon content of different components of selected biomass samples from proximate analysis.

From the table 4.1, it is found that the moisture content of Neem bark and new branch are highest (i.e., 11Wt. %) followed by groundnut husk (i.e., 10Wt. %) among all other selected samples. Babool bark has lowest (i.e., 7Wt. %) moisture content. The moisture content of various components of Neem and Babool samples are compared in Fig. 4.1 below.

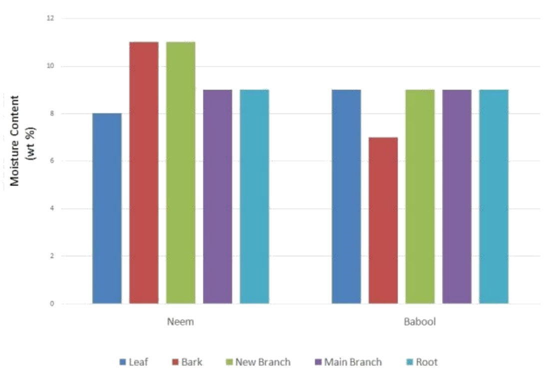

Fig. 4.1: Comparison of Moisture Content in Neem and Babool Samples.

Very high ash content is obtained in the case of Neem root (i.e., 17 Wt. %) followed by babool leaf (i.e., 11 Wt. %). The main branches of Babool are found to be lowest (i.e., 1 Wt. %). The ash content in different Neem and Babool samples are compared in the chart given below.

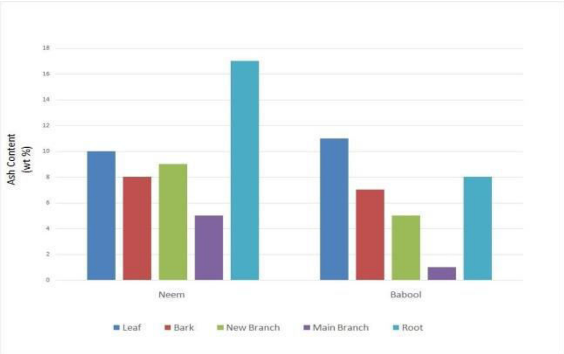

Fig. 4.2: Comparison of Ash Content in Neem and Babool Samples.

From all components of selected biomass samples the fixed carbon content is found to be highest in Coconut husk (i.e., 25 Wt. %) followed by Neem bark (i.e., 23 Wt. %). And fixed carbon content found lowest in case of leaves of Neem (i.e., 11 Wt. %). The fixed carbon content in Barks of Neem and Babool are found to be higher as compared to its other components. Also, the outer covers of Coconut, Groundnut, and Banana fruit shows comparatively higher fixed carbon content. Fixed carbon content in Neem and Biomass sample are compared in the chart in fig. 4.3.

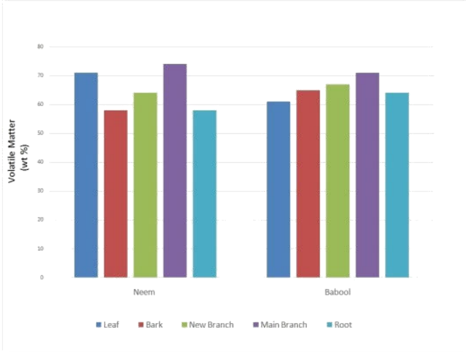

Fig. 4.3: Comparison of Fixed Carbon content in Neem and Babool Biomass samples

The table 4.1 shows that the branches have comparatively higher volatile matter than other components. Also, bark contains comparatively low volatile matter. Volatile matter is found to be highest in main branches of Neem (i.e., 74 Wt. %) followed by its leaves and the main branch of Babool and the husk of Groundnut has the lowest value of volatile matter (i.e., 57 Wt. %). A comparison of Volatile Matter Content in Neem and Biomass samples is shown in Fig. 4.4 below.

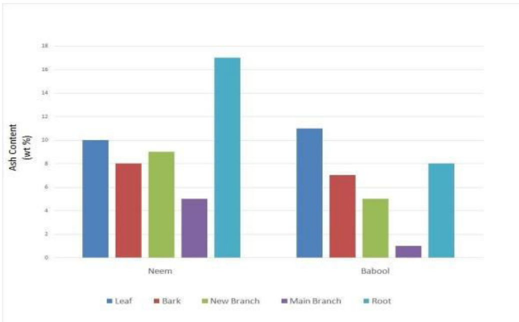

Fig. 4.4: Comparison of Volatile Matter Content in Neem and Babool Biomass samples

CONCLUSIONS

The following conclusions may be drawn from the results obtained from the present project work:

i. The root of Neem was found to have the highest ash content (17 wt.%) while main branches of Babool were found to be the lowest value (1 wt.%). Both the main branches of Neem and the new branches of Babool were also found to be lower (5 wt.%) in ash content followed by branches of Babool. Hence, these biomass species with lower ash content can be efficient for boiler operation.

ii. The volatile matter in the branches of Neem was found to be highest (74 wt.%) followed by both leaves of Neem and main branches of Babool(71 wt.%). The husk of Groundnut was found to be the lowest (57 wt.%) in volatile matter content.

iii. Out of all the tested biomass samples, Coconut husk has been found to have the highest (25 wt.%) fixed carbon content followed by Neem bark (23 wt.%).

iv. The energy value of Babool leaf is found to be highest followed by its root among all the selected biomass species. The energy value obtained in the case of all components of Babool biomass species is comparatively higher than the components of Neem biomass samples.

v. The bulk density of the bark of Babool biomass is found to be highest followed by Banana peel. So, a higher quantity of material or biomass fuel can be accommodated in a given volume of the reactor.

vi. The IDT and ST of all selected biomass samples were found to be much higher than the boiler operation temperature. The leaves of Neem biomass is expected to offer less ash-related problems in the boiler due to its highest IDT and ST.

vii. The calculation for the generation of 7300 MW of electricity indicated the 7234.532, 6811.524, 7349.375, 7228.739, and 6732.355 tonnes of Neem, Babool, Groundnut Husk, Banana peel and Coconut husk biomass required respectively. And 80.868, 154.236, 58.795, 407.23 and 100.95 hectare of land is required for Neem, Babool, Groundnut Husk, Banana peel and Coconut husk biomass respectively for the production of same 7300 MW of electricity. From the analysis of the present results, Coconut husk appears to be the best biomass for utilization in power generation.

References

[1] Energy Statistics (2013)., Ministry of Statistics and Programme Implementation, http://mospi.nic.in/mospi_new/upload/Energy_Statistics_2013.pdf.

[2] India State Forest Report (2013), Forest Survey of India, http://fsi.nic.in/cover_2013/sfr_forest_cover.pdf.

[3] Executive Summary (2011), International Energy Agency, http://www.iea.org/Textbase/npsum/solar2011SUM.pdf.

[4] Glassley, William E. (2010). Geothermal Energy: Renewable Energy and the Environment, CRC Press, ISBN 9781420075700.

[5] Co-firing of Biomass Residues for Electricity Generation in Grid Connected Power Plants (2009), CDM Executive Board, http://cdm.unfccc.int/EB/051/eb51_repan05.pdf.

[6] Key World Energy Statistics 2015 - International Energy Agency https://www.iea.org/publications/freepubli

cations/publication/KeyWorld_Statistics_2015.pdf
[7] Gluskoter, H., Increase in fossil fuel utilization in 21stCentury,USGS
[8] Walsh,J.H., resources and environment in the 21st Century: seeing past the phantoms: world energy council journal,july 1998.
[9] Ivanhoe, L.F., future world oil supplies,there is a finite limit, from world oil,1995.
[10] world fossil fuel reservesand projected depletion http://crc.nv.gov/docs/world%20fossil%20reserves.pdf
[11] Renewables 2014 Global Status Report - REN21 www.ren21.net/Portals/0/documents/.../2014/GSR2014_full%20report_low%20res.pdf
[12] Renewable 2013 - Global Status Report (2013), Renewable Energy Policy Network for the 21st Century, http://www.ren21.net/portals/0/documents/resources/gsr/2013/gsr2013_lowres.pdf.
[13] Annual Energy Outlook (2014), Energy Information Administration, http://www.eia.gov/forecasts/aeo/pdf/0383(2014).pdf.
[14] Energy statistics (2014), Ministry of Statistics and Programme Implementation, http://mospi.nic.in/mospi_new/upload/Energy_stats_2014.pdf.
[15] Annual Report (2014), Ministry of New and Renewable Energy, http://mnre.gov.in/file manager/annual-report/2013-2014/EN/overview.html.
[16] What is Woody Biomass? - Forest Bioenergy www.forestbioenergy.net/training.../fact.../fact-sheet-1-1-what-is-woody-biomass/
[17] Demirbas A. (2000), Biomass Resources for Energy and Chemical Industry, Energy Education Science & Technology, 5: pp. 21-45.
[18] AraKirakosyan and Peter B. Kaufman (2009-08-15). Recent Advances in Plant Biotechnology. p.169. ISBN 9781441901934. Retrieved 14 February 2013
[19] Kurchania A. K. (2014), Biomass Energy. In: Bashkar C., Bashkar S. and Dhillon R. S., Editors. Biomass Conversion, Berlin Heidelberg, Springer
[20] Demirbas A. (1998), Yields of Oil Products from Thermo-Chemical Biomass Conversion Processes, Energy Conversion Management
[21] Development benefits of clean energy in India: Biomass gasification prospects in India, (2007),. The William and Flora Hewlett Foundation, http://www.whrc.org/policy/pdf./cop13/hewlett-Report-FINAL.pdf.
[22] EPA Combined Heat and Power Partnership (2002),. United States Environmental Protection agency, .,http://www.epa.gov/chp/documents/biomass_chp_catalog_part5.pdf.
[23] Federal Technology Alert - A New Technology Demonstration Publication (2004), National Renewable Energy Laboratory, http://www.nrel.gov/docs/fy04osti/33811.pdf.
[24] Kurchania A. K., Panwar N. L.,and Pagar S. D.,(2010), Design and Performance Evaluation of Biogas Stove for Community Cooking Application, Sustainable Energy, 29(2):, pp. 116-123.,
[25] Biomass Co-firing (2013), IEA-ETSAP and IRENA Technology Brief E21, http://www.irena.org/DocumentDownloads/Publications/IRENA ETSAP%20Tech%20Brief%20E21%20Biomass%20Co-firing.pdf.
[26] World Energy Outlook (2011), International Energy Agency, http://www.iea.org/publications/freepublications/publication/weo2011_web.pdf.

DESIGN AND OPTIMIZATION OF SHELL AND TUBE HEAT EXCHANGER

N.Sneha
Mechanical dept.
Malla Reddy College of Engineering , Hyderabad, India.
snehadvr@gmail.com

N.Siddappa
Mechanical dept,
MallaReddy College of Engineering,Hyderabad,India
Siddappanyamagoud@gmail.com

Dr.P.Velmurugan
Mechanical dept.
MallaReddy College of Engineering,Hyderabad,India
Velmurugan_mech@mrce.in

***Abstract*—In the pre-sents, the most regular type of heat exchangers used extensively in oil refineries and large scale chemical processing industries are the Shell and Tube Heat Exchangers due to its nature of suitability for applications of high pressure. There lies an internal component in the exchangers that supports the tubes to attain rigidness in structure, to attain higher heat transfer coefficient, direct the flow across the tube bundles and prevent vibrations are the Baffles. The centre line distance between adjacent two Baffles is called Baffle Spacing (B).The segmental height to shell inside diameter, which is expressed in terms of percentage and provided on Baffles is called Baffle Cut(Bc). The variation of baffle cut ranges from 15% to 45% of shell inside diameter. To attain the better performances , researches showing their interests towards work on helical baffles than the single segmental baffle but it raises a problem in manufacturing costs, maintenance and set up costs. In heat exchanger design, mostly we focus on two important parameters such as cost and efficiency. So, for the development of thermal performance at low costs using shell and tube heat exchanger, the study is focused in providing some inclination over baffles to attain a reasonable pressure drop across the heat exchanger.**

The project, deals with initially Simulation which consists of modeling followed by meshing the heat exchanger design of basic geometry by adopting a software known as CFD package ANSYS 14.0. The main moto of the project is to develop a design of shell and tube heat exchanger consisting of baffles with various helix angles .Later we examine the intensity of flow and temperature field also determined within the shell at various points using ANSYS Software tools. The variation of helix angle over baffles ranges between 0 °to 20 °.The final reproduction will display how the variation taken place with respect to pressure flow velocity and temperature distribution in the shell due to provision of different helix angle . The pattern of flow in the shell side of heat exchanger with continuous helical baffles must be rotational and helical because of baffles geometry inside the shell, which finally shows a substantial raise in heat transfer coefficient per unit pressure drop across the heat exchanger.

Keywords—heat exchanger ;baffles ;helixangle ; pressure ;heat transfer coefficient.

I. INTRODUCTION

Heat exchanger is most useful equipment in the present large scale and small scale industries. It is a process of the heat transfer between two streams of body. This contains the heating and cooling process of the fluid or liquid in the present day. Present many industries using arrangement of helical baffles in heat exchangers. In this type there is nothing coincides of both hot and cooler fluids with each other because in between these separated pipes are constructed. This is better for compared to many other type, finally this type gives the better results. It is a one arrangement to give all quality of heat will be transfer in very fast and maintenance of all the working procedure in that of situation. OBJECTIVES

1. Analytical study.
2. To perform CFD reproductions of single stage and single segmental astounded shell-and-tube heat well exchanger with variable number of astounds and confound slant points by utilizing business CFD bundle FLUENT 14.5.
3. Examine the warmth exchange coefficient and weight drop on shell side by contrasting CFD results and the logical result.
4. Validate simulation results to analytical results.

In this present project, we tried to improve the heat transfer, pressure drop, velocity and temperature.

5. We used 10 degree and 20 degree baffle inclination angle orientation in single arrangements shell tube heat exchanger.
6. We used 6,8,10 and 12 number of hurdles' in single segmental shell and tube heat exchanger.
7. By using 6,8,10 and 12 number of baffles we made CFD simulation for flow inside the shell and implemented pressure drop variation, heat transfer, velocity and temperature for 10 and 20 degree baffle inclination orientation.
8. We made analytical calculations for the single segmental shell and tube heat exchanger compared with CFD calculations.

II. LITERATURE REVIEW

Lutcha and Nemcansky These are to try the new types of baffles, called the helical baffle, provide other improvement in the shell and tube. Literature survey is a one of methods to study about our project related papers in the world. To compare with that projects and what we are making, what is our target in base of preparation. Many scientists are study in glob what is need in present generation of industries.

Karls et al. his also study same working of our method similarly comparison is needs to calculating the results. In the present situation very high version of projects are doing in laboratory. We have taking to this type papers only in the purpose of references to study new model making. The recent days many of different methods will fixed in small and large scale industries.

Ender Ozden [3] according to this scantiest study, the shell side flow is very difficult in shell the tube heat exchanger due to many of leakages by pass stream between two types of zones. Space between baffles (B) dominos the structure of the upstream. Flow and heat transfer characteristics are very sensitive to baffle cut and baffle spacing also baffle inclination. Most the common baffles are single segmented baffles

Uday c kapale and satishchand:

A practical model for shell and tube drop has been developed by Uday C Kapale and Satish Chand [15]. The model incorporates on the effect of drop in inlet and outlet nozzle along losses in segments created by baffles.

Summary this literature gives various equations Dp calculation

$$\Delta Pn = \rho sun2$$

$$\Delta Pc = \frac{\rho_s u_{sc}^2 N_c f_s f_b}{2\sin\theta}\left(\frac{\mu_{sw}}{\mu_s}\right)^{0.14}$$

$$\Delta Pwz = \frac{2\rho_s u_{sc}^2 N_c f_l B_s}{2D_s}\left[\left(\frac{A_{sc}}{A_{wz}}\right)^2 - 1\right]\left(\frac{\mu_{sw}}{\mu_s}\right)^{0.14} + \frac{\rho_s k\, u_{wz}^2 B_s}{2D_s}$$

$$\Delta Pec = \rho_s f u_{sc}^2 N_c\left(1 + \frac{N_w}{N_c}\right) f_s f_b \left(\frac{\mu_{sw}}{\mu_s}\right)^{0.14}$$

Huadong and volker Local transfer and drop on the shell way of shell and pump heat exchanger of segmental baffles were investigated for different baffles spacing by Huadong Li and Volker Kottke [16]. The dispersion of the nearby warmth exchange coefficient on every tube surface inside of a completely created puzzle compartment were resolved and envisioned by method for mass exchange estimations. Per tube per column per compartment normal warmth exchange coefficient were drawn from the neighborhood values.

Simin Wang, Jian Wen, and YanzhongLi [17] are to studied on exchangers, what is configuration construction shell side. The gap between the baffle plates and shell is blood kids by the sealers, which effectively decreases the short circuit flow in the shell side. The after-effect of warmth exchange trial demonstrate that the shell side warmth exchange coefficient of the enhanced warmth exchanger expanded eighteen to twenty-five percentage, the general coefficient of warmth exchange expanded fifteen to nineteen percentage, and the energy productivity expanded by twelve to fourteen percentage. Weight misfortune expanded forty four to forty eight percentages with sealer establishment, yet augmentation of obliged influence dismissed contrasted and addition warmth flux. Warmth exchange execution enhanced warmth exchanger is strengthened, which undeniable advantage to improving of warmth.

SCOPE OF THE STUDY

To have the capacity to comprehend the reasons for the shell side outline shortcoming, the stream wonder inside the shell must be surely known.

Baffle cut and astounds dividend's distinguished as the most critical geometric parameter influencing both weight drop and warmth exchange qualities on the shell side outline

CFD procedure can be utilized both as a part, and warmth exchangers. Especially valuable beginning outline steps, lessening number of testing of model and giving a decent understanding in the vehicle sensation happening in the heat exchanger.

III. MODEL AND GEOMETRY OF HEAT EXCHANGER GEOMETRY

The making of helical baffles in different types angle of inclination using ansys software by computational fluid dynamics in the higher version of 14.5 present day this will be good running in all most industries in the world. First we are taking normal geometry in old days then making the our method, below diagram taking a normal diameter of shell in this we are making different angle of inclination.

Table 1. Geometrical values

NAME	GEOMETRY
length, L	620 mm
Inside diameter of shell, Di	100 mm
Outside diameter tube, Do	30 mm
No of tubes, Nt	7
No of baffles, Nb	6
Central baffles spacing, B	90 mm
Angle of inclination in degree	0 to 30 degree

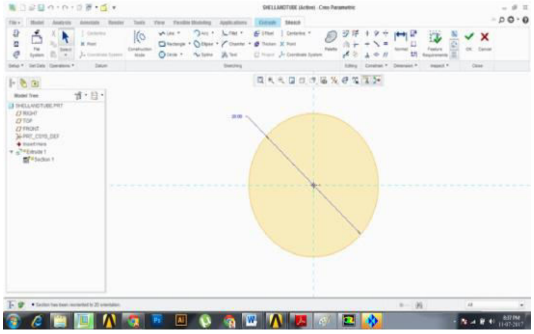

Extruded version of the circle using ansys software.

Extrude the circle to the appropriate length and make the 6 shells radially using the pattern

Model for straight baffles

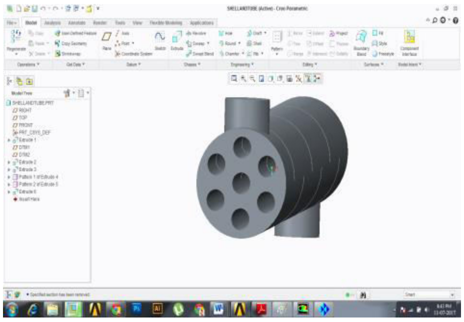

Fig 2.Straight baffles model

Model for straight or 0 degree baffle inclination angles in basic in present using many large industries in big cities of world.in this model we are making six tubes in 60 degree angles each of constructing holes. These are constructing in a one segmented shell and both two ends of this one inside and one outgoing tube will construct.

Making of 0 degree or straight baffles in single shell

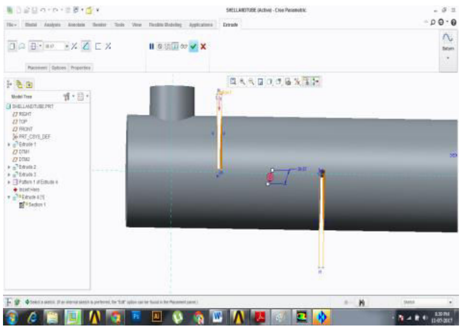

Fig 3.Model arrangements'

Pressure variation of straight baffles

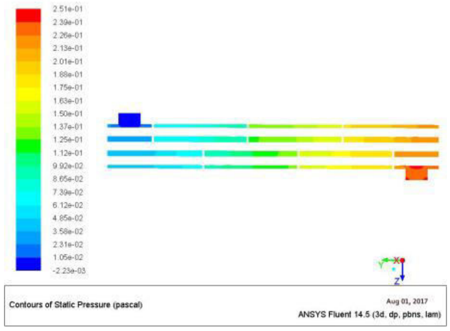

Fig 4.Pressure distribution for 0 degree baffle inclination.

Temperature variation of straight baffles

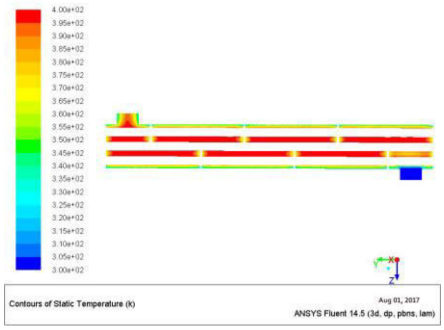

Fig 5. Temperature distribution for 0 degree baffle inclination

4.5 Temperature variation of outside tube

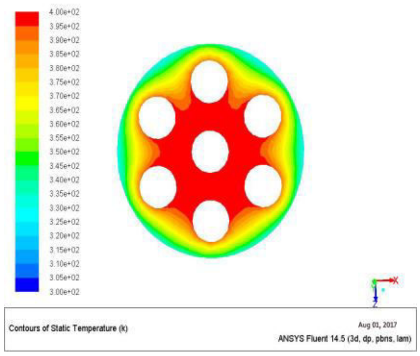

Fig 6. Static temperature for outside tube.

Velocity variation of straight baffles

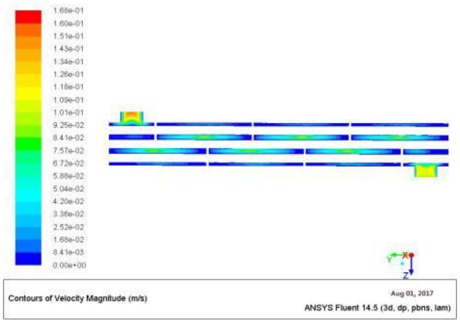

Fig 7. Velocity variations for 0 degree baffle inclination.

Velocity variation outside the tube

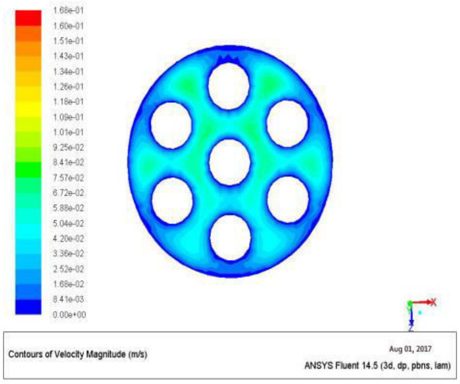

Fig 8.Static velocity for outside tube.

4.8 Model for helical baffles arrangements'

Making the helical baffles in heat exchangers for shell and tube by using CFD software of ansys fluent 14.5.To study variations of temperature pressure,mass flow rate and velocity of the shell and tube, also the rate of heat transfer. The model is design according to the tubular exchanger's manufacturers association (TEMA).

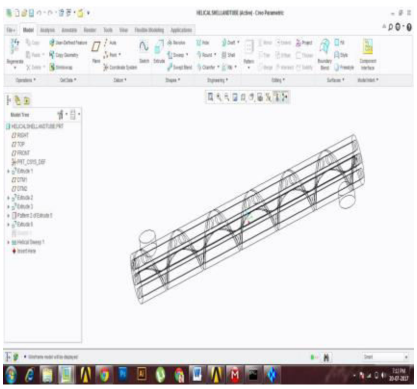

Fig 9. Isometric model for helical arrangement's

Meshing

In meshing there are two types, hex and tetrahedron cells. This mesh contains the mixed cells having both quadrilateral and triangular faces at the boundries.it reduces the numerical diffusion as much as possible by structured the well in design, near the wall region. Fine mesh will be better of one in meshing. This fine mesh finally the temperature and pressure gradients are finally mesh. In ansys 14.5 the meshing will be fine and well-structured in that the next procedure is depends.

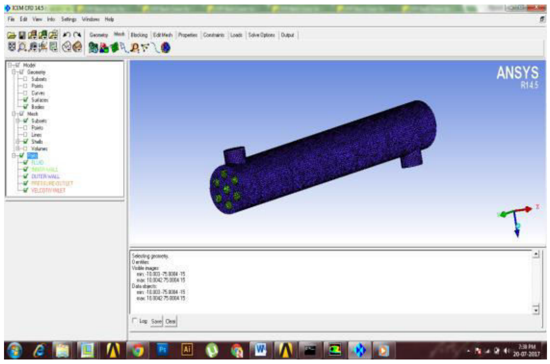

Fig 10. Meshing diagram.

IV. RESULTS AND DISCUSSIONS

Temperature Variation

Construction baffles in helical shape of the shell and tube heat transfer the temperature variation across the shell for different inclination of the baffles. The inclination angles from 0 degree to the 20 degree.

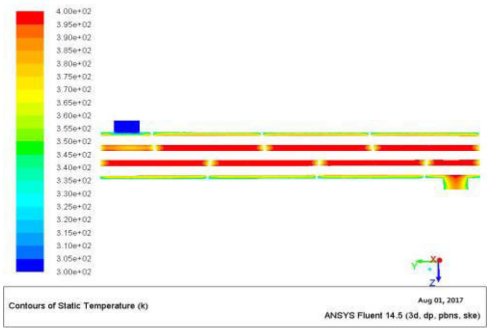

Fig 11. Temperature distribution for 10 degree baffles inclination in shell and tube.

Pressure Variation

The pressure variation of shell and tube in below fig, the pressure of the shell inside will be decreased when the baffle inclination will be increased. In the pressure variation the pressure drop will be decreased as same. The details of pressure in below graph show idea about the variation of the all.

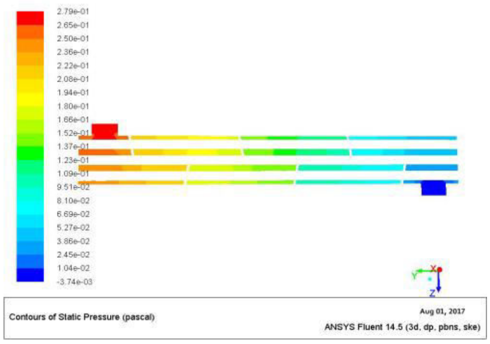

Fig 12.Pressure distribution for 10 degree baffles inclination in shell and tube.

Static Pressure

In the below graph says the variation of the static pressure in transfer of heat in our project making helical baffles in the 10 degree angle inclination. Showing the graph static pressure in Pascal vs. position of exchanger in our project. The static pressure will be decrease with increase the position of making baffles in heat transfers.

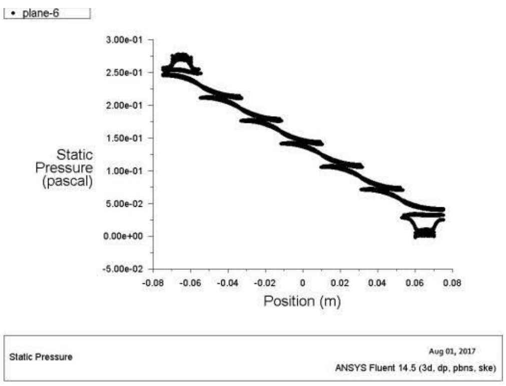

Fig 13. Static pressure for 10 degree baffles inclination in shell and tube.

Velocity Variation

The variation of velocity in the cross section of the heat transfer in shell and tube construction for helical baffles show in below fig, in variation of velocity input of the tube will be same in all the baffles inclination of the shell and tube i.e.1.2295m/s .The outlet of velocity is vary in shell baffle and turbulence will be occurs in the shell region.

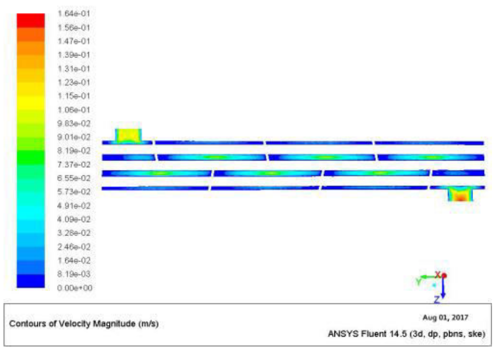

Fig 14. Velocity distribution for 10 degree baffles inclination.

For 20 Degree Baffle Inclination

Temperature Variation

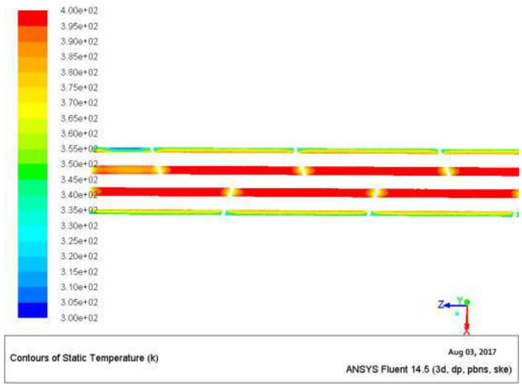

Fig 15. Temperature distribution for 20 degree baffles inclination in shell and tube.

Pressure Variation

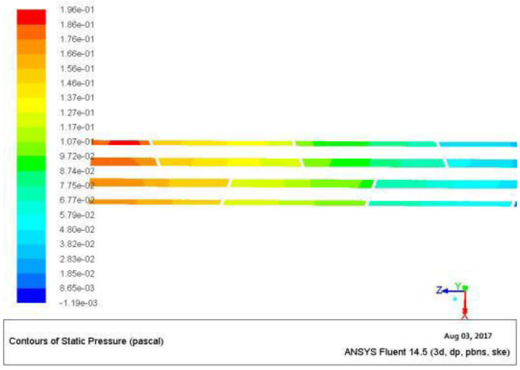

Fig16. Pressure distribution for 20 degree baffles inclination in shell and tube.

Velocity Variation

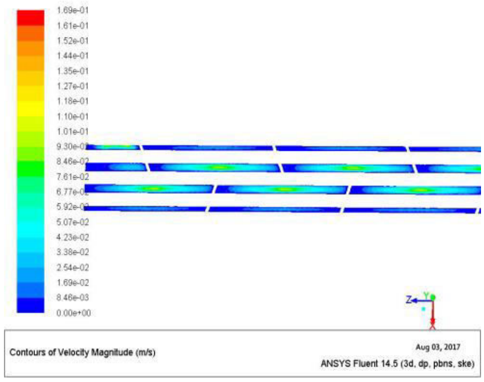

Fig17. Velocity distribution for 20 degree baffles inclination in shell and tube.

Static Pressure

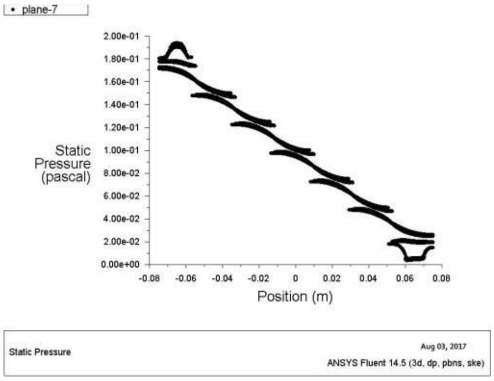

Fig 18. Static pressure for 20 degree baffles inclination in shell and tube.

Table 2. Outlet temperature of the shell side and tube side

Baffle inclination angles in (degree)	Outlet Temperature Shell Side	Outlet Temperature Tube Side
0	346	317
10	348	320
20	350	322

In the outgoing temperature of shell and incoming temperature of tube side increase with increased the baffle inclination angle of this type heat transfers in shell and tube heat exchangers. The shell side the temperature is above the 340K and in tube side below the 320K. The temperature of the shell side is higher than the tube side of the shell and tube heat exchanger.

Baffles inclination angles (in degree) V/s Temperature

Table 3. Pressure drop inside shell.

Baffle inclination angles in (degree)	Pressuredrop inside shell in(KPA)
0	233
10	232.5
20	230

Pressure drop V/s Baffle angle

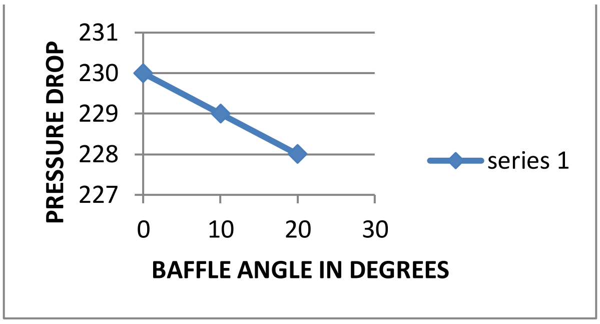

In shell side of the pressure drop will be decreased with the increase of the baffle inclination angles. The pressure drop will be decrease then the heat transfer is well in the shell and tube heat exchangers and also the good for efficiency of shell and tube.

Table 4. Velocity inside the shell in

Baffle inclination angles in (degree)	Velocity inside the shell in (m/sec)
0	4.2
10	5.9
20	6.34

Velocity vs. baffle inclination angles

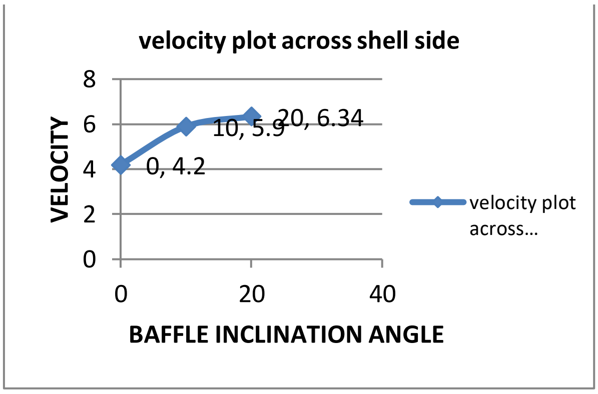

The velocity of the outlet shell increased with increase the baffle inclination angles. The more heat will be transfer in the tube the velocity also increases.

Heat Transfer Rate

The shell and tube heat exchanger the increase baffle inclination the heat transfer rate will be increase. For the better heat transfer rate,using helical baffles.

$Q = m*cp*(t1-t2)$

Q – Heat transfer rate across shell

m – Mass flow rate

cp – specific heat of water

Table 5. heat transfer rate across tube side

Baffe inclinations in degree	Shell outlet temperature	Tube outlet temperature	Pressure drop	Outlet velocity(m/s)	Heat transfer rate(Q) W/m square
0	346	317	233	4.2	3558
10	348	318	232.5	5.9	3972
20	350	320	230	6.34	4182

SNo	Baffle angles in degrees	Heat transfer rate across the tube side (m^2)
1	0	3558
2	10	3978
3	20	4183

Heat transfer rate vs baffle inclination angle

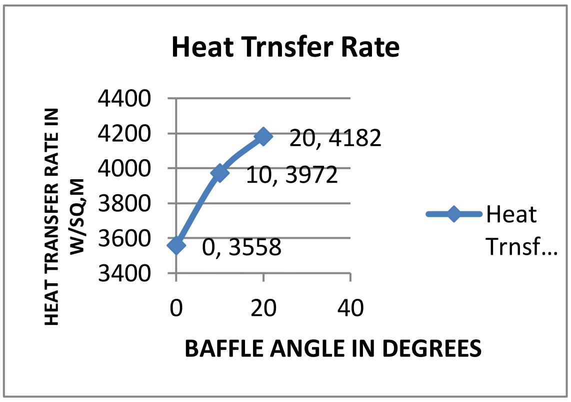

V. CONCLUSION

Design & construction of helical baffles in shell and tube heat exchanger helped to achieve the higher heat transfer rate and higher efficiency which is being tested by the application of ANSYS'- Fluent 14.5 higher version software. In the outgoing temperature of shell and incoming temperature of tube side increase with increased the baffle inclination angle of this type heat transfers in shell and tube heat exchangers. The shell side the temperature is above the 340 K and in tube side below the 320 K. The temperature of the shell side is higher than the tube side of the shell and tube heat exchanger. In shell side of the pressure drop will be decreased with the increase of the baffle inclination angles. The pressure drop will be decrease then the heat transfer is well in the shell and tube heat exchangers and also the good for efficiency of shell and tube.

SCOPE FOR FUTURE WORK

It is a cost consuming to use the conventional methods of design and development of shell and tube heat exchanger .Thus an alternative approach and most effective solution to the shell and tube heat exchanger design and optimization is by CFD Software Analysis. By knowing the velocity and pressure patterns across the details and by including various angles of helix and by incorporating number of baffles for different materials for components in shell and tube heat exchanger design and imported for analysis in CFD Soft ware to obtain more appropriate thermal characteristics and heat transfer rate.

VI.REFERENCES

1. Effect of baffle cut and baffle spacing on the shell side main stream by Ender Ozden.

2. Shell side pressure drop for fluid flow in shell and tube heat exchanger by Uday C Kapale and Satish Chand [15].

3. Effect of baffle spacing on pressure drop and local heat transfer in shell and tube heat exchanger for staggered tube arrangement by Huadong Li and Volker Kottke [16].

4. An experimental investigation of heat transfer enhancement for a shell-and-tube heat exchanger by Simin Wang, Jian Wen, and Yanzhong Li [17]

5. Transient heat exchanger response by Juan Yin, Michel K Jensen [18].

6. Shell and tube heat exchanger, Perry, Robert H. and Green, Don W.(1984). Perry's Chemical Engineers' Handbook, 6th Edition, McGraw-Hill.

7. More accurate exchanger shell-side pressure drop calculations by D. Gulley & associates, Tulska Oklahoma.

8. A Computer program for designing of shell and tube heat exchanger by Yusuf Ali Kara, Ozbilen guraras.

9. Design and rating shell and tube heat exchangers by John E. Edwards.

"STRUCTURAL ANALYSIS OF CARBON COMPOSITE LEAF SPRING WITH STEEL LEAF SPRING"

THUMATI.NINA, BANOTH.RAJENDRA PRASAD
Asst.professor, Department of Mechanical Engineering, Malla Reddy College Of Engineering, Telangana.

ABSTRACT: Expanding rivalry and development in car division has a tendency to adjust the current items by new and propelled material items. A suspension arrangement of vehicle is likewise a range where these developments are done consistently. Leaf springs are one of the most seasoned suspension segments that are as a rule still utilized broadly in autos. Weight diminishment is additionally offered because of significance via car producers. The vehicle business has indicated expanded enthusiasm for the utilization of composite leaf spring in the place of regular steel leaf spring because of its high quality to weight proportion. This work manages substitution of customary steel leaf spring of a light business vehicle with composite leaf spring utilizing Carbon/Epoxy. Measurements of the composite leaf spring are to be taken as same measurements of the regular leaf spring. The goal is to look at the heap conveying limit, stresses, redirection and weight reserve funds of carbon composite leaf spring with that of steel leaf spring

KEY WORDS: Laminated Composite leaf spring (LCLS); Static analysis ; Carbon/epoxy..

INTRODUCTION

In now a day the fuel efficiency and emission gas regulation of automobiles are two important issues. To fulfill this problem the automobile industries are trying to make new vehicle which can provide high efficiency with low cost. The best way to increase the fuel efficiency is to reduce the weight of the automobile. The weight reduction can be achieved primarily by the introduction of better material, design optimization and better manufacturing processes. The achievement of weight reduction with adequate improvement of mechanical properties has made composite a very good replacement material for conventional steel. In automobile car out of many components one of the components of automobile which can be easily replaced is leaf spring.

LITERATURE REVIEW

HISTORY/ORIGINS:

Over the last thirty years composite materials, plastics and ceramics have been the dominant emerging materials. The volume and number of applications of composite materials have grown steadily, penetrating and conquering new markets relentlessly. Modern composite materials constitute a significant proportion of the engineered materials market ranging from everyday products to sophisticated niche applications. While composites have already proven their worth as weight-saving materials, the current challenge is to make them cost effective. The efforts to produce economically attractive composite components have resulted in several innovative manufacturing techniques currently being used in the composites industry. Unlike conventional materials (e.g. steel), the properties of the composite material can be designed considering the structural aspects. The design of a structural component using composites involves both material and structural design. Composite properties (e.g. stiffness,) can be varied continuously over a broad range of values under the control of the designer. Careful selection of reinforcement type enables finished product characteristics to be tailored to almost any specific engineering requirement.

COMPOSITE MATERIALS:

A composite material is a macroscopic combination of two or more distinct materials, having a recognizable interface between them. Composites are used not only for their structural properties, but also for electrical, thermal, tribological, and environmental applications. Modern composite materials are usually optimized to achieve a particular balance of properties for a given range of applications. Many composite materials are composed of just two phases; one is termed the matrix, which is continuous and surrounds the other phase, often called the dispersed phase. The properties of composites are a function of the properties of the constituent phases, their relative amounts, and the geometry of the dispersed phase.

FIBER-REINFORCED COMPOSITES

The most commonly used composites in which the dispersed phase is in the form of a fiber. Design goals of fiber-reinforced composites often include high strength and/or stiffness on a weight basis. Fiber-reinforced composites with exceptionally high specific strengths and moduli have been produced that utilize low-density fiber and matrix materials.

Material	***Longitudinal Tensile Strength (MPa)***	***Transverse Tensile Strength (MPa)***
Glass-polyester	700	20
Carbon (high modulus)-epoxy	1000	35
Kevlar-epoxy	1200	20

LONGITUDINAL AND TRANSVERSE LOADING OF COMPOSITES

HAND LAY UP TECHNIQUE

Hand lay-up technique is the simplest method of composite processing. The processing steps are quite simple. First of all, a release gel is sprayed on the mold surface to avoid the sticking of polymer to the surface. Thin plastic sheets are used at the top and bottom of the mold plate to get good surface finish of the product. Reinforcement in the form of woven mats or chopped strand mats are cut as per the mold size and placed at the surface of mold after Perspex sheet. Then thermosetting polymer in liquid form is mixed thoroughly in suitable proportion with a prescribed hardener (curing agent) and poured onto the surface of mat already placed in the mold. The polymer is uniformly spread with the help of brush. Second layer of mat is then placed on the polymer surface and a roller is moved with a mild pressure on the mat-polymer layer to remove any air trapped as well as the excess polymer present. The process is repeated for each layer of polymer and mat, till the required layers are stacked.

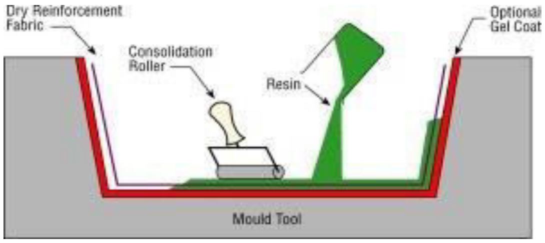

LEAF SPRING BY HAND LAYUP METHOD

Objective of the Work:

In the present scenario, weight reduction has been the main focus of automobile manufactures. The suspension leaf spring is one of the potential items for weight reduction in automobiles as it accounts for ten to twenty percent of the unsprung weight, which is considered to be the mass not supported by the leaf spring. The introduction of composite materials made it possible to reduce the weight of the leaf spring without any reduction on the load carrying capacity and stiffness. Studies were conducted on the application of composite structures for automobile for automobile suspension system. The leaf spring should absorb the vertical vibrations and impacts due to road irregularities by means of variations in the spring deflection so that the potential energy is stored in spring as strain energy and then released slowly. So, increasing the energy storage capability of a leaf spring ensures a more compliant suspension system. According to the studies, a material with maximum strength and minimum modulus of elasticity in the longitudinal direction is the most suitable material for a leaf spring. In the present work, a nine-leaf steel spring used in heavy vehicle is replaced with a composite multi leaf spring made of S2 Glass /Epoxy and Kevlar/Epoxy. The dimensions and the number of leaves for both steel leaf spring and composite leaf springs are considered to be the same. The objective is to compare their displacement, frequencies, deflections and weight savings of composite leaf spring

Design of Leaf Spring:

A spring is defined as an elastic machine element, which deflects under the action of the load and returns to its original shape when the load is removed. It can take any shape and form depending upon the application. The important functions and applications of springs are as follows: • Springs are used to absorb shocks and vibrations, e.g., vehicle suspension springs, railway buffer springs, buffer springs in elevators and vibration mounts for machinery. • Springs are used to store energy, e.g., springs used in clocks, toys, movie-cameras, circuit breakers and starters. • Springs are used to measure force, e.g., springs used in weighing balances and scales. • Springs are used to apply force and control motion.

DESIGN OF LEAF SPRING

CALCULATIONS FOR RADIUS AND LENGTHS OF LEAVES

Specifications of Ashok Leyland Viking

When n=10, Rear suspension
Number of leaf springs = 4
Overall length of the spring = 2L1 = 137.2cm = 1372mm
Width of leaves = 76.2 = 80mm
Number of full length leaves = 2 = nf
Number of graduated leaves = 8 = Ng
Number of springs = 10 (Ng+Nf)
Center load = 2W =115 tones = 11500kg

2W =11500 × 9.8 = 112700N
2W = 112700/4 = 28175N

$$2W = \frac{\text{total load}}{\text{no of springs}} = 28175N$$

W = 14087.5N

BENDING STRESS

$$\text{Bending stress}, \sigma = \frac{6\,W\,L_1}{nbt^2} = \frac{6 \times 14101.875 \times 686}{10 \times 80 \times 16^2} = 283.4146 \text{ N/mm2}$$

Bending stress, σ = 283.4146 N/mm2
Spring is simply supported beam
Width length = 2L
Central load =2W

Deflection for both full length and graduated leaves

$$y = \delta = \frac{6WL^3}{nebt^3} = \frac{6 \times 14101.875 \times 686^3}{10 \times 80 \times 86900 \times 16^3} = 95.923 \text{ mm}$$

RADIUS OF CURVATURE

$$R = \frac{{L_1}^2 + y^2}{2y} = \frac{686^2 + 95.923^2}{2 \times 95.923} = 2500.91 \text{ mm}$$

∴ Radius of curvature = 2500.91 mm

LENGTH OF LEAF SPRINGS

$2L_1$ = overall length of spring
Ineffective length l = width of band/distance between centers of u-tubes
Effective lengths $2L = 2L_1 - \frac{2}{3}l$ (when u bolts are used)
$L_1 = 1372$mm, $2L = 1372 - \frac{2}{3} \times 300 = 1172$mm
l= 300 (assume)

$$\text{Length of smallest leaf} = \frac{\text{effective length}}{n-1} + \text{ineffective length}$$

$$= \frac{1172}{9} + 300 = 430.22 \text{ mm(n=2)}$$

$$\text{Length of next leaf} = \frac{\text{effective length}}{n-1} \times 2 + \text{ineffective length}$$

$$= \frac{1172}{9} \times 2 + 300 = 560.44 \text{ mm}$$

$$\text{Length of 3rd leaf} = \frac{1172}{9} \times 3 + 300 = 690.66 \text{ mm}$$

$$\text{Length of 4rd leaf} = \frac{1172}{9} \times 4 + 300 = 820.88 \text{ mm}$$

$$\text{Length of 5rd leaf} = \frac{1172}{9} \times 5 + 300 = 951.1 \text{ mm}$$

$$\text{Length of 6rd leaf} = \frac{1172}{9} \times 6 + 300 = 1081.32 \text{ mm}$$

$$\text{Length of 7rd leaf} = \frac{1172}{9} \times 7 + 300 = 1211.54 \text{ mm}$$

$$\text{Length of 8rd leaf} = \frac{1172}{9} \times 8 + 300 = 1341.76 \text{ mm}$$

$$\text{Length of 9rd leaf} = \frac{1172}{9} \times 9 + 300 = 1471.98 \text{ mm}$$

Y = δ (the maximum deflection of spring is equal to camber(y) of spring)

$$L_1 = \frac{1372}{2} = 686\text{mm} \;;\; \delta = 95.923\text{mm}$$

Radius values

Radius of the first leaf = 2644.91 mm
Radius of the second leaf = 2628.91 mm
Radius of the third leaf = 2612.91 mm
Radius of the fourth leaf = 2596.91 mm
Radius of the fifth leaf = 2580.91 mm
Radius of the sixth leaf = 2564.91 mm
Radius of the seventh leaf= 2548.91 mm
Radius of the eighth leaf = 2532.91 mm
Radius of the ninth leaf = 2516.91 mm

ANALYSIS OF THE LEAF SPRING

Structural analysis is the most common application of the finite element engineering structures such as bridges and buildings, but also naval, aeronautical, and mechanical structures such as ship hulls, aircraft bodies, and machine housings, as well as mechanical components such as pistons, machine parts, and tools. The seven types of structural analyses available in the ANSYS family of products are explained below. The primary unknowns (nodal degrees of freedom) calculated in a structural analysis are displacements. Other quantities, such as strains, stresses, and reaction forces, are then derived from the nodal displacements. Structural analyses are available in the ANSYS Multi physics, ANSYS Mechanical, ANSYS Structural, and ANSYS Professional programs only.

CASE 1:- MATERIAL - MILD STEEL

MATERIAL PROPERTIES OF STEEL

Density	:	0.00000785kg/mm^3
Young's modulus	:	20000Mpa
Poissons ratio	:	0.3

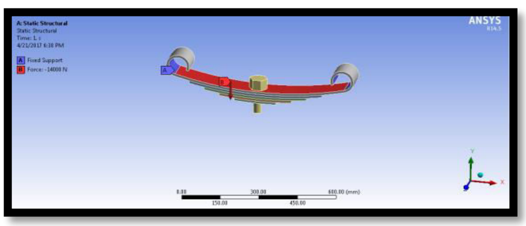

STATIC STRUCTURAL

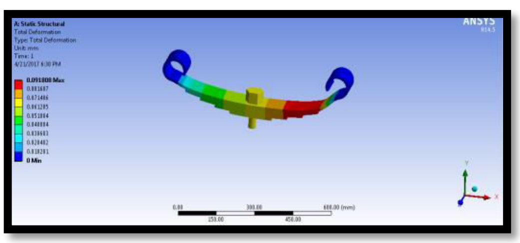

TOTAL DEFORMATION

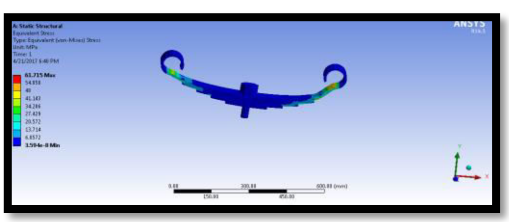

VON-MISES STRESS

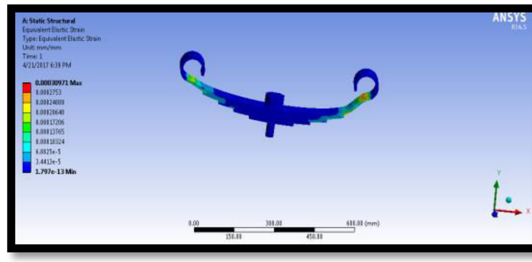

VON-MISES STRAIN

CASE 2:- MATERIAL - GLASS FIBRE

MATERIAL PROPERTIES OF GLASS FIBRE

Density	:	2.66-2.68 g/cc
Young's modulus	:	76-78 GPa
Poisson's ratio	:	0.3

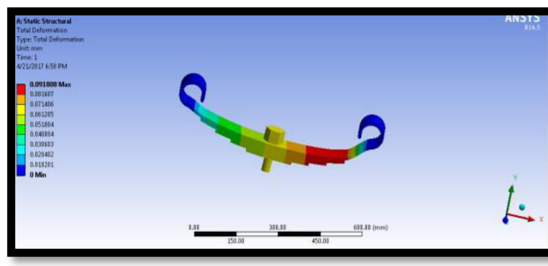

TOTAL DEFORMATION

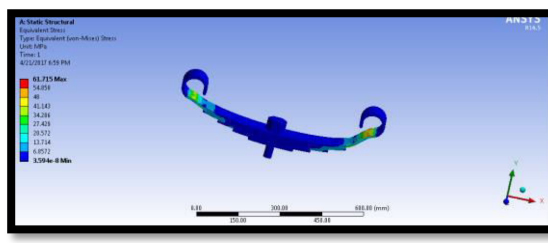

VON MISES STRESS

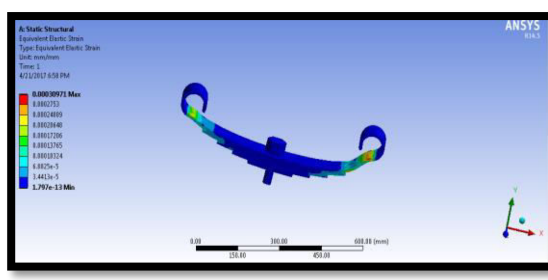

VON MISES STRAIN

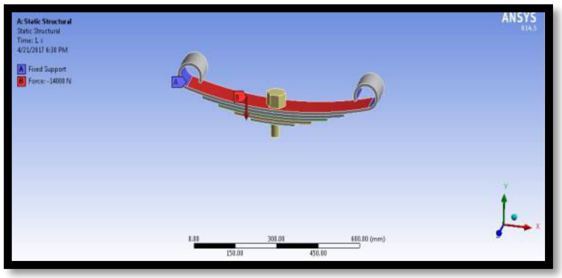

STATIC STRUCTURAL

RESULTS

STRUCTURAL ANALYSIS

COMPARISON BETWEEN MILD STEEL AND GLASS FIBRE

	Mild steel	**Glass fibre**
Deformation (mm)	0.091808	0.85182
STRESS (N/mm^2)	61.715	26.743
STRAIN	0.00030971	0.0029976

WEIGHTS COMPARISON

S.NO.	**MATERIAL**	**WEIGHT(IN KGS)**
1	**STEEL**	**2.450**
2	**E-GLASS/S2 GLASS**	**0.900**

V. CONCLUSION

A leaf spring is designed for Ashok Leyland Viking heavy vehicle. The data is collected from net for the specifications of the model. The leaf spring is designed for the load of 14087.5N. Theoretical calculations have been calculated for leaf spring dimensions at different cases like varying thickness, camber, span and no. of leaves by mathematical approach. In this thesis, analysis have been done by taking materials steel, carbon Epoxy.

REFERANCES

1. C. Madan Mohan Reddy, D. RavindraNaik, Dr M. Lakshmi Kantha, Study on analysis and testing of two wheeler suspension helical spring,

2. Slimane Metiche and Radhouane Masmoudi, Structural and thermal analysis of spring loaded safety valve using FEM, International journal of mechanical engineering and robotics research, 4(1), 430-434.

3. Pozhilarasu V. and T ParameshwaranPillai, Performance analysis of steel leaf spring with composite leaf spring and fabrication of composite leaf spring, International journal of engineering research and Science & Technology, 2(3), 102-109.

4. Aishwarya A.L., A. Eswarakumar, V.Balakrishna Murthy, Free vibration analysis of composite leaf springs, International journal of research in mechanical engineering &technology, 4(1), 95-97.

5. T. N. V. Ashok Kumar, E. VenkateswaraRao, S. V. Gopal Krishna, Design and Material Optimization of Heavy Vehicle Leaf Spring, International Journal of Research in Mechanical Engineering & Technology, 4(1), 80-88.

6. K.A. SaiAnuraag and BitraguntaVenkataSivaram, Comparison of Static, Dynamic & Shock Analysis for Two & Five Layered Composite Leaf Spring, Journal of Engineering Research and Applications, 2(5), 692-697.

7. E. Mahdi a, O.M.S. Alkoles a, A.M.S. Hamouda b, B.B. Sahari b, R. Yonus c, G. Goudah, Light composite elliptic springs for vehicle suspension, Composite Structures, 75, 24–28.

8. Y. N. V. Santhosh Kumar, M. VimalTeja, Design and Analysis of Composite Leaf Spring,Dept. of Mechanical Engineering, Nimra College of Engineering & Technology, Ibrahimpatnam, Vijayawada. (2012).

METHODS FOR IMPROVING PERFORMANCE OF HEAT TRANSFER IN PIPES – A REVIEW

M. Ravi kumar[1], VR. Palaniappan[2],M. Sabareesh[3]

[1] professor & [2], [3] UG students, Banari Amman institute of technology, Tamil Nadu

Abstract— **The working principle of Heat pipes are based on evaporation and condensation of a working fluid which transfers large amount of heat.Heat Pipes have their attention in various applications such as in Space craft thermal controls, cooling of computer systems, solar thermal water heating applications, and in various HVAC applications such as ventilation heat recovery. Design parameters such as inclination angle, length, working fluids, wick type and material determine the output of heat pipe. Hence the appropriate selection of the above parameters is important for the perfect design of heat pipe. A brief about the selection of parameters while considering a design of a heat pipe is done in this paper. Whilst the above parameters selection, criterions such as thermal resistance, overall heat transfer co-efficient and thermal efficiency are also weighed. Further, the scope for improvement of performance of heat pipe using nano fluids and insertion of fins to the heat pipe is discussed.**

Index Terms— Filling ratio, Heat Pipe, Heat transfer coefficient, Inclination angle, Nanofluids.

I. Introduction

A heat transfer device which transports heat effectively from a solid interface to another by using the principle of thermal conductivity and phase transition is known as a heat pipe. Initially at the hot interface the working fluid which is in liquid form is turned into vapour by absorbing heat when in contact with a thermally conductive solid. This vapour is then used to transport the latent heat to the cold interface after travelling along the heat pipe. The cycle is repeated by returning back the liquid to the hot interface by capillary action or centrifugal force. These are highly efficient thermal conductors because of the high heat transfer coefficients for boiling and condensation. Heat pipes are the available technologies which deal with the high density electronic cooling problem due to their high thermal conductivity, reliability and low weight. Heat pipes are two-phase heat transfer devices with high effective thermal conductivity. Due to the highheat transport capacity, heat exchanger with heat pipes has become much smaller than traditional heat exchangers in handling high heat fluxes.

Heat pipes are used for cooling purposes in a wide range of applications. Recently, it found its application in the field of manufacturing to control the process temperatures in die-casting, injection moulding and metal machining. In spacecraft Heat pipes and loop heat pipes are used extensively, since they don't require any power to operate, operate nearly isothermally, and can transport heat over long distances.

Many researchers have been carried out the improvement of the performance of heat pipe. Of the many factors considered, some important parameters that affected the performance of heat pipe are length and diameter, inclination angle, working fluid, filling ratio of working fluid as a percentage of evaporator volume, wick structure. Further gravity assisted heat pipes are more advantageous than anti-gravity heat pipes. Selection of working fluid is a fundamental parameter affecting heat pipe's performance. For normal applications, the working fluids are easily available and economical. They act as an ideal fluid having a low boiling point and high latent heat. Researchers [1] conducted experiments with commonly available and cheap working fluids such as acetone, ethanol, methanol and water. They showed water is the best candidate for high heat flux applications. Being cheaper and abundantly available water can be the first choice of preference. In the next step, to enhance the heat transfer performance, use of nano particles in the working fluids is another major segment. Researchers [4], [5], [6] studied the influence of titanium, copper and silver nano fluids on the performance. It was found that the use of nano fluids increased the thermal efficiency and reduced thermal resistance significantly when compared to bare working fluids. On average, a thermal efficiency of 60-65% can be achieved. Further the influence of hybrid nano fluids was investigated by [7], and they were able to reduce the thermal resistance by 59% and the capacity of heat pipe was increased beyond 250W.

In a new approach for advanced heat pipe performance, [10] studied the effect of finned structures on heat pipes. It was found that overall thermal performance enhanced significantly compared to non-finned heat pipes. This review recommends that the combined integrated performance of heat pipe with nanofluids and finned structures would result in ultimate maximum performance of heat pipe.

II. Heat Pipe Working Principle

A heat pipe as shown in Figure-1 consists of an evacuated container sealed at ends, a wick structure, and a small amount of working fluid in equilibrium with its own vapor. A heat pipe has three sections namely evaporator section, adiabatic (transport) section, and condenser section. The external heat load on the evaporator section causes the working fluid to vaporize. The resulting vapor pressure drives the vapor through the adiabatic section to the condenser section. In the adiabatic section, no heat is absorbed or rejected. The condensing section condenses the vapor and the latent heat of vaporization of the working fluid is rejected into the atmosphere. The condensed working fluid is then pumped back by capillary pressure generated in the wick structure. Transport of heat can be continuous as long as there is enough heat input to the evaporator section so that sufficient capillary pressure is generated to drive the condensed liquid back to the evaporator. Large quantities of heat can be transported through a small cross-sectional area over a considerable distance with no additional power input to the system using heat pipe when compared to other conventional methods of heat transfer.

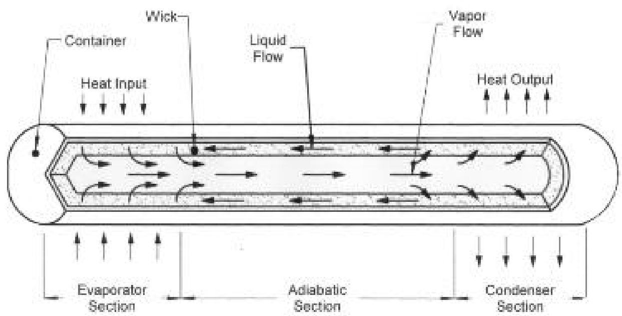

Fig.1. Heat pipe construction and working

Heat pipe operates on a closed two-phase cycle and utilizes the latent heat of vaporization to transfer heat with a very small temperature gradient. Heat pipe consists of three main parts, which are the vessel, wick structure and working fluid. The vessel or a container is normally constructed from glass, ceramics or metal. Where else wick structure is constructed from woven fibre glass, sintered metal powder, screen, wire meshes, or grooves. Finally, typical working fluids used vary from nitrogen or helium for low temperature heat pipes to lithium, potassium or sodium for high temperature. In order to fabricate a working heat pipe, all three parts are given equal importance to the material type, thermo physical properties and compatibility. Heat pipe is capable of creating its own capillary pressure at the evaporator end. This would cause a continuous flow of liquid in the wick and recirculate the liquid at the evaporator zone. Heat flows is assumed to be adiabatic through evaporator section and condenser section. Due to this reason, the vapour experiences a negligible temperature drop which proves that generally heat pipes exhibit thermal characteristics that are even better than a solid conductor of the same dimension. When considering the wick structure, the working fluid travels from the condenser section to the evaporator section. The working fluid should be evenly distributed over the evaporator section. In order to provide a proper flow path with low flow resistance, an open porous structure with high permeability is desirable. This is to ensure that the working fluid returns from the condenser to the evaporator.

III. Aim And Objective

The aim of the review is to compile the notable findings of researchers in the field of heat pipe design and serve guidelines and thumb rules to be considered in the design of heat pipes.

The objectives of the review is,

1) To filter the best candidate among the working fluids for common applications of heat pipes, so as to produce a cost effective design.
2) To analyse the performance of heat pipes with nanofluids and compare with bare working fuids.
3) To emphasize the scope for combined performance of nanofluids and finned structures in heat pipe.

IV. LITERATURE Review

Annamalai [1] discussed about experimental studies on porous wick flat plate heat pipe. In this study, the experimental analysis of the thermal performance of flat plate heat pipe of dimensions 133×133×35 mm was carried out for various heat input rates with different working fluids. Quantity of working fluid charged into the heat pipe is varied and its influence on performance was obtained. Different working fluids have been tested with heat pipe and their performance has been compared. At lower heat flux (1.38-2.73 W/m^2) the fluids such as acetone, ethanol, and methanol are better than water, whereas at higher heat flux (6.38 W/m^2) water is best candidature among these fluids considered. Water being more economical and easy availability will be a suitable choice of working fluid for high heat flux applications.

K. Mozumder [2] discussed about performance of Heat Pipe for Different Working Fluids and Fill Ratios. An attempt is made to design, fabricate and test a miniature heat pipe with 5 mm diameter and 150mm length with a thermal capacity of 10 W. Working fluids such as water, methanol and acetone were studied and compared. The performance of the heat pipe was quantified in terms of thermal resistance and overall heat transfer coefficient. The amount of liquid filled was varied and the variation of the performance parameters for varying liquid inventory is observed. Acetone with 100% fill ratio of evaporator volume shows the best result with minimum temperature difference across the evaporator and condenser. In case of water it was observed that it shows maximum value of heat transfer co-efficient and minimum value of thermal resistance at 85% fill ratio.

R.A. Hossain [3] presented the works on the Design, Fabrication and Experimental Study of Heat Transfer Characteristics of a Micro Heat Pipe. In this study the heat transfer characteristics, a micro heat pipe (MHP) of circular geometry having inner diameter 1.8mm and length 150 mm is designed and fabricated. An experimental investigation is carried out also to investigate the performance of the MHP with different experimental parameters like inclination angle, coolant flow rate, working fluid and heat input. Three different types of working fluids are used; acetone, ethanol and methanol. For each working fluid, heat transfer characteristics are determined experimentally for different inclination angle and different coolant flow rate at different heat input. Acetone is proved to be better as working fluid.

Paisarn Naphon [4] presented work on experimental investigation of titanium nano fluids on the heat pipe thermal efficiency. In this study the enhancement of heat pipe thermal efficiency with nano fluids with titanium particles was presented. The heat pipe is fabricated from the straight copper tube with the outer diameter and length of 15mm and 600 mm, respectively. The heat pipe with the de-ionic water, alcohol, and nano fluids (alcohol and nano particles) are tested. The mixtures of the pure alcohol and nano particles with the concentration of 0.01, 0.05, 0.10, 0.50 and 1.0% by volume are prepared using an ultrasonic homogenizer. The titanium nano particles with diameter of 21 nm are used in the present study which the mixtures of alcohol and nano particles are prepared using an ultrasonic homogenizer. Thermal efficiency of heat increases and reaches maximum upto a tilt angle of 60° for de-ionic water and 45° for alcohol. For de-ionic water thermal efficiency as a function of heat flux increases and reaches maximum when the percentage charge of water is 66%. For mixture of alcohol and titanium nano particles the optimal concentration of nano particles was 0.10 % for maximum efficiency. The maximum efficiency ranges from 65-70%.

R. Senthilkumar [5] studied about the experimental analysis of cylindrical heat pipe using Copper Nano fluid with an aqueous solution of N-hexanol. This study analyzes the thermal performance of heat pipe using copper nano fluid in n-Hexanol. The cylindrical heat pipe is filled with de-ionized water, copper nano fluid, an aqueous solution of n-Hexanol and copper nano particle in an aqueous solution of n- Hexanol separately and tested for its performance. The heat pipe body is made up of copper, with a length of 600 mm outside and inside diameter of 20 mm and 17.6 mm respectively. The use of n-Hexanol in de-ionized water and copper nano fluid enhances the performance of heat pipe. The variation of thermal efficiency with heat flux increases and reaches maximum upto a tilt angle of 45° for all working fluids. And for the same angle, the maximum efficiency is obtained in copper nanofluid – n-Hexanol mixture. Upto 65% efficiency is obtained. The thermal resistance of copper nano fluid in aqueous solution of n-Hexanol is nearly 80 to 90% less than the DI water.

Shung-Wen Kang [6] discussed about the experimental investigation of silver nano-fluid on heat pipe thermal performance. The outer diameter and length of the heat pipes used in these experiments were 6 mm and 200 mm, respectively. The heat pipe contained 211 µm wide 217 µm deep grooves. The nano fluid used in this study is an aqueous solution of 35 nm diameter silver nano-particles. The experiment was performed to measure the temperature distribution and to compare the heat pipe thermal resistance using nano-fluid and DI-water. The tested nano-particle concentrations ranged from 1 mg/l to 100 mg/l. At a same charge volume, the measured nano-fluid filled heat pipe temperature distribution demonstrated that the thermal resistance decreased 10–80% compared to DI-water at an input power of 30–60 W. DI-water diluted with 10 nm and 35 nm silver particles were used as working fluids and performance were evaluated. Comparing two nano-particle sizes with the thermal resistance value using DI-water, the maximum reduction was 50% (10 nm) and 80% (35 nm), respectively.

R. Ramachandran [7] discussed about the role of hybrid nano fluids in improving the thermal characteristics of screen mesh cylindrical heat pipes. Experiments were conducted to study the thermal performance of meshed wick heat pipe by varying the working fluid and heat input. The heat pipes were fabricated with commercially available straight copper tubes with outer diameter of 12.5 mm, inner diameter 11.5mm with a length 300mm. In this work four screen mesh wicked heat pipes were fabricated and tested. All the heat pipes were tested for heat input from 50W to 250W each with an increment of 50W in each step. The thermal resistance of all the heat pipes charged with different working fluids such as DI water, Al_2O_3/DI water nano fluid of volume concentration 0.1 % and hybrid nano fluid volume concentration 0.1%(with two different combinations of (Al_2O_3 50%- CuO 50%)/DI water and (Al_2O_3 25%- CuO 75%)/DI water) was determined. The maximum percentage reduction was found to be 58.87% for the hybrid nano fluid of (Al_2O_3 25%- CuO 75%)/DI water compared to base fluid. An important observation from the study is that, use of hybrid nano fluid can raise the operating range of the heat pipe beyond 250W which makes hybrid nano fluid as a potential substitute for the conventional working fluid.

Jung-Shun Chen [8] studied about the length and bending angle effects on the cooling performance of flat plate heat pipes. The effects of length and bending angle on the cooling performance of flat plate heat pipes (FPHPs) were examined experimentally in this study. All FPHPs had the same cross sectional area of 50 mm (width) by 2.5 mm (thickness). Experimental results showed that by increasing the length from 80 to 150 mm, to 200 mm, and to 300 mm, the minimum thermal resistance, Rth(min), increased by the factors of 2.4, 6.0, and 17.9,respectively from that of 0.103 K/W of the 80 mm FPHP. A rapid increase in Rth(min) occurred around the length of 150 mm. For the FPHPs with lengths smaller than 150 mm, Rth(min) could be smaller than 0.252 K/W. The maximum heat transport capability Qmax decreased quickly from 109.5 to 49.6W (a factor of about 0.452) when the length was increased from 80 to 150 mm, and then slowly decreased to the minimum value of 35W (a factor of about 0.318) for the length of 300 mm. In contrast, the results of bending angles showed that by increasing the bending angle, the thermal resistance decreased; Rth(min) reduced by a factor of about 3.3 from 0.6207 K/W of 0° bending to 0.1885 K/W of 90° bending. The corresponding maximum effective thermal conductivity, Keff(max), increased from 1933.4 to 6365.6 W/m K and Qmax increased from 45 to 85 W. This showed, a short FPHP performed better than those of longer ones and the thermal performance of FPHPs could be enhanced by proper bending.

Hamid Reza Goshayeshi [9] discussed about the experimental study on the effect of inclination angle on heat transfer enhancement of a ferro fluid in a closed loop oscillating heat pipe under magnetic field. The study uses a oscillating heat pipe of length 380mm, inner diameter 1.75mm and outer diameter 3mm. This paper elaborates on the findings of study on the effect of Fe_2O_3/Kerosene nano fluid to the copper closed-loop oscillating heat pipe under the magnetic field for inclination angles ranging from 0° to 90°, under different heat inputs (10–90 W). The heat pipe's heat transfer coefficient was measured without and with the magnetic field. It was shown that Fe_2O_3 nano particles could improve the thermal resistance and subsequently thermal performance as well as the pipe's heat transfer coefficient, especially under the magnetic field. The critical angle was 75°as the heat transfer coefficient increased due to higher inclination angle.

Saleh Almsater [10] discussed about the performance enhancement of high temperature latent heat thermal storage systems using heat pipes with and without fins for concentrating solar thermal power plants. This paper investigates an approach for reducing the thermal resistance by utilising axially finned heat pipes. A numerical model simulating the phase change material melting and solidification processes has been developed. The results show that by adding four axial fins and including the evaporation and condensation, the overall thermal performance of the storage system is enhanced significantly compared to having bare heat pipes. After 3 h a total of 106% increase in energy storage is obtained during the charging process. The results also show that the combined effect of incorporating the evaporation / condensation process and adding the fins leads to a threefold increase in the heat storage during the first 3 h. During the discharge process, there was a 79% increase in energy discharged and also the combined effect of incorporating the evaporation / condensation as well as adding the fins results in an almost four fold increase in the heat extracted within the first 3h.

R. Robinson Gnanadurai [11] presented about the investigation on the effect of cooling of the tool using heat pipe during hard turning with minimal fluid application. In this paper heat pipes were used as an auxiliary cooling source for a turning tool to enhance its cutting performance. The heat pipe used here was enveloped in electrolytic copper and the working fluid was water. Grooved type wick having an axial groove along the length of heat pipe was selected. The condenser the heat pipehad cooling fins of 0.5mm thickness over 75 mm length and 10mm width. Cooling the fins was done with a fan, blowing air at speed of 500m/min. Dissipation of heat from the cutting zone with heat pipes lead to overall reduction of cutting temperature which eliminated the thermal degradation of the cutting fluid, thus enhancing the lubrication. When heat pipe was introduced cutting temperature reduced by 22%, the tool wear reduced by 15%, the surface roughness reduced by 0.83% and cutting force was reduced by 2.9% when compared to the application with the absence of heat pipe.

Patrik Nemec [12] studied about the mathematical model for heat transfer limitations of heat pipe. In this paper a mathematical model was developed for calculating the heat transportation of heat pipes. It was carried out with various wick structures and working fluids. The effect of these parameters on the cooling effect of the heat pipe was evaluated. It was concluded that the critical limitations of the heat pipe performance was the entrainment limitation, capillary limitation which were basically influenced by the wick structure and the thermo physical properties of the fluid.

P.Gully [13] studied about the super fluid helium heat pipe. In this paper three super fluid helium heat pipes were subjected to thermal tests, of which two of them were designed with copper braids for larger transport capacity and the other with a smaller transport capacity eliminating the copper braids. The angle tilt was 60°. Conductance of the third heat pipe showed steep decrease when the temperature decreases. The longer heat pipe and the shorter one had same thermal performance in the temperature range 0.7 – 2.0 K. The longer heat pipe, at 1.7 K reached a heat transfer capacity of 6.2 mW and a thermal conductance of 600 mW/K for 4 mW transferred power.

M.G. Mousa [14] discussed about effect of nano fluid concentration on the performance of circular heat pipe. A simple small heat pipe is thermally tested with two working fluids; pure water and Al_2O_3-water based the nano fluid. In this study, effect of filling ratio, volume fraction of nano particles in fluid, and heat input rate on the thermal resistance is investigated. It was found that the thermal resistance decreased with increasing concentration of Al_2O_3-water based nano fluid.

Minghui Xie [15] revealed about the experimental investigation of heat transfer performance of rotating heat pipe. Here the experimental results of the rotating heat pipe and no heat pipe in terms of heat transfer. For both the cases test conditions were considered the same and the experiment was conducted for 45 minutes. When comparing both the cases, the temperature difference of rotating heat pipe was smaller than no heat pipe.

TABLE I
COMPARISON OF DIMENSIONS, WORKING FLUID AND RESULTS

Author	Dimensions	Working fluid	Results
Annamalai	Length – 133mm Width – 133mm Height – 35mm Flat heat Pipe	Acetone, ethanol, methanol and water.	At lower heat flux (1.38-2.73W/m^2) the fluids such as acetone, ethanol, and methanol are better than water, whereas at higher heat flux (6.38 W/m^2) water is best candidate.
K. Mozumder	Diameter – 5mm Length – 150mm	Water, methanol and acetone.	Optimal filling ratio for best performance for acetone and water are 100% and 85% respectively.
R.A. Hossain	Diameter – 1.8mm Length – 150mm	Acetone, ethanol, and methanol.	Acetone was the better working fluid.
PaisarnNaphon	Outer Dia – 15mm Length – 600mm	De-ionic water, alcohol and nanofluids (alcohol +titanium nano particles)	Thermal efficiency of heat increases and reaches maximum upto a tilt angle of 60° for de-ionic water and 45° for alcohol. For mixture of alcohol and titanium nano particles the optimal concentration of nano particles was 0.10 % for maximum efficiency. The maximum efficiency ranges from 65-70%.
R.Senthilkumar	Outer Dia – 20mm Inner Dia - 17.6mm Length – 600mm	De-ionized water, copper nano fluid, aqueous solution of n-Hexanol and copper nano particle in an aqueous solution of n- Hexanol.	The use of n-Hexanol in de-ionized water and copper nano fluid enhances the performance of heat pipe.
Shung-Wen Kang	Outer Dia – 6mm Length – 200mm	Silver nano-fluid (aqueous solution) and DI water.	Upto 80% reduction in thermal resistance obtained using silver nano fluids when compared to DI water.
Ramachandran.R	Outer Dia - 12.5mm Inner Dia - 11.5mm Length – 300mm	DI water, Al_2O_3 nanoparticle aqueous solution and hybrid nanofluid (Al_2O_3 –CuO) aqueous solution.	Hybrid nanofluid gives the maximum performance. They even extend the heat pipe capacity beyond 250W.
Jung-Shun Chen	Width – 50mm Thickness – 2.5mm Length – 80, 150, 200, 300 mm. Flat heat pipe	Acetone	A rapid increase in Rth(min) occurred around the length of 150 mm. Increasing the bending angle from 0° to 90° reduces the thermal resistance 3.3 times.
Hamid Reza Goshayeshi	Outer Dia -3mm Inner Dia - 1.75mm Length – 380mm	Fe_2O_3/Kerosene nano fluid under magnetic field.	Fe_2O_3 nano particles could improve the thermal resistance and subsequently thermal performance under magnetic field. The best performance is obtained at inclination angle of 75°.
Saleh Almsater	Outer Dia -3mm Inner Dia -2.5mm Length – 250mm	Ethonol and Methonol (50% filling ratio each)	Best performance was obtained with fin-inserted heat pipe at 45° inclination, and methanol as working fluid.
R. Robinson Gnanadurai	Outer Dia-6.3mm Inner Dia-5.3mm Length-90mm	Water (30% of whole volume)	Better performance of cutting tool when hard turned with heat pipes. Cutting temperature of the tool reduced by 22%, the tool wear reduced by 15% when adapting heat pipes while turning process.
PatrikNemec	Inner Dia-12.1mm Cross sectional Dia-10mm Length-320mm	Ethanol	Limitation values of a heat pipe depend only on the wick structures and the thermo physical property of the working fluid. Capillary limit is the maximum heat transport limitation of a heat pipe.
P. Gully	Inner Dia-4mm Outer Dia-6mm Volume-0.25mL	Helium	At 1.7 K Heat pipes with copper braid had transport capacity of 4.5 mW for a tilt angle of 60°. It reached 6 mW for a tilt angle of 0°. The thermal conductance of Heat pipe without copper braid at 0.5 mW heating power was200 W/K and 4 mW/K at 1.3 K and 0.7 K temperatures.

M.G. Mousa	Adiabatic Tube: Dia-20mm Length-40mm Evaporator and Condenser: Dia-40mm Height-60mm	Al_2O_3+Water	Nanoparticles of 40nm size were charged in water base fluid as the working fluid, which proved a decrease in thermal performance of the heat pipe when compared to setups with pure water as working fluids.
Yang Cai	Length-600mm Dia-42mm Rotational speed-400rpm	Ammonia	The temperature differences between the condenser and evaporator in both the cases of rotating heat pipe and no heat pipe is 4°C and 27°C. Heat transfer through the rotating heat pipe is larger.

V. Conclusion

In this paper effort has been made to review various work carried out by researchers in the field of heat pipe technology. Focus is made especially on factors influencing the performance of heat pipe. How factors such as inclination angle, working fluid and dimensions affect the heat transfer and thermal resistance and their optimal values are reviewed. This work could serve as a standard reference and gives important thumb rules to be used while designing heat pipe. Further the impact of nano fluids and hybrid nano fluids on the performance is also dealt in detail. Further, this promises for a new scope where combined effect of nano fluids and finned structures would result in ultimate maximum performance of heat pipe.

References

[1] Annamalai, Mani and Dhanabal, Somasundaram (2010). Experimental studies on porous wick flat plate heat pipe. International Refrigeration and Air Conditioning Conference. Paper1045.

[2] A. K. Mozumder1, A. F. Akon1, M. S. H. Chowdhury1 and S. C. Banik. (2010, December). Performance of Heat Pipe for Different Working Fluids and Fill Ratios. *Journal of Mechanical Engineering*. ME 41(2)

[3] R.A. Hossain, M.A.K Chowdhuri , C. M. Feroz Design (2010). Fabrication and Experimental Study of Heat Transfer Characteristics of a Micro Heat Pipe.J.heat and mass transfer. 24, 123-132.

[4] Paisarn Naphon, Pichai Assadamongkol, Teerapong Borirak (2008). Experimental investigation of titanium nano fluids on the heat pipe thermal efficiency. International Communications in Heat and Mass Transfer 35,1316–1319.

[5] R. Senthilkumar, S. Vaidyanathan, B. Sivaraman (2011). Experimental analysis of cylindrical heat pipe using Copper nano fluid with an aqueous solution of N-hexanol. Frontiers in Heat Pipes, 2(3), 1-5.

[6] Shung-Wen Kang , Wei-Chiang Wei , Sheng-Hong Tsai , Shih-Yu Yang. (2006). Experimental investigation of silver nano-fluid on heat pipe thermal performance. Applied Thermal Engineering. 26, 2377–2382.

[7] R Ramachandran, K Ganesan, Lazarus Godson Asirvatham . (2016).The role of hybrid nano fluids in improving the thermal characteristics of screen mesh cylindrical heat pipes. Thermal science, 20(6), 2027-2035.

[8] Jung-Shun Chen, Jung-Hua Chou. (2015). The length and bending angle effects on the cooling performance of flat plate heat pipes. International Journal of Heat and Mass Transfer, 90, 848–856.

[9] Hamid Reza Goshayeshi, MarjanGoodarzi, Mohammad Reza Safaei, MahidzalDahari. (2016). Experimental study on the effect of inclination angle on heat transfer enhancement of a ferro fluid in a closed loop oscillating heat pipe under magnetic field. Experimental Thermal and Fluid Science, 74, 265–270.

[10] SalehAlmsater, WasimSaman, Frank Bruno.(2016). Performance enhancement of high temperature latent heat thermal storage systems using heat pipes with and without fins for concentrating solar thermal power plants. Renewable Energy, 89,36-50.

[11] R. Robinson Gnanadurai, A.S. Varadarajan. (2016). Investigation on the effect of cooling of the tool using heat pipe during hard turning with minimal fluid application. Engineering Science and Technology, 19, 1190−1198.

[12] Patrik Nemec, Alexander Caja, Milan Malcho. (2013). Mathematical model for heat transfer limitations of heat pipe. Mathematical and Computer Modelling, 57, 126–136.

[13] P.Gully. (2015). Super fluid helium heat pipe.Physics Procedia, 67,625–630.

[14] M.G. Mousa. (2011). Effect of nano fluid concentration on the performance of circular heat pipe. Ain Shams Engineering Journal 2, 63–69.

[15] MinghuiXie, ZhihuXue,WeiQu, Wei Li. (2015). Experimental investigation of heat transfer performance of rotating heat pipe. Procedia Engineering, 99,746–751.

First A. Author received the B.E. degree in Mechanical Engineering from Coimbatore Institute of Technology in 1996 and M.Tech degree in Energy Engineering from Regional Engineering College in 2000 and PhD degree in Mechanical Engineering from Anna University in 2012. Presently working as a professor, Mechanical Engineering Department, Bannariamman Institute of Technology. In 2012, he received the award for best faculty adviser in Indian society of technical education for Tamilnadu – Puducherry section and published research work in 9 international journals.

Second B. Author currently pursuing BE Mechanical Engineering at Bannariamman Institute of Technology. He is the member of Indian society for heating, refrigerating and air-conditioning engineering and published a paper on cold storage system integrated with PCM.

Third C. Author received Diploma in Mechanical Engineering in PSG Polytechnic College at Coimbatore in 2015 and currently pursuing BE Mechanical Engineering at Bannari amman Institute of Technology. He is the member of Indian society for heating, refrigerating and air conditioning engineering and published a paper on cold storage system integrated with PCM.

THE POWER OUTPUT OF THE COMBINED CYCLE PLANT WITH OPTIMIZATION OF THE STEAM TURBINE EFFECT OUTPUT QUALITY

Lanka priyanka,
Assistant professor,
Department of Mechanical Engg.
Malla Reddy College of Engineering, secunderabad-500014
Email:- lohilakshmi.lakshmi@gmail.com

Nannoori swathi,
Assistant professor,
Department of Mechanical Engg.
Malla Reddy College of Engineering, secunderabad-500014
Email:-nannuriswathi4@gmail.com

Abstarct: **There is a thin hallway to a feasible arrangement going through the watchful strides to enhance the productivity of the (Resource Management) it gives earth cordial vitality. Warm power plants are more typical in many parts of vitality generation around the world. In this way, in this investigation ebb and flow explore and gave an exhaustive warm model framework consolidated cycle control plant with steam generator warm recuperation double weight. Since the nature of the yield of the steam turbine is highlighted prohibitive, and completed the improvement of three cases with various quality steam and talked about. In dissecting hand, exergy vitality and different segments of each of these three distinct cases evaluated and looked at. The outcomes demonstrate that it is truly imperative to keep up the nature of the steam turbine in a static port to 88% for the outcomes to be more reasonable, and enhanced information and practical and in fact suitable.**

I. INTRODUCTION

Energy is one of the main driving forces, helping to sustain human life. And it is available in various forms, for example, heat, light and electricity. Energy and won considerations on the economic and environmental impact much attention over the past three decades. Energy resources in the market and increasingly lower and higher prices with the progress of the industrial revolution. This is due to several terms reasons such growth of the world economy and depletion of energy resources, and environmental effects of production of this energy. Therefore, these energy issues now threatens many aspects of human life on this planet. existing concerns regarding the transfer of energy from thermal sources of electricity sources. In this sense, the central play a key role in the production of electricity. Among the different types of power plants and power plants combined cycle (CCPP) gained much attention due to the fact that is attractive in power generation due to high thermal efficiency instead of a gas turbine or steam energy individual plants. In addition, they are also important due to the relatively high energy efficiency, low emissions of pollutants and greenhouse gases, and operating Flexibility. The literature on this topic shows that several efforts optimal plant. And it is used to reduce energy consumption and improve annual earnings and other approaches. Unlike energy, exergy is a measure of energy efficiency that can be considered to assess, analyze and improve the system. Exergy analysis is used to determine the maximum system performance and determine its irreversibility. Therefore, the Exergy is a powerful tool for assessing the performance of the cycle, and is also one of the objectives usually went to the lack of studies of economic, technical and environmental viability. More recently, A set of tools as assessments of exergy, economic and environmental has received increasing attention throughout the term. Therefore, the way that considers all objectives, and offers a practical solution is currently required by the designers of the CCPP factory. In this regard, he conducted several studies [1-8] to investigate the combined cycle, but with some examples of multiple objectives of this plant, which represents the three main issues at one time would have made the best of our knowledge [2]. Exergy analysis is a useful tool to find the sites and the types and amounts of non-real efficiency (irreversibility) and suggest ways to improve overall system efficiency [2.9 to 12]. In the literature, there have been many studies associated exergy analysis of plants. Lior [13] proposed the concept of future power generation systems and the role of exergy analysis in its development. It illustrated some of the ideas to meet the demand for electricity in the light of the limitations of population growth and land use when the environmental impact of holding a bear. The following is Focus on Exergy, which will be essential in the design and development of this type of analysis operations. Finally discusses the surface modification is a generic term that is now applied to a large field of different techniques that can be used to achieve higher pay and improved performance reliability of industrial components. continuous quest to increase efficiency and productivity across the range of manufacturing and engineering industries has ensured that most modern components exposed to aggressive environments, are increasingly during a routine operation. So important it is the industrial components, and prone to more rapid deterioration as the parties could not withstand the rigors of harsh operating conditions and this has been taking huge losses to the economy of the industry. In a large overwhelming number of cases, there has been a rapid degradation tracking spare parts and ultimately failed to damage caused by harsh environments, as well as the high relative movement between the contact surfaces and corrosion media, and extreme heat and pressure League.

II. LITERATURE REVIEW

The objective of this literature review is to provide basic information on the topics to be discussed in this thesis, and emphasize the importance of this study. This treaty covers various aspects of ceramic tiles, with special reference to the characteristics of erosion wear.

Erosion of solid particles clothing materials solid particle erosion (SPE) is a typical situation where wear particles hitting against corrosion surfaces and increase the loss of material. During the particle momentum and trip takes kinetic energy that can be dissipated through impact, due to the interaction with the target surface. It is worth noting that the erosion of solid particles differs from other forms of corrosion, such as corrosive effect of liquid and semi-liquid erosion, cavitation erosion, etc. removal of material due to erosion of the solid particles is the result of a series of independent but basically similar effect events. Therefore, contact between the solid particles and the surface of a component is a very short period. From this point of view, and erosion is very different from other relevant documents such as sliding wear, abrasion, grinding and machining, where the connection between the tool / work piece abrasive and / goal is continuous processes.

In some cases, SPE is a useful phenomenon, as is the case in sandblast or water jet cutter with abrasive high speed, driving peening members fire patrol, cutting hard and brittle materials by aircraft war abrasive rock drilling [4-6], but it is a serious problem in many engineering systems, including aircraft steam turbine and piping and valves used in the transfer of the suspension of materials and combustion systems fluidized bed. Gas turbines and steam operating in environments where ingestion of solid particles is unavoidable. In industrial applications and power generation such as coal combustion boilers, turbines bed and fluidized gas, and solid particles are produced during the combustion of heavy oils, synthetic fuels, coal dust, etc., and cause erosion [23.24] which leads to damage of gas compressor Path, such as blades or vanes of the rotor components, resulting in gradual changes in surface finish, and engineering [25.26]. Similarly, the helicopter operating in the field of sand or dust generates a cloud of dust which is collected by the compressor leading to a progressive loss of minerals from each of the leading edges of the airfoils behind [27]. Therefore, erosion is expected to increasingly entrained solid particles in a gas or liquid medium that compromise the solid material at any speed. In both cases, the particles can be accelerated or slowed movement and orientation of the liquid can be changed. It faced the deterioration of materials due to erosion of the solid particles, either at room temperature or in a high temperature heat in a wide range of engineering industries

III. METHODOLOGY

Preparation of Substrates

Mild steel is the most common form of steel because its price is relatively low while it provides material properties that are acceptable for many applications. Low carbon steel contains approximately 0.05–0.15% carbon and mild steel contains 0.16–0.29% carbon; making it malleable and ductile, but it cannot be hardened by heat treatment. Mild steel has a relatively low tensile strength, but it is cheap and malleable; surface hardness can be increased through carburizing. It is often used when large quantities of steel are needed, for example as structural steel. The density of mild steel is approximately 7.85 g/cm^3 (7850 kg/m^3or 0.284 lb/in^3) and the Young's modulus is 210 GPa (30,000,000 psi).

Coating Material (Titania):

Titanium dioxide, also known as titanium(IV) oxide or titania, is the naturally occurring oxide of titanium, chemical formula TiO2. When used as a pigment, it is called titanium white, Pigment White 6, or CI 77891. Generally it comes in two different forms, rutile and anatase, Titanium dioxide occurs in nature as well-known minerals rutile, anatase and brookite. In this study, titania powder (procured from MERCEK Ltd.) are chosen as the raw materials for the deposition of coatings on substrates.

Driven by technological need and fuelled by exciting possibilities, novel methods for applying coatings, improvements in existing methods and new applications have proliferated in recent years. Surface modification technologies have grown rapidly, both in terms of finding better solutions and in the number of technology variants available, to offer a wide range of quality and cost. The significant increase in the availability of coating process of wide ranging complexity that are capable of depositing a plethora of coatings and handling components of diverse geometry today, ensures that components of all imaginable shape and size can be coated economically. Existing surface treatment and coating processes fall under three broad categories:

1. Overlay Coatings: This category incorporates a very wide variety of coating processes wherein a material different from the bulk is deposited on the substrate. The coating is distinct from the substrate in the as-coated condition and there exists a clear boundary at the substrate-coating interface. The adhesion of the coating to the substrate is a major issue in this process.

2. Diffusion Coatings: Chemical interaction of the coating-forming element(s) with the substrate by diffusion is involved in this category. New elements are diffused into the substrate surface, usually at elevated temperatures so that the composition and properties of outer layers are changed as compared to those of the bulk.

Thermal or Mechanical Modifications of Surfaces: In this case, the existing metallurgy of the component surface is changed in the near-surface region either by thermal or mechanical means, usually to increase its hardness

IV. RESULTS

Erosion wear characteristics of plasma sprayed 'titania' coatings have been investigated in this study following a plan of experiments based on the Taguchi technique which is used to acquire the erosion test data in a controlled way. This chapter reports the wear rates obtained from these erosion trials and presents a critical analysis of the test results. Further, erosion rate predictions following an ANN approach for different test conditions are presented. A correlation among various control factors influencing the erosion rate has also been proposed for predictive purpose. Possible wear mechanisms are identified from the scanning electron microscopy of the eroded surfaces.

Erosion Test Results and Taguchi Analysis

In Table 3.6, each of the columns, from second to fifth, represents a test parameter, whereas a row stands for a treatment or test condition, which is nothing but a combination of the parameter levels. The plan of the experiments is as follows: the second column is assigned to impact velocity (A), the third column to impingement angle (B), the fourth column to erodent size (C) and the fifth column to erodent temperature (D) respectively to estimate the erosion rate (Er).

V. CONCLUSION

This examination on strong molecule disintegration wear reaction of plasma showered titania coatings has prompted the accompanying particular conclusions:

Monetarily accessible titania is famously coat capable on mellow steel substrates utilizing barometrical plasma splashing method. Such coatings forces alluring covering qualities.

1. Solid molecule disintegration qualities of these coatings have been effectively examined utilizing Taguchi test outline. Huge control factors influencing the disintegration rate have been recognized through fruitful execution of this procedure. Effect speed, impingement edge and erodent measure in declining grouping are observed to be huge for limiting the disintegration rate of these coatings. Erodent temperature is distinguished as the slightest affecting control factor for disintegration rate.

2. All the coatings in this examination display fragile disintegration reaction with the pinnacle disintegration happening at typical effect (i.e. at 900 edge of impingement).

3. The utilization of a manufactured neural system model to reenact tries different things with parametric plan methodology is successful, productive and predicts the strong molecule disintegration reaction of such coatings under various test conditions inside and past the test space.

The test comes about help the capability of titania to be utilized as a wear safe covering material for testimony on gentle steel substrates.

REFERENCES

[1]. Bandopadhyaya P. P., (2000). *Processing and Characterization of Plasma Sprayed Ceramic Coatings on Steel Substrate*, Ph.D. Thesis, IIT, Kharagpur, India.

[2]. Taylor P. R., (2002). *Thermal Plasma Processing of Materials, Power Beamsand Materials Processing*, PBAMP 2002, Ed. A. K. Das et al., AlliedPublishers Pvt. Ltd., Mumbai, India, pp13-20.

[3]. Satapathy A., (2005). *Thermal Spray Coating of Red Mud on Metals*, Ph.D. Thesis, NIT, Rourkela, India.

[4]. Sundararajan G. and Roy M., (1997), *Solid particle erosion behaviour ofmetallic materials at room and elevated temperatures*, Trib. Int., v30 (5),pp339-359.

[5]. Finnie I. and Oh, H., (1966). *An analysis of rock drilling by erosion*, In: Proc. 1st Cong. Int. Soc. Rock Mech., Lisbon, v2, pp99–104.

[6]. Summers D. A., (1979). *Treatise on Materials Science and Technology* (Ed. Preece C.M.) Academic Press, New' York, v16, pp395

STUDY ON LIFECYCLE OF SOLAR PHOTOVOLTAICS POWER SYSTEMS

NAVEEN KUMAR K.L[1]
Assistant professor
Dept of mechanical engg
Malla reddy college of engineering
Email.naveen.nk45@gmail.com

Dr.VELMURUGAN.P[2]
Professor
Dept of mechanical engg
Malla reddy college of engineering
Email.velmurugan_mech@mrce.in

ABSTRACT

The usage of sun oriented vitality for power age – fundamentally through Solar PV – is blasting, without a doubt. Since 2000, the worldwide Solar PV industry has developed by around 45% every year all things considered, so introduced limit has been multiplying each a few years. All things being equal, Most places on earth get adequate daylight to make Solar PV an in fact reasonable alternative when combined with some type of vitality stockpiling. Life-cycle investigation is an important device for assessing the natural profile of an item or innovation from support to grave. Such life-cycle examination of vitality advancements are fundamental, particularly as material and vitality streams are frequently mixed, and disparate outflows into the earth may happen at various life-cycle-stages. sun oriented speaks to a little bit of aggregate worldwide power generation.The potential for the use of extra sunlight based vitality – and for sun based to assume an extensive part in worldwide vitality creation – is immense. the natural heap of photovoltaic power age framework (PV) amid its life cycle by vitality payback time (EPT) and Greenhouse Gas outflows are checked on through LCA concentrate to the condition of specialty of the photovoltaic innovations.

LITERATURE REVIEW

The investigation expands such examinations past the assembling stage and assesses the forthcoming support to-grave life-cycle effects of natural photograph voltaics contrasted and regular ones. Two frameworks (sun oriented housetop exhibit and compact sun powered charger) were outlined how extraordinary item incorporations, span of utilization and transfer courses influence potential natural benefits of natural photovoltaic while educating analysts on the prospects for proceeded with advancement and scaling-up this innovation.

The consequences of the life-cycle appraisal demonstrated that ecological benefits for natural photovoltaics stretch out past the make of the photovoltaic boards, with gauge support to-grave effects for both long haul utilizes (housetop clusters) and here and now utilizes (convenient chargers) by and large 55% and 70% lower than silicon gadgets, Evident vulnerabilities encompassing the OPV boards are the accepted lifetimes and efficiencies that will be accomplished at the mechanical scale. Expanding both are important to lessening the life-cycle effects of this innovation, however there is a non-straight relationship where increments in lifetimes and efficiencies brings about a lower rate of effects diminishments over the life-cycle. respectively(1).

Deciding the potential effect amid the entire existence of the framework, from crude materials supply to its finish of-life. The LCA has been completed by utilizing the LCA device created in the system of the International Energy Agency SHC Task. Results demonstrated that the valuable existence of the framework is a key parameter: for a helpful existence of 10 years, the traditional framework performs superior to anything the inexhaustible based one for every one of the areas. In any case, if a more drawn out life is accomplished (15 or 20 years), heavenly bodies indicate ecological preferred standpoint under all the climatic conditions: the natural benefits of utilizing a nearby planetary group amid the operation step balance the extra effect produced amid the other life-cycle steps(2).

The vitality examination technique turned out to be a solid approach for the assessment of the proficiency, viability and natural agreeableness of mechanical procedures under a worldwide scale point of view and may likely be connected to the PV examination as a supplement of customary vitality and monetary evaluations. Along these lines, this strategy was utilized as a part of this investigation to assess the manageability of a PV board reusing process. Moreover, his paper is intends to investigate the ramifications of methodological presumptions when Energy Accounting (EMA) handles squander administration frameworks, keeping in mind the end goal to address the weaknesses in this field Results unmistakably demonstrate that PV sun based power can be viewed as a develop innovation and can positively rival other sustainable and non-inexhaustible alternatives for power age. Be that as it may, proficiency enhancements of PV boards warm recuperation are as yet conceivable and may prompt further reduction of still too huge emergy expenses of the treatment procedure, not to discuss potential recuperation options, for example, concoction treatment for silicon cells and better upstream mechanical design(3).

sun oriented radiation has coordinate effect on techno-monetary and natural supportability of sun powered PV, consequently this innovation would be less appropriate for areas with less episode daylight. Albeit Northeast area does not profit by high sun powered irradiance, general supportability execution of sun oriented PV have all the earmarks of being fulfilling. Aside from diminishing carbon emanation and giving clean vitality to end clients, sun oriented PV can convey huge positive social effects to neighborhood groups, essentially however understanding fuel neediness which is very refreshing In any case, because of its high dependence on sponsorship and generally high capital speculation required, financing troubles had set up loads for arrangement of this innovation. Also, it should be noticed that unless substantial size of sun based PV establishment will occur, business openings produced by sun oriented PV is fairly limited(4).

The negative effect of clean amassing on photovoltaic boards suggests a drop in vitality efficiency of photovoltaic modules and in this way a decline of the relating vitality yield. Utilizing broad and nitty gritty true estimations, it is presumed that the normal power yield of any photovoltaic power plant is to a great extent influenced by the aggregation of tidy, particularly overlong eras. In the event that this influence is disregarded, it is nearly definite that solid contrast will show up between the genuine and the assessed vitality yield of these power frameworks.The clean thickness and size appropriation of airborne particles and fibers have been additionally examined and measured by an exceptionally delicate pressurized canned products measuring framework. The tidied module and another comparative clean module have been then presented to steady radiation and consistent temperature utilizing a sun oriented test system as light source. The affidavit of the tidy on the surface of the photovoltaic sun oriented modules demonstrated a lessening in both the short out current (Isc) and the yield control contrasted with similar parameters of the clean module(5).

Exemplification of PSC gadgets utilizing fantastic obstruction materials and basic epitome designs can significantly expand their lifetime under surrounding stockpiling conditions. Ca film tests showed the significant part of dampness/oxygen entrance by means of glue layers and around inserted electrical wire contacts, featuring the requirement for advance changes in embodiment designs to accomplish PSC lifetimes that meet business end-utilize prerequisites. Impedance spectroscopy estimations on non-typified PSC gadgets demonstrate that their inner protection increments amid presentation to surrounding dampness and oxygen conditions recommending that the loss of gadget execution is related with the arrangement of more resistive interfaces inside the gadget. These preparatory outcomes show the potential utility of impedance spectroscopy in explaining the debasement instrument of perovskite gadgets, and further investigations are in progress to better comprehend the corruption procedures of PSC devices(6).

Photovoltaic framework is an innovation for the generation of power from sustainable sources that is quickly developing on account of its capability to diminish the vitality utilization from customary sources and to diminish the air contamination. Amid the operational stage, there are no emanations and the main information is sunlight based power. Notwithstanding, it ought to be noticed that, considering the whole life cycle of a plant, photovoltaic frameworks, similar to some other methods for power creation, offer ascent to emanations that concentration particularly in the assembling stage and establishment of segments. In this examination, the natural heap of photovoltaic power age framework (PV) amid its life cycle by vitality payback time (EPT) and Greenhouse Gas emanations are evaluated through LCA concentrate to the condition of craft of the photovoltaic technologies(7).

The assessment of various parameters from an existence cycle point of view that influence environmental change alleviation. The essential goals are to evaluate the distinctive life cycle consequences for coming about ozone harming substance (GHG) outflows for power delivered by mc-Si boards for network associated frameworks . The investigation considers the impacts of vitality productivity measures, area of generation, establishment, building-incorporated alternatives, and climatic impacts. An existence cycle appraisal recommended that monocrystalline boards can create power with roughly ten times less GHG discharges than normal power blend. The consideration of building-coordinated applications lessens the life cycle affect much further by a factor of 3. With potential for critical GHG emanation decreases, mc-Si PV matrix associated power creation can fill in as a conceivable environmental change moderation technique [(8)].

The finish of-life phase of PV boards for the most part happens following 20 to 30 years of operation. This is because of the age ability of the boards diminishing over the long run; for the most part following 20 years they have debased to 80% of their unique rating. Notwithstanding, being a generally new industry this has not been completely tried. Every innovation sort has materials that can be reused so reusing the boards is a choice. Procedures to disassemble and recoup the materials of all board sorts have been produced over different scales[(9)].

PV modules are vigorously and ecologically exceptionally costly components. The vitality pay-back time (EPBT) was observed to be 1.85 years and the standardized ozone harming substance (GHG) outflows was assessed as 55.7 g-CO2/kW. These outcomes have additionally been contrasted and the other SPV power age systems[(10)].

Amid these stages, commotion and visual interruption, ozone harming substance outflows, water and soil contamination, vitality utilization, work mischances, affect on archeological destinations or on touchy biological communities, negative and positive financial impacts were measured. Research on the reusing of photovoltaic boards and assembling waste improves the recuperation of glass, cadmium and tellurium while limiting the life-cycle outflows and vitality utilize were contemplated by Fthenakis et al. in 2006. Amid that review, the recuperation of these things is the thing that makes the fabricate of photovoltaic modules more efficient as these things could be reused for future activities. An article by Tsoutsos, Frantzeskaki and Gekas (2005)[(11)].

Fast development of the volume of waste from PV cells is normal in the next years. The issue of its utilization seems to be themos timportant issue for future waste management systems.The examination depends on the LCA approach and the normal information accessible in particular databases for silicon standard PV cell is utilized. The practical unit incorporates parameters like: efficiency, sythesis, surface range. The exchange on the natural effect change because of the area of the PV creation and waste preparing plants is displayed The investigation of the PV cell life cycle situation exhibited in the article was performed utilizing the SIMAPRO programming and information from Eco concoct 3.0 database together with extra information got from other sources(12).

His expressed examination of the effect of dynamic changes in irradiance and temperature on the execution of various PV cell advances. The examination is planned to give important data about the reaction of three diverse PV cell innovations, for example, monocrystalline, multicrystalline and thin film modules to various air conditions and the investigation is completed by Sandia gauges. It is watched that all the three PV advances responded distinctively to various irradiance and temperature conditions, which thus impacted their vitality output(13).

Fast increment in the sending of photovoltaic establishments since the start of the century has prompted the worldwide limit surpassing 220GW expanding arrangement rates will prompt extensive volumes of waste photovoltaic modules later on and substantial volumes of decommissioned boards can be normal by the center of this century. Efficient end-of-life medicines will be expected to recoup important parts. Perovskite sun based cells were first announced a large portion of 10 years back and upgrades in efficiency of research facility scale gadgets have been accomplished at an exceptional pace. This Perspective talks about some essential natural, administrative, and down to earth viewpoints possibly emerging toward the finish of life of decommissioned perovskite sun oriented cells. With expanding PV organization rates, coming about waste volumes can be anticipated with a 20-to 30-year slack (14).

The objective of this investigation was to assess the ecological effects of vacuum, arrangement, and sans htlperovskite sun powered cell gadgets utilizing creation approaches that are amiable to huge scale fabricating. A correlation of natural effects was made with mono-Si as a kind of perspective point. We found that assembling of perovskite sun oriented modules causes 10– 30% lower impacts than assembling mono-Si PV. Be that as it may, if perovskite cells were to enter the market, their ecological effects would be higher than those of all business PV advancements predominantly in view of their shorter lifetimes. Monte Carlo investigation changing lifetime and efficiencies of perovskite cells demonstrated that sans htl structure could perform equivalent or superior to mono-Si cells with around 55% aggregate likelihood (15).

The impact of tidy on the execution of the half and half PV/warm authority was tentatively considered. The layer of the clean on the external surface of authority is diminishing the warm and electrical efficiency because of diminishing in the power of sunlight based radiation. The outlet air temperature achieved its most extreme incentive at 12 p. m. and after that dropped as a result of the diminishment in ingested radiation and increment in warm misfortunes. The outcomes demonstrated the warm efficiency diminished 13.4% if there should be an occurrence of clean presence on the external surface of gatherer.

Likewise, the most elevated electrical efficiency if there should arise an occurrence of clean authority was 10.24 % (16).

REFERENCES

1. Michael P. Tsanga, Guido W. Sonnemanna, Dario M. Bassani , “Life-cycle assessment of cradle-to-grave opportunities and environmental impacts of organic photovoltaic solar panels compared to conventional technologies” April 2016
2. Sonia Longo, Valeria Palombab, Marco Beccalia, Maurizio Celluraa, Salvatore Vasta, “Energy balance and life cycle assessment of small size residential solar heating and cooling systems equipped with adsorption chillers”year 2017
3. Corcelli F, RipaM ,Ulgiati S, ”End-of-life treatment of crystalline silicon photovoltaic panels. An emergy-based case study”. Year 2017
4. Tianqi Li, Anthony Paul Roskilly, Yaodong Wan “A Regional Life Cycle Sustainability Assessment Approach and its Application on Solar Photovoltaic” ICAE2016
5. MotasemSaidan , Abdul GhaniAlbaali , Emil Alasis , John K. Kaldellis, “Experimental study on the effect of dust deposition on solar photovoltaic panels in desert environment” year 2016
6. Hasitha C. Weerasinghea, YasminaDkhissi, Andrew D. Scullya, Rachel A. Carusoa, Yi-Bing Cheng, “Encapsulation for improving the lifetime oQ2 f flexible perovskite solar cells” October 2015
7. VishakhaBaharwani, NeetuMeena, AlkaDubey, Urmila Brighu4 and Jyotirmay Mathur5 “Life Cycle Analysis of Solar PV System: A Review” Volume 4, Number 2 (2014)
8. Noah Kittner, Shabbir H. Gheewala, and Richard Kamens, ‚"Life Cycle Considerations for Monocrystalline Photovoltaics in Thailand" year-2012
9. Author Luke Schwartfeger and Allan Miller “Environmental Aspects Of Photovoltaic Solar Power” year-2015
10. A. F. Sherwani, J. A. Usmani, Varun, Siddhartha “Life cycle assessment of 50 Kwp grid connected solar photovoltaic (SPV) system in India” year- 2011
11. Karen, Ann Brouwer, Chhaya Gupta, Shelton Honda, MahshadZargarian, “Methods And Concerns For Disposal Of Photovoltaic Solar Panels” year-2011
12. M. Bogackat, K. Pikon ́, M. Landrat,‚"Environmental impact of PV cell waste scenario”in year 2017
13. Premalatha L, Rahim N , “The Effect of Dynamic Weather Conditions on Three Types of PV Cell Technologies – A Comparative Analysis” year- 2017
14. Jeannette M. Kadro1 and Anders Hagfeldt1, “The End-of-Life of Perovskite PV” cell press
15. IlkeCelika, Zhaoning Song, Alexander J. Cimaroli, Yanfa Yan, Michael J. Heben, DefneApul,‚"Life Cycle Assessment (LCA) of perovskite PV cells projected from lab to fab”year-2017
16. Omer Khalil Ahmed, Zala Aziz Mohammed,‚"Dust effect on the performance of the hybrid PV/Thermal collector”year-2017.

DESIGN AND ANALYSIS OF STEAM BOILER USED IN THERMAL POWER PLANTS

Pranav Sarasan
M.tech Student
Department of Mechanical Engineering,
Mallareddy College of Engineering,
Email ID: pranavsamer@gmail.com

Maddineni Suresh Babu, M.Tech
Assistant Professor
Department of Mechanical Engineering,
Mallareddy College of Engineering,
Email ID: suresh4you247@gmail.com

Dr.P.Velmurgan, Ph.D
Professor
Department of Mechanical Engineering,
Mallareddy College of Engineering,
Email ID: velmurgan_mech@mrce.in

ABSTRACT

Steam boiler is a shut vessel in which water or other liquid is warmed under pressure and the steam discharged out is utilized for various warming applications. The primary contemplations of an boiler for a specific application are Thermal outline and investigation, Design for fabricate, physical size and cost.

In this postulation the steam stream in steam boiler tube is demonstrated utilizing PRO-E outline programming. The proposal worries with the warm and electronic liquid elements (CFD) investigation with various speeds. Warm examination is done for the steam boiler by steel, stainless steel& brass at various heat exchange coefficient esteems. These heat exchange coefficient esteems are taken from CFD investigation at various speeds.

In this postulation the CFD examination is utilized to decide the warmth exchange coefficient(h), warm or heat exchange rate(Q), mass stream rate(m), pressure drop(p). The thermal examination is utilized to decide the temperature dissemination and warmth transition for various materials. Here the 3D displaying is done in parametric programming Pro-Engineer and examination is done in ANSYS programming.

I. INTRODUCTION

STEAM BOILER: Steam boilers heat water to produce steam, which is then used to generate energy or heat for other processes.

Boilers are utilized to produce steam that at that point gives warmth or power. Water is changed over to steam in the evaporator. This steam goes through the warming device which can be any bit of hardware that requires steam for operation. The cooled steam is then consolidated into water and comes back to the kettle to begin the cycle once more.

Boilers are generally classified in to 2 types, they are

- fire tube boilers
- water tube boilers.

In Fire tube boiler, the hot gasses goes through number of tubes and water surrounds these tubes.

In water tube boiler, the water warmed inside and hot gasses encompass these tubes.

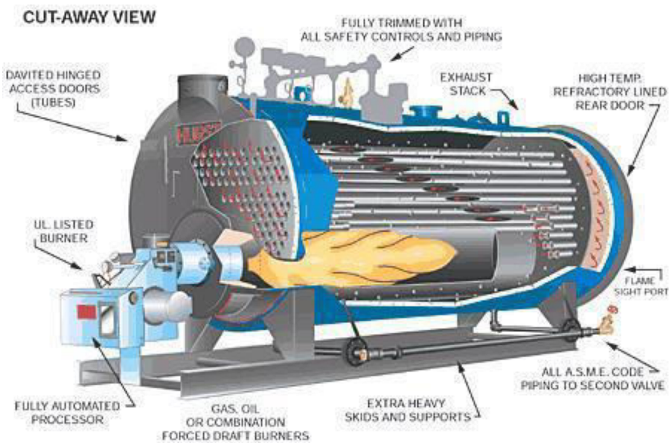

Figure 1 - FIRE TUBE BOILER

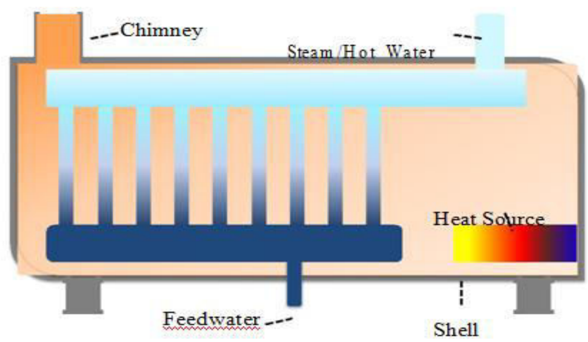

Figure 2 - WATER TUBE BOILER

II. MODELLING AND MESHING

The target of this venture is to influence a 3D to model of the steam evaporator and think about the CFD and warm conduct of the steam kettle by playing out the limited component analysis.3D demonstrating programming PRO-Engineer is utilized for planning and investigation programming (ANSYS) was utilized for CFD and warm examination.

The approach followed in the venture as takes after:

- Create a 3D model of the steam Boiler get together utilizing parametric programming genius build.
- Convert the surface model into Para strong document and import the model into ANSYS to do examination.
- Perform CFD investigation on the current model of the surface steam evaporator for Velocity bay to discover the mass stream rate, warm exchange rate, weight drop.
- Perform warm examination on the steam Boiler get together for warm loads.

PC helped outline (CAD), is likewise called as PC supported plan and drafting (CADD), is the utilization of PC devices for the procedure of plan and outline documentation. PC Aided Drafting clarify the technique for drafting with a PC. CADD programming offer the client with input-apparatuses for the working of streamlining configuration forms; drafting, documentation, and assembling forms. CADD yield is for the most part as electronic documents for printing or machining operations. The improvement of CADD-based programming is in straight relationship with the procedures it looks to conserve; industry-based programming (development, producing, and so forth.) normally utilizes vector-based (direct) situations while realistic based programming use raster-based (pixilated) conditions.

CADD conditions frequently draw in something beyond shapes. All through drafting of building or specialized illustrations, the yield of CAD ought to propose data, for example, forms, measurements ,materials and resistances, as indicated by application-particular tradition.

Computer aided design can be utilized to configuration bends and figures in two-dimensional (2D) space; or bends, surfaces, and solids in three-dimensional (3D) objects.

This product is usually utilized as a part of numerous applications, for example, aviation ventures, modern, car, shipbuilding and building plan, prosthetics, and so forth. Computer aided design is besides generally used to make PC liveliness for enhancements in films, publicizing and specialized manuals. The present universality and matchless quality of PCs implies that even aroma containers and cleanser allocator are composed utilizing methods incomprehensible by architects of the 1960s. Since of its immense financial significance, CAD has been a noteworthy main impetus for explore in computational geometry, PC designs (both equipment and programming), and discrete differential geometry.

The making of substance shape utilizing geometrical outline, by and large, is called PC supported geometric plan (CAGD).

Late PC helped outline programming bundles fluctuate from 2D vector-based drafting frameworks to 3D strong and surface modelers. Late CAD can typically permit revolutions in three measurements, permitting introduction of an outlined protest from any coveted edge, even from within watching out. A couple of CAD programming is equipped for dynamic mathematic demonstrating, in which case it might be advertised as CADD — PC supported plan and drafting.

This product is predominantly utilized for making apparatus ,devices, , outline and drafting of various sorts of structures, from little private sorts (houses) to the biggest business and modern structures (healing centers and industrial facilities).

It is essentially utilized for finish building of 3D models or potentially 2D illustrations of physical parts, however it is additionally utilized everywhere throughout the building procedure from theoretical plan and game plan of items, through quality and dynamic investigation of congregations to portrayal of assembling strategies for segments. It can likewise be utilized to configuration objects.

PTC CREO, already known as Pro/ENGINEER, is 3D demonstrating programming utilized as a part of mechanical building, assembling, outline, and in CAD drafting administration firm. It was the initial 3D CAD displaying applications that utilized an administer based parametric framework. Utilizing parameters, measurements and highlights to catch the conduct of the item, it can advance the improvement item and the outline itself. The name was changed in 2010 from Pro/ENGINEER Wildfire to CREO. Its name was given by the partnership who set up, Parametric Technology Company (PTC), amid the dispatch of its gathering of outline items that incorporate applications, for example, show amassing, 2D orthographic perspectives for specialized illustration, limited component investigation and that's only the tip of the iceberg.

PTC CREO says it can offer a more effective plan understanding than other demonstrating programming in view of its remarkable highlights including the joining of parametric and direct displaying in one stage. The total suite of uses traverses the range of item advancement, giving fashioners alternatives to use in each progression of the procedure. The product likewise has a more easy to use interface that gives a superior ordeal to creators. It likewise has community oriented limits that make it simple to share plans and roll out improvements.

There are incalculable advantages to utilizing PTC CREO. We'll investigate them in this two-section arrangement. In the first place up, the greatest preferred standpoint is expanded profitability on account of its proficient and adaptable outline abilities. It was intended to be less demanding to utilize and have highlights that take into consideration configuration procedures to move all the more rapidly, influencing a planner's efficiency to level increment.

Some portion of the reason profitability can be expanded is on account of the bundle offers devices for all periods of advancement, from the earliest starting point stages to the hands-on creation and assembling. Last stage changes are normal in outline strategies, yet PTC CREO can deal with it. Changes should be possible that are reflected in different parts of the procedure.

The community oriented capacity of the product additionally makes it less demanding and speedier to utilize. One reason it can process data all the more rapidly is a direct result of the interface amongst MCAD and ECAD outlines. Plans can be adjusted and featured between the electrical and mechanical originators taking a shot at the venture.

The time spared by utilizing PTC CREO isn't the main preferred standpoint. It has numerous methods for sparing expenses. For example, the cost of making another item can be brought down in light of the fact that the advancement procedure is abbreviated because of the mechanization of the era of acquainted assembling and administration expectations.

PTC likewise offers thorough preparing on the most proficient method to utilize the product. This can spare organizations by disposing of the need to enlist new workers. Their preparation program is accessible on the web and face to face, however materials are accessible to get to anytime.A remarkable component is that the product is accessible in 10 dialects. PTC knows they have individuals from everywhere throughout the world utilizing their product, so they offer it in different dialects so about any individual who needs to utilize it can do as such.

Models of steam boiler utilizing genius e rapidly spreading fire 5.0.The steam evaporator is demonstrated utilizing the given particulars and plan recipe from information book. The isometric perspective of steam kettle is appeared in underneath figure. The steam kettle external packaging body profile is outlined in sketcher and after that it is rotated up to 3600 edge utilizing spin choice and tubes are composed and collect to in steam evaporator utilizing expel choice.

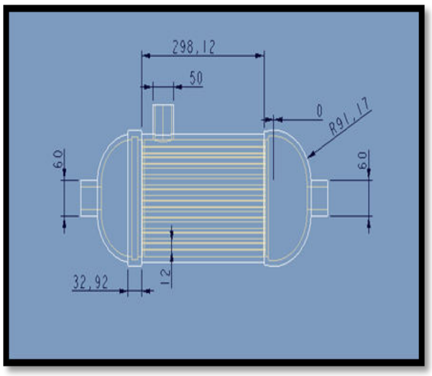

Figure 3 STEAM BOILER 2D MODEL

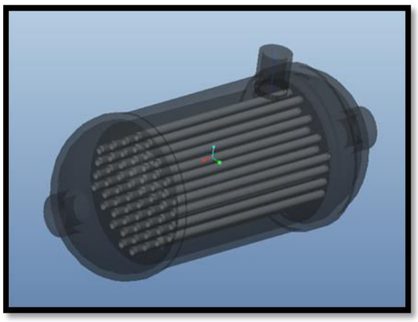

Figure 4 STEAM BOILER 3D MODEL

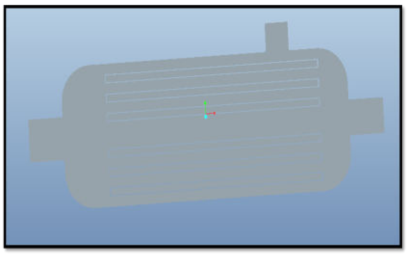

Figure 5 STEAM BOILER SURFACE MODEL

After designing the model, the cfd and thermal analysis can be carried outin ansys software.The CFD analysis is done by varying the inlet velocities of the steam in the boiler , for that importing the previously designed model.

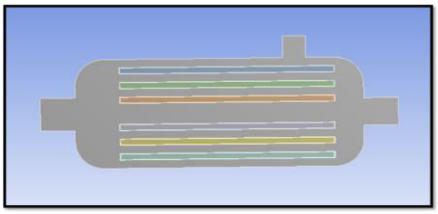

Figure 6 IMPORTED MODEL

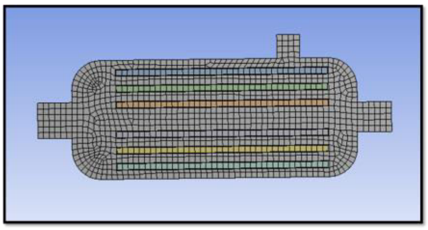

Figure 7 MESHED MODEL

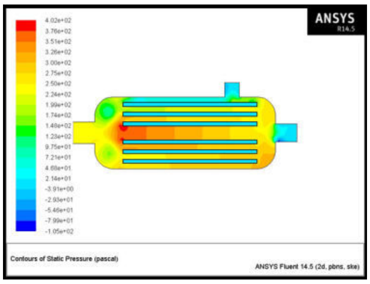

Figure 8 PRESSURE DISTRIBUTION

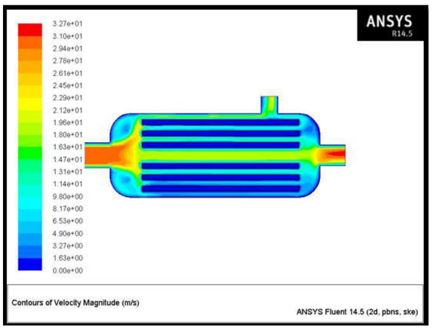

Figure 9 VELOCITY DISTRIBUTION

CFD examination is utilized to decide the heat exchange coefficient(h), warm or heat exchange rate(Q), mass stream rate(m), pressure drop(p).

The thermal examination is utilized to decide the temperature dissemination and warmth transition for various materials. In thermal analysis, the copper material for tube is kept constant. Steel, stainless steel and brass material are taken for boiler casing for finding the better material for the casing at different velocity conditions and different values of heat transfer coefficients taken out from the CFD analysis.

COPPER material properties

Thermal conductivity = 385w/m-k

Specific heat = 0.385j/g^{0}C

Density = 0.00000776kg/mm^3

STEEL material properties

Thermal conductivity = 93.0w/m-k

Specific heat = 0.669j/g^{0}C

Density = 0.0000075kg/mm^3

STAINLESS STEEL material properties

Thermal conductivity = 34.3w/m-k

Specific heat = 0.620j/g^{0}C

Density = 0.00000901kg/mm^3

BRASS material properties

Thermal conductivity = 233w/m-k

Specific heat = 0.380j/g^{0}C

Density = 0.00000760kg/mm^3

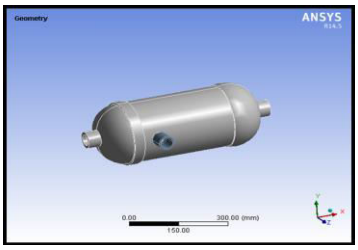

Figure 10 IMPORTED MODEL

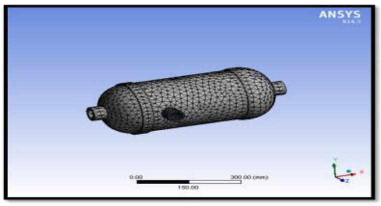

Figure 11 MESHED MODEL

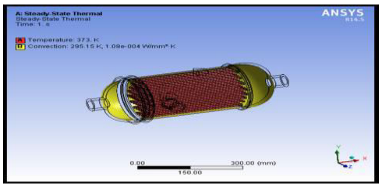

Figure 12 BOUNDARY CONDITIONS

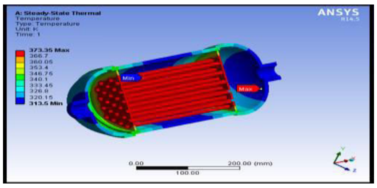

Figure13 TEMPERATURE DISTRIBUTION

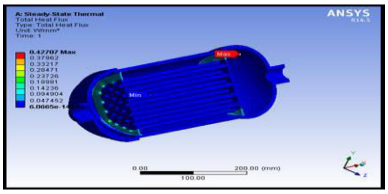

Figure14 HEAT FLUX

III. RESULTS AND DISCUSSIONS

CFD ANALYSIS RESULT TABLE

Velocity (m/s)	Pressure(Pa)	Velocity (m/s)	Heat transfer co-efficient (w/m^2-k)	Mass flow rate (kg/s)	Heat transfer Rate(W)
25	2.79e+02	2.73e+01	7.49e+01	0.0069018	1646.2891
30	4.02e+02	3.27e+01	8.66e+01	0.005703	1511.3906
35	5.47e+02	3.82e+01	9.83e+01	0.010582	2394.7773
40	7.13e+02	4.37e+01	1.09e+02	0.01201278	2719.8281

THERMAL ANALYSIS RESULT TABLE

Heat transfer coefficient (w/m^2-k)	result	Materials		
		steel	Stainless steel	brass
7.49e+01	Temperature(^{0}C)	373.35	373.48	373.26
	Heat flux(w/mm^2)	0.42707	0.17094	0.56179
8.66e+01	Temperature(^{0}C)	373.37	373.49	373.27
	Heat flux(w/mm^2)	0.45156	0.17639	0.60463
9.83e+01	Temperature(^{0}C)	373.39	373.5	373.29
	Heat flux(w/mm^2)	0.47265	0.18108	0.64226
1.09e+02	Temperature(^{0}C)	373.4	373.51	373.3
	Heat flux(w/mm^2)	0.4896	0.18485	0.67298

IV. CONCLUSION

In this postulation the steam stream in steam boiler tubes is demonstrated utilizing PRO-E outline programming. The proposition will concentrate on thermal and CFD investigation with various speeds (25, 30, 35& 40m/s). Warm investigation improved the situation the steam evaporator by steel, stainless steel and metal at various warmth exchange coefficient esteems. These qualities are taken from CFD investigation at various speeds. By watching the CFD investigation the pressure drop, speed, heat exchange coefficient, mass stream rate and heat exchange rate increments by expanding the channel velocities.

In thermal investigation, by taking diverse heat exchange coefficient esteems from CFD examination, It is observed that the Heat flux esteem is more for brass material than steel& stainless steel. We realize that heat transition is positive for the steam boilers utilizing as a part of energy plants. The productivity and execution of a steam evaporator is nearly relying on the estimation of heat flow. So we can reason that brass is the better material for a steam boiler utilized as a part of power plants than stainless steel and steel.

REFERENCES

1. Finite Element Analysis of Steam Boiler Used In Power Plants 1M. Suri Babu, 2 Dr.B.Subbaratnam 1M.Tech understudy, 2Professor, Dept of Mechanical Engineering, Kits, Markapur, A.P, India.
2. Structural and warm investigation of an evaporator utilizing limited component Analysis by D.Kondayya Department of Mechanical Engineering, Author Correspondence: Department of Mechancal Engineering, Sreenidhi Institute of Science and Technology, Ghatkesar, Hyderabad – 501301.
3. Analysis of New Boiler Technologies Dr Mike Inkson
4. A Study Analysis and Performance of High Pressure Boilers With its Accessories J. Suresh babu1,R.Latha2 ,B.Praveen3,V.Anil kumar4,R Rama kumar5,s.peerulla6 1 Assistant Professor in MED, K.S.R.M College of building, AP, India 2 3 4 5 6 Student, mechanical office, K.S.R.M College of designing, AP, India
5. Design and investigation of the model of evaporator for steam weight control 1Akanksha Bhoursae, 2 Jalpa Shah, 3Nishith Bhatt Institute of Technology, Nirma University, SG thruway, Ahmedabad-382481,India 3Essar steels limited,Hazira,Surat-394270,India
6. Lou Roussinos, P. E., "Heater Design and Efficiency" [online], Available: http://www.forestprod.org/drying06williamson .pd f, Accessed: September 1, 2010.
7. Murdock, K. L., "3ds max 9 Bible, Wiley Publishing Inc. Indianapolis, Indiana, 2007.
8. Nagpal, G. R., 1998, Power Plant Engineering, Khanna, Delhi.
9. Steam Pressure Reduction: Opportunities and Issues by U.S Deportment of vitality,
10. Rapid Start up Analysis of a Natural Circulation HRSG Boiler with a Vertical Steam Separator Design by M.J. Albrecht, W.A. Arnold, R. Jain and J.G. DeVitto,
11. Technological examinations and productivity investigation of a steam warm trade condenser:
12. Conceptual plan of a cross breed steam condenser by R K Kapooria and S kumar,
13. Developmental plan of a research facility fire tube Steam evaporator by I. O. OHIJEAGBON,
14. Steam boilers – care and operation by Robert. H. Kuss
15. Industrial boilers and warmth recuperation steam generators by V.Ganapathy

Study of Power Generation from Sewage Water

V.Veeranagulu
Assistant professor
Malla Reddy College of Engineering
Hyderabad, India
veeranagulu01@gmail.com

Y.Shailaja
Assistant professor
Malla Reddy College of Engineering
Hyderabad, India
shailajayarlagadda@gmail.com

Abstract—**This study is concerned with the feasibility of power generation using a hydraulic turbine from sewage flowing in pipes. This study indicates that the connection point have hydraulic potential that can be used for power generation throughout the year. It also demonstrates that the hydraulic turbine can be usefully employed for power generation from sewage flowing in the pipe at the connection points.**

Keywords—Hydraulic turbine, Sewage Power generation, Connection point, Hydraulic potential.

I. INTRODUCTION

Sewage is composed of rainwater and water discharged into sewers by humans and production activities. The sewer system contains wastewater and human waste from houses, offices, and factories. The approximate amount of wastewater generation is about 1800 MLD (Million Liters per Day). However, only 715 MLD of the wastewater can be treated. That's why most of the water is discharged into several lakes or the dry river bed of old Musi-River.

Hussain Sagar Sewage facilities comprise drainage facilities such as sewage pipes, treatment facilities such as treatment plants, and complementary facilities such as pump stations. The above mentioned estimation of the hydraulic energy potential seems to be restricted to the treated water discharged from treatment facilities

It is presumed that hydraulic energy potential is dispersed in sewage pipes around the city. Consequently, the utilization of sewage flowing in drainage facilities (sewage pipes) for power generation promises to realize small-scale distributed power generation, which could contribute to the local production of electric power for local consumption. However, such sewage power generation has never been conducted, and the hydraulic energy potential in the drain- age facilities has not yet been investigated.

In Telangana, hydropower is also receiving much attention because it is a promising renewable energy resource that is largely unaffected by the weather. As large-scale hydroelectric plants having outputs of more than 100 MW require huge dams and long conduits, few locations for such plants remain undeveloped. Thus, there is an increasing desire to realize micro-scale hydraulic power generation with an output of less than 100 kW. Such power generation can utilize small-scale hydropower, which is widely distributed in small rivers and irrigation canals in Telangana. Consequently, several small-scale hydraulic turbines have been developed. Such micro-hydraulic turbines are frequently blocked with foreign matter such as fallen leaves, twigs, and refuse and they occasionally lose their function. A filter installed upstream of the micro-hydraulic turbine can remove the foreign matter. However, such equipment increases the operation cost of micro-hydraulic turbines. We are engaged in the development of a hydraulic turbine with excellent performance in the passage of foreign matter. The runner has a circular hollow around the central axis so that foreign matter can pass through the runner. The efficiency and foreign matter passage performance of this hollow hydraulic turbine are being studied through laboratory experiments and demonstration experiments in a small river. Sewage contains hair and vegetable waste from home bath-rooms and kitchens, as well as human waste. To successfully generate power from sewage, it is essential that the hydraulic turbine is not blocked by foreign matter. Therefore, the hollow hydraulic turbine we are developing promises to be effective for sewage power generation applications.

The objective of this study is to search for possible hydraulic power generation from the sewage flowing in pipes. First, the present study focuses on the Hyderabad Sewerage water; it explores the sewage flow rate at the connection points over the course of a year to clarify the hydraulic energy potential of the sewage. Second, this study investigates the efficiency and foreign matter passage performance of the hollow hydraulic turbine in laboratory experiments that suppose the turbine to be installed in the sewage pipe at the connection points.

1. Flow duration and hydraulic potential of Hyderabad Sewerage

Outline of Hyderabad Sewerage

The Hyderabad Sewerage area is about 54 km2, the population is about 9,489,000, the approximate amount of wastewater generation is about 1800 MLD (Million Liters per Day) and the treatment capacity is 715 MLD.

Table 1: Reduction of E. Coli bacteria colonies in different STP`s

Sewage treatment plant	Inlet (cfu/ml)	Outlet (cfu/ml)	Reduction %
Amberpet	545	200	63
Malhapur	210	110	48
Kukatpalli	310	220	31

The Hyderabad Sewerage water is connected with public sewerage systems managed by HMWSSB. The connected part is called the connection point.

Flow duration at connection points

When constructing a hydraulic power plant, the daily mean water flow rate is measured in advance at the construction site over the course of a year to accurately estimate the power out-put. By arranging the daily mean water flow rates in descending order, a flow duration curve is constructed.

As the Hyderabad Sewerage water is a separated sewer system, only the sewage should flow in the sewage pipe; however, so-called "uncertain water," such as rainwater, is also considered to flow with the sewage in the pipe. The distance between the observation point and the connection point, Hussain Sagar, is about 7 km. In the months when precipitation is high, the sewage flow rate is also high. This trend is most marked in July and August. The reason that the maximum sewage flow rate is much higher than the mean, and fluctuates markedly, is that rainwater also flows in the sewage pipe. The mean and minimum flow rates are almost the same, but the maximum flow rate is much higher in July, August, September, and October. This may also be caused by rainwater flowing in the sewage pipe. This observation further confirms that rainwater increases the sewage flow rate.

Hydraulic potential at connection points

The hydraulic potential of fluid flowing with velocity u, that is,

P, is expressed as $P = \frac{1}{2} \rho Q u^2$

Where, ρ is the fluid density and Q is the flow rate.

The above mentioned hydraulic potential P can be converted to electric power by a generator driven by a hydraulic turbine. Considering the efficiencies of the generator and the hydraulic turbine, the electric power is evaluated to be $0.2P$. The electric power at the connection point at Hussain Sagar theoretically is 240 W. These values are assumed to remain unchanged throughout the year, because the change in the sewage flow rate is small. The power consumption of a ventilating fan with a diameter of around 250 mm is about 25 W, and that of an LED light bulb whose luminance is equivalent to a fluorescent lamp of 60 W is about 10 W. Thus, the electric power generated from the sewage can be used for ventilation and illumination at the connection points.

2. Hollow hydraulic turbine

A hydraulic turbine is needed to convert the hydraulic potential at the connection points into electric power. The sewage contains hair and vegetable waste from home bathrooms and kitchens, as well as human waste. Therefore, hydraulic turbines that will not be blocked by such foreign matter are urgently needed. Micro-hydraulic turbines, which can be installed in small rivers and irrigation canals for power generation, are frequently blocked by foreign matter, such as fallen leaves, twigs, and refuse. As such blockage causes a reduction in turbine performance; the development of a micro-hydraulic turbine with excellent foreign matter passage performance is desired. We are engaged in the development of a hydraulic turbine in which the runner has a circular hollow around the central axis so that foreign matter can pass through without blocking the hydraulic turbine. This hollow hydraulic turbine is considered to be useful for power generation from sewage. This study explores its applicability by means of laboratory experiments.

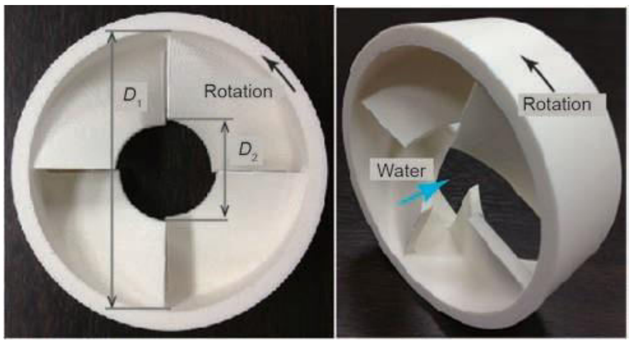

Fig. shows the cross-section of the hollow hydraulic turbine.

A circular pipe (hatched with red in the diagram) is inserted between two stationary pipes, with their axes on a line. The inserted pipe is supported by two bearings; thus, the pipe can rotate around the central axis. A runner (shown in blue in the diagram) is embedded within the inserted (rotational) pipe. When water flows in the pipe, the runner and the pipe rotate integrally around the axis. The inner diameter of the stationary and rotational pipes is 80 mm, and the axial length of the rotational pipe is 195 mm. A guide vane (shown in green) is mounted at the end of the stationary pipe, just upstream of the rotational pipe.

Fig. 8 shows an example of the runner. It has four blades, and a circular hollow is provided around the rotating (central) axis so that foreign matter included in the water can pass through the runner. The ratio of the hollow diameter D_2 to the pipe diameter D_1, which is 80 mm, is defined as the hollow ratio $\varepsilon = D_2/D_1$. The ε value for the runner is 0.375.

The runner is composed of a flat plate cascade. The width B is 23 mm, the thickness t is 5 mm, and the inlet and outlet angles, α_1 and α_2, respectively, are 70°. This study conducts pioneering experiments to explore the foreign matter passage performance of a hydraulic turbine. Since the runner is preliminarily designed in this study, the specifications could be modified to improve the performance.

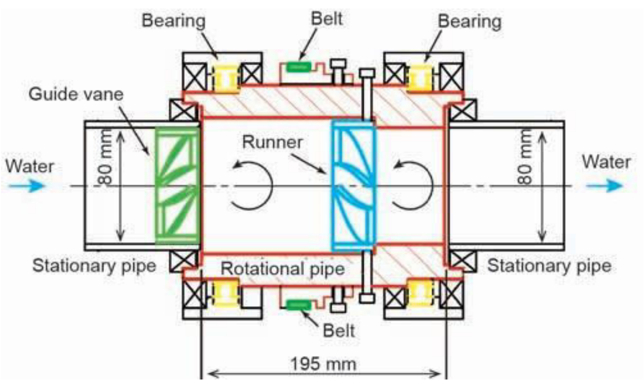

Cross-section of the hollow hydraulic turbine

3. Laboratory experiment with hollow micro-hydraulic turbine

Experimental method and conditions

To investigate the performance of the hydraulic turbine, laboratory experiments were conducted using the closed-loop test rig. Water in the tank is circulated by a pump and the circulated water drives the hydraulic turbine. The pipes upstream and downstream of the hydraulic turbine are made of transparent acrylic resin so that the behavior of foreign matter entrained in the loop can be observed. The pressures are measured at two points, 320 mm upstream and 183 mm downstream of the hydraulic turbine. The water flow rate is measured by a propeller-type flow meter mounted in a bypass pipe upstream of the pico-hydraulic turbine. To detect the turbine output, the torque is measured with a torque meter driven by the turbine. The rotational speed of the turbine, which is also measured by the torque meter, is controlled by a powder brake connected to the torque meter.

The efficiency of the hydraulic turbine, η, is defined as

$$n = T\omega / [Q (P - P)]$$

Where, T is the torque; ω is the angular velocity; Q is the flow rate; and $P1$ and $P2$ are the pressures upstream and downstream of the turbine, respectively.

Table
Blade specifications

	Value
Blade width B	23 mm
Blade thickness t	5 mm
Inlet angle α_1	70°
Outlet angle α_2	70°
Number of blades	4

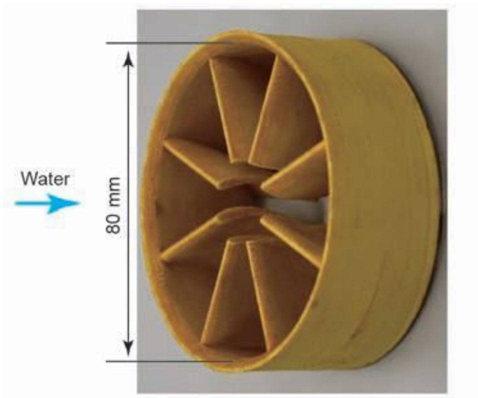

Guide vane with $\varepsilon = 0.25$.

This study investigates the turbine performance for four combinations of runners and guide vanes. The water flow rate Q is 0.01 $m^3 \cdot s^{-1}$.

To investigate the performance of the hydraulic turbine when installed in a sewage pipe under laboratory conditions, the foreign matter contained in sewage should be replaced with matter that is easily handled in the laboratory. The mass of solid matter included in 1 m^3 of domestic wastewater is estimated to be 0.2 kg, and 97% of human waste is considered to be moisture; thus, sewage is regarded as being almost all water. As the hair and fiber waste contained in sewage discharged from houses do not easily decompose, they flow down the sewage pipes.

There is concern that the micro-hydraulic turbine will be readily blocked by hair and waste. Therefore, this laboratory experiment used polyester fibers to simulate foreign matter in the sewage pipe. The diameter and mass of each spherically shaped fiber were about 20 mm and 0.2g, respectively. The fibers were released into the water from the outlet pipe of the tank, which was located upstream of the micro-hydraulic turbine. The time interval between the releases was 3 min.

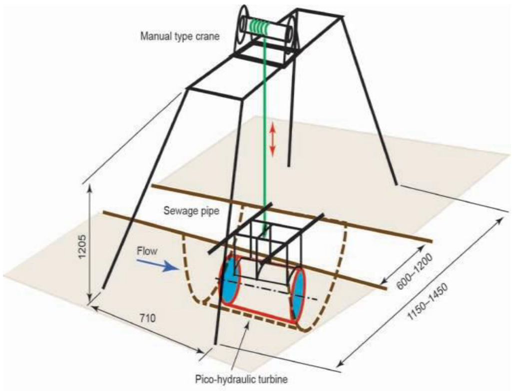

Install of hydraulic turbine in sewage pipe at connection point.

4. Conclusions

To search for possible micro-hydraulic power generation from sewage in pipes, the flow durations at connection point of the Hussain Sagar Sewerage were investigated, and the hydraulic potential of the sewage was estimated. The investigation indicates that the connection point at Hussain Sagar have hydraulic potential, which can be used for power generation throughout the year.

The efficiency and foreign matter passage performance of the hollow micro-hydraulic turbine were explored through laboratory experiments that supposed the micro-hydraulic turbine to be installed in the sewage pipe at the connection points. The exploration makes it clear that a runner with rounded blades and guide vanes with tapered blades can suppress the attachment of fibers to the micro-hydraulic turbine and, therefore, improve turbine efficiency. Consequently, it was found that the hollow micro-hydraulic turbine could be employed for power generation from sewage flowing in pipes.

A. References

[1] Japan Sewage Works Association. Wastewater works in Japan. Tokyo: Japan Sewage Works Association; 2015. Japanese.

[2] Systematization of resource/energy recycling [Internet]. Tokyo: Ministry of Land, Infrastructure, Transport and Tourism; c2008–16 [cited 2016 Apr 25]. Available from: http://www.mlit.go.jp/crd/sewerage/policy/09.html.

[3] Sato Y. Participatory irrigation management in Japan [Internet]. [cited 2016 Apr 25]. Available from: http://www.maff.go.jp/e/nousin/kaigai/inwepf/i_document/pdf/sympo_japan.pdf.

[4] Alexander KV, Giddens EP, Fuller AM. Axial-flow turbines for low head micro- hydro systems. Renew Energ 2009;34(1):35–47.

[5] Ikeda T, Iio S, Tatsuno K. Performance of nano-hydraulic turbine utilizing wa- terfalls. Renew Energ 2010;35(1):293–300.

[6] Singh P, Nestmann F. Experimental investigation of the influence of blade height and blade number on the performance of low head axial flow turbines. Renew Energ 2011;36(1):272–81.

Development of Layerless Additive Manufacturing Stereolithography Machine to Improve Surface Quality and Dimensional Accuracy

Y.Sajjan Rao[1]
Asst Professor
Mechanical Engg Department
Malla Reddy College of Engineering
sec-bad-10

I.Prasanna[2]
Asst Professor
Mechanical Engg Department
Malla Reddy College of Engineering
sec-bad-10

Abstract: Stereolithography (SLA) is an Additive Manufacturing (AM) process that has recently gained significant popularity in manufacturing research. The material used in SLA is a photocurable resin. SLA fabrication has conventionally been executed in a layered build process, which results in the staircase effect: a common problem in layered manufacturing giving a lower quality part surface due to created cusps on the surface. Manufacturing the part using a continuous build should theoretically eliminate this issue. A methodology for the design, development and calibration of a new layer less additive manufacturing system is introduced in this thesis. The methodology involves synchronizing the display of cross-sectional images with the platform elevation on an SLA machine and finding the optimal parameters in order to obtain a more dimensionally accurate and higher surface quality part. A variety of geometric features are constructed through experiments and their properties are examined to extract the most adequate fabrication parameters. The layer less process was found to reduce the staircase effect and the surface roughness on fabricated parts, as well as improve the ability of the machine to build complex features.

Introduction: Additive Manufacturing (AM) is a popular field of research in engineering, in which three dimensional shapes are constructed by adding material layer by layer (layered manufacturing). It is also commonly known as Three-Dimensional Printing (3DP), which has been an attractive research topic in manufacturing in recent years. There are several applications of 3DP, including but not limited to Fused Deposition Modeling (FDM), Selective Laser Sintering (SLS), Inkjet Printing (IP), Bioprinting (BP), and Stereolithography (SLA) [Gibson et al. 2010]. Demand for improving the surface quality and dimensional accuracy of fabricated three-dimensional parts is consistently increasing. This research pertains to the design and development of a specific SLA AM application, in which near-Ultraviolet (UV) light is used as a radiation source to project images of the cross-sections of a 3D model onto a build plate submerged in photocurable resin [Karsten et al. 2009]. The original setup constructs each layer of an object in sequence and builds parts in a bottom-up process. Layered manufacturing presents a well-known problem in 3DP known as the 2 staircase effect, which results in lower surface quality and can jeopardize the accuracy of manufactured parts. The motivation behind this research is to develop a solution to avoid the staircase effect resulting from the typical layered manufacturing processes. Surface quality involves the study of surface roughness and must not be improperly associated with surface integrity as having the same definition. Surface quality can include all of surface finish/roughness, waviness and lay of any fabricated surface, whereas surface integrity is the condition of a work piece after being used in a manufacturing process. Some of the parameters affecting surface integrity are tool wear, cutting speed, tool material, coatings, cutting angle and contact area. The challenges to achieve this objective are due to four major limitations in the design and development of the layerless manufacturing process: the material used for part construction, the radiation source used, the graphical device used and the complexity of the part desired, which all affect the capabilities of the machine and are dependent on one another. The material used in this research is MakerJuice Substance G+ photocurable resin, a liquid that hardens when exposed to specific types of light. This hardening is a chemical process also known as curing or photopolymerization. MakerJuice G+ is commercially available and reacts quickly to the light. The radiation source used is several near-UV Light-Emitting Diode (LED) units, rated at 405 nanometres and 3 Watts of power each, since the resin will only cure at wavelengths of 440 nanometres or less. The graphical device used is a monochrome Liquid Crystal Display (LCD) screen, which transfers a fraction of the power of the lights through a displayed shape and penetrates into the resin-filled container onto the build plate. A poor quality screen will transmit much less power, but the monochrome screen transmits five times as much power as multicolor. 3 The build process will take less time to complete and the quality of the part should be better. The optimal amount of time the light is exposed to the part, the exposure time, needs to be determined. In order to avoid the drawbacks of layered manufacturing including the stair-case effect, a layerless SLA system is designed and developed. This requires two tasks: Slicing Process - implementing a program to produce information from the cross-sections of a 3D model from a Stereolithography file (STL), and Dynamic Curing Process - synchronizing the transfer of slicing data with the elevation of the machine platform considering the optimum curing parameters. The input of the slicing process is either a text or binary STL file and the desired output is a video of the desired geometric model, showing its cross-sections for a length specified in the code as a frame rate. The frame rate of the video must then be synchronized with the constant feed rate of the machine by equating the time of the video to the time required for the curing process. The frame rate is computed based on the curing parameters of the machine, which are achieved using experimental studies. The elevator of the system is instructed by the G-code program to control the exact computed curing time required for layerless fabrication.

Literature Review: There have been many studies on AM processes and materials over the past three decades. Each AM process has its own set of specific applications and material usage. Materials used in AM processes cover a range of metals, plastics, glass, ceramics and biomaterials. Also, each material used has its own unique set of mechanical properties once fabricated. Among the typical AM processes, the masked projection Stereo lithography application is receiving significant attention in industry. This is particularly because of its build efficiency, speed and independence of the size of the part's cross-section as opposed to other AM processes. The research can be categorized based on the method of construction of the parts and the terminologies are vastly different for each separate application. There are still many topics of research to be investigated for these processes, and the interesting aspect is that there will always be a way to improve them based on rapidly developing technology. Increasing the surface quality of AM parts is one example of quality improvement, which is the first topic of the literature review. The next literature topicinvolves the review of mechanical properties of common AM applications, followed by literature on biomaterial AM applications and finally literature on stereo lithography AM applications.

Literature on The Surface Quality of Am Parts: In 2003, Pandey, Reddy and Dhande investigated a semi-empirical study on how to improve the surface finish of parts constructed using a Fused Deposition Modeling (FDM) AM process [Reddy and Dhande 2003]. The accessibility of certain locations on the prototyped part was addressed using a simple material removal method called Hot Cutter Machining (HCM). A fractional factorial design of experiments was adopted, involving two levels (low and high) with four factors (cutting speed, build orientation, rake angle and angle between cutting edge and layers). ANOVA was used to determine the significance of each variable investigated as well as the confidence level of the statistical model developed for the surface quality of the HCM surface. Results showed that the proposed machining method is able to produce a surface finish of the order of 0.3 μm with 87% confidence. Figure shows a depiction of the staircase effect and the important parameters involved with it.

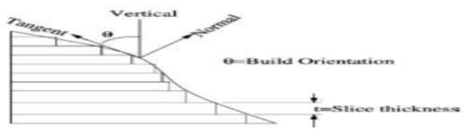

Figure: Staircase Effect on AM Produced Parts. [Rheddy and Dhande 2003]

The underlying problem with the staircase effect is with constructing layers during the build process. The larger the layer/slice thickness, the more inaccurate the approximation to the nominal profile on the prototyped surface and the greater the surface roughness. A new solution was proposed for solving the poor surface finish problem called adaptive slicing. In addition to this solution, an optimal part build orientation was proposed to improve on the quality even further. Models used to evaluate the part's average surface roughness and build time were developed and optimized using a real coded genetic algorithm. Results showed that by minimizing the weighted sum of the two objectives, namely build time and average part surface roughness, an optimal part deposition orientation could be selected.

In 2007, Barari, ElMaraghy and Knopf conducted research to reduce the uncertainty of a part's minimum deviation zone estimation [Barari et al. 2007]. An iterative search procedure was used in an integrated inspection system to estimate the minimum deviation zone Both actual and virtual inspection data were presented through experiments to reduce the uncertainty in the minimum deviation zone estimation.

In 2009, Ahn, Kweon, Kwon, Song and Lee did a study on the representation of an additive manufactured part's surface roughness using an FDM process [Ahn et al. 2009]. A new approach to model the surface roughness was presented in this work, using a theoretical model based on actual surface roughness distributions of FDM parts. The model expressed surface roughness distribution according to changes in surface angle by considering the main factors that significantly affect surface quality, namely surface angle, layer thickness, cross-sectional shape of the filament and the overlap interval. The model shaped the surface profile as an elliptical curve rather than a rectangular shape as it has been most commonly interpreted. Figure demonstrates the model of the surface profile used in the research, showing the current layer, the layer before and the layer after. The important variables used in relevant equations are shown in this depiction

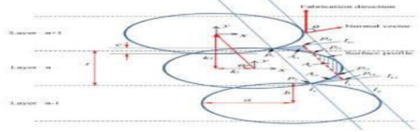

Fig:1 Schematic for Modeling the Surface Profile of the FDM-processed Part. [Ahn et al. 2009]

In 2014, Jamiolahmadi and Barari worked on a finite difference approach to analyze the surface topography of AM parts [Jamiolahmadi and Barari 2014]. The goal of the research was to provide a detailed reconstruction of the surface, something which had not been done previously, as the existing work only provided information regarding discrete points measured from the surface. Sample measured data points were taken to achieve this goal. The methodology used was a mapping method using a harmonic function with Drichlet boundary conditions. The methodology developed could be used for the surface texture modeling, surface quality analysis, surface quality inspection, and in planning for post-processing of the suitable surface finish processes. Figure 2.4 shows the reconstructed shape of the 3D surface using 90% of the initial points in the finite difference algorithm. The results showed that the estimation of the surface roughness using the proposed method proved to be very accurate to the actual shape.

The various approaches involved theoretical CAD and image models obtained from software and microscopic equipment, post-processing including chemical finishing and coating, mathematical optimization algorithms used in estimation, proposals of altering the build methods and build parameters, and finally comparison of known model data to a newly proposed model. The research showed extensive findings in working towards better surface quality and reducing the staircase effect, and also showed major improvement in estimation cost and analysis. There will always be a demand to improve the efficiency and quality of AM parts.

MECHANICAL PROPERTIES OF COMMON AM APPLICATIONS: In 1996, Giordano, Wu, Borland, L. Cima, Sachs and M. Cima demonstrated the ability of Three Dimensional Printing (3DP) to produce dense polymer parts from a powder bed [Giordano et al. 1996]. In 2005, Pfister, Walz, Laib and Mulhaupt used a powder blend of Polyacrylic Acid (PAA) with zinc oxide or a mix of zinc oxide and magnesium oxide to produce zinc polycarboxylate during 3D dispensing of an aqueous ink from AM processes [Pfister et al. 2005]. No postprocessing treatments were required and a high dimensional accuracy of the models was achieved. The mechanical properties improved with increasing PAA content, ink amount, and decreasing particle size of the sintered zinc oxide ceramic.

Biomaterial AM Applications: In 1999, Wheeler, Corey, Brewer and Branch provided an introduction of integrating cell growth with 3D printing technology [Wheeler et al. 1999]. Microcontact printing created precise patterns of proteins, which controlled growth of hippocampal neurons in culture. This additive, multi-mask technique permitted several different molecules to be patterned on the same substrate. The covalent linker technology permitted relatively long-term (two-week) compliance of neurons to the stamped pattern against a polyethylene glycol background. When polylysine was stamped adjacent to a laminin/polylysine mixture, neural somata and dendrites preferred the polylysine while axons prefer the mixture or the border between the two. There are no actual results on a 3D printing process in this paper, just fundamental theory.

In 2003, Yan, Wu, Zhang, Xiong and Lin discussed an important subject called biomanufacturing [Yan et al. 2003]. The hierarchy of bio-manufacturing (low grade: undegradable material used to perform permanent organ replacement, and high grade: biodegradable material 26 used to repair organ damage) was investigated by using an FDM AM process. The resulting bone and cartilage samples were tested on dogs and rabbits. The material used was a low grade biomaterial is HDPE (high density polyethylene), due to its ease of extruding, high melt index and high cohesiveness. It was found that the artificial cartilage planted in the rabbits for 3 months had developed well. The material used as a high grade biomaterial was a composite of Polylactic Acid (PLLA) and Tricalcium Phosphate (TCP). A composite was used to increase the mechanical strength and improve the regeneration properties of the material. It was found that the material had high porosity and similar properties to human bones.

Stereolithography AM Applications: In 1984, Otsubo, Amari and Watanabe performed a study of the curing of photoresin and the effect from varying light intensities, dynamic viscosity of the resin, sample/layer thickness and exposure energy on the sample area [Otsubo et al. 1984]. The ultraviolet light source used had a wavelength of 365 nm. Experiments were conducted with an oscillating plate rheometer. Results showed that the minimum exposure energy, required to initiate photopolymerization, increased with increasing sample thickness. Also, a sample thickness greater than 100 µm shows a substantial increase in the minimum exposure energy.

Methodology:A successful AM process must minimize all errors with the machine and its calibration and minimize them as much as possible. The design must be robust and reliable, the methods applied need to be consistent and practical, and the fabricated part as a result needs to be dimensionally accurate and have optimal surface quality. In order to modify the application of an AM process from layered to layerless (also known as continuous build), in which the machine does not cease its operation, the lift and retract sequence must be eliminated entirely. The layerless AM process should improve the quality of the part and also be faster in part production. There is limited knowledge and usage in industry for this process, and to better understand its behavior a new synchronization process is introduced.

The concepts behind the SLA AM process are discussed, including the curing mechanism, machine design, machine calibration and the layerless fabrication process.

Curing Mechanism: Before covering the machine design, it is important to understand the mechanism behind the curing functionality of the resin. The exact chemical structure of the G+ resin used is withheld from the public as a trade secret; however the Material Safety Data Sheet (MSDS) states that its composition contains greater than 60% of acrylate monomers. A monomer is a molecule and a chemical that is the primary ingredient in resin.

Machine Design: A schematic drawing of the machine is identifying all major components and their position in the system. The preliminary engineering design is provided in Appendix A. Some of the dimensions were modified later to accommodate a larger screen.

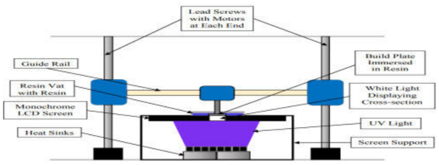

Fig:2 Schematic of SLA Machine Design.

The size of the SLA system, once constructed, is approximately a 500 mm cubic design. The 75 mm square build plate is super glued to a bolt fitted through a slot in the center piece, located on the horizontal double rail that is free to move along the rails. The bolt has two washers and two nuts in order to fasten the bolt to the center piece from both sides. Using the threaded lead screws, which are each attached to either side of the machine and to a stepper motor, the whole rail is permitted to travel in the vertical direction. A limit switch prevents any further movement which could cause damage to the components. Sitting on top of the LCD screen (black rectangular panel in the center of the machine) is the vat, which has been constructed by hand using only acrylic glass, acrylic glue, a coffee container and nonstick material called Sylgard 184 silicone elastomer.

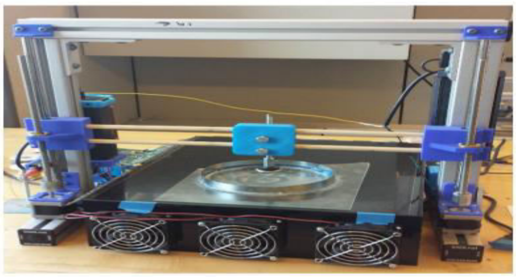

Fig3: Full-scale View of SLA Machine.

The frame structure of the machine is made of 8020 Aluminum, which is light and simple to work with. The dark blue components, consisting of mostly supports, hangers and guide pieces, are made of blue ABS (Acrylonitrile Butadiene Styrene) plastic. The light-blue center piece holding the build plate is made of PLA (Polylactic Acid) plastic. Both of these parts were fabricated using a BFB 3D Touch FDM 3D printer. The many fasteners used throughout the machine are made of steel, the heat sinks are made of aluminum, and the LCD screen holder (large black rectangle) is made from acrylic sheets.

Machine Calibration: Before printing, it was necessary to ensure the machine settings were optimal for the process. These settings were applied using the controlled software. Machine calibration was done with reference to a Vernier caliper and Coordinate-Measuring Machine (CMM) for measurements, 52 using the software, manual adjustment of machine components, and through several experiments. The experiments were conducted in order to understand what machine settings are optimal when manufacturing parts. Enclosed rings are printed by varying the internal diameter and external diameter to see how the resin expansion affects the dimensional accuracy of parts during the curing process. After this experiment, a more comprehensive shape is analyzed during the curing process, in which the exposure parameters exposure time, delay time and light intensity are varied. The optimal exposure parameters are selected from the sample that gives the highest dimensional accuracy. Finally, the last experiment validates the selected exposure parameters by printing larger 3D parts. A Rook is constructed at three different sizes and an Angle Cube is also constructed.

Controlling Software : To do proper 3D builds, software with manual settings is needed to run on a machine. The software is a very efficient, user-friendly, open-source type of software that is used to build 3D shapes using an SLA machine. There are four main features in this program, which can be switched between: 3D View, Slice View, Control, and Configure. The menu at the top of the interface shows eight different icons, which are seen in every feature. From left to right, these are Open File, Save File, Connect Machine, Disconnect Machine, Slice Model, Start/Resume Process, Pause Process, and Stop Process. Files consisting of stl, obj, 3ds, or amf extensions can be opened. The software also allows opening scene format files (cws extension), which is what all files will save as. A scene file contains all options saved in the program for printing. The graphic portion of the first screen, 3D View, shows the full model that is going to be fabricated.

Manual Calibration: Minimizing all possible errors before testing on an AM fabrication process is required. There are some calibration procedures that involve careful inspection and manual procedures, such as setting a level build plate, centering the build plate with the image, adjusting the home position of the build plate and finally re-sizing the build platform. Following these steps will result in a more consistent build every time the machine is operated.

Expansion of Enclosed and External Dimensions: Now that the machine is manually calibrated, the next step involves running several tests to select and validate the exposure parameters of the machine. One experiment includes the printing of enclosed parts (rings) and developing relationships between external dimensions, enclosed dimensions and dimensional accuracy. This is shown using a graphical method. The purpose of the experiment is to see how the resin expands externally and internally during curing 58 and how much this expansion affects dimensional accuracy of the manufactured parts. Each value recorded is an average of five measurements done using a Vernier caliper and a CMM to verify.

Optimal Exposure Parameter Selection: The optimal exposure parameters consist of the exposure time, the delay time and the light intensity. The delay time is a layered manufacturing term only, as it involves the total time after curing a layer that spans disabling the light source, lifting the build plate and retracting back down to a height that is one layer up from the previous layer that was cured. It is important to give the machine enough cooling time between the curing of each layer so the part quality will not be jeopardized. To find the optimal parameters for the machine, several samples of the same shape were printed with different specifications.

Complex 3D Parts (Rook and Anglecube): As found in the previous experiment, the optimal parameter setup of a 6-second layer cure time, a quadruple delay time (~55 seconds) and full light intensity is used to print the following parts. These parts contain more detailed features than any shape experimented with thus far, and present a final two parameters that require experimentation to find. These parameters are the lift speed (or the feed rate) and the lift height (between layers). Initially both of the parameters were set too high. They are more significant characteristics for longer build processes, where endurance of the machine becomes an important factor to consider.

LAYERLESS FABRICATION PROCESS: The developed layerless manufacturing SLA machine is conducted by completing two processes: Slicing Process - a software algorithm that produces information of the cross-sections of a 3D model from a Stereolithography file (STL), and Dynamic Curing Process – developing a G-cod instructional program for the machine to synchronize transfer of the slicing data with the elevation of the machine platform considering the optimum curing parameters.

The layerless AM process is achieved by synchronizing a video from the STL slicing program with manually generated G-Code used to control the curing process. The video is a dynamic representation of the cross-sectional views of the desired 3D model created by the CAD system. The rate of displaying the cross-sectional views is controlled by uses a very important variable called the frame rate, which determines the video's length. The units are frames per second, where Figure 3.15: AngleCube: (a) STL file, and (b) SLA print. (a) (b) 69 one frame means one cross-sectional view. The length of the video must be equal to the duration of the curing process, however certain specific parameters are necessary to obtain this relationship such as the minimum allowable machine feed rate, the optimal machine feed rate and the desired video frame rate.

STL Video Generation: The video is the baseline of the methodology for layer less manufacturing. There are two main scripts used. The first main file is an STL reader and slicer, which locates all of the faces and vertices of an STL file, and determines which vertices are connected using a line to construct the edge belonging to its respective triangle (face). The format of an STL file contains separate blocks associated with each triangle in the 3D model. These blocks consist of a normal vector indicating the triangle orientation and point coordinates associated with the vertices of the triangles. There are two types of STL files, which are text and binary.

Determination of Minimum Machine Feed Rate: The minimum machine feed rate can be determined by assigning a very small feed rate to the machine and operating for a specified lift height. The machine will be unable to work with the set feed rate, and therefore will regulate the setting to the minimum permitted speed of the motors.The manual G-Code must be saved as a text file before it can be sent to the machine.

Determination of Optimal Machine Feed Rate :The optimal feed rate calculated is then applied in the manual G-Code to the machine .The total time of the machine's operation is observed and the time is recorded as tprint. It is possible to obtain an optimal feed rate, which is lower than the minimum feed rate that was determined. If this situation occurs, the minimum feed rate is equal to the optimal feed rate.

Implementation of Machine Synchronization: Synchronization involves the implementation of one script and the use of manual G-Code in the controlling software. The process of the script is presented in pseudo-code as follows: Write video file Assign a frame rate based on the equations in 3.5 Open the video file From the first to last slice: Search through all intersection points: Check if points lie inside of the polygon or on its edge Find all interior points and points on the opposite side of the edge End Loop Set the figure handle with the required axis properties and figure properties Store the point data as an array of two columns For the length of the array Color interior points white and all points on opposite side of edge black End Loop Get the frame from the current figure Re-write the video initialized with a new one containing the frame Close the figure End Loop Close the video file This code is executed simultaneously with the manual G-code for machine synchronization.

CONCLUSION: A layerless manufacturing method is presented in this thesis by using synchronization between an STL reader code and an SLA 3D printing machine. The synchronization process involves writing a functional code and integrating the output video with the operation of the machine. By implementing this layerless approach, the layered manufacturing problem staircase effect is minimized and the surface quality of the part is improved with minimum dimensional error. The processes involved in the methodology were to understand the limitations and capabilities of the software used, explaining the design and functionality of the SLA machine, performing any necessary manual calibration of the machine to reduce part construction error and finally the approach behind the layerless AM process by implementing synchronization. Dimensional accuracy of the layer printing was improved by experimental study of the required compensation and scaling parameters which are used for calibration of the machine. In order to study the capability of the layerless process, several parts were printed, of which the focus was improving the surface quality, dimensional accuracy and reducing the staircase effect separately.

REFERENCES

1.[Gibson et al. 2010] Gibson, L., Rosen, D. W., Stucker, B., 2010, “Additive Manufacturing Technologies: Rapid Prototyping to Direct Digital Manufacturing”, Springer Science+Business, LLC, Springer New York Heidelberg Dordrecht London.

2. [Karsten et al. 2009] Karsten, R., Larston, B., Miller, K., 2009, “Characterizing the Efficiency of LED Curing”, Phoseon Technology, RadTech Europe.

3. [Pandey et al. 2003] Pandey, P. M., Reddy, N. V., Dhande, S. G., 2003, “Improvement of surface finish by staircase machining in fused deposition modeling”, Journal of Materials Processing Technology, Vol. 132, pp. 323-331.

4. [Barari et al. 2007] Barari, A., ElMaraghy, H. A., Knopf, G. K., 2007, “Search-Guided Sampling to Reduce Uncertainty of Minimum Deviation Zone Estimation”, ASME Journal of Computing Information Science and Engineering, Vol. 7, pp. 360-371, DOI: 10.1115/1.2798114.

5 [Jamiolahmadi and Barari 2014] Jamiolahmadi, S., Barari, A., 2014, “Surface Topography of Additive Manufacturing Parts Using a Finite Difference Approach”, Journal of Manufacturing Science and Engineering, Vol. 136, pp. 1-8, DOI: 10.1115/1.4028585.

6. [Giordano et al. 1996] Giordano, R.A., Wu, B.M., Borland, S.W., Cima, L.G., Sachs, E.M., Cima, M.J., 1996, “Mechanical properties of dense polylactic acid structures fabricated by three dimensional printing”. Journal of Biomaterial Science Polymer Edition, Vol. 8, No. 1, pp. 63-75

7 [Wheeler et al. 1999] Wheeler, B. C., Corey, J. M., Brewer, G. J., Branch, D. W., 1999, “Microcontact Printing for Precise Control of Nerve Cell Growth in Culture”, ASME Journal of Biomechanical Engineering, Vol. 121 pp. 73 – 76

8 [Yan et al. 2003] Yan, Y., Wu, R., Zhang, R., Xiong, Z., Lin, F., 2003, "Biomaterial forming research using RP technology", Rapid Prototyping Journal, Vol. 9 Iss 3 pp. 142 – 149

9 [Otsubo et al. 1986] Otsubo, Y., Amari, T., Watanabe, K., 1986, “Rheological Studies of Ultraviolet Curing with an Oscillating Plate Rheometer”, Department of Image Science and Technology, Faculty of Engineering, Chiba University, l-33, Yayoi-cho, Chiba-shi, 260 Japan.

EXHAUST MANIFOLD OPTIMIZATION OF BURNING MULTI-CYLINDER IC ENGINE BY USE OF THERMAL ANALYSIS

Sambasiva naidu
M.tech Student
Department of Mechanical Engineering,
Mallareddy College of Engineering,
Email ID: sambasiva370@gmail.com

B.S.Sai Deepika, M.Tech
Assistant Professor
Department of Mechanical Engineering,
Mallareddy College of Engineering,
Email ID: suryabogaram14@gmail.com

Dr.S.S.Gowda, Ph.D
Professor
Department of Mechanical Engineering,
Mallareddy College of Engineering,
Email ID:ssgouda105@gmail.com

***Abstract*— Exhaust manifold is one of the critical components of IC engine for improving the volumetric efficiency. The volumetric efficiency of the engine can be increased by reducing the backpressure in the exhaust manifold. This work analyzes the flow through two different models of exhaust manifold using CFD. The design of exhaust manifold is modified to get optimal geometry. The analysis results of two models are compared for back pressure. By comparing the results of two models the decrease in back pressure is found which ensure improvement in volumetric efficiency of the engine.**

Keywords*— *Exhaust Manifold, CFD, Multi-Cylinder SI Engine, Back Pressure.

I. INTRODUCTION

An exhaust manifold collects the exhaust gases from multiple cylinders into one pipe. It is attached downstream of the engine and is major relevance in multi-cylinder engines where there are multiple exhaust streams that have to be collected into a single pipe. When an engine starts its exhaust stroke, the piston moves up the cylinder bore, decreasing the total chamber volume. When the exhaust valve opens, the high pressure exhaust gas escapes into the exhaust manifold or header, creating an exhaust pulse comprising three main parts: The high pressure head is created by the large pressure difference between the exhaust in the combustion chamber and the atmospheric pressure outside of the exhaust system. As the exhaust gases equalize between the combustion chamber and the atmosphere, the difference in pressure decreases and the exhaust velocity decreases. This forms the medium-pressure body component of exhaust pulse. The r e ma i n i n g exhaust gas fo rms the lo w pressure tail component. This tail component may initially match ambient atmospheric pressure, but the momentum of the high and medium pressure components reduces the pressure in the combustion chamber to a lower than atmospheric level . This relatively low pressure helps to extract all the combustion products from the cylinder and induct the intake charge during the overlap period when both intake and exhaust valves are partially open. The effect is known as scavenging. Length, cross-sectional area, and shaping of the exhaust ports and pipe works influences the degree of scavenging effect. *Seenikannan et al.* [1] analyzed a Y section exhaust manifold system experimentally to improve engine performance. This paper investigates the effect of using various models of exhaust manifold on CI engine performance and exhaust emission. *Yasar Deger et.al* [2] had done CFD-FE-Analysis for the Exhaust Manifold of a Diesel Engine aiming to determine specific temperature and pressure distributions. The fluid flow and the heat transfer through the exhaust manifold were computed correspondingly by CFD analyses including the conjugate heat transfer. *Dr. Kutaiba et.al* [3] made an approach to estimate of flow characteristic in inlet and exhaust manifolds of internal combustion engines using a four-stroke variable compression ratio single cylinder gasoline engine. In the experimental work, the compression ratio was varied from 7 to 11 at variable speed with constant throttle opening, where engine performance was obtained. *Scheeringa* [4] studied analysis of Liquid cooled exhaust manifold using CFD. Detailed information of flow property distributions and heat transfer were obtained to improve the fundamental understandings of manifold operation. A number of computations were performed to investigate the parametric effects of operating conditions and geometry on the performance of manifolds. *Gopal et al.* [5] has conducted experimental analysis of flow through the exhaust manifold of a multi cylinder Petrol engine of a contessa engine of 20 hp at maximum speed of 2000 rpm and then analyzed using FLUENT [1].

II. BACK PRESSURE

Back pressure usually refers to the pressure exerted on a moving fluid by obstructions against its direction of flow. Back pressure caused by the exhaust system of an automotive engine has a negative effect on engine's performance as it will restrict the flow rate of the exhaust gasses. The result would be the engine not being able to expel the spent exhaust gasses fast enough to prevent spent exhaust gasses from contaminating the fresh air/fuel mixture that is drawn into the engine on the next intake stroke. Ultimately, this will result in reduced engine power.

III. CONSTRUCTION

The exhaust manifold system considered in the present case has 4 inlets connected to the exhaust port of the engines and a single outlet from where the flow is passed on to the exhaust system before ejection into the ambient. Due to lack of experimental data, an industrially available manifold geometry has been considered for the present analysis. It consists of the pipe diameter of 42 mm and total span of the manifold to be 0.6 m. The base model has the outlet placed besides the first port having smaller length of the curved pipe from the individual engine exhausts. The modified geometry has the outlet port placed in the middle with longer curved pipes from the individual engine exhausts, as shown in Figure.

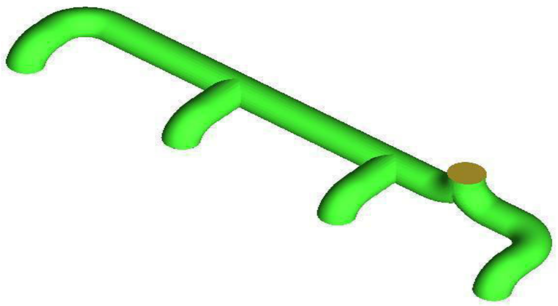

Fig-1: Base geometry of the exhaust manifold

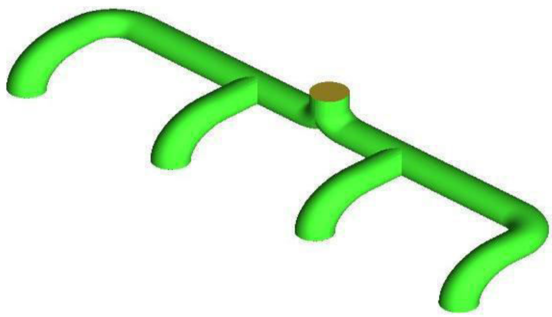

Fig-2: Modified geometry of the exhaust manifold

IV. METHODOLOGY

A steady state single phase single-species simulation with exhaust gas as the working fluid will be carried out for the two geometries at 4 different mass flow rates from each inlet to determine the pressure drop.

The geometry will be created using ANSYS ICEM CFD and a multi-block structured mesh will be created. ANSYS CFX will be used for doing the flow simulation under isothermal conditions. The overall analysis will be performed on ANSYS Workbench. A steady state single-species simulation will be carried out under isothermal conditions for exhaust gas. Turbulence will be modeled by *k*-ε RNG turbulence model appropriate to account for high velocities and strong streamline curvature in the flow domain. The reference pressure will be set at 1 atm and all pressure inputs and outputs will be obtained as gauge values with respect to this.

A. *MATERIAL*

Air will be the working fluid considered to be operating at 350 ^{0}C and 1.35 bar. The material properties under these conditions are:

Table-1: Properties of material

Property	Air
Density (kg/m^3)	0.7534
Viscosity (Pa.s)	3.0927 x 10^{-5}
Specific heat (J/kg-K)	1056.6434
Thermal conductivity (W/m-K) (not	0.0242

B. *BOUNDARY CONDITIONS*

The two models will be tested for 4 different engine loads corresponding to different mass-flow rates at each inlet:

Table-2: Boundary conditions

Cases	Engine load(kg)	Total exhaust mass flow rate (m/s)
i)	2	1.02
ii)	6	3.01
iii)	12	6.04
iv)	14	7.01
v	16	8.11
vi	18	9.55

V. RESULTS AND DISCUSSIONS

The models are analyzed using CFX and the results obtained are shown in the color Contours

A. *Pressure contours for the existing manifold*

The high pressure at the head is due to high pressure difference from exhaust in combustion chamber and atmosphere pressure. Fig shows, the pressure was not uniformly distributed in the existing manifold and the effect of non-uniformly distributed pressure gives an impact on the velocity of the flow of exhaust gases. The pressure flow through the outlet of the exhaust manifold should be uniformly distributed and so the new manifold design is drawn.

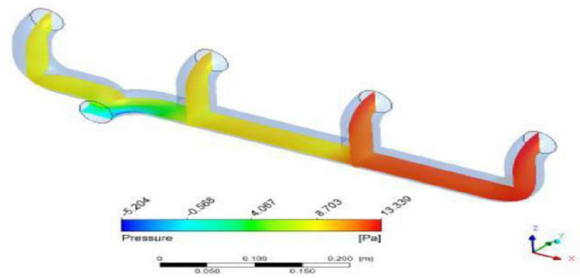

2 kg load

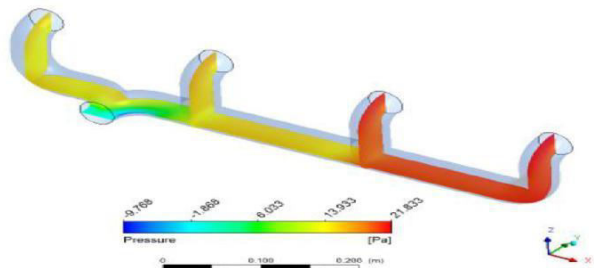

6 kg load

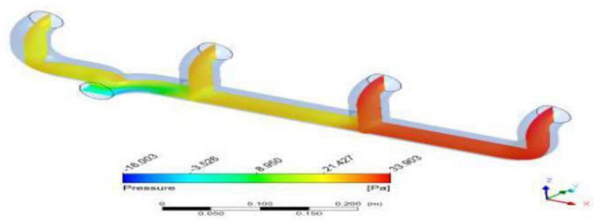

12 kg load

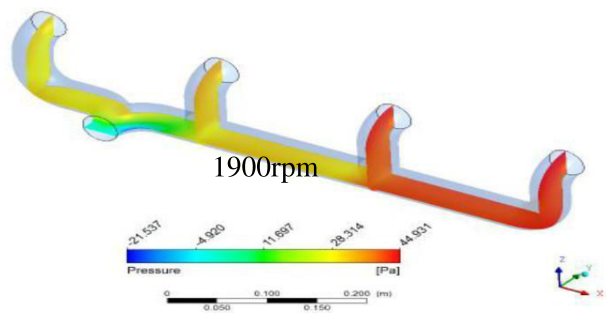

1900rpm

16 kg load

5.2 Pressure contours for the modified manifold

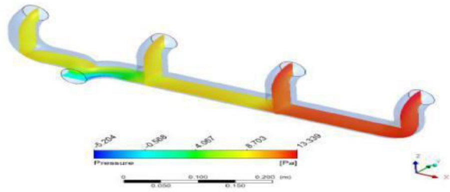

2 kg load

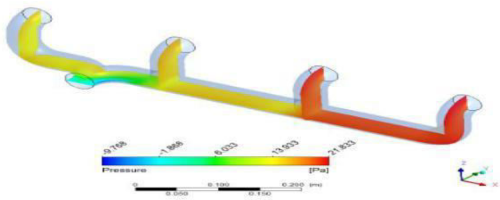

6 kg load

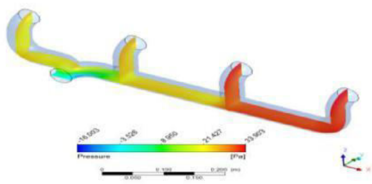

12 kg load

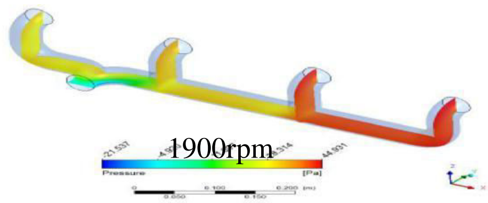

1900rpm

18 kg load

5.4 Velocity contours for the modified manifold

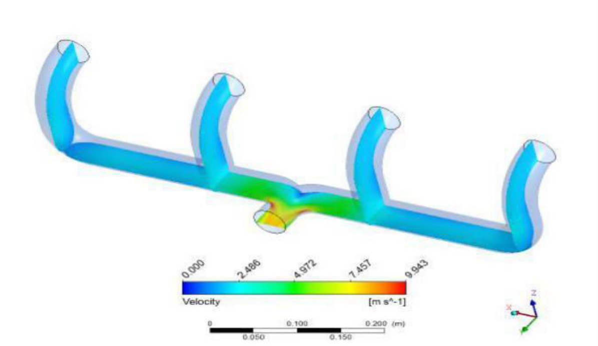

2 kg load

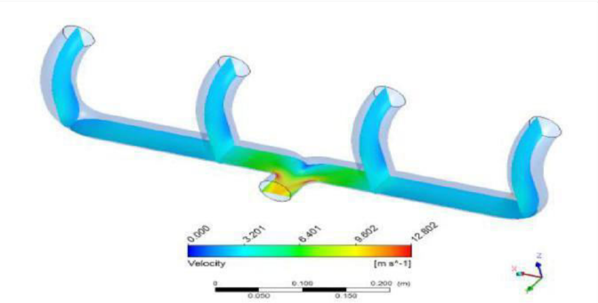

6 kg load

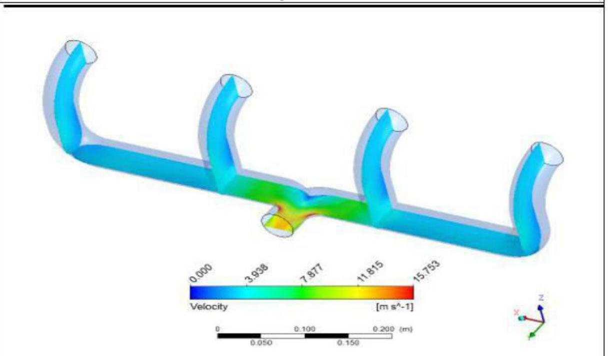

12 kg load

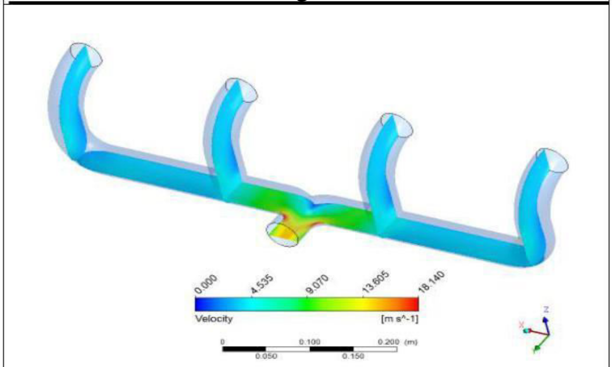

18 kg load

5.5 Pressure graphs

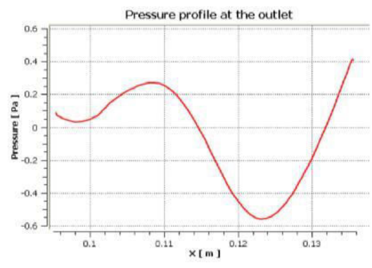

Base Model (2 kg)

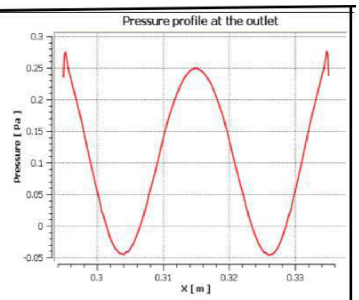

Modified Model (2 kg)

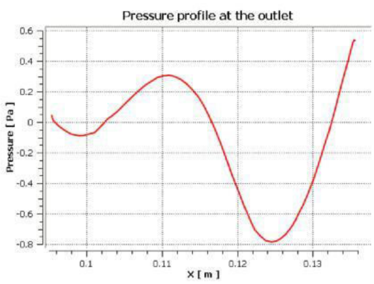

Base Model (6kg)

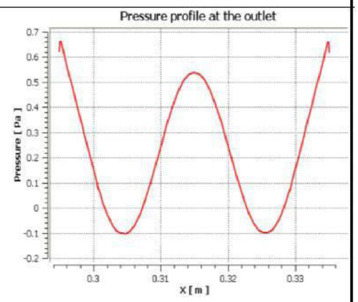

Modified Model (6kg)

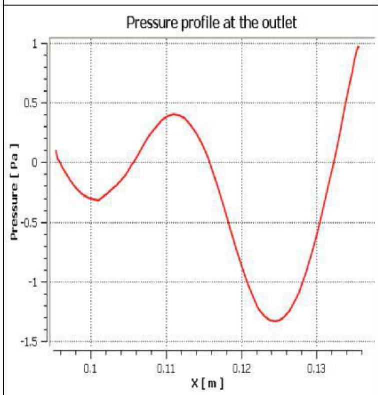

Base Model (12kg)

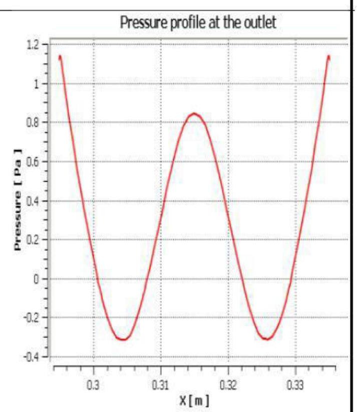

Modified Model (12 kg)

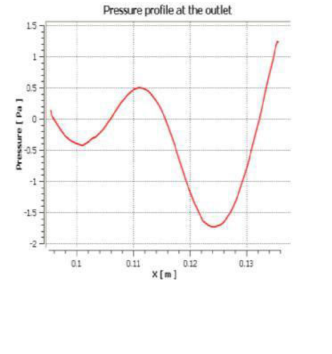	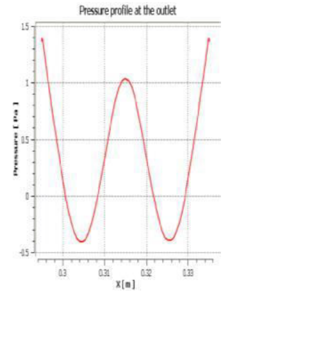
Base Model (14 kg)	**Modified Model (14 kg)**

5.6 Velocity graphs

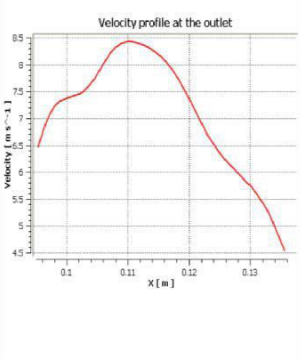	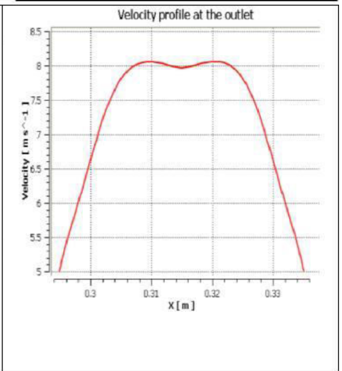
Base Model (16 kg)	**Modified Model (16 kg)**
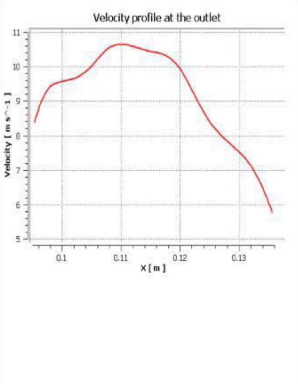	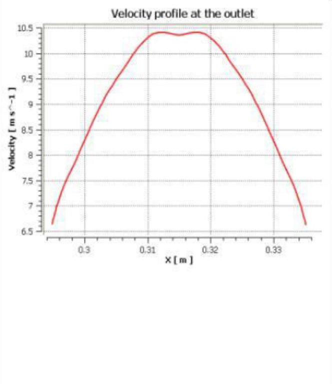
Base Model (18 kg)	**Modified Model (18 kg)**

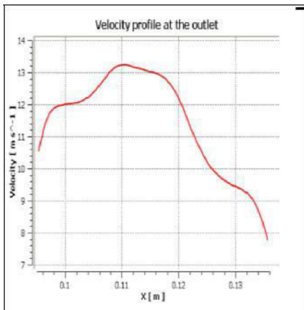	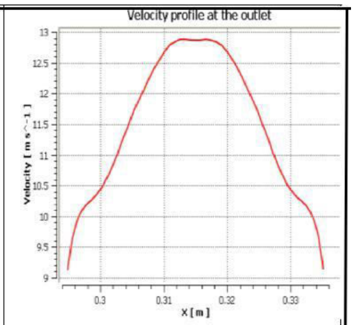
	Modified Model (16 kg)
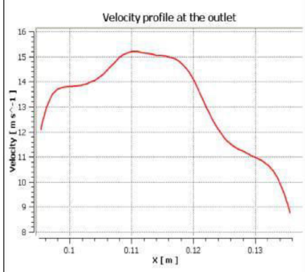	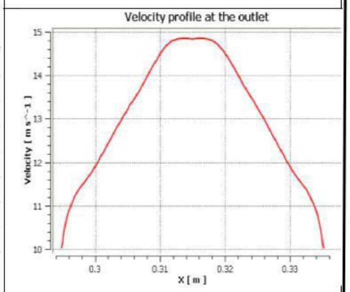
Base Model (18 kg)	**Modified Model (18 kg)**

5.7 Back Pressure Comparison

The graph shows that the back pressure is more in base model but it is less in case of modified model.

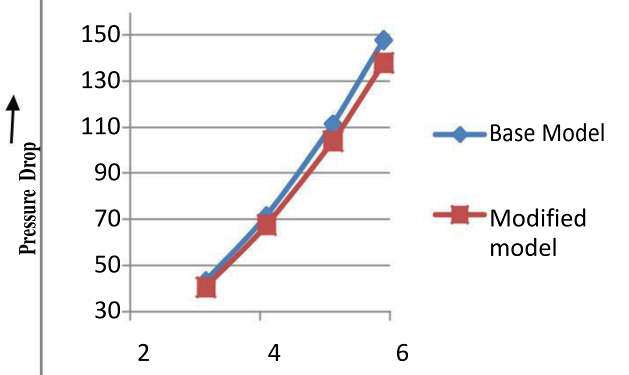

Mass flow rate

Fig-5.7: Comparison of Back Pressure

CONCLUSION

The flow analysis of exhaust manifold was performed. The existing manifold is modified by changing its geometry to get optimal geometry. Both old and new models are analyzed under same boundary conditions. The results of new model are compared with the existing model. Pressure and velocity graphs are drawn for the new model and are compared with existing model. The decrease in back pressure is shown by using contour and vector diagrams. The flow is made efficient by decreasing the exhaust gas back pressure in the newly modified model thus increasing the volumetric efficiency of the engine.

REFERENCES

1. Seenikannan P., Periyasamy V.M. and Nagaraj P. “An experimental analysis of a Y section exhaust manifold system with improved engine performance”.
2. Yasar Deger, Burkhard Simperl, and Luis P. Jimenez “Coupled CFD-FE-Analysis for the Exhaust Manifold of a Diesel Engine” Sulzer Innotec, Sulzer Markets and Technology Ltd, Winterthur, Switzerland.
3. Dr. Kutaiba J.M. AL-Khishali, Dr. Mahmoud A. Mashkour & Ehsan Shamil Omaraa “Analysis of Flow Characteristics In Inlet And Exhaust Manifolds of Experimental Gasoline Combustion In A VCR Engine”.
4. Scheeringa K. **“**Analysis of Liquid cooled exhaust manifold using CFD”.
5. Gopal P., Senthil Kumar T. and Kumaragurubaran B., “Analysis of Flow Through The Exhaust Manifold of a Multi Cylinder Petrol Engine for Improved Volumetric Efficiency” International Journal of Dynamics of Fluids ISSN 0973-1784 Volume 5 Number 1 (2009)
6. K.S. Umesh, V.K. Pravin and K. Rajagopal “CFD Analysis and Experimental Verification of Effect of Manifold Geometry on Volumetric efficiency and Back Pressure for Multi-cylinder SI Engine” International Journal of Engineering & Science Research IJESR/July 2013/ Vol-3/Issue-7/342-353

Modeling,Manufacturing and Analysis Of Crankshafts Using Ansys

V. Srinu[1] N. Kishore Kumar[2]

Assistant Professor Department of Mechanical Engineering Mallareddy college of Engineering Secunderbad -14

Abstract—**The crankshaft is the part of an engine that translates reciprocating linear piston motion into rotation. To convert the reciprocating motion into rotation, the crankshaft has "crankpins", additional bearing surfaces whose axis is offset from that of the crank, to which the "big ends" of the connecting rods from each cylinder**

It typically connects to a flywheel to reduce the pulsation characteristic of the four-stroke cycle, and sometimes a torsional damper at the opposite end, to reduce the torsional vibrations often caused along the length of the crankshaft by the cylinders farthest from the output end acting on the torsional elasticity of the metal

In this project Static and Modal Analysis was done on crankshafts of single cylinder four stroke engines by using Steel En36 and Cast iron Alloy. Static element analysis was performed on Crankshaft to obtain the Deformation and Stress at critical locations. Modal Analysis was done on the Crankshaft to obtain Mode Shapes and Natural Frequency of the crankshaft

Index Terms- **crankshaft, crankpins, cylinder, flywheel, Modal Analysis**

I. INTRODUCTION

Crank shaft is a large component with a complex geometry in the I.C engine, which converts the reciprocating displacement of the piston to a rotary motion with a four bar link mechanism. Crankshaft consisting of shaft parts, two journal bearings and one crankpin bearing. The Shaft parts which revolve in the main bearings, the crank pins to which the big end of the connecting rod are connected, the crank arms or webs which connect the crank pins and shaft parts. In addition, the linear displacement of an engine is not smooth; as the displacement is caused by the combustion chamber therefore the displacement has sudden shocks. The concept of using crankshaft is to change these sudden displacements to as smooth rotary output, which is the input to many devices such as generators, pumps and compressors. It should also be stated that the use of a flywheel helps in smoothing the shocks. Crankshaft experiences large forces from gas combustion. This force is applied to the top of the piston and since the connecting rod connects the piston to the crank shaft, the force will be transmitted to the crankshaft. The magnitude of the forces depends on many factors which consist of crank radius, connecting rod dimensions, and weight of the connecting rod, piston, piston rings, and pin. Combustion and inertia forces acting on the crankshaft. 1. Torsional load 2. Bending load. Crankshaft must be strong enough to take the downward force of the power stroke without excessive bending so the reliability and life of the internal combustion engine depend on the strength of the crankshaft largely. The crank pin is like a built in beam with a distributed load along its length that varies with crank positions. Each web is like a cantilever beam subjected to bending and twisting. 1. Bending moment which causes tensile and compressive stresses. 2. Twisting moment causes shear stress. There are many sources of failure in the engine one of the most common crankshaft failure is fatigue at the fillet areas due to the bending load causes by the combustion. The moment of combustion the load from the piston is transmitted to the crankpin, causing a large bending moment on the entire geometry of the crankshaft. At the root of the fillet areas stress concentrations exist and these high stress range locations are the points where cyclic loads could cause fatigue crank initiation leading to fracture.

II. MOTIVATION AND OBJECTIVES OF THE STUDY

This study was motivated by a need for a comparative study of forged steel and ductile cast iron crankshafts, which are the most commonly, used manufacturing processes for an automotive crankshaft. In addition, it was desired to develop an optimized geometry, material, and manufacturing procedure which will reduce the weight of the forged steel component for fuel efficiency and reduce the manufacturing cost due to high volume production of this component. In this section, these two competing manufacturing processes are explained and compared.This is followed by the optimization study of the forged steel crankshaft .The optimization process started with geometry optimization and was completed by considering modifications to the manufacturing process and using alternative materials.

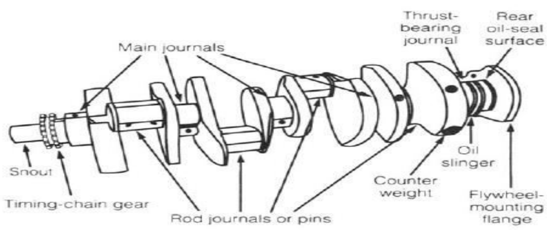

A. Modification to Manufacturing Process

As the next step for the optimization study it is tried to modify the production steps in order to reduce the cost or improve the performance of the current crankshaft. Further improvement of the performance could result in more geometry changes and weight reduction. The optimization in this section was investigated by considering adding compressive residual stress to the fillet area of the crankpin. Due to lack of experimental information, the magnitude of the residual stress that could be induced in the studied crankshaft geometry is not identified. It was shown in the studies by Kamimura , Park et al. and Chien et al. , as discussed in inducing compressive residual stress increases the fatigue strength of the crankshaft. Therefore, adding compressive residual stress on the fillet area of the current crankshaft increases its fatigue strength by 40% to 80% based on the material properties, crankshaft geometry, and applied rolling force. Effect of nitriding as a surface hardening process was discussed in the literature review in Section 2.5. Since the nitriding process is time consuming in comparison with other heat treatment processes, it was not considered as a modification to manufacturing process to increase the performance of the crankshaft. The effects of different surface hardening treatments such as quenching and tempering, ion-nitriding or fillet rolling on the fatigue properties were investigated in Pichard et al. research. Table 5.5 summarizes these effects. The fatigue bending moment for microalloyed 35MV7 steel without surface treatment was 1990 N.m. As could be seen in this table, the fatigue strength increases by 87% and 125% by fillet rolling forces of 9 kN and 12 kN, respectively. For short nitriding treatments, the fatigue limit of micro alloyed 35MV7 steel increased by about 135%.

B. *Modification Using Alternatives Materials*

One of the most common alternatives for the forged steel material is micro alloyed steel. Pichard et al. performed a study on a microalloyed (MA) steel with titanium addition specially adapted for the production of forged crankshafts and which does not require any post-forging treatment. The use of MA steel enables elimination of any further heat treatment, resulting in shorter manufacturing process and consequently an increase in the forged crankshaft productivity. The metallurgical choice of this MA steel for crankshaft applications was based on the 35MV7 steel grade, with a typical composition of 0.35C, 1.8Mn, 0.25Si, 0.12V, and micro-addition of Ti. Based on the results of their research, 35MV7 control-cooled micro alloyed steel shows similar tensile and rotating bending fatigue behavior as AISI 4142 quenched and tempered steel. In addition, the machinability of the micro-alloyed steel can be improved by about 40% in Turning and about 160% in drilling (Pichard et al. 1993).

The effect of using different material with the same surface treatments are summarized in Table 5.5. As could be seen in this table, the quenched and tempered 1042 steel with short nitriding treatment has 56% higher fatigue strength than the quenched and tempered alloyed ductile iron with the same nitriding time. The quenched and tempered 32CDV13 steel with 7 hour nitriding time has the highest fatigue strength, which is about 49% higher than quenched and tempered 1042 steel with shorter nitriding time. Cost reduction of 13% is obtained for the final crankshaft by replacing the traditional AISI 4142 steel with 35MV7 control-cooled micro-alloyed steel. This includes 10% savings on the unfinished piece, 15% mechanical operations and 15% saving on Ion Nitriding treatment (Pichard et al. 1993).

A comparison between the material properties used in the current crankshaft, AISI 1045 steel, and micro-alloyed steel 35MV7 indicates similar yield strengths, 12% higher tensile strength, and higher fatigue strength (by 21%) at 106 cycles for the micro-alloyed steel, as summarized in Table 5.6. Further study on the cost of final roduct is discussed in the cost analysis section.

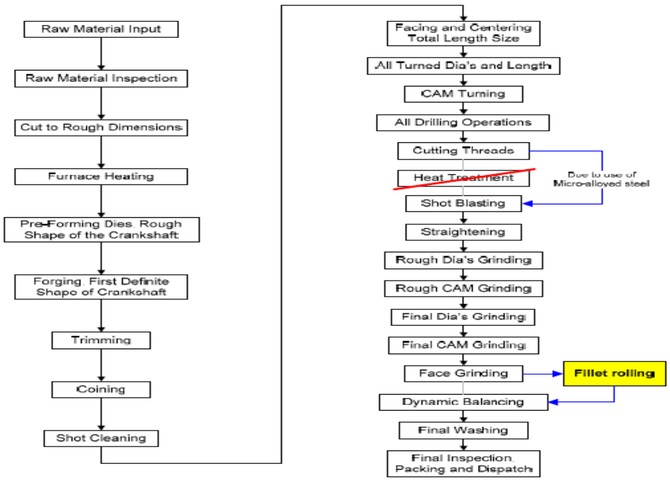

Modified manufacturing process for the forged steel crankshaft

III. GEOMETRIC MODELING AND FINITE ELEMENT ANALYSIS

A. *Modeling Software*

CatiaV5 R19 is an interactive Computer- Aided Design and Computer Aided Manufacturing system. The CAD functions automate the normal engineering, design and drafting capabilities found in today's manufacturing companies. The CAM functions provide NC programming for modern machine tools using the CatiaV5 R19 design model to describe the finished part. CatiaV5 R19 functions are divided into "applications" of common capabilities. These applications are supported by a prerequisite application called "CatiaV5 R19 Gateway".

CatiaV5R19 is fully three dimensional, double precision system that allows to accurately describing almost any geometric shape. By combining these shapes, one can design, analyze, and create drawings of products.

B. *Basic Procedure For Creating A 3-D Model In Catiav5 R19:*

Creation of a 3-D model in CatiaV5 R19 can be performed using three workbenches i.e., sketcher, modeling and assembly.

i) Sketcher:

Sketcher is used to create two-dimensional representations of profiles associated within the part. We can create a rough outline of curves, and then specify conditions called constraints to define the shapes more precisely and capture our design intent. Each curve is referred to as a sketch object.

ii) Creating a new sketch:

To create a new sketch, chose Start→Mechanical Design→Sketcher then select the reference plane or sketch plane in which the sketch is to be created

C. *SKETCH PLANE*

The sketch plane is the plane that the sketch is located on. The sketch plane menu has the following options:

Face/Plane: With this option, we can use the attachment face/plane icon to select a planar face or existing datum plane. If we select a datum plane, we can use the reverse direction button to reverse the direction of the normal to the plane.

XC-YC, YC-ZC, and ZC-XC: With these options, we can create a sketch on one of the WCS planes. If we use this method, a datum plane and two datum axes are created as below.

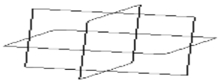

D. MODELING

i) Feature Creation

"Feature" is an all-encompassing term that refers to all solids, bodies and primitives used in CatiaV5 R19 Form Features are used to supply detail to the model in the form of standard feature types. These include hole, slot, groove, pocket, rib and pad. We can also create our own custom features using the User Defined option. All of these features are associative.

Reference Features allow creating reference planes, reference lines and reference points. These references can assist in creating features on cylinders, cones, spheres and revolved solid bodies. Reference planes can also aid in creating features at angles other than normal to the faces of a target solid. Dress up Feature options lets us modify existing solid bodies and features. These include a wide assortment of options such as edge fillet, variable fillet, chamfers, draft, offset face, shell and tapers.

Wire frame and Surface design lets us create surface and solid bodies. A surface body with zero thickness, and consists of a collection of faces and edges that do not close up to enclose a volume. Most Free Form Feature options create surface bodies..

ii) Creation Of Solid Bodies

We can create solid bodies by sweeping sketch and non-sketch geometry to create associative features or Creating primitives for the basic building blocks, then adding more specific features (for example, holes and slots).

Sweeping sketch and non-sketch geometry lets us to create a solid body with complex geometry. This method also gives us total control over the editing of the body. Editing is done by changing the swept creation parameters or by changing the sketch. Editing the sketch causes the swept feature to update to match the sketch."

Creating a solid body using primitive's results in a simple geometry solid body. Making changes to primitives is more difficult, because primitives cannot always be parametrically edited. We can use primitives when we do not need to be concerned with editing the model. Generally, however, it is to our advantage to create the model from a sketch.

iii) Design and Modeling of Crank Shaft

- Start – Mechanical Design – Part Design
- Select plane (side plane) and click on sketch icon.
- Open to sketcher work bench and draw the sketch (Circle dia 30mm) as shown fig below.

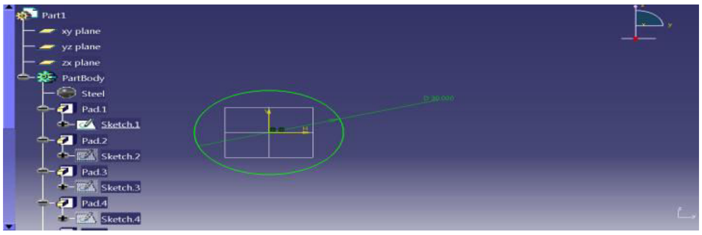

- Next exiting work bench and go to sketch base feature tool bar, select the pad icon, adding material normal to the sketch specify length. As shown fig below

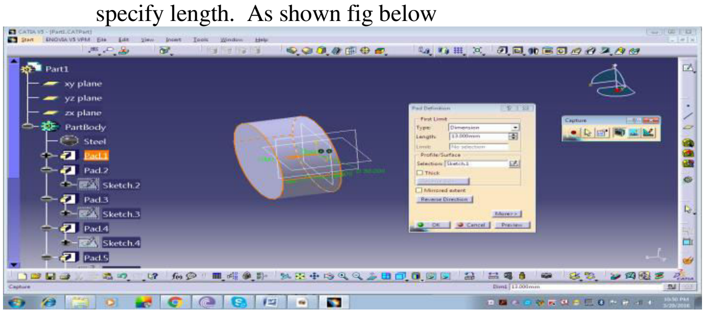

- Select the surface and click on sketcher icon, and draw the sketch of crank 2D drawing, as shown in the fig below.

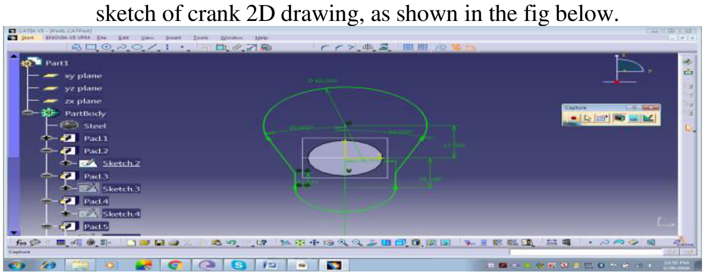

- Go to exiting work bench, and adding material normal to the sketch specify length as shown in fig below.

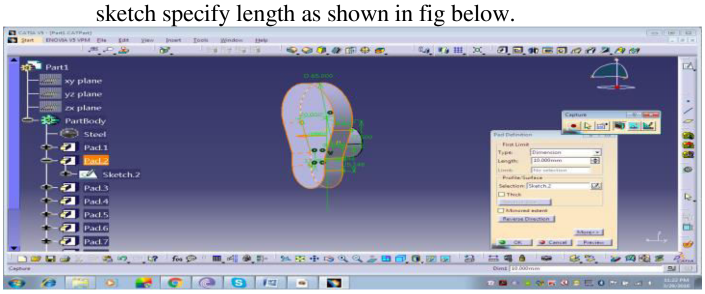

Final crank shaft with steel alloy material component and with out material component as shown in the fig below

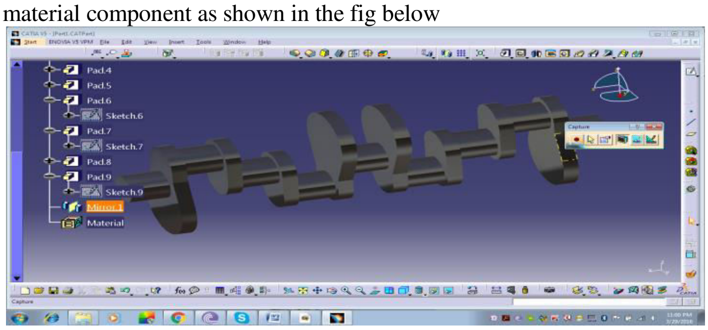

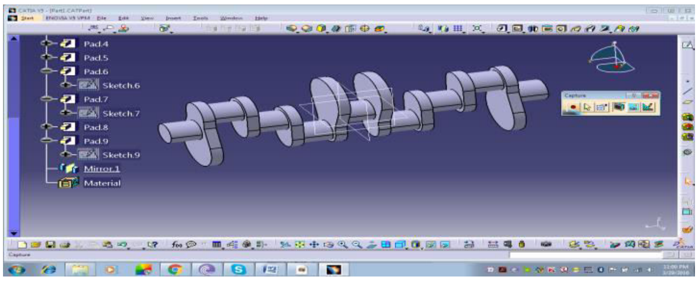

.

IV. FEA SOFTWARE – ANSYS

A. ANSYS Stands for Analysis System Product.

Dr. John Swanson founded ANSYS. Inc in 1970 with a vision to commercialize the concept of computer simulated engineering, establishing himself as one of the pioneers of Finite Element Analysis (FEA). ANSYS inc. supports the ongoing development of innovative technology and delivers flexible, enterprise wide engineering systems that enable companies to solve the full range of analysis problem, maximizing their existing investments in software and hardware. ANSYS Inc. continues its role as a technical innovator. It also supports a process-centric approach to design and manufacturing, allowing the users to avoid expensive and time-consuming “built and break” cycles. ANSYS analysis and simulation tools give customers ease-of-use, data compatibility, multi-platform support and coupled field multi-physics capabilities.

B. Reducing the design and manufacturing costs using ANSYS (FEA):

The ANSYS program allows engineers to construct computer models or transfer CAD models of structures, products, components, or systems, apply loads or other design performance conditions and study physical responses such as stress levels, temperature distribution or the impact of lector magnetic fields.

In some environments, prototype testing is undesirable or impossible. The ANSYS program has been used in several cases of this type including biomechanical applications such as high replacement intraocular lenses. Other representative applications range from heavy equipment components, to an integrated circuit chip, to the bit-holding system of a continuous coal-mining machine.

ANSYS design optimization enables the engineers to reduce the number of costly prototypes, tailor rigidity and flexibility to meet objectives and find the proper balancing geometric modifications.

Competitive companies look for ways to produce the highest quality product at the lowest cost. ANSYS (FEA) can help significantly by reducing the design and manufacturing costs and by giving engineers added confidence in the products they design. FEA is most effective when used at the conceptual design stage. It is also useful when used later in manufacturing process to verify the final design before prototyping

ix) Program availability:

The ANSYS program operates on Pentium based PCs running on Wndows95 or Windows NT and workstations and super computers primarily running on UNIX operating system. ANSYS Inc. continually works with new hardware platforms and operating systems.

C. Structural static analysis

A static analysis calculates the effects of steady loading condition on a structure, while ignoring inertia and damping effects such as those caused by time varying loads. A static analysis can, however include steady inertia loads (such as gravity and rotational velocity), and time varying loads that can be approximated as static equivalent loads (such as the static equivalent wind and seismic loads commonly defined in many building codes).

D. Procedure for ANSYS analysis

Static analysis is used to determine the displacements, stresses, strains and forces in structures or components due to loads that do not induce significant inertia and damping effects. Steady loading in response conditions are assumed. The kinds of loading that can be applied in a static analysis include externally applied forces and pressures, steady state inertial forces such as gravity or rotational velocity imposed (non-zero) displacements, temperatures (for thermal strain).

A static analysis can be either linear or nonlinear. In our present work we consider linear static analysis. The procedure for static analysis consists of these main steps:

- Building the model.
- Obtaining the solution.
- Reviewing the results**.**

i) Build the model:

In this step we specify the job name and analysis title use PREP7 to define the element types, element real constants, material properties and model geometry element types both linear and non-linear structural elements are allowed. The ANSYS element library contains over 80 different element types. A unique number and prefix identify each element type.

E.g. BEAM 94, PLANE 71, SOLID 96 and PIPE 16

Material properties:

Young’s modulus (EX) must be defined for a static analysis. If we plan to apply inertia loads(such as gravity) we define mass properties such as density(DENS). Similarly if we plan to apply thermal loads (temperatures) we define coefficient of thermal expansion (ALPX).

ii) Obtain the solution:

In this step we define the analysis type and options, apply loads and initiate the finite element solution. This involves three phases:

- **Pre – processor phase**
- **Solution phase**
- **Post-processor phase**

PRE – PROCESSOR:

Preprocessor has been developed so that the same program is available on micro, mini, super-mini and mainframe computer system. This slows easy transfer of models one system to other.

Preprocessor is an interactive model builder to prepare the FE (finite element) model and input data. The solution phase utilizes the input data developed by the preprocessor, and prepares the solution according to the problem definition. It creates input files to the temperature etc., on the screen in the form of contours.

GEOMETRICAL DEFINITIONS:

There are four different geometric entities in preprocessor namely key points, lines, areas and volumes. These entities can be used to obtain the geometric representation of the structure. All the entities are independent of other and have unique identification labels.

MODEL GENERATIONS:

Two different methods are used to generate a model:

- **Direct generation.**
- **Solid modeling**

With solid modeling we can describe we can describe the geometric boundaries of the model, establish controls over the size and desired shape of the elements and then instruct ANSYS program to generate all the nodes and elements automatically. By contrast, with the direct generation method, we determine the location of every node and size, shape and connectivity of every element prior to defining these entities in the ANSYS model. Although, some automatic data generation is possible (by using commands such as FILL, NGEN, EGEN etc) the direct generation method essentially a hands on numerical method that requires us to keep track of all the node numbers as we develop the finite element mesh. This detailed book keeping can become difficult for large models, giving scope for modeling errors. Solid modeling is usually more powerful and versatile than direct generation and is commonly preferred method of generating a model.

MESH GENERATION:

In the finite element analysis the basic concept is to analyze the structure, which is an assemblage of discrete pieces called elements, which are connected, together at a finite number of points called Nodes. Loading boundary conditions are then applied to these elements and nodes. A network of these elements is known as Mesh.

FINITE ELEMENT GENERATION:

The maximum amount of time in a finite element analysis is spent on generating elements and nodal data. Preprocessor allows the user to generate nodes and elements automatically at the same time allowing control over size and number of elements. There are various types of elements that can be mapped or generated on various geometric entities.

The elements developed by various automatic element generation capabilities of preprocessor can be checked element characteristics that may need to be verified before the finite element analysis for connectivity, distortion-index, etc.

Generally, automatic mesh generating capabilities of preprocessor are used rather than defining the nodes individually. If required, nodes can be defined easily by defining the allocations or by translating the existing nodes. Also one can plot, delete, or search nodes.

BOUNDARY CONDITIONS AND LOADING:

After completion of the finite element model it has to constrain and load has to be applied to the model. User can define constraints and loads in various ways. All constraints and loads are assigned set 1D. This helps the user to keep track of load cases.

MODEL DISPLAY:

During the construction and verification stages of the model it may be necessary to view it from different angles. It is useful to rotate the model with respect to the global system and view it from different angles. Preprocessor offers this capability. By windowing feature preprocessor allows the user to enlarge a specific area of the model for clarity and details. Preprocessor also provides features like smoothness, scaling, regions, active set, etc for efficient model viewing and editing.

MATERIAL DEFINITIONS:

All elements are defined by nodes, which have only their location defined. In the case of plate and shell elements there is no indication of thickness. This thickness can be given as element property. Property tables for a particular property set 1-D have to be input. Different types of elements have different properties for e.g.

Beams	: Cross sectional area, moment of inertia etc
Shells	: Thickness
Springs	: Stiffness
Solids	: None

The user also needs to define material properties of the elements. For linear static analysis, modules of elasticity and Poisson's ratio need to be provided. For heat transfer, coefficient of thermal expansion, densities etc are required. They can be given to the elements by the material property set to 1-D.

SOLUTION:

The solution phase deals with the solution of the problem according to the problem definitions. All the tedious work of formulating and assembling of matrices are done by the computer and finally displacements are stress values are given as output. Some of the capabilities of the ANSYS are linear static analysis, non-linear static analysis, transient dynamic analysis, etc.

POST – PROCESSOR:

It is a powerful user-friendly post-processing program using interactive color graphics. It has extensive plotting features for displaying the results obtained from the finite element analysis. One picture of the analysis results (i.e. the results in a visual form) can often reveal in seconds what would take an engineer hour to asses from a numerical output, say in tabular form. The engineer may also see the important aspects of the results that could be easily missed in a stack of numerical data.

Employing state of art image enhancement techniques, facilities viewing of:

- Contours of stresses, displacements, temperatures, etc.
- Deform geometric plots
- Animated deformed shapes
- Time-history plots
- Solid sectioning
- Hidden line plot

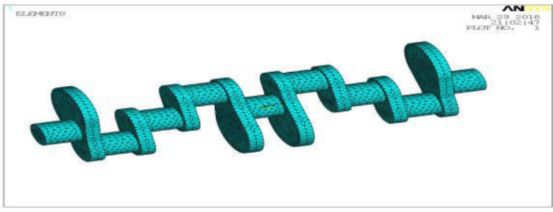

Fig: Mesh model of crankshaft

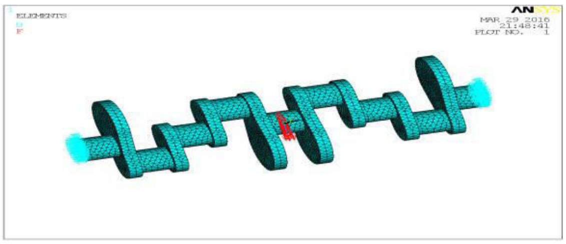

Fig. : Boundary conditions of Crank shaft

The above figure Shows that Working condition of the crank shaft At 2000 RPM.

V. RESULTS

A. Structural Analysis of Crankshaft with EN 36 Steel

The below diagram shows deformation of the crankshaft at 2000 RPM, maximum deformation is 0.293343 mm

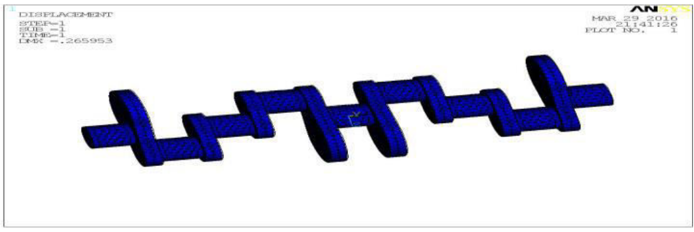

Fig.Deformation of crankshaft

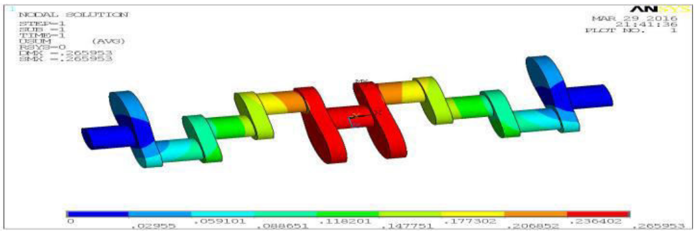

Fig.Vector sum of displacement of crankshaft

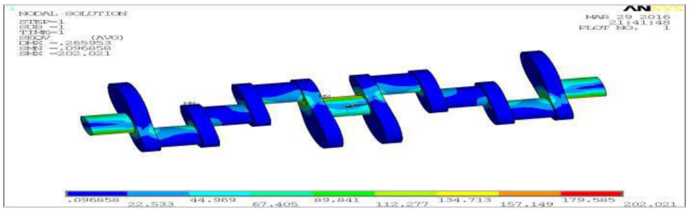

Fig.vonmises stress of crankshaft

B. Structural Analysis of Crankshaft with Cast iron Alloy

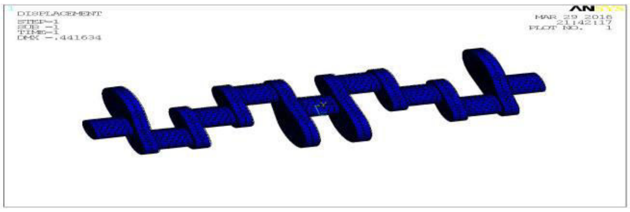

Fig.Deformation of crankshaft

The above diagram shows deformation of the crank shaft at 2000 RPM, maximum deformation is 0.372041 mm

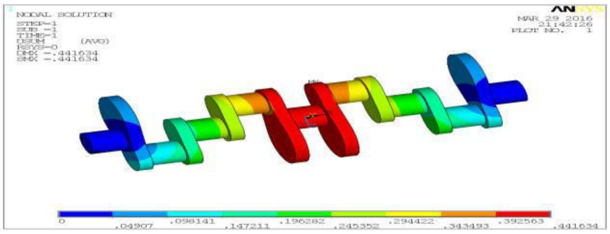

Fig.Vector sum of displacement of crankshaft

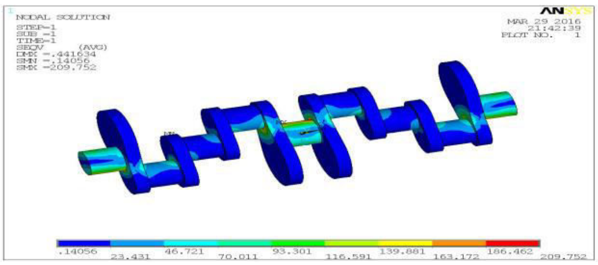

Fig.vonmises stress of crankshaft

C. Results of Static analysis

S. No	Material	Deformation, mm	Vonmises stresses, MPa
1	Steel En36	0.265	202.021
2	Cast Iron Alloy	0.4416	209.252

VI. CONCLUSION & FUTURE WORK

Steel En36 and Cast iron crankshaft were chosen for this Project, both of which belong to similar single cylinder four stroke air cooled gasoline engines. Static analysis and Modal analysis was performed based on of the slider crank mechanism consisting of the crankshaft.

The following conclusions can be drawn from the analysis:

i) Static analysis of the crankshaft results in more realistic stresses whereas all Stress are within the limits.
ii) From the results it is observed that Steel En36 is safer than cast iron Alloy. But both materials are within the elastic limits
iii) In the present investigation of static and Modal analysis is done on Crankshaft by using ANSYS package.
iv) Accurate stresses are critical input to fatigue analysis and optimization of the crankshaft

REFERENCES

1. Altan, T., Oh, S., and Gegel, H. L., 1983, “Metal Forming Fundamentals and Applications,” American Society for Metals, Metal Park, OH, USA.
2. Ando, S., Yamane, S., Doi, Y., Sakurai, H., and Meguro, H., 1992, “Method for Forming a Crankshaft,” US Patent No. 5115663, United States Patent.
3. Baxter, W. J., 1993, “Detection of Fatigue Damage in Crankshafts with the Gel Electrode,” SAE Technical Paper No. 930409, Society of Automotive Engineers, Warrendale, PA, USA.
4. Borges, A. C., Oliveira, L. C., and Neto, P. S., 2002, “Stress Distribution in a Crankshaft Crank Using a Geometrically Restricted Finite Element Model,” SAE Technical Paper No. 2002-01-2183, Society of Automotive Engineers, Warrendale, PA, USA.
5. Burrell, N. K., 1985, “Controlled Shot Peening of Automotive Components,” SAE Technical Paper No. 850365, Society of Automotive Engineers, Warrendale, PA, USA.
6. Chien, W. Y., Pan, J., Close, D., and Ho, S., 2005, “Fatigue Analysis of Crankshaft Sections Under Bending with Consideration of Residual Stresses,” International Journal of Fatigue, Vol. 27, pp. 1-19.
7. Fergusen, C. R., 1986, “Internal Combustion Engines, Applied Thermodynamics,” John Wiley and Sons, Inc., New York, NY, USA.
8. Guagliano, M., Terranova, A., and Vergani, L., 1993, “Theoretical and Experimental

EVALUATION OF THE STATE OF STRESS AT THE MIDDLE OF DAMAGED PLATE

M.Venkataswamy
Assistant professor
Dept. of Mechanical
Malla Reddy College of Engineering ,
Hyderabad, India.
Email ID: venkataswamy017@gmail.com

B.Bhaskar Naik
Assistant professor
Dept.of Mechanical
Malla Reddy College Of Engineering
Hyderabad,india
Email ID: bhaskarnaik308@gmail.com

ABSTRACT:

There are two, parallel ways to investigate the geometry effect on fracture toughness: experimental and computational analysis, the latter referring often to Finite Element Method (FEM). This investigation is at the middle of damaged plate of a finite length. Basically state of stress is calculated here analytically and computationally. ANSYS 11.0 is used as a computational tool. For different values of same pressure, state of stress is calculated and then compared with analytical results and good agreement is noted between both approaches.

Keywords: State of stress, Damaged length, Middle of Damaged Plate, ANSYS, and FEM.

1. INTRODUCTION

Fracture mechanics is a branch of science involving with micromechanics and strength of materials. Fracture mechanics is applied in order to obtain the fracture parameters of a cracked components or specimens, creating a singular stress field at the tip of the crack. Fracture toughness describes the ability to resist fracture and depends on component dimension, loading and material properties at the operating conditions. Problems are encountered with the size requirement. Usually low strength materials have high fracture toughness and so the minimum required specimen size for those materials may be very large, in some cases of the order of several meters. This leads to the need of larger testing machines which increases costs. On the other hand, in some cases the specimen size is limited due to manufacturing process or material availability. The stress intensity factor, K, is used in fracture mechanics to predict the stress state ("stress intensity") near the tip of a crack caused by a remote load or residual stresses. It is a theoretical construct usually applied to a homogeneous, linear elastic material and is useful for providing a failure criterion for brittle materials. The concept can also be applied to materials that exhibit small-scale yielding at a crack tip. The magnitude of K depends on sample geometry, the size and location of the crack, and the magnitude and the modal distribution of loads on the material.

2.LITERATURE REVIEW

To describe the behaviour of the crack growth the first milestone was set by Griffith [1] in his famous 1920 paper that quantitatively relates the flaw size to the fracture stresses. However, Griffith's approach is too primitive for engineering applications and is only good for brittle materials. For ductile materials, the milestone did not come about until Irwin developed the concept of strain energy release rate G in 1950s.When the strain energy release rate reaches the critical value, the crack will grow. Later, the strain energy release rate was replaced by the stress intensity factor K with a similar approach by other researchers. After the fundamentals of fracture mechanics were established around 1960, scientists began to concentrate on the plasticity of the crack tips. In 1968, Rice [2] modelled the plastic deformation as nonlinear elastic behaviour and extended the method of energy release rate to nonlinear materials. Hancock et al [3] presented constraint and toughness parameterized by a series of cracked specimen configurations tested to correlate the geometry dependence of crack tip constraint and fracture toughness in full plasticity. Yan et al [4] presented Effect of crack depth and specimen width on fracture toughness of a carbon steel in the ductile - brittle transition region The effects of crack depth. a/w and specimen width w on the fracture toughness and ductile- brittle transition have been investigated using three-point bend specimens. Finite element analysis is employed to obtain the stressstrain fields ahead of the crack tip. The results show that both normalized crack depth. a/w and specimen width (w) affect the fracture toughness and ductile-brittle fracture transition. An asymptotic approach to size effect on fracture toughness and fracture energy of composites by Hu [5] Size effect on fracture toughness and fracture energy of composites is investigated by a simple asymptotic approach. This asymptotic analysis based on the elastic/plastic fracture transition of a large plate with a small edge crack is extended to study fracture of composite.

3.FRACTURE MODES

There are three basic modes of fracture 1. Opening, 2. Sliding, 3. Tearing. Mode I: Opening Mode In this type of fracture, tensile stress are acting normal to the plane of crack, fig 3.1 shows the overview of fracture Mode I.

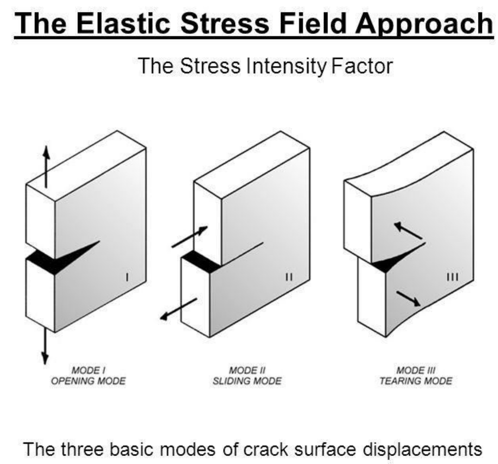

Parallel to the plane of the crack and parallel to the crack front as shown in fig 3.3. Our investigation is only mode I of fracture, opening. A central cracked plate of finite length is taken into consideration and analysis is done computationally and then compared with analytical results.

Intensity Factor and Crack Tip Stresses

Crack tips produce a 1/ r singularity. The stress fields near a crack tip of an isotropic linear elastic material can be expressed as a product of 1/ r and a function of θ with a scaling factor K [6]

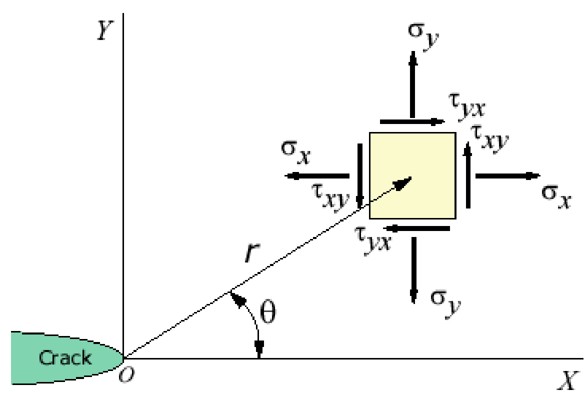

$$\lim_{y\to 0} \sigma_{ij} = \frac{K_I}{\sqrt{2\pi r}} f_{ij}(\theta) \quad \text{(Mode I)}$$
$$\lim_{y\to 0} \sigma_{ij} = \frac{K_{II}}{\sqrt{2\pi r}} f_{ij}(\theta) \quad \text{(Mode II)}$$
$$\lim_{y\to 0} \sigma_{ij} = \frac{K_{III}}{\sqrt{2\pi r}} f_{ij}(\theta) \quad \text{(Mode III)}$$

Where the superscripts and subscripts I, II, and III denote the three different modes that different loadings may be applied to a crack. The factor K is called the Stress Intensity Factor. The variables r and ө are the radius from the crack tip and the angle measured from the line ahead of the crack, respectively.

4.CLASSIFICATION OF FRACTURE MECHANICS

It is classified two types 1. Linear Elastic Fracture Mechanics (LEFM) e.g. Glass. 2. Elastic Plastic Fracture Mechanics (EPFM) e.g. Mild steel LEFM is valid only when the inelastic deformation is small compared to the size of the crack, what we called small-scale yielding. If large zones of plastic deformation develop before the crack grows, Elastic Plastic Fracture Mechanics (EPFM) must be used grows, Elastic Plastic Fracture Mechanics (EPFM) must be used.

5. PROBLEM SPECIFICATION

5.1 Consider a finite square plate in tension with a central crack. Material is assumed to be linear elastic, with a young's modulus E = 200 GPa and poison's ratio is 0.3 m. Width of specimen is 0.2 m and crack length is 0.02m. Calculate stress Intensity factor.

5.2 Analytical result :

Analytical solution given by W.D. Pilkey (formulas for stress, strain, structural Matrices) is

$$K_I = C\sigma\sqrt{\pi a},$$

Where, $C = (1 - 0.1\eta^2 + 0.96\eta^4)\sqrt{1/\cos(\pi\eta)}$,

$$\eta = \frac{a}{w}$$

5.3 Computational results Computational results are calculated by Modelling and meshing in Ansys 11.0 and then calculating stress intensity factor. We have taken ten cases for different pressure values and then calculate the stress intensity factor and then compared with respective analytical results and found good agreement between both values.

6. RESULTS AND DISCUSSIONS

6.1 Variation of stress intensity factor with : Variation of stress intensity factor KI can be seen in Table 6.1. Here both values of Stress intensity factor KI (i.e., analytical and computational) are compared. In fig 6.1 graphs can be seen between both the approaches.

TABLE 6.1: variation of stress intensity factor with σ

S.N.	σ (MPa)	K_I (ANALYTICAL) (MPa.m$^{1/2}$)	K_I (ANSYS) (MPa.m$^{1/2}$)	ERROR (%)
1.	100	25.0438106	26.524	5.9104
2.	120	30.05255772	31.821	5.8844
3.	140	35.06133484	37.124	5.8830
4.	160	40.07009696	42.427	5.8819
5.	180	45.07885908	47.731	5.8833
6.	200	50.0876212	53.034	5.8825
7.	220	55.09638332	58.338	5.8831
8.	240	60.10514545	63.641	5.8830
9.	260	65.1139075	68.945	5.8837
10.	280	70.12266969	74.248	5.8836

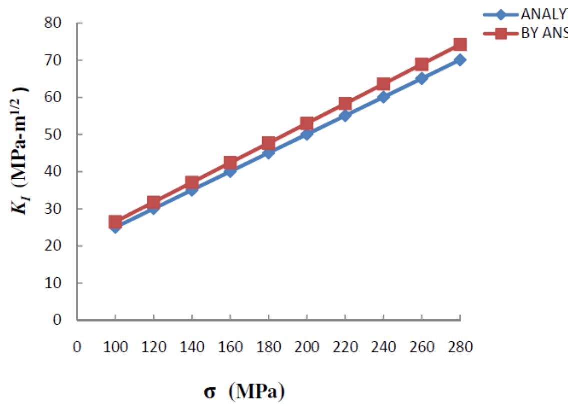

Figure 6.1: Variation of K_I with σ

Table 6.2: Variation of stress intensity factor with crack length at same load

S.N.	Crack length, a (m)	$K_{I\ (ANALYTICAL)}$ ($MPa.m^{1/2}$)	$K_{I\ (ANSYS)}$ ($MPa.m^{1/2}$)
1.	0.01	17.7202	18.019
2.	0.02	25.0438	26.524
3.	0.03	30.5921	34.559
4.	0.04	35.3627	43.243
5.	0.05	39.5360	52.107
6.	0.06	43.3658	55.137
7.	0.07	47.0001	63.179
8.	0.08	51.3101	68.426

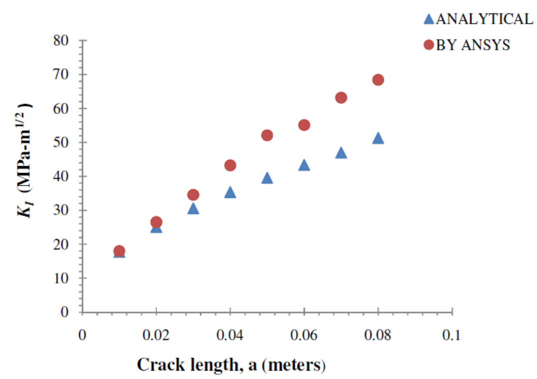

Figure 6.2: Variation of stress intensity factor with crack length

6.2 Variation of stress intensity factor with crack length at same load Variation of crack length can be seen in table 6.2. This is done by varying the crack length of specimen and then performed necessary calculation for KI (Analytical) and then compared with the KI (Ansys), which is computed by ANSYS. Variation between both the values can be seen in figure 6.2.

7. CONCLUSION

Study of fracture behaviour of materials is important as the materials may be subjected to extreme conditions like high temperature, high loading condition etc. In design of large structure, the measurement of fracture toughness is very typical due to their large sizes, therefore, the use of different scale specimens like compact tension. In this project work the ANSYS 11.0 used as computational tool for the analysis of static fracture mechanics problem. By the use of ANSYS 11.0, K estimated under different conditions such as different crack length and different load. After the calculation of K, J integral can be computed by computational tool ANSYS and after finding these parameters strain energy distribution can be estimated and this can be used as a very effective tool in fracture mechanics.

References

1. Griffith, A.A., “The phenomena of rupture and flow in solids”, Philosophical Transactions, Series A, Vol. 221, 1920, pp163-198

2. Rice J.R.,” a path independent integral and approximate analysis of strain concentration by notches and cracks”, Journal of Applied Mechanics, Vol.35, (1968), pp379-386

. 3. Hancock, J. W., Reuter, W. G., and Parks, D. M., “Constraint and Toughness Parameterized by T”, Constraint Effects in Fracture, ASTM STP 1171, E. M. Hackett, K.-H. Schwalbe, and R. H. Dodds, Eds., American Society for Testing and Materials, Philadelphia, (1993) 21-40

4. Yan, C.and Mai, Y.W., “Effect of crack depth and specimen width on fracture toughness of a carbon steel in the ductile - brittle transition region”, International Journal of Pressure Vessels and Piping, 77 (2000) 313-319.

5. Hu, X.Z., “An asymptotic approach to size effect on fracture toughness and fracture energy of composites”, Engineering Fracture Mechanics 69 (2002) 555– 564.

6. Hertzberge,R.W., “ Deformation and Fracture Mechanics of Engineering Materials”, 3rd Edition, John Wiley and Sons, Singapore, (1989)
7. W.D. Pilkey (formulas for stress, strain, structural Matrices).

MODELING AND STRUCTURAL ANALYSIS OF SPUR GEAR TOOTH WITH DIFFERENT MATERIAL

NILESH DHAKATE,
PG SCHOLOR,
Malla Reddy College of Engineering,
email : nilesh36mech@gmail.com.

M. VENKATASWAMY,
Assistant Professor,
Malla Reddy College of Engineering,
email : venkataswamy017@gmail.com.

ABSTRACT

Rigging is a standout amongst the most basic part in a mechanical power transmission framework, and most modern turning hardware The target of this proposal is to consider the different anxiety condition of apparatus tooth. The most widely recognized methods for transmitting power is Gears in the wooden mechanical world. They shift from a modest size utilized as a part of watches to bigger riggings utilized as a part of huge speed reducers, connect lifting system and rail street turn table drive. The riggings are key components of fundamental and helper instrument in many machines, for example, autos, tractors, metal cutting machine apparatuses moving factories facilitating and transmitting and transporting hardware, monstrous motors and so forth. In this venture outfit tooth is demonstrated in Ansys with separate measurements. Static investigation is carried on the tooth with the characterized material properties. Distortion, Stresses and vonmises stress will be shaped.

INTRODUCTION

Gears are ordinarily utilized for transmitting power. They grow high anxiety focus at the root and the point of contact. The weariness disappointment of apparatus tooth happens because of the rehashed worrying on the filets. A limited component model of Spur equip utilized as a part of the headstock of Lathe machine for control transmission is considered for investigation

The most astounding anxiety happens at two areas:

1. For the most part At contact point, where the power F acts and

2. At the filet locale close to the base of the tooth.

The surface disappointments happening chiefly because of contact weakness are setting and scoring. It is a wonder in which little particles are expelled from the surface of the tooth because of the high contact focuses on that are available between mating teeth. In reality the weakness disappointment of the tooth surface is Pitting. Hardness is theessential property of the rigging tooth that gives imperviousness to setting. At the end of the day, setting is asurface wearinessdisappointment because of numerousredundancies of high contact push, which happens on adapt tooth surfaces when a couple of teeth is transmitting power .Gear teeth bombs because of contact. Weakness is a typical marvel watched. Contact disappointment in gears is presently anticipated by contrasting the computed Hertz contact worry with tentatively decided admissible esteems for the given material. The technique for ascertaining gear contact worry by Hertz'scondition initially determined for contact between two barrels. The Hertz conditions talked about so far can be used to figure the contact stresses which win if there should arise an occurrence of tooth surfaces of two mating goad gears. In spite of the fact that an estimation, the contact parts of such riggings can be taken to be proportionate to those of barrels having similar radii of ebb and flow at the contact point as the heap transmitting gears have sweep of ebb and flow changes persistently if there should be an occurrence of involutes bend, and it changes pointedly in the region of the base circle.

Types of Gear:

- Spur Gear
- Helical Gear
- Spiral Gear
- Involute Gear

FINITE ELEMENT METHOD

Step by Step Procedure:

1. Discretization of the area
2. Fundamental Element Shapes
3. Size of Elements
4. Area of Nodes
5. Number of Elements

Advantages:

1. The utilization of partitioned sub locales or limited components for the trail arrangements allows a more prominent adaptability in considering continuation of complex shape.
2. As the limit conditions don't go into conditions for the individual limited components, one can utilize a similar field variable for both inner and limit

components.

3. The field variable models require not be changed when the limit conditions change.

Limitations:

1. Cracking and Fracture conduct.
2. Contact issues.
3. Bond disappointments of composite materials.
4. Non-Linear material conduct with work softening.

Applications:

1. Mechanical Design
2. Structural Engineering Structures
3. Air Craft structures
4. Warmth conduction
5. Atomic Engineering

PROCEDURE

STATIC ANALYSIS OF GEAR TOOTH USING GREY CAST IRON MATERIAL

PREFERENCES – **STRUCTURAL**:

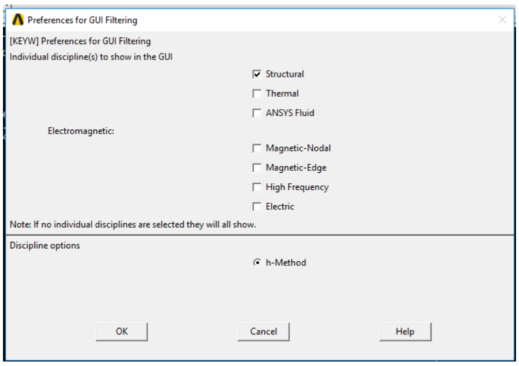

ELEMENT TYPE:

- ➢ Element type – ADD - SOLID -10 node 187

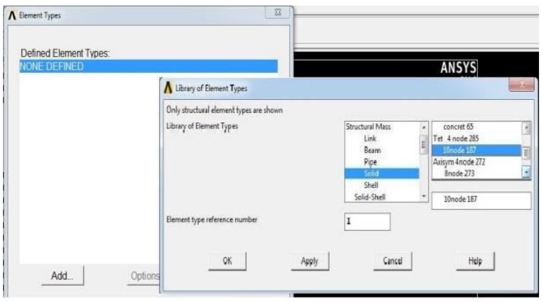

MATERIAL PROPERTIES

- ➢ STRUCTURAL -ISOTROPIC – EX = 2E5 , PRXY = 0.29

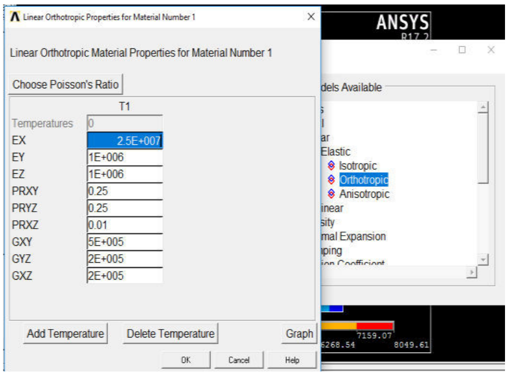

MODELING:

NODE	X – AXIS	Y - AXIS
1	0	0
2	2.4	0
3	0.68	2.25
4	1.72	2.25

LINE–STRAIGHT LINES – SELECT ALL

KEYPOINTS: LINES – LINE FILLET

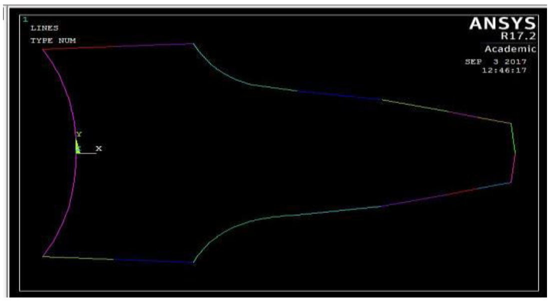

AREAS – ARBITRARY – THRU LINES

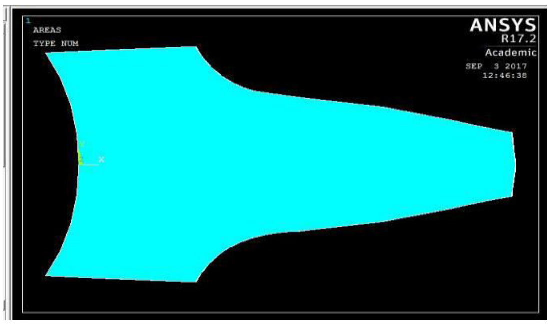

OPERATE – EXTRUDE – XYZ OFFSET, Z= 0.86

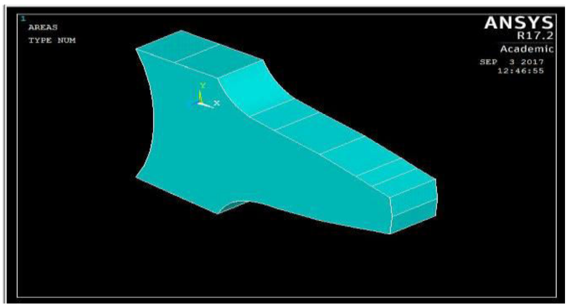

MESHING:

- **VOLUMES** – FREE – SELECT-VOLUME–OK.

LOADS:

DEFINE LOADS – APPLY -STRUCTURAL – DISPLACEMENT **-** ON AREAS **-** ALL DOF PRESSURE - ON AREAS

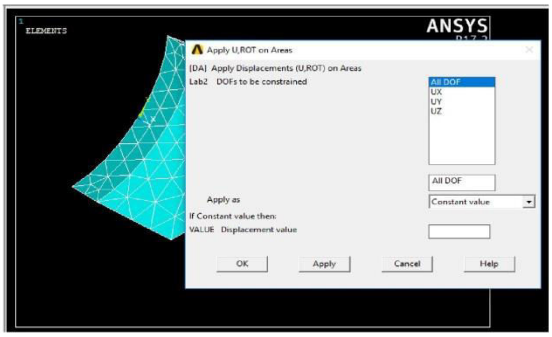

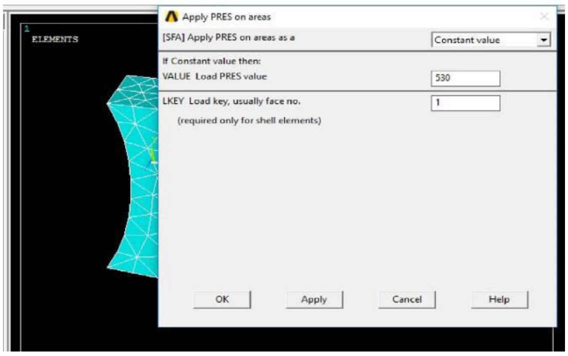

ANALYSIS TYPE:
SOLUTION:SOLVE

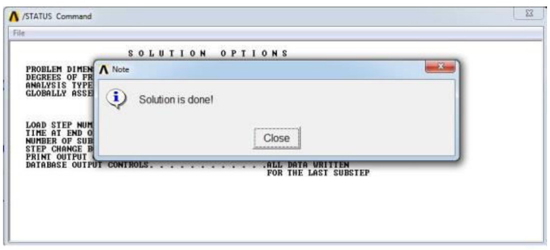

RESULTS:

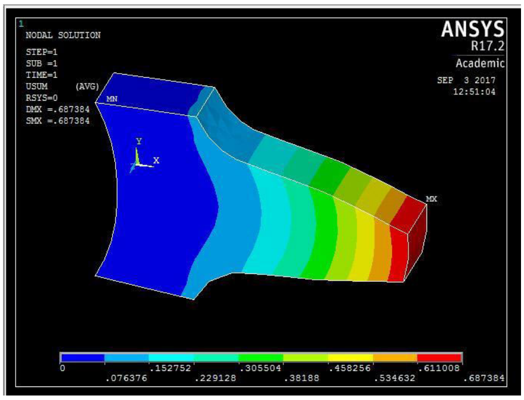

At Displacement Vector Sum

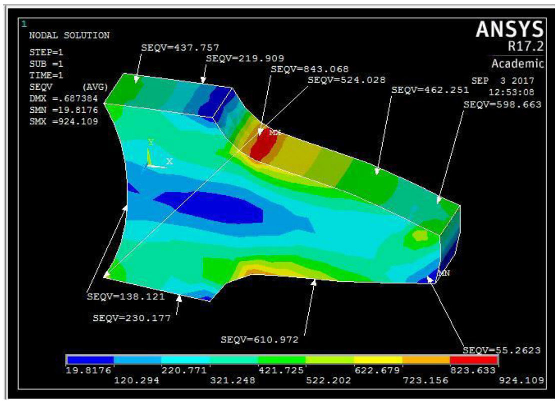

Von misses stress value

MODAL ANALYSIS OF GEAR TOOTH USING GREY CAST IRON MATERIAL

SOLUTION-ANALYSIS TYPE-NEW ANALYSIS-MODAL

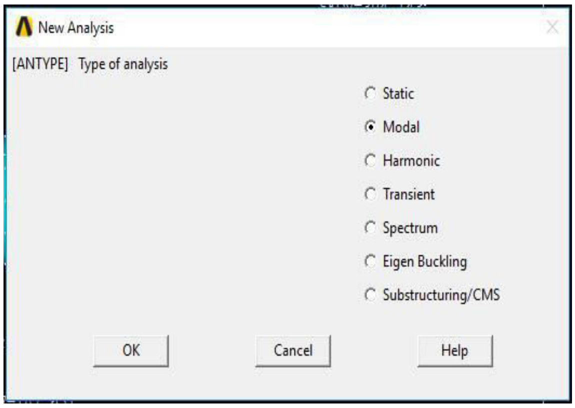

MODAL ANALYSIS-ANALYSIS OPTIONS

NUMBER OF MODES TO EXTRACT 3

NUMBER OF MODES TO EXPAND 3

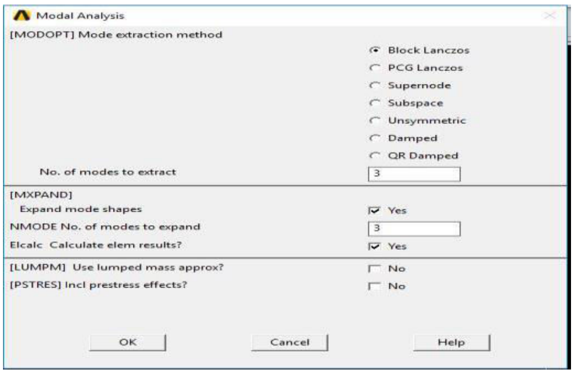

Frequency results

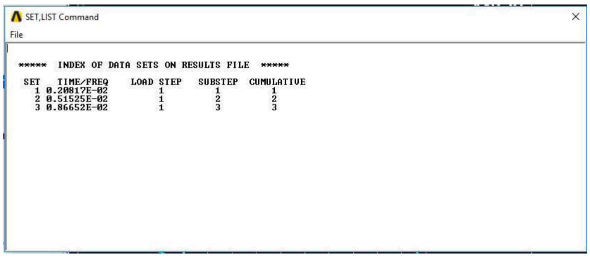

SET	TIME/FREQ	LOAD STEP	SUBSTEP	CUMULATIVE
1	0.20817E-02	1	1	1
2	0.51525E-02	1	2	2
3	0.86652E-02	1	3	3

MODAL ANALYSIS RESULTS

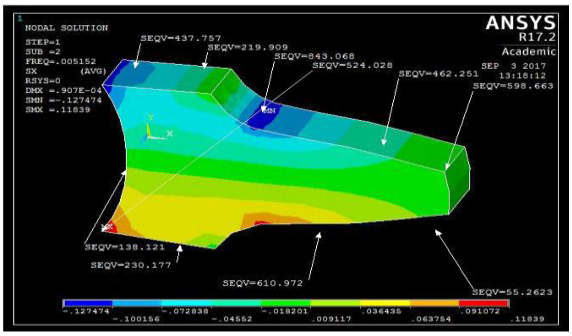

Vonmises stress at 1st frequency

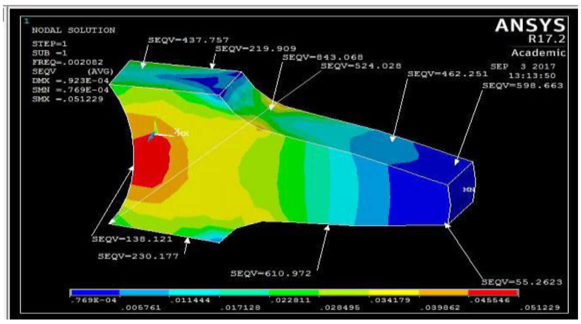

Vonmises stress at 2nd frequency

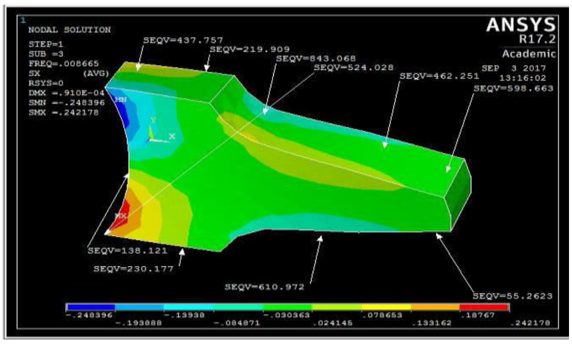

Vonmises stress at 3rd frequency

STATIC ANALYSIS OF GEAR TOOH USING CARBON STEEL MATERIAL

Material properties

Material = 20MnCr5
ex= 190e3 N/mm^2
prxy = 0.27
Density 8030 Kg/m^3

RESULTS

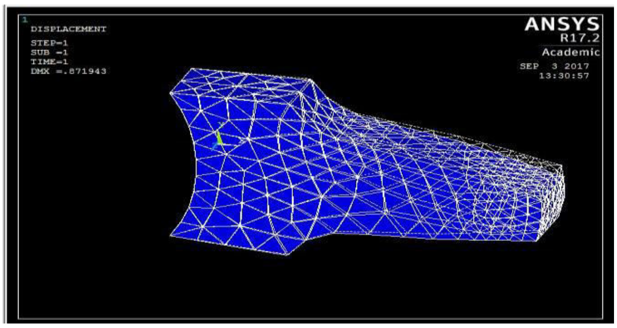

Deformed and unreformed shape

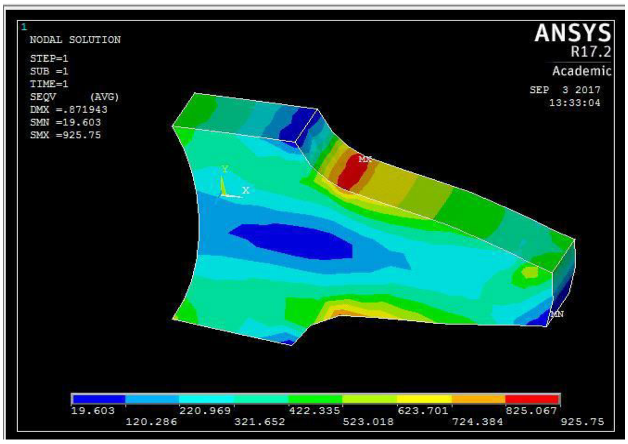

Von mises Stress values along geometry

MODAL ANALYSIS OF GEAR TOOTHUSING CARBON STEEL MATERIAL

Frequency results

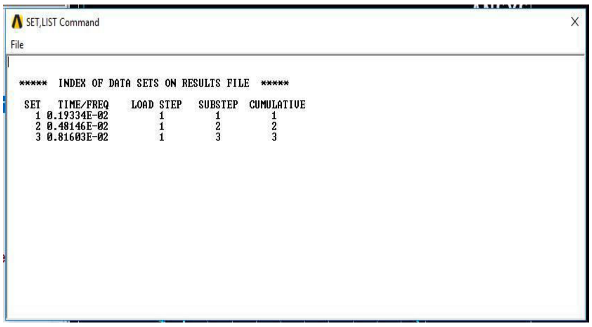

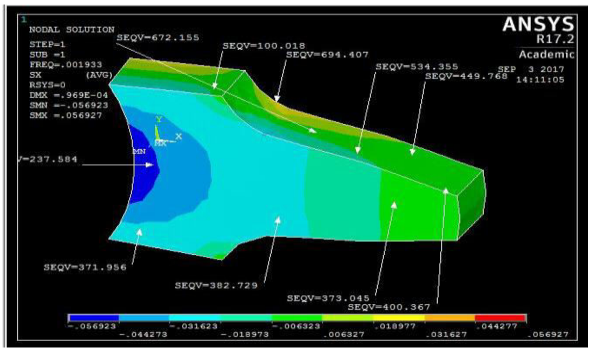

VonmisesStress values at 1st Frequency

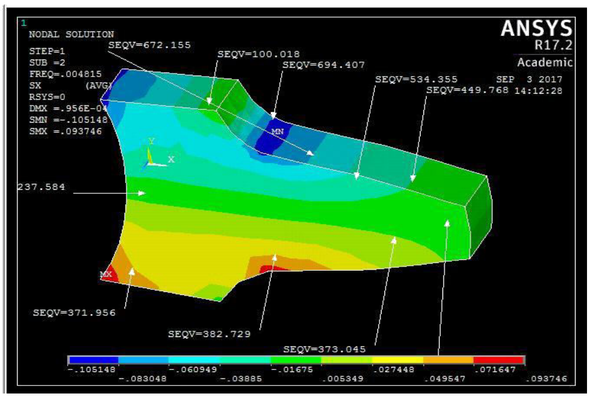

VonmisesStress values at 2nd Frequency

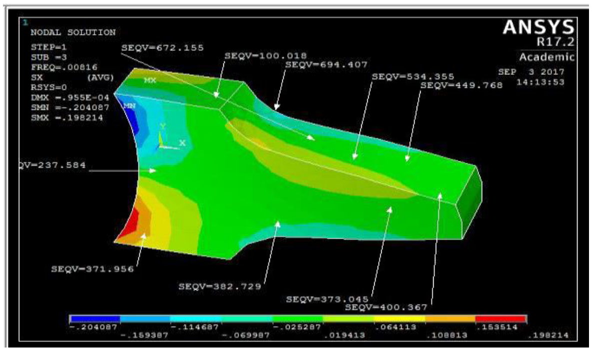

Vonmises Stress values at 3rdFrequency

RESULT:

Obtained Results After performing the static and modal analysisof a spur gear tooth with the 2 different materials.

MATERIAL	DEFORMATION	VONMISS STRESS
GRAY CAST IRON	0.687384	924.109
CARBON STEEL	0.871943	925.74

CONCLUSION

Gears are commonly used for transmitting power. They develop high stress concentration at the root and the point of contact. The repeated stressing on the fillets causes the fatigue failure of gear tooth. In this project the gear tooth is modeled with the respective dimensions and done both the static analysis and model analysis using steel material and grey cast iron materials. Found out the deformations of the body and contoured along with Vonmises stresses in all components in Static analysis as well as frequency response for both steel material and grey cast iron materials. In This I Concluded That Grey Cast Iron Material Is Suitable For Manufacturing Gear Tooth Because This Material Produces Less Stress And Deformation While Compared With Carbon Steel And This Material Provides Durability And also Ease Of Manufacture.

REFERENCES

- Theory of Machines, S.Chand and Khurmi, R. S.,
- https://en.wikipedia.org/wiki/Gear#CITEREFMcGraw-Hill2007
- Machine design by Khurmi, R. S
- Standard Handbook of Machine Design, Third Edition by Joseph E Shigley, Charles R.Mischke, Thomas Hunter Brown, Jr.
- Strength of Materials by R.K. Rajput

Wood Gas Generator with Integrated Boiler for Fueling Internal Combustion Engines by Using Wood Pyrolysis

P .Pavan Kumar[1], Dr.P Velmurgan[2],
[1]PG Scholar, [2]Professor Department of Mechanical Engineering, Malla Reddy College Of Engineering , Telangana.

Abstract—**Coal, wood and charcoal gasifiers have been used for operation of internal combustion engines in various applications since the beginning of this century. The utilization peaked during the Second World War when almost a million gasifiers were used all over the world, mainly vehicles operating on domestic solid fuels instead of gasoline. These gasifiers are mainly suitable for stationary engines like generators, gas stoves, and agriculture pump sets etc.Wood gas, the gas generated when wood, charcoal or coal is gasified with air, consists of 40 percent of combustible gases, mainly carbon monoxide, hydrogen and methane. The rest are non-combustible gas consists of mainly nitrogen, carbon dioxide and water vapor.**

KEY WORDS: Wood gas, Gasifier, Pyrolysis, Combustion, Biomass.

I. INTRODUCTION

WOOD GAS GENERATOR:

Wood gas generator is a gasification unit which converts timber or charcoal into wood gas, a syngas consisting of atmospheric nitrogen, carbon monoxide, hydrogen, traces of methane, and other gases, which - after cooling and filtering - can then be used to power an internal combustion engine or for other purposes. Historically wood gas generators were often mounted on vehicles, but present studies and developments concentrate mostly on stationary plants.

II. LITERATURE REVIEW

HISTORY/ORIGINS:

Gasification had been an important and common technology which was widely used to generate coal gas from coal mainly for lighting purposes during the 19th and early 20th century. When the first stationary internal combustion engines based on the Otto cycle became available in the 1870s, they began displacing steam engines as prime movers in many works requiring stationary motive power. Adoption accelerated after the Otto engine's patent expired in 1886. The potential and practical applicability of gasification to internal combustion engines were well-understood from the earliest days of their development.
In 1873, Thaddeus S. C. Lowe developed and patented the water gas process by which large amounts of hydrogen gas could be generated for residential and commercial use in heating and lighting. Unlike the common coal gas, or coke gas Which was used in municipal service, this gas provided a more efficient heating fuel.

During the late 19th century internal combustion engines were sometimes fueled by coal gas, and during the early 20th century many stationary engines switched to using producer gas created from coke which was substantially cheaper than coal gas which was based on the distillation (pyrolysis) of more expensive coal.
In about 1920 French inventor Georges Imbert created the 'Imbert' downdraft generator.

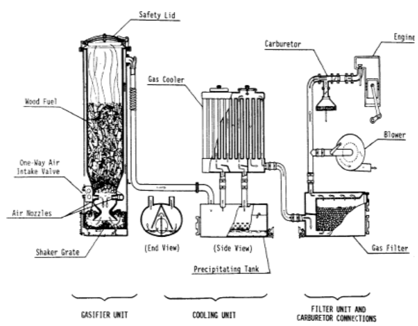

FIRST WOOD GASIFIER (IMBERT DESIGN)

This was quite popular during World War II in several European, African and Asian countries because the war prevented easy and cost-effective access to oil. In more recent times, wood gas has been suggested as a clean and efficient method to heat and cook in developing countries, or even to produce electricity when combined with an internal combustion engine. Compared to WWII technology, gasifiers have become less dependent on constant attention due to the use of sophisticated electronic control systems, but it remains difficult to get clean gas from them. Purification of the gas and feeding it into natural gas pipelines is one variant to link it to the existing refueling infrastructure. Liquefaction by the Fischer–Tropsch process is another possibility.
Efficiency of the gasifiers system is relatively high. The gasification stage converts about 75% of fuel energy content into a combustible gas that can be used as a fuel for internal combustion engines. Asked on long-term practical experiments and over 100,000 km drive The same source reports the following chemical composition by volume which most likely is also variable.

WOOD GAS:

Wood gas is a syngas fuel which can be used as a fuel for furnaces, stoves and vehicles in place of gasoline, diesel or other fuels. During the production process biomass or other carbon-containing materials are gasified within the oxygen-limited environment of a wood gas generator to produce hydrogen and carbon monoxide. These gases can then be burnt as a fuel within an oxygen rich environment to produce carbon dioxide, water and heat. In some gasifiers this process is preceded by pyrolysis, where the biomass or coal is first converted to char, releasing methane and tar rich in polycyclic aromatic hydrocarbons.

Wood gasifiers can power either spark ignition engines, where 100% of the normal fuel can be replaced with little change to the carburetion, or in a diesel engine, feeding the gas into the air inlet that is modified to have a throttle valve, if it didn't have it already. On diesel engines the diesel fuel is still needed to ignite the gas mixture, so a mechanically regulated diesel engine's "stop" linkage and probably "throttle" linkage must be modified to always give the engine a little bit of injected fuel (Often under the standard idle per-injection volume). Wood can be used to power cars with ordinary internal combustion engines if a wood gasifier is attached.

A wood gas producer
Nitrogen N_2: 50.9%
Carbon monoxide CO: 27.0%
Hydrogen H_2: 14.0%
Carbon dioxide CO_2: 4.5%
Methane CH_4: 3.0%
Oxygen O_2: 0.6%.

BY USING MATCH STICK SHOWING WOOD GAS

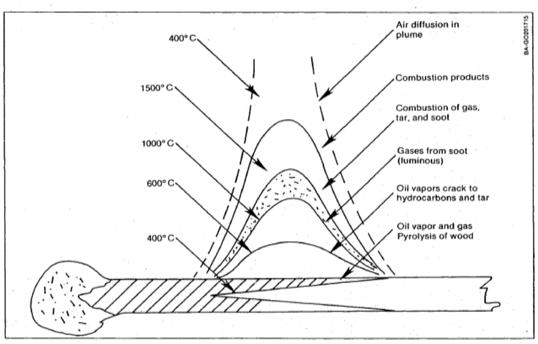

PYROLYSIS:

Pyrolysis is a thermo chemical decomposition of organic material at elevated temperatures in the absence of oxygen (or any halogen). It involves the simultaneous change of chemical composition and physical phase, and is irreversible. The word is coined from the Greek-derived elements pyro "fire" and lysis "separating".

Pyrolysis is a type of thermolysis, and is most commonly observed in organic materials exposed to high temperatures. It is one of the processes involved in charring wood, starting at 200–300 °C (390–570 °F). It also occurs in fires where solid fuels are burning or when vegetation comes into contact with lava in volcanic eruptions. In general, pyrolysis of organic substances produces gas and liquid products and leaves a solid residue richer in carbon content, char. Extreme pyrolysis, which leaves mostly carbon as the residue, is called carbonization.

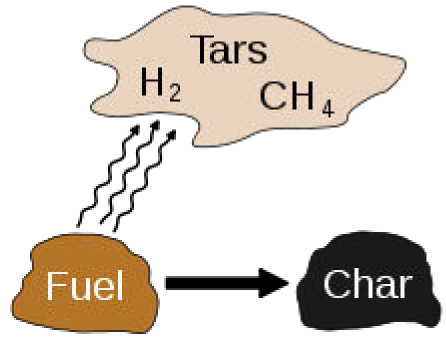

SYNGAS:

Syngas, or synthesis gas, is a fuel gas mixture consisting primarily of hydrogen, carbon monoxide, and very often some carbon dioxide. The name comes from its use as intermediates in creating synthetic natural gas (SNG) and for producing ammonia or methanol. Syngas is usually a product of gasification and the main application is electricity generation. Syngas is also used as an intermediate in producing synthetic petroleum for use as a fuel or lubricant via the Fischer–Tropsch process and previously the Mobil methanol to gasoline process. Syngas is combustible and often used as a fuel of internal combustion engines. It has less than half the energy density of natural gas.

When used as an intermediate in the large-scale, industrial synthesis of hydrogen (principally used in the production of ammonia), it is also produced from natural gas (via the steam reforming reaction) as follows:

$CH_4 + H_2O \rightarrow CO + 3\ H_2$

In order to produce more hydrogen from this mixture, more steam is added and the water gas shift reaction is carried out:

$CO + H_2O \rightarrow CO_2 + H_2$

The hydrogen must be separated from the CO_2 to be able to use it. This is primarily done by pressure swing adsorption (PSA), amine scrubbing, and membrane reactors.

TAR:

Tar obtained by the destructive distillation of wood either as a deposit from pyroligneous acid or as a residue from the distillation of the acid or of wood turpentine and used in the crude state as fuel or for preserving rope and wood and for caulking or fractionated to yield creosote, oils, and pitch

A tar-like substance can be produced from corn stalks by heating in a microwave. This process is known as pyrolysis.

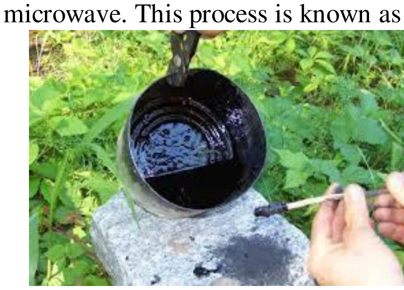

III. WOOD GAS PROCESS

THE HEAT REQUIRED ACCOMPLISHING GASIFICATION:

The heat required to accomplish gasification is generated in the combustion zone and the heat flows upwards with gas, starting the gasification processes.Where also a division of the different reaction zones is made. These four different zones will largely overlap in practice; still their differences will take a prominent place in the development of a model for the gasifier.

A description of the reactions that take place in each zone will be discussed next.

PROCESS IN GASIFICATION

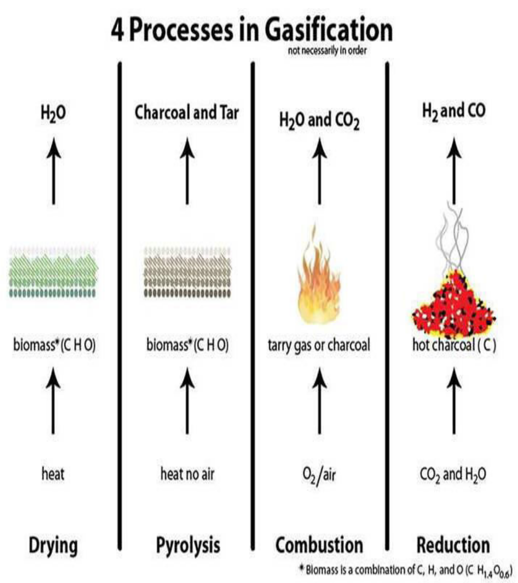

ZONES IN WOOD GASIFICATION

1. Combustion zone

The combustible substance of a solid fuel is usually composed of elements carbon, hydrogen and oxygen. In complete combustion carbon dioxide is obtained from carbon in fuel and water is obtained from the hydrogen, usually as steam. The combustion reaction is exothermic and yields a theoretical oxidation temperature of 1450^{0}C. The main reactions, Therefore, are:

$C + O_2 = CO2$ (+ 393 MJ/kg mole) (1)

$2H_2 + O_2 = 2H_2O$ (- 242 MJ/kg mole) (2)

2. Reaction zone

The products of partial combustion (water, carbon dioxide and uncombusted partially cracked pyrolysis products) now pass through a red-hot charcoal bed where the following reduction reactions take place.

REACTION CHEMISRY :

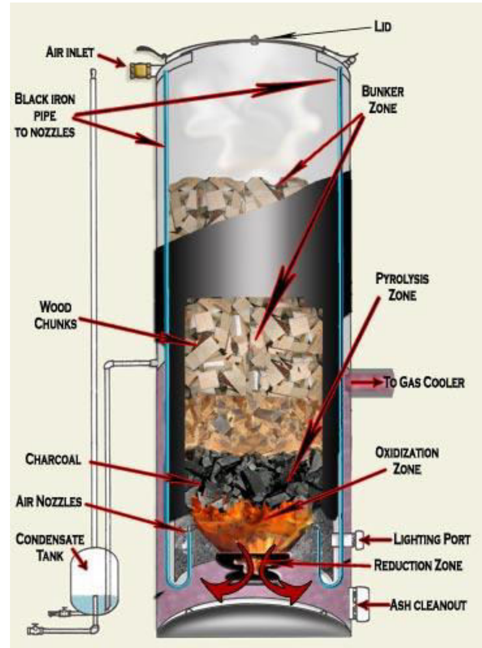

$C + CO_2 = 2CO$ (- 164.9 MJ/kg mole) (3)

$C + H_2O = CO + H_2$ (- 122.6 MJ/kg mole) (4)

$CO + H_2O = CO + H_2$ (+ 42 MJ/kg mole) (5)

$C + 2H_2 = CH4$ (+ 75 MJ/kg mole) (6)

$CO_2 + H_2 = CO + H_2O$ (- 42.3 MJ/kg mole) (7)

Reactions (3) and (4) are main reduction reactions and being endothermic have the capability of reducing gas temperature. Consequently the temperatures in the reduction zone are normally 800-1000^{0}C. Lower the reduction zone temperature (~ 700-800^{0}C), lower is the calorific value of gas.

3. Pyrolysis zone

Wood pyrolysis is an intricate process that is still not completely understood. The products depend upon temperature, pressure, residence time and heat losses. However following general remarks can be made about them.

Up to the temperature of 200^{0}C only water is driven off. Between 200 to 280^{0}C carbon dioxide, acetic acid and water are given off. The real pyrolysis, which takes place between 280 to 500^{0}C, produces large quantities of tar and gases containing carbon dioxide. Besides light tars, some methyl alcohol is also formed. Between 500-700^{0}C the gas production is small and contains H_2.

Thus it is easy to see that updraft gasifier will produce much more tar than downdraft one. In downdraft gasifier the tars have to go through combustion and reduction zone and are partially broken down.

4. Drying zone

Finally in the drying zone the main process is of drying of wood. Wood entering the gasifier has moisture content of 10-30%. Various experiments on different gasifiers in different conditions have shown that on an average the condensate formed is 6-10% of the weight of gasified wood[14]. Some organic acids also come out during the drying process. These acids give rise to corrosion of gasifiers.

HOW DOES THE GASIFIER WORK?

There are no pretty pictures or informative diagrams in this step. This is the stuff you need to read before attempting to build this project. Please don't skip it.

A biomass gasifier is a chemical reactor that converts wood, or other biomass substances, into a combustible gas. The formula is simple. **Biomass + Heat = Pyrolysis Byproducts**. Pyrolysis is a fancy-pants word that chemists use to describe the process of heat breaking down big molecules into smaller ones. In the gasifier we want to break big biomass molecules (mainly cellulose) down into smaller ones like Hydrogen and Carbon Monoxide.

Where does the heat come from? We get heat by partially combusting some of the biomass with a limited supply of Oxygen. The heat produced by the combustion then drives the pyrolysis reaction. A well built reactor will also convert combustion byproducts like CO_2 and water vapor into flammable CO and H_2 by passing them over a bed of hot charcoal, left over from the partial combustion, where they will get reduced.

Thus the gasifier converts most of the mass of the wood (or other biomass feedstock) into flammable gases with only some ash and unburned charcoal (bio-char) residue. That is the theory anyway. This is an extreme over-simplification of how the gasifier really works. Wood and other biomass is made of incredibly complex macro-molecules like Cellulose and Lignin that break down into hundreds or thousands of different smaller molecules as the reaction proceeds. There are thousands of different complex chemical reactions going on inside the reactor. The overall result though, if the gasifier is working well, is lots of clean, flammable gas.

Ideally, the gasifier would break down biomass into nothing but Hydrogen and Carbon Monoxide. Here in the real world though, things rarely work ideally. The dirty (literally) little secret about biomass gasification is tar production. Above I said that the macro-molecules that make up biomass get broken down into smaller molecules. Some of those smaller molecules are still pretty big though. If the gasifier is working well, these big breakdown by-products will be further "cracked" into smaller molecules. If the gasifier isn't working so well, these big molecules will wind up in the gas being produced. The first few iterations of this gasifier produced more tar than gas. The complete history of this design can be found on my web site at. Below is the most important of all chemical reactions a novice gasifier builder needs to know.

Biomass + Poorly Designed Gasifier = Tar!

I strongly recommend that anyone interested in gasifier technology do some research and read up on it. There is a lot more to this technology than I can present in an intractable.

SCHEMATIC OF THE GASIFIER

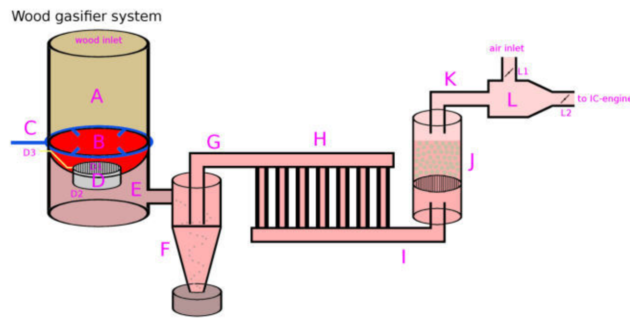

WHAT TO EXPECT FROM A WOOD GASIFIER SYSTEM:

Operation of modern spark ignition or compression ignition stationary engines with gasoline or diesel fuel is generally characterized by high reliability and minor efforts from the operator. Under normal circumstances the operator's role is limited to refueling and maintenance. There is little need for action and virtually no risk of getting dirty. Start and operation can infect be made fully automatic.

Anybody expecting something similar for wood gas operation of engines will to be disappointed.
Preparation of the system for starting can require half an hour or more. The fuel is bulky and difficult to handle. Frequent feeding of fuel is often required and these limits the time the engine can run unattended. Taking care of residues such as ashes, soot and tarry condensates is time-consuming and dirty.

It is necessary for most designs that the fuel properties are kept within fairly narrow ranges. This is not necessarily a more serious limitation than the need to use gasoline of super grade for high compression spark ignition engines rather than regular gasoline or diesel fuel. But in the case of gasifier operation, more of the responsibility for quality control of the fuel rests with the operator. The need for strict fuel specifications is well documented in the experiences reported from the Second World War. It is unfortunate that some commercial companies, with little practical experience, but trying to profit from the renewed interest in gasification, have advertised the possibility of using almost any kind of biomass even in gasifiers which will work well only with fuels meeting fairly strict standards. This has in some cases created unrealistic expectations and has led to disappointments with the technology.

Operation of wood gas engines can also be dangerous if the operator violates the safety rules or neglects the maintenance of the system. Poisoning accidents, explosions and fire shave been caused by unsafe designs or careless handling of the equipment. It may be assumed that modern systems are designed according to the best safety standards.

There has been some improvement of the technology, for instance of filter designs based on new materials, but the practical operating experience with these improved systems is limited. A consequence of this is that equipment failures caused by design mistakes, choice of the wrong materials, or incomplete instructions to the user on operation and maintenance, must be expected in the first period of reintroduction of wood gasifiers.

POSSIBILITIES OF USING PRODUCER GAS WITH DIFFERENT TYPES OF ENGINES:

Spark ignition engines, normally used with petrol-or kerosene, can be run on producer gasalone Diesel engines can be converted to full producer gas operation by lowering the compression ratio and the installation of a spark ignition system. Another possibility is to run normal unconverted diesel engine in a "dual fuel" mode, whereby the engine draws anything between 0 and 90 per cent of its power output from producer gas, the remaining diesel oil being necessary for ignition of the combustible gas/air mixture. The advantage of the latter system lies in its flexibility: in case of malfunctioning of the gasifier or lack of biomass fuel, an immediate change to full diesel operation is generally possible.

However, not all types of diesel engines can be converted to the above mode of operation. Compression ratios of ante-chamber and turbulence chamber diesel engines are too high for satisfactory dual fuel operation and use of producer gas in those engines leads to knocking caused by too high pressures combined with delayed ignition. Direct injection diesel engines have lower compression ratios and can generally be successfully converted.

GAS QUALITY REQUIREMENTS FOR TROUBLE-FREE OPERATION:

When a gasifier system is used in conjunction with an internal combustion engine, an important requirement is that the engine is supplied with a gas that is sufficiently free from dust, tars and acids. The tolerable amounts of these substances will vary depending on the type and outfit of the engine. The following values:

dust: lower than 50 mg/m³ gas preferably 5 mg/m³ gas
tars: lower than 500 mg/m³ gas
acids: lower than 50 mg/m³ gas (measured as acetic acid).

NEED FOR SELECTION OF THE RIGHT GASIFIER FOR EACH FUEL

residues(maize cobs, coconut shells, coconut husks, cereal straws, rice husks, etc.) and peat. Because those fuels differ greatly in their chemical, physical and morphological
Each type of gasifier will operate satisfactorily with respect to stability, gas quality, and efficiencyand pressure losses only within certain ranges of the fuel properties of which the most important are:

- Energy content
- Moisture content
- Volatile matter
- Ash content and ash chemical composition
- Reactivity
- Size and size distribution
- Bulk density
- Charring properties

COMPOSITION OF PRODUCER GAS FROM VARIOUS FUELS

Fuel	Gasification method	Volume Percentage					Calorific value MJ/m^3
		CO	H_2	CH_4	CO_2	N_2	
Charcoal	Downdraft	28-31	5-10	1-2	1-2	55-60	4.60-5.65
Wood with 12-20% moisture content	Downdraft	17-22	16-20	2-3	10-15	55-50	5.00-5.86
Wheat straw pellets	Downdraft	14-17	17-19	-	11-14	-	4.50
Coconut husks	Downdraft	16-20	17-19.5	-	10-15	-	5.80
Coconut shells	Downdraft	19-24	10-15	-	11-15	-	7.20
Pressed Sugarcane	Downdraft	15-18	15-18	-	12-14	-	5.30
Charcoal	Updraft	30	19.7	-	3.6	46	5.98
Corn cobs	Downdraft	18.6	16.5	6.4	-	-	6.29
Rice hulls pelleted	Downdraft	16.1	9.6	0.95	-	-	3.25
Cotton stalks cubed	Downdraft	15.7	11.7	3.4	-	-	4.32

IV. DOWNDRAUGHT OR CO-CURRENT GASIFIER

PROCESSES OCCURRING IN THE DOWN-DRAUGHT GASIFIER:

In the down-draught gasifier, schematically illustrated in, the fuel is introduced at the top, the air is normally introduced at some intermediate level and the gas is taken out at the bottom.

DOWNDRAUGHT OR CO-CURRENT GASIFIER

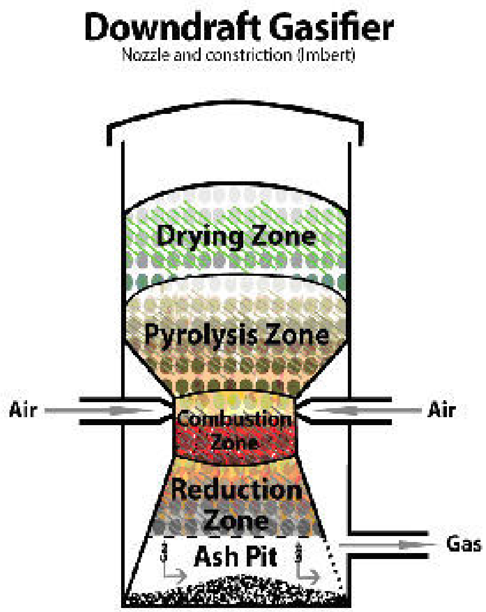

It is possible to distinguish four separate zones in the gasifier, each of which is characterized by one important step in the process of converting the fuel to a combustible gas. The processes in these four zones are examined below and the design basis will be discussed in the following section.

DESIGN:

This is the equipment belongs to the biomass gasification system

DESIGN

GAS CLEANING AND COOLING

GAS CLEANING:

Trouble free operation of an internal combustion engine using producer gas as fuel requires fairly clean gas.

As has been mentioned well designed downdraught gasifiers are able to meet the criteria for cleanliness at least over a fairly wide capacity range (i.e. from 20% -100% of full load). Up draught gasifiers in engine applications have to be fitted with bulky and expensive tar separating equipment. It is however possible to get the gas from up draught gasifiers up to specification as is reported. Methods are under development to reform the gas in a high temperature zone (secondary gasification), in order either to burn or crack the tars.

When suitable fuels are used, the gasifier and cleaner are well designed and the gasifier is operated above minimum capacity, tar contamination of the gas does not present a major problem.

Gas cooling mainly serves the purpose of increasing the density of the gas in order to maximize the amount of combustible gas entering the cylinder of the engine at each stroke ten percent temperature reduction of the gas increases the maximum output of the engine by almost two percent. Cooling also contributes to gas cleaning and makes it possible to avoid condensation of moisture in the gas after it is mixed with air before the engine intake.

GAS COOLING:

An excellent presentation of generator gas cooling theory . Major factors to be taken into consideration are the sensible heat in the gas, the water vapour content of the gas and its heat of condensation and the effects of fouling of the cooler. Generator gas coolers come in three broad categories: natural convection coolers, forced convection coolers and water coolers.

Natural convection coolers consist of a simple length of pipe. They are simple to use and clean and require no additional energy input. They can be rather bulky, though this problem can be partly offset by using fined pipe in order to increase the conductive surface. Forced convection coolers are equipped with a fan which forces the cooling air to flow around thetas pipes. This type of cooler can be much smaller than the natural convection coolers. Its disadvantages are the extra energy input to the fan and the necessity to use gas cooling pipes of small diameters, which can lead to fouling problems. The former can in some cases be offset by using the cooling air supplied by the engine fan.

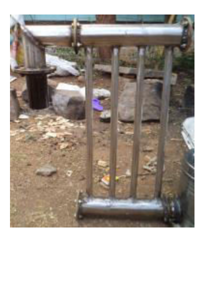

V. CONCLUSION

Very limited experience has been gained in gasification of biomass residues. Most extensively used and researched systems have been based on downdraft gasification. At present no reliable and economically feasible systems exist. Biggest challenge in gasification systems lies in developing reliable and economically cheap cooling and cleaning trains. Maximum usage of producer gas has been in driving internal combustion engine, both for agricultural as well as for automotive uses. However direct heat applications like grain drying etc. Are very attractive for agricultural systems.

By using this Down draft wood gasifier the emissions of a engine with petrol got carbon monoxide 7.8%,carbon dioxide 12.56%.oxygen 18%, where as wood gas emission got carbon monoxide 6%,carbon dioxide 15.28.oxygen 22%,wood gas blends with petrol got emissions has got carbon monoxide 5.8%,carbon dioxide 16%.oxygen 20%.A spark ignition engine running on producer gas on an average produces 0.55-0.75 kWh of energy from 1 kg of biomass. Compression ignition (diesel) engines cannot run completely on producer gas. Thus to produce 1 kWh of energy they consume 1 kg of biomass and 0.07 liters of diesel. Consequently they effect 80-85% diesel saving.

Hence by using this emission analysis conclude that wood gas becomes a future alternate fuel and this gas not harmful the atmosphere compare to petrol and diesel.

VI. ACKNOWLEDGMENT

I feel great pleasure in submitting this Paper on "WOOD GAS GENERATOR WITH INTEGRATED BIOLER FOR FUELING INTERNAL COMBUSTION ENGINES BY USING WOOD PYROLYSIS". I wish to express true sense of gratitude towards my Principal Dr. P.John Paul. And a special thanks to my H.O.D Shashikanth and Guide Dr.Velmurugan who at very discrete step in preparation of this Paper contributed his valuable guidance and help to solve every problem that arise. Also, most likely I would like to express my sincere gratitude towards my parents for always being there when I needed them the most. With all respect and gratitude, I would like to thank all the people, who have helped me directly or indirectly. I owe my all success to them.

VII. REFERENCES AND FOOTNOTES

1. Imbert gasifier first wood gasifierb .Imbert in1880

2. Kjellström, B. 1984. Hazards of producer gas operation: The Beijer Institute, Stockholm,Sweden.

3. Kaupp, A. 1982. The gasification characteristics of rice hulls for the generation ofelectricity and shaft power on a small (530 hp) scale, 1st Int. Prod. Gas Conf., Colombo, SriLanka.

4. Kissin, I. 1942. Gas producers for motor vehicles and their operation with forest fuels,Imperial Forestry Bureau, Oxford, U.K.

5. Axelsson, R. 1969a. Summary of laboratory tests withproducer gas operation of tractorMassey Ferguson 1100 (in Swedish). StatensMaskinprovningar, Umea, Sweden.

6. Axelsson, R. 1969b. Sweden. Summary of tests with producer gas truck Scania L80 (inSwedish).StatensMaskinprovningar, Umea,

7. Bailey, M.L. 1979. Gas producers for vehicles - An historical review. Department Scientific and Industrial Research, New Zealand.Rep. No.CD 2279.

8. Baja, L. 1983. Promotion of producer gas projects in the Philippines. Ibid.

9. Forest utilization contracts on public land, 1977 (E* F* S*)

10. Planning of forest roads and harvesting systems. 1977 (E* F* S*)

11. World list of forestry schools, 1977 (E/F/S*)

12. The marketing of tropical wood in South America, 1978 (E S*)

13. National parks planning, 1978 (E* F* S***)

14. Forestry for local community development 1978 (E* F* S*)

15. Wood chips, 1978 (C* E* S*)

Transient Thermal Analysis of I C Engine Exhaust valve

Prakash d chavan
Assistant Professor
Department of Mechanical Engg.
Malla Reddy College Of Engineering
Maisammaguda, Secunderabad -50014
Email:pakuchavan625@gmail.com

Rahul p tardale
Assistant Professor
Department of Mechanical Engg.
Malla Reddy College Of Engineering
Maisammaguda, Secunderabad -50014
Email:rahulpt407@gmail.com

Abstarct: **I C motors deliver deplete gasses at high temperatures and weights also. These hot gasses additionally go through the fumes valve, and the temperature valve, the valve situate, the power increment. To stay away from any harm to the fumes valve, and the warmth is exchanged from the fumes valve through the distinctive parts, particularly the consideration of the valve situate amid the cycle of opening and shutting since contact each. In this article, it is of restricted utilize component technique for displaying the fumes valve transient warm investigation. They are acquired from the temperature dispersion, warm and coming about weight in both opening and shutting. It conducts point by point investigation to gauge the limit states of the inside ignition motor. The model incorporates the fumes valve seat, manual, and spring. Investigation proceeds until the enduring condition of the state. In this examination, ANSYS and works for demonstrating and investigation of the fumes valve. It has been the improvement of an approach for dissecting the warm transient of the fumes valve.**

I. INTRODUCTION

With the depletion of conventional sources of fuel at a tremendous rate and increasing environmental pollution it has stimulated extensive research on alternative fuels and engine design. Development work oriented good fuel economy and low consumption of exhaust emissions often change the operating parameters, which is time and money consuming method. Instead of a simulation engine with a mathematical model it can easily be done to evaluate the effects of design changes in the operating parameters in a short period of time and inexpensive device. Modeling is a simple representation of complex real-world problem. Almost all real-world phenomena are complex and may take some simplifications. It is required to develop the simplest possible model, which includes the main features of this interesting phenomenon. Many models have been developed by many researchers to solve the combustion process is a complex homogeneous diesel [1-5]. Due to the complexity of engine operations and understanding it is not enough at a basic level, most incomplete engine models. The models used for design purposes, a complete understanding of the operations and to predict the behavior over a wide range of engine operating conditions. Theoretical models used in the case of internal combustion engines can be classified into two main groups: thermal models and models of fluid dynamics. Thermal models are mainly based on the first law of thermodynamics are used to analyze the performance characteristics of the engines. The pressure, temperature and other conditions necessary for the evaluation of crank angle or time characteristics. Engine friction and heat transfer is taken into account using The mathematical equations that were obtained from the experiments. These models are classified into two groups of an area, multi zone models and models. On the other hand, multi-zone models also computational fluid dynamics models is called. They are based on a numerical calculation of the equations of mass, momentum and energy and the preservation of species in any one or two or three dimensions for following the spread of flame or combustion front inside the combustion chamber of the engine. Two zone model is the burn area is one containing the pure air and the other consists of products of fuel combustion and calls burn area. And apply the first law of thermodynamics and equations of state in each of the two regions for the production of cylinder temperature and the change of the cylinder pressure. Using the model of two combustion zones has been the determination of the parameters of combustion and the formation of chemical Imbalance. Multidimensional models need information in detail many of the phenomena and calculating a timeline. A simple model area but does not account for the heterogeneity of diesel engines. Therefore, it is reasonable to choose the Bmntqtin model are simple and require a reasonably computer time. Defines biodiesel as fatty acid monoalkyl esters derived long chain vegetable oils or animal fats. It was observed from the literature [6-8] that the use of biodiesel in diesel engine results in a slight decrease in the strength of the brakes and a slight increase in fuel consumption. However, the lubricating properties of biodiesel are better than diesel fuel, which can help increase engine life. Exhaust emissions also less clean diesel biodiesel due to the presence of oxygen in the molecular structure of biodiesel process. Moreover, biodiesel is environmentally friendly, since biodiesel does not produce sulfur oxides and also that no increase in CO2 emissions worldwide.

II. LITERATURE REVIEW

The rapid development of computer technology and the use of complex simulation techniques to measure the impact of the basic processes of engine systems has encouraged. Progress through the current car engines have achieved would have been impossible without simulation models that offer these ideas [10-11] .Lyn and others. [12] analyzed the effects of the injection timing and the injection rate and fuel rate of the duration of the delay. A constant load increase speed increases the maximum pressure and temperature, due to reduced heat transfer, resulting in a slight decrease in the analysis period delay by Wong et al. [13]. semi-empirical relationship engineering applications based on a series of chemical reactions called also used "s work to find a firing rate [14-15]. But Weibe" Weibe employment picture is not able to predict the rate of fire during the first burning mixture. And therefore does not have to be twice Weibe "accurate direct fuel injection diesel predict function s [14,16]. Biodiesel has a relatively low flash point, high heating value, high density similar to that of petroleum diesel high viscosity. Several studies indicate that unburned hydrocarbons (HC) and carbon monoxide (CO) and sulfur levels are much lower in the exhaust gases while using bio-diesel fuel. However, a marked increase in the levels of nitrogen oxides and Male (NOx) with biodiesel [17-20]. The mixture of biodiesel reduces greenhouse gases such as CO2 levels. Additional benefits include exceptional lubricity, excellent biodegradability, high combustion efficiency and low toxicity compared to other fuels. [twenty-one] The combustion process in diesel engines are very complex due to the nature of the transient combustion and inhomogeneous, which is controlled mainly by the swirling fuel and air. High-speed photography studios and sample collection infrastructure cylinder has revealed some interesting phenomena of the combustion characteristics [10]. ignition delay in diesel engines has a direct impact on the efficiency of engine noise and exhaust emissions. There are a number of parameters that directly affect the identity of the period, including the cylinder pressure and temperature, the ratio of the spiral and misfire. The number of links used Arrhenius expression similar to Wolfer [22] proposed in 1938 as ignition delay is measured as a function of pressure and temperature. Watson [16] developed link identity by a diesel engine under the state of stability which is still used on a large scale conditions. Later Assanis and others.God. [23] developed a delayed start link to predict a delay in turbo direct injection of heavy diesel operating under steady engine and transient operation.

III. METHODOLOGY

The valves used in the IC engines are of three types: Poppet, mushroom valve, Sleeve valve or Rotary valve. Of these three types, Poppet valve is most commonly used. Since both the inlet and exhaust valves are subjected to high temperatures of 1930°C to 2200°C during the power stroke, therefore, it is necessary that the materials of the valves should withstand these temperatures. The temperature at the inlet valve is less compared to exhaust valve. Thus the inlet valve is generally made of nickel chromium alloy steel and exhaust valve is made of silchrome steel.

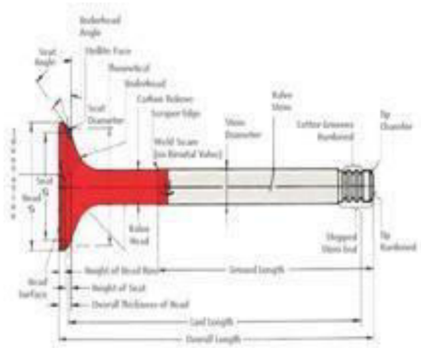

About Valves Engine Valve is one of the main parts which are used in all IC Engines. Each cylinder inthe engine has one inlet and one exhaust valve. Now a days engine are designed with multi valves viz., two inlet and one exhaust or Two inlet and Two exhaust valves which prevents air pollution and improves engine efficiency. Function of Inlet Valve The inlet which operates by the action of Tappet movement, allows air and fuel mixture into the cylinder. Function of Exhaust Valve The exhaust valve allows burnt gases to escape from the cylinder to atmosphere. Valve Efficiency Depends on the following characteristics like Hardness, Face roundness and sliding properties capable to withstand high temperature etc.

Design Calculations of Exhaust Valve

Figure 2: Exhaust Valve

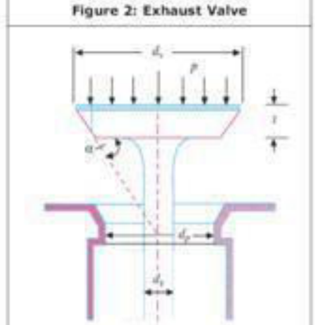

Description of the Physical System

The geometry of the exhaust valve is shownin Figure . The exhaust valve sits on thecylinder head of a combustion chamber. Theengine coolant liquid passes around thecylinder liner and the water passages in the cylinder head. The valve pops up and downto let the exhaust gases leave the combustionchamber.The up-and-down motion of the valvetakes place with the help of a rocker leverwhich is connected to the push rod. The pushrod rests over cams on the camshaft. Thevalve is spring loaded. The spring keeps thevalve connected to the camshaft during itsmotion. After the expansion process, theexhaust gases, at high temperature, arepurged through the exhaust valve and as aresult the temperature of the exhaust valveincreases. In order to avoid any damage tothe exhaust valve due to this hightemperature, heat must be continuouslytaken away from the valve. This is achievedwhen the valve is in contact with its seat. Asthe exhaust valves touch its seat, a significantdrop in exhaust valve temperature occurs.

Pressure-crank angle diagram

Figure 2 shows the measured and computed pressure trace and crank angle histories for the fuels tested at full load condition. In a compression ignition engine, cylinder pressure depends on the burned fuel fraction during the premixed burning phase which is the initial stage of combustion and the ability of the fuel to mix well with air and burn. High peak pressure and maximum rate of pressure rise are corresponding to large amount of fuel burned in premixed stage.

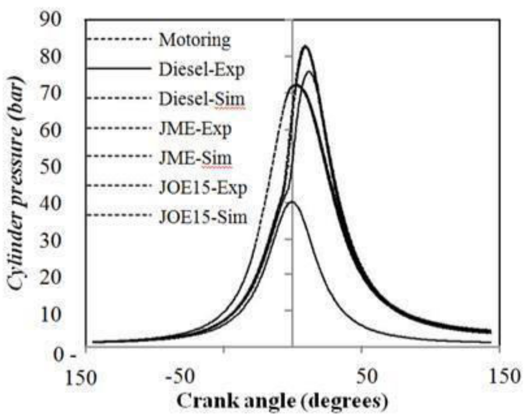

Figure 2: Variation of cylinder pressure with crank angle at full load.

It is observed from the experimental results that the peak pressure for diesel, JME and JOE15 are 75.72, 82.61 and 82.40 bar respectively. For the simulated conditions the peak pressure values are 71.76, 71.99 and 71.85 bar respectively. In both the cases the combustion of JME and JOE15 starts earlier than that of diesel fuel. Also the peak cylinder pressure of JME and JOE15 is marginally higher than that of diesel, as a result of high viscosity and low volatility.

Apparent or Net heat release rate

Figure 3 depicts the variation of apparent heat release with respect to crank angle for different fuels tested. The term apparent or net heat release rate is determined by deducting the heat transfer to cylinder walls, crevice volume, blow-by and the fuel injection effects from heat energy liberated by burning the fuel.

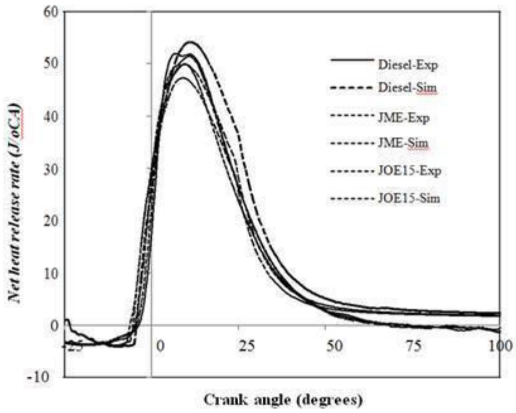

Figure 3: Variation of maximum heat release rate with crank angle.

The experimental results of maximum net heat release rate for diesel, JME and JOE15 are by about 52.01, 49.97 and 48.51 J/^{O}CA respectively at full load condition. At simulated conditions the values are by about 54.20, 49.93 and 47.31 J/^{O}CA for diesel, JME and JOE15 respectively. The intensity of premixed combustion phase for diesel is found to be more and whereas, this is lower in the case JME and JOE15. It is also seen that the quantity of diffusive combustion are found to be shorter for JME and JOE15 emulsion due to faster burning characteristics. Oxygen present in JME and quick evaporation nature of emulsified fuel JOE15 are the causes for faster burning process [27].

IV. CONCLUSIONS

The exploratory aftereffects of the pinnacle barrel weight of JME and JOE15 is barely higher than that of diesel, and comparable outcomes are gotten with recreated conditions.

The greatest warmth discharge rate of JME and JOE15 are lower than that of diesel fuel in both test and recreated conditions.

The NO emanations of diesel fuel are expanded with stack both in exploratory and reproduced conditions. Comparable patterns have been gotten with JME and JOE15.

The NO outflows of JOE15 are expanded and residue thickness is diminished with progressing of infusion timing and the qualities are in the other way around in impeded conditions.

The introduced model can foresee the burning and outflow qualities, for example, chamber weight, warm discharge, NO emanations and residue densities which are in great concurrence with the exploratory outcomes.

Dishonorable holding may happen prompting the lessened quality of the part and subsequently the segment will have a tendency to fall flat .

On the off chance that the steamed power is less then likewise the quality of the weld will be less in this manner expanding the propensity of the segment to fail.8.0 Manufacturing Results.

V. REFERENCES

[1] Rakopoulos C.D., and Giakoumis E. G., Simulation and analysis of a naturally aspirated IDI diesel engine under transient conditions comprising the effect of various dynamic and thermodynamic parameters, Energy Conversion and. Management, 39, (1998), 465-484.

[2] Singh B.P., and Sahoo P.K., A Simulation Model for Predicting the Performance of Bio Fuels Conventional Engine, Int.J. Emerging Technol. in Sci. Eng. , 5(3), (2012).18-31

[3] Rakopoulos C.D., Rakopoulos D.C., and Kyritsis D.C., Development and validation of a comprehensive two-zone model for combustion and emissions formation in a DI diesel engine, International Journal of Energy Research ,27,(2003),1221–1249.

[4] Prasath B. Rajendra, Tamilporai P., and Shabir F., Mohd, Analysis of combustion, performance and emission characteristics of low heat rejection engine using biodiesel, International.Journal of Thermal Sciences,49,(2010), 2483-2490.

[5] Sundarapandian S., and Devaradjane G., Performance and Emission Analysis of Bio Diesel Operated CI Engine, Journal of Engineering Computing and Architecture, 1(2), 2007.1-22.

[6] SrivastavaAnjana,PrasadRam, Triglycerides-based diesel fuels, J.Renewable and Sustainable Energy Reviews, 4,(2000), 111- 133.

[7] Barnwal B. K., Sharma M. P., Prospectus of Methyl Ester production from vegetable oils in India, J.Renewable and Sustainable energy reviews, 3,(2004), 212-217.

[8] PuhanSukumar,Vedaraman N., Sankaranarayanan G., Boppana V, Ram Bharat, Performance and emission study of Mahua oil ethyl ester in a 4-stroke natural aspirated direct injection diesel engine. J Renewable Energy, 30(8),(2005), 1269-1278.

[9] Monyem A., Van Gerpen J.H., The effect of biodiesel oxidation on engine performance and emissions, Biomass Energy, 20 ,(2001),pp:317–325.

[10] Heywood J. Internal combustion engines fundamentals. McGraw Hill book company; 1989.

[11] Ganesan V. Computer simulation of compression ignition engines. University Press (India) Ltd.; 2000.

[12] Lyn WT, Valdamanis. Effects of physical factors on ignition delay, SAE 680102, 1968

[13] Wong CL., Steere DE. The effects of diesel fuel properties and engine operating conditions on ignition delay. SAE 821231, 1982.

[14] Ghojel J I, Review of the development and applications of the Wiebe function: a tribute to the contribution of Ivan Wiebe to engine research, International Journal of Engine Research 11(2010),pp:297-312.

[15] Wiebe, I. I., Semi-empirical expression for combustion rate in engines, In Proceedings of Conference on Piston engines, USSR, 1956, pp. 185–191.

TRIBOLOGICAL PROPERTIES OF FLY ASH REINFORCED ALUMINIUM 6061 COMPOSITE

1) Niranjan J Nanjayyanamath Assistant Professor at Sri Dutta instituite of Engg and Science, Hyderabad.
2)Mahantesh S. Arakeri Lecturer at B.V.V.S Polytechnic(Autonomous) Bagalkot.
3) Santosh Balanayak Assistant Professor at Sri Dutta instituite of Engg and Science, Hyderabad.

***Abstract*— Aluminium 6061 alloy (Al6061) is most broadly used base material because of its unique blend of low density, high strength, good mechanical properties, higher corrosion resistance, low electrical resistance and better machinability. However its relatively poor wear resistance has restricted its use in certain tribological applications. In recent years, various fiber reinforced and particulate reinforced Al 6061 composites have shown significant enhancement in their mechanical as well as tribological properties. In view of the above, an attempt has been made to study the mechanical and tribological properties of fly ash reinforced Al 6061 composites, processed using the stir casting route. Three sets of composite samples were prepared with 5, 10 and 15 weight percentage of fly ash with particle sizes in the ranges of 5-20, 25-30 and 50-60 µm in each set. Wear tests of these composites were carried on pin on disc apparatus. It was found that as the content of fly ash increased from 0 to 10%, wear rate was decreased. With further increase in the distrubutionof fly ash up to 15 wt-%, wear rate increased. With the increase in particle size of the fly ash, wear rate decreased.**

Index Terms*— *Al6061, Fly ash, Tribological properties, Microstructure

I. INTRODUCTION

Aluminium based metal matrix composites (MMCs) are engineering materials that has the combination of various properties such as high specific strength, high specific stiffness and high hardness. Reinforced alloys show better resistance to wear compared to unreinforced alloys. Aluminium based MMCs are widely used in different structural applications such as helicopter parts, rotor vanes in compressors and in aero-engines [1]. High manufacturing cost of continuous fiber reinforced MMCs has led to the use of particle reinforced and whisker reinforced MMCs [2]. Particles such as mica, alumina (Al_2O_3), graphite, boron and silicon carbide (SiC) have been used as fillers with aluminium alloys. Fly ash from thermal power plants in India pose threat to surroundings causing health hazards. It is probable that, of 90mega tons (Mt) of coal combustion by-products generated per annum, only 25% is currently used, much of it is in the form of extenders in cement and in polymers; the remainder is ending up in land filling. It is expected that fly ash particles as reinforcement in aluminium alloys would promote yet another use of this by-product [3]. Tribological properties of components used in aircraft fittings, valves, pistons rings, brake drums, cam and follower play important role. Because light metal alloys usually have poor wear resistance, they require surface treatments like coating with oxides or nitrides.

II. TRIBOLOGICAL PROPERTIES

significant work have been conducted and found that they are designed to improve tribological properties of aluminium alloys. Uyyuru et al. [4] studied tribological behavior of Al–Si–SiCp composites / automobile brake pad system under dry sliding conditions using pin-on-disc machine where the aluminium MMC was used as disc, whereas the brake pad material forms the pin. They found that both wear rate and friction coefficient varied with applied normal load and sliding speed. With increase in the applied normal load, the wear rate was observed to increase whereas the friction coefficient decreased. However, both the wear rate and friction coefficient were observed to vary proportionally with the sliding speed. Anilkumar et al. [5] investigated the wear behavior of aluminium fly ash composites, containing fly ash in required quantities (10, 15, and 20 percent by weight) in weighed quantity of aluminium. They tested aluminium fly ash composite using a pin-on-disc wear testing machine with aluminium fly ash MMC as pin. They found that as the content of fly ash increased, the volumetric wear rate of the composite decreased.

Gurcan and Baker [6] investigated the wear resistance of four AA6061 MMCs together with the monolithic AA6061 alloy, all in the T6 condition, using a pin-on-disc test. In addition to the widely studied 20 volume percent Saffil MMCs, their investigation considered a hybrid of 11% Saffil + 20% SiCp and a high volume fraction SiCp MMC, AA6061 + 60% SiCp. The wear behaviour against P400 SiC grit adhesive bonded paper and against BS817M40 (EN24) steel were explored under an applied load of 9.8 N with a nominal contact pressure of 0.5 MPa. It was obsereved that after testing against SiC grit, AA6061 + Saffil showed little advantage over the monolithic alloy, but the other three composites had a significant improvement in wear resistance. The hybrid and the AA6061 + 60% SiC showed the best performance. Only small improvements were noted for AA6061 + Saffil and AA6061 + 20% SiC over the monolithic alloy, when tested against steel.

III. EXPERIMENTAL DETAILS

Al6061 has the good casting properties and due to its strength it is choosen as matrix material having chemical composition mentioned in Table 3.1. Fly ash collected from Raichur thermal power plant was used as filler material and its composition is given in Table 3.2.

Table3.1: Chemical composition of Al6061 alloy (wt-%)

Mg	Si	Fe	Cu	Ti	Cr	Zn	Mn	Al
0.91	0.76	0.24	0.21	0.08	0.11	0.05	0.04	balance

Table3.2: Chemical composition of Fly ash used in present study (wt-%)

Al_2O_3	SiO_2	Fe_2O_3	TiO_2	Loss of ignition
29,56	59.8	4.99	3.1	1.44

Tribological (wear) tests were conducted on samples with fly ash of particle size 25-30 microns and 50-60 microns. A pin on disc apparatus (Fig. 3.8) was used to investigate the dry sliding wear behavior of Aluminium alloy and its composites as per ASTM G99-95 standards. The specimen of size 8 x 8 x 4 mm was cut from samples, machined and then polished metallographically. The tests was carried out with the load 1 kg (9.81 N) and 3 kg (29.43 N) sliding speed 1.11 m/s, 2.086 m/s and sliding distance 1000, 1500 and 2000 m.

IV. RESULTS AND DISCUSSION

4.1 Microstructure

The microstructure shows the important features relating to wear performance of the alloy and its composites. The microstructure of MMCs was analyzed using scanning electron microscope (SEM) to study the distribution of fly ash in the matrix. The microstructure of as cast Al6061 and Al6061 with fly ash are shown in Figs. 4.1a-j. The distribution of reinforced particles was found to be reasonably uniform in all the samples without voids and discontinuities.

Figure 4.1(a) Microstructure of bare Al 6061

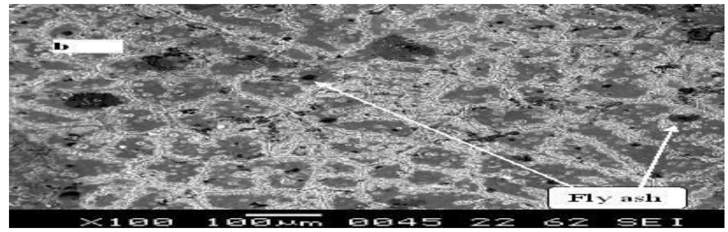

Figure 4.1(b) Microstructure of Al 6061 with 5 wt-% fly ash of particle size 5-20µm.

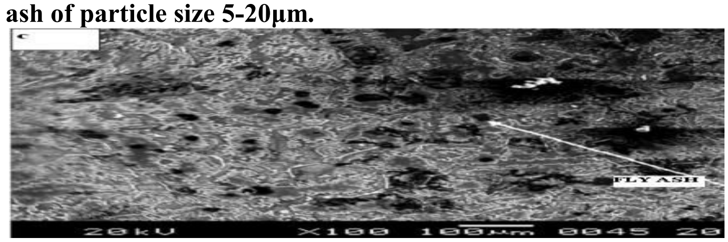

Figure 4.1(c) Microstructure of Al 6061with 10 wt-% of fly ash of particle size 5-20µm.

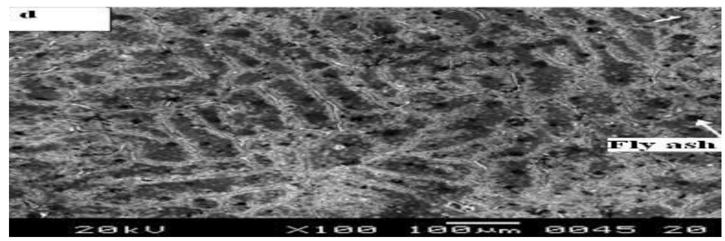

Figure 4.1(d) Microstructure of Al 6061with 15% weight fraction of fly ash of particle size 5-20µm.

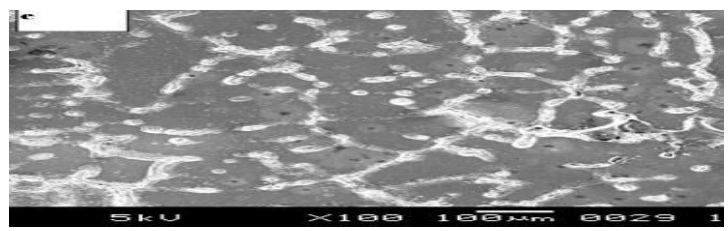

Figure 4.1(e) Microstructure of Al 6061with 5% weight fraction of fly ash of particle size 25-30µm.

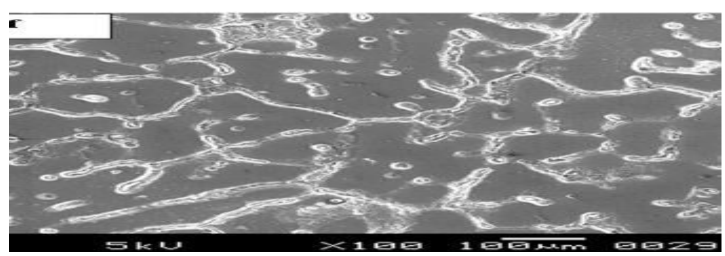

Figure 4.1(f) Microstructure of Al 6061with 10% weight fraction of fly ash of particle size 25-30µm.

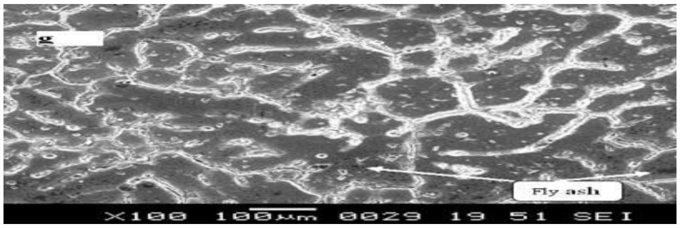

Figure 4.1(g) Microstructure of Al 6061with 15% weight fraction of fly ash of particle size 25-30µm.

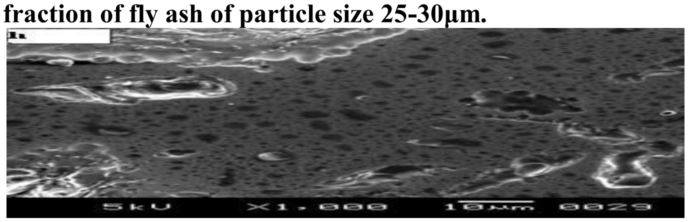

Figure 4.1(h) Microstructure of Al 6061with 5% weight fraction of fly ash of particle size 50-60µm.

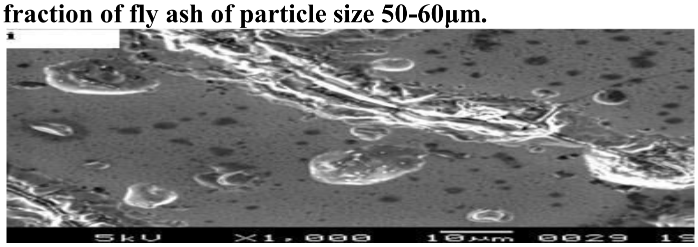

Figure 4.1(i) Microstructure of Al 6061with 10% weight fraction of fly ash of particle size 50-60µm.

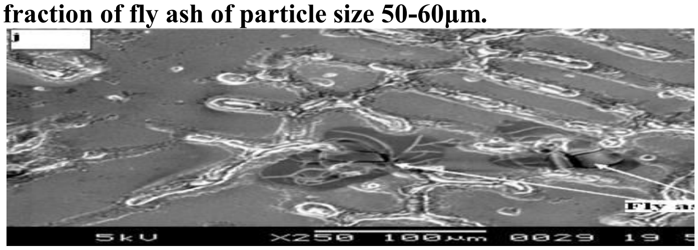

Figure 4.1(j) Microstructure of Al 6061with 15% weight fraction of fly ash of particle size 50-60µm.

Tribological tests were conducted on samples with fly ash of particle size 25-30 microns and 50-60 microns. The results of the variation of wear rate with the content of fly ash are shown in Figs. 4.6 - 4.13. Tables 4.5- 4.12 show the percentage development in wear rate of Al6061 alloy matrix by reinforcements. The percentage improvements with different weight fractions of reinforcements are also given. From the Figure 4.6 to 4.13 it is clear that as the weight fraction increases from 0% (pure Aluminium) to 10% wear rate decreases, having a minimum value at 10 wt-%, then it again increases. This may be due to the fact that strength and hardness of the composite increases till 10 wt-% and decreases afterwards, attaining the maximum value at 10 wt-%. This is due to the higher bonding between fly ash particles and Al alloy matrix.

Table 4.5 Results of variation of wear rate with weight percent of fly ash of particle size 25-30 µm; Load: 9.81 N; Sliding velocity: 1.11 m/s

Sliding distance (meters)	Weight percent of reinforcement	Wear rate
1000	0	3.0
	5	2.7
	10	2.9
	15	3.0
1500	0	3.6
	5	3.1
	10	3.0
	15	3.6
2000	0	3.6
	5	3.5
	10	2.5
	15	4.5

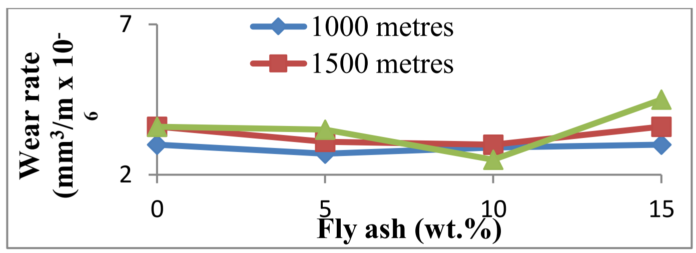

Fig.4.6 Variation of Wear rate with weight percent of fly ash of particle size 25-30 µm; Load: 9.81 N; Sliding velocity: 1.11 m/s

Table 4.6 Results of variation of wear rate with weight percent of fly ash of particle size 25-30 µm; Load: 9.81 N; Sliding velocity: 2.086 m/s

Sliding distance (meters)	Weight percent of reinforcement	Wear rate
1000	0	3.3
	5	2.9
	10	3.1
	15	3.5
1500	0	3.7
	5	3.2
	10	3.4
	15	3.8
2000	0	4.8
	5	4.3
	10	2.2
	15	2.8

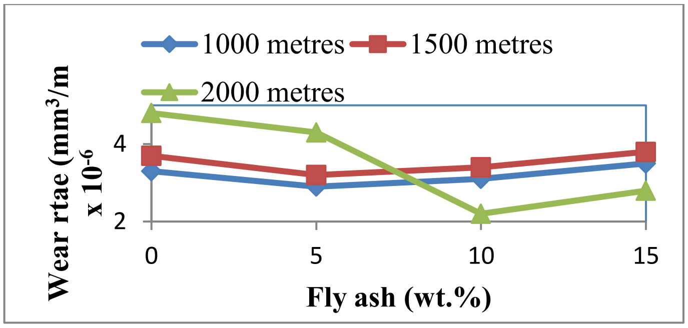

Fig.4.7 Variation of Wear rate with weight percent of fly ash of particle size 25-30 µm; Load: 9.81 N; Sliding velocity: 2.086 m/s

Table 4.7 Results of variation of wear rate with weight percent of fly ash of particle size 25-30 µm; Load: 29.43 N; Sliding velocity: 1.11 m/s

Sliding distance (meters)	Weight percent of reinforcement	Wear rate
1000	0	5.4
	5	4.8
	10	4.2
	15	5.4
1500	0	5.3
	5	4.6
	10	4.5
	15	5.7
2000	0	6.4
	5	5.3
	10	4.4
	15	4.7

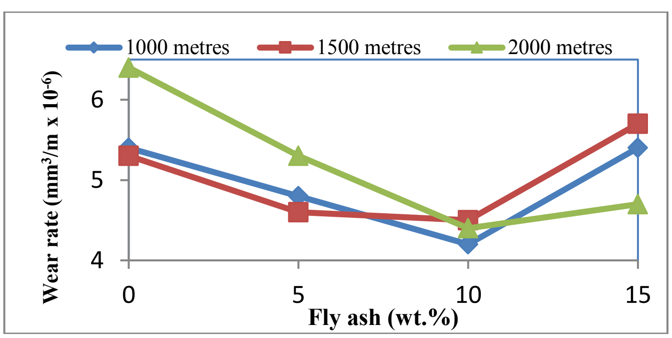

Fig.4.8 Variation of Wear rate with weight percent of fly ash of particle size 25-30 µm; Load: 29.43 N; Sliding velocity: 1.11 m/s

Table 4.8 Results of variation of wear rate with weight percent of fly ash of particle size 25-30 µm; Load: 29.43 N; Sliding velocity: 2.086 m/s

Sliding distance (meters)	Weight percent of reinforcement	Wear rate
1000	0	6.4
	5	4.3
	10	4.8
	15	6.8
1500	0	5.4
	5	4.9
	10	4.9
	15	5.5
2000	0	7.4
	5	5.5
	10	4.5
	15	5.5

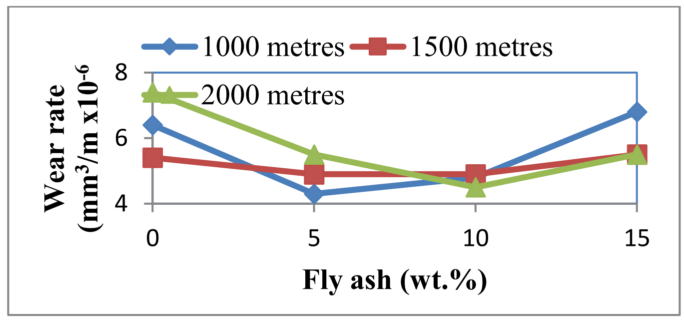

Fig.4.9 Variation of Wear rate with weight percent of fly ash of particle size 25-30 µm; Load: 29.43 N; Sliding velocity: 2.086 m/s

Table 4.9 Results of variation of wear rate with weight percent of fly ash of particle size 50-60µm; Load: 9.81 N; Sliding velocity: 1.11 m/s

Sliding distance (meters)	Weight percent of reinforcement	Wear rate
1000	0	3
	5	2.6
	10	3
	15	2.8
1500	0	3.6
	5	3.1
	10	2.8
	15	2.9
2000	0	3.6
	5	2.9
	10	2.4
	15	3.6

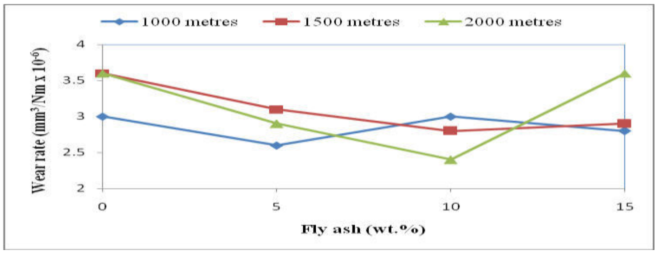

Fig.4.10 Variation of Wear rate with weight percent of fly ash of particle size 50-60µm; Load: 9.81 N; Sliding velocity: 1.11 m/s

Table 4.10 Results of variation of wear rate with weight percent of fly ash of particle size 50-60µm; Load: 9.81 N; sliding velocity: 2.086 m/s

Sliding distance (meters)	Weight percent of reinforcement	Wear rate
1000	0	3.3
	5	2.7
	10	2.6
	15	2.9
1500	0	3.7
	5	3.5
	10	3.3
	15	3.4
2000	0	4.8
	5	2.7
	10	2.2
	15	3.5

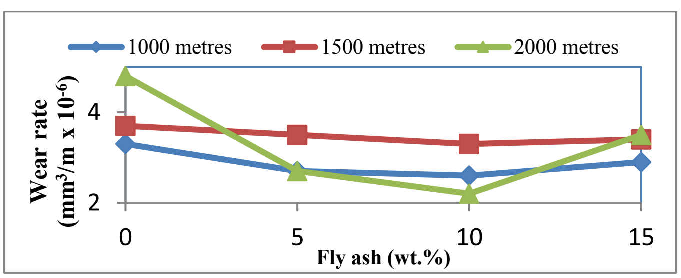

Fig.4.11 Variation of Wear rate with weight percent of fly ash of particle size 50-60µm; Load: 9.81 N; sliding velocity: 2.086 m/s

Table 4.11 Results of variation of wear rate with weight percent of fly ash of particle size 50-60µm; Load: 29.43 N; sliding velocity: 1.11 m/s

Sliding distance (meters)	Weight percent of reinforcement	Wear rate
1000	0	5.4
	5	4.2
	10	3.2
	15	4.4
1500	0	5.3
	5	4.5
	10	4.6
	15	5.4
2000	0	6.4
	5	6
	10	5
	15	4.5

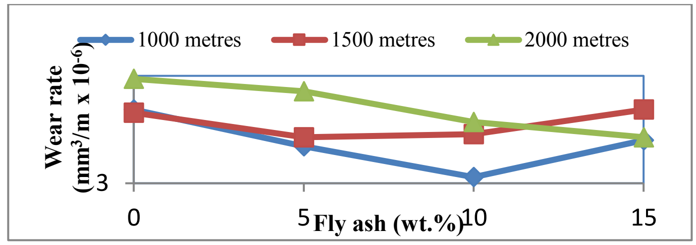

Fig.4.12 Variation of Wear rate with weight percent of fly ash of particle size 50-60 µm; Load: 29.43 N; Sliding velocity: 1.11 m/s

Table 4.12 Results of variation of wear rate with weight percent of fly ash of particle size 75-100 µm; Load: 29.43 N; Sliding velocity: 2.086 m/s

Sliding distance (m)	Content of reinforcement (wt-%)	Wear rate
1000	0	6.4
	5	6.2
	10	3.5
	15	4.9
1500	0	5.4
	5	4.5
	10	4.3
	15	5.7
2000	0	7.4
	5	6.6
	10	5.3
	15	5.9

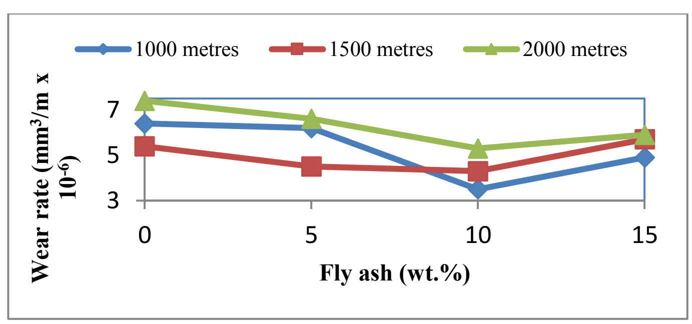

Fig. 4.13 Variation of wear rate with content of fly ash of particle size 50-60 µm; load 29.43 N; sliding velocity 2.086 m/s

Wear behaviour was conducted at room temperature are presented in Figs. 4.6-4.13. Assessment of wear properties of the fly ash as well as matrix in the interface region is important on these counts. These properties help to evaluate the integrity of the material, and to understand the material behavior under the condition of wear in critical components used in various applications. A normal load of 1kg and 3kg were used for all samples and they registered a gradual decrease in wear rate as the content of fly ash increased up to 10 wt-%. During wear test, thermal stress gradient may be generated within the sample and this gradient may produce cracks. Reinforcements in the form of fly ash can stop these cracks hence higher content of fly ash will lead to higher probability of stopping of cracks. Therefore, higher contents of fly ash show lower wear rate. During friction and wear process a considerable heat is generated between any two sliding surfaces. If the surface contains more content of fly ash i.e. 10 wt-%, the amount of heat generated will be less compared to material with lower fly ash.

If the sample contains more content of fly ash i.e. 15wt-% the amount of small cracks will be more and more of matrix is easy to break. In the present study, it is concluded that matrix worns out faster than fly ash. Hence, wear loss is caused mainly by matrix wear but fly ash only gets removed when matrix completely worns out. This could be revealed from SEM micrograph shown in Fig. 4.14.

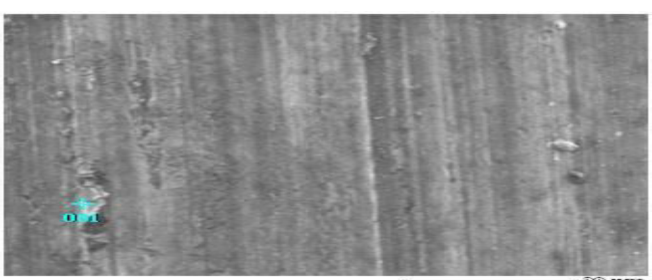

Fig. 4.14 Micrograph of worn surface of fly ash 50-60 µm and 15 wt-% at sliding velocity 2.086m/s, load 29.43 N, sliding distance 2000m

V. CONCLUSIONS

1. As the percentage of reinforcement fly ash was increased from 0% (pure Aluminium) to 10% wear rate decreases, having a minimum value at 10%, then it again increases.
2. Increasing the grain size of fly ash particle wear rate of composite decreases in most of the working conditions.
3. From the SEM analysis it has been concluded that as the fly ash content increases the distribution of fly ash evenly throughout the specimen.

REFERENCES

[1] S.K. Acharya P.K. Mahanta, and P.K Pattanaik, Wear behaviour of aluminium fly ash composite, *Journal of Institution of Engineers (1ndia)*, 83, 2002, 50-53.

[2] U. Cocen, K. Onel, Ductility and strength of extruded SiCp/aluminium alloy composites, *Composites Science and Technology,* 62,2002, 275-282.

[3] R. Kumar, A.K. Mahur, D. Sengupta, and R. Prasad, Radon activity and exhalation rates measurements in fly ash from a thermal power plant, *Radiation Measurements*, 40, 2005, 638–641.

[4] Uyyuru.R.K, Surappa.M.K, Brusethaug.S (2006). “Tribological behavior of Al-Si-SiCp composite/Automobile Brake Pad system under Dry Sliding conditions.” Tribology international. 1-9.

[5] Anilkumar H.C, H.Suresh Hebbar (2011), “Mechanical Properties of fly ash reinforced aluminium alloy (Al6061) composites is published in international journal of Mechanical and Material Engineering (IJMME), Vol. 6, No. 1, 41-45.

[6] Gurcan, A.B., Baker, T.N. (1995). “Wear behavior of AA6061 aluminium alloy and its composites.” Wear, 188, 185-191.

OPTIMIZATION OF TENSILE STRENGTH OF HYBRID GLASS/EPOXY COMPOSITE MATERIAL WITH WHITE CEMENT FILLER BY USING ANOVA

D. Harsha Vardhan[1], Dr. A. Ramesh[2] , Dr. B. Chandra Mohan Reddy[3], Dr Shiva Shankare Gowd.A. S [4]
[1]Asst. Professor& HOD, Dept. of ME, Sri Venkatreswara Institue of technology, Anantapr,A.P
harsha.mech360@gmai.com
[2] Professor& Principal, BIT Institute of Technology, Hindupur, Anantapr,A.P
prof_ramesh_epcet@yahoo.com
[3]Asst. Professor, Dept. of ME, Jawaharlal Nehru Technological Univerity-Anantapur,A.P.cmr_b@yahoo.com
[4] Prof and Dean Academics, Dept of Mech Engg., M R C E, HYDERABAD

ABSTRACT

Aim of current study is to obtain the maximum possible benefit from the combination of materials. The Glass Epoxy composite material with the white cement as filler is considered for the study. It has been observed that the percentage of filler will influence various mechanical properties and to achieve the maximum capable strength of the composite all the constituents should be in optimal combination. To estimate the optimal combination taguchi method is adopted. Based on Taguchi's L_9 orthogonal array, experiments were conducted for GFRP composite plates using epoxy composite with three different fiber orientation, fiber type and three different white cement filler (wt%) percentages. Tensile test was performed according to ASTM standard. Different parameters i.e., filler content (wt%) and Type of fiber, orientation of fiber angle are optimized using Taguchi method. Based on mean effective plots, the optimum levels of parameters have been identified, and significant contribution of parameters is determined by analysis of variance.

Keywords: *GFRP composites; Fabrication; Tensile strength; Taguchi; Design of Experiments; ANOVA*

1.0 INTRODUCTION

The current scenario globally many researchers are trying to develop the new materials, which can substitute the existing materials for the betterment in required aspects. The new material in the sense that the combination of the two different materials, will give more than 100 of different materials when they are completely soluble one in another. For combination of three different materials then we get more than 1000 types of different materials. According to hume-rothery rule of solid solubility many alloys are formed even new alloys are forming day by day. Even to achieve more than that an alloy can do, the researchers are combining the materials which are apart from the solubility, which leads to development of composite material. There will be one supporting material and one or more strengthening materials combined together forms a composite material. Supporting material named as matrix it may be metal, polymer or ceramic material. Strengthening materials may be natural earth reform materials or it may be artificially made. Artificially made are customized to requirement that it may have less weight to strength.

In order to achieve the strength requirement, instead of having one type of strengthening material, if it is made with more than one type of strengthening material named as hybrid composite material. Here hybridization leads to achieve the tailor-made properties for the application. In recent decade polymer based composite materials are attained more significance for their inherent characteristics and are quite economical.

Oxyde (%)	Portland cement
SiO_2	21.25
Al_2O_3	4.33
Fe_2O_3	1.85
TiO_2	0.13
CaO	64.30
MgO	1.81
So_3	3.70
K_2O	0.71
Na_2O	0.17
l.o.i	1.50

Figure 1 composition of white cement filler [10]

The strength of glass fiber reinforced composite material will vary with the filler material and percentage of filler in polymer and orientation of fiber. It is evident that from the literature FRP composite with hybridization will perform or exhibit better properties compared to base composite. The strength of the glass fiber reinforced composite material will reduce by addition of another natural fiber to the matrix in the process of hybridization [1-3] causes the reduction of actual strength by 20 to 25 % and improvement in ductility.. Another side literature shows that the strength of GFRP composite is increased by addition of another fiber like sisal [4], coir [5] or filler materials like carbon powder [6], ash[2] , carbon,SiO2 [7], up to some extent then strength reduced. Not only in epoxy based composites In Poplyproplline based composites also with the addition of polypropylene a CaCo3 will increase the strength and then after some extent properties decreased [8].The examination was carried out by T-test and analysis of variance (ANOVA) was performed in which process parameters were statistically significant [9], F. Michael Raj et al carried experiments on waste fishnet cross fiber characterization and found that the influencing parameter for each characteristic.

2.0 MATERIALS

2.1 Matrix:

The Epoxy resin(Araldite LY 556) as matrix ,a curing agent hardener is to be in a ratio of 10:1 to epoxy resin. The curing agent or hardener used tri-ethylene tetramine (HY-951) and Epoxy was supplied by Sree Industrial Composites, Hyderabad, India.

2.2 Filler:

As shown in figure1. White cement powder or Portland white cement is combination of oxides of silicon, alumina, Ferrous, Titanium, magnesium, calcium, sodium ,potassium etc., hence as it consists of many oxides forms, rather than considering single individual filler combination of all these white cement powder is taken for study . A white cement powder as filler material in 2 different proportions i.e. 5% and 10 % by weight was chosen for study.

2.3 Fiber:

To identify the influence of type of glass fiber three variations of were taken i.e longitudinal glass, cross ply glass and whisker glass fibers, also to examine the influence of fiber angle three variations in fiber angle is considered as 0degrees, 45degrees and 60degrees.

3.0 METHODOLOGY

3.1 Sample Preparation:

Hand layup technique was adopted for making of composite specimens, as per the ASTM standardsD638 [11], six sets of specimens prepared and tested for each sample. 297*210*5mm^3 mould was prepared for making composites, mould release spray was used for easy release of casted plate. The required dimensions were marked and sized the plate with help of vertical band saw.

Param eters	fiber angle	fiber type	filler percentage
Level1	0	1-	0
Level	45	2-(cross ply)	5
Level	60	3-(whisker)	10

Table 1 Level parameters table

3.2 Design of experiments:

Taguchi technique in design of experiments was adopted for Combination of materials in which samples were fabricated. To characterize the composite martial and to achieve optimal properties from the best combination of Epoxy/Glass and filler .Taguchi Technique was adopted with three parameters Fiber angle, Fiber Type and Filler Percentage for each parameter three levels were considered. For 3 input parameters and 3 levels of each, L9 orthogonal array was best suitable.

Specimen	fiber	fiber	filler
Specimen-	0	1	0
Specimen-	0	2	5
Specimen-	0	3	10
Specimen-	60	2	0
Specimen-	60	3	5
Specimen-	60	1	10
Specimen-	45	3	0
Specimen-	45	1	5
Specimen-	45	2	10

Table 2 shows parameters and 3 levels L9 orthogonal array

3.3 Tensile test:

The Tensile test is performed on specimens according to ASTM test standard D638 on a Universal Testing Machine. In each case three samples are taken and average value are recorded.

Specifications: Dimensions of Tensile Test Specimen as per ASTM D-638.

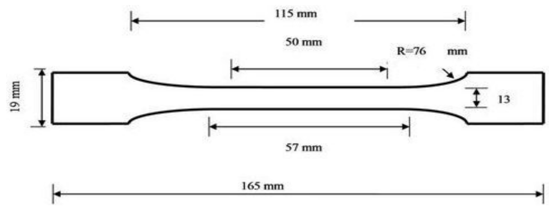

Figure 2 specifications of tensile test specimen

The tensile properties of the samples of sizes 165 mm long, 19 mm wide and 3.2 mm thick, as shown in Figure 3.9 were measured in accordance with ASTM: D638. The samples were tested at a cross head speed of 10 mm/min, using an UTM machine. The tensile test determines the overall strength of the given object. In a tensile test, the object fitted between two grippers at either end then slowly pulled apart until it breaks.

3.4 Optimization:

Taguchi method was used to optimize the input parameters. Based on mean effective plots, the optimum levels of parameters are to be identified. The present study makes an novel approach of applying taguchi method for constituents optimization in a material to achieve required mechanical property i.e tensile strength. As the work intended to maximize the tensile strength larger was better method adopted for optimization.

3.5 Analysis of variance:

Analysis of variance method was used to identify the most influencing parameter in an process, the current work carries three input parameters studying one output parameter i.e among the type of fiber, fiber angle, filler percentage which is most sensitive in output point of view, and what parameter will cause much fluctuation in output were analyzed..

3.5 Testing and validation:

The optimal combination of input parameters given by taguchi methods were verified by preparing six sets of new samples with optimal combination of parameters and were then tested as per ASTM standard. The results obtained were compared with system results

3.5 Morphology study:

Scanning electron micrographs (SEM) of optimal sample was taken to know the bonding between the matrix, fibre and filler. SEM was used to study the fracture behavior of fiber and fiber matrix integrations.

4.0 RESULTS & DISCUSSION

4.1 Experimentation:

The ability of a material to resist breaking under tensile stress is one of the most important and widely measured properties of materials used in structural applications. The force per unit area (N/mm^2) required to break a material was the ultimate tensile strength or tensile strength at breaking.

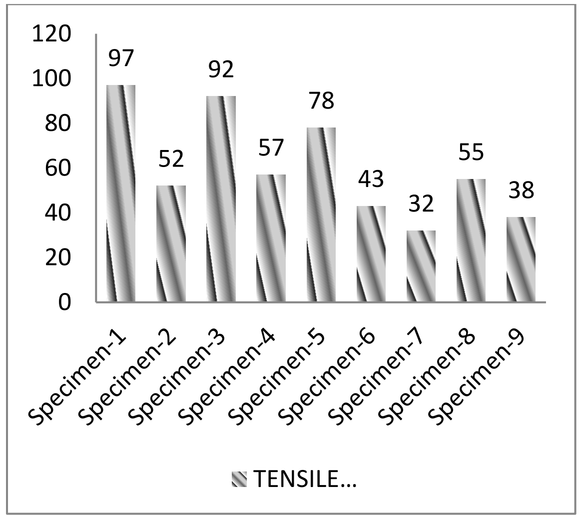

Figure 3 Average Tensile strength of each sample

Figure 3. Was evident for that the specimen1 (zero fibre angle-longitudinal-zero percent filler) has maximum strength; the presence of the filler is decreasing the strength of the material. For achieving the better combination, optimization was carried out.

s.n	FIBE	FIBE	FILLE	TENSIL	S/N
1	0	Long	0	97	39.7
2	0	wiske	5	52	34.2
3	0	crossp	10	92	39.2
4	60	wiske	0	57	35.0
5	60	crossp	5	78	37.8
6	60	Long	10	43	32.7
7	45	crossp	0	32	30.0
8	45	Long	5	55	34.8
9	45	wiske	10	38	31.6

Table 3: Signal to noise ratio for array tensile strength

4.2 Optimization of Tensile strength:

Analysis of the influence of each control factor (Fiber orientation angle, Type of Fiber, Filer Percentage) on the tensile strength was performed with a signal-to-noise (S/N) response table. The experimental design, results for tensile strength and S/N ratios are shown in Table 3.

Control factors	**Average s/n ratio (db)**				**Rank**
	Level 1	Level 2	Level 3	Max-min	
Fibre orientation angle (º)	37.75	32.16	35.23	5.58	1
Type of Fibre	35.71	35.75	33.68	2.07	2
Filer Percentage	34.93	35.66	34.55	1.11	3

Table 4 Response Table for Signal to Noise Ratios Larger is better

Main control factors	Optimum level	Optimum value
Fibre orientation angle (º)	1	0º
Type of Fibre	1	Longitudinal
Filer Percentage (%)	2	5 %

Table 5: optimum level of control factors for tensile strength

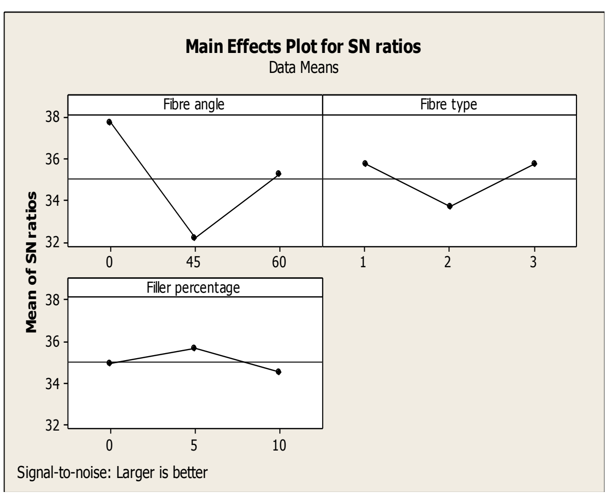

Figure 4: Main effect plots for Tensile strength for S/N ratio (dB)

Table 4 shows the S/N response table of Tensile strength. It indicates the S/N ratio at each level of control factor and how it was changed when settings of each control factor were changed from level 1 to level 2. The influence of interactions between control factors was neglected here. The control factor with the strongest influence was determined by difference value. The higher the difference, the more influential was the control factor.

Fig. 4.Shows the main effect plots for Tensile strength of the work piece for S/N ratios, respectively. The greater is the S/N ratio; the Larger is the variance of the tensile strength around the desired value. Optimal testing conditions of these control factors could be very easily determined from the response graph.

The best Tensile strength value was at the higher S/N value in the response graph. For main

Control factors, Table 5 indicate the optimum condition for the tested samples (*0 degrees Fiber angle, longitudinal fiber with 5 % of filler)*.

Thus, it could be concluded that the Tensile strength of hybrid Glass/ Epoxy/ White cement Composite material can be achieved and their optimal setting of control factors for tested samples is shown in Table 5.

4.3 Analysis of variance of Tensile strength:

The Analysis of variance (ANOVA) was used to investigate which design parameters significantly affect the quality characteristics of the Tensile strength of the material. The results of the ANOVA of Tensile strength of prepared composite materials are shown in Table 6. In addition to degree of freedom, mean of squares (MS), sum of squares (SS), F-ratio and P-values associated with each factor level were presented. This analysis was performed for a confidence level of 90%. The F value for each design parameters was calculated. The calculated value of the F showed a high influence of the Fiber orientation angle on the Tensile strength since

F-calculation was equal to 1.48, but Fiber type and Filler Percentage had also significant effects on the Tensile strength since F-test was equal to 0.40 and 0.02 respectively. The last column of the above table indicated the percentage of each factor contribution (P) on the total variation, thus exhibiting the degree of influence on the result. It was important to observe the P-values in the table. From the analysis of Table 6, the parameter Fiber orientation angle (P≈77.89%) showed a high significant effect. It was followed by fiber type (P≈21.06) and Filler Percentage ((P≈1.05%).

Source	Degree of freedom (d.f.)	Sum of squares (SS)	Adjustment of Sum of squares (Adj SS)	Adjustment of Mean of squares (Adj MS)	F-Calculation	Contribution,P (%)
Fibre angle	2	2214.6	2214.6	1107.3	1.48	77.89
Fibre type	2	596.8	596.8	298.4	0.40	21.06
Filler percentage	2	30.7	30.7	15.3	0.02	1.05
{	2	1492.7	1492.7	746.4		
Total	8	4334.8	-	-		100

Table 6: Results of ANOVA Tensile strength of material

4.4 Validation:

According to table5. From the results of control factors, higher Tensile strength was obtained for the material combination of 0 *degrees Fiber angle, longitudinal fiber with 5 % of filler*. The experimental work was carried out on the same hybrid Glass/ Epoxy/ White cement composite material using the determined optimal control factors. The Tensile strength was found to be about 118.2 MPa. The obtained value is more than the samples 1-9 it is shown in figure 5.

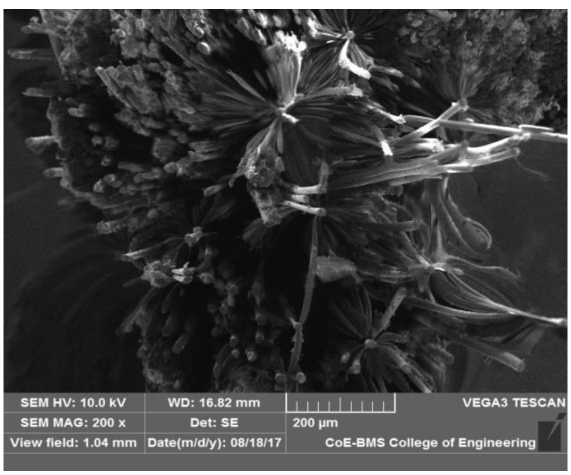

Figure 5: fiber breakage of optimized tensile test sample

4.5morphilogy:

The fiber peeling shows that the strong bonding of the matrix and fiber. Fiber was subjected to brittle failure and more depositors of the fillers are observed in figure 5. The matrix is observed that it is subjected to cup cone fracture but the fibers are undergone the brittle fracture.

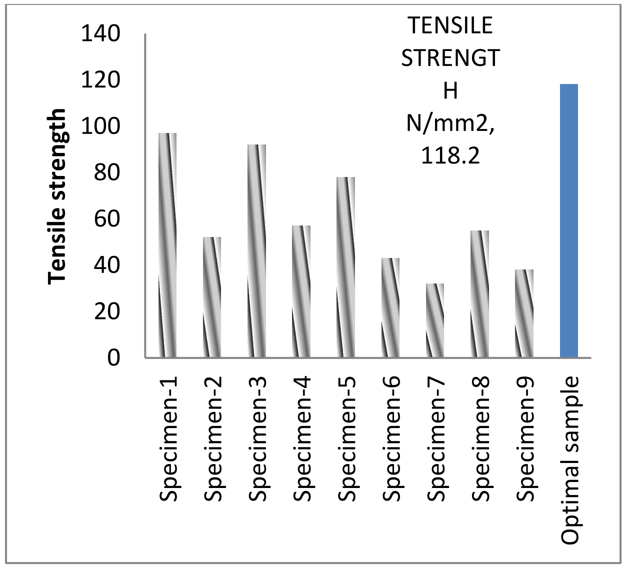

Figure 6 comparison of optimal solution

5.0 CONCLUSIONS

A detailed study has been conducted on the tensile strength of glass/epoxy composite on the basis of different weight concentration of filler, fiber alignment and fiber orientation. The study led to the conclusions mentioned below.

1. Epoxy resin reinforced with glass fiber were fabricated by hand lay-up method with different fiber angle, filler percentages and type of fiber as per L9 orthogonal array
2. Mechanical characterization was made to analyze the material behavior and parameters were optimizing by using taguchi method.
3. ANOVA is performed for each characterization to find most significant parameter.
4. The Tensile strength, as filler weight percentage in the material increases, there was increase in the tensile strength up to 5% then decreases .The fiber orientation plays most significant role in strength.
5. From the test data it was concluded that 5% of filler with longitudinal fiber at 0 degrees has good Tensile strength
6. Morphological studies showed that the good bonding of fiber, filler and matrix.

References

[1] R. Gujjala, S. Ojha, S.K. Acharya, and S.K. Pal, J. Compos. Mater., doi: 0021998313501924 (2013).

[2] G. Raghavendra,1 Shakuntala Ojha,2 S.K. Acharya,2 S.K. Pal, POLYMER COMPOSITES— DOI : 10.1002/pc (2014)

[3] P Sneha Latha1, M Venkateswara Rao2, VV Kiran Kumar3,G Raghavendra4, S Ojha5 and Ramu inala, Journal of Industrial Textiles 46(1) , DOI: 10.1177/1528083715569376

[4] R. S. Rana1 Ashish kumre2, Saraswati Rana3, and Rajesh Purohit4, 6th International Conference of Materials Processing and Characterization (ICMPC 2016), Materials Today: Proceedings 4 (2017) 5445–5451

[5] Rahul Shrivastavaa, Amit Telangb, R. S Ranac and Rajesh Purohitd, Materials Today: Proceedings 4 (2017) 3477–34832214-7853©2017 Elsevier Ltd. All rights reserve, 5th International Conference of Materials Processing and Characterization (ICMPC 2016).

[6] Shakuntala Ojha,1 Samir Kumar Acharya,1 Gujjala Raghavendra2 J. APPL. POLYM. SCI. 2015, DOI: 10.1002/APP.41211

[7] M.A. Agwa, M. Megahed* and A.A. Megahed, 10.1002/pat.4004, Polym. Adv. Technol. (2017)

[8] Haksung Lee1,2, Mongyoung Huh1, Jaeyoung Yoon1, Dasom Lee1, Seonyul Kim1 and Shinjae Kang1,2, Carbon Letters Vol. 22, 101-104 (2017), DOI::10.5714/CL.2017.22.101

[9] Kamil Şirin, Mehmet Balcan and Fatih Doğan (2012). The Influence of Filler Component on Mechanical Properties and hermal Analysis of PP-LDPE and PP-LDPE/DAP Ternary Composites, Polypropylene, Dr.Fatih Dogan (Ed.), ISBN: 978-953-51-0636-4, InTech,

[10] Tkaczewska, Ewelina. (2014). Effect of the superplasticizer type on the properties of the fly ash blended cement. Construction and Building Materials. 70. 388–393. 10.1016/j.conbuildmat.2014.07.096.

[11] ASTM D638-14, Standard Test Method for Tensile Properties of Plastics, ASTM International, West Conshohocken, PA, 2014, www.astm.org

MODELING AND STRUCTURAL ANALYSIS OF SPINDLE

C.P.Praneeth Kumar

M.Tech CAD/CAM
Department of Mechanical Engineering
Malla Reddy College of Engineering
Hyderbad-500100
Email-praneethroy99994@gmail.com
Ph: 8125405120

J.Chandra Sekhar
Assistant Professor
M.Tech CAD/CAM
Department of Mechanical Engineering
Malla Reddy College of Engineering
Hyderbad-500100
Email-chandu1439@gmail.com
Ph: 9550012358

ABSTRACT

In modern machine tool applications the performance of a machine tool is judged by its strength. The machine tool spindle has a profound impact on the overall machine performance. The work presented here provides machine tool spindle designers to develop spindles that are sufficiently stiff to meet their need.

In this we are using the dynamic analysis and the static analysis is use to calculate the deflection of spindle-bearing system. This analysis is to find out the deflections, stress induced.
and the frequencies of the mode shape for both steel material and 20MnCr5 material in machine tool spindle. This project is on the application of computer aided analysis using finite element method. The boundary conditions, loads, material properties are added according as per the design. The resultant of the deformation and stresses and the frequency of mode shapes obtained are reported and discussed

CHAPTER 1
INTRODUCTION

1.1 Introduction about spindle

In machine tools, a **spindle** is a rotating axis of the machine, which often has a shaft at its heart. The shaft itself is called as a spindle, but also, in shop-floor practice, to refer to the entire rotary unit, including not only the shaft itself, but its bearings and anything attached to it (chuck, etc.)

A machine tool may have several spindles, mainly the headstock and tailstock spindles on a bench lathe. The main spindle is usually the biggest one. References to “the spindle” without further qualification imply the main spindle. Some machine tools that specialize in high-volume mass production have a group of 4, 6, or even more main spindles. These are called **multi spindle** machines. For example, gang drills and many screw machines are multi spindle machines. A bench lathe has more than one spindle (counting the tailstock), it is not called a multi spindle machine; it has one main spindle.

Examples of spindles include:

- On lathe machine (whether wood lathe or metal lathe), the spindle is the heart of the headstock.
- In rotating-cutter wood working machinery, the spindle is the part on which shaped milling cutters are mounted for cutting features (such as rebates, beads, and curves) into the mould sand similar millwork.
- Similarly, in rotating-cutter metalworking machine tools (such as milling machines and drill press), the spindle is the shaft to which the tool (such as a drill bit or milling cutter) is attached.
- Varieties of spindles include grinding spindles , electric spindles, machine tool spindles, low-speed spindles, high speed spindles, and more.

Machine tool spindles are rotating components that are used to hold and drive cutting tools or work pieces on lathes, milling machines and other machine tools. They use belt, gear, motorized, hydraulic or pneumatic drives and are available in a variety of configurations. For example,
Cartridge assemblies are housed in a stationary enclosure while angled spindles are configured to allow right angle or adjustable tool rotation. Some machine tool spindles are housed in a solid block or box-like housing. Others are bolted down via flanges or feet at the bottom of the housing.
Most machine tool spindles that fit the heads of cutting tools feature a Morse taper or other standardized machine tool taper. Multiple spindle heads are used to speed machining operations and in repetitive precision work such as close-tolerance center holes. A variety of bearing types are used with machine tool spindles.
Selecting machine tool spindles requires an analysis of performance specifications, tool mounting, and spindle features. Performance specifications include:

- Operating speed
- Spindle power
- Maximum torque
- Input voltage

Tool mounting measurements such as outer diameter (OD) and inner diameter (ID) are measured in either English units such as inches or metric units such as centimeters.

Spindle interface size is the diameter of the cutting tool or the bore of the grinding wheel to which the spindle is mounted. Tool or work holder mounting style describes the spindle's mounting interface. Examples include standard, threaded, and flanged bores; arbors and shafts; collets and wheel collets; and external and internal tapers.

In terms of features, some machine tool spindles include air purging or automatic balancing options. Others include high frequency drives that are liquid cooled for improved heat dissipation. Spindles with coolant feeds are also available.

Machine tool spindles are used in a variety of applications.

- **Boring spindles** are used in the machining of internal diameters.
- **Drilling spindles** provide good thrust capacity and radial load ratings.
- **Grinding spindles** are used with grinding wheels for precision, size and surface finishing.
- **Wheel dressing spindles** are suitable for the truing, dressing, contouring, and re-profiling of abrasive grinding wheels.
- **Tapping spindles** are used with taps to create internal threads.
- **Tuning spindles** are designed for horizontal or vertical lathes and turning centers.
- **Hobbing spindles** are used in the cutting of gear tooth profiles.
- **Milling spindles** are used with a wide variety of machining tools and operations.

CHAPTER 2
FINITE ELEMENT METHOD

2.1 Introduction:

The basic idea in the Finite Element Method is to find the solution of complicated problem with relatively easy way. The Finite Element Method has been a powerful tool for the numerical solution of a wide range of engineering problems. Applications range from deformation and stress analysis of automotive, aircraft, building, defense, and missile and bridge structures to the field analysis of dynamics, stability, fracture mechanics, heat flux, fluid flow, magnetic flux, seepage and other flow problems. With the advances in computer technology and CAD systems, complex problems can be modeled with relative ease. Several alternate configurations can be tried out on a computer before the first prototype is built. The basics in engineering field are must to idealize the given structure for the required behavior. The proven knowledge in the computational aspects of the Finite Element Method is essential. In the Finite Element Method, the solution region is connected as built up of many small, interconnected sub regions called finite elements.

2.4 General Description of Finite Element Method:

STEP 1: Discretization of structure (domain)
The first step in the finite element method is to divide the structure or solution region into sub-divisions or elements.

STEP 2: Selection of a proper interpolation model.

Since the displacement (field variable) solution of a complex structure under any specified load conditions can't be predicted exactly. We assume some suitable solution within an element to approximate the unknown solution. The assumed solution must be simple from computational point of view, and it should satisfy certain convergence requirements.

STEP 3: Element stiffness matrices (characteristic matrices) and load vectors.
From the assumed displacement model the stiffness matrix [K(e)] and the load vector F(e) of element 'e' are to be derived by using either equilibrium conditions or a suitable variation principle.

STEP 4: Assemblage of element equations to obtain the overall equilibrium equations. Since the structure is composed of several finite elements, the individual element stiffness matrices and load vectors are to assembled in a suitable manner and the overall equilibrium equations have to be formulated as

$$[K]\, q = F$$

[K] is called assembled stiffness matrix, q is called the vector of nodal displacement and F is the vector of nodal forces of the complete structure.

STEP 5: Solution of system equations have to be modified to account for the boundary conditions of the problem. After incorporation of the boundary conditions, the equilibrium can be expressed as

$$[K]\, q = F$$

For linear problems, the vector 'q' can be solved very easily, But for non-linear analysis problems, the solution has to be obtained in a sequence of steps, each step involving the modification of the stiffness matrix [k] and /or the load vector F.

STEP 6: Computation of Element Stresses and Strains.
From the known nodal displacements, if required, the element stresses and strains can be computed by using the necessary equations of solid or structural mechanics.

CHAPTER 3
INTRODUCTION ABOUT ANSYS

INTRODUCTION TO ANSYS

3.1 BASIC METHODOLOGY OF ANSYS

Ansys is followed up by the method called Finite Element Modeling Methods (FEM)

Finite element method

The finite element method (FEM) (its practical application often known as finite element analysis (FEA) is a numerical technique for finding approximate solutions of partial differential

2

CHAPTER -4

PROCEDURE FOR ANALYSIS OF SPINDLE

MATERIAL PROPERTIES OF STEEL

- Modulus of elasticity, E=210,000 N/mm^2
- Shear Modulus, G=E/[2(1+V)] N/mm^2,81,000 N/mm^2
- Poisson's Ratio, V=0.3
- Density,=8050 Kg/m^3

DIMENSIONS OF THE MACHINE TOOL SPINDLE

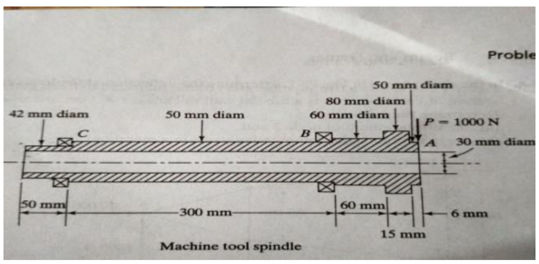

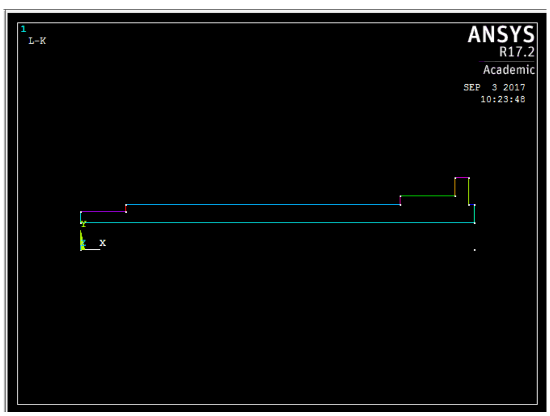

Fig.4.1 Lines through key points

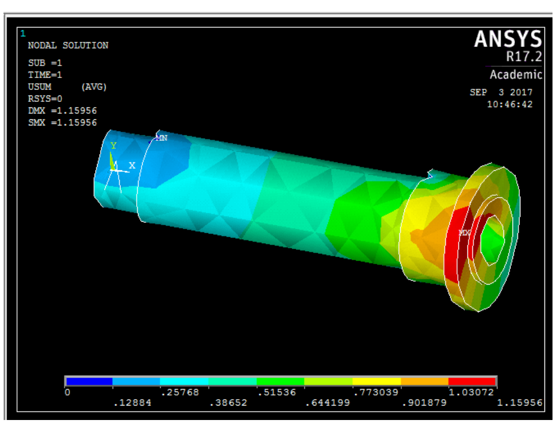

Fig.4.2 Deformation vector sum

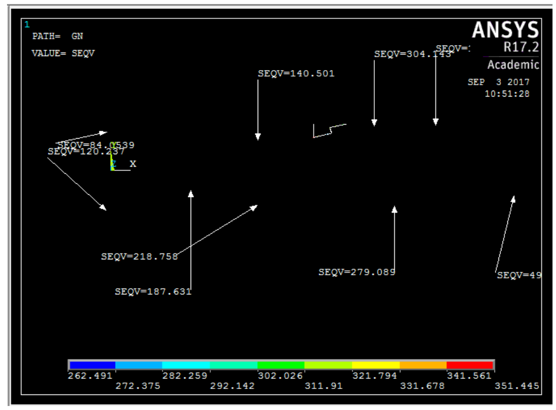

Fig.4.3 Von mises stress values

4.2 STATIC ANALYSIS OF SPINDLE USING 20MnCr5 MATERIAL

Material properties

- Material = 20MnCr5
- Modulus of Elasticity, Ex= 190e3 N/mm2
- Poisson's Ratio, Prxy = 0.27
- Density= 8030 Kg/m^3

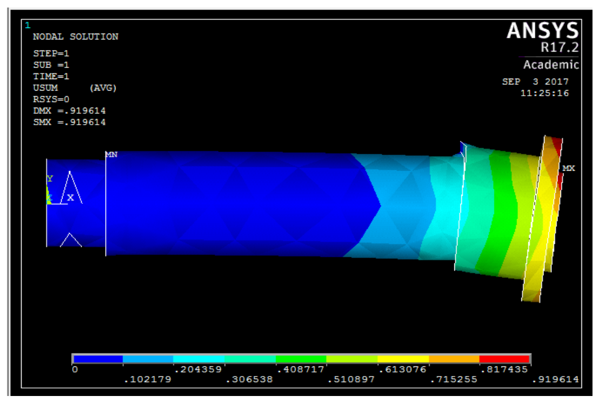

Fig.4.4 Deformation vector sum

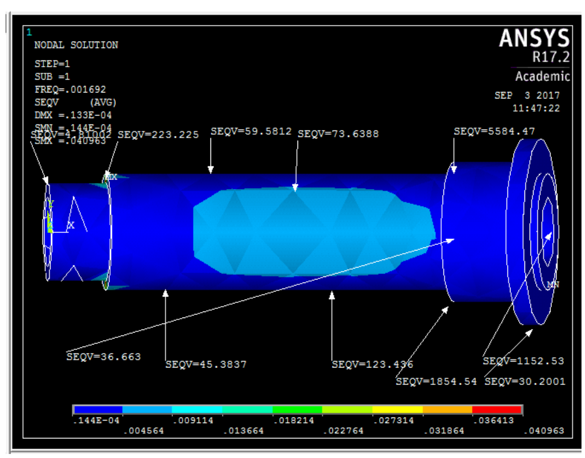

Fig.4.5 Von mises stress values

4.3 STATIC AND MODAL ANALYSIS FOR GREY CAST IRON

MATERIAL PROPERTIES

- Material = Grey Cast Iron
- Modulus of Elasticity, Ex= 26E6 psi
- Poisson's Ratio, Prxy = 0.29
- Density=75000 g/m

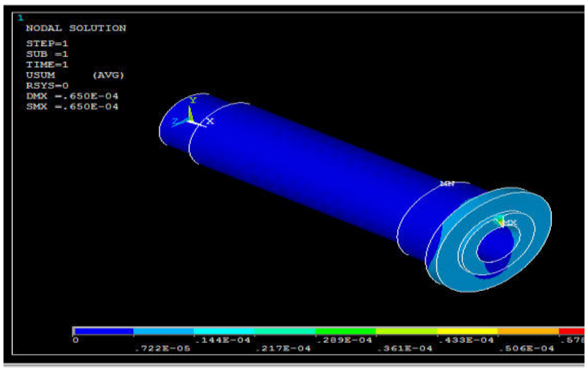

Chapter 5
RESULTS

BY COMPARING THE VALUES OF THREE MATERIAL

STEEL MATERIAL	20MnCr5 MATERIAL	GREY CAST IRON MATERIAL
DMX=1.15956	DMX=.919614	DMX=.650E-04
Von mises Stress 1)X=13117.9 2)Y=3756.95 3)Z=7324.1	Von mises Stress 1)X=5230.06 2)Y=3491.68 3)Z=3026.37	Von mises Stress 1)X=88.5825 2)Y=15.2686 3)Z=17.5574

CONCLUSION

The aim of this project is to model and to analysis on the Machine tool Spindle. Static analysis and Dynamic analysis is to calculate the deflection of spindle-bearing system. And it is performed by applying the loads and boundary conditions on the component using ANSYS by finite element method. The work presented here provides machine tool spindle designer to develop spindles that are sufficiently stiff to meet their need.

Total deformation and Von-Mises stresses and Displacement vector frequency are obtained by performing the analysis.

The three materials have been taken and both the static and dynamic analysis has been performed. And the results obtained by the materials has been noted and discussed

REFERENCES

[1]Thitima Jintanawan, "Effects of distributed bearing forces and bearing locations on rocking vibration of FDB (Fluid dynamic bearings) spindle systems", ASME Information Storage and Processing Systems Conference, 2005

[2]. Al-Shareef.K.J.H, Brandon. J.A, "Effects of variations in the design parameters on the dynamic performance of machine tool spindle-bearing systems", International Journal of Machine Tools and Manufacture, Vol 30, Pages 431–445, 1990.

[3]. Rathour. A. N, Darji P. H, "Design, development and analysis of high speed spindle: a review" Department of Mechanical Engineering, C. U. Shah College of Engineering and Technology, Surendranagar, Gujarat.

[4]. Machine tool design hand book by central machine tool institute, Bangalore.

[5]. Ball and roller bearing engineering by palmgren.A, Third edition 1959, burkank and co, Philadelphia

[6]. Luk, Y.W. and Mitchell, L.D, "System modeling and modification via modal IJSER analysis", Proceedings of the first Int

[7].Tirupathi R.Chandrupatla and Ashok D.Belegundu "Finite Elements in Engineering" Third Edition

[8] PRASAD RAO, T.H.V. Computer Aided Static and Dynamic Analysis of Machine Tool Spindle System. Proc. 8th AIMTDR Conf. (INDIA) pp 189–193.

[9] SKF (1962) "Engineering Data" and (1969) "Bearings in Machine Tools" Catalogue

[10] JANA, S (1974) Some aspects of Machine Tool Spindle Design, Machine Building Industry Vol.13.

DESIGN AND ANALYSIS OF HOLLOW EXHAUST VALVES IN INTERNAL COMBUSTION ENGINES

Ashish J
M.tech Student
Department of Mechanical Engineering,
Mallareddy College of Engineering,
Email ID: ashishjayan611@gmail.com

B.S.Sai Deepika, M.Tech
Assistant Professor
Department of Mechanical Engineering,
Mallareddy College of Engineering,
Email ID: suryabogaram14@gmail.com

Dr.P.Velmurgan, Ph.D
Professor
Department of Mechanical Engineering,
Mallareddy College of Engineering,
Email ID: velmurgan_mech@mrce.in

Abstract— **A motor valve is a mechanical gadget that manages the measure of fuel to a motor. It is a noteworthy piece of any motor structure and involve a stem and a head. Exhaust valve is precision motor component used to open and permit the consume gasses to debilitate from chambers. The leaders of the valves are subjected to the hoisted temperature of the blazing gasses. The Exhaust valves may achieve high temperature of 800^0C cherry red. It is fundamental that they ought not twist affected by the warmth, and that their seats ought not scale or erode, as in either case they would end up noticeably broken. The Exhaust valves are open to serve warm load and compound weakening. Exhaust valve open and close 2000 time for every mile.**

In this postulation, different outline of hollow exhaust valves are demonstrated utilizing CREO. The displayed exhaust valve plans 1) Hollow segment from tip of the stem to the base of it. 2) Hollow segment with a stem at centre. 3) Two parallel hollow segment with a beam at the inside. The hollow portion of the designs is filled with sodium which affect the heat dissipation property of valve. Investigation done in ANSYS.

Keywords: CFD, Hollow exhaust valve, Ansys

I. INTRODUCTION

An engine valve is a mechanical device that regulates the supply of fuel to the engine. This an important part of an engine system and comprised of a stem and head. It is precision engine component used to open the burned gases to exhaust from cylinders. The heads of the valves are subjected to high temperature of the burning gases. It should not warp or corrode under the influence of thermal loads and chemical corrosion.

Due to high temperature operating conditions, the material for exhaust valve should have 1. High strength and hardness to resist tensile loads and stem wear, 2. High hot strength and hardness to combat head cupping and wear of seats, 3. High fatigue and creep resistance, 4. Adequate corrosion resistance, 5. Least coefficient of thermal expansion to avoid excessive thermal stresses in the head, 6. High thermal conductivity for better heat dissipation. Process required for the exhaust valve essentially require high dimensional accuracy and heat treatment to guarantee complete fixing of the combustion chamber.

The aim of the present paper is to perform thermal analysis of various designs of hollow valves and to propose a suitable design and material which would improve the life of valves and is cost effective at mass production of the valves to be used in automotive engines.

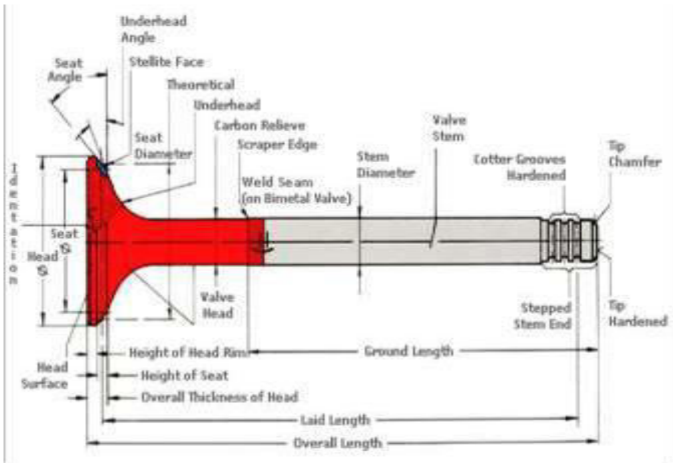

FIGURE 1: VALVE DIMENSIONS

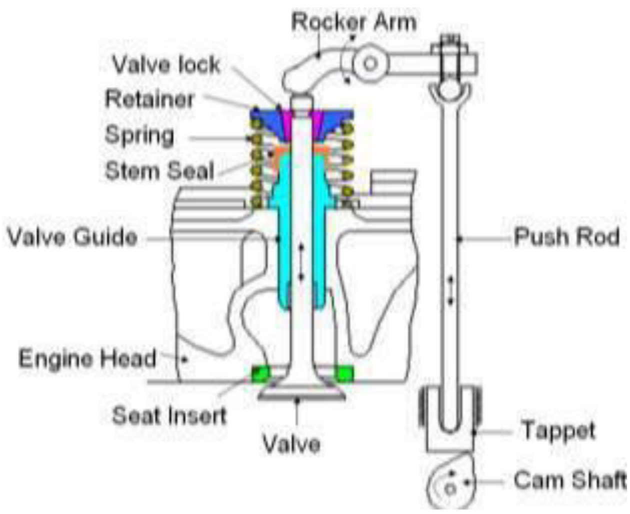

FIGURE 2: TYPICAL VALVE TRAIN ASSEMBLY

II.MODELLING AND MESHING OF VARIOUS DESIGNS OF HOLLOW VALVES

The various designs of hollow valves are designed using ProE (CREO) modeling software. The dimensions of the each design are as per the standard. Three models are made with two materials:-1) Stainless steel 2) Titanium alloy and corresponding thermal analysis is done in Ansys for each design with different materials. The material selected for this high temperature application was stainless steel and Titanium alloy which has got high strength and hardness to resist tensile loads and stem wear, high hot strength and hardness to combat head cupping and wear of seats, high fatigue and creep resistance, adequate corrosion resistance, least coefficient of thermal expansion to avoid excessive thermal stresses in the head, and high thermal conductivity for better heat dissipation. Hence stainless steel material was chosen as the exhaust material .Stainless Steels are iron-base alloys containing Chromium. Stainless steels contain less than 30% Cr and more than 50% Fe. They attain their stainless characteristics because of the formation of an invisible and adherent chromium-rich oxide surface film. This oxide establishes on the surface and heals itself in the presence of oxygen. Titanium alloy has a chemical composition of 6% aluminum, 4% vanadium, 0.25% (maximum) iron, 0.2% (maximum) oxygen, and the remainder titanium. Since sodium has got low specific gravity, a high specific heat, a low melting point, and a high boiling point, it is filled into the hollow spaces of the valves in order to carry away the heat effectively.

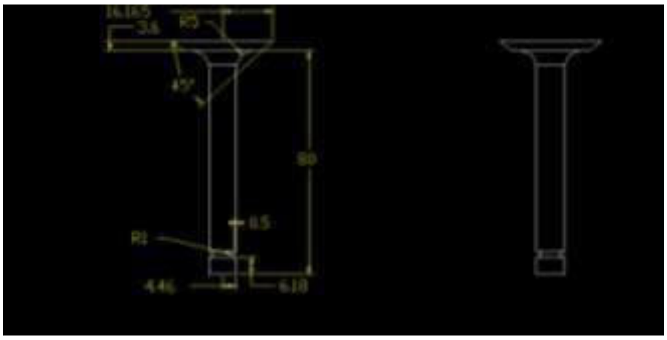

FIGURE 3 2D SKETCH OF EXHAUST VALVE

THREE DIFFERENT DESIGNED EXHAUST VALVE MODELS ARE SHOWN BELOW:

FIGURE 4: 1) HOLLOW EXHAUST VALVE

FIGURE 5: 2) VALVE WITH STEM AT CENTRE

FIGURE 6: 3) VALVE WITH BEAM AT CENTRE

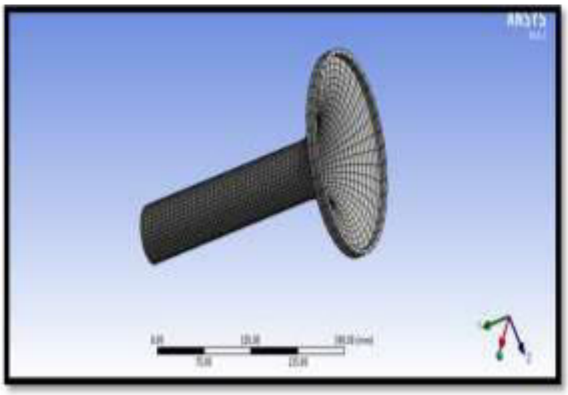

FIGURE 7: MESHED MODEL OF VALVE

The design 1 comprises of a hollow section from top of the stem to the bottom of it. Design 2 consists of a stem at the centre whereas design 3 has a beam at the centre from top of the stem to bottom. The hollow portions are filled with sodium. Although the design may be complex, the possibility of conduction and convection might improve the heat carrying capacity of the exhaust valve. CFD and thermal analysis is done for the designs with different materials at two velocities ie: 10 m/s and 12 m/s.

III. RESULTS & DISCUSSION:

CFD ANALYSIS RESULTS:

CASES	INLET VELOCITY (m/s)	PRESSURE (Pa)	HEAT TRANSFER COEFFICIENT (W/m²k)	MASS FLOW RATE (kg/sec)	HEAT TRANSFER RATE (w)
HOLLOW	10	7.26e+02	3.96e+03	0.0560321181	131988
	12	1.03e+03	4.64e+03	0.064642	152270
WITH STEM	10	7.27e+03	4.66e+04	0.0002	616.75
	12	1.01e+04	5.48e+03	0.00238	563
WITH BEAM	10	5.47e+04	3.60e+03	0.010732	25281
	12	7.98e+04	4.03e+03	0.0013766	3239.5

THERMAL ANALYSIS RESULTS:

FOR STAINLESS STEEL:

CASES	INLET VELOCITY (m/s)	TEMPERATURE (K)		HEAT FLUX(w/mm²)
		MIN	MAX	
HOLLOW	10	294.06	1073	1.6465
	12	294.02	1073	1.7157
WITH STEM	10	273.15	1073	1.9847
	12	273.15	1073	2.0601
WITH BEAM	10	255.6	1073	2.5624
	12	252.12	1073	2.6254

FOR TITANIUM ALLOY:

CASES	INLET VELOCITY (m/s)	TEMPERATURE (K)		HEAT FLUX(w/mm²)
		MIN	MAX	
HOLLOW	10	295.15	1073	3.2357
	12	295.15	1073	3.3732
WITH STEM	10	273.15	1073	2.5782
	12	273.15	1073	2.6771
WITH BEAM	10	266.37	1073	3.3572
	12	263.19	1073	3.4671

HEAT TRANSFER COEFFICIENT VS VELOCITY

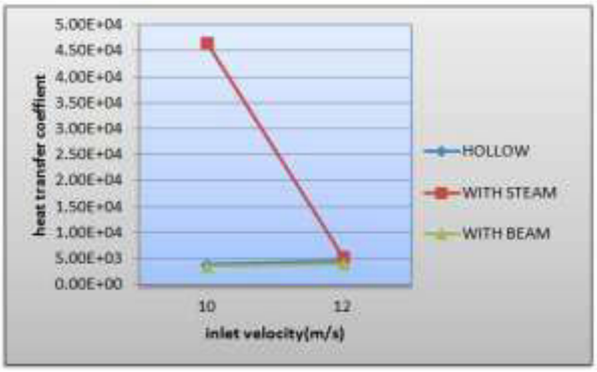

IV. CONCLUSION

* Henceforth three novel designs of the exhaust valve are outlined utilizing CREO. Thermal and CFD analysis of the designs are performed by ANSYS.
* In this postulation, different designs of exhaust valves are demonstrated utilizing CREO. The displayed exhaust valve designs are 1) Hollow segment from tip of the stem to the base of it. 2) Hollow segment with a stem at centre. 3) Two parallel hollow segment with a beam at the inside.
* By observing the CFD analysis the heat transfer coefficient values is more at exhaust valve with stem compare with hollow and with beam type valves.
* By observing the thermal analysis the heat flux value is more for Titanium alloy.
* So it can be concluded that with stem exhaust valve by the material Titanium Alloy is better performed.

HEAT FLUX FOR STAINLESS STEEL

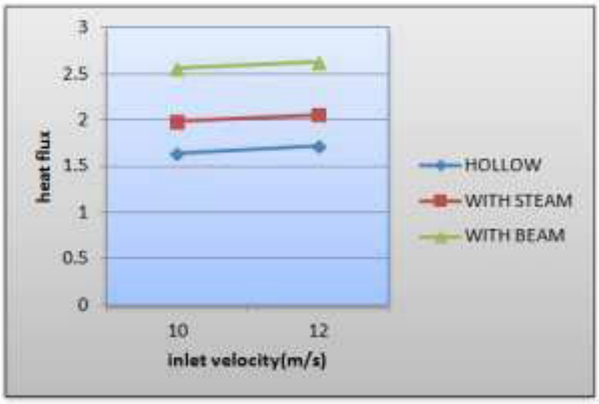

HEAT FLUX FOR TITANIUM ALLOY

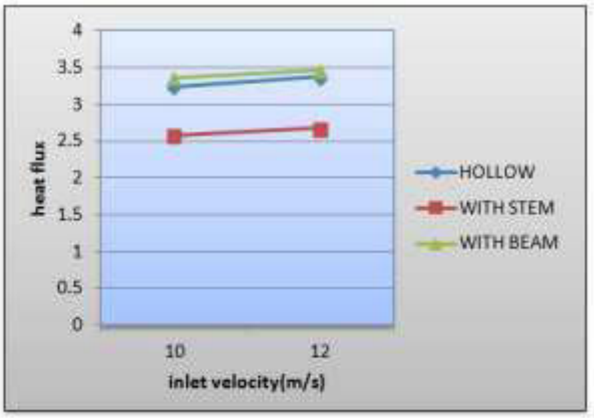

V.REFERENCES

1) J. M. Cherrie, Factors Influencing Valve Temperatures in Passenger Car Engines, SAE Paper 650484, 1965.
2) R. P. Worthen and T. N. Tunnecliffe, Temperature Controlled Engine Valves, SAE Paper 820501, 1982
3) Z. Johan, A. C. M. Moraes, J. C. Buell, and R. M. Ferencz, In-Cylinder Cold Flow Simulation Using a Finite Element Method, Comput. Meth. Appl. Mech. Eng., vol. 190,pp. 3069–3080, 2001.
4) R. Prasad and N. K. Samria, Heat Transfer and Stress Fields in the Inlet and Exhaust Valves of a Semi-adiabatic Diesel Engine, Comput. Struct. vol. 34, no. 5, pp. 765–777, 1990.
5) R. Prasad and N. K. Samria, Transient Heat Transfer Studies on a Diesel Engine Valve,Int. J. Mech. Sci., vol. 33, no. 3, pp. 179–195, 1991.
6) C. R. Ferguson and A. T. Kirkpatrick, Internal Combustion Engines, 2nd ed., Wiley, New York, 2001.
7) A. C. Alkidas, Intake-Valve Temperature and the Factors Affecting It, SAE Paper 971729, 1997.
8) J. Cowart and W. Cheng, Intake Valve Thermal Behavior during Steady-State and Transient Engine Operation, SAE Paper 1999-01-3643, 1999.
9) R. P. Worthen and D. G. Rauen, Measurement of Valve Temperatures and Strain in a Firing Engine, SAE Paper 860356, 1986.
10) H. Cheng-Hung and J. Tzann-Ming, Inverse Problem of Determining the Periodic Thermal Contact Conductance between Exhaust Valve and Seat in an Internal Combustion

DESIGN AND ANALYSIS OF COMBUSTION CHAMBER IN I.C ENGINE

G DANRAJ KUMAR
PG scholar
Dept. of Mechanical Engineering
Malla reddy college of engineering
dhanraj2984@gmail.com

LANKA PRIYANKA
assistant professor
Dept. of Mechanical Engineering
Malla reddy college of engineering
lohilakshmi.lakshmi@gmail.com

P.VELMURUGAN
professor
Dept. of Mechanical Engineering
Malla reddy college of engineering
velmurugan_mech@mrce.in

ABSTRACT

Inside ignition motors are seen each day in autos, trucks, and transports. The name inside ignition alludes additionally to gas turbines aside from that the name is typically connected to responding inward ignition (I.C.) motors like the ones found in ordinary cars. There are essentially two sorts of I.C. start motors, those which require a start plug, and those that depend on pressure of a fluid. Start motors take a blend of fuel and air, pack it, and light it utilizing a start plug. In this proposal, the ignition chamber is composed by the ic motor determinations and broke down for its warmth exchange rate utilizing Finite Element investigation programming ANSYS. Displaying will be done in CREO parametric programming. CFD investigation to decide the weight drop, speed, warm exchange rate and mass stream rate with distinctive liquids (ethanol, methanol, ethylene, Propyl and gasoil).Thermal examination is to decide the warmth exchange rate per unit zone i.e. warm motion and temperature dissemination for two materials steel and cast iron.

Keywords: Internal combustion, CREO, ANSYS 14.5

1. INTRODUCTION:

ICEs typically comprise reciprocating piston engines, rotary engines, gas turbines and jet turbines. The combustion process increases the internal energy of a gas, which translates into an increase in temperature, pressure, or volume depending on the configuration. In an enclosure, for example the cylinder of a reciprocating engine, the volume is controlled and the combustion creates an increase in pressure.

In a continuous flow system, for example a jet engine combustor, the pressure is controlled and the combustion creates an increase in volume. This increase in pressure or volume can be used to do work, for example, to move a piston on a crankshaft or a turbine disc in a gas turbine. If the gas velocity changes, thrust is produced, such as in the nozzle of a rocket engine.

Literature work:

Owing to the need identified and the innovative idea considered, literature review has been carried out. This has identified the Technology which is available or unavailable for the realization of the concept considered for the present work.

[1] Simulation And CFD Analysis Of Various Combustion Chamber Geometry Of A C.I Engine Using CFX(Dr. Abdul Siddique),2016.

[2] Design and Analysis of an Internal Combustion Engine Piston Head to Increase the Torque on Crankshaft(Nagasundaram.S),2016.

[3] Internal Combustion Free Piston Engines(ujjawal.k.saha),2004.

[4] Design And Analysis Of Internal Combustion Compressed Air Hydrid Engine (INCO)(Sourabh.N.Mahendrakar),2014.

2. Concept and Definition:

In this thesis, different alternate fuels are analyzed for their performance in the combustion chamber of an IC engine. The Alternate fuels are ethanol, methanol, ethylene, propyl and gas oil. 3D model of the combustion chamber of an IC engine is done in CREO parametric software. In ANSYS, CFD analysis is done on the combustion chamber of an IC engine for alternate fuels and thermal analysis is done for two materials steel and cast iron.

The following dimensional are taken from previous journal.

Parameter	**Magnitude**
Crank shaft speed	1550rpm
Crank radius	56mm
bore	85mm
stroke	85mm
fuel	Diesel,$C_{10}H_{26}$

Materials Used:

Steel	
Young's modulus	205000 mpa
Poisson's ratio	0.3
Density	7850kg/m^3

Cast iron	
Young's modulus	110000 mpa
Poisson's ratio	0.28
Density	7200kg/m^3

Thermal Analysis of Combustion Chamber:
Material Steel:-

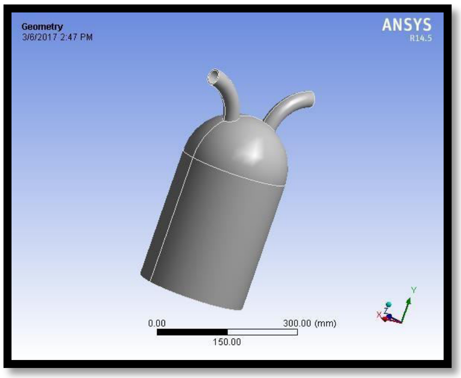

Fig1 Imported model

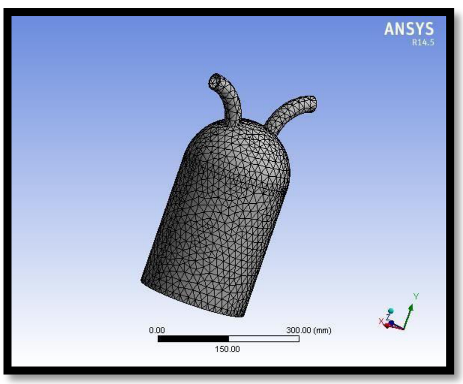

Fig2 Mesh model

FEA representing a real project as a "mesh" a series of small, regularly shaped tetrahedron connected elements, as shown in above fig. And then setting up and solving huge arrays of simultaneous equations. The finer the mesh, the more accurate the results but more computing power is required.

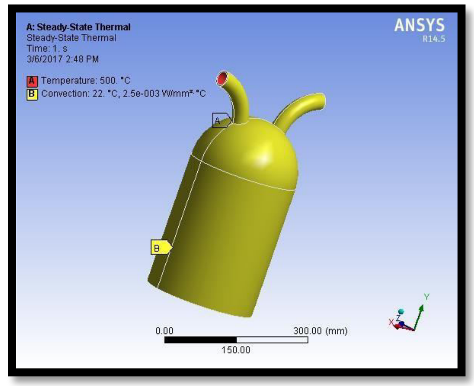

Fig3 Boundary conditions

T=500

A Temperature 500^0 C, B Convection 22^0 C

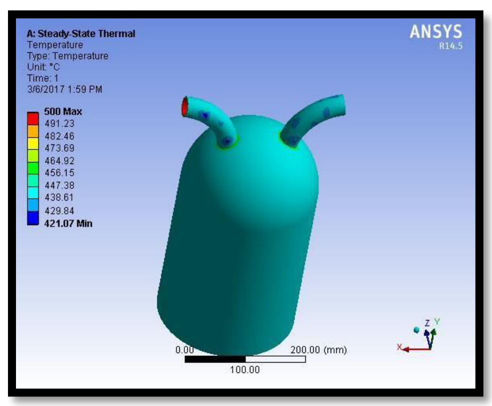

Fig4 Temperature

According to the contour plot, the temperature distribution maximum at tubes because the steam passing inside of the tube. So we are applying the temperature inside of the tube and applying the convection except inside the tubes.

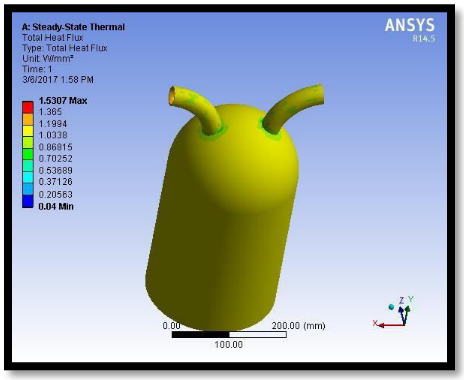

Fig 5 Heat flux

According to the contour plot, the maximum heat flux at inside the tubes because the steam passing inside of the tube. So we are applying the temperature inside of the tube and applying the convection except inside the tubes. Then the maximum heat flux at inside the tubes and minimum heat flux at combustion chamber casing and outside of the tubes. According to the above contour plot, the maximum heat flux is 1.5307 w/mm^2 and minimum heat flux is 0.04 w/mm^2.

MATERIAL-CAST IRON

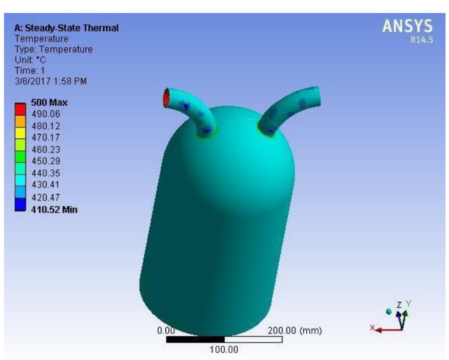

Fig 6 Temperature

So we are applying the temperature inside of the tube and applying the convection except

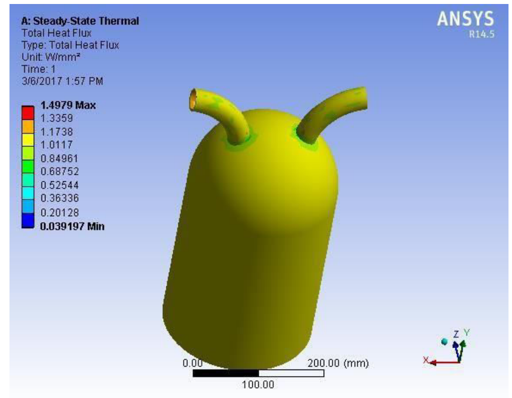

inside the tubes. Then the maximum temperature at tubes minimum temperature at combustion chamber casing.

Fig 7 Heat flux

So we are applying the temperature inside of the tube and applying the convection except inside the tubes. Then the maximum heat flux at inside the tubes and minimum heat flux at combustion chamber casing and outside of the tubes. According to the above contour plot, the maximum heat flux is 1.4979 w/mm^2 and minimum heat flux is 0.039197 w/mm^2.

3. CFD ANALYSIS OFCOMBUSTION CHAMBER

FLUID ANALYSIS:
1.Propyl Velocity – 120

Fig 8 Pressure

According to the above contour plot, the maximum pressure is 3.71e+06Pa and minimum static pressure is -1.53e+07Pa.

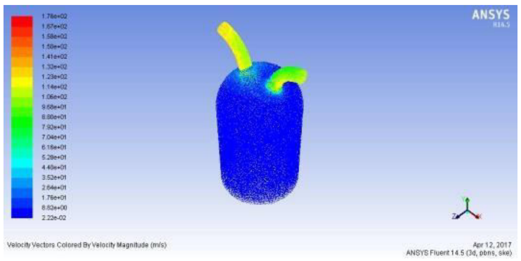

Fig 9 Velocity

According to the above contour plot, the maximum velocity is 1.76e+02m/s and minimum velocity is 2.22e-02m/s.

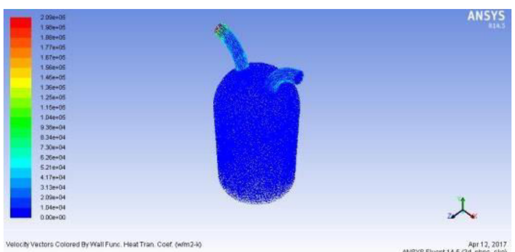

Fig10 Heat transfer coefficient

According to the above contour plot, the maximum heat transfer coefficient is 2.09e+05w/m^2-k and minimum heat transfer coefficient is 0.00e+00 w/m^2-k.

HEAT TRANSFER RATE:

Total Heat Transfer Rate	(w)
inlet	21641068
outlet	-18097492
wall-____msbr	-142817.3
Net	3400758.7

MASS FLOW RATE:

Mass Flow Rate	(kg/s)
inlet	92.979073
interior-____msbr	-336.4798
outlet	-79.01432
wall-____msbr	0
Net	13.964752

2. Fluid-Gasoil

Pressure: The maximum pressure is 1.195e+07Pa and minimum static pressure is -7.907e+06Pa.

Velocity: The maximum velocity is 1.586e+02m/s and minimum velocity is 1.866e-02m/s.

Heat transfer coefficient: The maximum heat transfer coefficient is 3.578e+04w/m^2-k and minimum heat transfer coefficient is 0.00e+00 w/m^2-k.

Heat transfer rate:

Total Heat Transfer Rate	(w)
inlet	17480826
outlet	-15103444
wall-____msbr	-52488.648
Net	2324893.4

Mass flow rate:

Mass Flow Rate	(kg/s)
inlet	98.184021
interior-____msbr	-345.0722
outlet	-85.153641
wall-____msbr	0
Net	13.03038

3. Fluid- Ethanol

Pressure: The maximum pressure is 3.07e+06Pa and minimum static pressure is -1.35e+07Pa.

Velocity: The maximum velocity is 1.48e+02m/s and minimum velocity is 7.10e-03m/s.

Heat transfer coefficient: The maximum heat transfer coefficient is 7.90e+04w/m^2-k and minimum heat transfer coefficient is 0.00e+00 w/m^2-k.

Heat transfer rate:

Pressure: The maximum pressure is 2.87e+06Pa and minimum static pressure is -9.60e+07Pa.

Velocity: The maximum velocity is 1.69e+02m/s and minimum velocity is 2.09e-03m/s.

Heat transfer coefficient: The maximum heat transfer coefficient is 8.09e+04w/m^2-k and minimum heat transfer coefficient is 0.00e+00 w/m^2-k.

Heat transfer rate:

Total Heat Transfer Rate	(w)
inlet	19940684
outlet	-17191628
wall-____msbr	-82784.781
Net	2666271.2

Velocity: The maximum velocity is 1.59e+02m/s and minimum velocity is 9.74e-03m/s.

Heat transfer coefficient: The maximum

Total Heat Transfer Rate	(w)
inlet	17897942
outlet	-14643287
wall-____msbr	-82538.547
Net	3172116.5

Mass flow rate:

Mass Flow Rate	(kg/s)
inlet	89.600609
interior-____msbr	-276.47824
outlet	-73.86158
wall-____msbr	0
Net	15.739029

4. Fluid- Methanol

Mass flow rate:

Mass Flow Rate	(kg/s)
inlet	93.333954
interior-____msbr	-228.94684
outlet	-81.425613
wall-____msbr	0
Net	11.90834

5. Fluid- Ethylene

Pressure: The maximum pressure is 8.41e+03Pa and minimum static pressure is -1.54e+04Pa.

heat transfer coefficient is 6.99e+02w/m^2-k and minimum heat transfer coefficient is 0.00e+00 w/m^2-k.

Heat transfer rate:

```
Total Heat Transfer Rate                (w)
-------------------------  --------------------
                   inlet            9584.0059
                  outlet           -7270.9004
            wall-___msbr           -1015.6625
         ----------------  --------------------
                     Net             1297.443
```

Mass flow rate:

```
     Mass Flow Rate                 (kg/s)
-------------------  --------------------
              inlet           0.11829399
   interior-____msbr         -0.41831699
             outlet         -0.099765703
       wall-____msbr                    0
   ----------------  --------------------
                Net          0.018528283
```

4. RESULT AND DISCUSSION:

4.1 Thermal Analysis:

Material	Temperature		Heat Flux
	Min	Max	
Steel	**421.07**	**500**	**1.5307**
Cast Iron	**410.52**	**500**	**1.4979**

4.2 CFD ANALYSIS RESULTS TABLE

Fluids	Pressure(pa)	Velocity (m/s)
ethanol	$3.07e^{+06}$	$1.48e^{+02}$
methanol	$2.87e^{+06}$	$1.69\ e^{+02}$
ethylene	$8.41e^{+03}$	$1.59\ e^{+02}$
propyl	$3.71e^{+06}$	$1.76\ e^{+02}$
Gas oil	$1.195e^{+07}$	$1.586\ e^{+02}$

Heat transfer coefficient(w/ m2-k)	Heat transfer rate(W)	Mass flow rate(kg/s)
$7.90e^{+04}$	3172116.5	15.739029
$8.09e^{+04}$	2666271.2	11.90834
$6.99\ e^{+02}$	1297.443	0.018528
$2.09\ e^{+05}$	3400758.7	13.964752
$3.578\ e^{+04}$	2324893.4	13.03038

5. CONCLUSIONS:

The combustion process increases the internal energy of a gas, which translates into an increase in temperature, pressure, or volume depending on the configuration. In an enclosure, for example the cylinder of a reciprocating engine, the volume is controlled and the combustion creates an increase in pressure.

The burning procedure builds the inside vitality of a gas, which converts into an expansion in temperature, weight, or volume relying upon the arrangement. In a fenced in area, for instance the barrel of a responding motor, the volume is controlled and the burning makes an expansion in weight. In a ceaseless stream framework, for instance a fly motor combustor, the weight is controlled and the burning makes an expansion in volume. This expansion in weight or volume can be utilized to do work, for instance, to move a cylinder on a crankshaft or a turbine plate in a gas turbine. In the event that the gas speed changes, push is created, for example, in the spout of a rocket motor. By watching the CFD examination the weight drop, speeds and warmth exchange rate esteems are expanding by expanding the speed. The warm examination is to decide the warmth transition of the ignition chamber the warmth motion more for steel contrast and cast press material. So it can be finished up the warmth exchange rate more for PROPYL liquid, when warm exchange rate will more than the motor proficiency will increment.

6. REFERENCES:

[1]. AIRCRAFT PROPULSION By FAROOKI

[2]. MODELING OF COMBUSTION SYSTEMS: A Practical Approach By Joseph Colcannon .

[3]. COMBUSTION CHAMBERS FOR JET PROPULSION ENGINES By V. S. And L. S. Skubachevskii Zuyev

[4]. DEVELOPMENT OF AERO GAS TURBINE ANNULAR COMBUSTOR: BY Dr. C. Darinath combustion Group.

[5]. Gas Turbains And Jet Propulsion - M.J. Sable

[6]. Some Relevent Data From Wikipedia.

[7]. CFD Analysis Of Rocket Engine Combustion Chambers By J. Steelant In ESTEC, 9-10th Of October 2003.

[8]. Optimization Of Combustion Chamber For Diesel Engine Using Kriging Model By Shinkyu JEONG In JFST V-1,no-2,2006.

DESIGN OF MAIN LANDING GEAR AND STRESS ANALYSIS

1. M MAHEEDHAR ,M.tech CAD/CAM **2. C. SHASHIKANTH** Assistant Professor, MECH Dept
MALLA REDDY COLLEGE OF ENGINEERING
Maisammaguda, Dhulapally, Secunderabad, Hyderabad, India

ABSTRACT

The Landing gears of an aircraft forms an integral part of the aircraft structure. This is a complex structure capable of transferring large aircraft loads on to the ground. It is one of the mission's most critical part and is also the component that will causes the most trouble in aircraft design. Main load carrying member of landing gear "Leg" is considered for the design and analysis. The estimated loads acting on the Main Leg are analyzed for different Ground loads data.CAD Model is generated by using CATIA modeling tool for FEM analysis. Ground Loads are evaluated by using empirical formulae as per MIL guidelines. These evaluated loads are used as an input loads to carry out Finite Element Analysis (FEM). Stress analysis is carried out by using Patran software for different Ground loads. For different Ground loads, reaction at each component of Landing gear is also calculated by making free body diagram and by using moment arm method.The design of LEG has been validated by estimating the stresses experienced by the leg for given load conditions. Factor of Safeties & reserve factor were calculated against yield strength and UTS established from FE results. Factor of Safety obtained from the analysis are found to be within the acceptable levels and hence the design of the Leg is safe with respect to strength requirement.

Introduction

In aviation, the undercarriage or landing gear is the structure (usually wheels) that supports an aircraft on the ground and allows it to taxi. Landing gear usually includes wheels equipped with shock absorbers for solid ground, but some aircraft are equipped with skis for snow or floats for water, and/or skids. Landing Gear is a complex structure capable of reacting the largest local loads on the aircraft. Its function is to convert a relatively airborne vehicle into a rather awkward and clumsy ground vehicle. In one brief moment, the landing gear must make the best of returning the aircraft from its natural environment to hostile environment – the earth.

Landing Gear Purpose

The purpose of landing gear is

- To absorb horizontal and vertical energy during touchdown
- Facilitate ground maneuver
- Stop the aircraft during runway operation
- Provide adequate tail down angle for takeoff rotation
- To provide the aircraft with stable support while on the ground.

Additionally, landing gear enables the aircraft to roll up to its take-off position and to take off without the use of a launching catapult trolley, as well as to carry its own means of retaining forward motion, or braking, without resort to external arresting equipment.

The landing gear of an aircraft supports it during ground maneuvering operations, by providing a suitable suspension system and also cushions the landing impact. It features a shock strut, which dissipates the kinetic energy associated with the vertical velocity on landing, and provides ease and stability for ground maneuvering.

Types of landing gears

There are two basic types of landing gear:

1. Cantilever (Telescopic)
2. Articulated.

A Cantilever configuration is most widely used, and it is without question the most cost and weight efficient. The name comes from the fixit of shock strut cylinder to aircraft. It supports drag and side loads An Articulated gear finds application where the ground clearance is low, or where stowage is limited. It offers maintenance advantage, since the shock strut can be removed in the field without major effort. It is pin ended and does not support drag and side load Semi-articulated gear is similar to fully articulated except the cylinder also acts as a structural member.Apart from this, there are Main landing gears and Nose Landing Gears. Main Landing Gear is present at the back, to which brakes are fixed and on which the aircraft lands. Nose Landing Gear is fixed at the front, which plays a major role in steering the aircraft.

Parts of Landing gear

- Shock Absorber
- Locks
    - Uplocks and Downlocks
- Breaks
- Anti-Skid Controls
- Wheel
- Steering
- Tyres
- Retraction System
- Doors and Fairings
- Axle
- Bearing

General Arrangement of Landing Gear

- **Tail Wheel Layout**

Advantages:

1. Location of auxiliary wheel in a relatively unimportant part of fuselage.
2. A minimum auxiliary wheel weight when disposed well at the rear of the aircraft.
3. Dissipation of some (Perhaps 25%) of the total forward energy in air drag due to the tail down altitude when landing. Energy, which would otherwise have to be absorbed by the brakes.
4. he location of the main brake wheel in front of the center of gravity of the aircraft means that the wheel loading is increased when the brakes is applied. This tends to prevent troubles due to locking of the wheels and means that automatic skid detecting devices are not needed to reduce tire wear.

Disadvantage:

1. Heavy braking can cause over-turning of the aircraft and the degree of braking Permitted must be restricted to safe values.
2. Brake drag forces, being applied forward to center of gravity cause a tendency for the aircraft to swing around.
3. On touchdown, the aircraft tail drags; this increase incidence causing a tendency for aerodynamic bouncing or ‘ballooning’, which is particularly, serious on deck loading aircraft, which have to touchdown before striking the ouster cable.
4. The pilot’s visibility during taxing is poor.

Nose Wheel Layout

Advantage:

1. Heavy braking cannot cause overturning.
2. The a/c when landing particularly in a cross wind, or with drift, is inherently stable as the c.g. is ahead of the main wheel.
3. At touchdown as the a/c pitches forward, spoiling the wing lift and eliminating any risk of aerodynamic brake
4. Pilot’s visibility is maximum at all time.
5. Floor line of a/c is always being horizontal which is advantageous for freight loading or to the passengers.

Disadvantage:

1. Retraction of nose wheel is often awkward.
2. Very little of the forward energy of the a/c is dissipated by air drag.
3. Thus, brake has to deal with most of it.
4. Skidding and making more desirable automatic brake antiskid devices.

Notwithstanding these disadvantages the nose wheel-landing layout is the most widely adopted layout.

Materials used for Landing Gear

- **Commonly used Materials**

Initial Calculation

For load analysis of Landing Gear, spin up case

during landing is considered

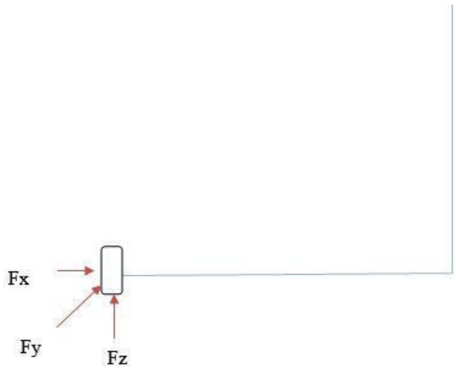

Free Body Diagram for Load Analysis

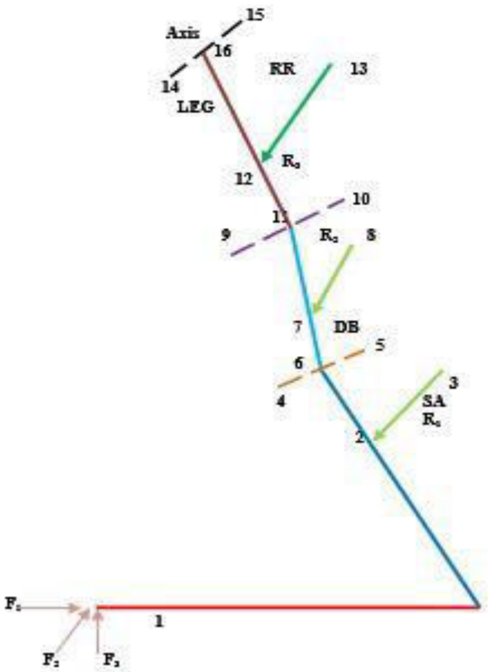

Coordinates of different landing gear points shown in FBD

Point	X	Y	Z	R
1	8443.833	-1114.754	-1309.38	
2	8304.6914	-928.4073	-1139.03	
3	8035	-710	-470	
4	8069.876	-1005.706	-1130.23	
5	8069.876	-835.5383	-1130.23	
6	8069.876	-935.8306	-1130.23	
7	806.876	-835.5383	-1130.23	
8	8026.7285	-343.4802	-520.259	
9	8015.5449	-934.5686	-1016	
10	8099.9111	-934.5723	-1005.64	
11	8057.728	-934.5704	-1010.82	
12	8126.8335	-609.5605	-690.206	
13	8264.3291	-516.0161	-577.515	
14	8033.7881	-578.9711	-430.991	
15	7981.9775	-432.5017	-502.429	
16	8020	-540	-450	

Position vectors & Direction cosine

Position vector	X	Y	Z	R
r (1-6)	373.957	-178.9236	-179.153	
r (2-6)	234.8154	7.42328	-8.801	
DC (2-3)	0.35783353	-0.289788	-0.88768	
DC (4-5)	0	1	0	
5	8069.876	-835.5383	-1130.23	
6	8069.876	-935.8306	-1130.23	
7	806.876	-835.5383	-1130.23	
8	8026.7285	-343.4802	-520.259	
9	8015.5449	-934.5686	-1016	
10	8099.9111	-934.5723	-1005.64	
11	8057.728	-934.5704	-1010.82	
12	8126.8335	-609.5605	-690.206	
13	8264.3291	-516.0161	-577.515	
14	8033.7881	-578.9711	-430.991	
15	7981.9775	-432.5017	-502.429	
16	8020	-540	-450	

Calculation of Shock Absorber reaction

Calculation of Direction Bar reaction

Calculation of Radius Rod reaction

Stress Analysis of Leg

The main landing gear- leg is analyzed for the loads for which the landing gear will experience in its service. These loads are static in nature and experienced under spin up case underground load condition. Classical approach is followed to get the reaction forces that are acting on main landing gear –leg. Detailed calculation is shown in chapter 5.

Below shown are the stress plots for the main landing gear-lug

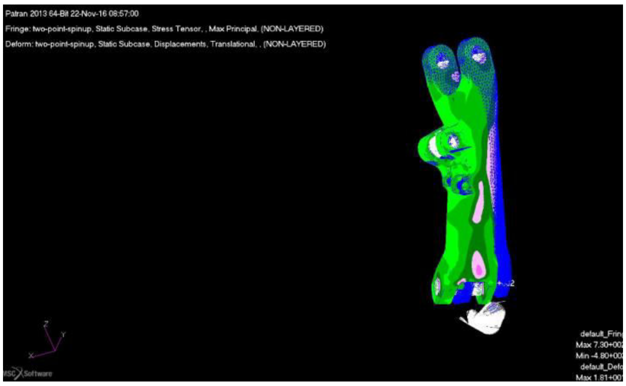

The above figure shows the maximum principal stress plot of main landing gear-leg. The maximum stress observed is 720 MPa. But this stress is spurious observed at load application region. Hence this stress is ignored and the next critical location is observed at point which is around 370 MPa. For aluminum alloy the UTS value is 480 MPa. Hence reserve factor against observed critical location is 1.3 (480/370=1.3).From the calculation shown above the reserve factor observed is greater than 1. Hence the component is fit for the purpose.

Von-Mises stress plot is also shown below to depict the stress distribution on main landing gear-leg.

Conclusion

This design is an attempt to the usage of the oleo pneumatic shock absorber for the main landing gear shock strut. Stroke of the shock absorber depends on the sink rate1. To justify the shock absorber design drop test must be performed. Mc Adams software used to simulate real drop test behavior in conceptual design phase. Based on this characteristic optimum orifice diameter found. Solid model created using CATIA software.Stress Analysis by patron software using fem analysis. The given material is safe for the stresses induced. Ground and landing loads and it is found within the limits

BIBLIOGRAPHY

1. Norman S. Currey "Aircraft Landing Gear Design: Principle and Practices 1st Edition, American Institute of Aeronautics and Aeronautices".

2. Oleo Pneumatic Shock Absorber Design for Light Aircraft Author: Dr. Mohammed Abdul Wasay Usmani, and Goh Kwong Thong Aerospace Engineering Department, University Putra Malaysia.

3. .Aircraft Landing Gear Design Principles and Practices Norman S. Currey Lockheed Aeronautical Systems Company Marietta, Georgia

4. Air frames and systems Jeppesen Gmbh Frankfurter Strasee 233, 63263 Neu-Isenburg Germany

5. Landing gear design by H.G.CONWAY London champman and hall ltd 37 essex street,w.c.2 1958

THERMAL TRANSIENT ANALYSIS OF FINS WITH DIFFERENT PROFILES

Lingasani Tejaswini
M.Tech CAD/CAM
Department of Mechanical Engineering
Malla Reddy College of Engineering &Technology
Hyderbad-500100

Assistant Professor **C. SHASHIKANTH**
M.Tech CAD/CAM
Department of Mechanical Engineering
Malla Reddy College of Engineering & Technology
Hyderbad-500100

ABSTRACT

Consideration of FIN in Heat transfer mostly depends on Space, cost consideration, manufacturing techniques, weight and thermal characteristics. In the present study, a detailed work has been carried out to develop a finite element methodology to estimate the temperature distribution for transient heat transfer and thermal stresses induced. Finite element method (FEM) was used to compute the temperatures. An extensive study was carried out using ANSYS, a powerful platform for finite element analysis.

Transient analysis is carried out for the fins of different profiles under the convection and a specified base temperature condition. Thermal conductivity of the fin material is specified. A constant temperature condition is applied at the base of the fin. Comparative study is being done among the fins of different profiles to find out the best profile under the conditions. In results temperature distributions at different times at a node, temperature distributions along the fin, thermal stress distribution of thermal gradients and heat flux values of fin for different profile sections were discussed and reported.

CHAPTER - 1
1. INTRODUCTION

Fins are extended surfaces which can provide a considerable available area for heat transfer between a solid and a fluid. For proper prediction and control of the fin performance, It is essential to perceive the temperature distribution of fins under transient or unsteady thermal condition for proper prediction and control of the fin performance.

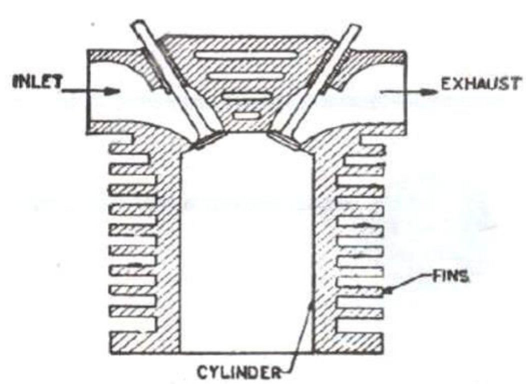

Fig: 1.1 Fins

1.1 Fin

In the study of heat transfer, fins are surfaces that extend from an object to increase the rate of heat transfer to or from the environment by increasing convection.

The amount of conduction, convection, or radiation of an object determines the amount of heat it transfers. Increasing the temperature gradient between the object and the environment, increasing the convection heat transfer coefficient, or increasing the surface area of the object increases the heat transfer. Sometimes it is not feasible or economical to change the first two options. Thus, adding a fin to an object increases the surface area and can sometimes be an economical solution to heat transfer problems.

1.2 TYPES OF FINS

- RECTANGULAR FINS
- TRIANGULAR FINS
- CIRCULAR FINS
- PIN FINS

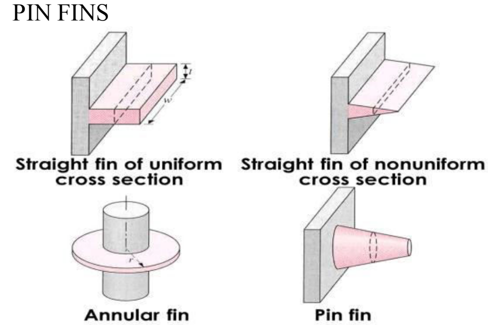

Fig: 1.2 Types of fins

SPECIAL CASES:

Consider 3 cases of constant area fins

- Specified temperature at base, semi-infinite fin
- Finite fin, specified temperature at the base, insulated tip
- Finite fin, specified temperature at the base, heat transfer at the tip

1.3. APPLICATIONS OF FINS:

Air-cooled heat exchangers, variety of sensible, condensing, and boiling services in shell and tube exchangers

CHAPTER 2
FINITE ELEMENT METHOD

2.1 FEM

The finite element method (FEM) is a numerical technique for finding approximate solutions to boundary value problems or partial differential equations. It is also referred to as finite element analysis (FEA).

The subdivision of a whole domain into simpler parts has several advantages:

- Accurate representation of complex geometry
- Inclusion of dissimilar material properties
- Easy representation of the total solution
- Capture of local effects.

A typical work out of the method involves

(1) Dividing the domain of the problem into a collection of sub domains called finite elements, with each sub domain represented by a set of element equations to the original problem, followed by
(2) Systematically recombining all sets of element equations into a global system of equations for the final calculation.
(3) The global system of equations has known solution techniques, and can be calculated from the initial values of the original problem to obtain a numerical answer.

FEM is applied for structural analysis, solid mechanics, Dynamics, thermal analysis, electrical analysis and biomaterials..

2.2 Benefits of FEA:

With FEA we can:

✓ Predict and improve product performance and reliability
✓ Reduce physical prototyping and testing
✓ Evaluate different designs and materials
✓ Optimize FEA Software

CHAPTER - 3
INTRODUCTION TO ANSYS

Ansys is commercial finite-element analysis software with the capability to analyze a wide range of different problems such as elasticity, fluid flow, transient heat transfer, can all be solved by the Finite element method in ANSYS.

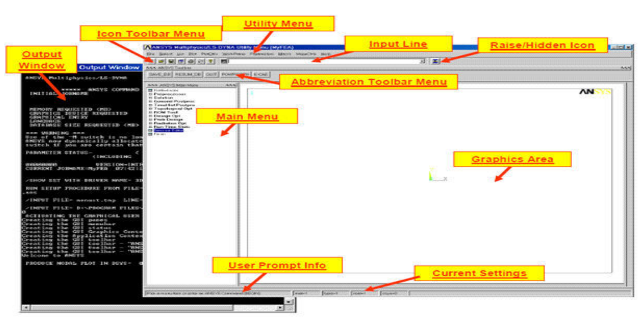

Fig: 3.1 Output window of ansys

Ansys user interface is divided into 4 sections.

- ANSYS Utility Menu
- ANSYS Toolbar Menu
- ANSYS Main Menu
- Display window

CHAPTER 4

TRANSIENT ANALYSIS OF FINS USING ANSYS

PROCEDURE FOR TRANSIENT ANALYSIS OF FINS OF DIFFERENT PROFILES:

4.1 PREFERNCES - Thermal

4.2 ELEMENT TYPE – ADD/EDIT/DELETE –

Tet 10node 87

4.3 MATERIAL PROPERTIES OF Aluminium alloy 6061

- Select the conductivity value 167 W/m-k
- Select specific heat as 1.256 e+3
- Select density as 2700 kg/ m3

4.4 MODELLING OF TRIANGULAR FIN

- Select the key points and entering nodes as 1(0, 0), 2(12, 0), 3(0, 30), 4(12, 30), 5(12, 19), 6(37, 15), 7(12, 11)

4.5 LINES – STRAIGHT LINES – SELECT ALL KEYPOINTS

4.6 CREATE – AREAS – ARBITRARY – BY LINES, extruding the area by extrusion option and meshing by free meshing

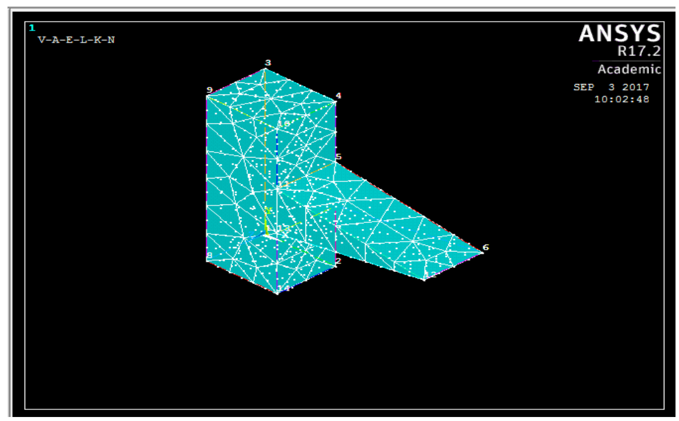

Fig:4.1. Meshing after volume

4.7 SOLUTION

Select the analysis type - new analysis – select Transient

4.8 SOLUTION CONTROLS

- Select the time at end load step as 650 seconds
- Select time sub step as 1

4.9 DEFINE LOADS

- Apply the temperature 598k at the entry surface of fin
- Enter the film coefficient 0.00083
- Enter the bulk Temperature as 140

4.10 LOAD SETUP

- Select the time frequency at end of load step as 650sec
- Select the amplitude decay in ON mode

4.11 GENERAL POST PROC

In read results, we will select the set of time data and will plot results.

CHAPTER -5

RESULTS

5.1 Results for Triangular Profile:

- Plot results – contour plot – nodal temperature / thermal gradients components in X, Y, Z directions / heat flux / heat flow

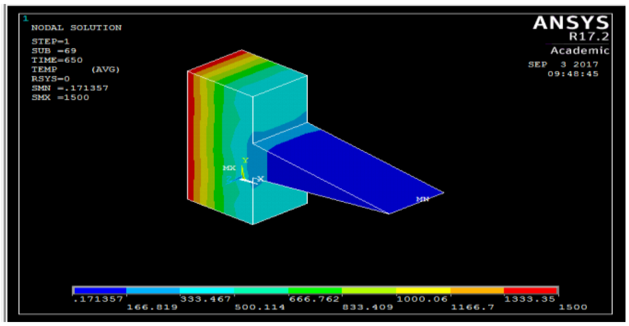

Fig 5.1 Nodal Temperature

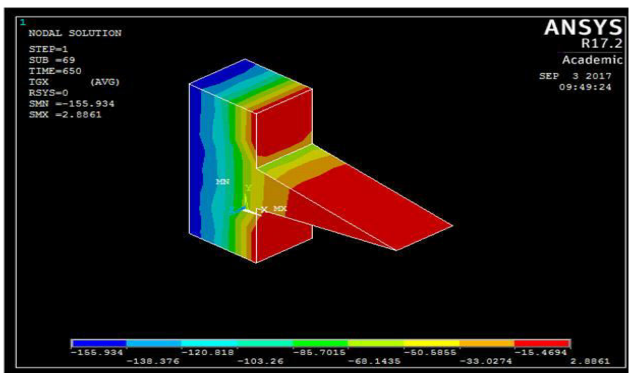

Fig 5.2: Thermal gradient component in X- Direction

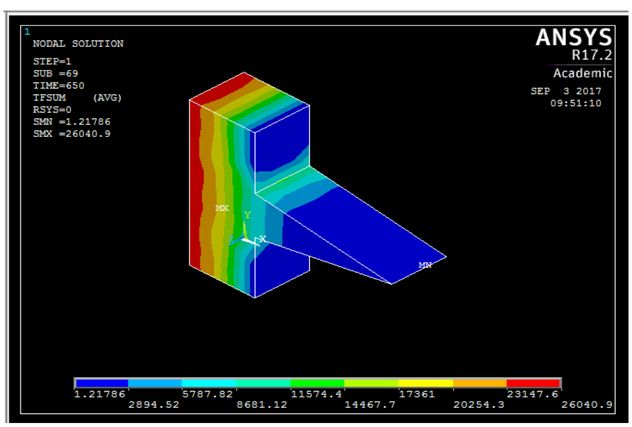

Fig 5.3: Thermal flux

5.2 Results for Rectangular profile:

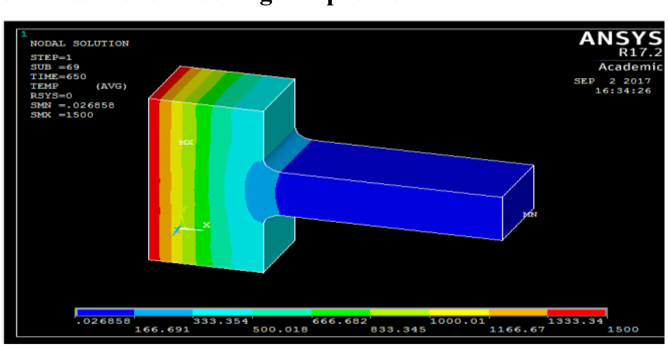

Fig 5.4 Nodal temperature

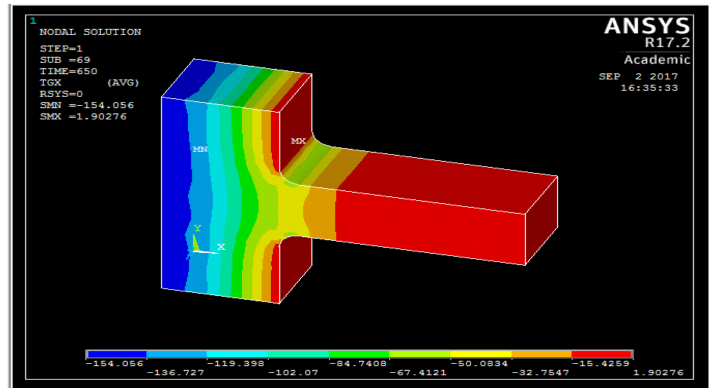

Fig 5.5. Thermal gradient component in X - Direction

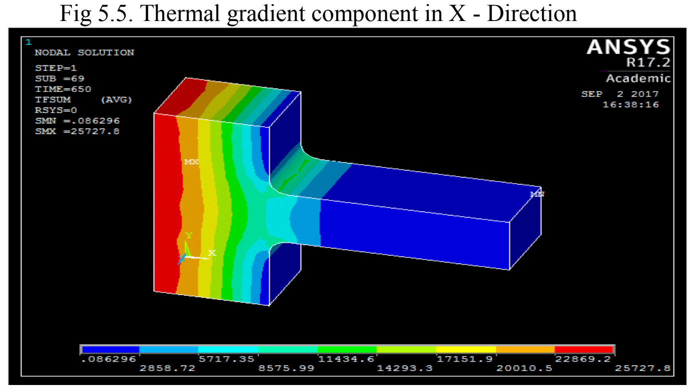

Fig 5.6. Thermal flux

5.3 Results for Circular profile:

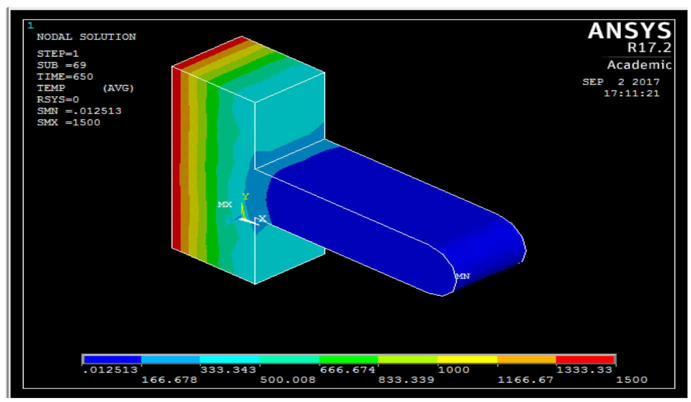

Fig 5.7. Nodal temperature

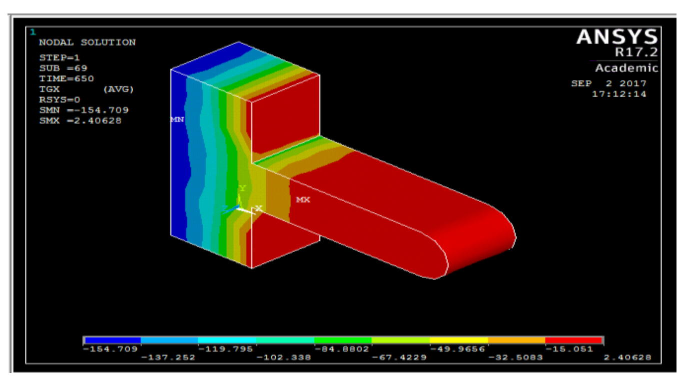

Fig 5.8. Thermal gradient component in X - Direction

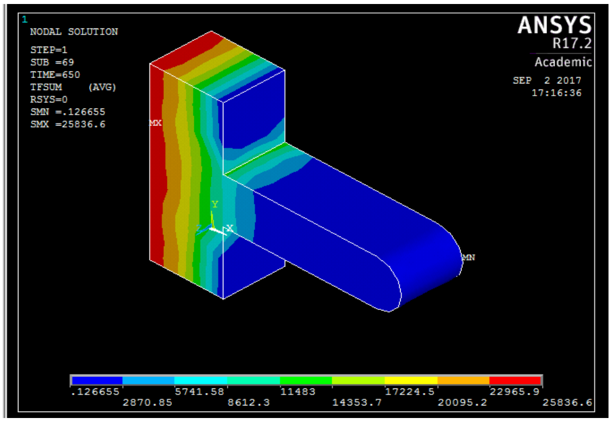

Fig 5.9. Thermal Flux

5.4 Plotting results in a table for three Fin profiles:

Profile	Thermal gradient along the fin		Thermal flux	
	SMX	SMN	SMX	SMN
Triangular profile	2.8861	-155.934	26040.9	1.2178
Rectangular profile	1.9027	-154.056	25727.8	0.08629
Circular profile	2.406	-154.709	25836.6	0.1266

Table 5.1. Results

5.5 Thermal gradient trend over different profiles of fins

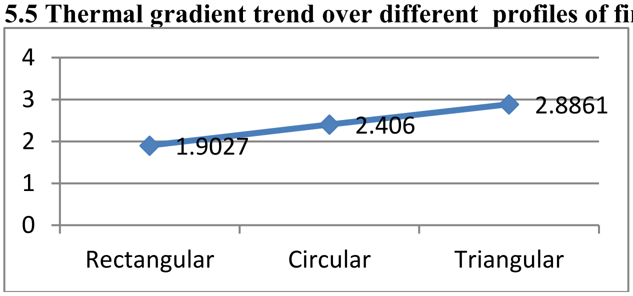

Graph 5.1. Thermal Gradient vs Profiles

5.6 Thermal flux trend over different profiles of fins:

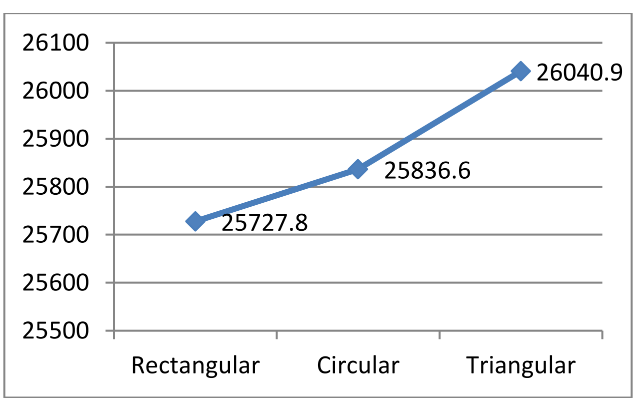

Graph 5.2. Thermal Flux vs Profiles

CONCLUSION

In present work, a Fin body is modeled in three different profiles named rectangular, circular triangular profile and thermal Transient analysis is done by using Ansys.

By varying the geometry profiles, thickness and the weight of the fin body reduces thereby increasing the heat transfer rate and efficiency of the fin . Triangular fins are having less thickness compared to circular and rectangular fins. And also weight of the triangular fins is less compared to circular and rectangular fins.

Each and every individual subset defined to total 650 subsets assumed in Solver control . For every subset respective time, Nodal temperature plotted in Graphs and contoured the Nodal solutions for the temperatures, thermal gradients, heat flux and heat flows.

In both the graphs 6.7, 6.8, triangular fins are showing upper trend than other two profiles. Therefore triangular fins has more heat transfer rate than circular and rectangular fins.

REFERENCES

1. Donaldson A B and Shouman A R (1972), “Unsteady-State Temperature Distribution in a Convecting Finof Constant Area”, Appl. Sci. Res., Vol. 26, Nos. 1-2, pp. 75-85.
2. Sonn, A. Bar-cohen, “Optimum cylindrical pin fin”, ASME J. Heat Transfer,vol.103, pp. 814–815, 1981.
3. P. Razelos, B.R. Satyaprakash, “Analysis and optimization of convective trapezoidal profile longitudinal fins”, ASME J. Heat Transfer, vol. 115, pp. 461–463, 1993.
4. Mao J and Rooke S (1994), “Transient Analysis of Extended Surfaces with Convective Tip”, Int. Commun. Heat Mass Transf., Vol. 21, pp. 85-94.
5. Aziz A and Kraus A D (1995), “Transient Heat Transfer in Extended Surfaces”, Appl. Mech. Rev., Vol. 48, No. 3, pp. 317-349.
6. Kevin D. Cole , B. Wilson (2009), “ Analysis of Flux-Base Fins for Estimation of Heat Transfer Coefficient”, Published in International Journal of Heat and Mass Transfer 52:1-2 pp. 92–99.
7. Moradi and H. Ahmadikia (2010), “Analytical Solution for Different Profiles of Fin with Temperature Dependent Thermal conductivity”
8. Raseelo J Moitsheki, Charis Harley (2011), “Transient heat transfer in longitudinal fins of various profiles with temperature-dependent thermal conductivity and heat transfer coefficient ”, journal of physics, Vol. 77, No. 3 pp. 519–532.
9. Dipankar Bhanja, Pabitra Kumar Mandal (2013), “Thermal analysis of porous pin fin used for electroniccooling”, International Conference on Design and Manufacturing, Procedia Engineering 64 pp.956 – 965.
10. Y. Pratapa Reddy, Dr.Ch. Srinivasa Rao (2015), “Temperature Distribution Analysis of Composite Pin fin by experimental and finite element methodnhng

International Conference on Future Technologies in Mechanical Engineering (ICFTME) - ISBN 978-93-85100-09-3

DESIGN AND STRUCTURAL ANALYSIS OF COMPOSITE LEAF SPRING

Kiran Kumar Allaka[1] C.Shashikanth[2]

Address for Correspondence

[1]kiran1510@gmal.com, [2] csk262000@gmail.com

Department of Mechanical Engineering, MALLA REDDY COLLEGE OF ENGINEERING

(Under MALLAREDDY GROUP OF INSTITUTIONS)

Maisammaguda, Dhulapally (Post Via Kompally)

Secunderabad- 500 100, Telangana State

ABSTRACT

Reducing weight while increasing or maintaining strength of products is getting to be highly important research issue in this modern world. Composite materials are one of the material families which are attracting researchers and being solutions of such issue. In this paper we discuss the design parameters and analysis of composite leaf spring.

The objective is to compare the stresses, deformations and weight saving of Composite Leaf Spring with that of Steel and Aluminum Leaf Spring. The design constraint is stiffness. The Automobile Industry has great interest for replacement of steel leaf spring with that of composite leaf spring, since the composite materials has high strength to weight ratio, good corrosion resistance.The materials selected were Glass Fiber Reinforced Polymer (E-glass Epoxy), steel and Aluminum. The design parameters were selected and analyzed with the objective of minimizing weight of the Composite Leaf Spring as compared to the Steel Leaf Spring and Aluminum Leaf Spring.

1.0 INTRODUCTION

Semi-elliptic leaf springs are almost universally used for suspension in light and heavy commercial vehicles. For cars also, these are widely used in rear suspension

The spring consists of a number of leaves called blades. The blades are varying in length. The blades are us usually given an initial curvature or cambered so that they will tend to straighten under the load. The leaf spring is based upon the theory of a beam of uniform strength. The lengthiest blade has eyes on its ends. This blade is called main or master leaf, the remaining blades are called graduated leaves. All the blades are bound together by means of steel straps.

The spring is mounted on the axle of the vehicle. The entire vehicle load is rests on the leaf spring. The front end of the spring is connected to the frame with a simple pin joint, while the rear end of the spring is connected with a shackle. Shackle is the flexible link which connects between leaf spring rear eye and frame. When the vehicle comes across a projection on the road surface, the wheel moves up, this leads to deflecting the spring. This changes the length between the spring eyes.

1.1 Suspension System

The automobile chassis is mounted on the axles, not direct but some form of springs. This is done to isolate the vehicle body from the road shocks, which may be in the form of bounce, pitch, roll or sway. These tendencies give rise to an uncomfortable ride and also cause additional stress in the automobile frame anybody. All the part, which performs the function of isolating the automobile from the road shocks, is collectively called a suspension system. It includes the springing device used and various mountings for the same.

Broadly speaking, suspension system consists of a spring and a damper. The energy of road shock causes the spring to oscillate. These oscillations are restricted to a reasonable level by the damper which is more commonly called a shock absorber.

1.2 Objective of Suspension

2. To prevent the road shocks from being transmitted to the vehicle components.
3. To safeguard the occupants from road shocks.
4. To preserve the stability of the vehicle in pitting or rolling, while in motion.

1.3 Types of Leaf Springs

Fig: Types of leaf springs

2.0 MATERIALS FOR LEAF SPRING

2.1 Composite Material:

A composite is a material that is formed by combining two or more materials to achieve some superior properties. Almost all the materials which we see around us are composites. Some of them like woods, bones, stones, etc. are natural composites, as they are either grown in nature or developed by natural processes. Wood is a fibrous material consisting of thread-like hollow elongated organic cellulose that normally constitutes about 60-70% of wood of which approximately 30-40% is crystalline, insoluble in water, and the rest is amorphous and soluble in water. Cellulose fibres are flexible but possess high strength. The more closely packed cellulose provides higher density and higher strength.

2.2 Properties of Materials for Leaf Spring

The material used for leaf spring is usually a plain carbon steel having 0.90 to 1.0% carbon. The leaves are heat treated after the forming process. The heat treatment of spring steel produces greater strength and therefore greater load capacity, greater range of deflection and better fatigue properties.

For automobiles: 50Cr 1, 50 Cr 1 V 23, and 55 Si 2 Mn 90 all used in hardened and tempered state.

In this project Steel , Aluminum and E-Glass Epoxy composite materials has been used for analysis of leaf spring. The properties of these materials mentioned below.

Physical Properties of Steel:

Property	Name
Youngs modulus (E)	200000MPa
Poission ratio	0.3
Density	7800 kg/m^3

Physical Properties of Aluminum:

Property	Name
Youngs modulus (E)	70000MPa
Poission ratio	0.3
Density	2700 kg/m^3

Orthotropic Properties of E-Glass Epoxy composite material

PROPERTIY	VALUE
Longitudinal strength(Ex)	34000MPa
Transverse strength (Ey)	6530 MPa
Transverse strength (Ez)	6530MPa
Longitudinal shear strength(Gxy)	2433 MPa
Transverse shear strength (Gyz)	1698MPa
Transverse shear strength (Gzx)	2433 MPa
Poisson ratio (PRXY)	0.217
Poisson ratio (PRYZ)	0.366
Poisson ratio (PRZX)	0.217
Mass density of the material (ρ), kg/mm3	2.6x10-6

3.0 CONSTRUCTION OF LEAF SPRING

A leaf spring commonly used in automobiles is of semi-elliptical form as shown in Fig 6.1

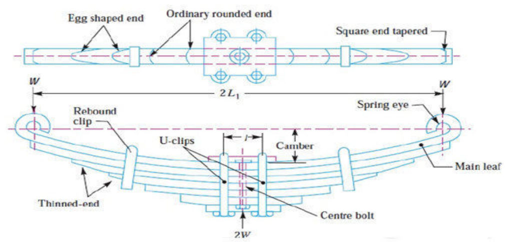

Fig: Construction of leaf spring

It is built up of a number of plates (known as leaves). The leaves are usually given an initial curvature or cambered so that they will tend to straighten under the load. The leaves are held together by means of a band shrunk around them at the centre or by a bolt passing through the centre. Since the band exerts stiffening and strengthening effect, therefore the effective length of the spring for bending will be overall length of the spring *minus* width of band. In case of a centre bolt, two-third distance between centres of *U* -bolt should be subtracted from the overall length of the spring in order to find effective length. The spring is clamped to the axle housing by means of *U* -bolts.

The longest leaf known as main leaf or master leaf has its ends formed in the shape of an eye through which the bolts are passed to secure the spring to its supports. Usually the eyes, through which the spring is attached to the hanger or shackle, are provided with bushings of some antifriction material such as bronze or rubber. The other leaves of the spring are known as graduated leaves. In order to prevent digging in the adjacent leaves, the ends of the graduated leaves are trimmed in various forms as shown in (Fig. 6.1) Since the master leaf has to with stand vertical bending loads as well as loads due to sideways of the vehicle and twisting, therefore due to the presence of stresses caused by these loads, it is usual to provide two full length leaves and the rest graduate d leaves as shown in Fig 6.1. Rebound clips are located at intermediate positions in the length of the spring, so that the graduated leaves also share the stresses induced in the full length leaves when the spring rebounds.

4.0 DESIGN SELECTION OF LEAF SPRING

4.1 Design Selection

The leaf spring behaves like a simply supported beam and the flexural analysis is done considering it as a simply supported beam. The simply supported beam is subjected to both bending stress and transverse shear stress. Flexural rigidity is an important parameter in the leaf spring design and test out to increase from two ends to the center.

4.1.1 Constant Thickness, Varying Width Design

In this design the thickness is kept constant over the entire length of the leaf spring while the width varies from a minimum at the two ends to a maximum at the centre.

4.1.2 Constant Width, Varying Thickness Design

In this design the width is kept constant over the entire length of the leaf spring while the thickness varies from a minimum at the two ends to a maximum at the centre.

4.1.3 Constant Cross-Selection Design

In this design both thickness and width are varied throughout the leaf spring such that the cross-section area remains constant along the length of the leaf spring.

Out of the above mentioned design concepts, the constant cross-section design method is selected due to the following reasons:-

- Due to its capability for mass production and accommodation of continuous reinforcement of fibres.
- Since the cross-section area is constant throughout the leaf spring, same quantity of reinforcement fibre and resin can be fed continuously during manufacture.
- Also this is quite suitable for filament winding process.

4.2 Terminology in leaf spring:

2L – Length of span or overall length of spring

l - Width of band or distance between centres of U bolts. It is the in effective length of the spring

t = Thickness of the leave, and

b= Width of the leaves

Length of smallest leaf = $\frac{\text{Effectivelength}}{n-1}$ + Ineffective length

Length of next leaf = $\frac{\text{Effectivelength}}{n-1}$ x 2 + Ineffective length

Similarly, length of (n-1)th leaf

= $\frac{\text{Effectivelength}}{n-1}$ x (n-1) + Ineffective length

The nth leaf will be the master leaf and it is of full length

4.3 Standard sizes of Automobile Suspension Springs:

Following are the standard sizes for the automobile suspension springs:

1) Standard nominal widths are : 32, 40, 45, 50, 55, 60, 65, 70, 75, 80, 85, 90, 100 and 125mm

2) Standard nominal thicknesses are : 3.2, 4.5, 5.6, 6.5, 7, 7.5, 8, 9, 10, 11, 12, 14 and 16mm

4.4 Assumptions and calculations for leaf spring:

Here weight and initial measurements of four wheeler "TATA ACE" Light commercial vehicle is taken.

Kerb weight of vehicle = 2070Kg,

Load carrying capacity = 1121Kg

Gross weight of the vehicle = 2070 + 1121 = 3191Kg

Taking factor of safety (FS) = 1.15

Total Load = 3191 x 1.15 = 3670 Kgf = 36000 N = 36 KN; [1 kgf= 9.81N]

Load acting on single side (F) = 36000/4 = 9000N (2W)

No: of leaves in the leaf spring = 1

Span of the spring 2L = 1300mm

Width of the leaf (b) = 100mm

Thickness of the leaf (t) = 16mm

Bending stress = $\frac{6\,WL}{n.b.t^2}$

Deflection = $\frac{4\,WL^3}{n.E.b.t^3}$

5.0 PROCEDURE OF STRUCTURAL ANALYSIS

5.1.1 2-D Drawing of Leaf:

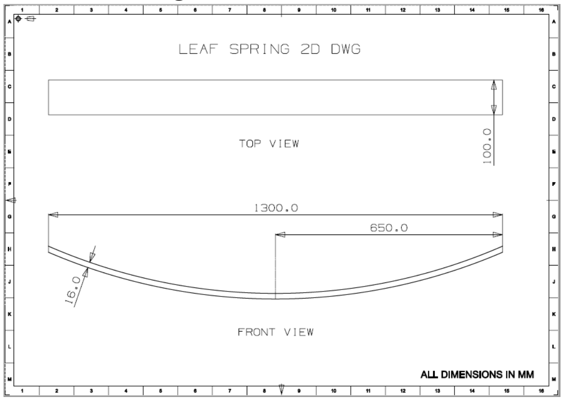

5.1.2 3-D Model:

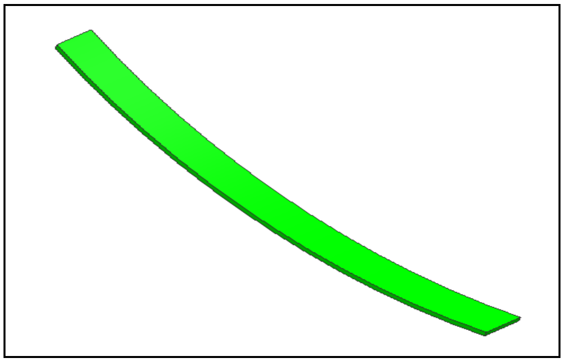

5.1.3 Finite element Model:

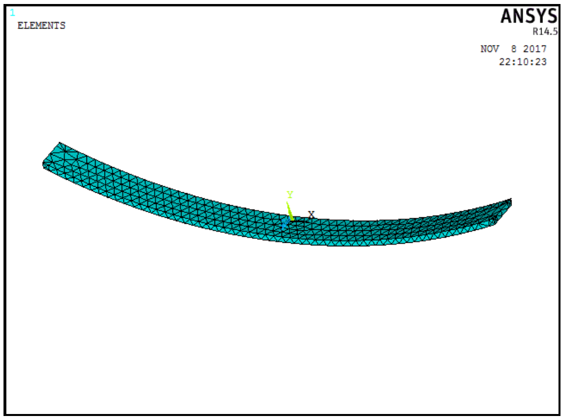

5.1.4 Displacement & Force:

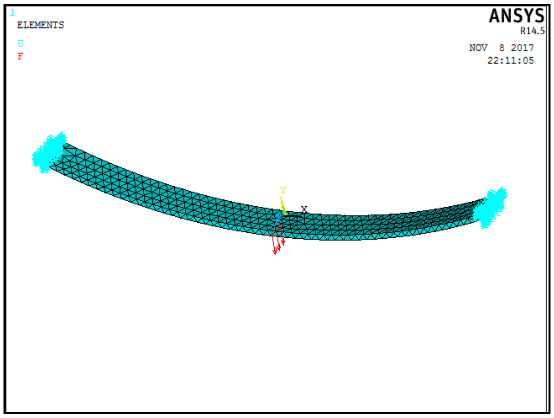

5.1.5 Resultant Deformation in E-Glass Epoxy:

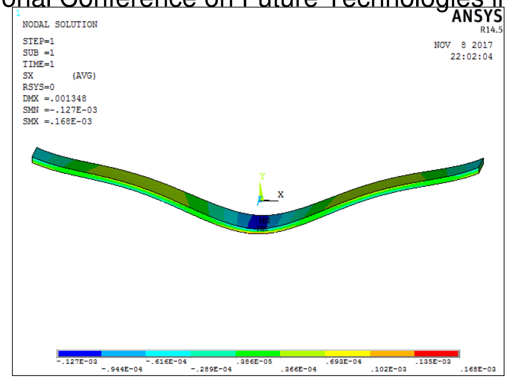

5.1.6 Vonmises Stress Results for E-Glass Epoxy:

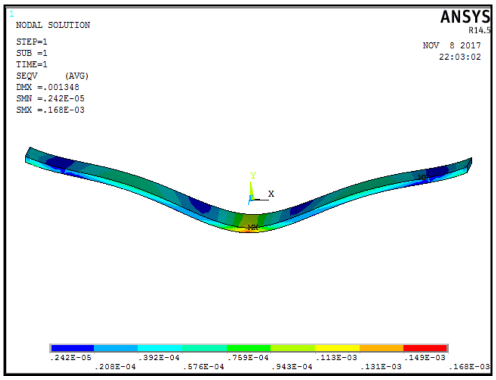

5.1.7 Resultant Deformation in Steel:

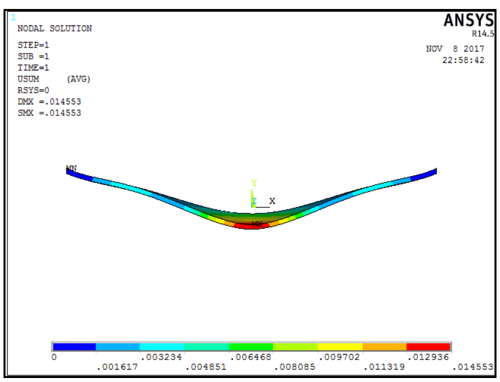

5.1.8 Vonmises Stress Results for Steel:

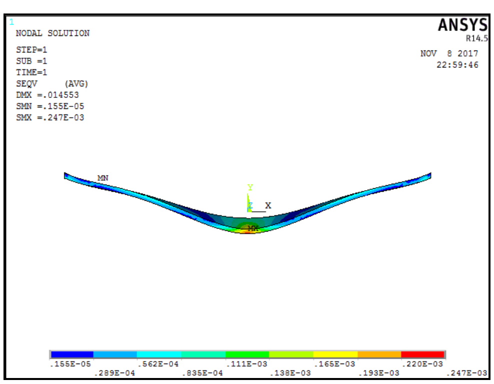

5.1.9 Resultant Deformation in Aluminium:

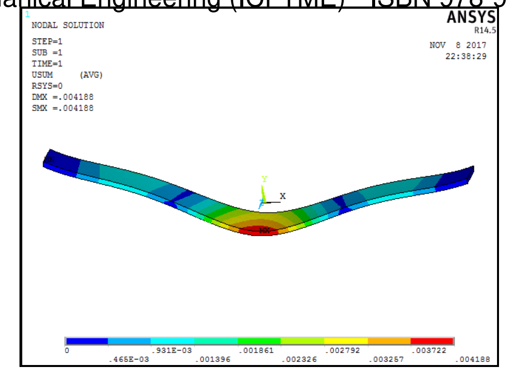

5.1.10 Vonmises Stress Results for E-Glass Epoxy:

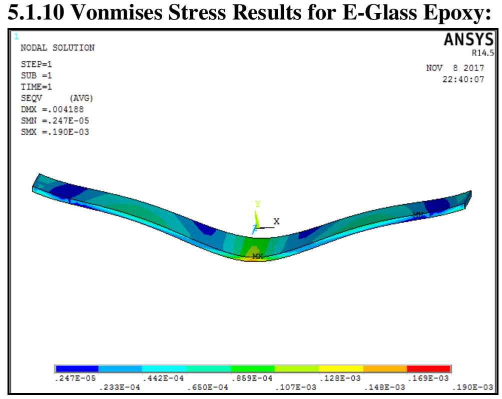

6.0 CONCLUSIONS

In the present work, the dimensions of a composite leaf spring of a light weight vehicle are chosen, modelled using **NX** and analyzed using **ANSYS**.

A load of 9000N was applied at the base in the middle of the leaf spring in the Y-direction. Later a leaf spring of uniform thickness and width was modelled so as to obtain the displacement of leaf spring. **E-Glass Epoxy composite material, Steel and Aluminium** has been used for analysis of Leaf Spring and Static analysis has been performed.

6.1 Results comparison between the materials Steel, Aluminium and E-Glass Epoxy composite material:

Material	Steel	Al	E-Glass Epoxy	Reduction by E-Glass Epoxy
Total Load (2W) Applied	9000N	9000N	9000N	-
Weght (Kg)	16.3	5.9	5.4	67%
Max Resultant Displacement (mm)	0.01450	0.004188	0.001348	7%
Von mises Stress (Mpa)	0.247×10^{-3}	0.190×10^{-3}	0.168×10^{-3}	32%

Table: Results comparison

There is a minimum displacement & lower stress of E-glass/epoxy, and all the values are nearly equal and are below the camber length for a given load of 9000N these values are without crack of the leaf spring.

A study has been made on composite leaf spring reduces the weight by 67% for E- Glass Epoxy over Steel leaf spring.

From the static analysis results, we see that the von-misses stress in the E-Glass/Epoxy composite leaf spring has lower stresses in leaf spring.

Finally this project concludes from above table that the static analysis results it is found that under the same static load conditions deflection and stresses of steel leaf spring and composite leaf spring are found with the great difference. Deflection of composite leaf spring is less as compared to steel leaf spring with the same loading condition. At maximum load condition also composite leaf spring shows the minimum deflection as compared to steel Leaf Spring. Composite leaf spring can be used on smooth roads with very high performance expectations. Hence it is concluded that E-Glass/Epoxy material can be used for the leaf spring.

The project carried out by us will make an impressing mark in the field of automobile. While carrying out this project we are able to study about the analyzing software (ANSYS) to develop our basic knowledge to know about the industrial design.

***REFERENCES*:**

1. Design and analysis of composite leaf spring in light vehicle [international journal of engineering research (ijmer)],[vol.2, issue.1, jan-feb 2012]

2. Design and analysis of a leaf spring for automobile suspension system review [International journal of emerging technology and advanced engineering], [volume 3, issue 6, june 2013]

3. Performance analysis of two mono leaf spring used for maruti 800 vehicles [International journal of innovative technology and exploring engineering] [issn: 2278-3075, volume-2, issue-1, december 2012]

4. Performance analysis of steel leaf spring with composite leaf spring and fabrication of composite leaf spring [international journal of engineering research and science &technology (ijerst) [vol. 2, no. 3, august 2013]

5. Analysis of natural fiber composite leaf spring[international journal of latest trends in engineering and technology] vol. 3 issue 1 september 2013mono composite leaf spring for light weight vehicle – design, end joint analysis and testing[mechanical engineering department, psg college of technology] vol. 12, no. 3. 2006

6. “A textbook of machine design” by R.S.Khurmi and J.K.Gupta.

7. William D callister. “Fundamentals of material science and engineering”. Fifth edition, john wiley& sons, inc 1985.

8. International journal & magazine of engineering, technology, management and research (ijmetmr) january 2016.
9. "Machine design" Dr N C Pandya and Dr C S Shah.

10. "Elements of fracture mechanics" by Prashantkumar.

11. A textbook of "strength of materials" by R.K,Bansala.

12. An introduction to the Finite Element Method (Engineering Series) Hardcover – January 11, 2005

STUDY ON INCREMENTAL SHEET METAL FORMING

Gudipaka Soujanya[1]

[1]Assistant professor, Department of Mechanical Engineering, Malla reddy college of engineering, Hyderabad, Telangana, India

Vishwagna Ramya[2]

[2] Assistant professor, Department of Mechanical Engineering, Malla reddy college of engineering, Hyderabad, Telangana, India.

ABSTRACT

Unique ISF (incremental sheet metal forming) has superb flexibility to customary processing machines and requires least utilization of complex tooling, dies and shaping press, which influences the procedure to savvy and simple to computerize for different applications. It is a method which utilizes CNC apparatuses to form sheet metals. The technique isn't relevant for large scale manufacturing yet observed to be extremely valuable in little group quality creation. This paper gives the data on essentials of incremental sheet metal forming, impact of different parameters, for example, step size, Tool radius and forming angle. This examination likewise incorporates the applications and points of interest of ISF in different fields.

Keywords: Incremental sheet forming (ISF), Tool radius and forming angle.

INTRODUCTION

Besides being a noteworthy industry, metal framing is the foundation of current manufacturing industry. It is a mass maker of semi-completed and completed products, which is practical to embrace innovative work ventures. Roll forming and Deep drawing illustration being the most prevalent sheet metal shaping procedure were found for the prerequisites of large scale manufacturing. For both small batch and prototype productions the design of heavy die and punches is only misuse of material, time and money. Another creation strategy called incremental sheet forming (ISF) is being produced to repay these three factors.

Incremental sheet forming is a procedure for deforming sheet metals by the localized deformations.These disfigurements are continued by the utilization of well ordered incremental encourage to the deforming tool.

FUNDAMENTAL SETUP OF ISF:

Simple geometry tool is mounted on a CNC machine having three degrees of freedom (X, Y and Z hub). The sheet is mounted in an apparatus which permits shaping of the sheet into the hole of the apparatus as appeared in fig.1.

The tool is proceeded onward the sheet and it forces twisting locally on the sheet in a successive way according to the offered program to CNC. The way along which the tool should move is specifically characterized from a CAD definition. The tool path is picked in view of the required profundity of vertical sustain. Supporting tools or dies are utilized beneath the sheet metal when the geometrical structure of the item is muddled.

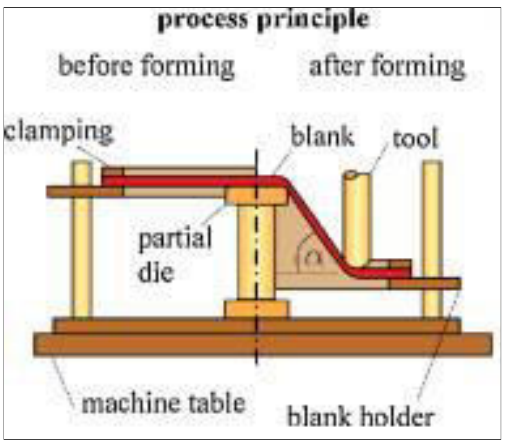

Fig : 1 Schematic portrayal of SPIF

The impact of the principle parameters on formability has been examined by a great deal of scientists. But with respect to the impact of hardware estimate conclusions are not steady. However in the conclusions the outcome has been discovered by expanding sheet thickness and decreasing tool size estimate it was discovered the lessening in vertical advance size each of the tend to increment in formability.

SORTS OF INCREMENTAL SHEET FORMING:

Single point incremental framing:

Single point incremental forming (SPIF) is a new innovative and achievable answer for the fast prototyping and the assembling of small batch sheets.

SPIF is a free frame sheet forming in which inverse side of the sheet is bolstered by a faceplate and it is disfigured utilizing a hemi round tipped tool through little incremental distortions as appeared in fig.2, the tool diameter can differ from 5 to 20mm. The procedure is conveyed at room temperature requires a CNC machine, a circular headed tool and a straightforward help to settle the sheet being shaped.

Two point incremental forming:

In Two point incremental forming (TPIF) the blank is clipped in the blank holder which can be adjusted in the z pivot. In this procedure a partial and full die supports the sheet.

In TPIF with partial die on the tool moves more than one surface of the sheet metal and the other surface of sheet is bolstered by pass on to get the coveted shape as appeared in fig 2. Whereas on account of TPIF with full die, the other surface of sheet is bolstered with die to get the coveted shape and the size as appeared in fig 2. The cost of this procedure is high because of the cost related with the die material (aluminum, steel and wood) and manufacture.

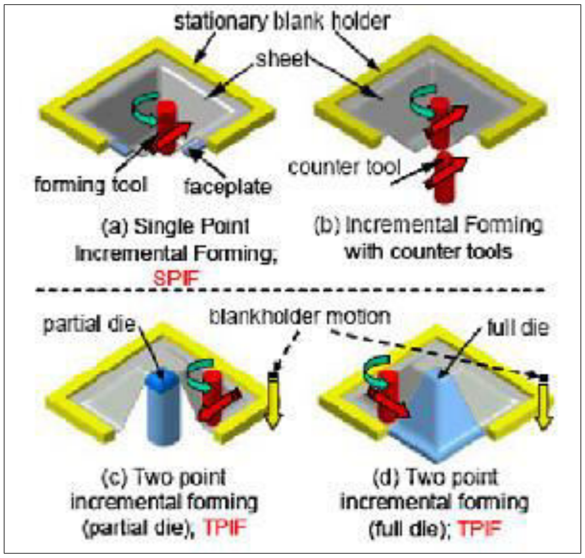

Fig.2 Single and Two point incremental framing process

LITERATURE REVIEW

The enormous writing audit has been done on late progression in Incremental Sheet Forming (ISF). Single point incremental forming (SPIF) is a sheet metal shaping procedure that permits fabricating parts without improvement of complex tools in examination with stamping process [1].

Expanding stretching and shear opposite to the tool bearing record for contrasts between the sine law and measured divider thickness for SPIF and TPIF. The forecast of thickness conveyance is near that acquired on the genuine part [1].

ISF process depends firmly on the shaping tool path which impacts significantly the part geometry and sheet thickness circulation [2].

Tisza, et al.[3] has expressed that because of the extraordinary incremental nature of deformation process, essentially higher deformation can be accomplished contrasted with ordinary sheet metal shaping procedures and it additionally takes after from its one of a kind twisting qualities that materials with bring down formability in traditional forming might be produced in a financial way.

Step size: The impact of step estimate is as yet a dubious parameter. Ham and jewiet [4] in their two new trial plans in SPIF considered the formability of AA3003 sheets and found that the progression measure impacted formability. The probability of the part to be formed was enhanced by diminished advance size. Hussian et al [5] researched the impact of step estimate on the formability of economically pure titanium blank and found that as step measure builds the formability diminishes directly. Decultot et al[6] in his experimental investigation of surface 3D advanced picture relationship, in shaping of an AW-5086-H111-review aluminum combination, found that the formability of work piece was diminished with the expansion of incremental advance size. It can be presumed that there is a hole of comprehension because of step estimate in ISF. So as to discover the connection between step estimate and the formability of various materials more research should be completed.

Tool radius: Hussain et al [5]. Assessed the formability of a Cp Ti sheet in frosty ISF process with a specific end goal to research the impact of tool diameter across on the formability. He found that by changing the tool diameter across up to three levels i.e. 8, 12 and 16 mm, by expanding the tool size the formability roughly diminishes. Jun-chao et al[7]. Contemplated the impact of tool diameter on the thickness and found that the little connection to the area of least thickness was appeared by the instrument estimate and furthermore if a regular apparatus way is utilized the base thickness is nearly connected with tool diameter. The impact of tool diameter across on the greatest shaping plot for SPIF of aluminum AA3003 sheets was represented by Ham and Jeswiet [4]. They found that because of the convergence of friction heat at the forming tool tip, higher formability happened with littler forming tools.

Forming angle: In SPIF, the greatest shaping edge is thought to be a standout amongst the most critical criteria to measure the material's formability limit. Numerous examinations has been discovered that numerous parameters bigly affect the wall angle, e.g. tool diameter and tool path, so as to decide the scope of their impacts on the wall angle additionally examine is required.

APPLICATIONS:

- ISF innovation was basically produced for the necessities of automobile and aeronautic trade. Over the time, different branches have perceived the advantages of this innovation and presently effectively connected in many fields.
- In the field of automobile industry, ISF is utilized for quick prototyping of warmth vibration shield silencer lodging for trucks and so forth.
- In the field of pharmaceutical, SPIF is utilized to create thin walled uniquely designed metal parts, for example, denture plate, skull bone prosthesis and lower leg bolster.
- In airplane business, parts like instrument board, body board, and traveler situate cover and so forth are created.

POINTS OF INTEREST

- As the die is disposed of in this manufacturing procedure the cost per piece is diminished.
- The formability of metal materials under the restricted deformation forced by incremental forming is superior to in conventional deep drawing, better formability.
- Uniform thickness appropriation.
- Complex shapes can be formed.
- Blunders in traditional process can be dispensed with in this procedure like tearing, wrinkling and so on. Higher adaptability and enhanced quality.

CONCLUSION:

The ISF procedure can be effortlessly utilized for producing perplexing, little shapes and bigger forming angles with legitimate forming strategy. Without planning and assembling of lower and upper die, figured out items can be produced. ISF can accomplish great surface complete and close net shape.

REFERENCES

[1] Thibaud S, Hmida RB, Richard F, Malécot P (2012) A fully parametric toolbox for the simulation of single point incremental sheet forming process: numerical feasibility and experimental validation. Simul Model Pract Theor 29:32–43

[2] Azaouzi M, Lebaal N (2012) Tool path optimization for single point incremental sheet forming using response surface method. Simul Model Pract Theor 24:49–58 [3] M. Tisza , "General overview of sheet incremental forming" Journal of achievements in materials and Manufacturing Engineering, Volume 55 issue 1 pp. 113-120, 2012.

[4] Ham M, Jeswiet J (2006) Single point incremental forming and the forming criteria for AA3003. CIRPAnnManuf Technol 55(1):241–244

[5] Hussain G, Gao L, Zhang ZY (2008) Formability evaluation of a pure titanium sheet in the cold incremental forming process. Int J Adv Manuf Technol 37:920–926

[6] Decultot N, Robert L, Velay V, Bernhart G (2010) Single point incremental sheet forming investigated by in-process 3D digital image correlation. EPJ Web Conf 6:1100

[7] Jun-chao L, Chong L, Zhou T-g (2012) Thickness distribution and mechanical property of sheet metal incremental forming based on numerical simulation. Trans Nonferrous Metals Soc China22:s54–s60

The CFD Analysis Of Engine Combustion Characteristics

M.VeeraReddy Asst.professor, Department of Mechanical Engg Malla Reddy College of Engineering,mudela123@gmail.com

T.Suresh Asst.professor, Department of Mechanical Engg, Malla Reddy College of Engineering, tsuresh330@gmail.com

.

Abstarct: **Computational fluid dynamics code (CFD) Fluidity used to model the compound The phenomenon of combustion pressure Engine ignition. Temperature profile and nitrogen oxides Produced within the combustion chamber Compared with traditional jatropha Diesel.The simulation results obtained Experimentally verified for both jatropha and test conventional diesel diesel engines. Simulation is fluid in use Ansys- Mixture combustion model is to respond to the real needs The parameters in the combustion cylinder.Two Combustion chamber dimensions network simulation distortion is used.**

Keywords—CFD Analysis,combustion,fluidity,jatropha diesel, simulation

I. INTRODUCTION

Since the beginning of civilization, it has provided the combustion of fuels for most of our energy needs. Tgreater still providing 70% [3] of its current capacity of the planet. Therefore, combustion technology remains the main energy in the foreseeable future. The combustion phenomenon is the conversion of the energy trapped in various types of chemically fuel heat model (and light). This energy can be used to increase the generation of steam and electricity, Tricity, heating, transport and cooking area, and many other applications. It can happen fuel used in domestic and industrial equipment combustion in any of the three phases that occur naturally (solids, liquids and gases). This fuel must react with oxygen, which occur in gaseous form. But also it must be converted into gaseous form before undergoing combustion reactions. This conversion occurs through evaporation of the liquid fuel or solid fuel outgassing at high temperatures.

At the molecular level, which can be of two reagents undergo a change in electronic form to form or break the links leading to a chemical reaction. They have to be thoroughly mixed and Esna implementation cient combustion. Therefore bringing the two reactants, namely. Fuel and oxygen, in proximity to each other at the molecular level, forming part of the challenge for the design of any combustion equipment. Research hill experience provides useful data that can be used in the design of this equipment in trying to theoretical developments to explain the experimental behavior BE-observed. Numerical simulations give predictability needed for the design of combustion systems. And the use of experimental results and theoretical and proposals on the development of numerical simulation successfully. Most fuels used in combustion applications are a mixture of several chemical types. Each of these species reacts with oxygen to release its own heat reemployment. Such reactions do not occur, such as the process from step one, but make up many of the initial steps involving many intermediate species. All these steps intermediate species necessary to understand the behavior of fuel combustion. Several decades of research have achieved mathematical and numerical method .For treatment of the complex nature of chemical reactions. These include the disarmament of the kinetic model of chemical glue, accounts balance and solving equations of balance of species in the simple flow equipment. The fluid flow may have additional properties, such as compressible, swirling, and is stable with respect to time or any of the groups from above. Ff flow characteristics ect shape and extent of the fuel particles and oxidant contact one another. Therefore, in addition to know the details of the chemistry and behavior of operations problems, it is also necessary to have the descriptive approach to simulate the interactions between the two countries (viz. The chemical interaction agitation). combustion reactions often result in many contaminants such as soot, nitrogen oxides and sulfur oxides. an accurate prediction of these contaminants that all details of the chemical reactions are inserted into the flow simulation is required. This becomes a turbulent flow cases integrals. And it can be used to simulate the response of simplistic give good results with respect to the release of heat patterns approach and flow but not grasp the ignition delay and the formation of pollutants time details. Along similar lines, can be complex shapes (such as Monte Carlo) modeling turbulent flow is also to be exhaustive. There are several methods for modeling the precise details of agitation alone, and chemical reactions, and there alone, and the development of a simplified plan the previous days more complex and intensive studies numerically latter approach. He described some of them in the following chapters. However, its design and following thoughtful and optimization in the industry today, and the balance of accuracy is required for an account. Approach that focuses on a single detail of this phenomenon can be misleading or does not serve the general purpose of simulation studies

II. LITERATURE REVIEW

The Process work in a simulation of the combustion process in diesel engines compression ignition (CI) using low ILDM mechanism automatically using technology in the three-dimensional model CFD. While the conditions in the diesel engine online characterized by high pressure and temperature, and a similar approach can be used to simulate the combustion process it is similar to mixing systems.

The compression ignition engines of the diesel engine, in which inspirited only air in the cylinder, unlike spark ignition engines, where air and fuel mixture is inspir-ited. The fuel is injected directly into the combustion chamber in the form of a mist of liquid. combustion chamber of the diesel engine is composed of a cylindrical piston. And inspirited air in the intake stroke (at the beginning of the session) in the case of at-

atmospheric (more if the engine is turbocharged) when the piston is at bottom dead center, the intake valve is open. In the compression stroke, the piston compresses the air trapped inside the room, and raise it to a high temperature, and finally to the top dead center (TDC). The compression ratio in spark-ignition engines are in the range of 12 to 24, much higher than in SI engines. Compressed air can be up to 80-100 atm. The temperature can be up to 800 to 1000 K at this point. Shortly before the piston reaches the body, liquid fuel sprayed into the combustion chamber. Due to the high temperature (greater ignition point fuel), fuel ignition engine. Time from the start of injection (SOI) and ignition and the occurrence of so-called time delay ignition. In the expansion stroke, in the light of the flame propagation through the combustion chamber, the heat is released from the fuel. (BDC), and the hot exhaust gases are pressed towards the extended piston BDC. Therefore, the energy is converted into mechanical motion of the piston, which has also resulted in the crankshaft and used to transport in a car or electricity generation etc. integrity arrival combustion piston BDC, reflecting the start address of the exhaust stroke. The release of the exhaust valves open and the flue gases. With this the cycle is completed and start fondling the

following entry in the final part of the session.

There are many aspects to be considered for CFD simulation in a diesel engine, which are listed below.

- combustion occurs at high pressures and flow can not be assumed that the tablet.
- simulation requires a base turbulent flow in three dimensions.
- heat transfer due to radiation, convection and conduction to be considered.
- model require liquid spray droplets for mass and heat transfer with the continuous phase, as well as breaking and coalescence.
- suitable for predicting the weather so self- ignition.
- models and polluting chemical and abundant species.
- transmission networks to simulate the movement of the piston.

Each of the above considerations suggest that these simulations are, however, a complicated-com useful exercise.

The presence of the species in the flow interaction requires the inclusion of additional points in the equations change. This is because the terms of the source of all kinds and the energy released due to a reaction. And it is subject to changes in the concentration of species and the heat released due to a reaction rate kinetic equations. Turbulent flows in the reaction, these conditions sources pose a problem because they are not in a closed form. A closure method where the source can be integrated by using a statistical approach, where the formulation of the probability density function (PDF) on the terms of any source. This method is chosen for the job. If a large number of species present in the flow, and this approach can be costly in terms of numbers. Therefore technique, described as ILDM (essentially low dimensional manifold), to reduce the reaction system offers variable representation can be used. A mathematical method for the separation of the reactions in the fast and slow reactive groups on the basis of analysis of making the value of the Jacobi matrix in terms of the source.

III.METHODOLOGY

The experiment was performed in a single cylinder four-stroke diesel engine air cooled vertical 5.9 kW nominal power and nominal

minute 1500 RPM speed. Precise measurements of the degree of exhaust heat, The rate of fuel flow. emissions biodiesel And measured using diesel gas analyzer. speed continuous pregnancy test has been performed on Motor and previous measurements Taken under different loads. The experiment showed that the above scheme. Establish airbox has a size of about 500 Times the size of the engine cylinder. The idea is To make the free flow of air from any pulse full engine axis AC generator load applications .Electrical Using the engine alternator. Temperature and It is measured by using the exhaust gas emissions Thermal and gas analyzer, respectively. While performing the experiment conditions of the room It remained constant and adequate ventilation He offered to make the surrounding free Exhaust emissions, which may affect emissions Read.

IV.RESULTS

The results of any simulation is only as good as some input for modeling code. Compared with experimental data can reveal the accuracy and validity of the results. A set of experimental data for the engine 3406 Caterpillar heavy trucks available [159] for this purpose. It is given this engine specifications in the following section. The amounts include pressure measurement

average and the average temperature, shutter speed, and the concentrations of nitrogen oxides and soot. Additional qualitative description of the engine can be performed by analyzing propagation of flame, the flame shape, and the numerical rates dissipate sites ignition and ignition delay.

In any CFD simulation, it is very important to ensure that the results do not depend on the network used. This can be achieved by using more consistent, respectively density, and stood on the step and then no change was found in the results. And the use of networks three di ff Erent density in this study, and found suitable for medium dense networks accounts. A brief description in the next section. E ff ect of the many parameters studied is clear from the following addresses sections.

Engine Specifications and network

54 kW simulator diesel engine at 2,100 rpm (revolutions per minute) were classified. And considering the design of the initial conditions in Tables 7.1 and 7.1 for details. Available for

download partial cycle with the condition in 1600. minute stays on all the walls under constant temperature data experi mental. Measuring air temperature error of about 10 to 15 K input, which is adjusted to suit the temperature in the injection simulation experience in a state of cold flow. Ho stirring time mogeneous

closing the intake valve, which occur in the - 137o ATDC (after top dead center) is assumed. the exhaust valve opens 130o ATDC, and not only perform simulations for these events between the two valves. The initial values of the parameters of his turbulence calculated based on the recommended level of turbulence by 10%. And the value of ǫ is calculated as the value of freedom of movement and a length of

1.432 cm. The results do not pay attention to these values as previously reported [33].

Use 1/6 the sector to take advantage of the symmetry league, which was established as a result of injector nozzles 6 as it reduces the time required for the account. Numeric

Bore	137.16 mm
Stroke	165.1 mm
Connecting Rod Length	263 mm
Engine Speed	1600 rpm
Number of Nozzle Orifices	6
Injection Timing	-7°, -4°, -1°, 2°, 5° ATDC
Duration of Injection	19.75°
Fuel Injected	0.168 g/cycle
Cylinder Wall Temperature	433 K
Piston Wall Temperature	553 K
Head Temperature	523 K
Initial Gas Temperature	361±15 K
Spray Temperature	341 K

Table 7.1: Caterpillar-3401 engine specifications.

Initial Gas Composition (g/cm^3)			
O_2	N_2	CO_2	H_2O
4.6012×10^{-4}	1.5337×10^{-3}	2.8579×10^{-6}	1.2579×10^{-6}

Table 7.2: Engine conditions at the time of inlet valve closure.

V. CONCLUSION

Simulating turbulent flows is a difficult problem. Having reactions adds more complexity to this challenge. The ability to achieve such a complex within the limits of computing resources and lifetime challenge are industrially reasonable results it is the main objective of this work. Results and

discussion in the previous chapter leads to the conclusion that ILDM provides reasonable to integrate kinetic rate laws for the complex interaction mechanism in the probabilistic description of turbulent flows form. Choice of reaction variables may be slightly ff ect accuracy of the results. model based on the results raised to fully automatic container (including low temperature reactions HC) gives delay times similar to the appointed ignition temperature formations release time measured experimentally. Intro-duction of RNG model as ǫ wall and enhance heat transfer equation translates into better heat transfer expectations and consistent with literature disorder. It can also be concluded that the Zeldovich mechanism for predicting nitrogen oxides when used in concentrations of reactive intermediate species which have been obtained from ILDM can improve the accuracy of the accounts for approximately

10 to 20%. Similarly, the expectations of soot, using the model of phenomena including ILDM soot precursors, can be obtained within 20 to 30% of those obtained experimentally. The formation of nitrogen oxides in the inclination equally flame in contrast to soot, tops in emerging areas of the flame. Soot increases rapidly after injection, and I saw a little peak after peak fuel focus seems to indicate that the formsoot, especially in areas rich flame. In all temperature characteristics, there can be observed a deviation of laboratory values before the start of injection. Initially it was thought that this could be due to the assumption that the ideal gas law. The implementation of the best equation of state (Radash-Kwong or Soave) could not fill this gap, and can not solve the problem. a reassessment of the relationship of pressure and heat is required to address this issue. In short, all important parameters to know. temperature and pressure and heat release rate as well as nitrogen oxides and soot contaminants

satisfactorily predicted. Despite his comment on the numerical ILDM remain outside the scope of this Workplaces and public observations about the functions can be done. And to allow simultaneous use of remote zero (balance), in addition to regular programming go a long way to address the question of where is the source where there ILDM points. The need to use the one-step reaction or a point shape and inaccuracies that come with it, then it can be ignored. There are several reasons for this, but the lack of correspondence between the experimental data and attributed the results of the simulation, and. Assuming a uniform ILDM for use with all cases is one pressure. When a one-step model is used when ILDM countries can not find it, it is done NO and soot accounts using only PDF degrees of temperature. Moreover, the concentrations of intermediate species and obtain the cells are not added to each, but only used for accounts NO and soot. This is to avoid errors in the overall balance to calculate the chemical in one step.

Despite being a good Affordable way FF it is more valuable than a simple demonstration purpose, integrating ILDM to simulate the turbulent flow of the reaction is still plagued by many di culties ISNA dispute, and the robustness of the method is LG more doubtful. The results can only be obtained with many of the numerical limitations. One such limitation is the assumption of the probability distributions of statistical independence T, ξ and directed from a distance. Standardization and analysis of the time scale used to address this assumption induces the numerical weakness in the code element Simo-. It may be the future work includes the implementation of a way to remove this assumption common PDF files directly calculated. Remains in the account in terms of ff-mail ORT Compu tational for a procedure of this kind to be seen. However, one should consider the fact that this work is limited to the application in an unstable state of the state where the difference in the

REFERENCES:

[1] I. Mayeres, S. Proost. Why do we still have Diesel cars in Europe? In EAERE 2000 Annual Conference, 30 June - 2 July 2000, pp 1–22, University of Crete, Department of Economics, Rethymnon, Greece,. 2000.

[2] C. Hibbs. Diesel auto sales trending to exceed gasoline in Eu- rope in 2006. PriceWaterhouseCoopers Report, available at http://www.greencarcongress.com/2006/01/diesel_auto_sale.html,

[3] N. Blackaby. Once bitten, twice shy. Power Engineering International **8**, pp 20–22, 2005.

[4] N. Peters. Turbulent combustion. Cambridge University Press, New York, NY, 2000.

[5] R. Klein. Numerics in combustion. Von Karman Institute, Belgium, 1999.

[6] R.B. Bird, W.E. Stewart, E.N. Lightfoot. Transport phenomenon. John Wiley & Sons, New York, 1960.

[7] F.A. Williams. Combustion theory. Addison-Wesley, New York, 1985.

DESIGN, COMPARISON AND THERMAL ANALYSYS OF PIN FINS IN A WEDGE DUCT

Jis Mathew, jissmathew1990@gmail.com, +917558930803
M.tech in Thermal Engineering, Department of Mechanical Engineering, Malla Reddy College of Engineering
Secunderabad, India

ABSTRACT

This project titled "Design, comparison and thermal analysis of pin fins in a wedge duct" presents design, numerical comparison of the flow and heat transfer characteristics of circular and elliptical in line pin fins in a wedge duct with different types of coolants. Pin fins at the trailing edge of the turbine blade connecting the upper end wall and lower end wall , con not only effectively improve the heat transfer rate, but also improves the strength of the blade trailing edge. Blade cooling improves the overall efficiency and improve the power output of the turbo engine. Because proper blade cooling can increase the turbine inlet temperature, since blade can withstand more temperature. Here in this project we are studying the effect of air and steam as coolant. Analysis done at two different duct Reynolds number. Geometric model of elliptic and circular pin fins was created by CATIA V5 and mesh generated using ANSYS ICEM-CFD. Required results are obtained with the help of ANSYS CFX-15:0. Validation of the numerical results obtained in this project is done with the help of experimental results published by J.J.Hwang and C.C.Lui in 2001. This project result is showing that elliptical pin having better thermal performance when compared with circular pin fins.

KEY WORD-Pin fin cooling

I. INTRODUCTION

I.1 BLADE COOLING

Blade cooling is the most effective way of maintaining high operating temperatures making use of the available material. Based on the cooling site blade cooling is classified as external cooling and internal cooling. According to the cooling medium it is classified as liquid cooling and air cooling [1].

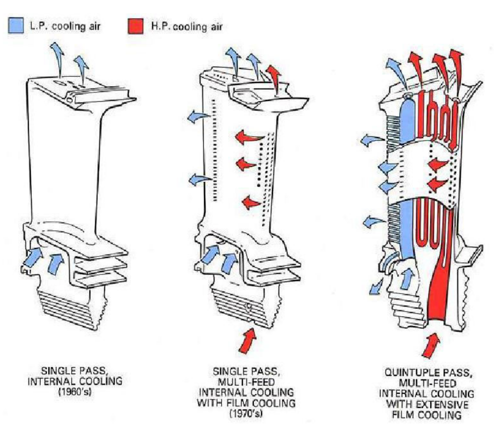

SINGLE PASS, INTERNAL COOLING (1960's)

SINGLE PASS, MULTI-FEED INTERNAL COOLING WITH FILM COOLING (1970's)

QUINTUPLE PASS, MULTI-FEED INTERNAL COOLING WITH EXTENSIVE FILM COOLING

I.2 PIN FIN COOLING

Trailing edge of the blade is very thin in nature, so cooing in this area is very complicated. Here comes the use of pin fin technique, which helps in cooling of the turbine blades trailing edge area.

Pin fins are designed in such a way that, it is connecting the upper end walls and the lower end walls. Implementation pin fin at the trailing edge of the turbine. Blade, not only increase the internal heat transfer but also increase the strength of the blade, mainly at the trailing edge. Trailing edge region of the blade is in a form of wedge, since the blade is designed in such a way that to increase the aerodynamic efficiency. Blade thickness is gradually reducing from the leading edge to the trailing edge. Coolants first flowing through the wedge trailing edge with pin fin cooling and eject at the slot of the trailing edge. Thereafter this coolant mixes with the main stream. Here heat transfer characteristics in a convergent pin fin channel are analyzed. Trailing edge portion of a gas turbine engine blade posses a small wedge angle. So here we are analyzing the pin fins arranged in a wedge duct. Circular pin fin arrangement and elliptical pin fin arrangement are taken into consideration for the analysis.

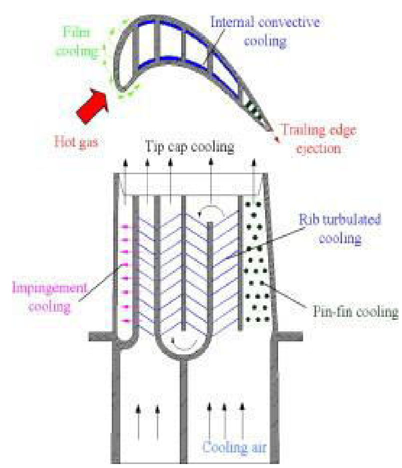

Pin fins were installed at the trailing edge of the blade, they can intensify the mixing of the fluid by triggering walls and this improves the heat transfer performance. Pin fins are extending from top end wall to bottom end wall. At the ends of the pin fins, vortex generation occurs and this improves the end wall heat transfer characteristics. At the junction of pin fin with end walls will tend to initiate horse shoe vortices and this tend to enhance the regional end wall heat transfer rate [2]. In this project we are using types of pin fin arrangements.

1. Circular pin fins

2. Elliptical pin fins

Heat transfer performance of circular pin fins and elliptical pin fins are analyzed and compared here. Here in this paper, for analysis elliptical and circulars pin fins placed in a wedge duct is taken into consideration. In most cases the cooling fluid used is the air extracted from the compressor inlet in real gas turbine. This method of extracting a portion of air from the compressor reduces the total amount of air entering in the combustor. Thus reduces the overall thermal efficiency of a gas turbine engine. Even though this problem still exists, this type of extraction of air from the compressor still remains in practice because it is the easy method of cooling [3]. Using steam as a coolant can considerably reduce the problem of extracted air on the thermal efficiency steam also has a high specific and thermal conductivity [6]. Gao experimentally investigated the flow and heat transfer characteristics of steam in rectangular ducts with pin fins and nozzle vanes. These investigations show that comparing air as coolant and steam as coolant, steam possesses more heat transfer rate. Mist as a coolant. This coolant shows a higher heat transfer characteristics. There occurs a higher effective specific heat for this coolant because of the latent heat of evaporation. Also water droplets were attached to the end walls also evaporated. This evaporation also reduces the heat of the end walls [5].

II. GEOMETRIC MODEL

Here, for this project study, the geometrical calculation and computational configuration is taken from Ref. [2]. This consists of extended inlet and outlet sections and pin fins arranged in the wedge duct. Entrance section is extended for the purpose of making a stable and uniform velocity distribution of the flow to the pin fins, where the extended exit section for resisting the back flow.

Here, 25 inline pins with each diameter of 12 mm is arranged in such a way that spacing between the fins are same. Pins height between upper and lower end walls varies as pin fin height to diameter ratio from 1.3 to 3.6. This height to diameter ratio variation from first row of pin fin to the last row.

A structured mesh of the model is created with the help of ANSYS ICEM CFD.15.0. While creating the mesh an O-grid applied around the pin fins and grid requirement technique adopted at both lower and upper end walls. For getting rear-wall resolution, value of y+ must be below 1. This is to meet the requirement (insisted by ANSYS CFX 15.0 Solver) quality checking of the method geometry must be done after meshing. Here, for structures meshed quality must be more than 0.5 and for unstructured it must be more than 0.1.

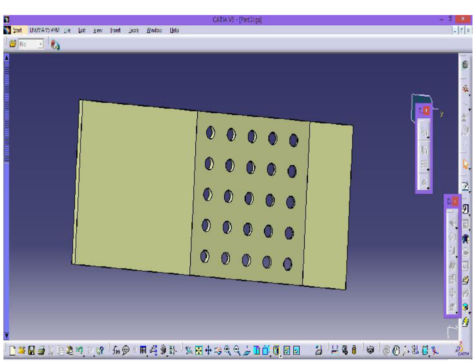

III. METHODOLOGY

3D model of elliptical pin-fin and circular pin-fin model is developed by CATIA V5. The necessary calculations for the pin fin geometry developed by Microsoft excel, with the help of the ref journal [7]. The model is then exported to ANSYS ICEM-CFD 15:0 for geometric meshing purpose. First structured mesh has created. There after structured mesh was converted to unstructured mesh. Then the finite element model has been taken into ANSYS CFX for applying boundary conditions and for obtaining the result. Boundary conditions applied in the module ANSYS CFX –Pre 15:0. After that using run command analysis has carried out. Here required number of iterations to be carried , residual target etc given in solver control, solver control box given in fig. Result obtained with the help of ANSYS CFX-Post 15:0.

IV. DESIGN CALCULATIONS

Model consists of a wedge duct having pin fins arranged in line. Also geometric model have an extended entrance and exit sections. Extended entrance section to make an uniform flow entering into the wedge duct. Also provides a stable flow. Extended outlet section is for avoiding back flow. Twenty five pin fin arranged in a wedge duct. Each row contains five pin fins each. Total number of rows is five. The pin length to diameter ratio varies from 1.3 to 3.6. Table below shows the necessary calculation values required for creating the geometric model.

2	Parameters	Relation	Value	Unit
3	Diameter of Pin-Fin		12	mm
4	Le length of the entrance section (mm)	Le/D=13.33	159.96	mm
5	Lo length of the outlet section (mm)	Lo/D=5	60	mm
6	H1 height of the entrance of the wedge duct (mm)	H1/D=3.6	43.2	mm
7	H2 height of the exit of the wedge duct (mm)	H2/D=1	12	mm
8	Sx longitude space between the pins (mm)	Sx/D=2.5	30	mm
9	Sv transverse space between the pins (mm	Sy/D=2.5	30	mm
10	W endwall width (mm)	W/D=13.33	159.96	mm
11	L endwall length (mm)	L/D=13.33	159.96	mm

A	B	C	D	E
	DESIGN,COMPARISON & THERMAL ANALYSIS OF PIN FINS IN A WEDGE DUCT			
	Parameters	Relation	Value	Unit
	1 dimeter of fin	b=1.18182a	a=11,b=13	mm
	2 Le, length of inlet section	Le/a=14.509	159.6	mm
	3 Lo, length of outlet section	Lo/a=5.455	60	mm
	4 H1, height of the entrance of the wedge duct	H1/a=3.93	43.2	mm
	5 H2, height of the exit of the wedge duct	H2/a=1.091	12	mm
	6 Sx, longitudinal space between fins	Sx/a=2.7272	30	mm
	7 Sv, transverse space between the pins	Sv/a=2.7272	30	mm
	8 W,Endwall width	W/a=14.509	159.6	mm
	9 L, endwall length	L/a=14.509	159.6	mm

Design calculations of circular and elliptical pin fins are shown in the above figures.

Pin fin arrangement on the wall shown in fig.

Here circular pin fin arrangement on the lower end wall is shown.

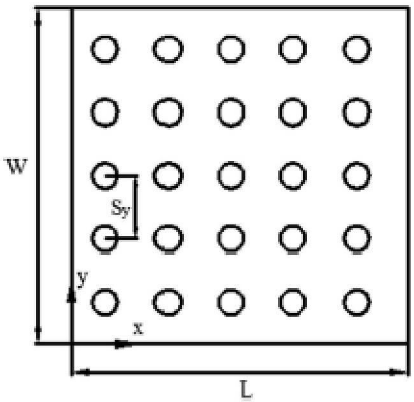

IV.1 FINITE VOLUME MODEL IN ANSYS ICEM CFD

ANSYS ICEM-CFD is using mainly for creating mesh. ICEM means Integrated Computer aided Engineering and Manufacturing. We can do computational fluid dynamics and finite element analysis in ICEM CFD. Here in this project we are going through CFD analysis. ICEM-CFD specially used for meshing purposes. In ICEM CFD more tools are available for meshing .so we can easily generate the mesh with proper accuracy and so easily. Nowadays most of the companies using ICEM-CFD for mesh generation purposes. In ICEM-CFD structured mesh consist of Quad and Hex shaped elements. Where As unstructured mesh consist of Tri, Tetra, Pyramid, Prism and even Quad and Hex elements. Hybrid mesh is a combination of both structured mesh and unstructured mesh. At some particular portions we will do structured mesh. We are creating structured mesh where high accuracy and high quality is required. For generating structured mesh, we needed more time. Because Quad and HEXA shapes are unable to generate near sharp edges, over curved surfaces etc. so on those areas we need special tools like O-grid generator, move vertex option etc for dividing the sharp area. After that we capture the Quad and HEXA shapes on those special regions. For structured mesh solving time is less when compared with unstructured mesh. Here each element having particular address. Thus we can easily take the previous iteration results. Address having i, j, k format for 3D mesh and i,j format for 2D mesh. Unstructured mesh has no address. For unstructured mesh instead of address cell to cell numbering is provided. Thus unstructured mesh needed more solving time. Because every time we need to check all the previous iteration results. In ICEM-CFD initially we will create structured mesh for getting more accurate solution and after that we will change this already created structured mesh into unstructured mesh.

Meshed geometries are shown figures. CATIA designed geometries are meshed using ANSYS ICEM-CFD. Structure meshing is used initially for meshing purposes. There after it is converted into unstructured mesh after checking the quality of the mesh. If desired quality is satisfied it can be used for analysis purpose and for obtaining results.

Circular fin is transferred into ANSYS ICEM-CFD after converting the CATIA geometry into .IGS or STEP FILE.O-Grid generation is a special one to capture special shape with quad and hex shape in structure meshing. O-Grid formed blocks are shown in fig.4.9. O-grid generation is necessary for getting the proper alignment of the blocks with respect to the geometry that we designed.

Quality checking of the mesh generated geometry is very important before we are going to analysis. Because we need to know that whether our shape properly created or not. For structured mesh accuracy or quality should be at least 0.5. For unstructured mesh it is 0.1.

IV.2 CFX SOLVER MANAGER

We are giving necessary boundary conditions for analysis. Here we are always keeping the end wall temperature as constant. And it was 39 and 150 for case 1 and 2 respectively. Velocity given is the value that obtained after finding the corresponding velocity for air and steam flow at different duct Reynolds number such as 20,000 and 50,000. According to given boundary condition in CFX Pre solver manager solve the equations based on RANS method. RANS method means Reynolds Average Navier –Stokes Equation. Here seven equations solved.

1. Conservation of mass having one equation

2. Conservation of momentum having three equations.

3. Conservation of energy having one equation.

4. Turbulence model having two equations.

Once we reach the RMS (Root Mean Square) value, that time our result will generate. Then a graph will generate. This graph never says whether our result is right or wrong. This graph only gives an idea that whether our result is stable or not. If the graph is converging, then our result is stable. If graph is not converging then our result is unstable. Result graphs that we are getting after successive result generation shown in figure. These graphs consist of three portions momentum and mass transfer consisting a graph, heat transfer and then turbulence model. Converging results required for understanding whether our results are stable or not. Here the results are converging.

IV.3 ANSYS CFX CFD-Post

ANSYS CFX CFD-Post using to see the results that we obtained after successive solver run. Here we will see the results in two different ways.

1. Quantitative way

2. Qualitative way.

Quantitative results means, in contour or color plots we can see the results.

Qualitative means, it is graph like results.

CFD-Post result was shown in below figure.

V. VALIDATION

Result that we obtained from ANSYS CFD-Post is discussed here. These results are compared with the previously done experiments. This comparison is done for the validation of results that we obtained in this project. For validation we are comparing our numerical results with the experimental results that presented in the paper “Measurement of end wall heat transfer and pressure drop in a pin-fin wedge duct”. This paper is published by J.J.Hwang and C.C. Lui 15th march 2001 [7].

V.1. TEMPRATURE DIFFERENCE INFLUENCE ON HEAT TRANSFER

How temperature difference is affecting heat transfer is discussed here. Temperature difference of cooling air flow and heat transfer on the pin fin placed in the wedge duct is analyzed. Temperature difference can be stated as the difference in temperature between inlet and wall temperature. That is,

$\Delta T = T_1 - T_W$
Here, ΔT for case 1 is 26k
ΔT For case 2 50k
ΔT For case 3 steam is 50k
Three different case are analyzed here.
1. In case 1 inlet temperature is 65 degree Celsius.

2. In case 2 inlet temperature is 100 degree Celsius.

3. In case 3 inlet temperature is 100 degree Celsius.
Two different coolants are used
1. Air as coolant for case 1and case 2 2. Steam as coolant for case 3

These all above mentioned cases are similar for both circular pin-fin and elliptical pin-fin. ΔT for the case 1 is same for the experimental condition. Thus our project validation is carried out by comparing our results with the experimental condition. Here high nusselt number region is found out at the front area of the pin-fin and also at some portions those are little away from the trail area of the pin-fins.
Pin produces two vortexes. Mainly primary and secondary horse shoe vortexes. This produces two branches. And thus causing the coolant to come in contact with the hotter bottom surface. This contact initiates heat transfer between coolant and walls. Nusselt number decreases at the tail area of the circular pin fin and elliptical pin fin. This happened because of the back flow occurring at the tail area of the pin fins. Effect of heat transfer for ΔT=26k case1 is little better than that of ΔT=50k case 2. This found mainly near the side walls of second row and third row of pin fins arranged in the wedge duct [7].
Area averaged nusselts number also seen little high for case 1 when we compared with the case 2 results. Numerical data obtained for ΔT=50k slightly better agreement with the data found by experiment for Reynolds number higher than 30,000. For Reynolds number lower than 30,000 numerical data that we obtained is consistent with experimental data. Data found, such as area averaged nusselts number for first to 5th row is matching with the experimental results. Thus, totally we can say that numerical results for case 1 is ΔT=26k and ΔT=50k is satisfying when compared with experimental results and thus our validation has been done successfully. The stagnation points are obtained at the leading edge of the pin fins. This significantly enhances the heat transfer near the stagnation point formed at the leading edge of the pin fins. As a result of this increment in heat transfer local nusselts number also increased. Velocity is high in front of the leading edge of the pin fins and at the portion where boundary layer separation occurs. Where velocity is higher at those regions temperature is lower.
The results that we obtained after analyzing the results from ANSYS CFD-Post are given below. These results presented in both contour pattern and graph format. Contour pattern for quantitative analysis. Graph like format for qualitative analysis.

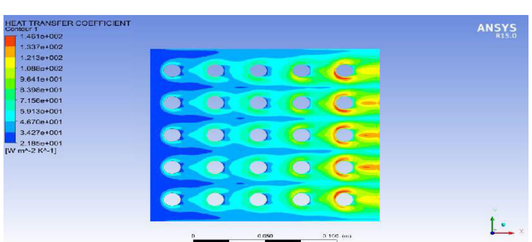

Heat transfer coefficient for circular pin fin at 65 degree Celsius

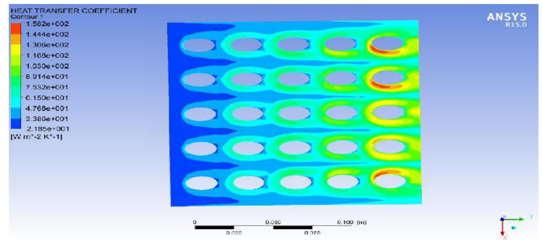

Heat transfer coefficient for elliptical pin fin at 65 degree Celsius

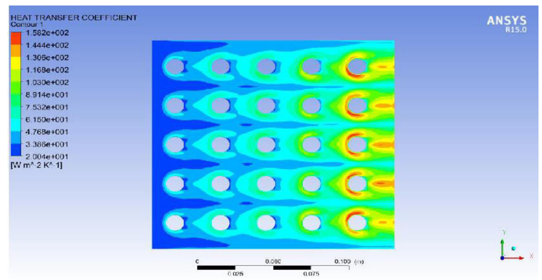

Heat transfer coefficient of circular pin fin at 100 degree Celsius when air as coolant.

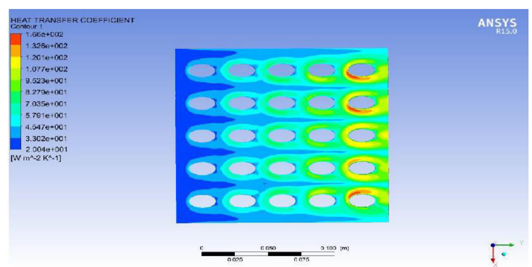

Heat transfer coefficient for elliptical pin fin at 100 degree Celsius when air as coolant.

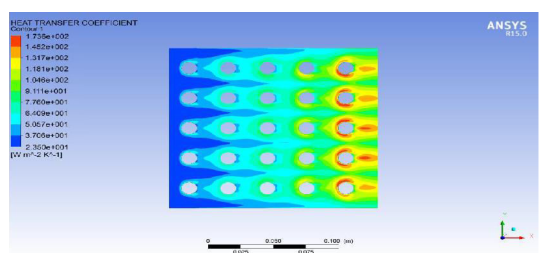

Heat transfer coefficient of circular pin fin at 100 degree Celsius when steam as the coolant.

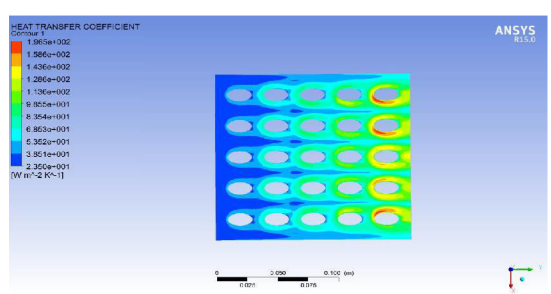

Heat transfer coefficient for elliptic pin fin at 100 degree Celsius when steam as coolant.

The above results are showing that heat transfer coefficient is increasing when we are going from the inlet section to the outlet. That is, heat transfer coefficient is increasing when we are moving from the first row to the fifth row. Pressure is decreasing from the front portion to the rear portion. Local pressure distribution is decreasing as we are moving from the first row to the fifth row of the pin fin arranged in the wedge duct. Pressure loss is more for circular pin fin when compared with elliptical pin fin. These are the general result discussion that has been carried out in this paper.

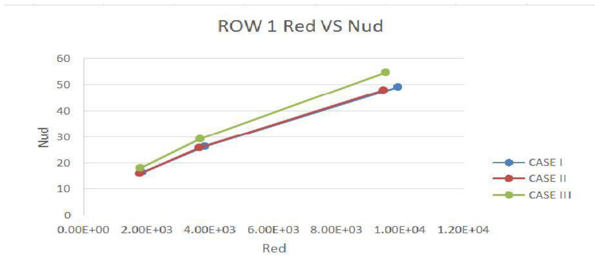

Re vs Nu for elliptical pin fin 1st row.

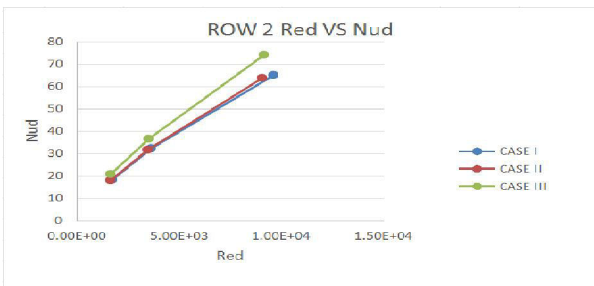

Re vs Nu for elliptical pin fin 2nd row

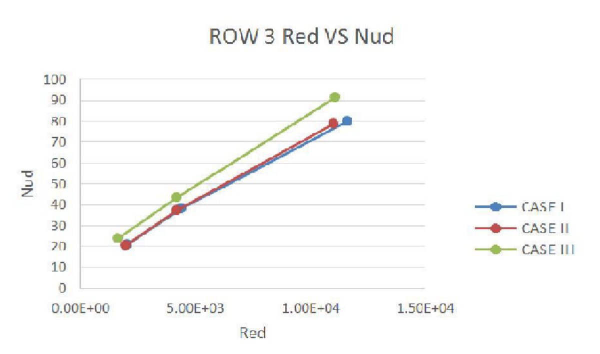

Re vs Nu for elliptical pin fin 3rd row

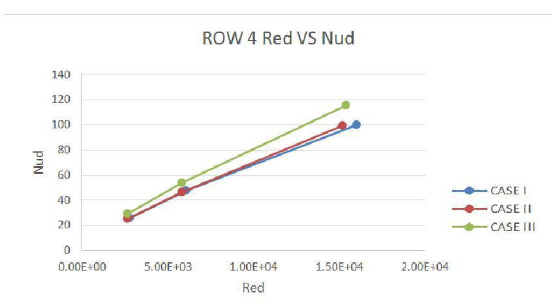

Re vs Nu for elliptical pin 4th row

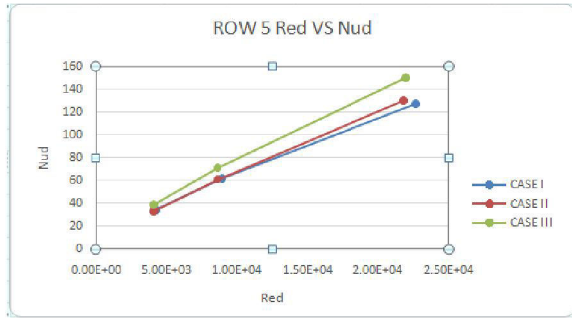

Re vs Nu for elliptical pin fin 5th row.

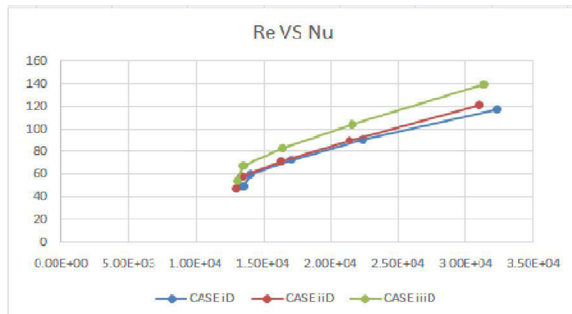

Re VS Nu for elliptical pin fin over all duct case.

Heat transfer effect at the first row is more noticeable when compare with the other rows. And also we can see that local nusselts number increases as row increases. Effect of heat transfer at the downstream of the last row and around the pin fin considerably enhanced. When we are using steam as coolant it can take the full advantage of good thermal conductivity coefficient and large specific heat. Thus we can see that heat transfer effect on the upper and lower end walls are increase significantly.

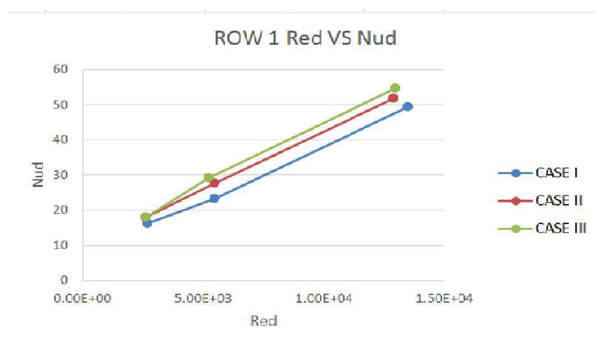

Red vs Nud for circular pin row 1

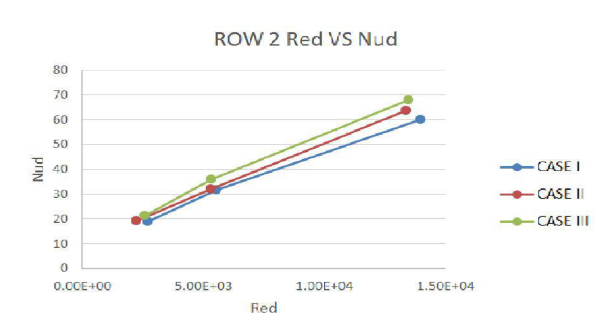

Red vs Nud for circular pin fin row 2

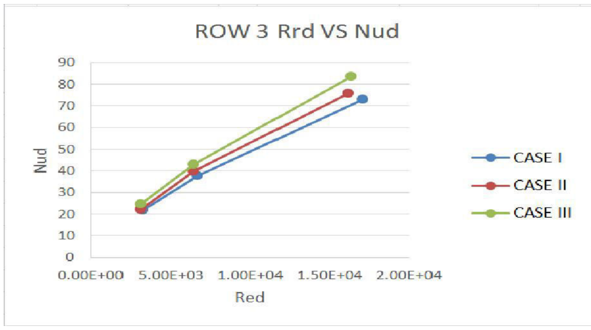

Red vs Nud for circular pin row 3

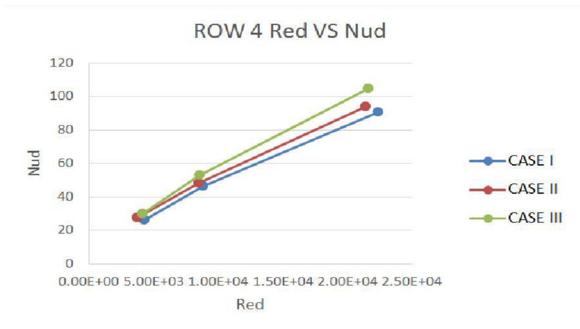

Red vs Nud for circular pin fin row 4

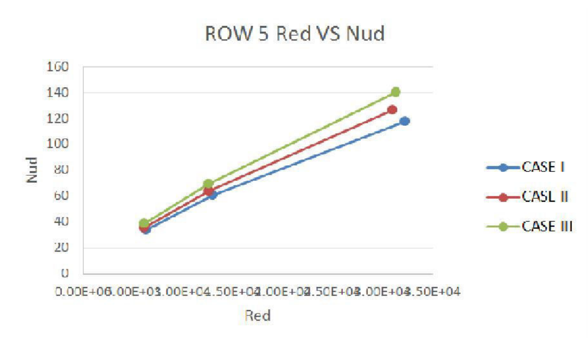

Red vs Nud for circular pin fin row 5

By analyzing all these results we can understand that steam as coolant having more thermal performance than air. Distribution of temperature near the wall especially near the last rows of our pin fins placed in the wedge duct is improved. As Reynolds number is increasing nusselts number also increasing.

VI. CONCLUSION

Numerical comparison of thermal analysis of elliptical pin fin and circular pin fin arranged in a wedge duct has been carried and following conclusions can be drawn from the numerical investigations.

For circular pin-fin at Re 20000 air 65 degree Celsius having more nusselts number when compare with air at 100 degree Celsius.

When comparing coolant cases of steam and air. Steam shows more thermal performance than air. When comparing steam performance coefficient of steam increased by almost 17%.

When elliptical pin fins and circular pins compared, elliptical pin fins having more thermal performance. In a straight wedge duct, due to the flow acceleration effects heat transfer coefficients of the end wall increase with the increasing row number.

We know that velocity is inversely proportional to temperature and pressure. When velocity of the flowing coolant is less coolant flows more time on the pin fins. There by reducing the temperature of the blade. Since coolant contact time with the end wall is high heat transfer rate also becomes high.

Performance of steam as coolant is high when compared with air as coolant. Steam has water droplets. This water droplets are also absorbs heat from blade or end walls. Thus reducing or keeping the temperature of the blade wall at a desired value.

VII. References

[1] V.Ganeshan, “Gas turbines” Third Edition, Tata McGraw Hill,2010

[2] Saravanamutto0,H.Cohen,GFC Rogers, “Gas Turbine Theory” Fifth edition, Pearson

[3] S.L.Dixon and C.A Hall, “fluid mechanics and thermodynamics of turbomachinery”, Seventh edition,Butterworth-Heinemann.

[4] Yunus A Cengel; Afshin J. Ghajar , “Heat and Mass Transfer: Fundamentals and Applications.”, Fifth Edition inSI Units, Special Indian Edition, , Tata McGraw Hill.

[5] P.K.Nag, “Engineering Thermodynamics”, Fifth Edition,2013, , Tata McGraw Hill.

[6] R.K.Rajput, “Fluid Mechanics and Hydraulic Machines.”, Sixth Edition, S.Chand Publications.

[7] J.J. Hwang, C.C. Lui, “Measurement of end wall heat transfer and pressure drop in a pin–fin wedge duct.” Int. J. Heat Mass Transfer 45 (2002) 877–889.

[8] E.M. Sparrow, J.W. Ramsey, “Heat transfer and pressure drop for a staggered Wall-attached array of cylinders with tip clearance.” Int. J. Heat Mass Transfer 21 (1978) 1369–1377.

[9] A. Zukauskas, “Heat transfer from tubes in cross flow.”Adv. Heat Transfer 8 (1972) 93–160.

[10] C. Wang, “Internal cooling of blades and vanes on gas turbine.” Project Report, 2013.

[11] S.W. Chang, A.W. Lees, “End wall heat transfer and pressure drop in scale roughened Pin–fin channels.” Int. J. Therm. Sci. 49 (2010) 702–713.

[12] M.K. Chyu, V. Natarajan, “Heat transfer on the base surface of three-dimensional protruding elements.” Int. J. Heat Mass Transfer 39 (1996) 2925–2935.

[13] S.Y. Won, G.I. Mahmood, P.M. Ligrani, “Spatially-resolved heat transfer and flow Structure in a rectangular channel with pin fins.” Int. J. Heat Mass Transfer 47 (2004) 1731–1743.

[14] D.E. Metzger, R.A. Berry, J.P. Bronson, “Developing heat transfer in rectangular ducts with staggered arrays of short pin fins.” In: ASME Paper No. 81-WA/HT-6, ASME Winter Annual Meeting, Washington, DC, 1981.

[15]M.R Vijayalakshmi & Ashok kumar mondal gtre,drdo. “Over view of NDT methods applied on an aero engine turbine rotor blade.”

[16]R.S Amano, “Advances in gas turbine blade cooling technology.” University of Wisconsin- USA.

MODELING AND ANALYSIS OF COMPOSITE PLATE USING DIFFERENT ANSYS ELEMENTS

1. **GINNARAM VISHNUVARDHAN,**M.tech CAD/CAM **2. I.PRASANNA,** Assistant Professor, MECH Dept
vishnuginnaram@gmail.com, prasannabobba81@gmail.com
MALLA REDDY COLLEGE OF ENGINEERING
Maisammaguda, Dhulapally, Secunderabad,Hyderabad,India

ABSTRACT

Composite materials (likewise called arrangement materials or abbreviated to composites) are materials produced using at least two constituent materials with altogether unique physical or synthetic properties, that when consolidated, create a material with qualities not quite the same as the individual segments. The individual parts stay partitioned and particular inside the completed structure. The new material might be favored for some reasons: basic illustrations incorporate materials which are more grounded, lighter or more affordable when contrasted with conventional materials. In this venture the basic examination. A square cross employ overlaid plate is subjected with the particular limit conditions and accepting axisyymentry properties and orthotropic material properties. The diversions, stresses, and extensive outcomes are gotten and plotted.

INTRODUCTION

A composite material is made by consolidating at least two materials – frequently ones that have altogether different properties. The two materials cooperate to give the composite special properties. In any case, inside the composite you can without much of a stretch distinguish the distinctive materials one from the other as they do notdissolve or mix into each other.A composite material can be characterized as a mix of a network and a support, which when consolidated gives properties better than the properties of the individual parts.

Uses of composites on airplane include:

• Fairings
• Flight control surfaces
• Landing gear entryways
• Leading and trailing edge boards on the wing and stabilizer
• Interior parts
• Floor bars and planks of flooring
• Vertical and level stabilizer essential structure on extensive airplane
• Primary wing and fuselage structure on new era extensive airplane
• Turbine motor fan sharp edges
• Propellers

Significant Components of a Laminate:

- Quality Characteristics
- Fiber Orientation
- Twist Clock
- Fiber Forms
- Wandering
- Unidirectional (Tape)
- Bidirectional (Fabric)
- Nonwoven (Knitted or Stitched)

Types of Fiber:

- Fiberglass
- Carbon/Graphite
- Boron
- Fired Fibers
- Lightning Protection Fibers

Matrix Materials:

- Thermosetting Resins
- Polyester Resins
- Vinyl Ester Resin
- Phenolic Resin
- Epoxy
- Polyimides
- Polybenzimidazoles (PBI)
- Bismaleimides (BMI)
- Thermoplastic Resin
- Semicrystalline Thermoplastics
- Indistinct Thermoplastics
- Polyether Ether Ketone (PEEK)

FINITE ELEMENT METHOD

Step by Step Procedure:

1. Discretization of the area
2. Fundamental Element Shapes
3. Size of Elements
4. Area of Nodes
5. Number of Elements

Advantages:

1. The utilization of partitioned sub locales or limited components for the trail arrangements allows a more prominent adaptability in considering continuation of complex shape.
2. As the limit conditions don't go into conditions for the individual limited components, one can utilize a similar field variable for both inner and limit components.
3. The field variable models require not be changed when the limit conditions change.

Limitations:

1. Cracking and Fracture conduct.
2. Contact issues.
3. Bond disappointments of composite materials.
4. Non-Linear material conduct with work softening.

Applications:

1. Mechanical Design
2. Structural Engineering Structures
3. Air Craft structures
4. Warmth conduction
5. Atomic Engineering

PROCEDURE

PREFERENCES – **STRUCTURAL**:

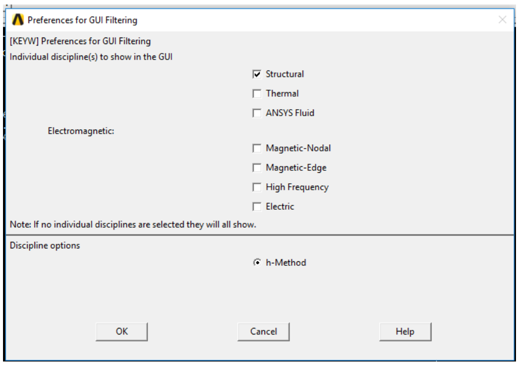

ELEMENT TYPE:

➢ Element type – ADD - SOLID -shell 190

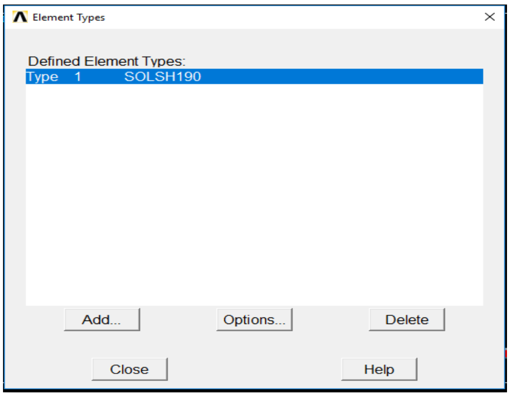

MATERIAL PROPERTIES

➢ STRUCTURAL -LINEAR – ELASTIC - ORTHOTROPIC

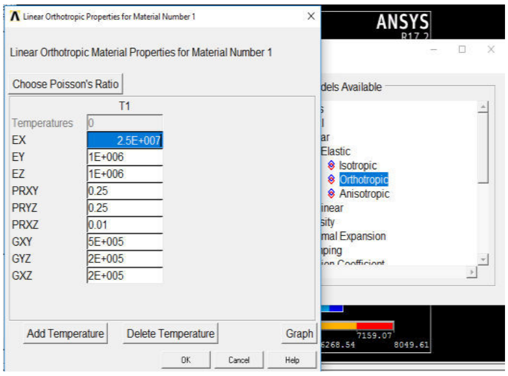

SECTIONS:

➢ **SHELL -** ADD/EDIT

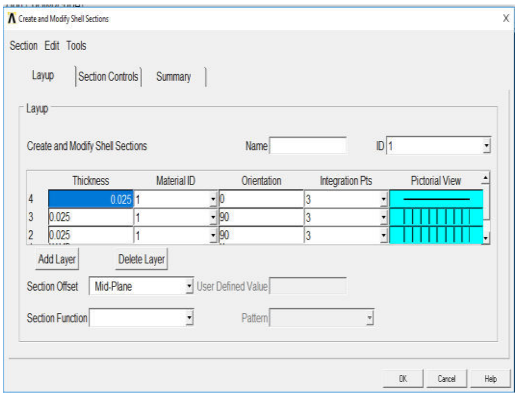

MODELING:

➢ **CREATE –** VOLUMES – BLOCK - BY DIMENSIONS

MESHING:

➢ **VOLUMES –** FREE – SELECT-VOLUME – OK.

LOADS:

➢ **DEFINE LOADS** – APPLY - STRUCTURAL – DISPLACEMENT **-** ON AREAS **-** SELECT THE AREA A4 - UX , UZ & AREA A6 - UY , UZ

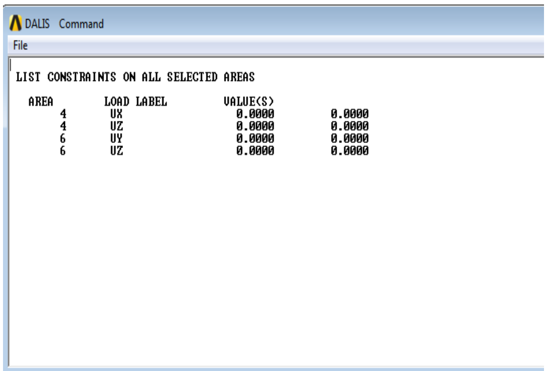

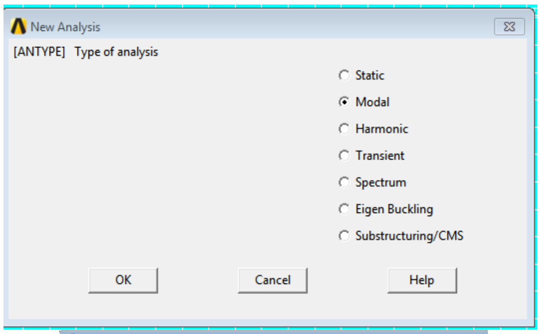

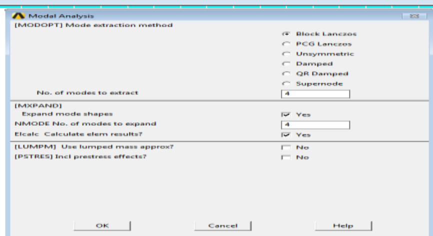

ANALYSIS TYPE:
SOLUTION:

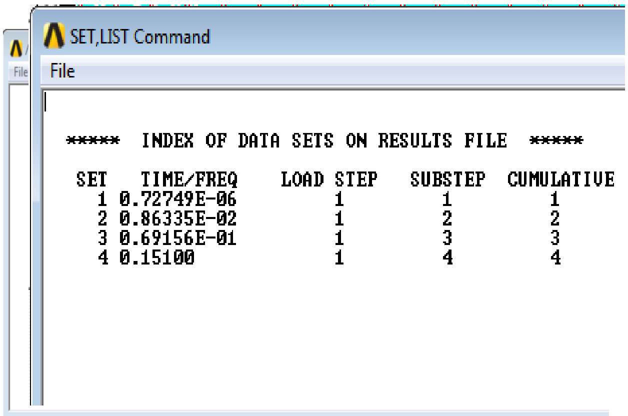
SET,LIST Command
File

```
*****  INDEX OF DATA SETS ON RESULTS FILE  *****

 SET   TIME/FREQ    LOAD STEP   SUBSTEP  CUMULATIVE
   1 0.72749E-06        1          1          1
   2 0.86335E-02        1          2          2
   3 0.69156E-01        1          3          3
   4 0.15100            1          4          4
```

SOLVE - CURRENT LS – OK

RESULTS

SOLSH 190:

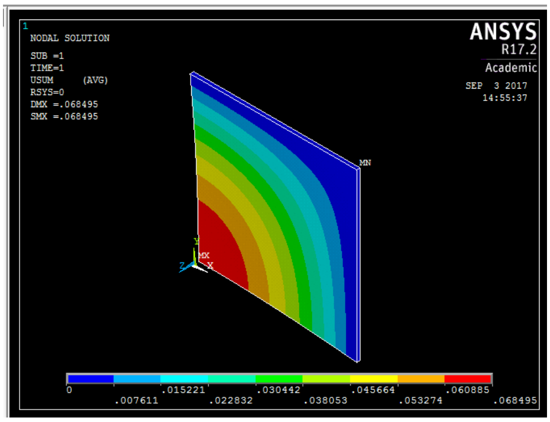

Fig shows total displacement value

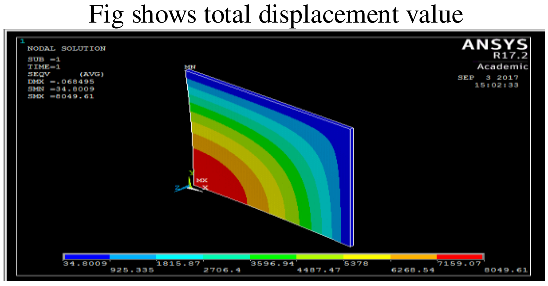

Fig shows Von misses stress value

SOLID 10NODE187:

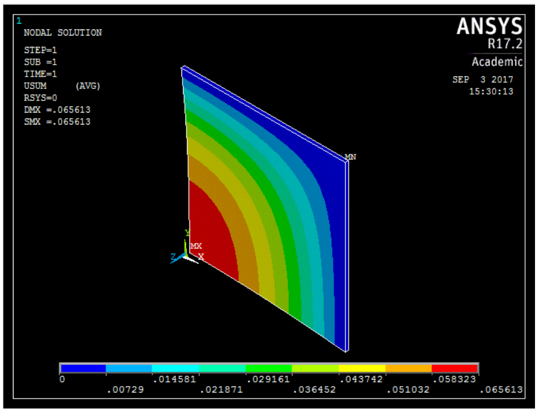

Fig shows total displacement value

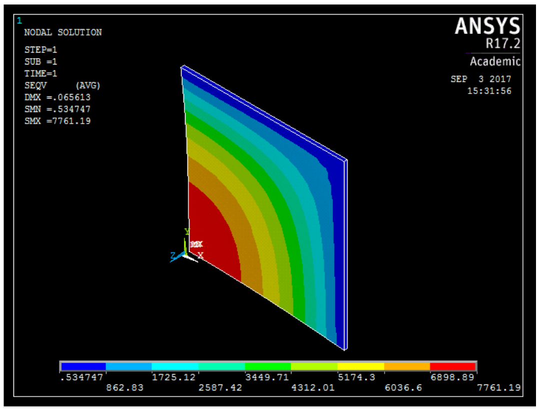

Fig shows Von misses stress value

BRICK8 NODE185:

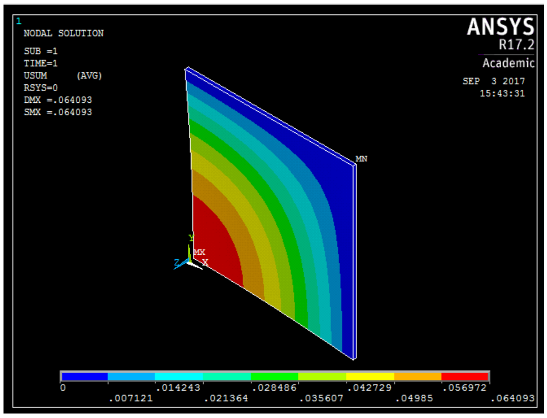

Fig shows total displacement value

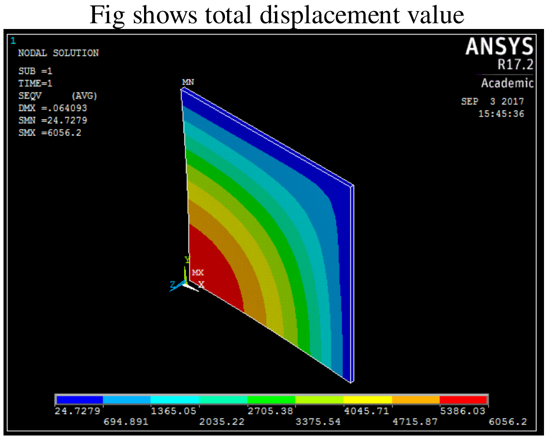

Fig shows Von misses stress value

RESULT:

After performing the model analysis with the 3 different element types.

Element type	Vonmisses stress
Solid shell90	8049.61
Solid 10 node 187	7761.19
Brick node 185	6056.2

CONCLUSION

Composite material can be characterized as a mix of a grid and a support, which when joined gives properties better than the properties of the individual parts. On account of a composite, the support is the strands and is utilized to strengthen the framework as far as quality and firmness. In this undertaking composite material expected with the characterized orthotropic material properties . Rectangular plane territory is displayed and compelled with dislodging and outer burdens are connected. Distortions and streses were created and mode shapes with frequencies of time from the body were recorded and diagrams are plotted.

- Following results shows the maximum vonmisses stress after application of 3 different element types.
- From the above 3 element types brick node 185 has got 6056.2 has suitable element for developing the plate.

REFERENCES

[1] Anderson RA. "Flexural vibration of uniform shafts as indicated by the Timoshenko hypothesis", ASME, J Appl.Mech; 1951; 20; 504– 510.
[2] Dalph CL. "On the Timoshenko hypothesis of transverse shaft vibrations", Quart J. Appl. Math; 1954; 12; 175– 187.
[3] Hermann G. "Constrained vibration of Timoshenko shafts" Trans ASME J Appl. Mech 1955; 77:53– 6.
[4] Archer J. "Steady lattice definition for auxiliary investigation utilizing limited component strategies", AIAAJ; 1965; 1910– 1928.
[5] Cowper GR. "On the exactness of Timoshenko's pillar hypothesis", ASME, J. Eng. Mech. Div. 1968; 94; 1447– 1453.
[6] Davis R, Henshell RD, Wanburton GB. "A Timoshenko shaft component. J Sound Vibrat", 1972; 22; 475– 487.
[7] Abarcar R.R. "Cunniff PF. The vibration of cantilever light emissions fortified material", J. Compos Mater; 1972; 6; 504– 517.
[8] Thomas DL, "Wilson JM, Wilson RR. Timoshenko shaft limited components", J Sound Vibrat 1973; 31; 315– 30.
[9] Teh LS, "Hung CC. The vibration of light emissions fortified material" J. Sound Vibrat 1977; 51; 467– 473.
[10] Dawe DJ. "A limited component for vibration examination of Timonshenko shafts", J Sound Vibrat; 1978; 60; 11– 20.
[11] Kant T, "Gupta A. A limited component demonstrate for a high request shear deformable shaft hypothesis", J Sound Vibrat; 1988; 125; 193– 202.
[12] Lee KH, Senthilnathan NR, Lim SP, Chow ST. An enhanced crisscross model for the bowing of overlaid composite plates. Composite Structures; 1990; 15; 137– 148.

MODELING AND ANALYSIS OF PRESSURE VESSEL AT WELDED JOINTS FOR DIFFERENT WELD EFFICIENCIES

Sali.sairam ; Sali.sairam329@gmail.com ; +917382351109
I.PRASANNA; prasannabobba81@gmail.com;+918885214054

ABSTRACT

Pressure vessel cylinders find wide applications in thermal and nuclear power plants, process and chemical industries, in space and ocean depths, and fluid supply systems in industries. Good design practice is allowable pressure for weld strength expressed as weld efficiency. Efficiency is defined as the ratio of longitudinal (axial) strength of a welded joint to the longitudinal strength of pipe or tank shell.

In this thesis, the pressure vessel is designed according to the weld efficiency and analyzed for its strength using Finite Element analysis software ANSYS. Mathematical correlations will be considered for the design of pressure vessel whose design parameters are specified by a company according to the required weld efficiency. Modeling will be done in Pro/Engineer. Structural and fatigue analysis will be done in ANSYS on the welded joint of pressure vessel for different weld efficiencies.

1.1 Introduction to pressure vessels:

The term pressure vessel referred to those reservoirs or containers, which are subjected to internal or external pressures. The pressure vessels are used to store fluids under pressure. The fluid being stored may undergo a change of state inside the pressure vessels as in case of steam boilers or it may combine with other reagents as in chemical plants. Pressure vessels find wide applications in thermal and nuclear power plants, process and chemical industries, in space and ocean depths, and in water, steam, gas and air supply system in industries.

The material of a pressure vessel may be brittle such as cast iron, or ductile such as mild steel.

1.2 HIGH PRESSURE VESSELS:

High Pressure vessels are used for a pressure range of 15 N/mm^2 to a maximum of 300 N/mm^2. These are essentially thick walled cylindrical vessels, ranging in size from small tubes to several meters diameter. Both the size of the vessel and the pressure involved will dictate the type of construction used.

The following are few methods of construction of high-pressure vessels.

1. A solid wall vessel produced by forging or boring a solid rod of metal.
2. A cylinder formed by bending a sheet of metal with longitudinal weld.
3. A vessel built up by wire winding around a central cylinder. The wire is wound under tension around a cylinder of about 6 to 10 mm thick.
4. A vessel built up by wrapping a series of sheets of relatively thin metal tightly round one another over a core tube, and holding each sheet with a longitudinal weld.

Types of High Pressure Vessels

Solid Wall Vessel

Multi Layered Cylindrical Vessel

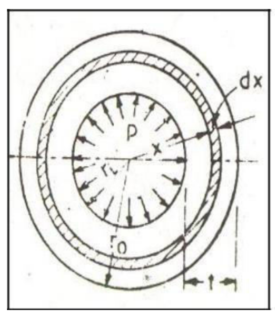

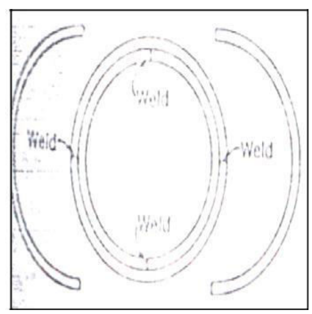

DESIGN PAREMETERS:

The design of solid pressure vessel includes,

(a) Design of Vessel thickness
(b) Design of Dished ends thickness.
(c) Calculation of Hydrostatic Test Pressure
(d) Calculation of Bursting Pressure

DESIGN OF VESSEL THICKNESS (t):

The Vessel holds the fluid under pressure and the tangential stress is taken as design stress. A joint in the longitudinal direction, which is considered in terms of joint efficiency, forms the Vessel.

The thickness of the Vessel is calculated from the equation

$$t \quad R_i \, [\sqrt{\frac{(S\,J \quad P)}{(SJ - P)}} \text{ -1]} \quad C.A$$

$$t \quad 1143 \, [\sqrt{\frac{(123 \times 1 \quad 21)}{(123 \times 1 - 21)}} \text{ -1]} \quad 3.0$$

= 219 mm

Thickness of Solid Wall Vessel, t = 219 mm

DESIGN OF HEMISPHERICAL DISHED END:

The thickness of the dished end is given by

$$t_d \quad \frac{P\,R_i}{2\,S\,J \quad 0.2\,P} \quad C.A$$

$$t_d \quad \frac{21 \times 1143}{2 \times 123 \times 1.0 \; 0.2 \times 21} \quad 3.0$$

= 102.26 mm

Adopted Thickness of the dished end is, t_d = 219 mm.

CALCULATION OF HYDROSTATIC TEST PRESSURE

The hydrostatic pressure is taken as 1.3 times the design pressure.

$$P_H \quad 1.3\text{x Design Pressure}$$

= 1.3 * 21

= 27.3 N/mm^2

STRESS DEVELOPED DURING HYDROSTATIC TEST: (i) In Vessel

The Stress developed inside the vessel is calculated from the equation,

$$tR_i \, [\sqrt{\frac{(S\,J \quad P)}{(SJ - P)}} \text{ -1]}$$

$$219 \; 1143 \, [\sqrt{\frac{(S * 1.0 \quad 27.3)}{(S * 1.0 - 27.3)}} \text{ -1]}$$

S = 157.33 N/mm^2.

The stress developed (157.33 N/mm^2) is less than the allowable stress value (267.6N/mm^2)

In Dished End

The Stress developed inside the Dish is given by the equation,

$$S_{HD} \quad \frac{27.3 \times 1143 \quad 0.2 \times 27.3 \times 219}{2 \times 219}$$

$$S_{Hd} \quad \frac{P_H \; R_i \quad 0.2\,P_H \; t}{2 * t}$$

=73.97 N/mm^2

The stress developed (73.97 N/mm^2) is less than the allowable stress value (267.6N/mm^2)

CALCULATION OF BURSTING PRESSURE (P_B):

U.T.S is Ultimate Tensile Strength of the material = 492 N/mm^2

K = Outer Diameter / Inner Diameter
= 2724 / 2286 = 1.191

The bursting pressure is calculated as per Lame's method

$$P_B \quad U.T.S \times \frac{K^2 - 1}{K^2 \quad 1} \quad 85.37 \text{ N/mm}^2$$

Stress Developed During Bursting Test :

The Stress developed inside the Dished ends is given by the equation,

$$S_{Bd} \quad \frac{P_B \; R_i \quad 0.2\,P_B \; t}{2 \times t}$$

$$S_{HD} \quad \frac{85.37 \times 1143 \quad 0.2 \times 85.37 \times 219}{2 \times 219}$$

S = 231 .06 N/mm^2

The stress developed (231.06 N/mm^2) is less than the allowable stress value (267.6 N/mm^2).

Hence it is safe.

DIFFERENT MODULES IN PRO/ENGINEER

- PART DESIGN
- ASSEMBLY
- DRAWING
- SHEETMETAL
- MANUFACTURING

CHAPTER 4

STATIC ANALYSIS OF PRESSURE VESSEL

4.1 CASES

Case 1: welding efficiency -1.0

Case 2: weld

USED MATERIALS

Steel
S2 glass fiber
E –glass fiber

Material properties of steel

Young's modulus=205000Mpa

Poisson's ratio=0.3

Density=0.0000078kg/mm^3

Material properties of S2 glass fiber

Young's modulus=89000Mpa

Poisson's ratio=0.23

Density=0.00000249kg/mm^3

Material properties of e-glass fiber

Young's modulus=80000Mpa

Poisson's ratio=0.21

Density=0.00000255kg/mm^3

CASE 1: WELDING EFFICIENCY -1.0

MATERIAL -STEEL

Used software for this project work bench

Open work bench in Ansys 14.5

Select static structural>select geometry>import IGES model>OK

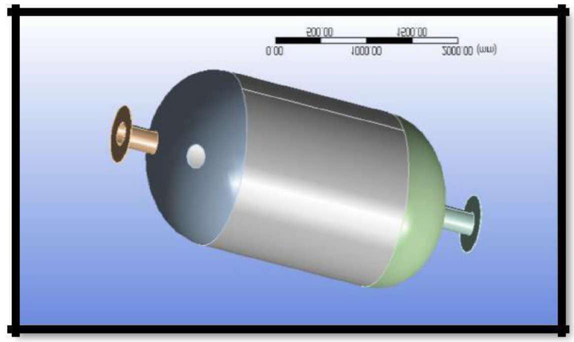

Fig 4.1 Pressure vessel (steel)

Click on model>select EDIT

Select model >apply materials to all the objects (different materials also) Mesh> generate mesh>ok

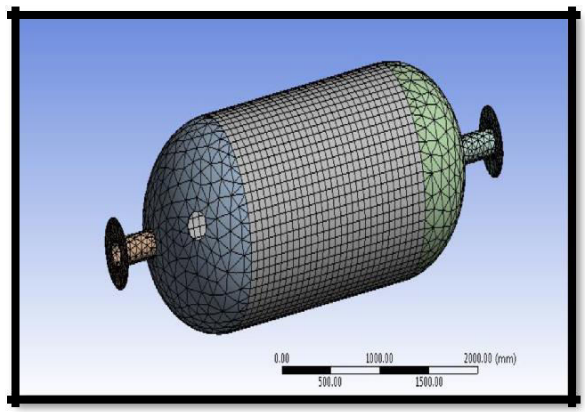

Fig 4.2 Mesh Generation

Finite element analysis or FEA representing a real project as a "mesh" a series of small, regularly shaped tetrahedron connected elements, as shown in the above fig. And then setting up and solving huge arrays of simultaneous equations. The finer the mesh, the more accurate the results but more computing power is required.

Static structural A5>insert>select displacement>select fixed areas>ok

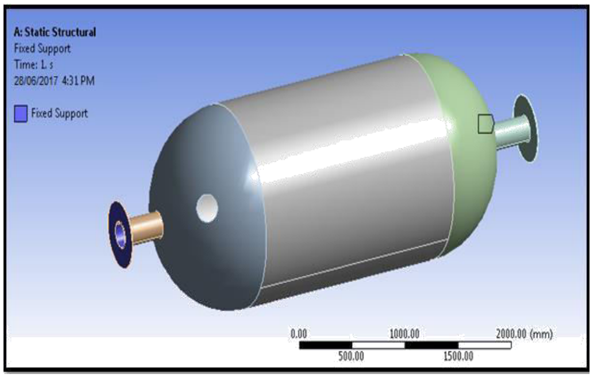

Fig 4.3 Selection of fixed area

>Select pressure>select pressure areas> enter pressure value

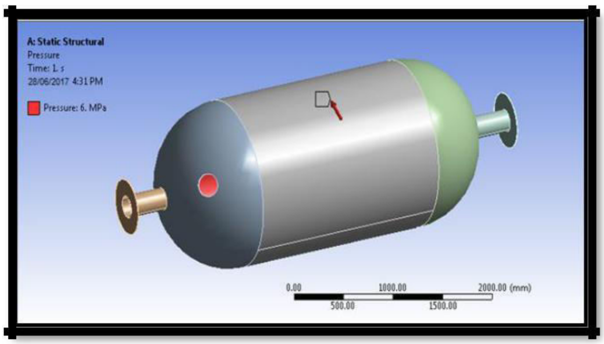

Fig 4.4 Giving pressure to the vessel **Deformation**

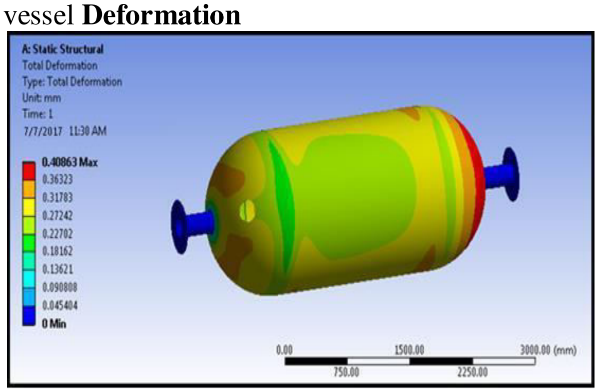

Fig 4.5 Deformation of Pressure vessel maximum deformation is 0.40863 mm and minimum deformation is 0.045404 mm.

Stress

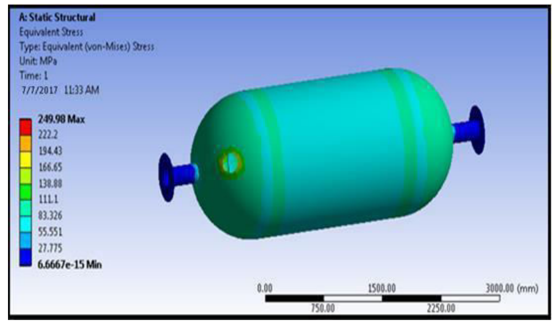

Fig 4.6 Stress Analysis

maximum stress is 249.98 N/mm^2 and minimum is 6.6667e-15.

Strain

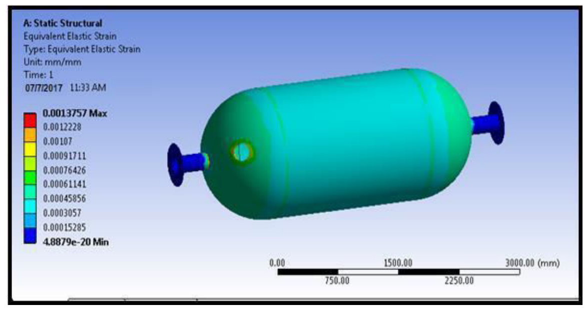

Fig 4.7 Strain Analysis

maximum strain is 0.0013757 and minimum is 4.88e-20.

MATERIAL –S2 GLASS FIBER

Deformation

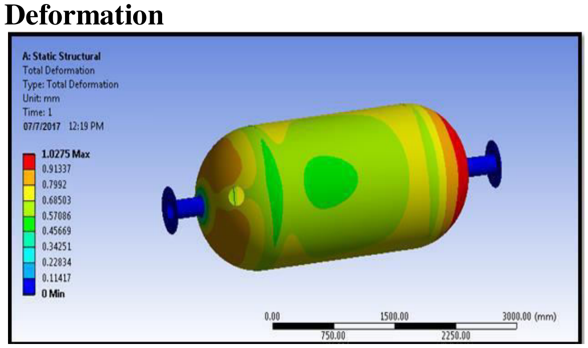

Fig 4.8 Deformation of Pressure vessel

maximum deformation is 1.0275mm and minimum deformation is 0.11417 mm.

Stress

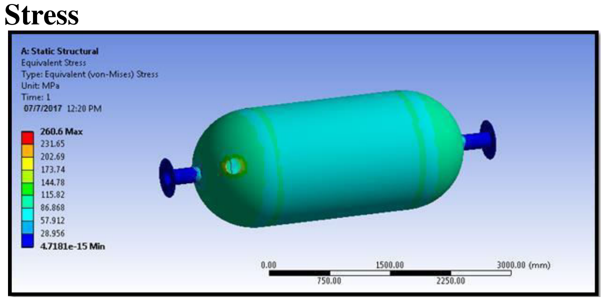

Fig 4.9 Stress Analysis

maximum stress is 260.6 N/mm^2 and minimum is 4.7181e-15.

Strain

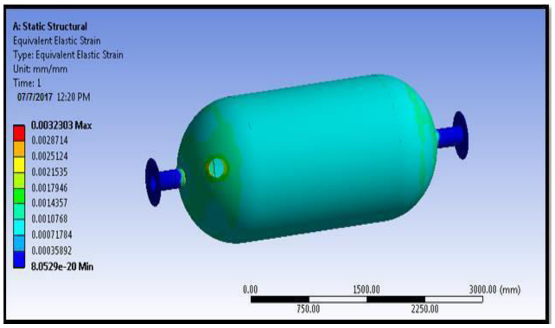

Fig 4.10 Strain Analysis

According To the Counter Plot, the maximum strain is inside of the pressure vessel and minimum strain at nozzles of the pressure vessel. The maximum strain is 0.0032303 and minimum is 8.0529e-20.

MATERIAL –E GLASS FIBER Deformation

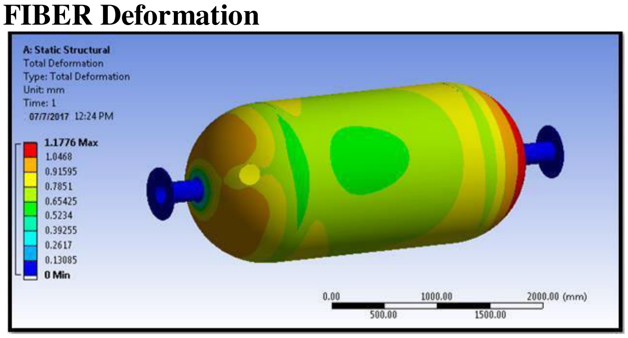

Fig 4.11 Deformation of Pressure vessel

maximum deformation is 1.1776 mm and minimum deformation is 0.13085 mm.

Stress

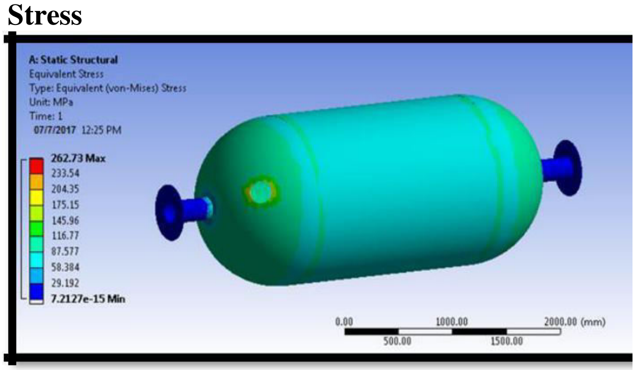

Fig 4.12 Stress Analysis

maximum stress is 262.73 N/mm^2 and minimum is 7.2127e-15.

Strain

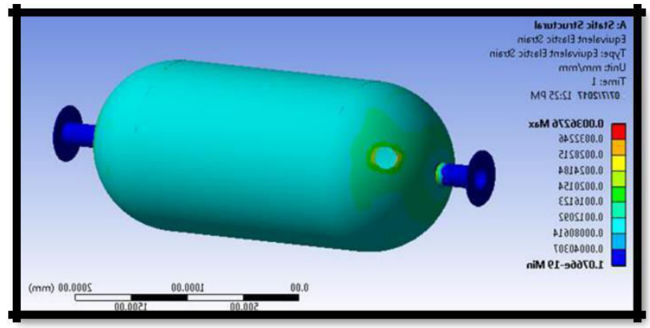

Fig 4.13 Strain Analysis

maximum strain is 0.0036276 and minimum is 1.0766e-19.

CASE 2: WELDING EFFICIENCY -0.85

Similarly at weld efficiency 0.85 also I have done the same thing for the following materials and I found the results as,

MATERIAL -STEEL

Deformation

Similarly at weld efficiency 0.85, maximum deformation is 0.29397 mm and minimum deformation is 0.032663 mm.

Stress

maximum stress is 84.938 N/mm^2 and minimum is 2.8489e-15.

Strain

maximum strain is 0.00041433 and minimum is 5.5923e-20.

MATERIAL –S2 GLASS Deformation

maximum deformation is 0.66446 mm and minimum deformation is 0.073829 mm.

Stress

maximum stress is 85.529 N/mm^2 and minimum is 3.3929e-15.

Strain

maximum strain is 0.000961 and minimum is 3.9697e-20.

MATERIAL –E GLASS FIBER

Deformation

maximum deformation is 0.73561mm and minimum deformation is 0.081735 mm.

Stress

maximum stress is 85.691 N/mm^2 and minimum is 4.0675e-15.

Strain

maximum strain is 0.0010711 and minimum is 5.245e-20.

CHAPTER 5
FATIGUE ANALYSIS OF PRESSURE VESSEL

5.1 CASE 1: WELDING EFFICIENCY -1.0
5.1.1 MATERIAL -
STEEL Life
maximum life is 1e10 and minimum life is 1.1745e8.
Damage
maximum damage is 8.5139 and minimum life is 0.1.
Safety factor
Safety factor of Pressure maximum safety factor is 15 and minimum life is 0.55205
5.1.2 MATERIAL –S2 GLASS
Life
Maximum life is 1e10 and minimum life is1.0185e8.

Damage
maximum damage is 9.8187 and minimum life is 0.1.
Safety factor
maximum safety factor is 15 and minimum life is 052954.
5.1.3 MATERIAL –E GLASS
FIBER Life
maximum life is 1e10 and minimum life is 9.9144e
Damage
maximum damage is 10.086 and minimum life is 0.1.
Safety factor
maximum safety factor is 15 and minimum life is 0.52525

5.2 CASE 2: WELDING EFFICIENCY -0.85

Similarly at weld efficiency 0.85 also I have done the same thing for the following materials and I found the results as,
5.2.1 MATERIAL -
STEEL Life
maximum life is 1e10 and minimum life is 3.4361e8.
Damage
maximum damage is 2.9103 and minimum life is 0.1.
Safety factor
maximum safety factor is 15 and minimum life is 0.74737
MATERIAL –S2 GLASS
Life
maximum life is 1e10 and minimum life is 3.3499e8
Damage
maximum damage is 2.9852 and minimum life is 0.1.
Safety factor
maximum safety factor is 15 and minimum life is 0.74221.
5.2.3 MATERIAL –E GLASS

FIBER Life

maximum life is 1e10 and minimum life is 3.3266e8
Damage
maximum damage is 3.006 and minimum life is 0.1.
Safety factor
maximum safety factor is 15 and minimum life is 0.7408.
CHAPTER 6
LINEAR LAYER STATIC ANALYSIS OF PRESSURE VESSEL
6.1 CASE 1: WELDING EFFICIENCY -1.0
6.1.2 MATERIAL -STEEL
3 LAYERS
Used software for this project work
bench Open work bench in Ansys 14.5

Select static structural>select geometry>import IGES model>OK

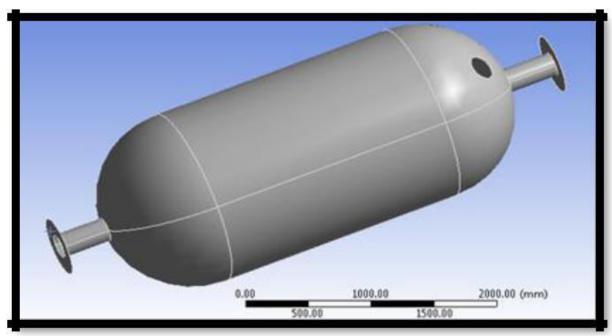

Fig 6.1 Modeling of Pressure
vessel Click on model>select EDIT
Select geometry> right lick >layered selection>select object>work sheet >entered no.of layers

Select model >apply materials to all the objects (different materials also)

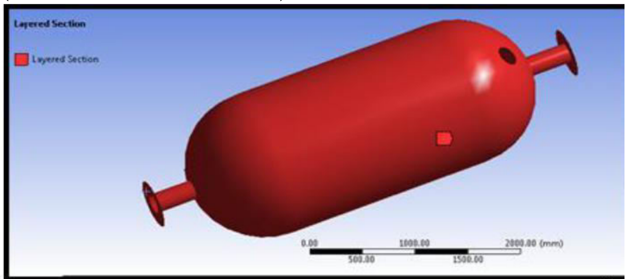

Layer	Material	Thickness (mm)	Angle (°)
(+Z)			
3	Structural Steel	15.98	-90
2	s2	15.98	0
1	e glass	15.98	90
(-Z)			

Fig 6.2 Layered selection

Mesh> generate mesh>ok

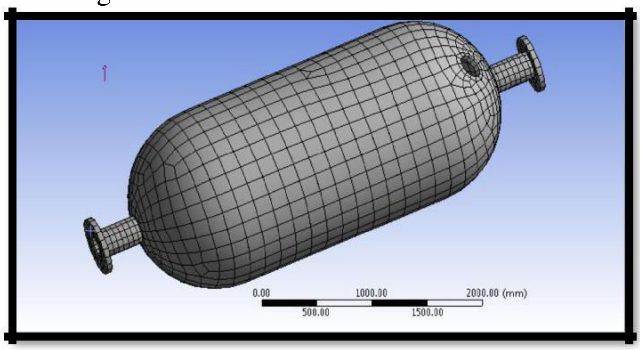

Fig 6.3 mesh generation

Finite element analysis or FEA representing a real project as a "mesh" a series of small, regularly shaped tetrahedron connected elements, as shown in the above fig. And then setting up and solving huge arrays of simultaneous equations. The finer the mesh, the more accurate the results but more computing power is required.

Static structural A5>insert>select .displacement>select

fixed areas>ok

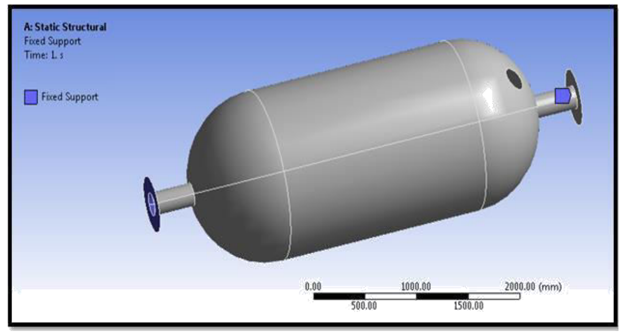

Fig 6.4 selection of fixed area

>Select pressure>select pressure areas> enter pressure value

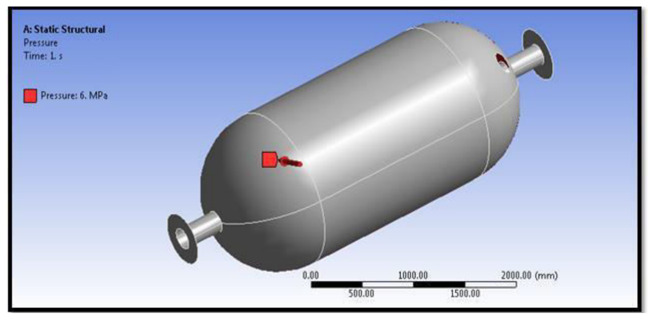


``````Fig 6.5 Entering the pressure value

Solution A6>insert>total deformation>right click on total deformation>select evaluate all result Insert>stress>equivalent (von misses)>right click on equivalent >select evaluate all results
Insert>strain>equivalent (von misses)>right click on equivalent >select evaluate all results.

**Deformation**

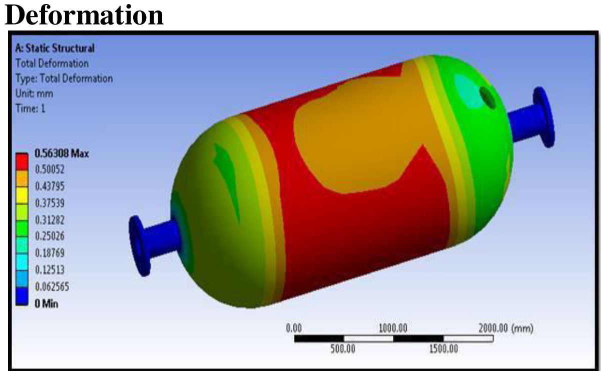


Fig 6.6 Deformation of Pressure vessel
``````

maximum deformation is 0.56308 mm and minimum deformation is 0.062565 mm.

Stress

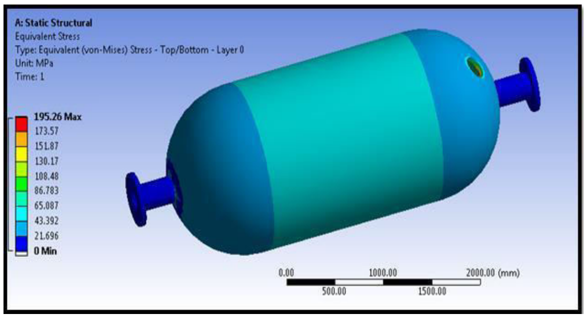

Fig 6.7 Stress Analysis

maximum stress is 195.26 N/mm^2 and minimum is 21.696.

Strain

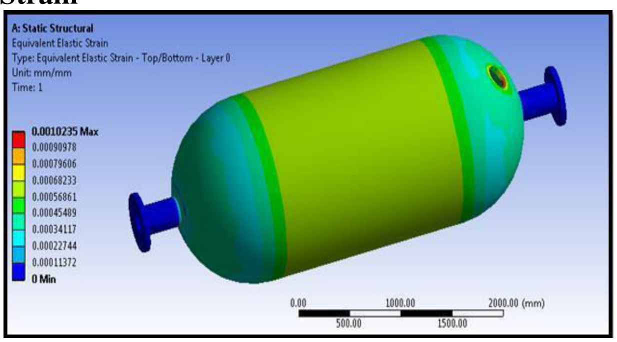

Fig 6.8 Strain Analysis

maximum deformation is 0.5684 mm and minimum deformation is 0.063156 mm.maximum strain is 0.0010235 and minimum is 0.00011372.

6 LAYERS

Layer stacking

Layer	Material	Thickness (mm)	Angle (°)
(+Z)			
6	Structural Steel	7.9	-90
5	s2	7.9	0
4	e glass	7.9	0
3	Structural Steel	7.9	0
2	s2	7.9	0
1	e glass	7.9	90
(-Z)			

Deformation

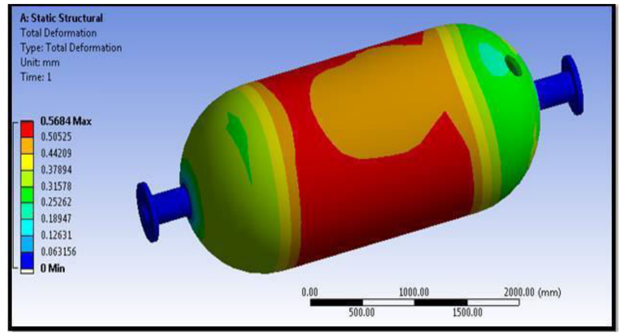

Fig 6.9 Deformation of Pressure vessel

Stress

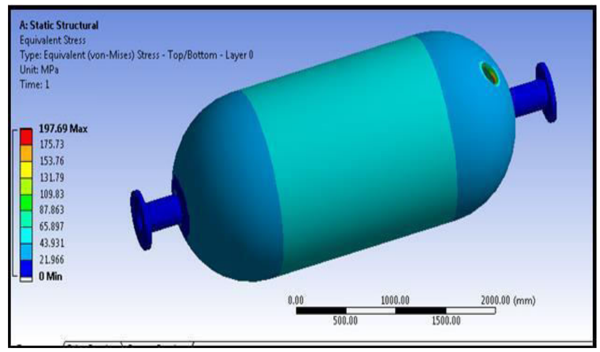

Fig 6.10 Stress Analysis

maximum stress is 197.69 N/mm^2 and minimum is 21.966.

Strain

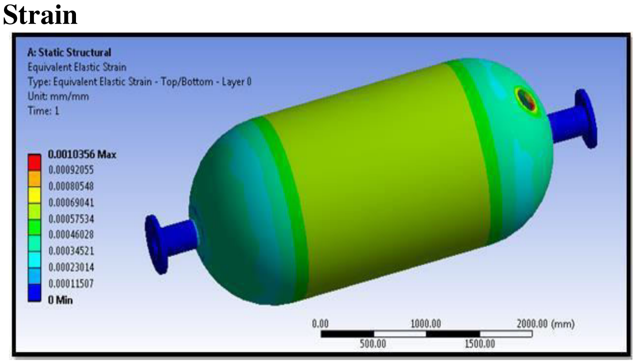

Fig 6.11 Strain Analysis

maximum strain is 0.0010356 and minimum is 0.00011507

9 layers Layer stacking

Layer	Material	Thickness (mm)	Angle (°)
(+Z)			
9	Structural Steel	5.32	-90
8	s2	5.32	0
7	e glass	5.32	0
6	Structural Steel	5.32	0
5	s2	5.32	0
4	e glass	5.32	0
3	Structural Steel	5.32	0
2	s2	5.32	0
1	e glass	5.32	90
(-Z)			

Deformation

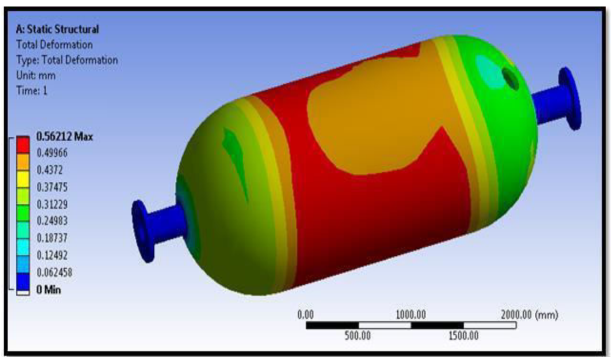

Fig 6.12 Deformation of Pressure vessel

maximum deformation is 0.56212 mm and minimum deformation is 0.062458 mm

Stress

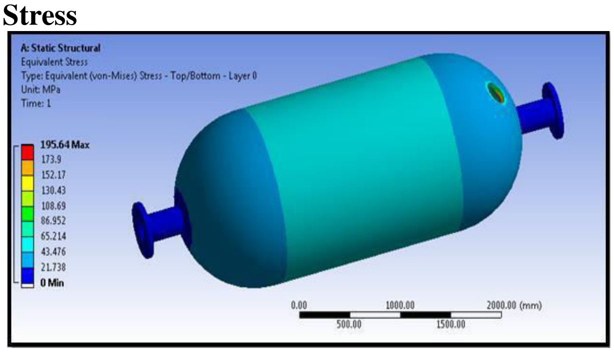

Fig 6.13 Stress Analysis

maximum stress is 195.64 N/mm^2 and minimum is 21.738.

Strain

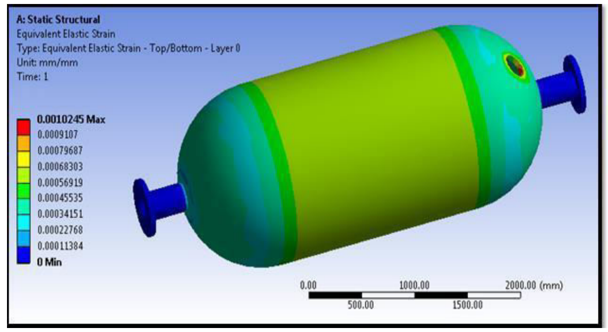

Fig 6.14 Strain Analysis

maximum strain is 0.0010245 and minimum is 0.00011384

12 layers

Layer stacking

Layer	Material	Thickness (mm)	Angle (°)
(+Z)			
12	Structural Steel	3.995	-90
11	s2	3.995	0
10	e glass	3.995	0
9	Structural Steel	3.995	0
8	s2	3.995	0
7	e glass	3.995	0
6	Structural Steel	3.995	0
5	s2	3.995	0
4	e glass	3.995	0
3	Structural Steel	3.995	0
2	s2	3.995	0
1	e glass	3.995	90
(-Z)			

Deformation

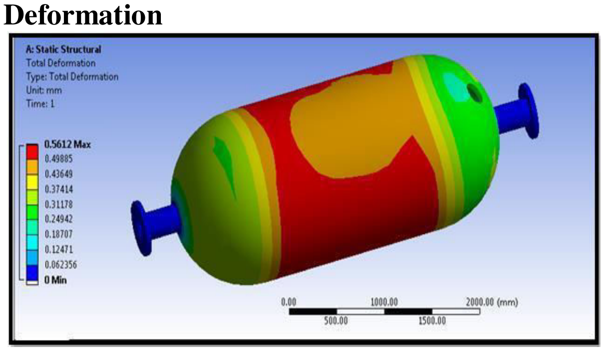

Fig 6.15 Deformation of Pressure vessel

maximum deformation is 0.5612 mm and minimum deformation is 0.062356 mm.

Stress

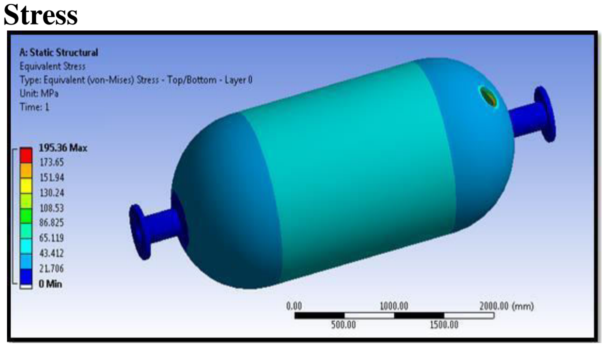

Fig 6.16 Stress Analysis

maximum stress is 195.36 N/mm^2 and minimum is 21.706.

Strain

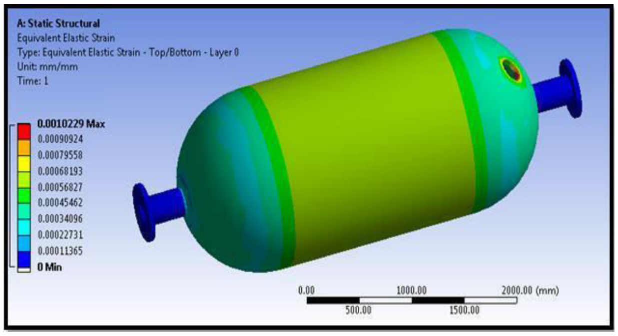

Fig 6.17 Strain Analysis

maximum strain is 0.0010229 and minimum is 0.00011365

6.2 CASE 2: WELDING EFFICIENCY -0.85

6.2.1 MATERIAL -STEEL

3 LAYERS

Deformation

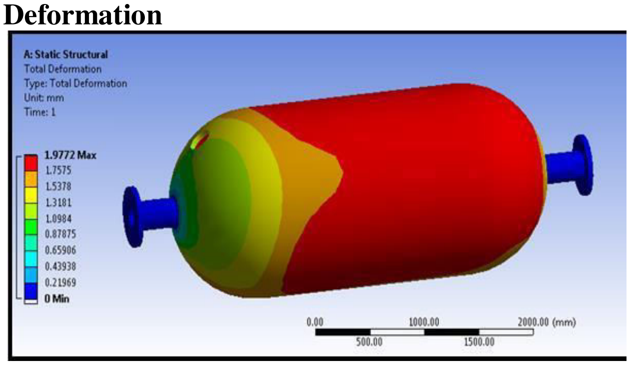

Fig 6.18 Deformation of Pressure vessel

maximum deformation is 1.9772 mm and minimum deformation is 0.21969 mm.

Stress

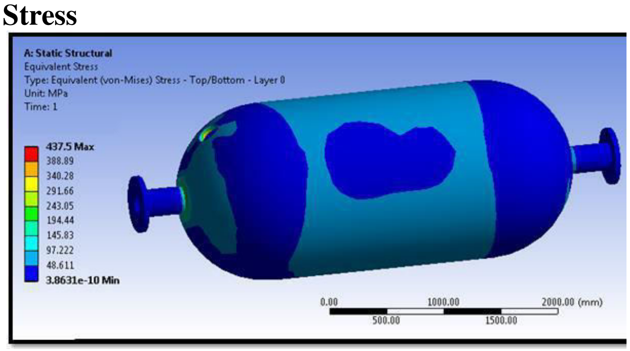

Fig 6.19 Stress Analysis

maximum stress is 437.5 N/mm^2 and minimum is 3.8631e-10.

Strain

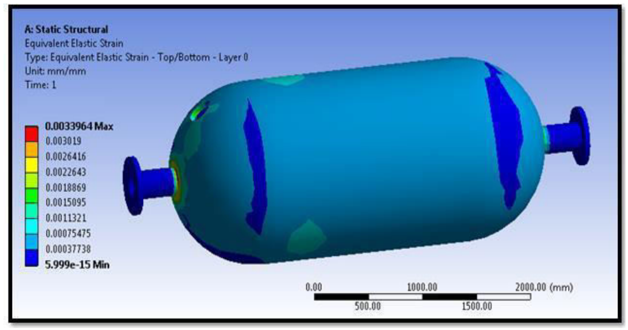

Fig 6.20 Strain Analysis

maximum strain is 0.0033964 and minimum is 5.999e-15

6 LAYERS

Deformation

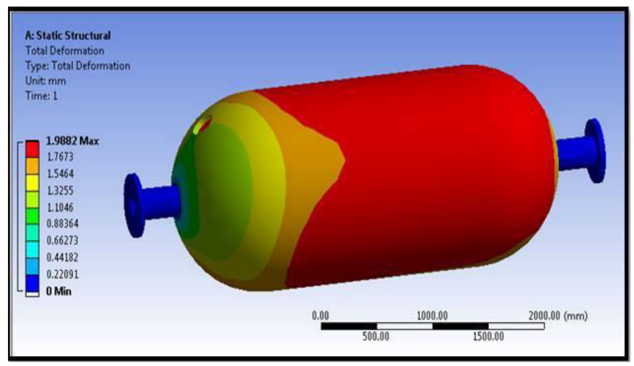

Fig 6.21 Deformation of Pressure vessel

maximum deformation is 1.9882 mm and minimum deformation is 0.22091 mm.

Stress

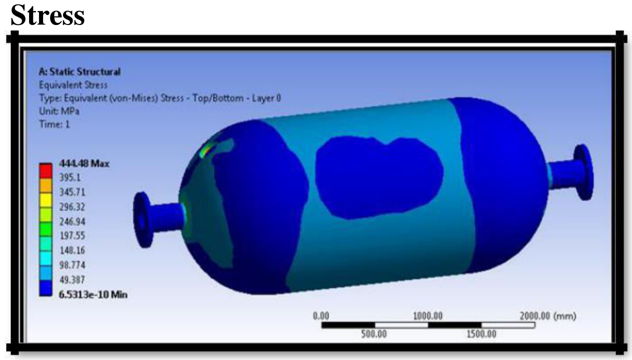

Fig 6.22 Stress Analysis

maximum stress is 444.48 N/mm^2 and minimum is 6.5313e-10.

Strain

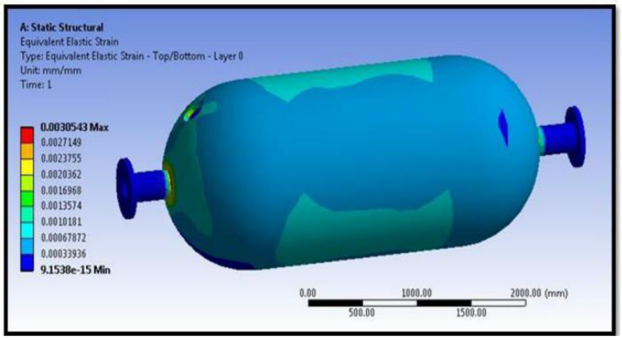

Fig 6.23 Strain Analysis

maximum strain is0.0030543 and minimum is 9.1538e-15

9 LAYERS

Deformation

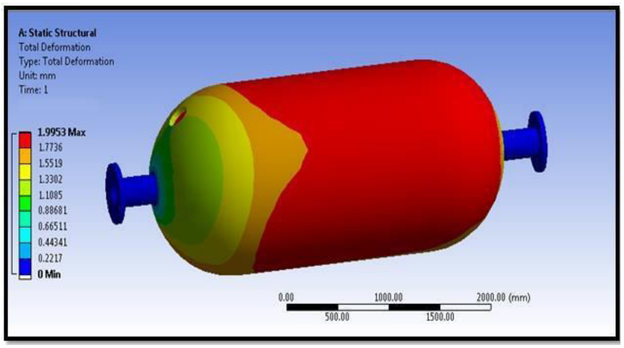

s Fig 6.24 Deformation of Pressure vessel

maximum deformation is 1.9953 mm and minimum deformation is 0.2217 mm.

Stress

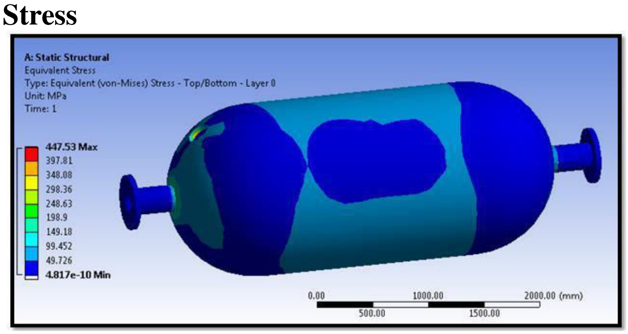

Fig 6.25 Stress Analysis

maximum stress is 447.53 N/mm^2 and minimum is 4.817e-10.

Strain

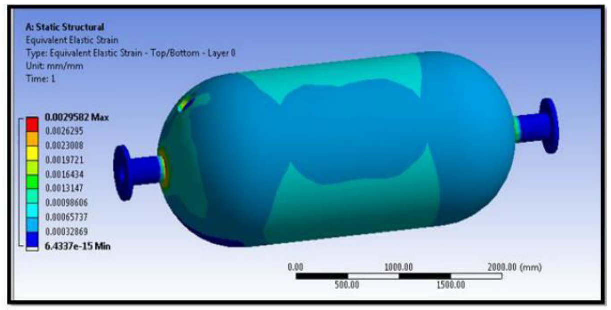

Fig 6.26 Strain Analysis

maximum strain is 0.0029582 and minimum is 6.4337e-15

12 LAYERS

Deformation

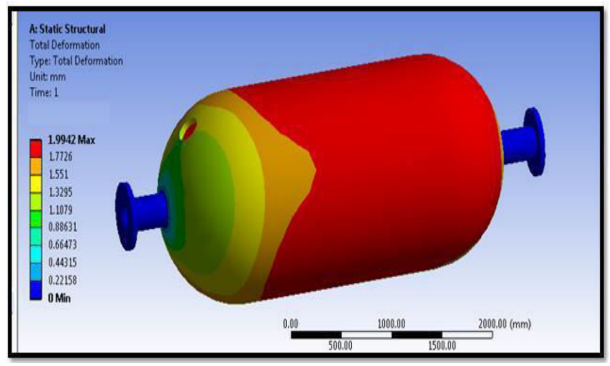

Fig 6.27 Deformation of Pressure vessel

maximum deformation is 1.9942 mm and minimum deformation is 0.022158 mm.

Stress

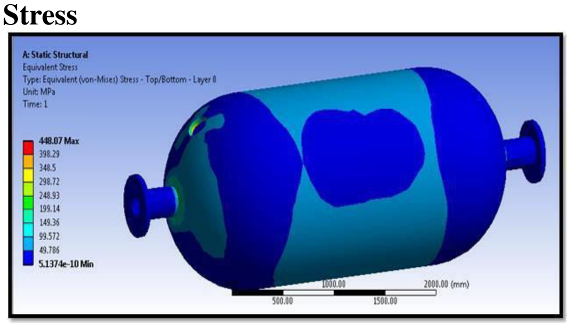

Fig 6.28 Stress Analysis

maximum stress is 448.07 N/mm^2 and minimum is5.1374e-10.

Strain

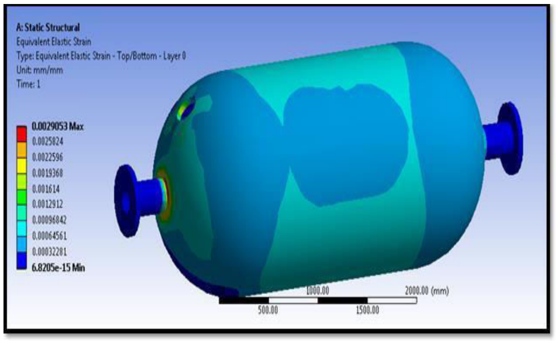

Fig 6.29 Strain Analysis

maximum strain is 0.0029053 and minimum is 6.8205e-15

CHAPTER 7

RESULT TABLES

TABLE 1: LINEAR LAYER STATIC ANALYSIS RESULT TABLES

Cases	**Layer stacking**	**Deformation (mm)**	**Stress (N/mm^2)**	**Strain**
Welding efficiency - 1.0	**3**	0.56308	195.26	0.0010235
	6	0.5684	197.69	0.0010356
	9	0.56212	195.64	0.0010245
	12	0.5612	195.36	0.0010229
Welding efficiency - 0.85	**3**	1.9772	437.5	0.0033964
	6	1.9882	444.48	0.0030543
	9	1.9953	447.53	0.0029582
	12	1.9942	448.07	0.0029053

TABLE 2:

STATIC ANALYSIS RESULT TABLES

Cases	**Material**	**Deformation (mm)**	**Stress (N/mm^2)**	**Strain**
Welding efficiency - 1.0	**Steel**	0.40863	249.98	0.0013757
	S2 glass fiber	1.0275	260.6	0.0032303
	E glass fiber	1.177	262.73	0.0036296
Welding efficiency - 0.85	**Steel**	0.29397	84.938	0.00041433
	S2 glass fiber	0.66446	85.529	0.000961
	E glass fiber	0.73561	85.691	0.0010711

TABLE 3: FATIGUE ANALYSIS RESULT TABLES

Cases	**Material**	**Life**	**Damage**	**Safety factor**	
				Min	**Max**
Welding efficiency - 1.0	**Steel**	1 e10	8.5139	0.55205	15
	S2 glass fiber	1 e10	9.81887	0.52954	15
	E glass fiber	1 e10	10.086	0.52525	15
Welding efficiency - 0.85	**Steel**	1 e10	2.9103	0.74737	15
	S2 glass fiber	1 e10	2.9852	0.74221	15
	E glass fiber	1 e10	3.006	0.7408	15

CHAPTER 8
CONCLUSION

By observing the static analysis the stress values are increased by increasing the welding efficiency. The stress values are less for steel material compare with S2 glass fiber and e-glass fiber. But s-2 glass has more yield strength compared with steel.

By observing the fatigue analysis the safety factor values increases by decreasing the welding efficiency 0.85.

So it can be concluded the s2 glass fiber material is better material for pressure vessel at welding efficiency 0.85.

REFERENCES

[1] Introduction to Finite Element in Engineering,Chandrapatala, Belgunda, third edition PHI;
2012; pp276-286

[2] Design of Machine Elements, V.B. Bhandari; Tata McGraw Hill Publication;2012;

[3] Mechanical System Design, R.B. Patil; Tech. Max Publication; 2012;

[4] Finite Element Analysis – Theory and Applications with ANSYS, SaeedMoaveni; 1999;

[5] Pressure Vessel Design Guides & Procedures. G. GhanbariM.A.Liaghat, 2000;

[6] Calculations of Plastic Collapse Load of Pressure Vessel Using Fea, Peng-FeiLiu,Jin; Institute of Chemical Machinery and Process Equipment, Zhejiang University, Hangzhou 310027, China)

[7] Stress Concentration At Openings In Pressure Vessels – A Review, AvinashKharat1, V.V. Kulkarni2; Research Scholar, Dept. of Production Engineering, K. I. T."S.

[8] Stresses In A Pressurized Ribbed Cylindrical Shell with A Reinforced Hole, A. J.Durelii& V. J. Parks The Journal of Strain Analysis For Engineering Design, 1973, 8, Pp-140-150.;

[9] Pressure Vessel - User's Design SpeciCation, Derek Shuman1, Sara C_Arcel2 A. Mart__Nez2 Berkeley Ca, Usa 2instituto De Fsica Corpuscular (Ific), Csic, Univ. De Valencia, Valencia, Spain, 2 April 2012

[10] Stress Analysis of Reactor Nozzle to Head Junction, A. Hardik B. Nayak and B.R. R. Trivedi; A. Assistant Professor,

DESIGN AND ANALYSIS OF AIRCRAFT WIND SHIELD BY USING FSI TECHNIQUE

KHAZA FAZAL MAHAMMAD
Pg Scholar Mallareddy College Of Engineering
Fazalaffu@Gmail.Com

M. VENKATASWAMY
Assistant Professor,
Mallareddy College Of Engineering
Venkataswamy017@Gmail.Com

ABSTRACT.
The windshield or windscreen of a flying machine, auto, transport, motorbike or cable car is the front window. Windshield is a vital get together of a flying machine and some ace highlights are relied upon its quality. The vital quality attributes of windshield are perceivability through the overhang, structure inflexibility, affect resistance, dependability of the inward instruments, and the delicacy of development. The most generally utilized material for light coach air ship windshield is Glass. In the present work, it is proposed to substitute the current glass for a light mentor. In the present work two unique materials were considered to be specific polymethyl- methacrylate and poly vinyl butyl for windshield

INTRODUCTION

1. WINDSHIELD

The windshield (North America) or windscreen (Commonwealth nations) of an air ship, auto, transport, motorbike or cable car is the front window. Current windshields are for the most part made of covered security glass, a sort of treated glass, which comprises of two (commonly) bended sheets of glass with a plastic layer overlaid between them for wellbeing, and are reinforced into the window outline. Motorbike windshields are regularly had of high-effect acrylic plastic.

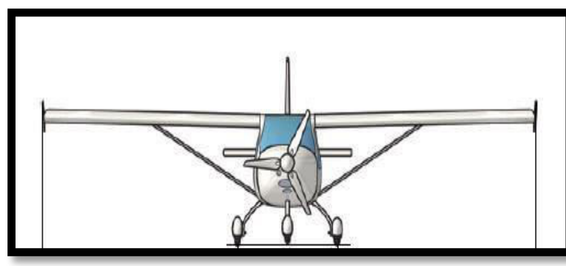

Fig.1.1 Aircraft

1.4 WINDSHIELD MAIN STRUCTURE

After essential fuselage structure were composed, it had been clear where precisely windshield structure must be adjusted. It was chosen principle casing to be comprised of profiles which would be made by innovation of sheet metal banding. Hunting down existing windshield outline profiles [2] it was discovered how it may look. Fundamental windshield structure comprises of five little casings and furthermore extra little sheet metal pieces which are altogether associated with outlines by the bolts.

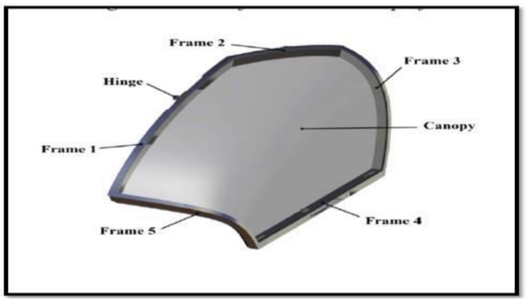

Fig.1.4 Isometric view of windshield main structure

PROBLEM DESCRIPTION AND METHODOLOGY

Dynamic analysis was carried out by Computational Fluid Dynamics (CFD), Fluid-Solid-Interaction (FSI) approach and ANSYS in order to evaluate fluid pressure, stress distribution and deformation in windshield with different air speeds. The analysis is carried out for all the three different materials at various air speeds of 900,800,600 and 400km/hr.

In the present work two different materials were considered namely polymethyl-methacrylate and poly vinyl butyl for windshield.

Windshield modeling was done in 3D using Pro/Engineer software.

Speed (km/hr)	Velocity (m/s)	materials
900	250	**Glass, polymethyl methacrylate & Poly vinyl butyl**
800	222.22	
600	166.66	
400	111.11	

INTRODUCTION TO CFD :

Computational fluid dynamics, usually abbreviated as CFD, is a branch of fluid mechanics that uses numerical methods and algorithms to solve and analyze problems that involve fluid flows. Computers are used to perform the calculations required to simulate the interaction of liquids and gases with surfaces defined by boundary conditions. With high-speed supercomputers, better solutions can be achieved. Ongoing research yields software that improves the accuracy and speed of complex simulation scenarios such as transonic or turbulent flows. Initial experimental validation of such software is performed using a wind tunnel with the final validation coming in full-scale testing, e.g. flight tests.

DIFFERENT MODULES IN PRO/ENGINEER

- PART DESIGN
- ASSEMBLY
- DRAWING
- SHEETMETAL

RESULTS AND DISCUSSIONS
MODELS OF WINDSHIELD USING PRO-E WILDFIRE 5.0
2D DRAWING

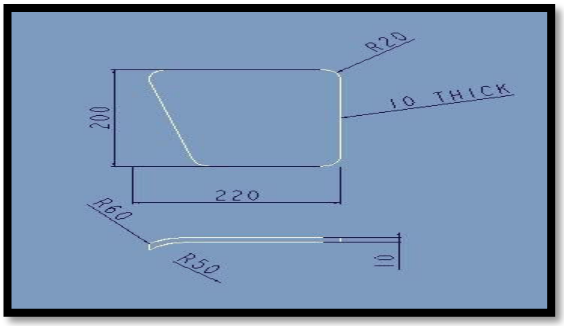

CFD & Structural analysis of windshield (FSI -Fluid Structure Interface)

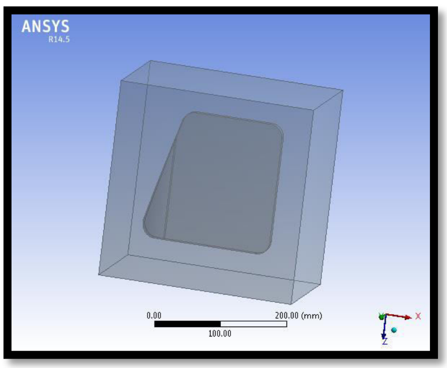

→→ Select mesh on work bench → right click →edit → select mesh on left side part tree → right click → generate mesh →

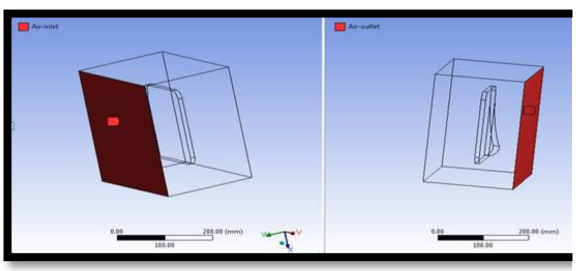

Air Inlet **Air outlet**

Update project>setup>edit>model>select>energy equation (on)>ok
Materials> Materials > new >create or edit >specify fluid material or specify properties > ok
Select fluid

Boundary conditions>inlet>enter required inlet values
Inlet air Velocity

Speed (km/hr)	Velocity (m/s)
900	250
800	222.22
600	166.66
400	111.11

Pressure=101325Pa
Temperature=313K
Solution > Solution Initialization > Hybrid Initialization >done
Run calculations > no of iterations = 100> calculate > calculation complete>ok
Results>edit>select contours>ok>select location (inlet, outlet, wall.etc)>select pressure>apply

SPEED – 900 km/hr

According to the above contour plot, the maximum velocity magnitude of the wind shield at inside of the boundary and minimum velocity magnitude at outside of the boundary. According to the above contour plot, the maximum velocity is 2.51e+02m/s and minimum velocity is 1.28e+01m/s.

STRESS

3

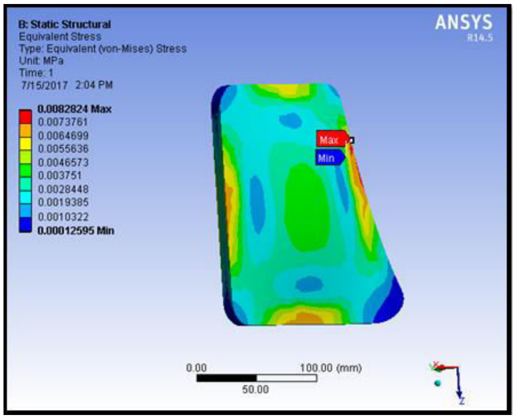

When the loads i.e. pressure and velocity applied on wind shield, the maximum stress value is 0.0082824MPa at one side of the edge of the wind shield and minimum stress is 0.00012595MPa.

STRAIN

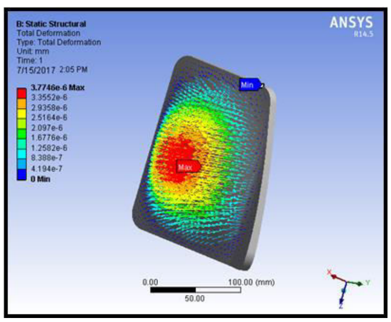

When the loads i.e. pressure and velocity applied on wind shield, the maximum strain value is 1.2947e-7 at one side of the edge of the wind shield and minimum strain is 2.7565e-9.

MATERIAL- POLYMETHYL METHACRYLATE

DEFORMATION

STRESS

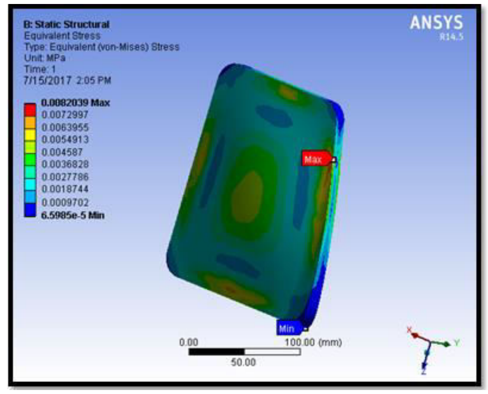

STRAIN

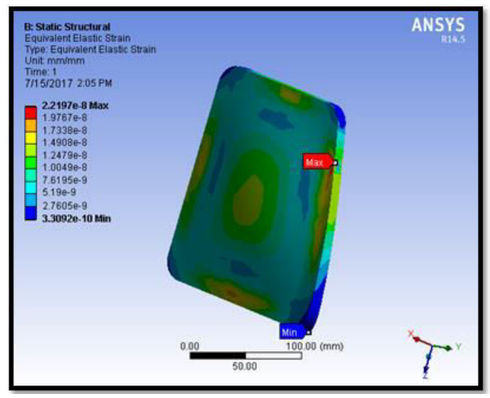

MATERIAL- POLY VINYL BUTYLDEFORMATION

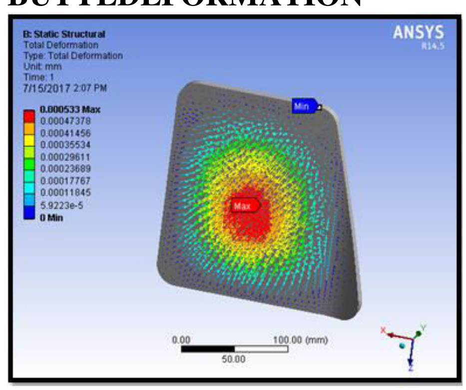

STRESS

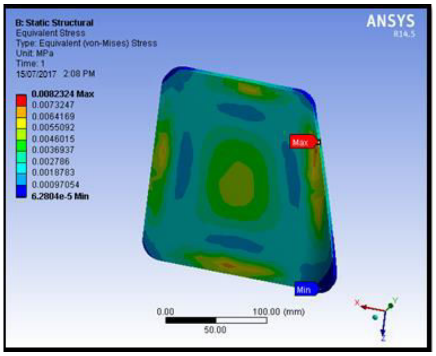

STRAIN

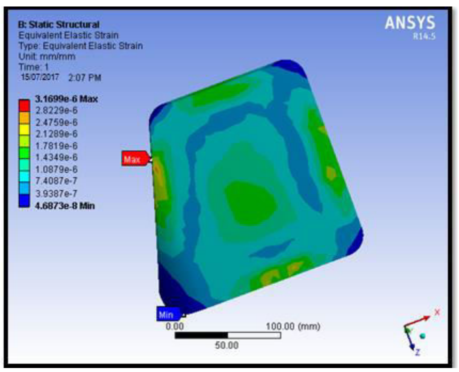

SPEED – 800 km/hr

PRESSURE CONTOUR

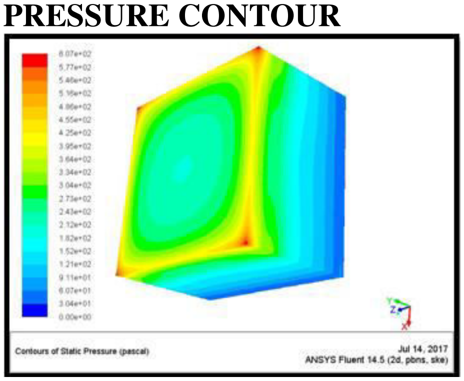

VELOCITY MAGNITUDE

MATERIAL- GLASS

DEFORMATION

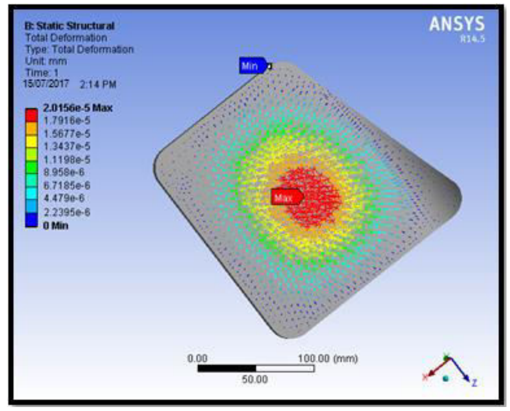

STRESS

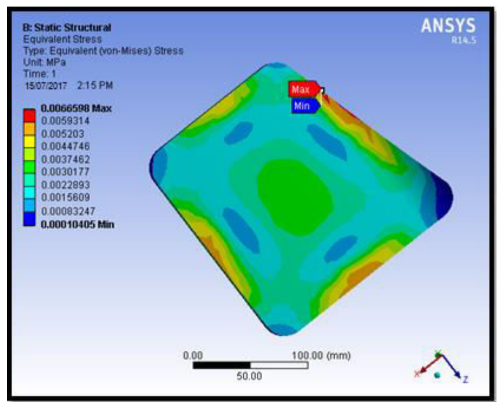

STRAIN

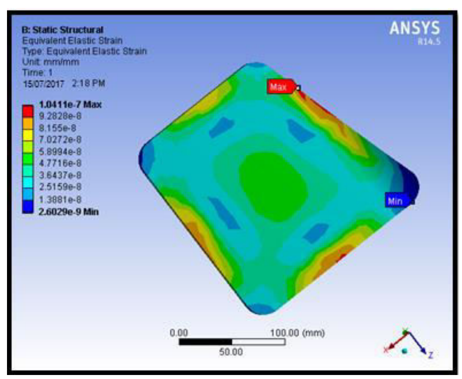

MATERIAL- POLYMETHYL METHACRYLATE

DEFORMATION

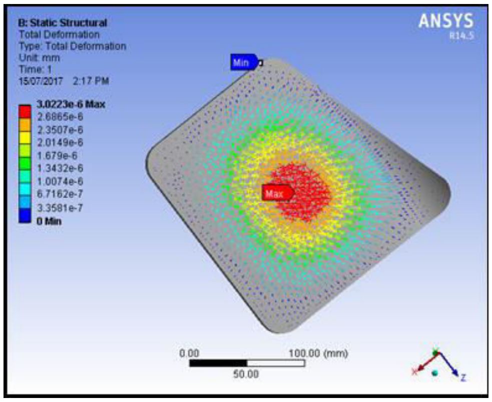

STRESS

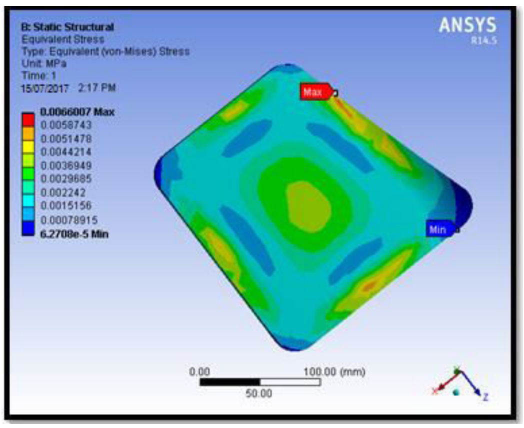

STRAIN

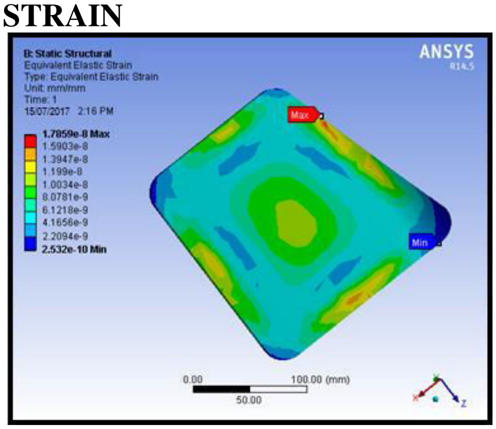

MATERIAL- POLY VINYL BUTYL

DEFORMATION

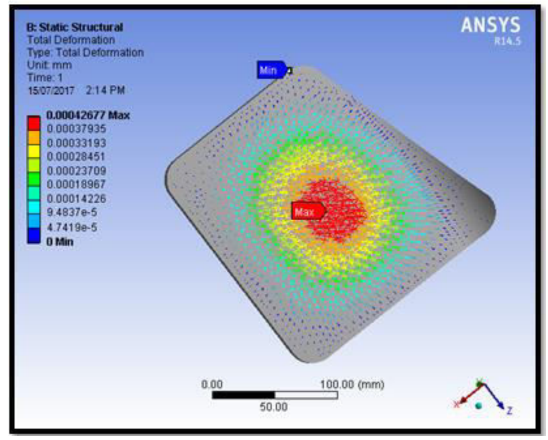

STRESS

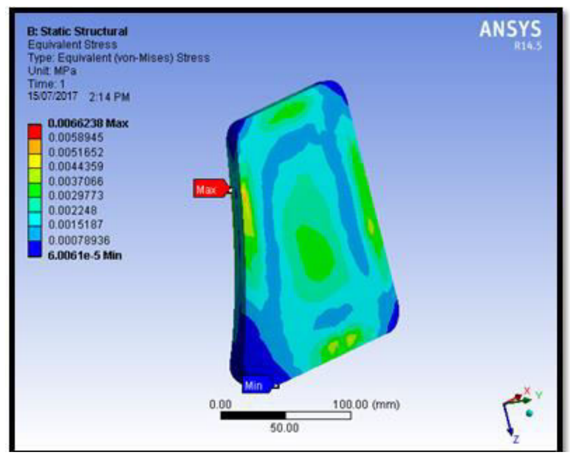

STRAIN

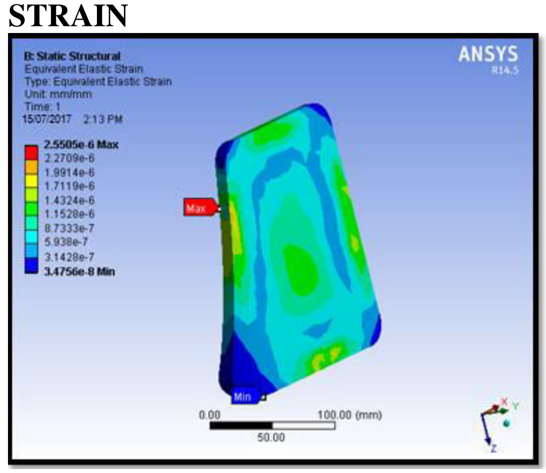

SPEED – 600 km/hr

PRESSURE CONTOUR

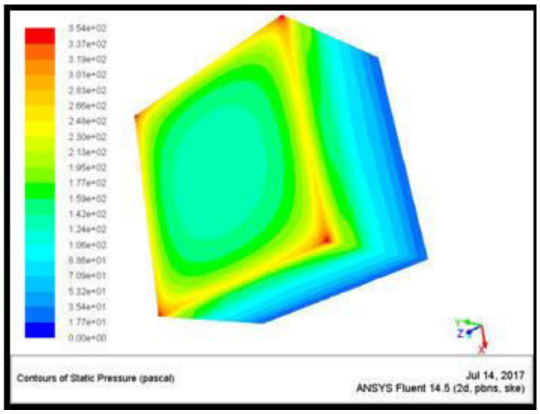

VELOCITY MAGNITUDE

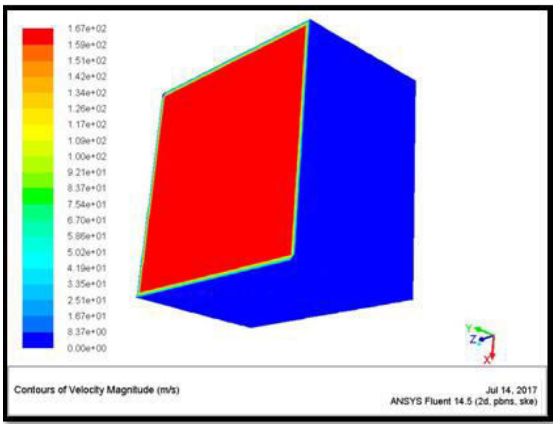

MATERIAL- GLASSDEFORMATION

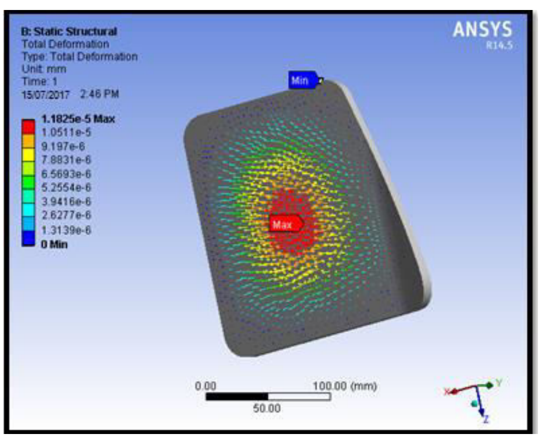

STRESS

MATERIAL- POLYMETHYL METHACRYLATE

DEFORMATION

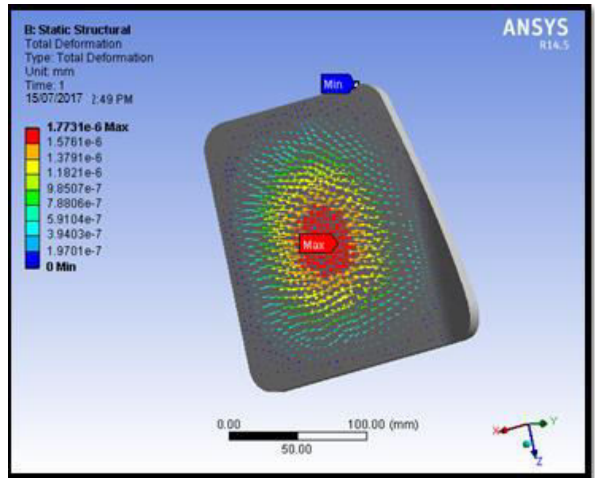

STRESS

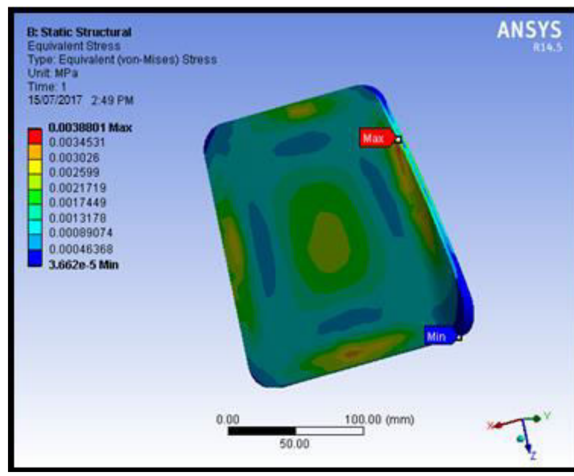

STRAIN

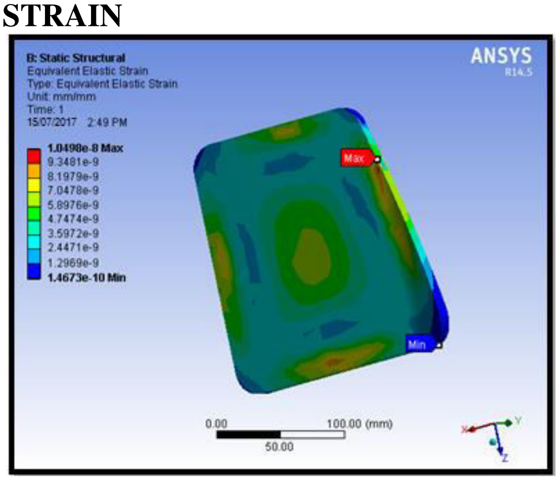

MATERIAL- POLY VINYL BUTYLDEFORMATION

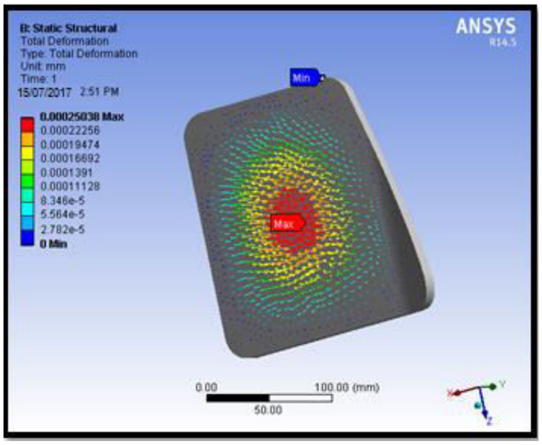

STRESS

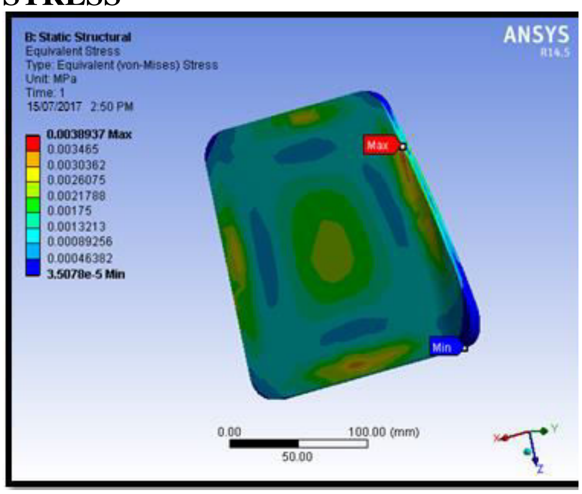

STRAIN

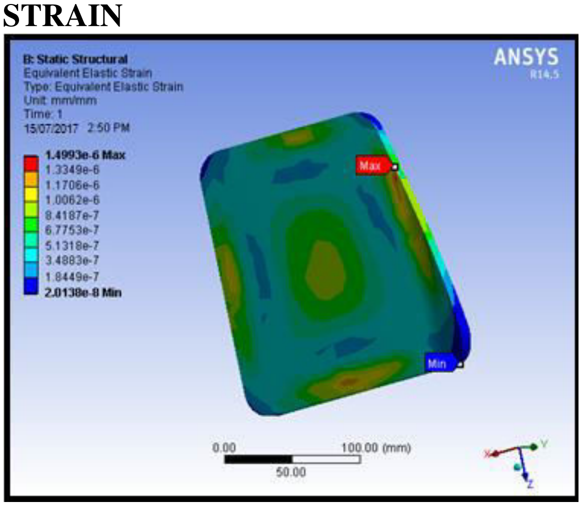

SPEED – 400 km/hr

PRESSURE CONTOUR

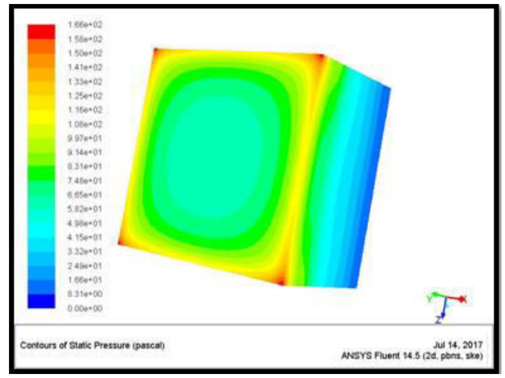

VELOCITY MAGNITUDE

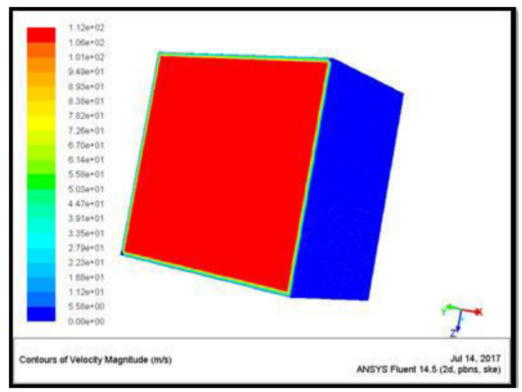

MATERIAL- GLASSDEFORMATION

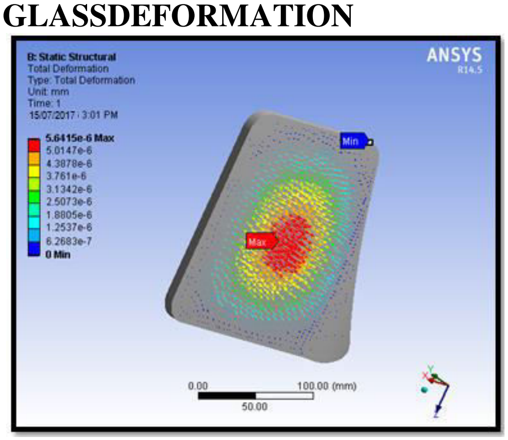

STRESS

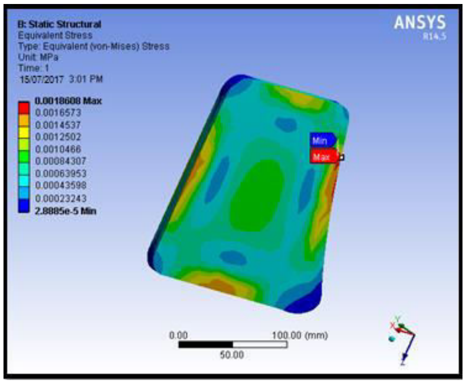

STRAIN

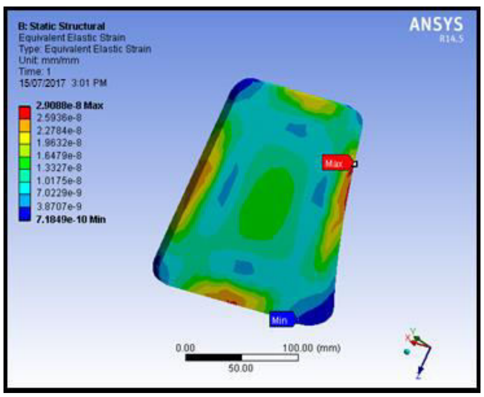

MATERIAL- POLYMETHYL METHACRYLATE

DEFORMATION

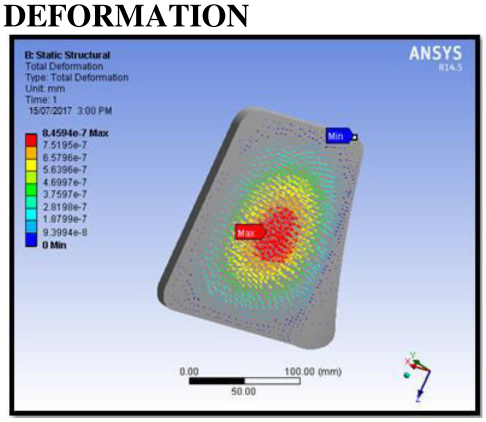

STRESS

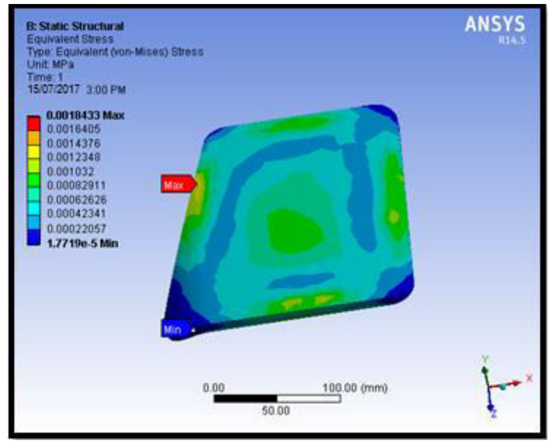

STRAIN

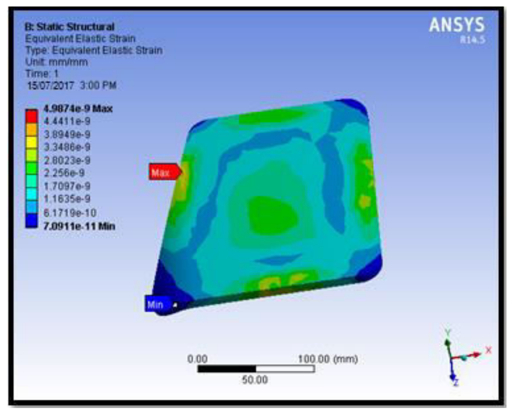

MATERIAL- POLY VINYL BUTYL

DEFORMATION

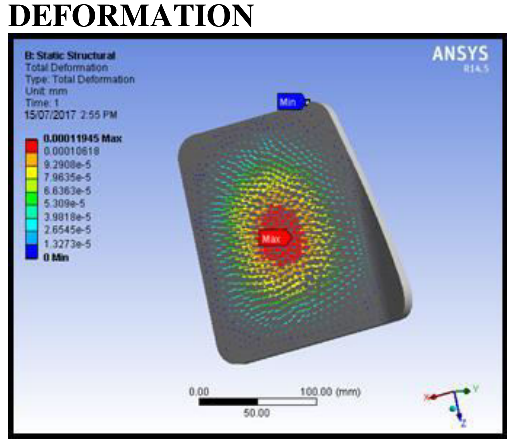

STRESS

Speed km/hr	materials	Deformation(mm)	Stress(MPa)	strain
900	Glass	2.5173e-5	0.0082824	1.2947e-7
	polymethyl methacrylate	3.7746e-6	0.0082039	2.2197e-8
	Poly vinyl butyl	0.000533	0.0082324	3.1699e-6
800	Glass	2.0156e-5	0.0066598	1.041e-7
	polymethyl methacrylate	3.0223e-6	0.0066007	1.7859e-8
	Poly vinyl butyl	0.00042677	0.0066238	2.5505e-6
600	Glass	1.1825e-5	0.0039146	6.1193e-8
	polymethyl methacrylate	1.7731e-6	0.0038801	1.0498e-8
	Poly vinyl butyl	0.00025038	0.0038937	1.4993e-6
400	Glass	5.6415e-6	0.0018608	2.9088e-8
	polymethyl methacrylate	8.4594e-7	0.0018433	4.9874e-9
	Poly vinyl butyl	0.00011945	0.0018498	7.1224e-7

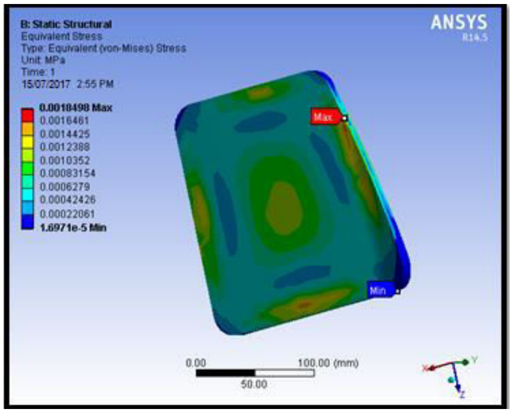

STRAIN

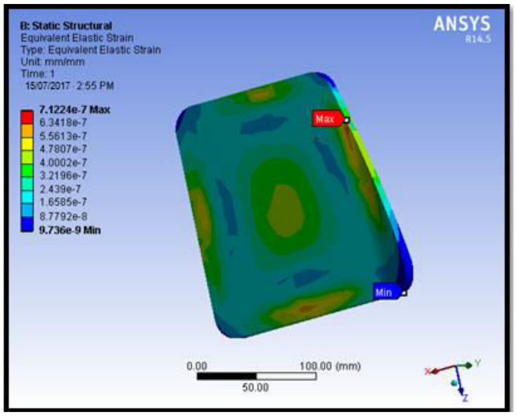

Chapter-6

Results

CFD RESULT TABLE

Speed km/hr	Pressure(Pa)	Velocity(m/s)
900	7.51e+02	2.51e+02
800	6.07e+02	2.23e+02
600	3.54e+02	1.67e+02
400	1.66e+02	1.12e+02

STATIC ANALYSIS RESULT TABLE

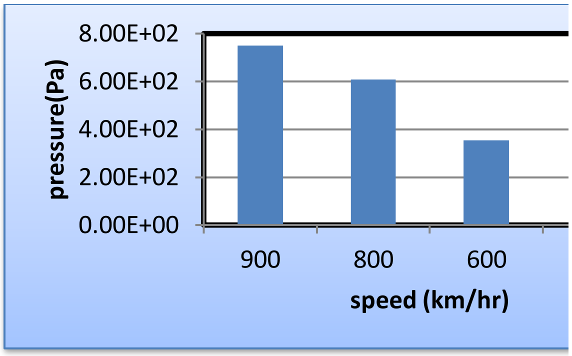

A plot between maximum pressure and speeds by FSI approach is shown in above fig. From the plot the variation of maximum static pressure is observed. Maximum static pressure increases by increasing speeds.

Velocity plot

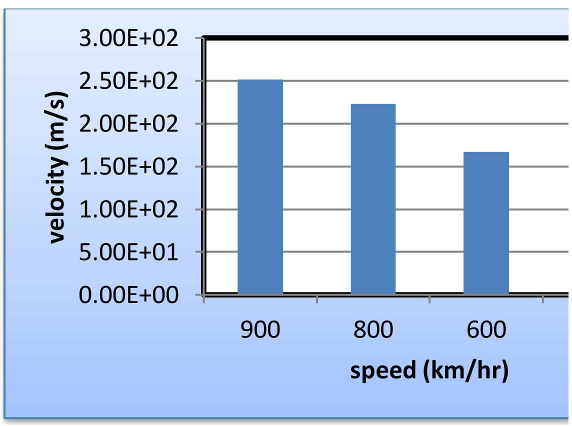

A plot between maximum velocity and speeds by FSI approach is shown in above fig. From the plot the variation of maximum velocity is observed. Maximum velocity increases by increasing in speeds.

Deformation plot

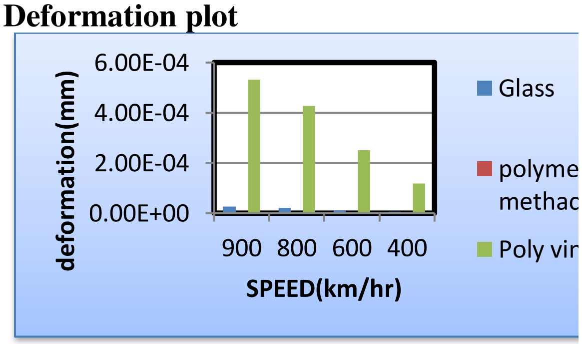

Stress plot

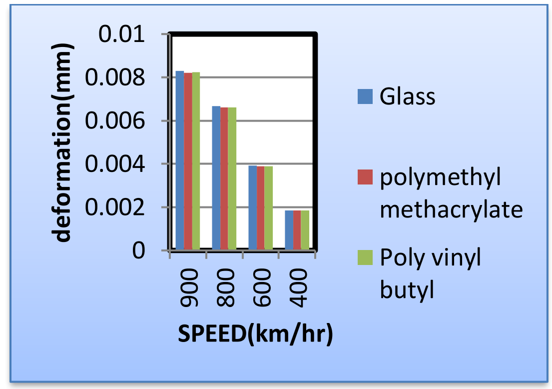

Chapter-7
CONCLUSIONS

In this report,

.By observing the CFD analysis the pressure drop and velocity increases by increasing the speed km/hr.

By observing the static analysis, the stress values are decreases by decreasing the speeds, the taken different pressure values are from CFD analysis. The stress value is less for polymethyl methacrylate material than glassand poly vinyl butyl

So we can conclude the polymethyl methacrylate material is better for wind shield.

SCOPE FOR FUTURE WORK:

The same analysis can be done for the other thermoplastic materials which are less in weight like Polyurethane, polyester, polypropylene.

The same analysis can be done at other speeds of the aircraft.

REFERENCES
JOURNAL PAPERS

1. Ahmed mukhtar.,bojan,šekutkovski, sonjapetrović, aleksandarbojanić “windshield design for the light trainer aircraft”, accepted and published in International Journal of Recent Trends in Mechanical Engineering (IJRTME),Vol.3(2011) No 1, ISSN 1821-1259 ,pp. 61-64 , 28.03.2011
2. Uzair Ahmed Dar, Weihong Zhang, YingjieXu “fe analysis of dynamic response of aircraft windshield against bird impact” accepted and published in International Journal of Aerospace Engineering (IJAE),Volume 2013 (2013), Article ID 171768, 12 pages
3. Wang Xinjun, FengZhenzhou, Wang Fusheng, YueZhufeng “Dynamic response analysis of bird strike on aircraft windshield based on damage-modified nonlinear visco elastic constitutive relation” accepted and published in ChineseJournal of Aeronautics (CJA),Volume 1 ,Issue 1 31 July 200
4. Reza Hedayati, Saeed Ziaei-Rad,

MODELING AND STRUCTURAL ANALYSIS OF DISK BRAKE

Mohammad Raziuddin
DEPARTMENT OF MECHANICAL ENGINEERING
MALLA REDDY COLLEGE OF ENGINEERING
Maisammaguda, Dhulapally, Telangana, India.

ABSTRACT

Noise and vibration associated with the braking process in passenger automobiles has become an important economic and technological problem in the industry. The knowledge of natural frequencies of components is of great interest in the study of response of structures to various excitations. Hence a brake disc plate with central hole, fixed at inner edge and free at outer edge is chosen and its dynamic response is investigated. The objective of current work is to analyze the static and vibration characteristics like stresses, deformations and mode frequency, mode shapes of brake disc with drilled holes of diameter. FEM software package is used for static analysis and model analysis of brake discs. The disc brake is modeled using commercial computer aided design (CAD) software, Ansys.

1. Introduction:

In today's growing automotive market the competition for better performance vehicle is growing enormously. The racing fans involved will surely know the importance of a good brake system not only for safety but also for staying competitive. The disc brake is a device for slowing or stopping the rotation of a wheel. A brake disc usually made of cast iron or ceramic composites includes carbon, Kevlar and silica, is connected to the wheel and the axle, to stop the wheel]. A friction material in the form of brake pads is forced mechanically, hydraulically, pneumatically or electromagnetically against both sides of the disc. This friction causes the disc and attached wheel to slow or stop. Generally, the methodologies like regenerative braking and friction braking system are used in a vehicle. A friction brake generates frictional forces as two or more surfaces rub against each other, to reduce movement. Based on the design configurations, vehicle friction brakes can be grouped into drum and disc brakes. If brake disc are in solid body the heat transfer rate is low. Time taken for cooling the disc is low. If brake disc are in solid body, the area of contact between disc and pads are more. In disc brake system a ventilated disc is widely used in automobile braking system for improved cooling during braking in which the area of contact between disc and pads remains same.

1.1 General Description of Finite Element Method:

The step by step procedure for static structural problem can be stated as follows

STEP 1: Discretization of structure (domain)

The first step in the finite element method is to divide the structure or solution region into subdivisions or elements.

STEP 2: Selection of a proper interpolation model. Since the displacement (field variable) solution of a complex structure under any specified load conditions can't be predicted exactly. We assume some suitable solution within an element to approximate the unknown solution. The assumed solution must be simple from computational point of view, and it should satisfy certain convergence requirements.

STEP 3: Element stiffness matrices (characteristic matrices) and load vectors.

From the assumed displacement model the stiffness matrix [K (e)] and the load vector F (e) of element 'e' are to be derived by using either equilibrium conditions or a suitable variation principle.

STEP 4: Assemblage of element equations to obtain the overall equilibrium equations. Since the structure is composed of several finite elements, the individual element stiffness matrices and load vectors are to assembled in a suitable manner and the overall equilibrium equations have to be

formulated as

[K] q = F

[K] is called assembled stiffness matrix, q is called the vector of nodal displacement and F is the Vector of nodal forces of the complete structure.

STEP 5: Solution of system equations have to be modified to account for the boundary conditions of the problem. After incorporation of the boundary conditions, the equilibrium can be expressed as

[K] q = F

For linear problems, the vector 'q' can be solved very easily, but for non-linear analysis problems, the solution has to be obtained in a sequence of steps, each step involving the modification of the stiffness matrix [k] and /or the load vector F.

STEP 6: Computation of Element Stresses and Strains. From the known nodal displacements, if required, the element stresses and strains can be computed by using the necessary equations of solid or structural mechanics.

1.2Limitations of Finite Element Method:

The finite element method does not accommodate few complex phenomena such as

1. Cracking and Fracture behavior.
2. Contact problems.
3. Bond failures of composite materials.

Applications of FEM:

1. Mechanical Design
2. Civil Engineering Structures
3. Air Craft structures
4. Heat conduction
5. Nuclear Engineering

2. ANSYS: A Finite-element analysis

2.1 BASIC METHODOLOGY OF ANSYS

Ansys is followed up by the method called Finite Element Modeling Methods (FEM).

Finite element method:

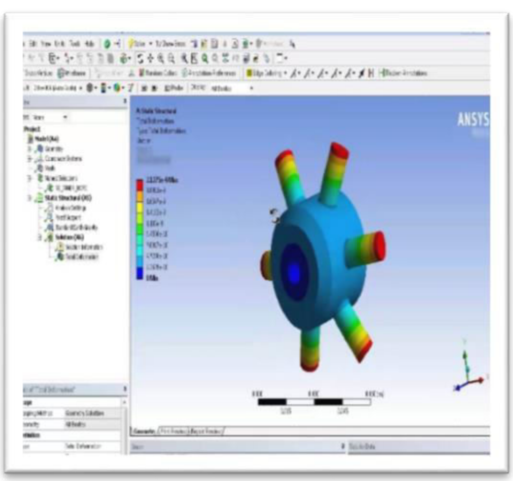

2.1 user interface of Ansy

2.1.1 PREPROCESSOR

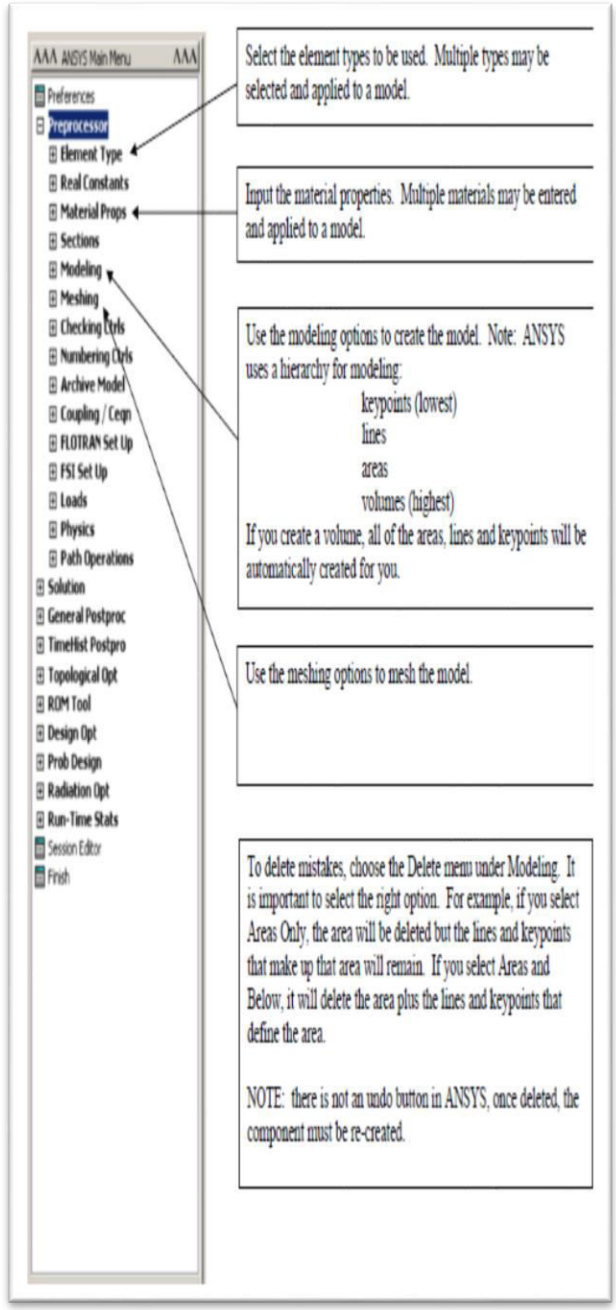

2.1.2 POST PROCESSING

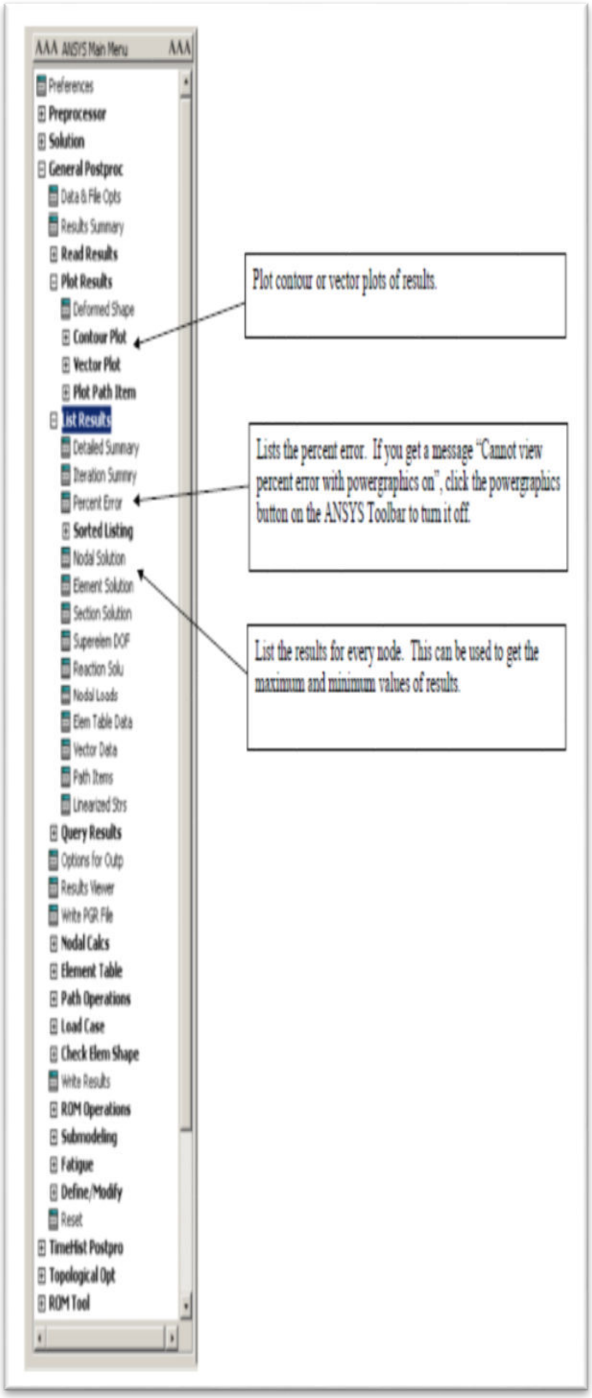

3. MATERIAL PROPERTIES: -

Properties	Carbon-carbon composites	Mar aging steel	Cast iron
Density (Kg/M^3)	1800	8100	7100
Young's Modulus (GPA)	95	210	125
Poisson Ratio	0.31	0.3	0.25
Thermal Conductivity (W/M-K)	40	25.5	54.5
Specific Heat (J/Kg-K)	755	813	586
Coefficient of Friction	0.3	0.8	0.2

4. PROCEDURE FOR ANALYSIS OF DISC BRAKE:

1. STATIC ANALYSIS OF DISC BRAKE USING CARBON STEEL MATERIAL

PREFERENCES – STRUCTURAL

Element: type 10 node solid 187

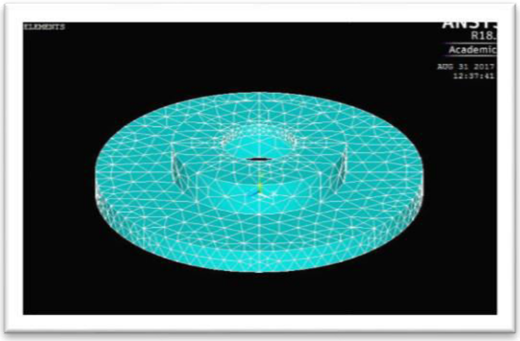

Fig.4.1 Mesh model

APPLIED LOAD

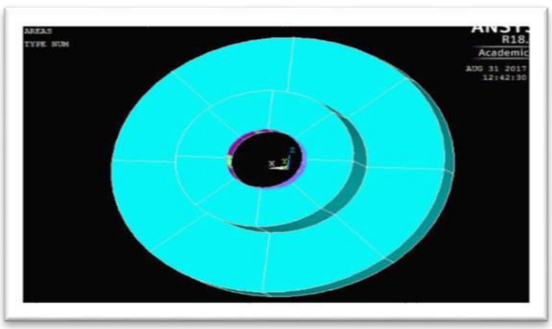

Fig.4.2 Applied pressure

RESULTS

PLOT RESULTS - CONTOURED PLOT- VONMISES STRESS- AT X COMPONENT

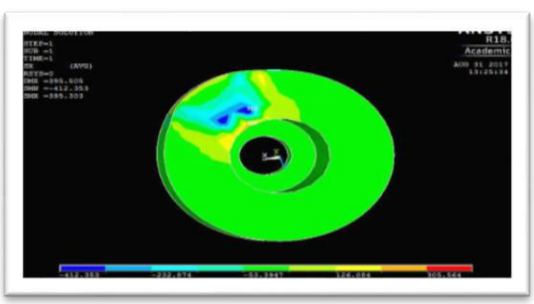

Fig.4.3 Stress values along X-axis

PLOT RESULTS - CONTOURED PLOT- VONMISES STRESS- AT YCOMPONENT

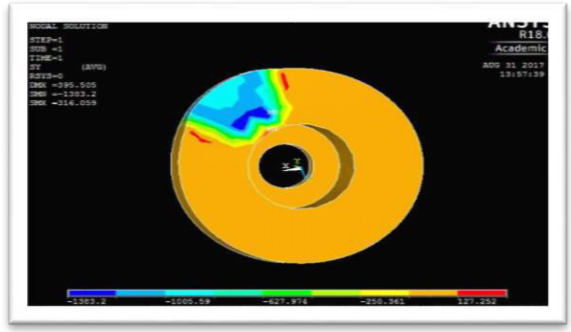

Fig.4.4 Stress values along Y-axis

PLOT RESULTS - CONTOURED PLOT- VONMISES STRESS- AT Z COMPONENT

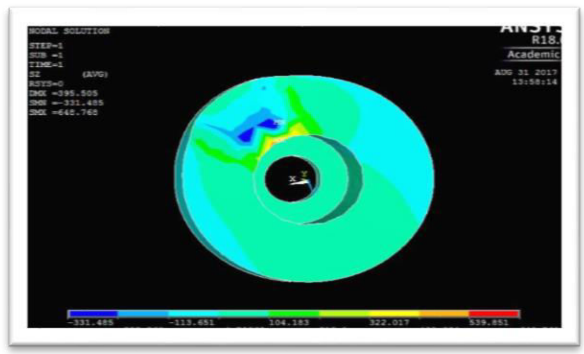

Fig.4.5 Stress values along Z-axis

4.1 MODEL ANALYSIS OF DISC BRAKE USING CARBON STEEL MATERIAL

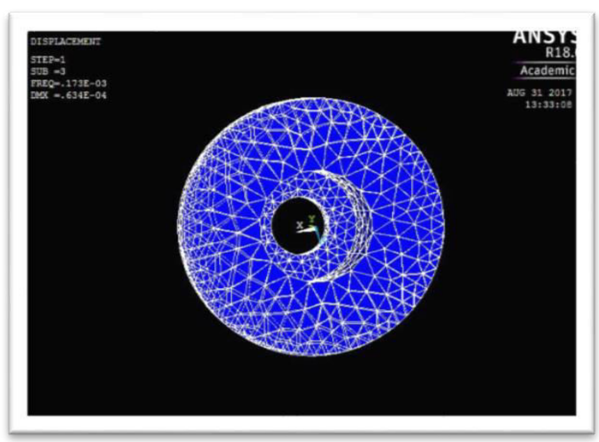

Fig.4.6 Mode shape

4.2 STATIC ANALYSIS OF DISC BRAKE USING MARAGING STEEL

PLOT RESULTS - CONTOURED PLOT- VONMISES STRESS- AT X COMPONENT

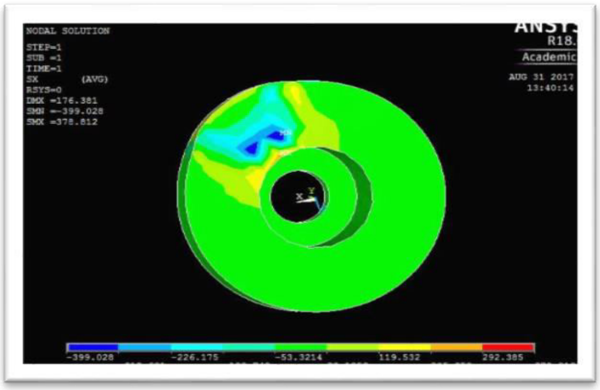

Fig.4.7 Stress values along X-axis

PLOT RESULTS - CONTOURED PLOT- VONMISES STRESS- AT Y COMPONENT

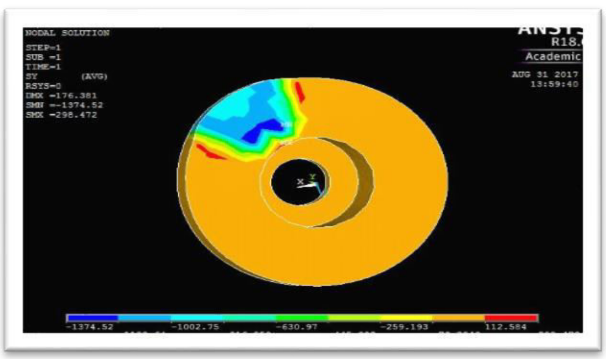

Fig.4.8 Stress values along Y-axis

PLOT RESULTS - CONTOURED PLOT- VONMISES STRESS- AT Z COMPONENT

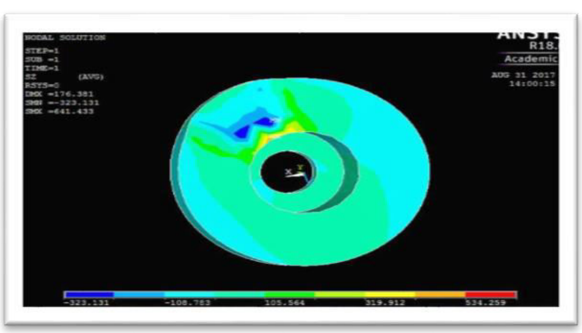

Fig.4.9 Stress values along Z-axis

VON MISES STRESS

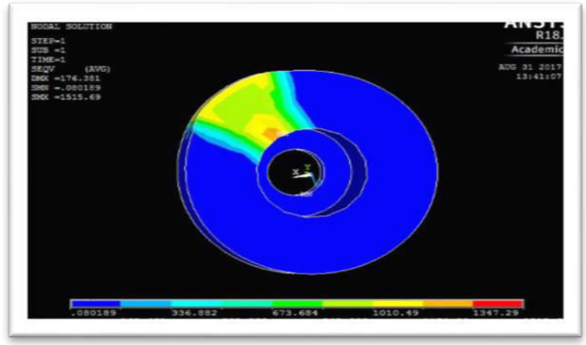

Fig.4.10 Von mises Stress values

Stress along geometry

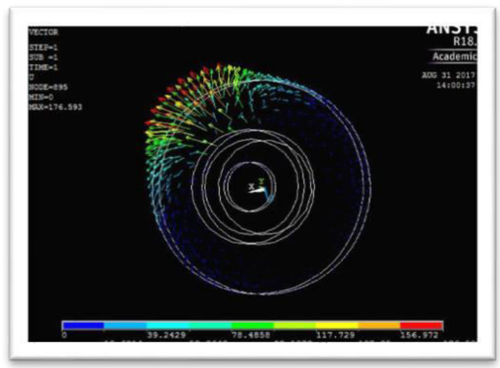

Fig.4.11 Stress along geometry

4.3 MODEL ANALYSIS OF DISC BRAKE USING MARAGING STEEL MATERIAL

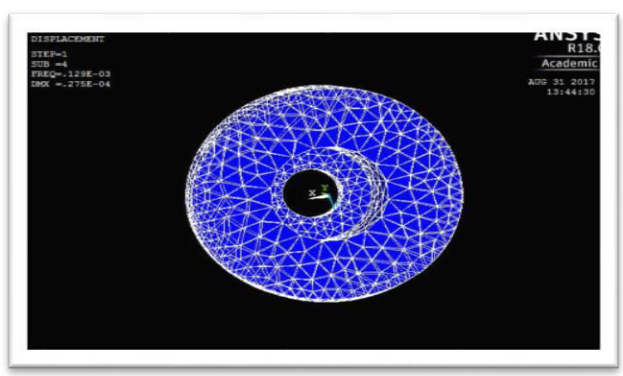

Fig 4.12 Mode shape

4.4 STATIC ANALYSIS OF DISC BRAKE USING CAST IRON

PLOT RESULTS - CONTOURED PLOT- VONMISES STRESS- AT X COMPONENT

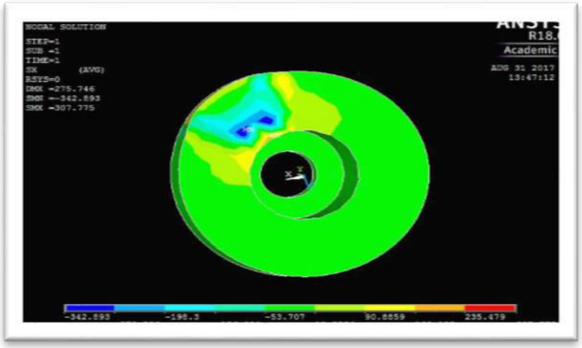

Fig.4.13 Stress values along X-axis

PLOT RESULTS - CONTOURED PLOT- VONMISES STRESS- AT Y COMPONENT

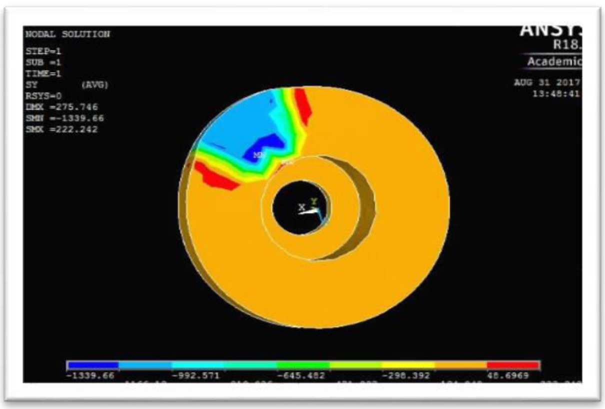

Fig.4.14 Stress values along Y-axis

PLOT RESULTS - CONTOURED PLOT- VONMISES STRESS- AT Z COMPONENT

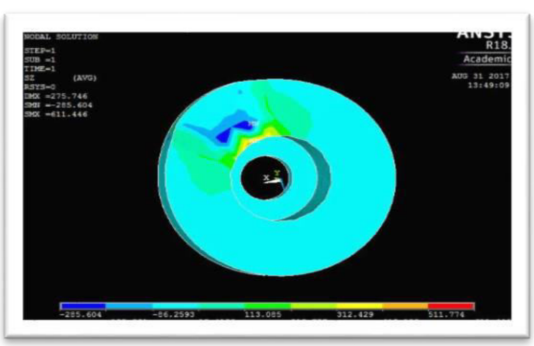

Fig.4.15 Stress values along Z-axis

VON MISES STRESS

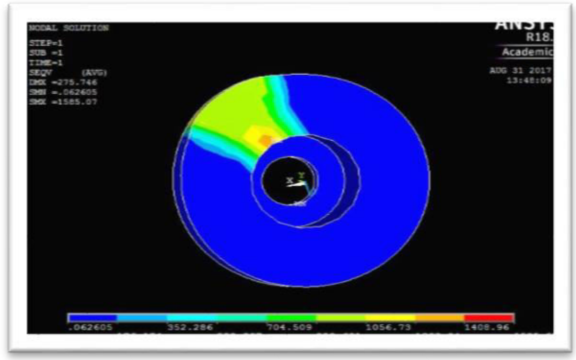

Fig.4.16 Vonmises Stress values

Stress along geometry

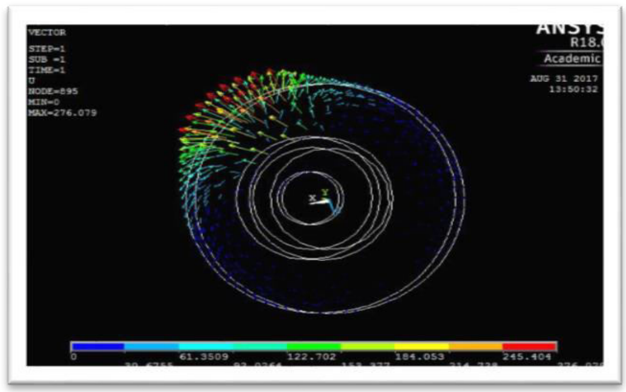

Fig.4.17 Stress along geometry

4.5 MODEL ANALYSIS OF DISC BRAKE USING CAST IRON MATERIAL

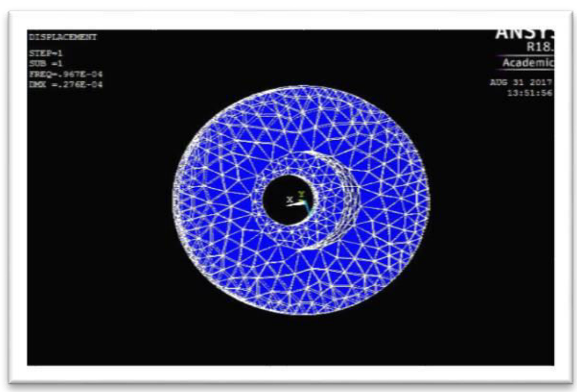

Fig.4.18 Mode shape 1

Results Comparison: -

The table gives the results of the three materials Carbon-Carbon Composites, Mar aging Steel and Cast Iron proposed and shows that Mar aging Steel gives less deformation and stress when the loads are applied. Therefore, Mar aging Steel material is preferred over the existing materials.

Material	Displacement (m)		Von Mises Stress (N/m^2)	
	Solid	Ventilated	Solid	Ventilated
Carbon-Carbon Composites	0.07633	0.000838	$0.551E^{-08}$	$0.247\ E^{-07}$
Maraging Steel	0.032735	0.000373	$0.540\ E^{-08}$	$0.247\ E^{-07}$
Cast Iron	0.065491	0.000574	$0.585\ E^{-08}$	$0.249\ E^{-07}$

CONCLUSION:

A brake usually made of Steel or cast iron or ceramic composites includes carbon, Kevlar and silica, is connected to the wheel and the axle, to stop the wheel]. A friction material in the form of brake pads is forced mechanically, hydraulically, pneumatically or electromagnetically against both sides of the disc. This friction causes the disc and attached wheel to slow or stop. Generally, the methodologies like regenerative braking and friction braking system are used in a vehicle. In this project complete Brake pedal is modeled and static analysis is done for carbon steel, maraging steel and cast iron. Applied all kind of boundary conditions on modal and response of the body is recorded in the form of deformations , stresses and all Vonmises stresses contoured plotted. Also modal analysis was done for frequency response for carbon steel, maraging steel and cast iron.

REFERENCES:

[1] ISBN-10: 1932709444 ISBN-13: 978- 1932709445 Pro/ENGINEER Wildfire 4.0 for Designers textbook is a comprehensive textbook that introduces the users to Pro/ENGINEER Wildfire 4.0,

[2] Machine Design Edition: 14th. Author: R.S. Khurmi & J.K. Gupta

[3] Analysis of Ventilated Disc Brake Squeal Using a 10 DOF Model," SAE Technical Paper 2012-01-1827, 2012.

[4] A Textbook of Machine Design by R S Khurmi and GUPTA.

[5] G. Babukanth & M. Vimal Teja. Transient Analysis of Disk Brake By using Ansys Software.

[6] Ali Belhocine, MostefaBouchetara. Thermal analysis of a solid brake disc, Applied Thermal Engineering 32 (2012) 59-67.

[7] V. M. M. Thilak, R. Krishnaraj, Dr. M.S akthivel, K. Kanthavel, Deepan Marudachalam M.G, R. Palani. Transient Thermal and Structural Analysis of the Rotor Disc of Disc Brake, International Journal of Scientific & Engineering Research Volume 2, Issue 8, August-2011.

[8] Finite Element Analysis for Engineering &Tech. Author, T. Chandrupatla. Edition, illustrated. Publisher, Universities Press, 2004.ISBN, 8173714274.

[9]ISBN-10: 1932709444 ISBN-13: 978- 1932709445 Pro/ENGINEER Wildfire 4.0 for Designers textbook is a comprehensive textbook that introduces the users to Pro/ENGINEER Wildfire 4.0,

DESIGN AND ANALYSIS OF A DIESEL ENGINE NOZZLE

Libin Thomas, PG Scholoar
Department of Mechanical Engineering,Mallareddy College of Engineering, Secunderabad-India

Dr.S.S.Gowda,Professor
Department of Mechanical Engineering,Mallareddy College of Engineering
Secunderabad-India

ABSTRACT

The nozzle is used to transform the chemical energy into kinetic energy in the combustion chamber. The nozzle converts the high pressure, high temperature and low velocity gas in the combustion chamber into high velocity gas of lower pressure and lower temperature. Nozzle is designed to control the rate of flow, velocity, direction, mass, shape, and the pressure of the stream that exhaust from the nozzle exit.

Nozzle is designed based on its mission in which its used, its shape and size are the important factors depending in the study of its performance characteristic. Since heating of the propellant in the combustion chamber is possible convergent nozzle is used mostly

In this thesis we use convergent divergent nozzle with different nozzle diameter and different fluids at different velocities are used. We modelled convergent divergent nozzle changing with different nozzle diameters and its analysed with different mass flow rates to determine the pressure fall, heat transfer coefficient, and velocity and heat transfer rate for the fluid by CFD technique.

I. INTRODUCTION

The primary challenges towards developing new diesel engines for traveller cars be the strict future emission legislation together with the customer's demands for steady rising performance. For instance, the emission limitations of Tier a pair of Bin five needs a complicated once treatment system and a sturdy combustion method that minimizes emissions within the method of them being shaped. Advancements within the technology of Diesel Injection (DI) systems have contend in necessary role within the enhancements that are created up to the current purpose. Combining the reduction in nozzle passage diameters through increased flow characteristics with inflated injection pressures provides a chance to develop engines that includes high power density and reduced emissions. the first downside to those fashionable spray hole geometries is that they typically suffer a discount of power output throughout long run operation.Alternative studies have known these important formations of deposits because the main reason for this behaviour.

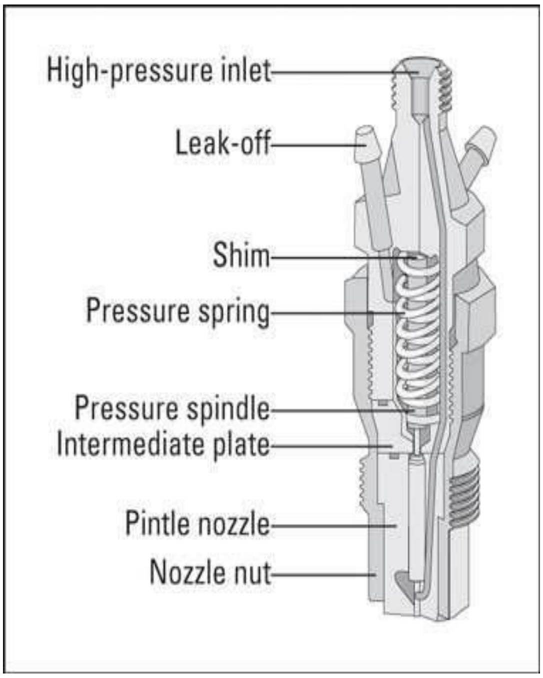

Fig 1 MODERN FUEL INJECTORS

Basic mechanisms are often wont to make a case for the formation and removal of deposits in burning engines These mechanisms act severally of the situation of shaped deposits (e.g. injection nozzles, heat changer) and of the combustion method (e.g. IDI, DI; diesel or gasoline).

The model delineate within the study illustrates the interaction of a wall with the introduction flow regime. The transport of particles to the wall is predicated on the method of thermophiles is that this process ends up in the force of gas particles within the direction of the temperature depression. It's amplified with associate degree increasing temperature differential between wall (cold) and fluid (hot). This method results is associate degree increasing concentration of deposit-building particles close to the wall.

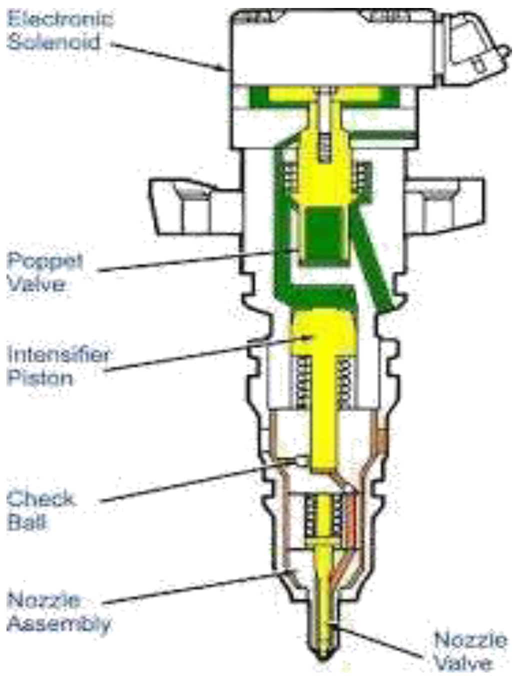

Fig 2 ANATOMY OF A FUEL INJECTOR

High a pair of turbulence close to the wall could scale back the force of the aerosol once more to a norm, compensating for associate degree inflated temperature distinction. The deposits area unit composed of connected particles (solid and liquid) and gas (Figure 1.1).

Condensation and surface assimilation of vaporous compounds at the cold wall promotes the formation method. At this time, the expansion of the deposits is currently principally influenced by the sticking out, impaction and incorporation of particles The surface assimilation of vaporous elements and therefore the chemical reactions (as shift, dehydration and chemical change, etc.), result in the compaction of the deposits]. The removal of deposits has analogous physical mechanisms.

The mechanism is reaction destroying the organic compounds within the coating Evaporation and action scale back the vaporous fraction dissolved within the deposits. Abrasion is caused by robust mechanics forces and breaking-off, attributable to warmth changes, leading to heterogeneous extensions of the wall and deposit layer.

The corresponding cutting off stresses initiates the breaking-off method the soluble fraction of the deposits is washed off by solvents (e.g. water as solvent for salt compounds)

II. MODELLING AND MESHING

Computer-aided design (CAD) is use to help the creation, modification, analysis, or improvement of a style. CAD package is improving the productivity of the designer, improve the standard of style, improve communications through documentation, and a total change in the production. CAD output is usually within the type of electronic files with printable form, machining, or alternative producing operations. The term CADD (Computer aided Design and Drafting) is also used.

The use in coming up with electronic systems is thought as electronic style automation, or EDA. In engineering style it's called mechanical style automation (MDA) or computer-aided drafting (CAD), which has the method of making a technical drawing with the utilization of pc package.

CAD package for mechanical style uses either vector-based graphics to show the objects of ancient drafting, or may additionally turn out formation graphics showing the look of designed objects. However, it involves quite simply shapes. The output of CAD should convey data, like materials, dimensions, processes, tolerances and boundary conditions in keeping with application-specific conventions if we are doing the drafting manually.

CAD is also wont to style curves and figures in two-dimensional (2D) space; or curves, surfaces, and solids in three-dimensional (3D) house.

CAD is a crucial industrial art extensively utilized in several applications, as well as automotive, building, and region industries, industrial and bailiwick style, medical specialty, and plenty of additional. CAD is additionally wide wont to turn out pc animation for computer graphics in movies, advertising and technical manuals, typically referred to as DCC digital content creation.

The fashionable presence and power of computers implies that even fragrance bottles and shampoo dispensers area unit designed victimization techniques exceptional by engineers of the Nineteen Sixties. Attributable to its monumental economic importance, CAD has been a serious propulsion for analysis in procedure pure mathematics, camera work (both hardware and software), and separate differential pure mathematics.

PTC CREO, early to called Pro/ENGINEER, is 3D modeling package utilized in engineering science, design, producing, and in CAD drafting service companies. PTC CREO is the one among the primary 3D CAD modeling applications that used a rule-based constant quantity system. Victimization parameters, dimensions and options to capture the behavior of the merchandise, it will optimize the event product in addition because the style itself.

The name was modified in 2010 from Pro/ENGINEER configuration to CREO. It had been announced by the corporate UN agency developed it, constant quantity Technology Company (PTC). The product have additional features of applications like assembly modelling, second writing views for technical drawing, finite part analysis and additional.

PTC CREO says it offers an additional economical style expertise than alternative modeling package attributable to its distinctive options as well as the mixing of constant quantity and direct modeling are handling software that is its main advantage. The entire suite of applications periods the spectrum of development, gives importance in designers choices to use in every step of the method. The package conjointly features an additional user friendly interface that has a more realistic expertise for designers. It conjointly has cooperative capacities that build it simple to share styles and build changes.

There are innumerable advantages to victimisation PTC CREO. We'll take a glance at them during this two-part series.

First up, the most important advantage is hyperbolic productivity attributable to its economical and versatile style capabilities. it had been styled to be easier to use and have options that leave design processes to maneuver additional quickly, creating a designer's productivity level increase.

Part of the explanation productivity are often hyperbolic is as a result of the package offers tools for all phases of development, from the start stages to the active creation and producing. Late stage changes area unit common within the style method, however PTC CREO will handle it. Changes are often created that area unit mirrored in alternative elements of the method.

The cooperative capability of the package conjointly makes it easier and quicker to use. One among the explanations it will method data additional quickly is attributable to the interface between MCAD and ECAD styles. styles are often altered and highlighted between the electrical and mechanical designers acting on the project.

The time saved by victimisation PTC CREO isn't the sole advantage. it's many ways of saving prices. as an example, the price of making a replacement product are often lowered as a result of the event method is shortened owing to the automation of the generation of associative producing and repair deliverables.

PTC conjointly offers comprehensive coaching on a way to use the package. this may save businesses by eliminating the necessity to rent new workers. Their educational program is on the market on-line and in-person, however materials area unit on the market to access anytime.

A unique feature is that the package is on the market in ten languages. PTC is aware of they need folks from everywhere the globe victimisation their package, in order that they provide it in multiple languages therefore nearly anyone UN agency desires to use it's able to do therefore.

Fig 3 NOZZLE WITH 50DIA

Fig 4 NOZZLE WITH 40DIA

Fig 5 NOZZLE WITH 30DIA

CFD analysis is carried out at fluid with different inlet velocity conditions.

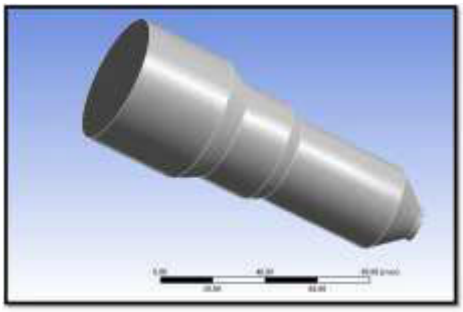

Fig 6 IMPORTED MODEL

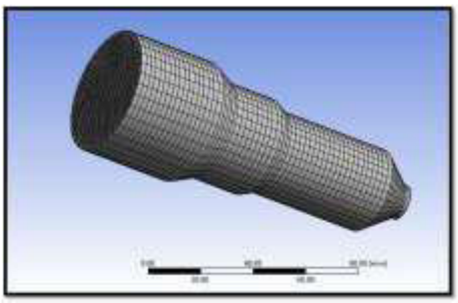

Fig 7 MESHED MODEL OF NOZZLE

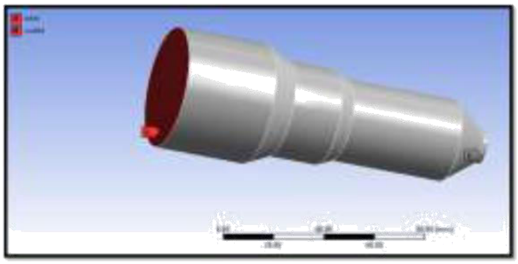

Fig 8 INLET AND OUT LET CONDITIONS

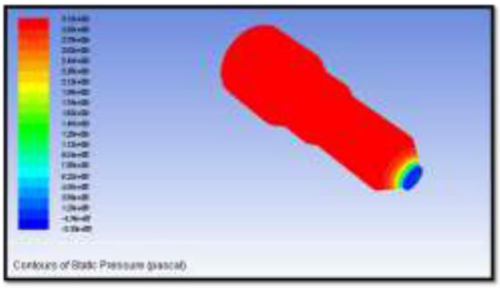

Fig 9 PRESSURE DISTRIBUTION

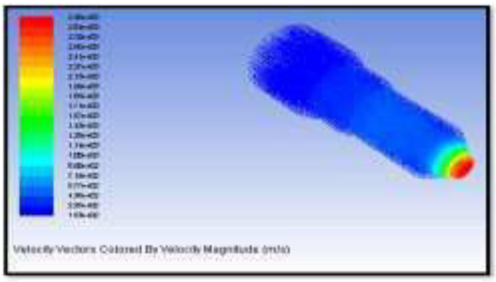

Fig 10 VELOCITY DISTRIBUTION

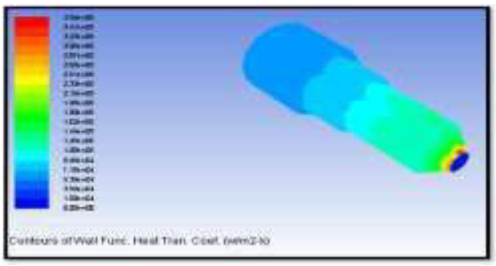

Fig 11 HEAT TRANSFER COEFFICIENT

For thermal, fatigue and static analysis for different materials such as aluminum and brass, importing the respective model from the CFD analysis.

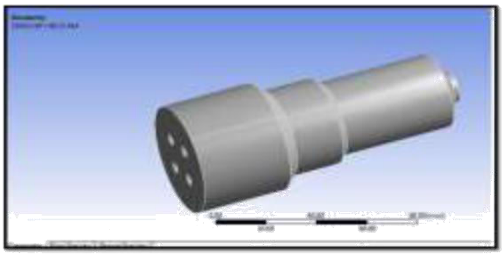

Fig 12 IMPORTED MODEL

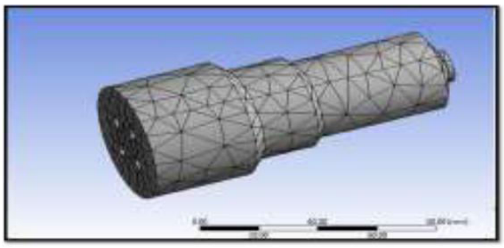

Fig 13 MESHED MODEL

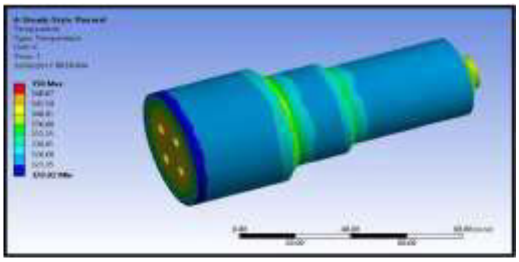

Fig 14 TEMPERATURE DISTRIBUTION

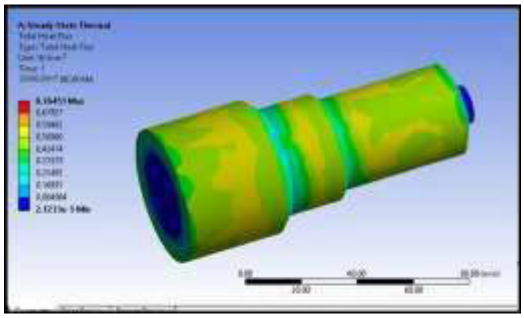

Fig 15 HEAT FLUX DISTRIBUTION

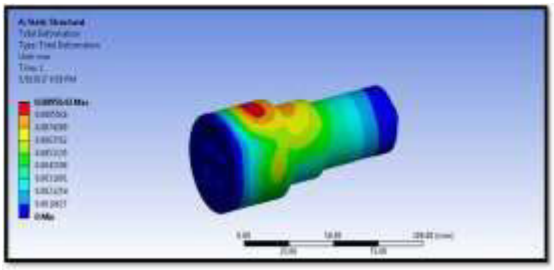

Fig 16 DEFORMATION DISTRIBUTION

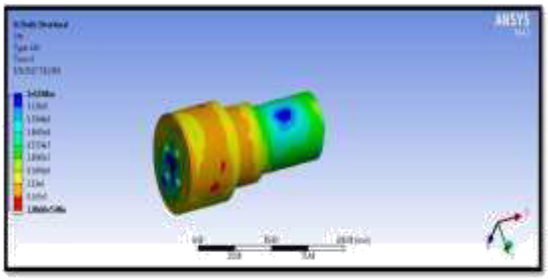

Fig 17 LIFE SPAN

III. RESULTS AND DISCUSSIONS

CFD ANALYSIS RESULT TABLE

Nozzle dia.	Inlet velocity (m/s)	Pressure (Pa)	Velocity (m/s)	Heat transfer coefficient (w/m2-k)	Mass flow rate (kg/s)	Heat transfer (W)
50	200	3.12e+09	2.98e+03	3.59e+05	1.138945	11540.5
	300	6.96e+09	4.46e+03	5.10e+05	0.289245	2927.5
	400	1.25e+10	5.99e+03	6.56e+06	3.087343	31294
40	200	4.53e+09	3.58e+03	3.76e+05	1.0457764	10600
	300	1.03e+10	5.38e+03	5.36e+05	2.192199	22219
	400	1.83e+10	7.17e+03	6.80e+05	2.9847107	30249
30	200	1.04e+10	5.36e+03	6.90e+05	0.16120148	1634.3125
	300	2.34e+10	8.05e+03	8.05e+03	0.44642	4520.625
	400	4.18e+10	1.07e+04	1.25e+06	0.8333587	8450.75

THERMAL ANALYSIS RESULT TABLE

Material	Temperature (K)		Heat flux(W/mm^2)
	Min	Max	
Brass	320.02	350	0.76451
Aluminum	323.59	350	0.87036

IV. CONCLUSION

Nozzles come in a variety of shapes and sizes depending on the mission of the rocket, this is very important for the understanding of the performance characteristics of rocket. Convergent divergent nozzle is the most commonly used nozzle since in using it the propellant can be heated in combustion chamber.In this thesis the convergent divergent nozzle changing the different nozzle diameters and different fluids at different velocities. We modeled convergent divergent nozzle changing with different nozzle diameters.

By observing the CFD analysis of diesel engine nozzle the pressure, velocity, heat transfer rate and mass flow rate values are increases by increasing the inlet velocities and decreasing the nozzle dia.

By observing the thermal analysis, heat flux is more for aluminum alloy compared with brass material.

So it can be concluded the diesel engine nozzle efficiency were more when the nozzle dia. decreases.

REFERENCES

[1] J.B. Heywood, “Internal Combustion Engine Fundamentals”,McGraw-Hill Book Co, pp 493-494, 1988.

[2] D. Ing. H. Tschöke, “Diesel distributor fuel-injection pumps”, Robert Bosch GmbH, pp 12-53, 1999.

[3] B. Challen R. Baranescu, “Diesel Engine Reference Book” Reed Educational and Professional Publishing Ltd., Second Edition, pp.260-301, 1999.

[4] M. Volmajer, B. Kegl, “Experimental and numerical analysis of fuel flow in the diesel engine injection nozzle" , Journal of Kones. Combustion Engines, Vol. 8, No. 1-2, 2001.

[5] Z. Li, M. Kokkolaras, D. Jung, Panos Y. Papalambros and D. N. Assanis, “An Optimization Study of Manufacturing Variation Effects on Diesel Injector Design with Emphasis on Emissions”, SAE International, 2004.

[6] A.J.Von Wielligh, “Influence of fuel quality on diesel injector failures”, Fifth International Colloquium Fuels, Germany, 2005. Property Unit Jatropha oil Jatropha Oil methyl ester Diesel Density at 15°C kg/m3 918 880 850 Viscosity at 40°C mm2 /s 35.4 4.84 2.60 Flash point °C 186 162 70 International Journal of Innovations in Engineering and Technology (IJIET) Vol. 2 Issue 1 February 2013 76 ISSN: 2319 – 1058

[7] LI Minghai, CUI Hongjiang, W.Juan, G. Ying, “Improvement of fuel injection system of locomotive diesel engine”, Journal of Environmental Sciences, pp. S139-S141, 2009.

[8] B. Paul, V. Ganesan, “Flow field development in a direct injection diesel engine with different manifolds” International Journal of Engineering, Science and Technology Vol. 2, No. 1, pp. 80-91, 2010.

[9] K. K.Khatri, D. Sharma, S. L. Soni, S. Kumar, D Tanwar, “Investigation of Optimum Fuel Injection Timing of Direct Injection CI Engine Operated on Preheated Karanj-Diesel Blend” Jordan Journal of Mechanical and Industrial Engineering Volume 4, pp. 629-640, 2010. 1M.Tech understudy, 2Professor, Dept of Mechanical Engineering, Kits, Markapur, A.P, India.

1. Finite Element Analysis of Steam Boiler Used In Power Plants 1M. Suri Babu, 2 Dr.B.Subbaratnam 1M.Tech understudy, 2Professor, Dept of Mechanical Engineering, Kits, Markapur, A.P, India.
2. Structural and warm investigation of an evaporator utilizing limited component Analysis by D.Kondayya Department of Mechanical Engineering, Author Correspondence: Department of Mechancal Engineering, Sreenidhi Institute of Science and Technology, Ghatkesar, Hyderabad – 501301.
3. Analysis of New Boiler Technologies Dr Mike Inkson
4. A Study Analysis and Performance of High Pressure Boilers With its Accessories J. Suresh babu1,R.Latha2 ,B.Praveen3,V.Anil kumar4,R Rama kumar5,s.peerulla6 1 Assistant Professor in MED, K.S.R.M College of building, AP, India 2 3 4 5 6 Student, mechanical office, K.S.R.M College of designing, AP, India
5. Design and investigation of the model of evaporator for steam weight control 1Akanksha Bhoursae, 2 Jalpa Shah, 3Nishith Bhatt Institute of Technology, Nirma University, SG thruway, Ahmedabad-382481,India 3Essar steels limited,Hazira,Surat-394270,India
6. Lou Roussinos, P. E., "Heater Design and Efficiency" [online], Available: http://www.forestprod.org/drying06williamson .pd f, Accessed: September 1, 2010.
7. Murdock, K. L., "3ds max 9 Bible, Wiley Publishing Inc. Indianapolis, Indiana, 2007.
8. Nagpal, G. R., 1998, Power Plant Engineering, Khanna, Delhi.
9. Steam Pressure Reduction: Opportunities and Issues by U.S Deportment of vitality,
10. Rapid Start up Analysis of a Natural Circulation HRSG Boiler with a Vertical Steam Separator Design by M.J. Albrecht, W.A. Arnold, R. Jain and J.G. DeVitto,
11. Technological examinations and productivity investigation of a steam warm trade condenser:
12. Conceptual plan of a cross breed steam condenser by R K Kapooria and S kumar,
13. Developmental plan of a research facility fire tube Steam evaporator by I. O. OHIJEAGBON,
14. Steam boilers – care and operation by Robert. H. Kuss
15. Industrial boilers and warmth recuperation steam generators by V.Ganapathy

TEMPERATURE DISTRIBUTION AND THERMAL STRESS CALCULATON OF TURBINE DISC OF AN AEROJET ENGINE

Rani Jain M,M.tech, Department of Mechanical Engineering, Mallareddy College of Engineering, Secunderabad-India

ABSTRACT

The turbine blades are responsible for extracting energy from the high temperature gas produced by the combustor. These turbine blades are supported by turbine disc. Operating the turbine blades and disc at high temperature would provide better efficiency and maximum work output. Withstanding of gas turbine blades and disc for the elongation is a major consideration in their design, because they are subjected to high tangential, axial, centrifugal forces during their working conditions.

This project summarizes the design and analysis of turbine disc, on which NX 8.5 is used for modeling the turbine disc, ANSYS APDL 16 software is used for analysis of model generated by Finite Element Modeling of disc by hypermesh

I.INTRODUCTION

THE NECESSITY AND SIGNIFICANCE OF DISC THERMAL DESIGN AND THERMAL STRESS ANALYSIS: Gas turbine engines are operating on high pressure ratios. Efficiency and work output of an engine is depends on compression ratios, turbine inlet temperature etc. The pressure and temperature are high at the turbine inlet and combustion chamber exit. Turbine is a power producing device which converts thermal energy into mechanical power output. Therefore the pressure and temperature reduces during their operation. The compressor and turbine blades are mounted on discs. The turbine blades are extracting energy from the high temperature gas produced by the combustor. Operating the blade and disc at high temperature provide better efficiency and work output. The blade and disc are subjected to different forces like tangential, axial, centrifugal etc which leads to stresses. The disc must have strength to withstand all the forces and stresses acting on it without failure and it should have long life.

Also, additional stresses acting on the disc due to engine over rotational speed. The material used in the disc which withstands all forces and stresses. The blades are dissipating heat into the disc. The disc receives heat from hot mainstream gas through blade on the rim and cool air from secondary air on the bore. This results in high thermal gradient and stresses. The disc also withstand excessive thermal stresses acting on it without failure.

The disc withstanding different stresses like thermal, centrifugal, tangential, axial etc without failure. Therefore the designer must take care of the material and the properties .

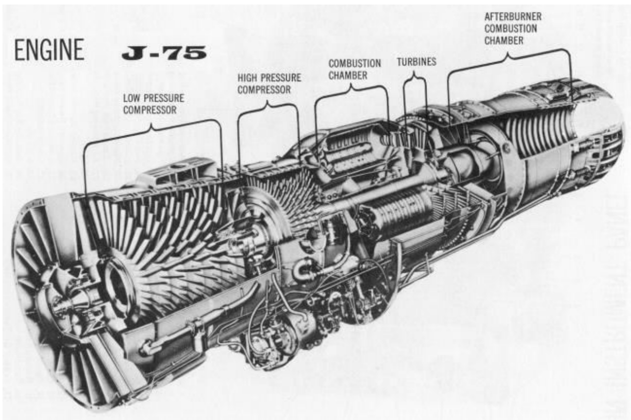

Figure 1 - layout of jet engine

This report describes the Temperature distribution and Thermal stress analysis of high pressure turbine disc of a jet engine .Analysing temperature distribution and thermal stress of UDIMET 720 and INCONEL 718.The analysis has been carried out by using finite element software ,ANSYSAPDL.The analysis and results are described in this report.

NX 8.5 is used to design the model, meshing is done by HYPERMESH and ANSYS APDLL is used for analysis.

Turbine disks are the most massive and expensive rotating components in gas turbine engines. They therefore have the highest kinetic energy, and a disk failure cannot be survived in most aerospace applications. Advanced engine disk design is thus faced with the need to develop new disk materials for improved temperature and performance capabilities combined with realistic, reliable durability models to ensure the highest levels of safety. The disk alloy team is involved in the development of improved powder metallurgy disk superalloys in the areas of composition, processing, microstructure, properties, and durability.

I1.MODELLING AND MESHING

The NX software integrates knowledge-based principles, industrial design, geometric modeling, advanced analysis, graphic simulation, and concurrent engineering. The software has powerful hybrid modeling capabilities by integrating constraint-based feature modeling and explicit geometric modeling. In addition to modeling standard geometry parts, it allows the user to design complex free-form shapes such as airfoils and manifolds. It also merges solid and surface modeling techniques into one powerful tool set.

By using NX 8.5 design the turbine disc. The mainstream hot gas flowing into the turbine disc. The disc receives heat from blade by convection and which is convected to the rim. The blades mounted on the disc at the rim receives heat by conduction. The disc transferring heat to the other parts by conduction. The heat received by secondary air from the hot gas and it cools by convection. Hot gases and secondary air is balanced at steady conditions.

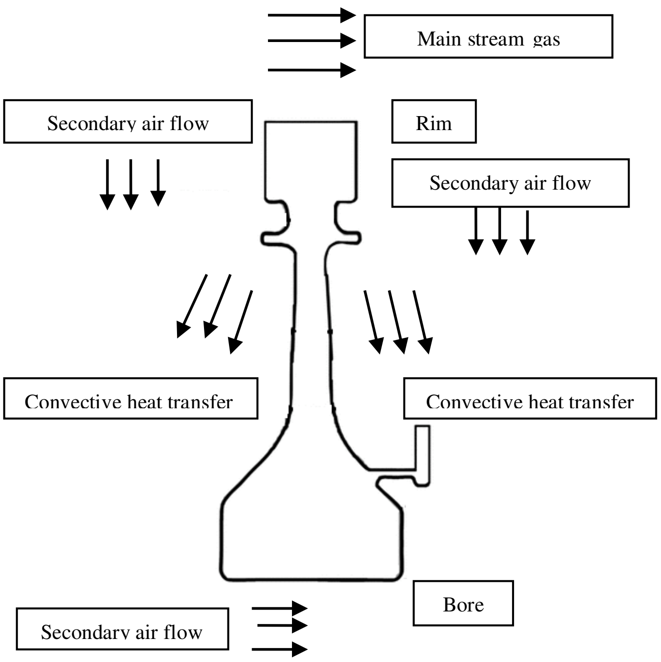

Figure 2-Turbine disc model

Hypermesh is a high-performance finite element pre- and post-processor for major finite element solvers, which allows engineers to analyze design conditions in a highly interactive and visual environment. Hypermesh's user-interface is easy to learn and supports the direct use of CAD geometry and existing finite element models, providing robust interoperability and efficiency. Advanced automation tools within Hypermesh allow users to optimize meshes from a set of quality criteria, change existing meshes through morphing, and generate mid-surfaces from models of varying thickness.

Finite Element Method is the discretization (elements and nodes) of a contentious system withinfinite number of degrees of freedom to finite number of degrees of freedom.Depending upon the nature of products such as small or big size and simple or complicated shapeetc, they are subjected to simple inspection or vigorous inspection which may included sometheoretical analysis also .Usually three methods are adopted for analyzing engineering products toevaluate their mechanical and other properties .They are

1. Experimental methods
2. Analytical methods
3. Numerical methods

This project is done by using quard meshing, I prefer quad mesh because it gives more accuratesolution than Tria .It is because Tria element having high stiffness than quad element. But Triaelement meshing is easier than quad meshing.

Before meshing we want to perform geometric cleanup and splitting to get a good quality mesh.While meshing we want to take care about the element size fine mesh or course mesh because if weare doing fine mesh we will get more accurate results but it will take large time to solve ,So mostprobably we are preferred course mesh and doing fine mesh over the critical regions.

Plane 55 is used as element type finite element modeling.PLANE55 can be used as a plane element or as an axisymmetric ring element with a 2-D thermal conduction capability. The element has four nodes with a single degree of freedom, temperature, at each node.

The element is applicable to a 2-D, steady-state or transient thermal analysis. The element can also compensate for mass transport heat flow from a constant velocity field. If the model containing the temperature element is also to be analyzed structurally, the element should be replaced by an equivalent structural element (such as PLANE182).A similar element with midside node capability is PLANE77. A similar axisymmetric element which accepts nonaxisymmetric loading is PLANE75.

The finite element analysis method requires the following major steps:

• Discretization of the domain into a finite number of subdomains (elements).
• Selection of interpolation functions.
• Development of the element matrix for the subdomain (element).
• Assembly of the element matrices for each subdomain to obtain the global
matrix for the entire domain,
• Imposition of the boundary conditions.
• Solution of equations.
• Additional computations (if desired).

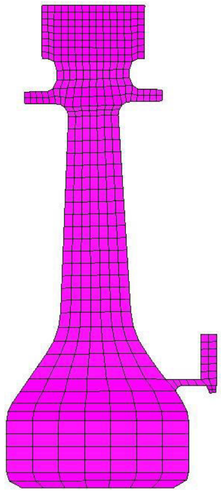

Figure 3-Turbine disc configuration

This FEA model is then connected to thermal analysis Systems .We need to give the engineering data related to the material for thermal analysis. The engineering data required thermal analysis thermal conductivity , thermal expansion coefficient, etc. At first we will run the cfd part and generate the solution such temperature. Then this temperature imported to thermal analysis. In setup we apply the boundary condition and give solve to obtain the result output.

ANSYS Workbench is a project management tool. It can be considered as the top – level interface linking all our software tools. Workbench handles the passing of data between ANSYS Geometry/Mesh/Solver/Post Processing tools.Dragging an analysis system to the project desktop lays out a workflow, comprising all the steps needed for a typical analysis. Workflow is from top to bottom. However an analysis could equally well be prepared by selecting the individual component systems that are needed for the analysis, and then linking them together with connectors.

The Finite element model is exported into the solver desk ANSYSs APDL 14 after assigning the element type. In ANSYS APDL 14 applied equation and write cdb file, this cdb file is open in ANSYS Workbench fea modeler .
UDIMET 720 and INCONEL 718 is used for the turbine disc material.

UDIMET 720

Super alloys or high performance alloys are available in a variety of shapes and contain elements in different combinations to obtain a specific result. These alloys are of three types that include iron-based, cobalt-based and nickel-based alloys. Super alloys have good oxidation and creep resistance and can be strengthened by precipitation hardening, solid-solution hardening and work hardening methods. They can also function under high mechanical stress and high temperatures and also in places that require high surface stability.

Element	Content (%)
Nickel, Ni	55.16-59.705
Chromium, Cr	15.5-16.5
Cobalt, Co	14.0-15.5
Titanium, Ti	4.75-5.25
Molybdenum, Mo	2.75-3.25
Aluminum, Al	2.25-2.75
Tungsten, W	1.00-1.50
Zirconium, Zr	0.0250-0.0500
Boron, B	0.0100-0.0200
Carbon, C	0.0100-0.0200

Chemical properties of UDIMET 720

INCONEL 718

Inconel 718 is a nickel-chromium-molybdenum alloy designed to resist a wide range of severely corrosive environments, pitting and crevice corrosion. This nickel steel alloy also displays exceptionally high yield, tensile, and creep-rupture properties at high temperatures. This nickel alloy is used from cryogenic temperatures up to long term service at 1200° F. One of the distinguishing features of Inconel 718's composition is the addition of niobium to permit age hardening which allows annealing and welding without spontaneous hardening during heating and cooling. The addition of niobium acts with the molybdenum to stiffen the alloy's matrix and provide high strength without a strengthening heat treatment. Other popular nickel-chromium alloys are age hardened through the addition of aluminum and titanium. This nickel steel alloy is readily fabricated and may be welded in either the annealed or precipitation (age) hardened condition.

Element	Percentage
Carbon	0.08 max
Manganese	0.35 max
Phosphorus	0.015 max
Sulfur	0.015 max
Silicon	0.35 max
Chromium	17-21
Nickel	50-55
Molybdenum	2.80-3.30
Columbium	4.75-5.50
Titanium	0.65-1.15
Aluminum	0.20-0.80
Cobalt	1.00 max
Boron	0.006 max
Copper	0.30 max
Tantalum	0.05 max
Iron	Balance

Chemical properties of INCONEL 718

III.RESULTS AND CONCLUSION

Results obtained from ANSYS APDL for temperature distribution and stress calculations of both UDIMET 720 and INCONEL 718 are shown below.

UDIMET 720

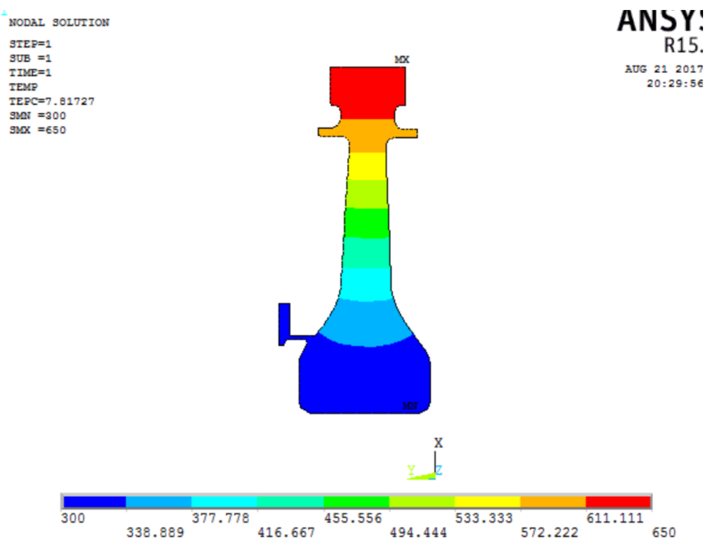

Figure 4-Temperature distribution of UDIMET 720

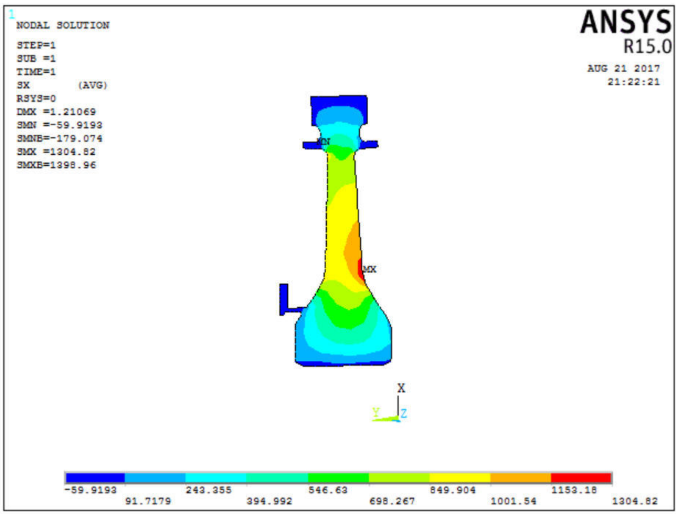

Figure 6-Radial stress of UDIMET 720

INCONEL 718

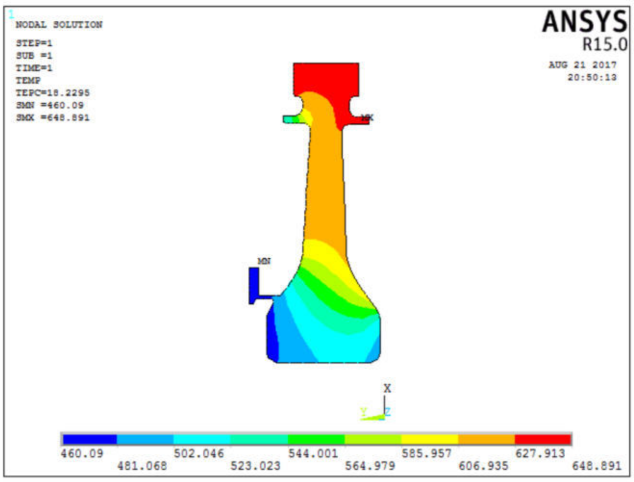

Figure 5-Temperature distribution of INCONEL 718

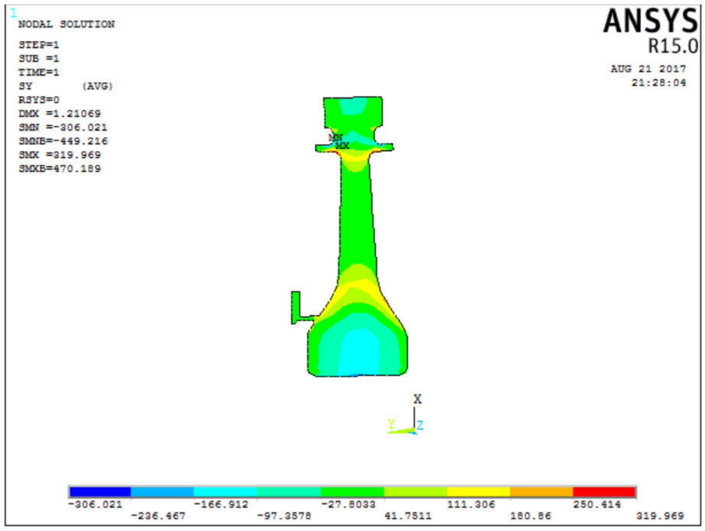

Figure 7-Tangential stress of UDIMET 7

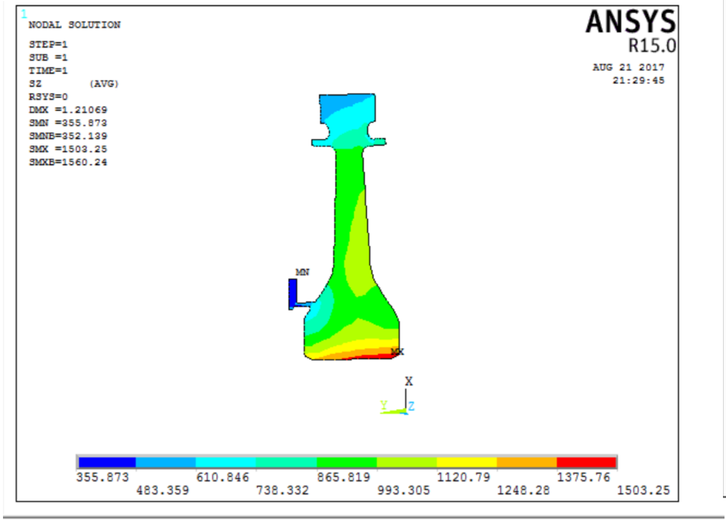

Figure 8-Axial stress of UDIMET 720

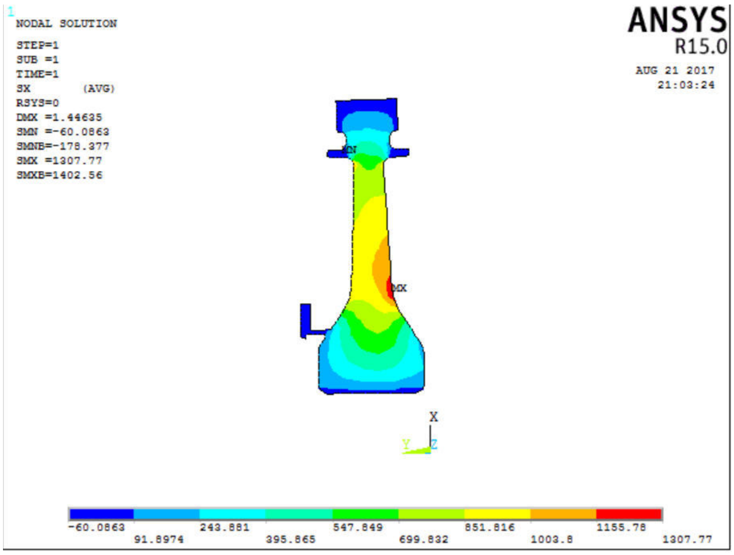

Figure 10-Radial stress of INCONEL 718

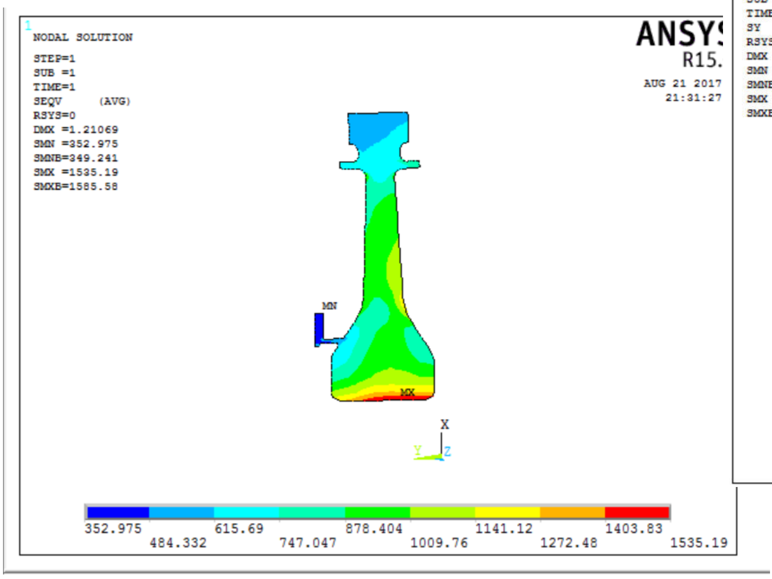

Figure 9-Vonmises stress of UDIMET 720

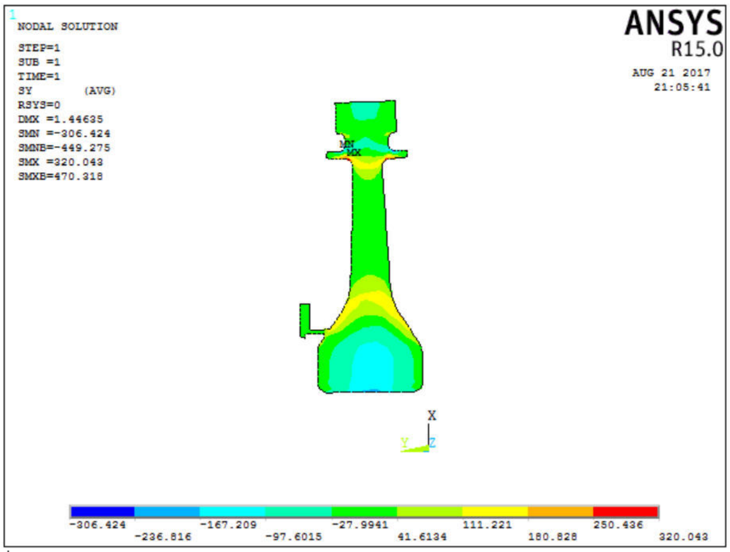

Figure 11-Tangential stressof INCONEL 718

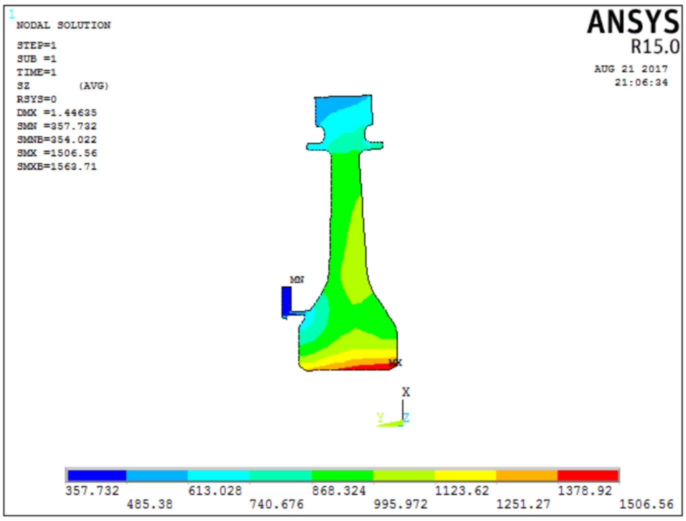

Figure 12-Axial stress of INCONEL 718

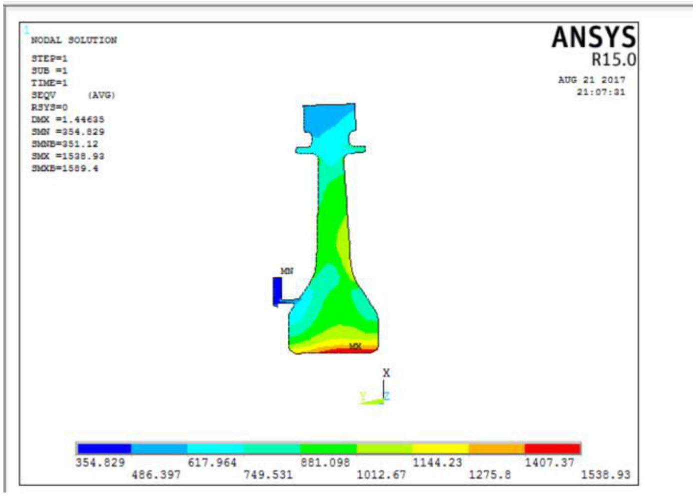

Figure 13-Vonmises stress of INCONEL 718

.RESULT TABLE

RESULT TABLEMATERIAL	RADIAL STRESS (MPa)	TANGENTIAL STRESS (MPa)	AXIAL STRESS (MPa)	VONMISES STRESS (MPa)
UDIMET 720	1304.82	319.969	1503.25	1535.19
INCONEL 718	1307.77	320.03	1506.56	1538.93

The thermal stress acting on UDIMET 720 is lesser than INCONEL 718.

1. Finite analysis of gas turbine disc is carried using PLANE55.The temperature has an important effect on turbine disc.
2. Temperature and rotation depends on stress and material properties. Stress is in most cases function of external loads and geometry.
3.UDIMET 720 is the best material for turbine disc than INCONEL 718,because of its better thermal properties.
4. Temperature gradient is directly proportional to heat transfer rate .i.e. if the temperature gradient is high, the heat transfer rate is also high.
5. Heat transfer rate is also depends on material properties.

REFERENCES

1.D.Bohn,E.Deuker,R.Emunds, V. Gorzelitz, “Experimental And Theoretical Investigation Of Heat Tranfer In Closed Gas Filled Rotating Annuli”.
2.J.Ramesh, C.VijayaBhaskar Reddy, Dr. B. Jayachandraiah,, “Design And Analysis Of Hp Steam Turbine Casing For Transient State Condition ”.
3.GantaNagaraju, Venkata Ramesh Mamilla, M. V. Mallikarjun,“ Design Optimization And Static & Thermal Analysis Of Gas Turbine Blade”.
4.Shilpa P. Bhorkar, Dr. A.V. Vanalkar,“ Transient Thermal Analysis Of A Steam Turbine Rotor”.

5.Arun Joe, M.Lr.ChaitanayaLahari,“Temperature Calculation And Stress Analysis Of Gas Turbine Engine Rotor Blade”.

6.R.S.Bunker,D.E.Metzger,S.Witting“Local Heat Transfer In Turbine Disc Cavities”.

7.J.X.Chen,X.Gan,J.M.Owen,“Heat Transfer From Air-Cooled Contra Rotating Discs”.

8.Michael Ebert,WeiShyy,SiddharthThakur,CorinSegal,“Heat Transfer And Fluid Flow In Rotating Cavities”.

9.Z.X.Yuan, N.Saniei,X.T.Yan,“Turbulent Heat Transfer On The Stationary Disc In A Rotor-Stator System”.

10G. D. Singh And S. Rawtani,“.International Engineering Service”.

10.Vijay A. Gaikwad, PravinLohote ,“Review On Fir Tree Joint F Turbine Disc N Aero Engine”.

11."The Jet Engine"-Rolls Royce,(1996).

12. S.S Rao, (1999)" The Finite Element Method In Engineering", Bh Publications New Delhi,3rd edition.

13.P.V.Krishnakanth,G.NarasaRaju ,R.Saisrinu(2013)," Structural And Thermal Analysis Of Gas Turbine By Using FEM"

14.OlegRojkov(2007),"Strategy For Turbine Blade Meshing Using Hypermesh"

15.H.I.H,Saravanamutto,Gordon Frederck Crichton Rogers,"Gas Turbine Theory"

16. J.Ramesh,C.VijayaBhaskar Reddy, Dr. B. Jayachandraiah ," Design And Analysis Of HP Steam Turbine Casing For Transient State Condition "

17.GantaNagaraju ,Venkata Ramesh Mamilla, M.V.Mallikarjundesign" Optimization And Static & Thermal Analysis Of Gas Turbine Blade".

18.F. E. Sczerzenie , G. E. Maurer," Development Of Ljdimet 720 For High Strength Disk Applications "

19.*LK, Rastogi V, Gupta P (2017).* "Study Of Corrosive Fatigue And Life Enhancement Of Low Pressure Steam Turbine Blade Using Friction Dampers". *Journal Of Mechanical Science And Technology*

20. Koff, Bernard L. (2003). "Gas Turbine Technology Overview - A Designer's Perspective". AIAA/ICAS International Air And Space Symposium And Exposition.

21. *Takeshi, Takashi, Kuniyuki, Ken-Ichi, Masato.* "Development Of CMC Turbine Parts For Aero Engines"

22.Halbig, Jaskowiak, Kiser, Zhu (June 2013). "Evaluation Of Ceramic Matrix Composite Technology For Aircraft Turbine Engine Applications" "Ceramic Matrix Composites Allow GE Jet Engines To Fly Longer - GE Reports". *GE Reports.*

22.Schilke, P. W. (2004)." Advanced Gas Turbine Materials And Coatings".

23.Mackay, Rebecca A, (2007) "Low-Density, Creep-Resistant Superalloys Developed For Turbine Blades. NASA Glenn's Research & Technology".

24.Ming C Leu, Akul Joshi"NX For Engineering Design "**.**

25.Frank p incopera ,David p dewitt" Fundamentals of heat and mass transfer".

MICRO ELECTRO MECHANICAL SYSTEMS

SONNAITENKAM VINAY
PG scholar
Dept. Of mechanical Engineering
Malla reddy college of engineering
Hyderabad, Telangana
Email: vinaysonnaitenkam@gmail.com

Dr. E RAJITH
Professor
Dept. Of mechanical Engineering
Crescent college of engineering
Tamil nadu

Abstract-"Micromechatronic is the synergistic integration of microelectromechanical systems, electronic technologies and precision mechatronics with high added value."

This field is the study of small mechanical devices and systems .they range in size from a few microns to a few millimeters. This field is called by a wide variety of names in different parts of the world: micro electro mechanical systems (MEMS), micromechanics, Microsystems technology (MST), micro machines .this field which encompasses all aspects of science and technology, is involved with things one smaller scale. Creative people from all technical disciplines have important contributions to make.

MEMS is a relatively new technology which exploits the existing microelectronics infrastructure to create complex machines with micron feature sizes .these machines can have many functions, including sensing, communication and actuation. Extensive application of these devices exists in both commercial and defense systems.

I. INTRODUCTION

Microelectromechanical systems or MEMS are integrated micro devices or systems combining electrical and mechanical components .they are fabricated using integrated circuit(IC) batch processing techniques and can range in size from micrometers to millimeters. These systems can sense control and actuate on the micro scale and function individually or in arrays to generate effects on the micro scale.

"The field of micro electro mechanical system (MEMS) is based on the use of integrated circuit (IC) fabrication techniques to create devices capable of acting as mechanical, electrical, and chemical transducers for applications in areas such as automotive and medical industries."

Fig.1 MEMS

It can be difficult for one to imagine the size of MEMS device. The general size of MEMS is on the order of microns (10 power-6 meter). The main characteristic of MEMS is their small size. Due to their size, MEMS cannot be seen with the unaided eye. An optical microscope is usually required for one to be able to see them.

In this paper, we will discuss the field of MEMS in 3 parts:

First, it will discuss a general manufacturing process and fabrications involved in MEMS devices. Second, it will discuss the advantages and disadvantages using MEMS devices. Lastly, it will discuss important applications of MEMS devices in automotive industry.

II. MANUFACTURING PROCESS OF MEMS

Today, we have the capability to produce almost any type of MEMS devices. To fully understand what MEMS are, we must first understand the basic of the MEMS manufacturing process, fabrication process, and their material compositions.

2.1 MATERIALS

MEMS are generally made from a material called polycrystalline silicon which is a common material also used to make integrated circuits. Frequently, polycrystalline silicon is doped with other materials like germanium or phosphate to enhance the materials properties. Sometimes, copper or aluminium is plated onto the polycrystalline silicon to allow electrical conduction between different parts of the MEMS devices. Now, that we understand the material composition of MEMS devices.

2.2 PHOTOLITHOGRAPHY

Photolithography is the basic technique used to define the shape of micro machine structures in the three techniques outlined below. The technique is essentially the same as that used in the microelectronics industry, which will be described here. The differences in the photolithographic techniques for Excimer laser micromachining and LIGA will be outlined in the relevant sections.

Figure shows a thin film of some material (eg. silicon dioxide) on a substrate of some other material (eg. silicon wafer). It is desired that some of the silicon dioxide (oxide) is selectively removed so that it only remains in particular areas on the silicon wafer. Firstly, a mask is produced. This will typically be a chromium pattern on a glass plate. The wafer is then coated with a polymer which is sensitive to ultraviolet light called a photo resist. Ultraviolet light is then shone through the mask onto the photo resist. The photo resist is then developed which transfers the pattern on the mask to the photo resist layer. There are two types of photo resist, termed positive and negative photo resist. Where the ultraviolet light strikes the positive resist it weakens the polymer, so that when the image is developed the resist is washed away where the light struck it – transferring a positive image of the mask to the resist layer.

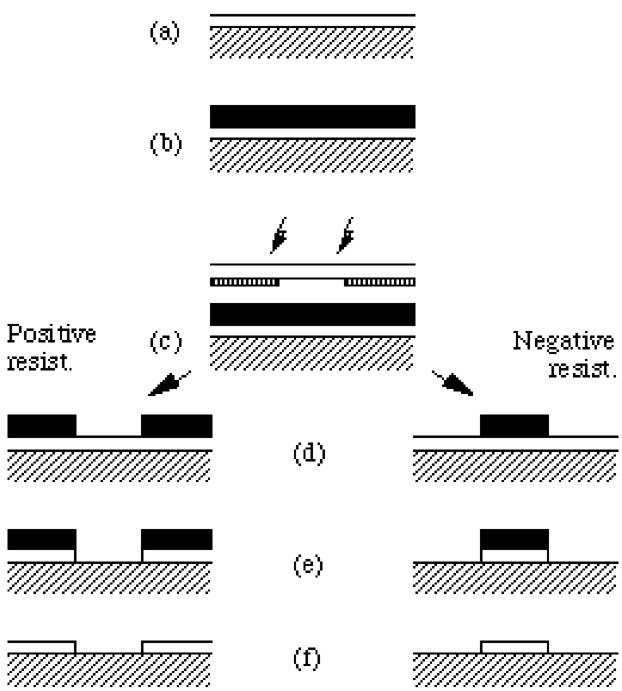

Fig.2 PHOTOLITHOGRAPHY

The opposite occurs with the negative resist. Where the ultraviolet light strikes negative resist it strengthens the polymer, so when developed the resist that was not exposed to ultraviolet light is washed away – a negative image of the mask is transferred to the resist.

A chemical (or some other method) is used to remove the oxide where it is exposed through the openings in the resist. Finally, the resist is removed leaving the patterned oxide.

2.3 SILICON MICROMACHINING

There are number of basic techniques that can be used to pattern thin films that have been deposited on a silicon wafer, and to shape the wafer itself, to form a set of basic microstructures (bulk micromachining). The techniques for depositing and patterning thin films can be used to produce quite complex microstructures on the surface of silicon wafer (surface silicon micromachining). Electrochemical etching techniques are being investigated to extend the set of basic silicon micromachining techniques. Silicon bonding techniques can also be utilized to extend the structures produced by silicon micromachining techniques into multilayer structures.

III. Excimer laser micromachining

Excimer lasers produce relatively wide beams of ultraviolet laser light. One interesting application of these lasers is their use in micromachining organic materials (plastics, polymers, etc). This is because the excimer laser doesn't remove material by burning or vaporizing it, unlike other types of laser, so the material adjacent to the area machined is not melted or distorted by heating effects. system the mask is placed in contact with the material being machined, and the laser light is shone through it. A more sophisticated and versatile method involves When machining organic materials the laser is pulsed on and off, removing material with each pulse. The amount of material removed is dependent on the material itself, the length of the pulse, and the intensity (fluency) of the laser light. Structures with vertical sides can be created. By adjusting the optics it is possible to produce structures with tapered sidewalls.

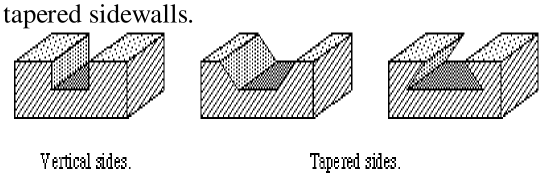

FIG.4 EXCIMER LASER MICROMACHINING

Below certain threshold fluency, dependent on the material, the laser light has no effect. As the fluency is increased above the threshold, the depth of material removed per pulse is also increased.

It is possible to accurately control the depth of the cut by counting the number of pulses. Quite deep cuts (hundreds of microns) can be made using the excimer laser. The shape of the structures produced is controlled by using chrome on quartz mask, like the masks produced for photolithography. In the simplest projecting the image of the mask onto the material. Material is selectively removed where the laser light strikes it.

IV. FABRICATION PROCESS IN MEMS

4.1 ADVANCED MICRO SYSTEMS FABRICATION TECHNOLOGIES

- Plastics Technologies
- Glass Technologies
- Silicon Technologies
- Metals Technologies

4.2 PRECISION MACHINING TECHNOLOGIES

- Jet Deposition Technologies
- Laser Sintering Technologies
- Jet Molding Technologies
- Electrical Discharge Machining
- Micro milling / drilling
- 3-D Micro Fabrication Technologies

CASE STYDY

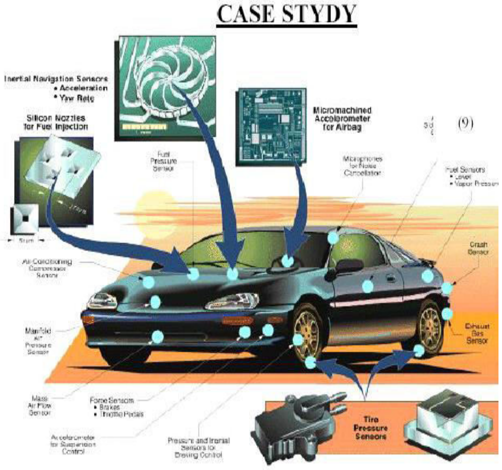

FIG 5 COMPLEXITY OF FABRICATION

4.3 EMERGING SILICON MICRO FABRICATION TECHNOLOGIES

- Deep Reactive Ion Etching
- Electroplated Photo resist
- Integration of Piezoelectric Devices

V. ADVANTAGES AND DISADVANTAGES OF MEMS

5.1 ADVANTAGES OF MEMS

There are four main advantages of using MEMS rather than ordinary large scale machinery.

- Ease of production.
- MEMS can be mass-produced and are inexpensive to make.
- Ease of parts alteration.
- Higher reliability than their macro scale counterparts

5.2 DISADVANTAGES OF MEMS

- Due to their size, it is physically impossible for MEMS to transfer any significant power.
- MEMS are made up of Poly-Si (a brittle material), so they cannot be loaded with large forces.

To overcome the disadvantages, many MEMS researchers are working hard to improve MEMS material strength and ability to transfer mechanical power. Nevertheless, MEMS still have countless number of applications as stated below.

VI. APPLICATION OF MEMS

- ❖ Inertial navigation units on a chip for munitions guidance and personal navigation.
- ❖ Electromechanical signal processing for ultra-small and ultra low-power wireless communications.
- ❖ Distributed unattended sensors for asset tracking, environmental monitoring, and security surveillance.
- ❖ Integrated fluidic systems for miniature analytical instruments, propellant, and combustion control.
- ❖ Weapons safing, arming, and fuzing.
- ❖ Embedded sensors and actuators for condition-based maintenance.
- ❖ Mass data storage devices for high density and low power.
- ❖ Integrated micro-optomechanical components for identify-friend-or-foe

systems, displays, and fiber-optic switches.

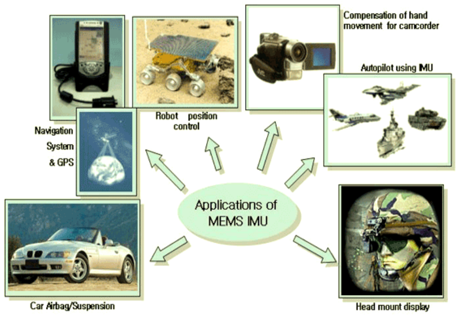

FIG.6 **APPLICATION OF MEMS**

6.1 MEMS Sensors Are Driving the Automotive Industry

- Vehicle Dynamic Control
- Rollover Detection
- Electronic Parking Brake Systems
- Vehicle Navigation Systems
- The Sensor Cluster

CONCLUSION

Thus hereby we concluded our presentation in the topic of MEMS which is going to be the future of the modern technical field in the growth of micro sensor based applications such as automotive industries, wireless communication, security systems, bio medical instrumentation and in armed forces.

REFERENCE

1. Nexus Market Analysis for MEMS and Microsystems III, 2005 - 2009
2. Think Small!, issue 2, volume 2, July 2007, Wicht Technologie Consulting
3. Lab-on-Chip and Microfluidics Technologies' Capability to Reduce Costs and Time-to-Market Drive Uptake in Drug Development and Clinical Diagnostics, Frost & Sullivan, July 2007

4. Smith, J.H. et. al., Embedded Micromechanical Devices for the Monolithic Integration of MEMS with CMOS, Proc. 1995 IEDM, pp. 609-612
5. Rewards and Risks of Moving into New Applications: Case Study Accelerometers, Henne van Heeren, Jeremie Bouchaud, Richard Dixon and Patric Salomon, MSTnews, February 2007
6. 2005 Electromechanical Switches – Global Market Demand Analysis. www.vdc-corp.com
7. Emerging Markets for Microfluidic Applications, Yole Developpement, June 2007
8. MEMS in Medicine, Ken Gilleo, www.et-trends.com
9. Diagnostic Report 2007, Cambridge Consultants, www.cambridgeconsultants.com
10. IEEE Robotics & Automation magazine, March 2003.

NUMERICAL ANALYSIS OF HEAT TRANSFER AND FLOW FRICTION THROUGH A PIN FIN CHANNEL SECTION

SHIJILA P V[1], SHASHIKUMAR S[2], Dr. S S GOWDA[3]

[1]PG Scholar, [2]Assistance Professor, [3] Professor

Department of Mechanical engineering, MallaReddy College of Engineering

Abstract

A numerical study was conducted to investigate the flow friction and heat transfer performance in rectangular channels with pin fins in the Reynolds number range of 8200–54,000. The study aims at improving the cooling design for the gas turbine components such as combustion chamber and turbine blades. The pin fins are enhancing the heat transfer and also increase the structure integrity and stiffness. The friction factor and Nusselts number of the pin fin channels have been obtained and compared with the previously published data and also with the result obtained by using correlations correspondence to the smooth channel. CATIA software is used for the modeling of the test section and NUMECA is used for its grid generation, analysis and post processing purpose. By this study observed that the presence of pin fin is increases the heat transfer rate through the channel. It is obtained by, when the fluid flows across the pin fins arrays unsteady vertical shedding induced from the pin. Hence this produce high turbulence level in the flow and it enhance the convective heat transfer performance. The frictional factor also is higher for pin fin channel than the smooth channel. The Reynolds numbers also have a role in the heat transfer rate. The heat transfer rate is increases with increasing the Reynolds number. For analyzing different turbulence model gives different result. k-ϵ turbulence model gives a matching result with the previously published paper. The pin fin is a easy method for improving heat transfer rate.

Key words: Heat transfer, pin fin, flow friction, NUMECA, CATIA

1. INTRODUCTION

Heat is the major source of energy; it can be converted into mechanical energy through gas turbines and power plants. Gas turbine output is used for different types of work. Maximum amount of heat energy converted into mechanical work by improving the efficiency of the gas turbine engine. In the turbine component, entering flow temperature is high then the thermal efficiency of the whole engine is also become very high. . But its temperature value is limited by the material which is used for the turbine blade manufacturing. This limitation is overcome by providing cooling technique to the turbine blades. By using pin fins in the turbine blades heat transfer rate increases as well as it provides stiffness to the blade. In this project, the numerical analysis of heat transfer performance and friction factor of a flow through a test channel section with pin fin are carried out. Yu Rao [1] $et.al$ conducted a study on the title "Experimental study of pressure loss and heat transfer in the pin fin an pin fin dimple channel with various dimple depths". In this paper they included experimental as well as numerical study. Their conclusion also the same that the heat transfer rate can be improved by providing pin fins. The flow friction due to the presence of pin fin can be reduced by providing dimples. Earlier they started studies regarding this pin fin heat transfer.

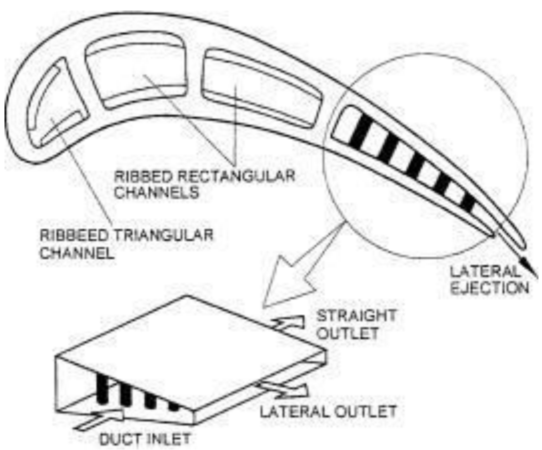

Figure 1.1 Pin Fin Arrangements in a Blade Section

The flow passes through a rectangular test section which is having staggered arranged pin fins. Inlet and outlet is provided for this test section for getting smooth steady flow through the section. The model is created by using CATIA V5. The pre-processing, solving and analysis is done by using the software NUMECA. Then the output result is compared with the experimental data which is already available and the correlations.

2. MODELLING AND MESHING

The numerical analysis of heat transfer through the rectangular test section is done by using the software package NUMECA. This is CFD software in which finite volume method is used. The model is made by using the software CATIA V5. For the entire work, NUMECA is used with the interface between different platforms of it.

For this work the three dimensional model of the test channel section is created by using CATIA software corresponding to the geometry criteria. The test section contains pin-fins arranged in staggered manner and also having an inlet and outlet section having same cross section of the test channel. Best surface modelling capabilities and tools, in-built cam operation feature are some of the advantages of this software. It is a user friendly software. It having a huge library of material is then solid works. It can be used in different fields like, electrical, mechanical, civil, aerospace, automobile etc. CATIA is also proved that it is an efficient one.

The geometry chosen for this experiment is a rectangular cross sectional channel with pin fins which are arranged in staggered manner. The geometry is same throughout the experiment for different Reynolds number. An inlet and outlet section also provided to this test section for proper mixing of the flow. The total length of the channel is 645mm, in which 160mm for outlet section and 245m length for test section. The breadth and width for all sections are 120mm and 10mm respectively. Total number of rows is 10 and the pin fins are arranged in staggered manner. The diameter of the pin fins are 10mm and the height to diameter ratio is 1. The hydraulic diameter to pin fin diameter ratio is 1.85

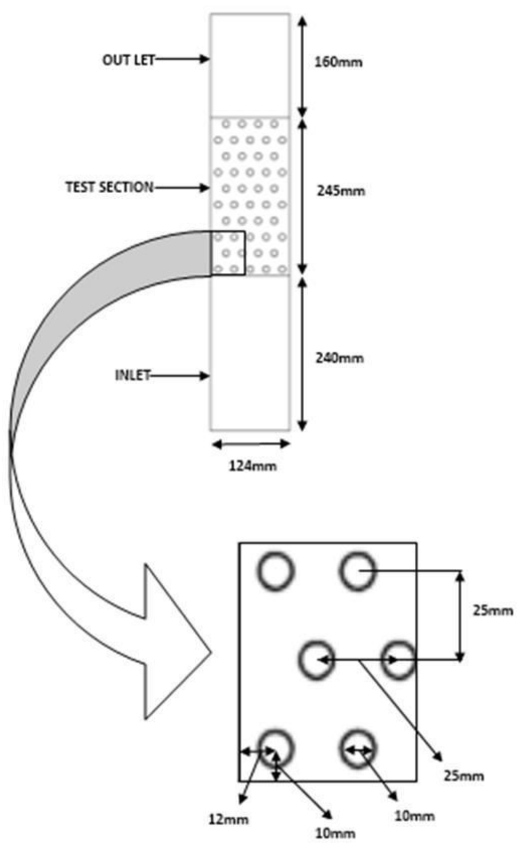

The model section in XYZ axis is as shown in below.

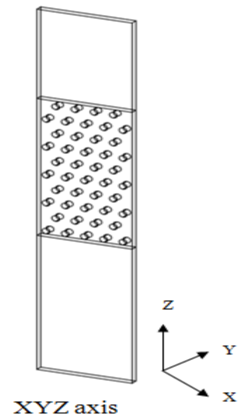

The CFD software NUMECA is used here for the preprocessing solving and post processing work. In this study auto mesh is done by using HXPRESS NUMECA tool. Here the values corresponding to,

Number of refinements = 4

Reference length = .0185

The kinematics viscosity and reference velocity are depends the Reynolds number.

Total number of cells	Whole section	11722663
	Inlet and Outlet	6392560
	Test section	5330103
Total number of vertices	Whole section	6265349
	Inlet and Outlet	668491
	Test section	5596858

Number of Mesh cells obtained is given in the above table.

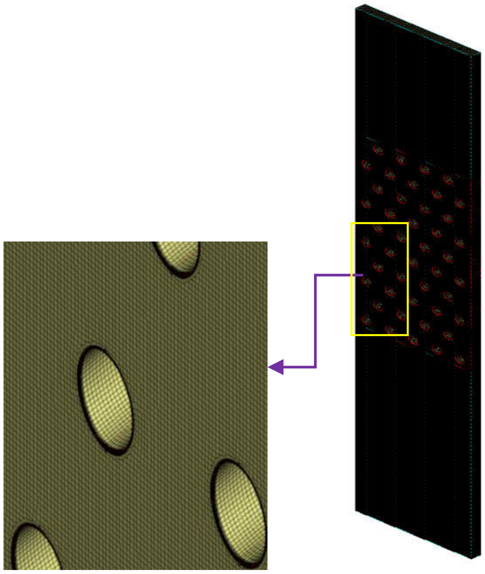

3. NUMERICAL METHODS

The important basic equations used for the current study are:

Continuity equation: $\frac{\partial uj}{\partial xj} = 0$

Momentum Equation:

$$\frac{\partial \rho uiuj}{\partial xj} = -\frac{\partial p}{\partial xi} + \frac{\partial}{\partial xj}\left((\mu + \mu t)\left(\frac{\partial uj}{\partial xi} + \frac{\partial ui}{\partial xj}\right)\right)$$

Energy equation:

$$\partial uiT/\partial xi = \partial/\partial xi \; ((\mu/Pr + \mu t/Prt) \;\; \partial T/\partial xi)$$

The equation for k and ϵ:

$$\frac{\partial(\rho U_j k)}{\partial x} = \frac{\partial}{\partial x_j}\left[\sigma_k(\mu + \mu_t)\frac{\partial k}{\partial x_j}\right] + P_K - \rho\epsilon$$

$$\frac{\partial(\rho U_j \epsilon)}{\partial x_j} = \frac{\partial}{\partial x_j}\left[\sigma_\epsilon(\mu + \mu_t)\frac{\partial \epsilon}{\partial x_j}\right] + \quad C_{\epsilon 1}\frac{\epsilon}{k}P_k - C_{\epsilon 2}\rho\frac{\epsilon^2}{k} - \mathrm{R}$$

Where, $\sigma_k = 1.0,\ \sigma_\epsilon = 1.3, C_{\epsilon 1} = 1.42, C_{\epsilon 2} = 1.68$.

Heat transfer rate can be calculated by using the Nusselts number. **Nusselts number** can be defined as, it is the ratio of convective to conductive heat transfer across (normal to) the boundary. In heat transfer at boundary (surface) with in a fluid, Nusselt number have important role. It is a dimensional number.

- The Nusselts number close to 1, namely, convection and conduction of similar magnitude, is characteristics of slug flow or laminar flow.
- A large Nusselts number corresponds to more active convection, with turbulent flow typically in the 100-1000 range.

$$\text{Nu} = \frac{\text{Total heat transfer}}{\text{Conductive heat transfer}}$$

$$\mathbf{Nu} = \frac{\mathbf{hL}}{\boldsymbol{\lambda}}$$

Here,

$$\mathbf{h} = \frac{\mathbf{Q}}{\mathbf{AT_{lm}}}$$

and

$$T_{lm} = \frac{T_{out} - T_{in}}{\ln\left[\frac{T_w - T_{in}}{T_w - T_{out}}\right]}$$

The concept of hydraulic diameter allows the use of relationships developed for circular pipes with noncircular conduits.

Hydraulic diameter, $D_h = \frac{4A}{P}$

4. RESULTS

The flow which passes through the pin fin channel is analysed by using the CFD software (NUMECA). The numerical results of inlet and outlet temperature, pressure, the bottom wall temperature, the Nusselts number and friction factor for different Reynolds number are given in the table.

Re	Tin(K)	Tout(K)	Pin(Pa)	Pout(Pa)	Tw(K)	Tm(K)	Nu	f
8200	297.583	305.635	101532	101311	348.751	309.502	81.302	0.5743
15639	297.632	303.046	102017	101240	330.633	305.646	131.863	0.5551
36700	297.656	301.734	104327	101123	314.413	303.693	264.79	0.4157
50500	297.672	300.874	105836	101046	303.785	302.413	351.889	0.3282
80800	297.706	298.987	109149	100877	280.45	299.603	543.128	0.2214

Table 5.3 Output Result

The figure given below shows the wall temperature distribution in the lower surface of the test section where the heat flux is given, corresponding to the Reynolds numbers 15639.

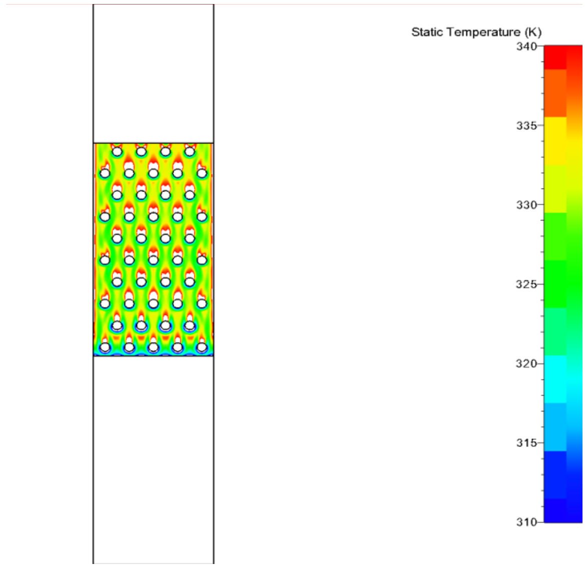

The flow velocity distribution is changes due to the presence of pin fin. At the wall boundary the reverse flow will occur due to the presence of boundary layer. The figure given below shows the velocity vector of the flow at a cut section by the YZ plane.

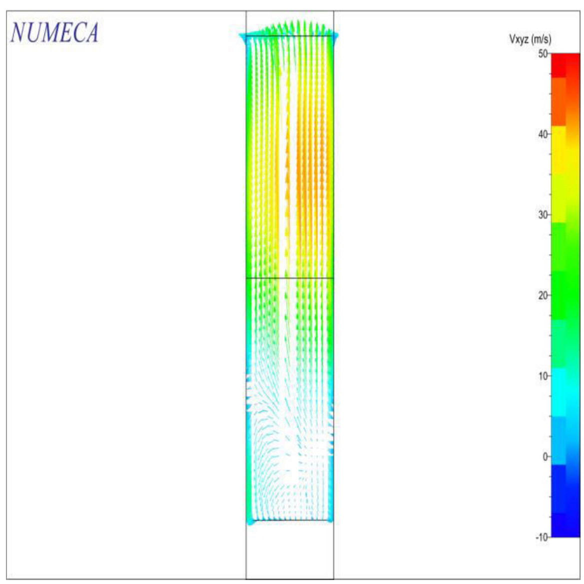

The figure given below shows the mean temperature distribution of the back wall of the test section where the heat fluxes is given, corresponding to the Reynolds number 15639.

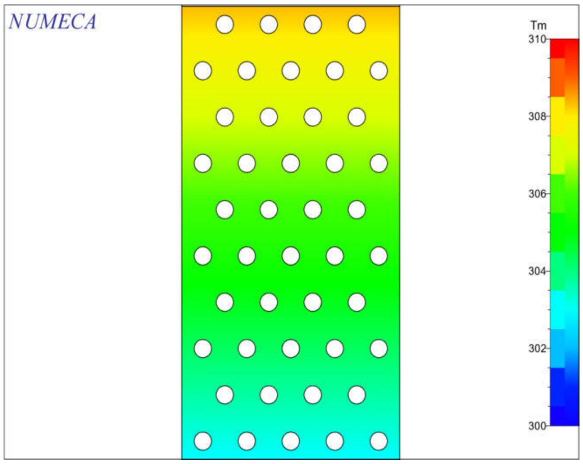

COMPARISON OF RESULTS

1. Nusselts Number

The Nusselts number is represents the heat transfer rate of the flow which is passes through a solid surface. Here the flow is passes through test channel which is having pin fins. Based on the value of the Nusselt number we can explain about the heat transfer rate through it. The figure given below shows the Nusselts number distribution at the bottom wall of the test section where heat flux is given corresponding to the Reynolds number 15639.

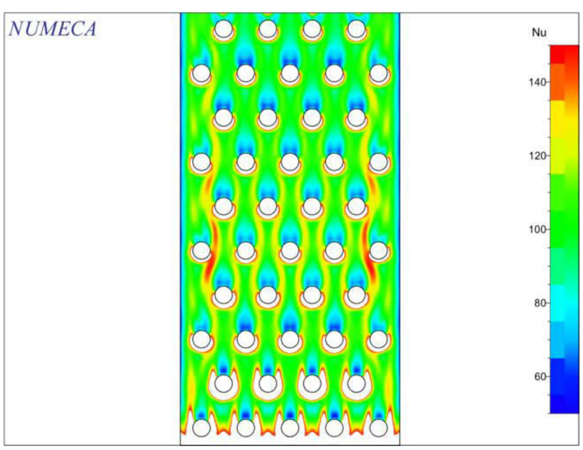

The figure given below shows the Nusselts number variation of pin fin channel with the Reynolds number corresponding to the numerical study and result of the Rao's numerical study.

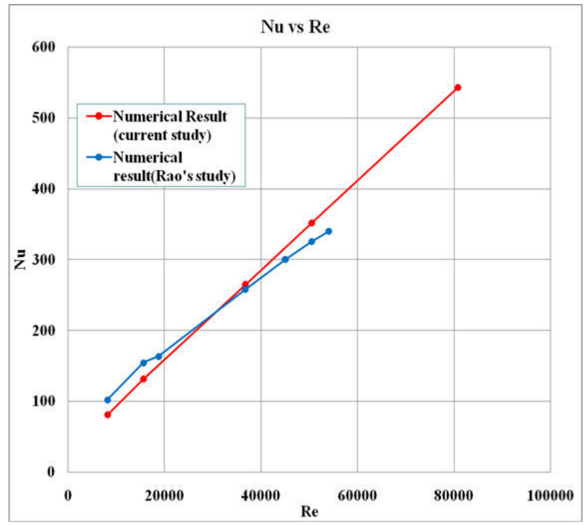

The result is almost matching in both cases. The small deviation occurred due to the some errors. In both cases the heat transfer rate is increases with the Reynolds number. Heat transfer rate of pin fin channel depends the value of Reynolds number.

The result of current study also can be compare with some correlations. Here, consider the correlation corresponding to the Nusselts number of smooth circular channel. Kay and Crawford's correlation for the circular duct fully developed turbulent flow is given by

$$Nu = 0.022 \times Re^{0.8} \times Pr^{0.5}$$

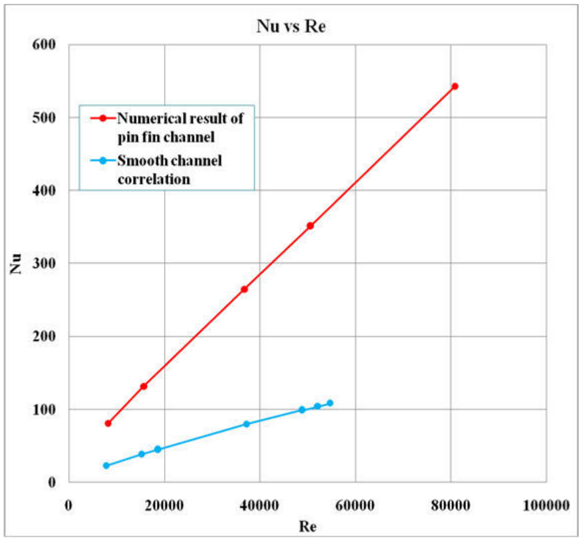

2. Friction factor

The friction factor is also considered under the study. Here, compare the friction factor for the current channel with the previously published paper as well as with the correlation for the smooth channel. The equation used to calculate the friction factor for the current study is given below.

$$f = \frac{2\Delta PD_h}{\rho U^2 L}$$

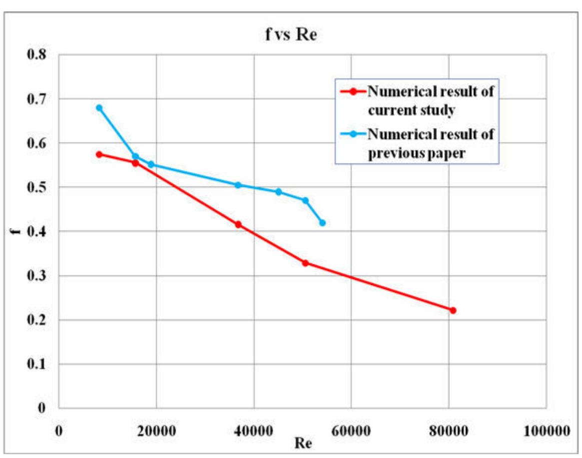

The presence of pin fin increases the friction factor. This can be analyzing by comparing the current friction factor result with friction factor of smooth channel obtained from correlation. The graphical representation of the above mentioned result is shown below. The Blasius correlation for the fully developed turbulent flow in circular ducts is given below which is used for the above mentioned comparison.

$$f = 0.316 \times Re^{-0.25}$$

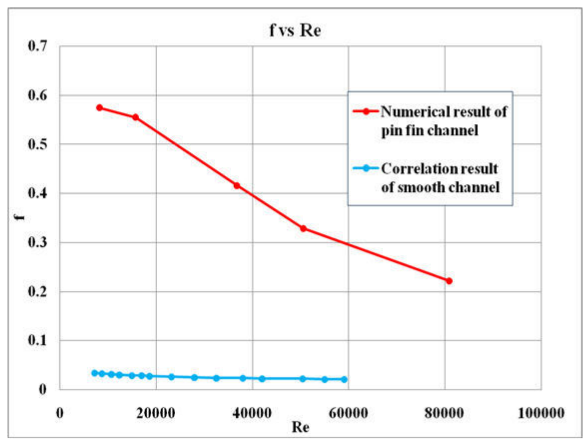

5. CONCUSION

In the paper, a comparative numerical study was conducted on the flow friction and heat transfer of pin fin channel. The friction factor and Nussels number of the pin fin channel have been obtained and compared with the previously published data of the pin fin channel and correlation of the smooth circular pipe for the Reynolds number range of 8200 – 80800. The output result obtained from the current study helps to obtained several conclusion. And also the work carried out can be extended for further studies.

The important conclusions obtained from the current study are;

- CFD analysis is a very easy and accurate method used for the heat transfer as well as the fluid flow analysis.

- Different flow model and fluid model can be analyzing by using the CFD software NUMECA.

- The Nusselts number obtained for the pin fin channel is almost matching with the previously published data.

- The Nusselts number is higher for the pin fin channel. Hence conclude that, the presence of pin fin increases the heat transfer rate. Due to this reason pin fins can be used as a cooling technique for the turbine blade.

- The main causes responsible for the heat transfer enhancement are, the characteristics in the distribution of the flow velocity and the turbulence level in the flow.

- The rate of heat transfer is increases with the increase of Reynolds number. The Nusselts number is higher for higher Reynolds number.

- For the smooth channel also the Nusselts number is increases with the increase in the Reynolds number.

- In the different flow models k-ε turbulence model is better than the Spallart – Allmaras turbulence model. k-ε model gives a matching result with previously published paper result.

- The friction factor is higher for the pin fin channel than the smooth channel. The presence of the pin fin causes increased rate friction. Hence there is disadvantage for using the pin fin is that the frictional loss is higher if pin fin is present.

- The friction factor is slightly reduces by increasing the Reynolds number for pin fin channel. For smooth channel the variation of friction factor is negligible with the Reynolds number.

Nomenclature

h	Convective heat transfer coefficient.
L	Characteristic length.
λ	Thermal conductivity
$\frac{Q}{A}$	Heat flux.
T_{lm}	Logarithmic mean temperature
T_{in}	Inlet temperature.
T_{out}	Outlet temperature.
T_w	Wall temperature.
A	Flow area.
P	Wetted perimeter
Pr	Prandtl number
F	Friction factor

ΔP Change in pressure

L The length of the test channel section

U Velocity of the flow

References

1. Experimental study of pressure loss and heat transfer in the pin fin an pin fin dimple channel with various dimple depths [Yu Rao, Chaoyi Wan YaminXu]
2. A numerical study on comparison on thermal performance of in-line pin-fins in wedge duct with tree kinds of coolant. [Gaoliang Liao, Xinjun Wang, Jun Li, Feng Zhang]
3. Comparison of Pin Surface Heat Transfer in Arrays of Oblong and Cylindrical Pin Fins [Kathryn L. Kirsch, Jason K. Ostanek, Karen A. Thole]
4. Trailing Edge Film Cooling of Gas Turbine Airfoils—External Cooling Performance of Various Internal Pin Fin Configurations [T. Horbach, A. Schulz, H.-J. Bauer]
5. Heat transfers from pin-fin arrays experiencing forced convection [M. Tahata, Z.H. Kodah, B.A. Jarrah, S.D. Probert]
6. Numerical analysis of flow structures and heat transfer characteristics in square channels with different internal-protruded dimple geometrics. [Gongnan Xie, Jian Liu, Philip M. Ligrani, Weihong Zhang]
7. Spatially-resolved heat transfer and flow structure in a rectangular channel with pin fins. [S.Y. Won, G.I. Mahmood, P.M. Ligrani]
8. Performance analysis of rectangular ducts with staggered square pin fins [O.N. Sara]
9. Comparison of Heat Transfer Prediction for Various Turbulence Models in a Pin Fin Channel [Mark Ricklick, Cassandra Carpenter]
10. A Numerical Study of the Flow and Heat Transfer in the Pin Fin-Dimple Channels With Various Dimple Depths[Yu Rao , Chaun N, Ligae Xe]
11. .Numerical study of turbulent heat transfer in 3D pin-fin channels: Validation of a quick procedure to estimate mean values in quasi-periodic flows [J.F.Mitre, L.M. Santana, R.B. Damian, J. Su, P.L.C. Lage]
12. Thermal performance of a pin-fin assembly [R. F. Babus'Haq, K. Akintunde, and S. D. Probert]
13. Augmented heat transfer in a pin fin channel with short or long ejection holes [T. K. KUMARAN, J. C. HAN and S. C. LAU]
14. Heat Transfer From Low Aspect Ratio Pin Fins [Michael E. Lyall, Alan A. Thrift, Karen A. Thole, Atul Kohli]
15. An experimental and computational investigation of thermal air flows through perforated pin heat sinks [Amer. Al-Damook,N. Kapur, J.L. Summers H.M.Thompson]
16. Measurement of end wall heat transfer and pressure drop in a pin fin wedge duct. [Jenn-Jiang Hwang, chau-Chin Lui]
17. Numerical heat transfer and fluid flow [Suhas V, Patankar]

18. Computational Fluid Dynamics: Principles and Applications [J. Blazek]
19. User guide of the Software CATIAV5
20. User guide and theory guide of the software NUMECA.
21. Practical approach of Computational Fluid Dynamics [Y. Chau]
22. Numerical and Experimental Investigation of Turning Flow Effects on Innovative Pin Fin Arrangements for Trailing Edge Cooling Configurations [C. Bianchini, B. Facchini, F. Simonetti, L. Tarchi, S. Zecchi]
23. Second law analysis of rectangular channels with square Pin-fins [O. N Sara, S. Yaplcl, M. Ytlmaz]
24. GTRE public site
25. Wikipedia
26. Google search
27. Computational Fluid Dynamics [John D. Anderson]
28. Fundamentals of Heat and Mass transfer [P.K.Nag]

THE COMPRESSED AIR VEHICLE

A. Happy
Mallareddy College of engineering
Hyderabad, India
Email:happy.angelika5@gmail.com

P. Johnpaul
Mallareddy College of engineering
Hyderabad, India
Email:jppulipati@yahoo.com

Abstract—**While developing of compressed air vehicle, control of compressed air parameters like temperature, energy density, requirement of input power, energy release and emission control have to be mastered for the development of a safe, light and cost effective compressed air vehicle in near future.This paper describes the design and construction of a viable experimental pneumatic driven vehicle. The main aim is to find ways to drive efficiently by using alternative energy, not necessary cheaper, but more environmental friendly in increasing polluted metropolis. This is done by taking the emission source from the vehicle's tail pipe to the central electrical generating plant. Emission control measures at a central generating plant may be more effective and less costly than treating the emissions of widely dispersed vehicles. Where low emissions sources are available like: Aeolian, water, solar, and nitrogen byproducts; net production of pollutants can be reduced. The results used in this study are obtained by designing, building and testing experimental configurations of compressed-air/gas vehicles.**

Keywords-pneumatic vehicle, compressed air, chassis, ackermann condition, pollutant, CO2

I INTRODUCTION

A **compressed-air vehicle** (**CAV**) is powered by an air engine, using compressed air, which is stored in a tank. Instead of mixing fuel with air and burning it in the engine to drive pistons with hot expanding gases, compressed-air vehicles use the expansion of compressed air to drive the pistons. The first compressed air vehicle was established in France by a Polish engineer Louis Mekarski in 1870 was tested in Paris in 1876.The working principle of Mekarski's engine was the use of energy stored in compressed air to increase gas the efficiency of S.I.engine.It is experimentally found that the efficiency of the vehicle ranges from 72-95%. So this can be considered as one of the preferable choices to run the vehicle.

Compressed-air technology reduces the cost of vehicle production by about 20%, because there is no need to build a cooling system, fuel tank, Ignition Systems or silencers.Hydro-carbons and carbon monoxide and CO_2, SO_2 are the major pollutants released by the combustion of fuels.

II. MODE OF USE

A. *Design of chassis*

Chassis is made by arc welding at various sections for the Rectangular cross sections. It includes:

•Lap joint welds •Butt welds •T joint welds

The end joints re butt welded and some internal angular sections are lap welded. The steering column support is given by welding a hollow shaft with a T weld to the front frame of the chassis.

The steering of a vehicle is so arranged that the front wheels will roll truly without any lateral slip. The function of the steering system is to convert the rotary movement of the steering wheel into angular turn of the front wheels. To keep effective control on the moving vehicle throughout its range of speed irrespective of the load and road conditions. The steering system of a vehicle should fulfill the following requirements:

1. It should multiply the effort applied on the steering wheel by the drivers.

2. The mechanism should have self-adjusting effect so that when the driver releases the steering wheel after negotiating the turn, the wheel should try to achieve straight ahead position.

3. It should not transmit road shocks to steering wheel.

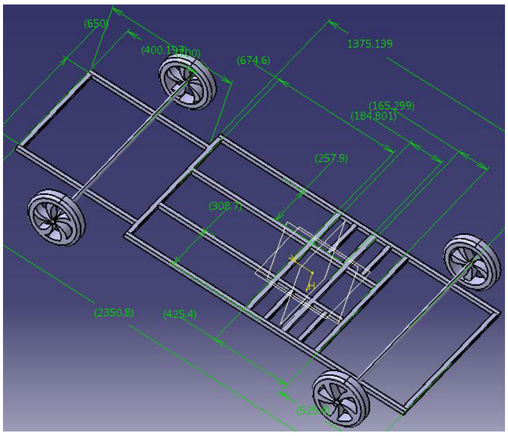

B. Storage tank

The storage tank may be made of metal or composite materials. The fiber materials are considerably lighter than metals but generally more expensive. Metal tanks can withstand a large number of pressure cycles, but must be checked for corrosion periodically.

C. Steering report

Types of steering gear mechanism used:

1. Davis steering gear mechanism
2. Ackermann steering gear mechanism

The main difference between the two steering gear mechanisms is that the Davis steering has sliding pairs, whereas the Ackermann steering has only turning pairs. The sliding pair has more friction than the turning pair; therefore the Davis steering gear will wear out earlier and become inaccurate after certain time. The Ackermann steering gear is not mathematically accurate except in three positions, contrary to the Davis steering gear which is mathematically correct in all positions. However, the Ackermann steering gear is preferred to the Davis steering gear.

The ACKERMAN steering system consists of steering wheel, steering column, rack and pinion and a linkage system. The vehicle is controlled by the behavior of the steering gear with the spring loaded rack and pinion.

Rack and pinion steering gear being compact and light package with kinematic ally stiffer characteristics is commonly employed on passenger vehicle cars. For simplicity, we have chosen to purchase a pre-assembled rack n pinion unit.

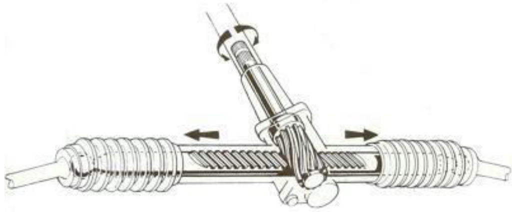

STEERING DIAGRAM WITH RACK AND PINION

D. Steering set-up with thyroids

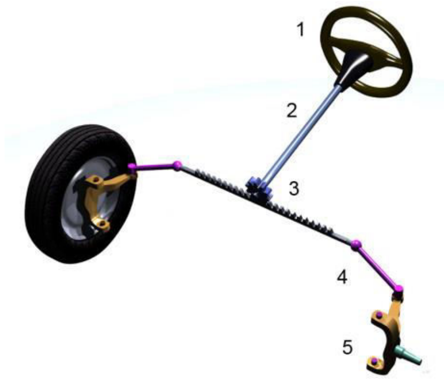

E. Selection of steering system

vehicle	Turning radius	Turning ratio	Tie rod length
Maruthi 800	173.228 inches	16:1	3.602362 inches

F. Brushless direct current motor with arrangement

G. Engine specifications

Displacement (cc)	125
Cylinders	1
Max Power (kw)	10
Maximum Torque N-m	11
Bore (mm)	52
Stroke (mm)	58
Valves Per Cylinder	2
Fuel Delivery System	Carburetor
Fuel Type	Petrol
Ignition	Digital CDI
Spark Plugs(Per Cylinder)	1
Cooling System	Air Cooled

Transmission :

Gearbox Type	Manual
No Of Gears	5
Transmission Type	Chain Drive
Clutch	Multi plate Wet Type
Battery	12V-3Ah

H . Calculations

Ackermann condition:
$(1/\tan\varpi) - (1/\tan\beta) = B/L$

ϖ = turn angle of the wheel on the outside of turn
β = turn angle of the wheel on the inside of the turn
B = wheel base
L = track length

b = distance from rear axle to centre of mass
Turning Circle:
(Track width/2) + Wheel base / sin (Average steer angle)

As for the steering ratio the ϴ=33.75 Degrees.

MOTOR SPECIFICATIONS:
POWER = 650 WATTS
SPEED = 1000 R.P.M
VOLTAGE = 48 VOLTS
WEIGHT = 6.53 KG

FORMULA: POWER=2∏NT/60 WATTS

TORQUE=650×60÷2×∏×1000 = 6.207 N-M

POWER= 2×3.14×1000×6.207÷60 = 649.995 WATTS

POWER= 650WATTS (APRX..)

WEIGHT OF THE MOTOR = 6.53 KGS

III. APPLICATIONS

Low manufacture and maintenance costs as well as easy maintenance.

- The air tank may be refilled more often and in less time than batteries can be recharged, with re-filling rates comparable to liquid fuels.
- Lighter vehicles cause less damage to roads, resulting in lower maintenance cost.
- Vehicle doesn't just need to know about its surroundings, it also needs to make predictions about how other vehicles, people, and objects around it will move. Especially on city streets where there are a lot more pedestrians and there is significantly more traffic.
- Compressed-air technology reduces the cost of vehicle production by about 20%, because there is no need to build a cooling system, fuel tank, Ignition Systems or silencers.
- The engine can be massively reduced in size

IV.CONCLUSIONS AND FUTURE WORK

Possible improvements:

Compressed-air vehicles operate according to a thermodynamic process because air cools down when expanding and heats up when being compressed. Since it is not practical to use a theoretically ideal process, losses occur and improvements may involve reducing these, e.g., by using large heat exchangers in order to use heat from the ambient air and at the same time provide air cooling in the passenger compartment. At the other end, the heat produced during compression can be stored in water systems, physical or chemical systems and reused later.

It may be possible to store compressed air at lower pressure using an absorption material within the tank. Absorption materials like Activated carbon,or a metal organic framework is used for storing compressed natural gas at 500 psi instead of 4500 psi, which amounts to a large energy saving.

The principal disadvantage is the indirect use of energy. Energy is used to compress air, which in turn provides the energy to run the motor. Any conversion of energy between forms results in loss. For conventional combustion motor cars, the energy is lost when oil is converted to usable fuel – including drilling, refinement, labor, storage, eventually transportation to the end-user. For compressed-air cars, energy is lost when electrical energy is converted to compressed air, and when fuel, either coal, natural gas or nuclear, is burned to drive the electrical generators. Energy collectors such as dams, wind turbines and solar collectors are expensive and have their own problems in manufacture, pollution, transport and maintenance.

Here’s what to expect:

- Much like electrical vehicles, air powered vehicles would ultimately be powered through the electrical grid which makes it easier to focus on reducing pollution from one source, as opposed to the millions of vehicles on the road.
- Compressed-air technology reduces the cost of vehicle production by about 20%, because there is no need to build a cooling system, fuel tank, Ignition Systems or silencers.
- Hydro-carbons and carbon monoxide and CO_2, SO_2 are the major pollutants released by the combustion of fuels.
- Low manufacture and maintenance costs as well as easy maintenance.
- The air tank may be refilled more often and in less time than batteries can be recharged, with re-filling rates comparable to liquid fuels.
- Lighter vehicles cause less damage to roads, resulting in lower maintenance cost.

REFERENCES

[1] https://en.wikipedia.org/wiki/Compressed-air_vehicle

[2] "History and Directory of Electric Cars from 1834 to 1987". Didik.com. Retrieved 2009-09-19.

[3] "What About Compressed Air Cars?". TreeHugger. Retrieved 2010-10-13.

[4] "Engineair".Engineair. Retrieved 2010-10-13.

[5] MrNGovind-MrSSanyasiRao-MrManishkumarBehera-38.pdf

[6] "National Science Foundation (NSF) News – From Farm Waste to Fuel Tanks – US National Science Foundation (NSF)".nsf.gov. Retrieved 2010-10-13.

[7] Ma Shengqian. "Metal-Organic Framework from an Anthracene Derivative Containing Nanoscopic Cages Exhibiting High Methane Uptake". Journal of the American Chemical Society. **130**: 1012–1016. doi:10.1021/ja0771639.

[8] "Tata Motors' air-powered car project still on, to be launch ready in 3 years". Auto Car Professional. Retrieved 24 August 2017.

[9] Compressed-Air Propulsion

[10] Scientific American cover 1916-11-25

[11] "TramwayInformation". Tramwayinfo.com. Retrieved 2010-10-13

PERFORMANCE STUDY ON SOLAR STEEL WITH WATER COOLING

PAPAI REDDY PG SCHOLAR
Mechanical Engineering Department,
MRCE COLLEGE
MAISAMMAGUDA.

Dr.R.Kuppusamy
Mechanical Engineering Department,
REC COLLEGE
Karnataka-570014

ABSTRACT

A solitary bowl sun oriented still is a straightforward gadget to create drinking water from effortlessly accessible saline water. Due to its low efficiency it isn't prominently utilized. A great deal of research work is embraced to enhance the efficiency of the still. Warmth move in a sun based still mostly relies upon the temperature contrast between the evaporative water surface and the gathering surface for a given surface region. An endeavor has been had to expand the temperature effect by diminishing the consolidating surface temperature. In such manner two comparable, single bowl twofold incline sunlight based stills are taken for our examination. Experimentation is performed in the premises of SHIATS-DU Allahabad. 17% pick up is recorded in the distillate yield due to cooled gathering spread.

Key words: Solar Still, Heat and Mass Transfer.

INTRODUCTION

Oceans are inexhaustible sources of water covering three fourth of the earth surface. But water in the oceans is of high salinity. Water shortage problems can be addressed by desalination of this water. Separation of salts from sea water requires lot of energy, which when produced from fossile fuel, can cause harm to the environment. Sea water desalination using solar energy gives viable solution to this problem.

Solar energy can be used for sea water desalination either by producing the thermal energy required to drive the phase change processes or by generating the electricity required to drive the membrane processes. The energy required for various desalination processes, as obtained from a survey of manufacturer's data that the process with the smallest energy requirement is Reverse Osmosis with energy recovery. But this is only viable for very large systems due to the high cost of the energy recovery turbine. The next lowest is the RO without energy recovery and the MEB system. A comparison of the desalination equipment cost and the sea water treatment requirement as obtained from a survey of manufacturers data, The cheapest of all the systems considered is the solar still. This is the direct collection system which is very simple to construct and operate. The disadvantage of this process is the very low yield [1].The production capacity of a simple type solar still is in the range of 2-5 $L/m^2/day$ only. Number of methods is available to improve the productivity of single basin solar still. The required output from the still is the condensed water from the glass cover. The condensation is higher when the condensing heat transfer from the glass and the evaporation heat transfer from the basin water are high. Heat transfer within the solar still mainly depends on the evaporative surface area and the temperature difference between the evaporative surface temperature and the condensing surface temperature. In order to maximize the existing temperature difference between the water and the condensing surface, an attempt has been made to cool down the condensing surface by flowing water on the condensing surface. The glass cover temperature is reduced by a film of cooling water continuously flowing over the glass [2] or intermittent flow of cooling water on the cover [3].The wind velocity is also affecting the cover temperature. At higher wind velocity the convective heat transfer from the cover to atmosphere increases due to increase in convective heat transfer coefficient between cover and atmosphere. This effect increases the condensing and evaporation rate and productivity of the still [4, 5].

EXPERIMENTAL SETUP

Figure 1 shows the photographs of two similar double slope solar stills kept on a single platform. The second photograph shows cooling of condensing cover by water flow arrangement. The experimental setup consists of a passive solar distillation unit with a glazing glass cover inclined at 26^0 having an area of 0.048m x 0.096 m. This tilted glass cover (3 mm thick) served as solar energy transmitter as well as a condensing surface for the vapor generated in the basin. To intercept the maximum insolation, the still was oriented in the East-West direction. Glass basin, made up of galvanized iron sheet, has an effective area of 0.72 m^2. The basin of the distiller was blackened to increase the solar energy absorption. A distillate channel was provided at each end of the basin. For the collection of distillate output, a hole was drilled in each of the channels and plastic pipes were fixed through them with an adhesive (Araldite). An inlet pipe and outlet pipe was provided at the top of the side wall of the still and at the bottom of the basin tray for feeding saline water into the basin and draining water from still for cleaning purpose, respectively. Rubber gasket was fixed all along the edges of the still. The glass panes of 3 mm thickness were used as covers for the still. All these arrangements are made to make the still air tight. A water tank of capacity 500 liter is kept at a height of 2 m to supply cooling water, to cool down the glass covers as in the photograph. The basin water gets evaporated and condensed on the inner surface of glass cover. It runs down the lower edge of the glass cover. The distillate was collected in a bottle and then measured by a graduated cylinder. The system has the capability to collect distillates from two sides of the still (i.e. East and West sides). Thermocouples were located in different places of the still. They record different temperature, such as inside glass cover, water temperature in the basin temperature and ambient temperature. In order to study the effect of salinity of the water locally available, table salt was used at various salinities. All Experiments were conducted during the month of September 2011 on several days. The experimental data is used to obtain the internal heat and mass transfer coefficient for double slope solar still.

Procedure:

The experiments were conducted on different thirty five days in the campus of the Sam Higginbottom Institute of Agriculture, Technology and Sciences Allahabad, India. All experiments were started at 08:30 AM local time and lasted for 05:00 PM. The following parameters were measured for every 30 minutes for a period of 8:30 hrs .Inner glass temperature, vapor temperature, water temperature, ambient temperature and distillate output.Water, glass and vapor temperatures were recorded with the help of calibrated copper constant thermocouples and a digital temperature indicator having a least count 1^0C. The ambient temperature is measured by a calibrated mercury (ZEAL) thermometer having a least count 1^0C. The distillate output was recorded with the help of a measuring cylinder of least count 1 ml. The solar intensity was measured with the help of a calibrated solarimeter of a least count of 2mW/cm^2. The hourly variation of all above mentioned parameters were used to evaluate average values of each for further numerical computation.

Fig 1: Two similar double slope solar stills on single platform

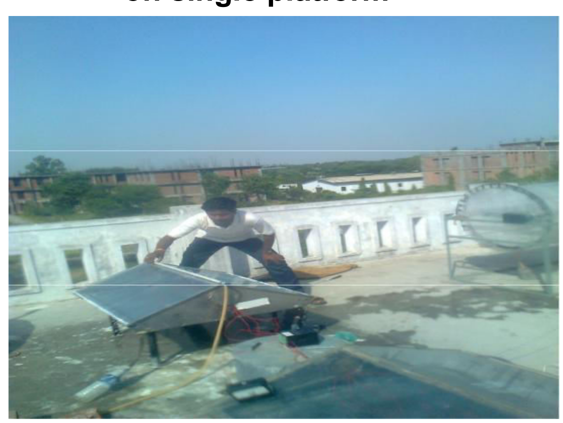

Fig 2 Water cooling of the condensing cover

Observations recorded after 10:00 AM are shown because the temperature difference between the basin water and the glass cover are positive. Due to higher glass cover temperature and lower basin water temperature in the morning, the temperature difference between basin water and glass cover is negative. Fig 3 shows the variation of solar intensity falling on the east and west side of the glass cover. As it is expected solar intensity on the east side is higher in the morning, and the maximum intensity is recorded at 11:30 AM. Fig 3 to 5 shows hourly average values of h_{cw}, h_{ew} , $h_{cw\ Dunk}$ and $h_{ew\ Dunk}$ calculated by using 8 hrs of experimental data. A TURBO C++ program was used to calculate the values of constants C and n used in the relation $Nu=C(\ GrPr)^{n}$.and convective and evaporative heat transfer coefficients by the present model and by the Dunkle model also. It is clear from fig 4 and fig 6 that the effect of cooling of condensing cover increases the convective and evaporative heat transfer coefficient.

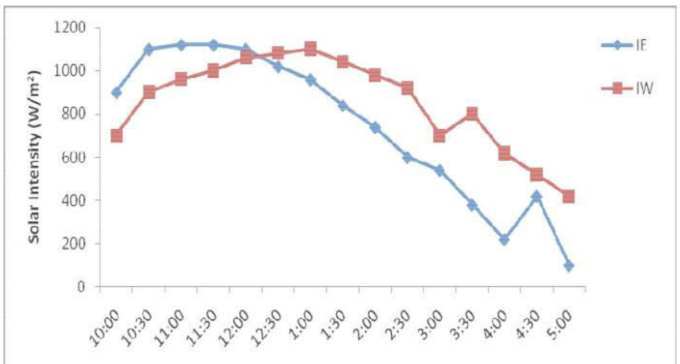

Fig. 3 Variation of solar intensity of east side and west side of the glass cover for solar stills with cooled and without cooled condensing cover

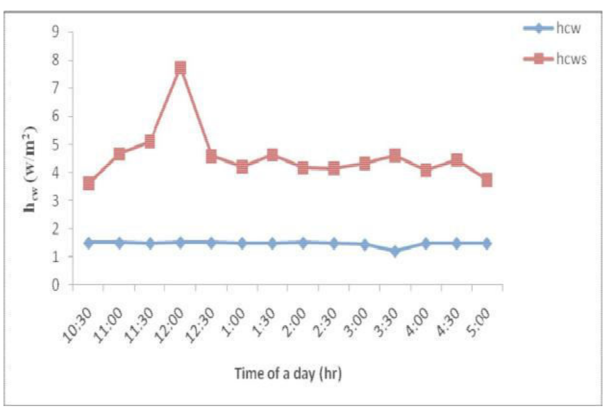

Fig. 4 Variation of convective heat transfer coefficient for solar stills with cooled and without cooled condensing cover

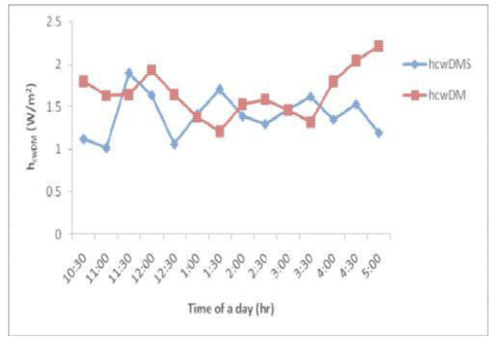

Fig. 5 Variation of convective heat transfer coefficient calculated by Dunkle model for solar stills with cooled and without cooled condensing cover

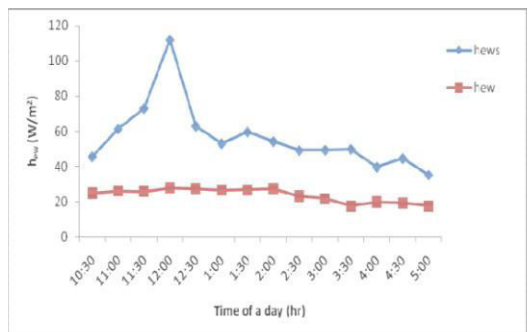

Fig.6 Variation of evaporative heat transfer coefficient for solar stills with cooled and without cooled condensing cover

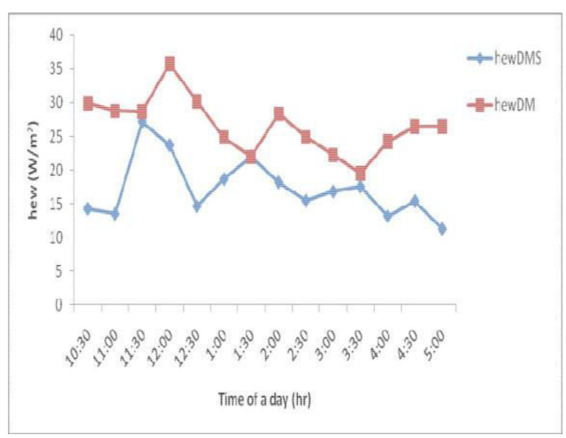

Fig.7 Variation of evaporative heat transfer coefficient calculated by Dunkle model for solar

stills with cooled and without cooled condensing cover

CONCLUSION

A simple method to enhance the solar still productivity and still efficiency is proposed. The water film cooling method is used to modify the glass cover temperature in order to increase the rate of condensation. For experimentation two, double slope solar still of same size are taken and kept on a single platform for the purpose of comparative study. The average daily productivity of the still was 1.424 kg without glass cover cooling and 1.667 kg with cooling of the glass cover. The effect of film cooling on the thermal efficiency of solar still was also studied. It is observed that the thermal efficiency of the still is improved by 4%.

REFERENCES

1. Soteris Kalogirou (1998), Use of parabolic trough solar energy collectors for sea water desalination, Applied Energy, 60, pp 65-88
2. B.A.K. Abu-Hijleh, Enhanced solar still performance using water film cooling of the glass cover, Desalination, 107 (1996) 235–244.
3. G.N. Tiwari, Madhuri and H.P. Garg, Effect of water flow over the glass cover of a single basin solar still with an intermittent flow of waste hot water in the basin, Ener. Convers. Manag., 25 (1985) 315–322.
4. H. Yousef and Mousa Abu-Arabi, Modelling and performance analysis of a regenerative solar desalination unit, Appl. Therm. Eng., 24 (2004) 1061–1072.
5. A A El-Sebaii, Effect of wind speed on some designs of solar stills, Ener.Conversion and Management. 41(2000) 523-538.
6. Ajeet Kumar Rai, Ashish Kumar and Vinod Kumar Verma, “Effect of Water Depth and Still Orientation on Productivity of Passive Solar Still”, International Journal of Mechanical Engineering & Technology (IJMET), Volume 3, Issue 2, 2012, pp. 740 - 753, ISSN Print: 0976 – 6340, ISSN Online: 0976 – 6359.
7. Ajeet Kumar Rai, Vivek Sachan and Bhawani Nandan, “Experimental Study of Evaporation in a Tubular Solar Still”, International Journal of Mechanical Engineering & Technology (IJMET), Volume 4, Issue 2, 2013, pp. 1 - 9, ISSN Print: 0976 – 6340, ISSN Online: 0976 – 6359.
8. Nattadon Pannucharoenwong and Chawisorn Phukapak, “The Performance of Heat Absorber from Zinc on the Efficiency of Double Slope Solar Still”, International Journal of Mechanical Engineering & Technology (IJMET), Volume 4, Issue 2, 2013, pp. 530 - 541, ISSN Print: 0976 – 6340, ISSN Online: 0976 – 6359.
9. Ajeet Kumar Rai, Vivek Sachan and Maheep Kumar, “Experimental Investigation of a Double Slope Solar Still with a Latent Heat Storage Medium”, International Journal of Mechanical Engineering & Technology (IJMET), Volume 4, Issue 1, 2013, pp. 22 - 29, ISSN Print: 0976 – 6340, ISSN Online: 0976 – 6359.
10. Hitesh N Panchal, Dr. Manish Doshi, Anup Patel and Keyursinh Thakor, “Experimental Investigation on Coupling Evacuated Heat Pipe Collector on Single Basin Single Slope Solar Still Productivity”, International Journal of Mechanical Engineering & Technology (IJMET), Volume 2, Issue 1, 2011, pp. 1 - 9, ISSN Print: 0976 – 6340, ISSN Online: 0976 – 6359.
11. Dr P.Ravinder Reddy, Dr K.Srihari and Dr S. Raji Reddy, “Combined Heat and Mass Transfer in MHD Three-Dimensional Porous Flow with Periodic Permeability & Heat Absorption”, International Journal of Mechanical Engineering & Technology (IJMET), Volume 3, Issue 2, 2012, pp. 573 - 593, ISSN Print: 0976 – 6340, ISSN Online: 0976 – 6359.
12. Ajeet Kumar Rai, Shahbaz Ahmad and Sarfaraj Ahamad Idrisi, “Design, Fabrication and Heat Transfer Study of Green House Dryer”, International Journal of Mechanical Engineering & Technology (IJMET), Volume 4, Issue 4, 2013, pp. 1 - 7, ISSN Print: 0976 – 6340, ISSN Online: 0976 – 6359.

Optimization of Drilling Parameters on Hemp Fibre Reinforced Composite Using Taguchi and Anova

Ms Sriveni[1],
Research scholar
Dept. of Mechanical Engg,
MRCE college
Maisammaguda

Dr.Kandasamy[2]
Professor
Dept. of Mechanical Engg,
Reva universicity
karnataka

ABSTRACT

Common fiber composites today are supplanting manufactured fiber composites because of predominant properties of characteristic strands, for example, low thickness, high particular quality and modulus, relative nonabrasiveness, simplicity of fiber surface alteration, and wide accessibility. Boring is frequently required to encourage the gathering of the parts to get the last item. Be that as it may, boring composite materials introduce various issues, for example, delamination related with the attributes of the material and with the utilized cutting parameters. The present examination is an endeavor to ponder the components and blend of variables that impact the dalamination of the penetrated unidirectional hemp fiber fortified composites utilizing Taguchi and ANOVA investigation and to accomplish the conditions for least delamination. Affirmation tests were directed to check the anticipated ideal parameters with the test comes about.

Keywords: Delamination, Drilling, Hemp fiber reinforced polymer composite, Taguchi.

1. INTRODUCTION

Natural fibers like jute, hemp, sisal, coconut (coir) and bamboo in their natural form as well as several waste cellulosic products such as shell flour, wood flour and pulp have been used as reinforcing agents of different thermosetting and thermoplastic composites. Several authors have reported the chemical composition, properties of natural fibers and their composites by incorporating the fibre in different matrices before and after treatment by different methods [1–5].

The manufacturing of the natural fiber reinforced composite can broadly be classified as primary and secondary manufacturing. The primary manufacturing results in a near-net shape of the final product. The various primary manufacturing processes are hand lay-up, pultrusion, filament winding, vacuum bag molding and resin transfer molding. Although most of the composite products are made to a near-net shape, a certain degree of intricacy in the product design necessitates the development of the composite product in parts. The independently manufactured parts are then finally assembled to get the final composite product. Machining thus becomes imperative to ascertain the structural integrity of complex composite products. Hole making is one of the important machining operations to facilitate the assembly operations. Though a number of approaches have been used for making holes in composite laminates, conventional drilling till date is the most widely acceptable and frequently practiced machining operation for hole making. Conventional drilling however results in damage in the form of delamination, micro cracks, fiber pull out and matrix burning around the hole and may ultimately cause variation in the strength of the component with a drilled hole.

Koenig et al. [6] studied in 1985 the machining of fiber reinforced plastics and concluded that a high feed rate of drilling will cause a crack around the exit edge of the hole. Miller Hocheng and Puw [7] in 1992 presented a study of the chip formation and assess the machinability of two composite materials and concluded that from cutting chips the former presents a large amount of deformation in chip formation, while the latter tends to fracture. Chambers and Bishop [8] in 1995 investigated the effect of the cutting parameters on drilling carbon/epoxy and carbon/peek and concluded that the drilling of carbon composites is dependent upon the characteristics of the matrix and the helical PCD drill geometry gave the best overall performance.

Lin et al. [9] in 1996, carried out a study on drilling of carbon fiber reinforced composite at high speed and concluded that an increase of the cutting velocity leads a increasing of the drill wear. In this way the fact of increasing the wear of drill causes a rising of thrust force. Wen-Chou Chen [10] in 1997 studied the variations of cutting forces with or without onset delamination during the drilling operations and concluded that the delamination free drilling processes may be obtained by the proper selections of tool geometry and drilling parameters. Piquet et al. [11] in 2000 carried out a study of drilling thin carbon/epoxy laminates with two types of drills, a helical drill and a drill of special geometry, and concluded that both drills leads a damage at the entrance in the wall and the exit of the hole, with the exception of special geometry drill which is possible a significant reduction in the final damage. Enemuoh et al. [12] in 2001, realize that with the application of the technique of Taguchi and other methods, were possible to achieve the cutting parameters that allowed the absence of damage in the drilling of fiber reinforced plastics.

In order to understand the effects of process parameters on the delamination, a large number of machining experiments have to be performed and analyzed mathematical models to be built on the same. Modeling of the formation of delaminations is highly complex and expensive. Hence, empirical/statistical approaches are widely used over the conventional mathematical models. In this paper, an approach based on the Taguchi method is used to determine the desired optimum cutting parameters for minimized appearance of delaminations in drilled unidirectional hemp fiber reinforced composites.

2. EXPERIMENTAL SET-UP AND MACHINING CONDITIONS

HFRP specimen preparations

The composite materials used in the tests are made with hemp fiber reinforcement. The resin polyester possessing a modulus of 3.25 GPa and density 1350 kg/m^3 was used in preparing the specimens with hand lay-up process. Required numbers of layers were stacked to give intended thickness and a fiber volume fraction, which was determined later to 0.52 using weight loss method.

Machining set-up

The carbide drill bit used in the experiments was of 5mm diameter. Drilling tests were conducted on CNC machining center supplied by MTAB, India. The laminate composite specimen was held in a rigid fixture attached to the machine table. The experimental set-up is as shown by the schematic in Fig. 1.

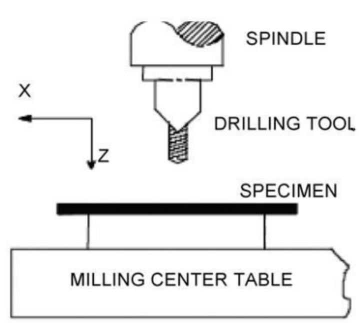

Fig. 1. Schematic diagram of experimental set-up.

Design of experiments

The cutting speed and the feed rate are the two most important parameters that characterize the drilling operation and have been selected for investigation. The feed rate and the speed are the two parameters under investigation in the present study. A L9 orthogonal array is selected for the present investigation. The factors and their respective levels are shown in Table 1. The treatment of experimental results is based on the analysis of variance (ANOVA). The analysis of variance of the experimental data for the Peel up delamination and Push down delamination generated during drilling of UD-HFRP is done to study the relative significance of the cutting speed and the feed rate.

Table 1 Levels of the variables used in the experiment.

Process parameters	Low (1)	Center (2)	High (3)
Speed (A) in rpm	1000	1500	2000
Feed (B) in mm/min	100	200	300

MEASUREMENT OF DELAMINATION FACTOR

To determine the differing extent of intrinsic hole machining defects (delamination) caused by drilling, both the upper (Peel up delamination) and lower (Push down delamination) surfaces of each specimens were examined using The Mitutoyo TM 500 toolmakers' microscope of 1µm resolution with 30X magnification was employed to measure the delamination damage of holes and each trial was replicated twice, as it can be observed in Fig. 2. The value of delamination factor (F_d) can be obtained by the following equation:

$$F_d = D_{max} / D \quad (1)$$

where, D_{max} is the maximum diameter of the damage around the hole periphery and D is diameter of the drill.

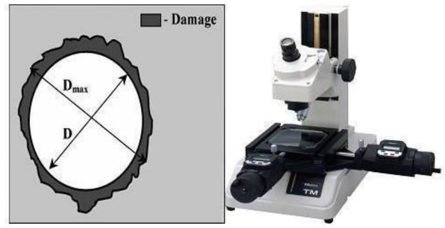

Fig.2. Measurement of the maximum diameter (D_{max}) with a tool maker's microscope.

The average readings of two trials of delamination factor were taken as process response. Table 2 presents the experimental layout plan and the computed values of delamination factor.

Table 2
Design and experimental results of the L9 orthogonal array experiment

Sl. no.	Factors A	B	Push down delamination Trial 1	Trial 2	Peel up delamination Trial 1	Trial 2
1	1	1	2.00	1.80	1.80	1.60
2	1	2	2.80	2.60	2.40	2.20
3	1	3	3.60	3.50	2.80	2.40
4	2	1	1.20	1.00	1.00	0.80
5	2	2	1.60	1.80	1.40	1.20
6	2	3	2.20	2.00	1.80	2.20
7	3	1	0.70	0.80	0.30	0.40
8	3	2	1.60	1.80	0.80	0.96
9	3	3	1.70	2.00	1.0	1.25

4. EXPERIMENTAL RESULTS AND DATA ANALYSIS

Analysis of S/N ratio

In the Taguchi method, the term 'signal' represents the desirable value (mean) for the output characteristic and the term 'noise' represents the undesirable value (S.D.) for the output characteristic. Therefore, the S/N ratio is the ratio of the mean to the S.D. Taguchi uses the S/N ratio to measure the quality character deviating from the desired value. The S/N ratio η is defined as To obtain optimal cutting performance, the-lower-the-better quality characteristics for delamination should be taken for obtaining optimal cutting performance. The optimum process design is achieved when the S/N ratio is maximized. Since – log is a monotonically decreasing the function, it implies that we should maximize. The M.S.D. for the-lower-the-better quality characteristic can be expressed as:

The response obtained from experiments was analyzed using response table and graphical representation of mean effects and interaction effect of parameters on the quality characteristics. Table (3) shows the experimental results for delamination factors of push down delamination and peel up delamination and the corresponding S/N ratio using Eqs.

The S/N response graph for push down and peel up delaminations are shown in Figure (3). Regardless of the-lower-the-better of the-higher-the-better quality characteristic, the greater S/N ratio corresponds to the smaller variance of the output characteristic around the desired value (Eqs. (2) and (3)). Therefore, based on the S/N, the optimal parameters for peel up delamination are the feed rate at level 1 (100 mm/min), the cutting speed at level 3 (2000rpm). Similarly, the optimum parameters for push down delamination are the feed rate at level 1 (100 mm/min), the cutting speed at level 3 (2000 rpm).

4.2. Analysis of variance:

The purpose of the analysis of variance (ANOVA) is to investigate the design parameters significantly affect the quality characteristic of a product or process. This is accomplished by separating the total variability of the S/N ratios, which is measured by the sum of the squared deviations from the total mean S/N ratio, into contributions by each of the design parameters. Statistically, there is a tool called an F test named after Fisher to see which design parameters has a significant effect on the quality characteristic. In performing the F test, the mean of squared deviations due to each design parameter needs to be calculated. Then, the F value for each design parameter is simply the ratio of the mean of squared deviations to the mean of squared error. Usually, when $F > 4$, it means that the change of the design parameter has a significant effect on the quality characteristic.

From Table 4, which gives ANOVA response results, it can be found that cutting speed and feed rate are the significant parameters affecting the peel up delamination and feed rate and cutting speed are the significant parameters affecting the push down delamination. Figure (4) illustrate the interaction plots for different S/N ratios for push down and peel delaminations.

5. CONCLUSIONS

From the analysis of results in drilling of HFRP composite plates using conceptual S/N ratio approach, ANOVA and response surfaces, the following can be concluded from the present study within the range of the experiments.

(1) As seen in this study, the Taguchi method provides a systematic and efficient methodology for the design optimization of the process parameters resulting in the minimum delamination with far less effect than would be required for most optimization techniques.

(2) Based on the S/N, the optimal parameters for the minimum peel up delamination are the feed rate at level 1 (100 mm/min), the cutting speed at level 3 (2000 rpm).

(3) Similarly, the optimum parameters for the minimum push down delamination are the feed rate at level 1 (100 mm/min), the cutting speed at level 3 (2000 rpm).

(4) The feed rate and cutting parameters influences the push down and peel up delaminations. Therefore, the feed rate and cutting speed seems to be the most critical parameters and should be selected carefully in order to reduce all kinds of damages.

(5) Conceptual S/N ratio and ANOVA approaches for data analysis draw similar conclusion.

REFERENCES

- Jain S, Kumar R, Jindal UC. Mechanical behavior of bamboo and bamboo composite. J Mater Sci 1992; 27:4598–604.
- Varghese S, Kuriakose B, Thomas S. Stress relaxation in short sisal-fibre reinforced natural rubber composites. J Appl Polym Sci 1994; 53:1051–60.
- Geethamma VG, Joseph R, Thomas S. Short coir fibre-reinforced natural rubber composites: effects of fibre length, orientation and alkali treatment. J App Polym Sci 1995;55:583–94.
- Ahlblad G, Kron A, Stenberg B. Effects of plasma treatment on mechanical properties of rubber/cellulose fibre composites. Polym Int 1994; 33:103–9.
- Li Y, Mai Y-W, Lin Y. Sisal fibre and its composites: a review of recent developments. Compos Sci Technol 2000; 60:2037–55.
- Koenig W, Wulf C, Grass P, Willerscheid H. Machining of fiber reinforced plastics. Manufact Tech CIRP Ann 1985; 34(2):537–48.
- Miller JA. Drilling graphite/epoxy at Lockheed. Am Mach Autom Manufact 1987; 70–1.
- Chambers A, Bishop G. The drilling of carbon fibre polymer matrix composites. Process Manufact 1995; III, 565–72. Lin SC, Chen IK. Drilling of carbon fiber-reinforced composite material at high speed. Int J Mac Tools Manufact 1996; 156–62.
- Chen W. Some experimental investigations in the drilling of carbon fibre-reinforced plastic (CFRP) composite laminates. Int J Mach Tools Manufact 1997; 37(8):1097– 108.
- Piquet R, Ferret B, Lachaud F, Swider P. Experimental analysis of drilling damage in thin carbon/epoxy laminate using special drills. Int J Mac Tools Manufact 2000; 1107–15.
- Ugo Enemuoh E, Sherif El-Gizawy A, Chukwujekwu Okafor A. An approach for development of damage-free drilling of carbon fiber reinforced thermosets. Int J Mac Tools Manufact 2001; 1795–814.

Future power plant –a review on variable compression ratio engine

Ms Renuka[1],
Dept. of Mechanical Engg,
MRCE college
maisammaguda

A. Kulkarni[2]
Dept. of Mechanical Engg,
Reva universicity
Bangalore

ABSTRACT

Progressively stringent discharge and mileage benchmarks have since quite a while ago remained a wellspring of difficulties for explore in car motor innovation advancement towards the all the more thermally productive and less contaminating motor. Variable pressure proportion (VCR) innovation has for some time been perceived as a technique for enhancing the vehicle motor execution, proficiency, efficiency with decreased emanation. The primary element of the VCR motor is to work at various pressure proportion, by changing the ignition chamber volume, contingent upon the vehicle execution needs. This paper takes audit of all the geometric methodologies and arrangements used to accomplish VCR with its one of a kind highlights, considers the consequences of earlier research and its relating business obstructions.

Keywords: compression, ratio, polluting engine, emission

INTRODUCTION

Worldwide pressure to reduce automotive fuel consumption and CO2 emissions is leading to the introduction of various new technologies for the automotive engine.The concept of variable compression ratio (VCR) promises improved engine performance, efficiency, and reduced emissions.VCR is identified as the key enabling technology of downsized engines. The search for a feasible VCR engine has been driven by the compromise between WOT (Wide Open Throttle) and part-throttle which exists on any fixed CR engine.At low power levels, the VCR engine operates at a higher compression ratio to capture high fuel efficiency benefits, while at high power levels the engine operates at low compression ratio to prevent knock. The optimum compression ratio is determined as a function of one or more vehicle operating parameters such as inlet air temperature, engine coolant temperature, exhaust gas temperature, engine knock, fuel type, octane rating of fuel, etc.[1]

NEED FOR VCR

One of the key features affecting thermal efficiency is the compression ratio, which is always a compromise in fixed compression ratio spark ignition (SI) engines. If the compression ratio is higher than the designed limit, the fuel will pre-ignitecausing knocking, which could damage the engine.[2] Generally, the operating conditions of SI engines vary widely, such as stop and go city traffic, highway motoring at constant speed, or high-speed freeway driving. Unfortunately, most of the time SI engines in city driving conditions operate at relatively low power levels under slow accelerations, low speeds, or light loads, which lead to low thermal efficiency and hence higher fuel consumption. As the engine load decreases, the temperature in the end gas drops, so that high compression ratio could be employed without the risk of knocking in naturally aspirated or boosted engines. Raising the compression ratio from 8 to 14 produces an efficiency gain from 50 to 65 per cent (a 15 per cent gain), whereas going from 16 to 20 produces a gain from 67 to 70 per cent (a 3 per cent gain). Figure 2.1 shows the effects of compression ratio with respect to thermal efficiency.

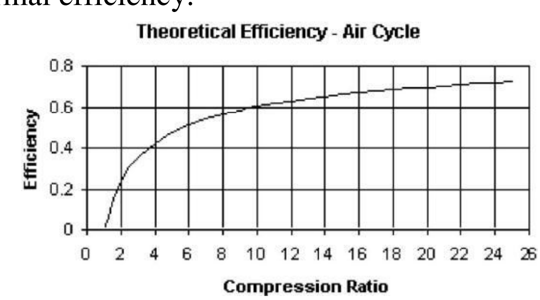

Fig.2. Effect of compression ratio on thermal efficiency

VARIOUS VCR APPROACHES

Designing and successfully developing a production practical, VCR engine has long been a challenge to the automobile industry. Many innovative patents have been filed and different designs developed to modify the compression ratio. A few approaches are discussed below:-

Moving the Crankshaft Axis

FEV, Germany has chosen to alter the position of the crankshaft. In their engine, crankshaft bearings are carried in an eccentrically mounted carrier that can rotate to raise or lower the top dead centre (TDC) positions of the pistons in the cylinders The compression ratio is adjustable by varying the rotation of the eccentric carrier. Mounting the crankshaft on eccentric bearings is simple in that the reciprocating assembly itself is unchanged. In fact, the engine requires an offset fixed-position output shaft; a coupling is required between the movable crankshaft end and the fixed output shaft. The compression ratio is adaptable from 8 to 14 approximately by varying the rotation of the eccentric carriers through 55° [4].

Modification of the connecting rod geometry.

The Nissan project uses a multi-link system to achieve VCR by inserting a control linkage system between the connecting rod and the crankshaft, and connecting this to an actuator shaft, so that the compression ratio can be varied. This project was incorporated in a four-cylinder engine without major modification of the engine block. The shorter crank throw allowed room for the link system, which was anchored by an eccentric rotary actuator. Compression was varied from 10 to 15 approximately by a 70° rotation of the actuator, while at TDC, the piston position was changed by 3.1 mm Examining the details of multi-link system operation reveals some advantages. The most striking advantage is that of maximum piston accelerations. Tension forces acting through the connecting rod and piston at TDC represent one of the factors limiting piston speed, so a geometry that reduces the peak piston acceleration would allow either an increase in sustainable engine speed or an increasing stroke, either of which is useful in terms of increasing power output [5]

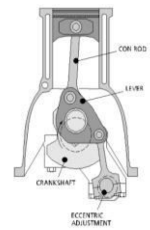

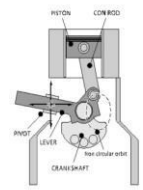

Fig.Nissan VCR Engine
Fig.Mayflower e3 VCR Engine

Moving the cylinder head

The moving head concept (Saab Automobile AB) combines a cylinder head with cylinder liners into a monohead construction, which pivots with respect to the remainder of the engine. The lower half of the block includes the crankcase and engine mounts, and carries the crankshaft, gear box, oil cooler, and auxiliaries. The upper half includes the cylinders, their liners, camshafts, and an integrally cast cylinder head. This part is referred to as the monohead. Saab has enabled a tilting motion to adjust the effective height of the piston crown at TDC. The linkage serves to tilt the monohead relative to the crankcase in order to vary the TDC position of the piston. By means of actuator and linkage mechanism the compression ratio can be varied from 8 to 14. A screw type supercharger provides a 2:1 boost pressure when wide open throttle conditions occur [5]. This system gives wide fuel flexibility, with reduced CO_2 emissions proportional to fuel consumption. Saab recognized that the fuel efficiency of the VCR engine would be low without high-pressure supercharging.

Ford has patented a means to vary combustion chamber volume by using a secondary piston or valve. The piston could be maintained at an intermediate position, corresponding to the optimum compression ratio for a particular condition. The volume of the combustion chamber is increased to reduce the compression ratio by moving a small secondary piston which communicates with the chamber [5], however, this would require a finite length bore in which the piston could travel, which raises questions of sealing, packaging, and durability.

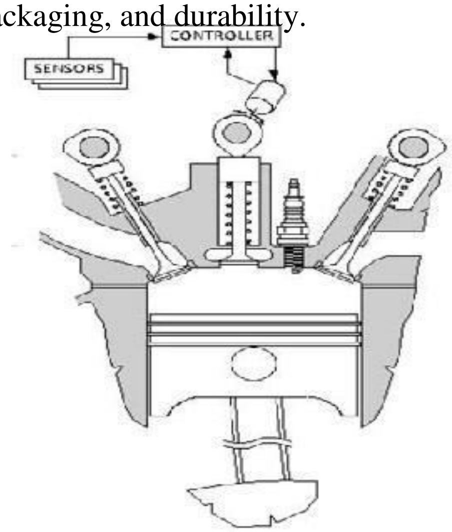

Fig.3.4.1 Ford VCR Engine

Varying combustion chamber geometry compromises the area available for intake and exhaust valves, while moving the cylinder head and barrel is feasible in a research engine but harder to accomplish in a production vehicle. The cylinder head cooling needs to be improved by an efficient cooling system and the auxiliary piston needs proper lubrication for efficient functioning of the VCR engine.12

Variation of piston deck height

The Daimler-Benz VCR piston design shows variation in compression height of the piston and offers potentially the most attractive route to a production VCR engine, since it requires relatively minor changes to the base engine architecture when compared to other options . Unfortunately, it requires a significant increase in reciprocating mass and, more importantly, a means to activate the height variation within a high-speed reciprocating assembly.

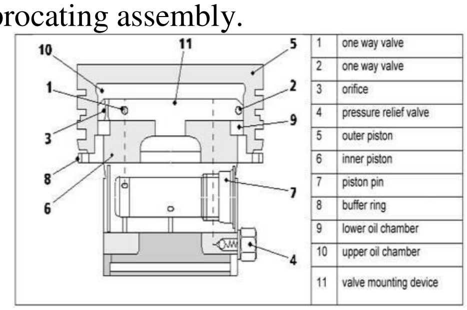

Fig. Daimler Benz VCR Piston

This is typically proposed by means of hydraulics using the engine lubricating oil; however, reliable control of the necessary oil flow represents a major challenge. This is claimed to reduce the peak firing loads so that the compression ratio variation becomes self-acting rather than externally controlled. A side-effect would be the momentary variation in clearance volume during the combustion event, which would, in turn, increase, then reduce the volume available to the expanding gases.

The University of Michigan developed a pressure-reactive piston for SI engines. The pressure-reactive piston assembly consists of a piston crown and a separate piston skirt, with a set of springs contained between them

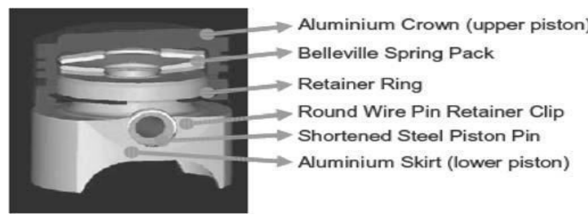

Fig.3.5.2. Pressure Reactive Piston Cross Section

This piston configuration allows the piston crown to deflect in response to the cylinder pressure. As a piston crown deflects, the cylinder clearance volume increases, lowering the effective compression ratio and reducing peak cylinder pressure. This mechanism effectively limits the peak pressures at high loads without an additional control device, while allowing the engine to operate at high compression ratio during low load conditions [8], It can be easily adapted to the conventional engine with only changes to piston and connecting rod design. Brake specific fuel consumption improvements of the pressure-reactive piston engine over baseline engine at light loads ranges from 8 to 18 per cent. The pressure-reactive piston shows higher heat transfer losses because of higher surface-to-volume ratio and produces higher hydrocarbon emission at part load owing to higher compression ratio and more crevice volume (piston crown design).

Moving the crankpins

Gomecsys has proposed to move the crankpins eccentrically to effect a stroke change at TDC. Figure 3.6.1 shows the Gomecsys VCR engine in which moveable crankpins form an eccentric sleeve around the conventional crankpins and are driven by a large gear.

Gomecsys VCR Engine

Differences in the TDC position may vary up to 10 mm with a rotation of the ring-gear of only 40°. By rotating the ring-gear slightly to the right or to the left, while the crankshaft is at the TDC position at the end of the compression stroke, the position of the eccentric can be lifted or lowered. Note that lifting the eccentric at one TDC automatically causes the other TDC to be lowered accordingly. In order to effectively downsize the engine, a two-cylinder inline engine is a perfect solution for small cars; the two-cylinder Go Engine concept is small and lightweight, and total power train costs are comparable with a small four-cylinder engine. Applications involving staggered crankpin geometry would be less elegant, requiring multiple gear drives.

BENEFITS OF VCR

Hence the important benefits of the VCR engine can be summarized as follows: —

1. Optimum combustion efficiency in the whole load and speed range.
2. Low fuel consumption and low exhaust emissions.
3. The VCR provides better control over pollutant generation and after-treatment than a conventional fixed compression ratio (FCR) engine, also extends the life expectancy of a three way catalytic converter.
4. As the geometrical volumetric ratio is under control on VCR engines, the engine always operates below the knock limit, whatever the load.
5. The VCR engine provides excellent fuel flexibility, since the compression ratio can be varied and adjusted to suit the properties of the fuel, and therefore the engine will always run at the compression ratio best suited to the fuel being used for bi-fuel (compressed natural gas (CNG)/gasoline) power-trains, the realization of VCR is of specific interest. High fuel flexibility, with optimal combustion efficiency.
6. Very smooth idle and full load accelerations are achieved.
7. It provides better indicated thermal efficiency than that of FCR engines.
8. It allows for a significant idle speed reduction because of reduced misfiring and cyclic irregularities, resulting in low vibration levels.
9. Reduction in low-frequency noise because of constant peak pressures.
10. Smoother combustion because the rate of heat release is the same (short) both at low and high compression ratios.
11. Cold starting emissions can be reduced greatly by early catalyst warm-up in the catalytic converter.
12. Improvement in the low end torque of a petrol engine without the risk of detonation.
13. Potential technology for future high-boosting super lean burn engines.
14. Low CO_2 emissions by down-sizing for the same power output.
15. Good idling performance at low ambient temperatures.
16. Constant frictional losses owing to almost constant peak pressures.

COMMERCIAL BARRIERS

Variable compression ratio engines have not yet reached the market, despite patents and experiments dating back over decades. Indeed, several prototypes of VCR engines and vehicles have been tested. In many cases, the deviation from conventional production engine structure or layout represents a significant commercial barrier to widespread adoption of the technology. Some of the commercial barriers are listed below:-

- The available methods require major changes to the base engine architecture or layout and represent significant commercial barriers to widespread adoption of the technology.
- 2.Introduction of additional elements within the crowded combustion chamber environment threatens to compromise ideal geometry and layout of the valves and ports.
- Engine-out emissions performance is likely to be undermined by additional crevice volumes which obstruct complete burning, thereby increasing hydrocarbon emissions.
- There is a significant increase in reciprocating mass in the case of a variable height piston.
- Some approaches lead to an increase in vibrations owing to intermediate members in the connecting rod.
- In some cases, reworking of the entire engine structure is necessary.
- Variable compression ratio designs consist of multilink rod-crank mechanisms, which may also present a near-to-sinusoidal motion unfavorable to cylinder filling at low speeds and fine-scale turbulence.

ECONOMICS OF VCR ENGINE

Choosing an appropriate VCR technology is a decisive step to determine the cost of VCR implementation in future vehicle. The different available VCR technologies have to be compared by focusing on all the positive and negative impacts on engine components and their operations. The benefits of VCR also include increased power density, reduced number of cylinders, sophisticated injection technologies, and complex after-treatment Indeed, to be marketable, the VCR technology has to present indispensable features such as robustness, durability, easy integration into all vehicles and low noise and vibration levels.The real potential of VCR engines will be realized when they are used in combination with down-sizing and supercharging.

CONCLUSION

The VCR engine has great potential for improving part-load thermal efficiency, more efficient operation, ability to down size the engine, multi fuel flexibility. and reducing the harmful emissions. when compared to other competing technologies. The main obstacles to adoption of VCR are incompatibility with major components in current production and difficulties of combining VCR and non-VCR manufacturing within existing plant.

The Potential of these technologies needs to be evaluated by a trade -off between cost and consumption benefit. It is potentially one of the profitable sources to investigate for the automotive industry.

REFERENCES

- Taylor, C. F. *"The internal-combustion engine in theory and practice"*, 1960 (MIT Press, Cambridge, Massachusetts).Heywood, J. B. *Internal combustion engine fundamentals*, 1995 (McGraw Hill Book Co., USA).
- KSchwaderlapp, M.(Habermann, K., and Yapici, K. *Variable compression ratio - a design solution for fuel economy concepts.* SAE paper 2002-01-1103, 2002.
- Martyn Roberts *" Benefits and Challenges of Variable Compression Ration (VCR)"*
- SAE, Paper No. 03P-227 (2002
- Mfaoteki, K., Aoyama, S., Ushijima, K., Hiyoshi, R., Takemura, S., Fujimoto, H., and Arai, T. *A study of a variable compression ratio system with a multi-link mechanism.* SAE paper 2003-01-0921, 2003.
- Gooijer, B. and Gomecsys, B. V. Technical document, February 2002, available from www. gomecsys.com.

EXPERIMENTAL INVESTIGATION OF A DOUBLE SLOPE SOLAR STILL WITH LATENT HEAT STORAGE MEDIUM

Ms B.Simran[1],
PG Scholar,
[1 2]Dept of Mechanical Engg,
MRCE college,Hyderabad,Telangana.

Dr.P.Velmurugan[2] ,
Professor

ABSTRACT--- Single basin star still could be a terribly straightforward star device used for changing out there briny or water into contemporary water. This device are often made-up simply with domestically out here materials. the upkeep is additionally low cost and no mean labor is needed. The device could also be an appropriate answer to resolve water draw back however due to its low productivity it's not popularly used. variety of works square measure undertaken to boost the productivity of the still. the utilization of heat energy storage system exploitation state change|natural action|action|activity} material (PCMs) is an efficient method of storing thermal energy and has the advantage of high energy density and therefore the equal nature of the storage process. Double slope single basin star still is experimented by adding a heat reservoir within the basin exploitation atomic number 30 NitrateHexahydrate.

Single basin solar still is a very simple solar device used for converting available brackish or water into fresh drinking water. This device can be fabricated easily with locally available materials. The maintenance is also cheap and no skilled labor is required. The device may be a suitable solution to solve drinking water problem but because of its low productivity it is not popularly used. Number of works are undertaken to improve the productivity of the still. The use of latent heat storage system using phase change material (PCMs) is an effective way of storing thermal energy and has the advantage of high energy density and the isothermal nature of the storage process. Double slope single basin solar still is experimented by adding a heat reservoir in the basin using Zinc Nitrate Hexahydrate. It is a material which changes its phase during addition and removal of heat. It is observe that an increment of 33.5 % is observed in the collection of distillate when the still is used with PCM as Zinc Nitrate Hexahydrate.

Key Words: double Slope Solar Still, Phase Change Materials

INTRODUCTION

Water is the primary source of life. Next to oxygen, fresh water is the most important substance for sustaining human life. Water shortage is a worldwide problem, where 40% of the world population is suffering from water scarcity [1]. Although Water is one of the most abundant resources on Earth, covering approximately three-quarters of the planet's surface. About 97% of the Earth's water is salt water in the oceans. 3% of all fresh water is in ground water, lakes and rivers, which supply most of that needed by humans and animals.

However, rapid industrial-growth and the population explosion world-wide have resulted in a large escalation of the demand for fresh water. Added to this is the problem of pollution of rivers and lakes by industrial wastes and the large amounts of sewage discharged. On a global scale, man-made pollution of natural sources of water is becoming the single largest cause for fresh-water shortages. Besides the only inexhaustible sources of water are the oceans. Their main drawback, however, is the high salinity of such water. It would be attractive to tackle the water-shortage problem with desalination of this water, which may be mixed with brackish water increase the amount of fresh water and reduce the concentration of salts to around500 ppm .

Solar distillation has been practiced for many generations. All desalination methods require fossil fuel or electrical energy but solar distillation is one of many processes that can be used to produce fresh water by using the heat of the sun directly in a simple equipment to purify water. The equipment, commonly called a solar still . Solar still is most simple device to get potable/fresh distilled water from impure water. Among other available designs of solar still, the Double Slope Solar Still is most popular. The construction and design of this solar still is simple. The problem is poor productivity. A large number of attempts are made to improve the productivity from solar still. Studies are performed to predict the performance of solar still [5]. Effect of variation of parameters on the total output is also studied by various researchers.They have analyzed the effect of water depth on the performance of DSS. Due to intermittent nature of solar energy, distillate production is not continuous and night time production is almost nil. By using energy storage mediums, distillate may be produced during non-Sunshine hours. These energy storage systems may store heat energy in two ways (i) Sensible Heat (ii) Latent Heat. Thermal energy can be stored as a change in internal energy of a material as sensible heat, latent heat or combination of these two. In sensible heat storage (SHS), thermal energy is stored by raising the temperature of a solid or liquid. SHS utilizes the heat capacity and the change in temperature of the material during the process of charging and discharging. The amount of heat stored depends on the specific heat of the medium, the temperature change and the amount of storage material .

Storage media. Latent Heat storage systems are having advantage of their isothermal nature of storing heat energy. Kuznik et. has given a good explanation of how PCM stores and releases latent heat. The external heat supplied to a PCM is spent in breaking the internal bonds of lattice and thereby it absorbs a huge amount of latent heat at phase temperature. Abhat et.al. has given a detailed classification of PCMs along with their properties. Dinser and Rosen have also exercised the same. A large number of phase change materials (organic, inorganic and eutectic) are available in any required temperature range. El-Sebaii et al and Shukla et al have used phase change material as a energy storage medium to study the performance of a single slope solar still. In the present study, performance of a double slope solar still with **Zinc Nitrate Hexahydrate** as PCM has been investigated in outdoor conditions in the month of October. Thermophysical properties of Zinc Nitrate Hexahydrate are given. Melting temperature 36.1^0C specific heat (solid) 1.34 kJ/kg^{0}C, specific heat (liquid) 2.26kJ/kg^{0}C, Latent Heat of fusion 147.0 kJ/kg, Thermal conductivity 0.464W/mK at 39.9^0C.

EXPERIMENTAL SET-UP AND PROCEDURE

Set-up

Figure 1 shows the photograph of two Double Slope Solar Still of same size and shape. One DSS is without PCM and another DSS is having PCM in the basin. The DSS consist of a passive solar distillation unit with a glazing glass cover inclined at 26^0 having an area of 0.048m x 0.096 m. The tilted glass covers are of 3 mm thickness, Transmit solar energy and work as an insulator of heat. It works as a condensing surface for the vapor generated in the basin. Still basin, made up of Galvanized Iron, has an effective area of 0.72 m^2. The basin of the distiller was blackened to increase the absorptive of the basin liner. A distillate channel was provided at each end of the basin for the collection of distillate output, a hole was drilled in each of the channels and plastic pipes were fixed through them with an adhesive (Araldite). An inlet pipe and outlet pipe was provided at the top of the side wall of the still and at the bottom of the basin tray for feeding saline water into the basin and draining water from still for cleaning purpose, respectively. All arrangements are made to make the still air tight. Water gets evaporated and condensed on the inner surface of glass cover. It runs down the lower edge of the glass cover. The distillate was collected in a bottle and then measured by a graduated cylinder. The distillate is collected from two sides of the still. Phase Change Material is filled in the tubes and placed in the basin of the still. Tubes are made of aluminum to offer little resistance to the heat transfer between water and PCM. Tubes are of dia 10 mm and length as that of the basin inner side. Thermocouples were attached in different locations of the still to record the temperatures of inside glass cover, water temperature in the basin and ambient temperature. All experimental data are used to obtain the internal heat and mass transfer coefficient for double slope solar still. The effect of use of phase change material is also studied by comparative analysis.

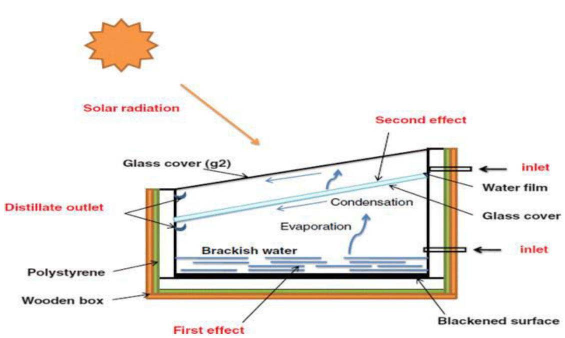

Fig.1 Photograph showing experimental set-up (Double Slope Solar Still with and without PCM)

Procedure

The experiments were conducted in the campus of Sam Higginbottom Institute of Agriculture, Technology and Sciences- Deemed University, Allahabad, India. All experiments were started at 08:30 AM at local time and lasted for 08.30 hours. Water, glass, water vapor and PCM temperatures were recorded with the help of calibrated Copper – Constantan thermocouples having a least count of 1^0C. The ambient temperature is measured by a calibrated mercury (ZEAL) thermometer having a least count 1^0C. The distillate output was recorded with the help of a measuring cylinder of least count 1 ml. The solar intensity was measured with the help of calibrated solarimeter of a least count of 2 mW/cm^2. The hourly variation of all above mentioned parameters were used to evaluate average values of each for further numerical computation.

PRODUCTIVITY AND EFFICIENCY OF THE SOLAR STILL

Energy balance equations are written for the different components of a double slope solar still without PCM in the basin, and with PCM in the basin .

The hourly and daily productivity of solar still is

$$M_{ewh} = h_{ewh}\,(T_w - T_{gin})/L \qquad (5)$$

$$M_{ewd} = \sum 24\ \mathrm{hrs}\, m_{ewh} \qquad (6)$$

The instantaneous efficiency of the solar still is:

$$\eta_i = [\,h_{ewh}\,(T_w - T_{gin})/I\,(t)]\times 100\% \qquad (7)$$

$$\eta_d = [M_{ewd}\ h_{ew}/(A_p \sum I)(\Delta t)]\times 100\% \qquad (8)$$

2. RESULTS AND DISCUSSION

Variation of solar intensity falling on the east and west side glass covers of the double slope solar still for a particular day (17-10-12). It is observed that the solar intensity falling through east side glass cover is higher till 01:30 hrs. Maximum value is observed around11:00 hrs on east glass cover.

Variation of east glass cover temperatures of DSS with PCM and without PCM is shown in fig 2. It is observed that the DSS with PCM tubes will have higher glass cover temperature in comparison to that of without PCM. This difference is higher in afternoon session. This is due to thermal inertial effect produced by PCM tubes. This is also true for the west side glass cover. A slight rise in temperature of the west side glass cover with PCM is shown in fig.3. This little difference is due to low solar intensity on west side glass cover.

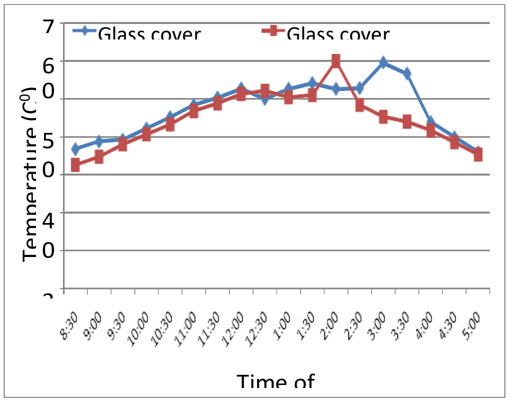

Fig. 2. Variation of West glass covers temperatures of DSS with PCM and without PCM

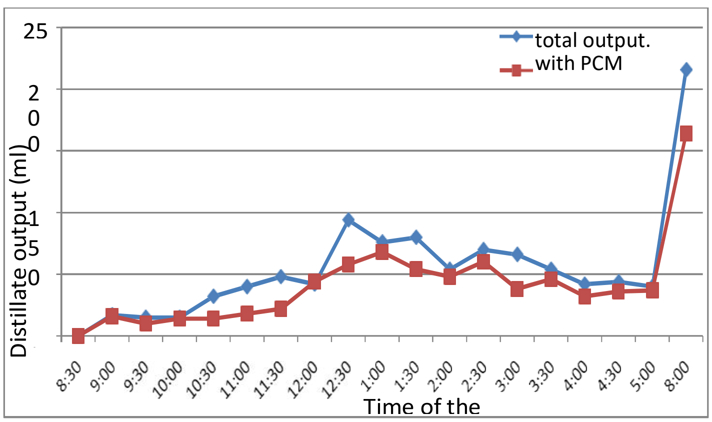

Fig.3.Variation of total distillate output from DSS with PCM and without PCM

Hourly distillate output is measured in the daytime only from 08:30 AM till 5:00 PM. Last reading shows total distillate collected during 5:00 PM to 8:00 AM. From fig.3, it is clear that output will increase due to use of PCM as heat reservoir. Total gain of 33.5% is observed in output. Where daytime gain is 34.7% and nocturnal gain is of 31.7%.

CONCLUSION

This study explores the possibility of using latent heat energy storage mediums in conventional solar still to ensure the continuous production of fresh water even after sunset. Result shows that productivity increases by 30 to 35% with Zinc Nitrate Hexahydrate as PCM. This can be further improved by a PCM with high latent heat of fusion and increasing the mass of the PCM in the basin.

REFERENCES

[1]Abdullah S., Badranb O. & Abu-Khaderc M. M. (2008), Performance evaluation of a modified design of a single slope solar still. Desalination 219pp. 222–230

[2]MalikMAS,Tiwari GN, Kumar A, Sodha MS.Solar distillation.Oxford: Pergamon Press,1985.

[3] Tiwari, G.N., Tiwari, A.(2007), Solar Distillation Practice for Water Desalination Systems, Anamaya, New Delhi,.

[4] Argaw N. (2001),"Renewable Energy in Water and Wastewater Treatment Applications". National Renewable Energy Laboratory

[5] Shukla S.K. and Rai A. K. (2008), "Analytical thermal modeling of double slope solar still using inner glass cover temperature" Thermal Science,vol 12,(3), 139-152.

[6] Rai Ajeet Kumar, Kumar Ashish and Verma Vinod Kumar (2012), "Effect of water depth and still orientation on productivity of passive solar still"IJMET, vol 3, (2), 740-753.

[7] Rai Ajeet Kumar, Kumar Ashish (2012)," A Review on phase change materials and their applications"IJARET, vol. 3,(2), 214-225.

[8] Lorsch HG, Kauffman KW, Denton JC, "Thermal Energy Storage for Heating and Air Conditioning, Future energy production system". Heat Mass Transfer Processes; 1: pp 69-85 (1976).

[9] Lane GA, Glew DN, Clark EC, Rossow HE, Quigley SW, Drake SS, et al. "Heat of fusion system for solar energy storage subsystems for the heating and cooling of building". Chalottesville, Virginia, USA, 1975.

[10] Humphries WR, Griggs EI. " A designing handbook for phase change thermal control and energy storage devices." NASA Technical Paper, p. 1074, (1977).

[11] Kuznik F., Virgone, J. and Noel, J.: Optimization of a phase change material wallboard for building use. Applied Thermal Engineering 28 (2008), 1291-1298.

[12] A. Abhat, Low temperature latent heat thermal energy storage: heat storage materials, Solar Energy30, pp 313-332 (1983).

THERMAL PERFORMANCE CHARACTERIZATION OF R134 AND BUTANE CHARGED TWO PHASE CLOSED THERMOSYPHONS

A.RANJITH
PG Scholar,
Dept. of Mechanical Engineering
Malla Reddy college of Engineering,
Hyderabad-500100
ranjith.education02@gmail.com

A.SRAVEENA
B.Sc Physics
Vasavi Degree college
Bhoopalapally-506169
ranjith.education02@gmail.com

DR. S.S.GOWDA
Professor
Dept. of Mechanical Engineering
Malla Reddy college of Engineering,
Hyderabad-500100

ABSTRACT:

Experimentally determined correlations for, the evaporator and condenser heat transfer coefficients and the maximum heat transfer rate of two-phase closed thermosyphons using R134a and butane as working fluids are given. Two-phase closed thermosyphons of inside diameters 74.9, 77.3, 20.2and 37,9 mm and lengths of 2.0 and 6.2 m were tested for vertical and inclined (45') orientations and an evaporator liquid charge fill ratio of 50%.The correlations for the evaporator heat transfer coefficient and the maximum heat transfer rate can be used with reasonable confidence in analytical thermal performance correlations. The condenser heat transfer correlation show a significance scatter. The experimental results are also compared with other published correlations

Key words: heat pipes, butane, propane, R134, evaporator

1. Introduction:

A heat pipe consists of a sealed pipe lined with a working structure, in which a small amount of working fluid is present, and can be divided into an evaporator or heat addition section and condenser or heat rejection section. When heat is added to the evaporator region, the working fluid present in the wicking structure is heated, vaporizes and flows to the cooler condenser section and condenses, giving up its latent heat of vaporization. The capillary forces in the wicking structure then pump the condensate back to the evaporator. Two-phase closed thermosyphons or thermosyphons, on the other hand , are essentially heat pipes but without the working structure and thus gravity to return the condensate back to the evaporator. To ensure that the condensate can return to the evaporator the evaporator section must thus be situated below the condenser section.It has been shown that in the presence of gravity,thermosyphons are preferred to heat pipes owing to the fact that the wick structure in the heat pipe could produce an additional resistance to the flow of condensate'. Figure 1 illustrates the principle difference between a heat pipe and a thermosyphon. One of the main reasons why thermosyphons are becoming ever more popular is the fact that they have a very high effective thermal conductance. As an example, thermosyphons are able to conduct up to 1000 times more heat, under favorable conditions, than a solid copper pipe of the same diameter3. They are also particularly suitable for use in heat recovery heat exchangers to recover heat from low-grade waste streams to preheat incoming streams at ambient temperatures. There are many such applications to be found in the food processing and industrial process industries. As conventional energy resources diminishing energy prices increase it is becoming more attractive to consider recovering the waste heat from streams of typically up to 80'C temperature to pre-heat incoming streams from external Conditions at incoming temperatures. Refrigerant R134a and butane were chosen as the working fluids as both these fluids have low ozone depletion and global warming potentials and this makes them attractive working fluids. Rl34a is increasing in popularity in the refrigeration industry and in certain countries legislation prescribes its use. Butane is relatively cheap and is commercially available. Gas lighter fuel, sold in supermarkets, is a mass percentage mixture of 50% n-butane, 25% iso-butane and 25% propane. The Saturated vapor pressure of both butane and Rl34a at room Temperatures is significantly higher than atmospheric pressure and relatively small vapor specific volumes (approximately220kPa and 0.18 milk respectively for n-butane)4. This has an important practical implication, as it obviates the need of a high quality vacuum pump to charge the system. After charging, the non-condensable gases may be removed by boiling-off a little of the liquid charge. The successful removal of the noncondensable gasses using this method can be verified by Checking that the working fluid temperature at the top of the condenser is only slightly less than the temperature in the evaporator. Limited research has been undertaken using R134as whilst no formal database on the heat transfer of butane as a thermosyphon working fluid is available. Water has arguably superior thermal properties, but with a sub-atmospheric saturated pressure at room temperature of only 2.4 kPa would require high quality vacuum equipment to charge the system at room temperatures. Also, because water has a large specific volume of 58m/k low saturation temperatures, it is considerably more sensitive to the thermally insulating effect of non-condensable gas, is it collects on the surface on which the condensation is taking place. The important thermal characteristics, unique to two-phase closed thermosyphons, needed to theoretically or analytically characterize their performance include the internal evaporator and condenser heat transfer coefficients and the maximum heat transfer rate at different inclination angles and liquid charge fill ratios. It is thus the expressed objective of this paper to experimentally determine these thermal characteristics for a number of closed two phase thennosyphons of varying diameters for cooling temperatures in the region of 5 to 20C and heating temperatures of up to 80'C for both Rl34a and butane As working fluids. These test conditions and temperatures being particularly suitable for recovering heat from low-grade waste streams to preheat an incoming stream at ambient conditions and are typical for thermosyphons that might be included in heat recovery heat exchangers for heat recovery applications in many food processing and industrial processes. Further, these experimentally determined heat transfer coefficients will be presented as correlations suitable for use in performance calculations and will also be compared with other published thermal performance correlations.

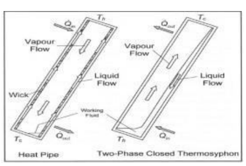

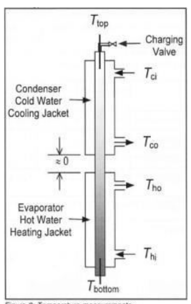

Figure 2: Temperature measurements

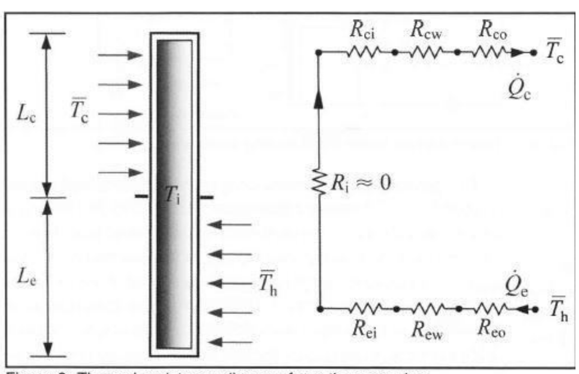

Figure 3: Thermal resistance diagram for a thermosyphon

2. Theory

For a single two-phase closed thermosyphon, as indicated in Figure, and for the thermal resistance diagram shown in Figure3, heat is transferred from a heat source, Through the evaporator wall, into the working fluid and then out through the condenser to the heat sink. This Heat transfer rate may thus be conveniently expressed in terms of a temperature difference and the sum of a series of thermal resistances as knowing the heating and cooling water inlet and outlet temperatures and the mass flow rates of the heating and cooling streams. the evaporator and condenser section heat transfer rates can be calculated in accordance with the consorted right hand terms equations (2) and (3) account for the heat that is not transferred to the working fluid in the evaporator and from the working fluid in the condenser but that which is lost or gained from the environment through the heating/cooling jacket walls as well as through the structure supporting the thermosyphon. The free convection and radioactive heat transfer coefficients determined using correlations obtained from Mills6. The wall temperature used was the wave rage of the heating and cooling water temperatures. Equation (1) may be rearranged to give the internal heat transfer coefficients for the evaporator and condenser

Sections of the thermosyphon as Knowing the inside working fluid temperatures and the heating and cooling water inlet and outlet temperatures the average temperature and may be calculated. Knowing the wall thermal conductivity, the wall thermal resistances may also be calculated. The external heat transfer coefficients may also be determined using well-known correlations provided by textbooks such as Millsu, as shown in equation (6).This correlation agrees with most of the available experimental data to within20%o.6 The internal heat transfer coefficients are more problematic and would have to be determined experimentally using equations 4 and 5. Experimental Set-up and procedur Four different diameter thermosyphons (three copper and one304 stainless steel) were tested. Table 1 gives their basic dimensions. The diameters of the copper thermosyphons correspond to typically available sizes used in the air conditioning and refrigeration industries. The lengths were chosen such that a maximum heat transfer rate could be achieved. The thermosyphons were fitted with tubular jackets (see Figure 2) through which heating and cooling water could be circulated using a hot and cold water supply system shown in Figure 4.The thermosyphon support structures could be inclined at different angles. In all cases a liquid charge fill ratio of 50% was used, at inclinations of 45^0 and 90" to the horizontal and cooling water temperatures of between 5 to 20'C and heating water temperatures of up to 80"C. Circulating water mass flow rates were determined by measuring the time it took for a known volume of water to flow. Temperature measurements using type-T thermocouple s were recorded every 30 s using a Schlumberger (SI35951A IMP) data logger and a test run continued until the maximum heat transfer rate, or when the heating water temperature reached 80'C.Figure 5 is typical of the different temperature measurements as a function of time for a test run. It is seen that as the temperature difference between the hot and cold environment increases, the heat transfer rate increases until the maximum heat transfer rate is reached. At this point, transfer rate tends to remain constant even though the heating. Temperature is further increased, or the cold temperature is decreased. The heat For each test run, equally spaced data points up to but not including the maximum heat transfer rate were selected to form a data set of 45 data points. For the four diameters and two inclination angles a data set of 360 (45x4x2) points was generated for each of the working fluids. To determine the correlations for the maximum heat transfer rate data sets of 17 points for each of the working fluids were generated. To demonstrate compliance with the conservation of energy the condenser heat transfer rate and evaporator heat transfer rate compared with each other. Figure 6 gives the condenser heat transfer rate as a function of the evaporator heat transfer rate for both working fluids But only for the vertical orientations. Similarly for figure 7 but now for 45^0 inclined orientations. Over the full range of heat transfer rates there is a correspondence of within + 10%. Values of this order are deemed acceptable considering the complexity of the physical processes occurring in the thermosyphon. The heat transfer rate inside the condenser section is not necessarily in phase with that of the evaporator section and unstable phenomena such as near-dry out oscillation, geyser boiling and flooding oscillation often occur during normal operation of two-phase closed thermosyphons. The type-T thermocouples used for

The investigation has an uncertainty of 0.1ºCin temperature measurements. The Schlumberger data logger introduced a further error of less than 0.3ºC. A potentially large effort may be introduced into temperature measurements by flow-phenomena such as capitation or thermal stratification off low occurring at the locations of insertion of the thermocouples. Care was thus taken to ensure that these types of errors did not occur. The device used for charging the thermosyphons measured the volume of working fluid transferred with an error less than 1.0x 10 6m'(1 m/). This corresponds to amass inaccuracy of approximately 0.0005 kg for liquid butane under operating conditions. Mass flow rates of heating and cooling water were determined by means of volumetric measurements over a timed interval. The uncertain ties in volumetric measurements (approximately $0.0001m^3$), and time measurements (approximately 0.01 seconds) used to determine mass flow rates of heating and cooling water yield an uncertainty of less than 0.01 kg/s for these quantities.

	Material	d_i [mm]	d_o [mm]	L_e [m]	L_c [m]
5/8"-Thermosyphon	Copper	14.90	15.88	1.00	1.00
3/4"-Thermosyphon	Copper	17.27	19.05	1.03	1.03
7/8"-Thermosyphon	Copper	20.19	22.22	1.03	1.03
5/4"-Thermosyphon	Stainless Steel	31.90	34.90	1.20	5.00

Table 1: Sizes and dimensions of the experimental thermosyphons

EQUATIONS:

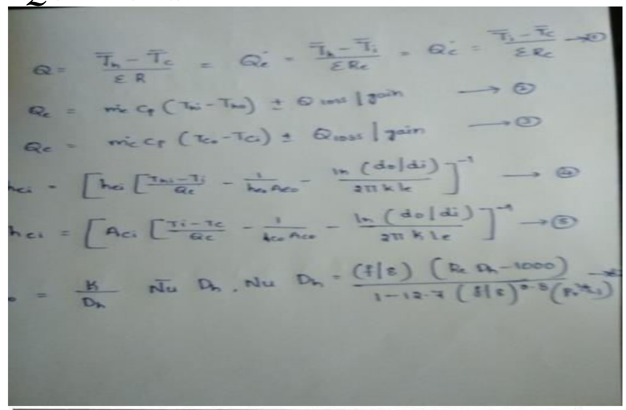

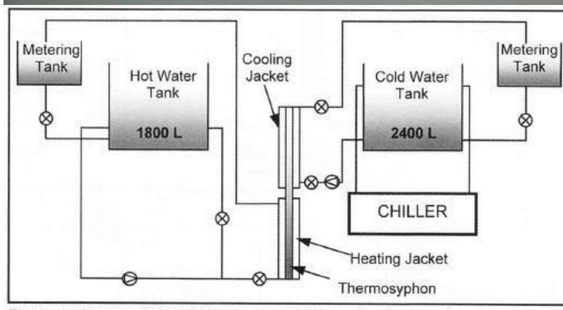

Figure 4: Thermosyphon heating and cooling water tank systems

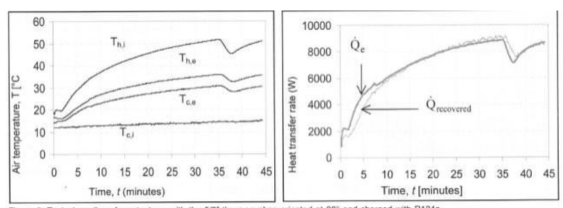

Figure 5: Typical readings for a test run with the 5/8"-thermosyphon oriented at 90° and charged with R134a

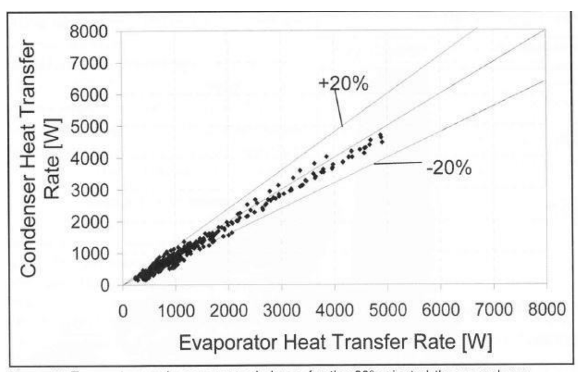

Figure 6: Evaporator-condenser energy balance for the 90° oriented thermosyphons

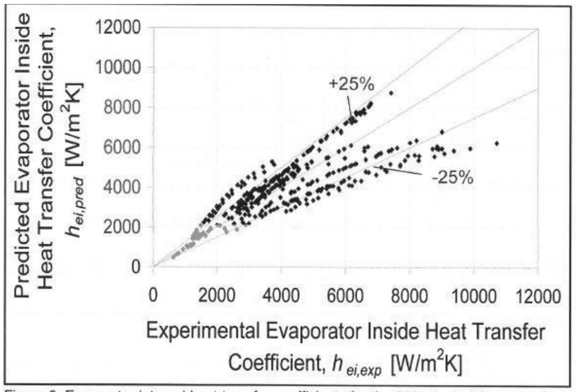

Figure 8: Evaporator internal heat transfer coefficients for the 90° oriented thermosyphons

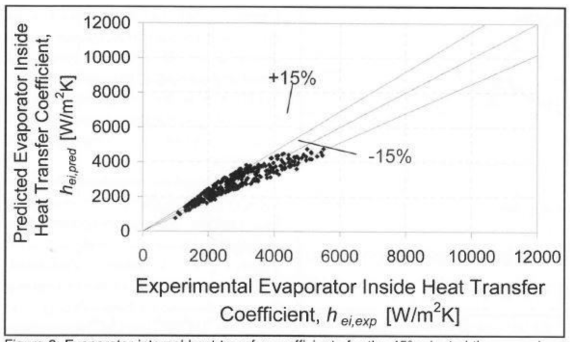

Figure 9: Evaporator internal heat transfer coefficients for the 45° oriented thermosyphons

4. Results

Multi-linear regression was used to correlate the heat transfer coefficients and the maximum heat transfer rate in terms of the independent variables. The form of the correlations was chosen as a power series ..... This form of equation was chosen because it is simple, and similar forms have been used successfully for many broadly similar correlations in the past6.

4.1 Evaporator heat transfer coefficient

The evaporator heat transfer coefficient was correlated in terms of, essentially, the heat transfer rate, the temperature difference between the wall and the working fluid, and the fluid properties of the different working fluids (butane and R 134a) for the two orientations by power series as shown in equations (7) and(8) .The non-dimensional Kutateladze and Jacob numbers were chosen to represent the independent variables, as using these two numbers gave the best correlation coefficients. Use of additional terms in the power series did not significantly improve the correlation coefficient. Although four different diameters were tested, the diameters did not significantly influence the evaporator heat transfer coefficient. Figures 8 and 9 illustrate the comparison between the predicted and experimentally determined internal evaporator heat transfer coefficients for vertical and inclined operation. For the vertical operation, 78% of the predicted values fell within 25% of the experimental values and for the inclined operation, 82% the values fell within l5%. It is interesting to note that, for the same temperature difference between the hot and the cold strafes', the evaporator heat transfer Coefficient is significantly higher for the vertical case compared with the inclined case. For the smaller diameter thermosyphon, the heat transfer coefficient for the inclined thermosyphons was some 30% lower and for the larger diameter 5/4" - thermosyphon, 70%lower. This is attributed to the fact that condensate returns to the evaporator more evenly around the periphery of a vertically orientated pipe and hence it is easier to maintain a better wetted evaporator surface. On the other hand, for the inclined case, condensate returns to the evaporator section essentially as a rivulet flowing in the bottom on the pipe and hence less able to adequately wet the entire evaporator section surface. Predicted evaporator section internal heat transfer coefficients using equations (l) and (8) as well as a number of published correlations are compared with the experimentally determined values for the vertical and inclined orientations in Figures 10 and 11. From the figures, it can be seen that the predictions obtained with the El-Genk and Saber correlations are relatively inaccurate. This may be attributed to the fact that although the heat flux in both experimental set-ups was of a similar order of magnitude and range, their experimental data does not include R134a or butane as the working fluid. The thermosyphons from which the correlations were generated may also have had differing geometries (diameters and lengths) to those pertaining to this paper. Equations (7) and (8).

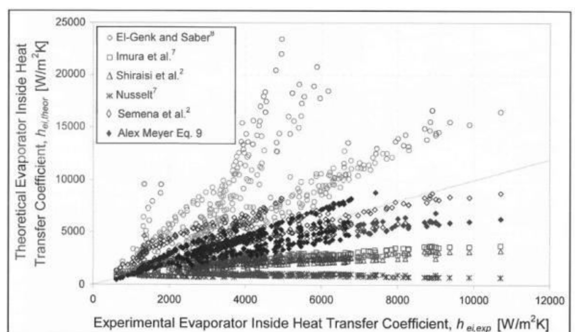

Figure 10: Comparison between theoretically determined evaporator internal heat transfer coefficients for the 90°oriented thermosyphons

EQUATIONS PART 2:

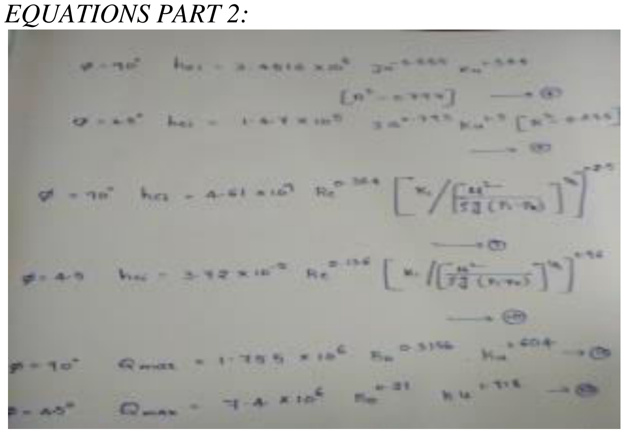

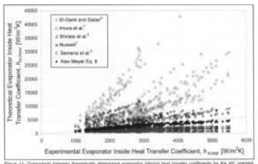

Figure 11: Comparison between theoretically determined evaporator internal heat transfer coefficients for the 45° oriented thermosyphons

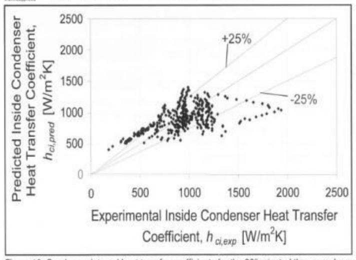

Figure 12: Condenser internal heat transfer coefficients for the 90° oriented thermosyphons

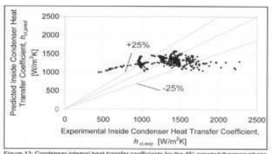

Figure 13: Condenser internal heat transfer coefficients for the 45° oriented thermosyphons

4.2 Condenser heat transfer coefficient

The independent variables, as is common for film-wise condensation, were taken as a Reynolds number and a property grouping based on the Kutateladze number6 as shown in equations (9)and (10).Predictions using equation (9) for vertical case with relatively low correlation coefficient of R2 = 0.425 could be argued as being more-or-less reasonable as shown in Figure 12 where 6l.l% of the predicted values fall within the+25%limts. Equations (l0) .for the inclined case on the other hand with the low regression coefficient of 0.121 and shown in Figure 13 cannot really be expected as being able to accurately predict the heat transfer coefficient even though 74.4% the values fall within +25 Volts'. The low correlation coefficients are a result of the condenser internal heat transfer coefficients remaining relatively insensitive to the variables usually used to correlate condensation in vertical and inclined pipes. On average the condenser section internal heat transfer coefficients for the inclined orientation is some 50% higher than for the vertical orientation. This is to be expected as the average condensate film thickness for a relatively long pipe decreases as the pipe angle to the horizontal decreases. The heat transfer coefficient for a laminar film may be approximated by the thermal conductivity divided by the film thickness, and hence the smaller the film thickness the larger the heat transfer coefficient. The predicted condenser internal heat transfer coefficients using equations (9) and (l0) are compared with published correlations in Figures 14 and 15. None of the correlations are seen to accurately predict the experimentally determined values. Although equations (9) and (10) show a correspondence with Nusselt theory correlations' is seen that the Wang correlation significantly over-predicts the predicted correlation given by equations (9) and (10) for both the vertical and inclined operations.

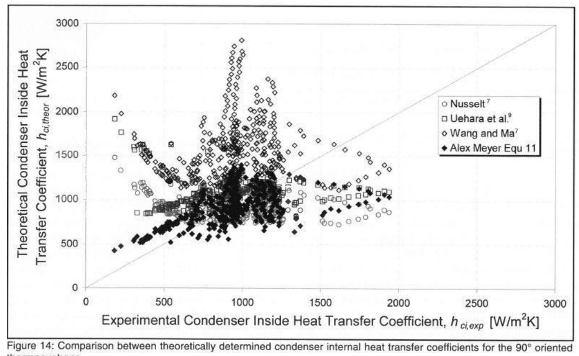

Figure 14: Comparison between theoretically determined condenser internal heat transfer coefficients for the 90° oriented thermosyphons

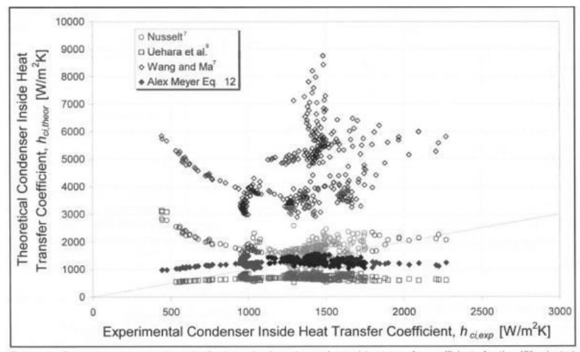

Figure 15: Comparison between theoretically determined condenser internal heat transfer coefficients for the 45° oriented thermosyphons

4.3 Maximum heat transfer rate

As the temperature difference between the heating and the cooling water increases so too does the heat transfer rate. However, there is a point of operation at which the heat transfer rate is at a maximum, beyond which it cannot increase, despite any further increase in the temperature difference. This is due to the phenomenon known as flooding, which occurs when high velocity vapor hinders the return of liquid from the condenser section to the evaporator section of the thermosyphont. For athermosyphon using an electrical heating element to provide a constant heating rate to the evaporator, the heat transfer rate may eventually drop to zero as the temperature difference increases beyond this point, due to burnout or melting. However for temperature controlled thermosyphons such as those used in this investigation, a slight drop in the average heat transfer rate is observed but it will not decrease to zero, and large fluctuations in the instantaneous heat transfer rate, as the liquid vapor interface becomes unstable. This can be observed in Figure 5. The maximum heat transfer rates as defined above for the vertical and inclined orientations of the two-phase closed thermospythons were found to be highly dependent on the diameter and the heat transfer rate and hence are given in terms of a Bond and a Kutateladze number respectively, as shown in equations (11) and (12).Figures 16 and 17 compare the predicted values using these equations with the experimentally determined values. As can be seen in these figures, and also by the relatively high correlation coefficients that were obtained, equations (11) and (I2) reflect the maximum heat transfer rate of the tested thermosyphons reasonably well. As expectedr0 the maximum heat transfer rate for the inclined thermosyphon is some 40% higher than for the verticalthermosyphon. It is however interesting to note that if the maximum heat transfer rate has not been attained that for the same temperature difference between the heat source and the heat sink that the heat transferred by both the vertical the inclined thermosyphons is essentially the same. The reason for this is that the increased condenser heat transfer coefficient for the inclined case is offset by the decreased evaporator heat transfer coefficient and vice versa for the vertical.

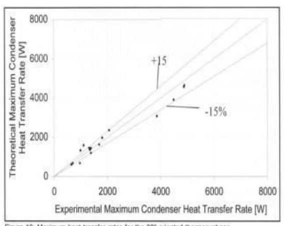

Figure 16: Maximum heat transfer rates for the 90° oriented thermosyphons

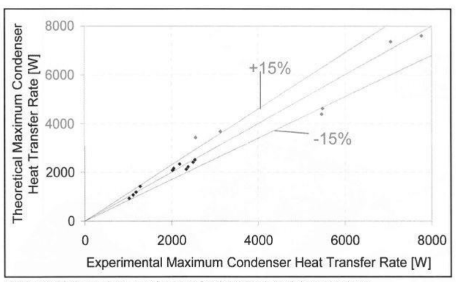

Figure 17: Maximum heat transfer rates for the 45° oriented thermosyphons

Conclusions

The energy balances between the evaporator and condenser Heat transfer rates fell within a reasonable percentage of about for both the vertical and inclined orientations. Considering the complex phenomena occurring inside a thermosyphon and the fact the evaporator heat transfer rate is necessarily out of phase with the condenser heat transfer rate it is argued that the experimental energy balances that were obtained are typical of what can be expected and hence the experimentally determined evaporator and condenser heat transfer rates for Rl34a and butane may be used with reasonable confidence. Correlations for the vertical and inclined operation for different thermosyphon geometries with R134a and butane as charge fluids are given by equations (7) to (I2).It is found that the evaporator vertical heat transfer coefficient is slightly higher compared with the inclined case for the same temperature difference between the heat source and the heat sink. It is however found that as the temperature difference increases, the vertical orientation reaches its maximum heat transfer rate at a lower temperature difference. The evaporator heat transfer coefficients and the maximum heat transfer rate correlations as given by equations (7) and (8) and (11) and (12) respectively with their relatively high correlations coefficients, may be used with relative confidence. The correlation coefficients for equations (9) and (10) are low and these correlations based on only the film theory of condensation are rather imprecise. It is thus concluded that this is not a suitable basis for this sort of correlation, and that a better understanding of the physical nature of the complex processes in the condenser section of thermosyphon is required to more accurately predict internal heat transfer coefficients for the condenser
Section.

References

1. Dunn DP and Relay D, Heat Pipes. 4th Ed., Pergamum, 1994.
2. Pioro LS and Pioro IL, Industrial Two-phase Thermosyphons, Bagel House, 1997.
3. Russwurm AE, Q-pipes add a new dimension to waste Heat Recovery, Part I. Heating, Air Conditioning A Refrigeration (Now Refrigeration and Air-conditioning), January 1980,27-39.
4. ASHRAE, Handbook of Fundamentals American Society of Heating, Refrigeration and Air-Conditioning Engineers atlanta, 2001.

HEAT TRANSFER ALONG VERTICAL INSULATED CHIMNEY

K.SANDHYA
[sandi.sandhya123@gmail.com]
Dept. of Mechanical Engineering, Mall Reddy College of engineering, Maisammaguda,HYD

M.SURESH BABU
[suresh4you247@gmail.com]
Dept. of Mechanical Engineering, Mall Reddy College of engineering, Maisammaguda,HYD

ABSTRACT

Chimney, which form the last component of a system using a flue gas such as boiler, play a vital role in maintaining efficiency, draft, etc, of a system and also in minimizing the atmospheric pollution. The hot gases occupy larger volume than before. The weight of gases per cubic meter becomes less. For the purpose of the structural design of the steel chimney, the height and diameter of chimney. Chimneys are required to carry vertically and discharge, gaseous products of combustion, chemical waste gases, and exhaust air from an industry to the atmosphere In this thesis, chimney will be designed considering with insulation and without insulation. 3D model of the chimney is done in CREO Parametric software and fluid-structural and thermal analysis is done on the chimney in ANSYS software. A simplified model of chimneys with various insulation materials (concrete and carbon epoxy).Static analysis is to determine the deformation, stress and strain for chimney with insulation and without insulation. Thermal analysis to determine the heat flux of the chimney with different materials to different models.CFD analysis to determine the pressure drop, velocity, heat transfer coefficient, mass flow rate and heat transfer rate.

Keywords

Chimney, Flue Gases, Heat transfer rate.

I. Introduction

A chimney is a structure that provides ventilation for hot flue gases or smoke from a boiler, stove, furnace or fireplace to the outside atmosphere. Chimneys are typically vertical, or as near as possible to vertical, to ensure that the gases flow smoothly, drawing air into the combustion in what is known as the stack, or chimney effect. The space inside a chimney is called a flue. Chimneys may be found in buildings, steam locomotives and ships. In the United States, the term smokestack (colloquially, stack) is also used when referring to locomotive chimneys or ship chimneys, and the term funnel can also be used.

The height of a chimney influences its ability to transfer flue gases to the external environment via stack effect. Additionally, the dispersion of pollutants at higher altitudes can reduce their impact on the immediate surroundings. In the case of chemically aggressive output, a sufficiently tall chimney can allow for partial or complete self-neutralization of airborne chemicals before they reach ground level. The dispersion of pollutants over a greater area can reduce their concentrations and facilitate compliance with regulatory limits.

fig:1.1 chimney diagram

II. Literature Review

1.Seismic Analysis and Design of Industrial Chimneys: Slenderness ratio H/Dinf, radius ratio Rsup/Rinf, thickness ratio Esup/Einf and thickness diameter ratio Dinf/Einf

2. Analysis of Self Supported Steel Chimney as Per Indian Standard: To ensure a desired failure mode design code (IS-6533: 1989 Part 2)

3. Analysis and Computational Study of a High Chimney Tower for Solar Energy the "Autodesk Robot structural analysis professional"

4. Dynamic Soil-Structure Interaction Analysis of Tall Multy-Flue Chimneys under Aerodynamic and Seismic Force: . JEEVAN T, SOWJANYA G. V (2014

III. Problem Description & Methodology

The objective of this project is to make a 3D model of the chimney and study the thermal and static behavior of the chimney by performing the finite element analysis. 3D modelling software (PRO-Engineer) was used for designing different geometrics and analysis software (ANSYS) was used for thermal and static analysis.

The methodology followed in the project is as follows:

1.During pre-processing

The geometry (physical bounds) of the problem is defined.

The volume occupied by the fluid is divided into discrete cells (the mesh). The mesh may be uniform or non-uniform.

2.The physical modeling is defined – for example, the equations of motion + enthalpy + radiation + species conservation

3.Boundary conditions are defined. This involves specifying the fluid behaviour and properties at the boundaries of the problem. For transient problems, the initial conditions are also defined.

The simulation is started and the equations are solved iteratively as a steady-state or transient.

Finally a postprocessor is used for the analysis and visualization of the resulting solution.

IV. Introduction to CAD

Throughout the history of our industrial society, many inventions have been patented and whole new technologies have evolved. Perhaps the single development that has impacted manufacturing more quickly and significantly than any previous technology is the digital computer.

A. Introduction to PRO/Engineer

Pro/ENGINEER, PTC's parametric, integrated 3D CAD/CAM/ CAE solution, is used by discrete manufacturers for mechanical engineering, design and manufacturing. Created by Dr. Samuel P. Geisberg in the mid-1980s, Pro/ENGINEER was the industry's first successful parametric, 3D CAD modeling system. The parametric modeling approach uses parameters, dimensions, features and relationships to capture intended product behavior and create a recipe which enables design automation and the optimization of

B. Introduction to Finite Element Method

Finite Element Method (FEM) is also called as Finite Element Analysis (FEA). Finite Element Method is a basic analysis technique for resolving and substituting complicated problems by simpler ones, obtaining approximate solutions Finite element method being a flexible tool is used in various industries to

solve several practical engineering problems. In finite element method it is feasible to generate the relative results. ANSYS is an

Engineering Simulation Software (computer aided Engineering). Its tools cover Thermal, Static, Dynamic, and Fatigue finite element analysis along with other tools all designed to help with the development of the product. The company was founded in 1970 by Dr. John A. Swanson as Swanson Analysis Systems, Inc. SASI. Its primary purpose was to develop and market finite element analysis software for structural physics that could simulate static (stationary), dynamic (moving) and heat transfer (thermal) problems.

IV. Modelling and Analysis

A. Models of Narrow Plate Using Pro-e

The vertical narrow plate is modeled using the given specifications and design formula from data book. The isometric view of vertical

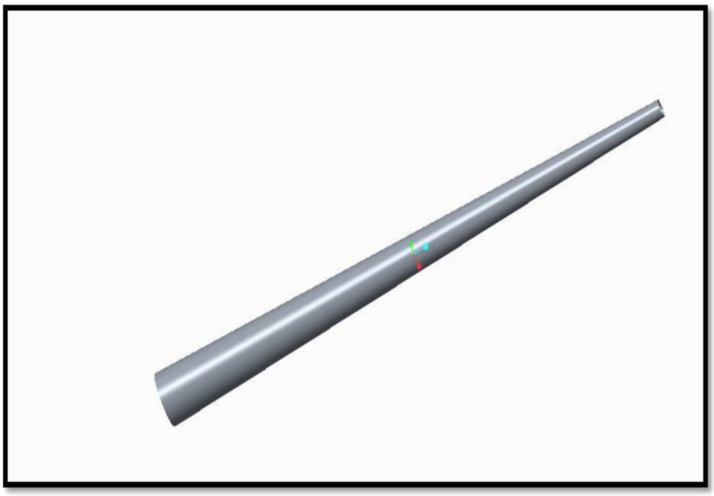

3D Model of chimney

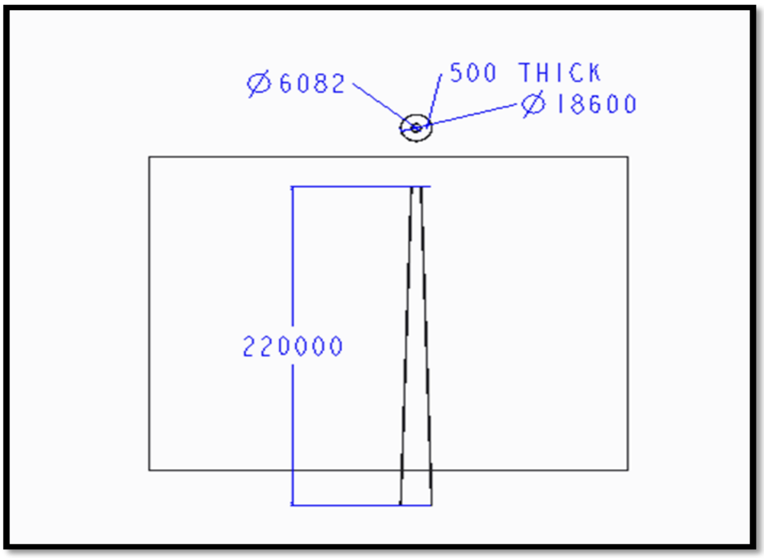

2D model of chimney

B.Static Analysis of Chimney With insulation Material carbon epoxy: Deformation

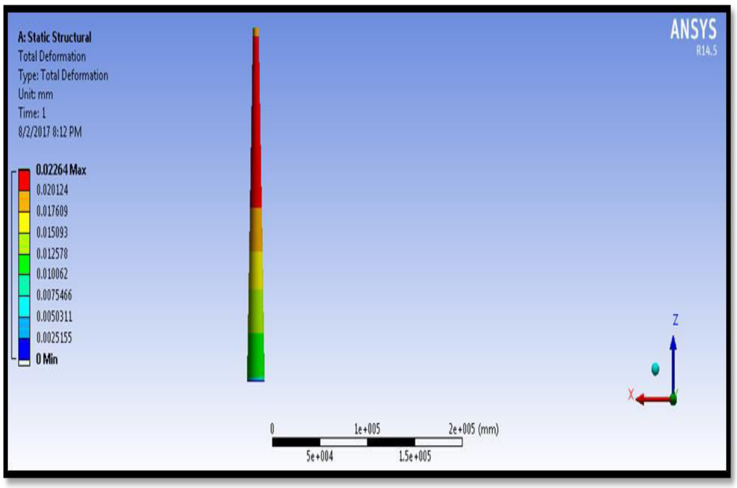

Stress:

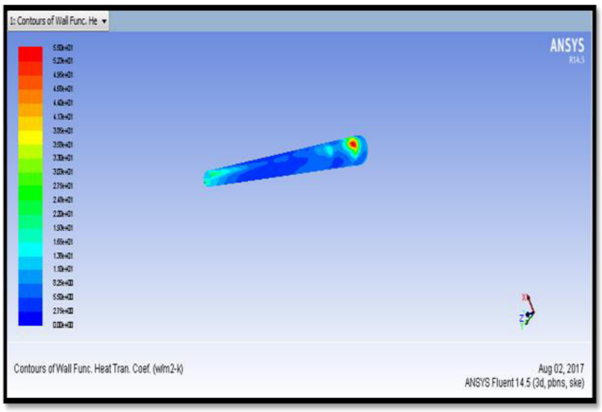

Strain:

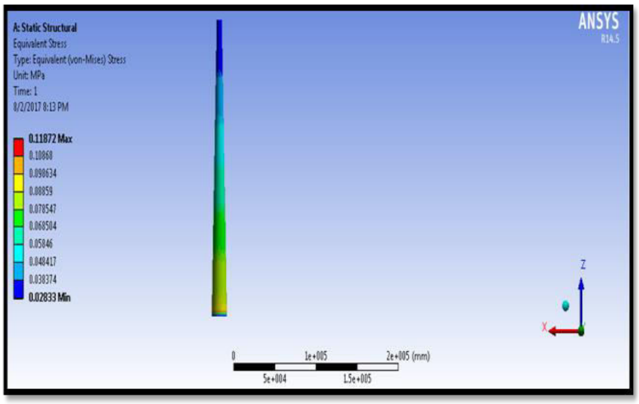

C.Thermal Analysis of chimney wth insulation

Material carbon epoxy:

Heat flux:

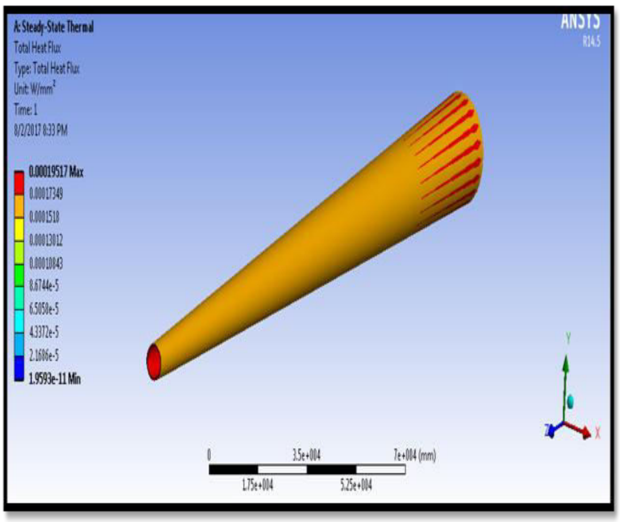

Temperature:

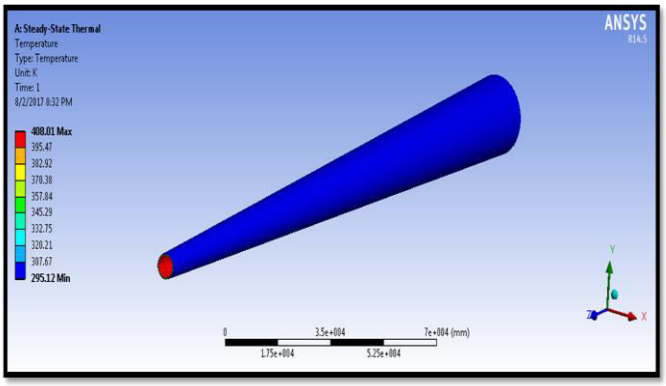

D.CFD Analysis of chimney AT VELOCITY-25m/s:

Pressure:

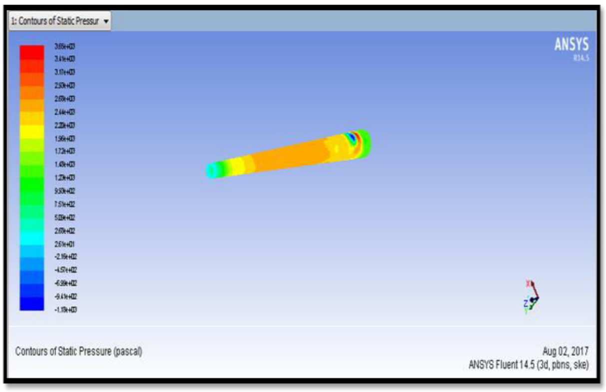

VELOCITY:

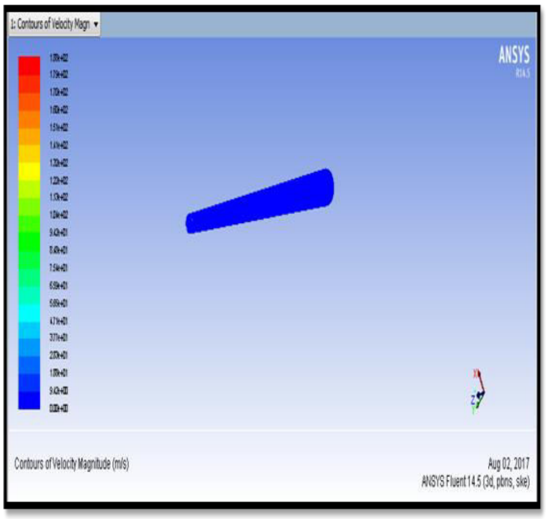

V. Results and Discussion

A. Static Analysis Result Table:

Cases	Material	Deformation (mm)	Stress (N/mm^2)	Strain
Without insulation	Concrete	0.10631	0.13931	4.64e-6
	Carbon epoxy	0.02264	0.11872	1.696e-6
With insulation	Concrete	0.077796	0.10321	3.19e e-6
	Carbon epoxy	0.021326	0.099309	1.4187e-6

B. Thermal Analysis Results Table:

Cases	Material	Temperature (k)		Heat flux (w/mm2)
		Min	Max	
Without insulation	Concrete	295.16	408	0.00017788
	Carbon epoxy	295.16	408	0.000161517
With insulation	Concrete	295.12	408.01	0.00017488
	Carbon epoxy	295.12	408.01	0.00019612

CFD Analysiis Result Table:

Inlet velocity(m/s)	Pressure (Pa)	Velocity (m/s)	Temperature (k)	Heat transfer coefficient w/m^2K	Mass flow rate (Kg/sec)	Heat transfer rate(w)
15	1.13e+03	1.36e+02	4.13e+02	5.50e+01	86.634321	3076241.8
20	2.18e+03	2.21e+02	4.10e+02	7.16e+01	118.02872	3744.563
25	3.66e+03	1.88e+02	4.08e+02	9.55e+01	148.25006	4430918.5

VI. Conclusion And Referrence:

In this thesis, chimney will be designed considering with insulation and without insulation. The Bureau of Indian Standards (BIS) design codes procedures will be used for the design of the chimney. The chimney was considered as a cantilever beam with annular cross section.3D model of the chimney is done in CREO Parametric software and fluid-structural and thermal analysis is done on the chimney in ANSYS software. A simplified model of chimneys with various insulation materials (concrete and carbon epoxy).Static analysis is to determine the deformation, stress and strain for chimney with insulation and without insulation.

References:

[1] M R Tabeshpour, "Non linear Dynamic Analysis of Chimney-like towers", Asian Journal of Civil Dynamic Analysis of RCC Chimney- A Review (IJSRD/Vol. 4/Issue 02/2016/037) All rights reserved by www.ijsrd.com 120 Engineering (Building and Housing), vol.13, NO.1 (2012), pp.97-112.

[2] Victor bochicchio, “Design of chimney with GRP liner for low and high temperature operation”, Vol-22, no-1, pp-1-5.

[3] M Shivaji and V S N Raju, "Dynamic analysis of RCC Chimneys ", pp.1-14.

[4] Anurag Jain, Behnam arya, Charles Goddard and Jon Galsworthy, "Non linear Dynamic Analysis of an Industrial Chimney's Pile foundation system for huricane loading", 11th Americas conference on wind engineering -sanjuan, Pucrto rico, June-22-26, 2019.

[5] K.S.Babu Narayan, Subhas .C. Yaragal, and Yukio Tamura, “Interaction Envelops for Limit State Design Chimneys”, The fourth International Symposium on computational Wind Engineering (cwe2006), Yokohama, 2006, pp 439-442.

[6] B.R. Jayalekshmi, S.V. Jisha, R.Shivshankar, "Wind load Analysis of Tall Chimneys with Piled Raft foundation

considering the Flexibility of Soil", International Journal of Advance Structural Engineering (2015), pp.95-115.

[7] Negar Sadegh Pour, Indrajit chowdhary, "Dynamic soil structure interaction analysis of tall multy-flue chimneys under aerodynamic and seismic force", The 12th International Conference of International Association for Computer Methods and Advances in Geomechanics (IACMAG). 1-6 Oct, 2008, Goa, India, pp.2696-2703.

[8] Jeevan T, Sowjanya G V, "Soil Structure Interaction on 100m Tall Industrial Chimney under Seismic Load", International Journal of Engineering Research and Technology (IJERT), vol.3, issue 8, Aug 2014, pp.782-789.

[9] Ganeshkumar T, Shruthi H.K, "Soil structure interaction effect on 200m tall industrial chimney under seismic load", International Journal of Civil & Structural Engineering research, Vol.2, issue 1, pp.111-118.

[10] Doris Mehta, Nishant J Gandhi, "Time Response Study of Tall Chimneys, under the effect of Soil Structure Interaction and long period Earthquake Impulse", The 14th World Conference Earthquake Engineering Oct 12-17, 2018, Beijing, China.

[11] Jisha S V, Dr B R Jayalekshmi, Dr R Shivashankar, "Across Wind Response of Tall Reinforced Concrete Chimneys Considering the Flexibility of Soil" International Journal of Engineering Research and Technology (IJERT) Volume-1, issue-8, october-2012, pp.1-8.

[12] Sreerath S, Anooja Basheer,"Comparison of Wind & Seismic Effects on a Reinforced Concrete Chimney", IJETT, vol 28, No 7, Oct 2015, pp.365-368

PERFORMANCE ANALYSIS OF TWO STROKE PETROL ENGINE ON BASIS OF VARIATION IN CARBURETTOR MAIN JET DAIMETER

ABHILASH.P
Department of Mechanical Engineering
MALLA REDDY COLLEGE OF ENGINEERING

Dr. P.VEL MURUGAN
Professor,
Department of Mechanical Engineering
MALLA REDDY COLLEGE OF ENGINEERING

***Abstract*- 2s cars are the use of for cars walking. We maximum gain is that 2s engine has revolutions for every rev it's has one running stroke. Because of that working stroke it gives extra pickup and electricity, with that power we are the usage of in mechanical devices to utilise that power. Mainly we are the use of right here fuel engines to work efficient and overall performance to examine how a whole lot it's miles imparting and therefore changing the diameter of car by Gasoline will deliver less carbon particles as compared to different fuel based totally vehicles. Mostly I am used right here the 2s fuel engine for higher end result and estimate the warmth analysis and speed and mass transfer rate.**

In this project, a main jet of carburettor is intended and sculptured in 3D modelling software package CREO constant quantity. Since the planning of main jet of carburettor is advanced, and potency is directly associated with material performance, material choice is of prime importance. During this project, totally different materials and different nozzle diameters (15,20 and 25mm) by acting thermal analysis on the most jet of carburetor for each the styles with Sir Joshua Reynolds numbers (4000& 6000).

In this project, CFD technique is used to research the flow the fluid over the rotary engine blade. Analysis is completed in ANSYS

1. Introduction

Here the car by introduced for the charge entering so that it gives to combustion chamber and it sucks and make compression to give enough work stroke. Every motorbike engine, from the easy single-cylinder two-stroke, to the foremost subtle multi-cylinder four-stroke, depends on 2 terribly precise items of accessory instrumentation. the primary of those, the ignition, is of obvious importance as a result of it provides the exactly-timed spark that ensures that combustion happens at exactly the correct moment. The second piece of kit will fairly be thought of to be of even larger importance, for while not it, the engine can't be run or controlled. It is, in fact the carburetor. Throughout each engine cycle, be it two- or four-stroke, the carburetor should feed the engine with an exact quantity of fuel, mixed with Associate in Nursing equally precise quantity of air. Moreover, as loading on the engine varies, this fuel mixture should be varied to compensate. Once the engine is cold the quantitative relation of fuel to air should be altered radically; once inactivity, the carburetor should perform automatically; and once it's wanted to extend the speed of the engine, some suggests that of dominant the carburetor's operation to fine limits should be contrived. it'll already be apparent that the carburetor should be capable of acting a large vary of functions with nice accuracy and consistency, permitting induction to require place as usually as 10 thousand-fold each minute or perhaps additional. Equally vital, it should be sturdy, to endure extremes of temperature and vibration and wide variations of climate. Carburetors have for the most part instrumentation.

2.SPECIFICATION OF CARBURRETOR

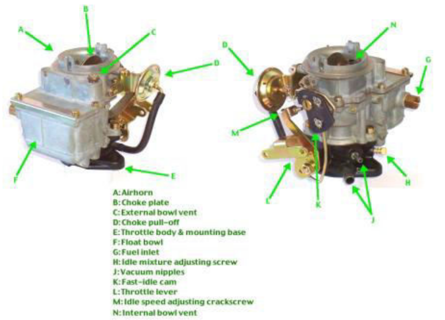

Fig1: Specification Of Carburetor

Principles

When carburetors rectangular degree utilized in craft with piston engines, unique styles and options square measure required to prevent gasoline entering at some stage in opposite flight. Previous cars run on 2s vehicles only in systematic order of mechanical system known as a stress car by, have draft carburetor style.

Outboard motor carburetors square measure generally side draft, as a result of they have to be stacked one on prime of the opposite so as to put those in the cylinders in a very vertically cast.

Beginning in the nineteen thirties draft carbies is the most fashionable sort outboard motor car by measures side draft.

A square degree of carby will make the confined carbies to make stepping into the chamber to offer energy stroke in that means it generally it's enough power what we required. Here we used modern carby,to restrict the glide of fee into chamber why because we must get the mileage to car and particularly mileage will depends on carburetor.

Operations of Carburetor in two different fields

Actually carburetor is used in two types of uses so called that fixed and variable carbies.Here in the fixed carby this structure is used anywhere and everywhere we can see on roads of running vehicles also. This implementation is quite different. Below figure shows the common used carby on mainly heavy vehicles.

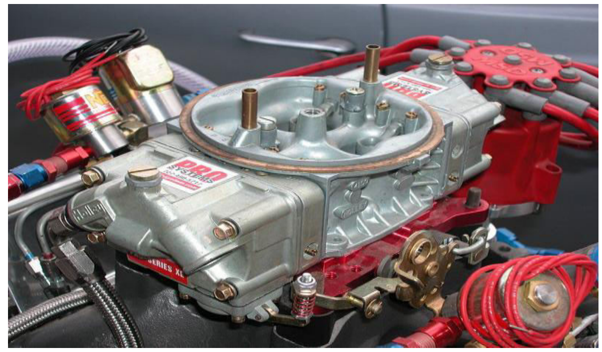

Fig2: Four-barrel carburetor gives big performance.

In operation mechanical tool waft proper amount stay within range like proportions equally and samely to get high power to deliver the chamber.

1. Cold Begin.
2. Hot Beginning.
3. Zero load or slow-moving.
4. Giving power.
5. More power / high power at full gate opening.
6. Cruising at component valve opening.

In addition, modern carburetors are required to do this while maintaining low rates of exhaust emissions.

Basics:

A mechanical device called Carby basically includes companion diploma that within fashion of the element that suits for handing over the fee. It in particular have the choke valve to enter the fee and restricts the drift. By the gravity the gas enters into gas cabin by means of go with the flow location and whilst gas fills the valve closes the port. As the fuel occurring passes into chamber the gasoline takes into the cabin. Throttle valve will pass charge into combustion chamber. By the opening of throttle valve the charge enters. Throttle is connected to the principle acceleration cable for velocity cause. Air is entered from top of the carby body. Fuel is entered from the center component. At throttle each mixes to shape a price in ratio.

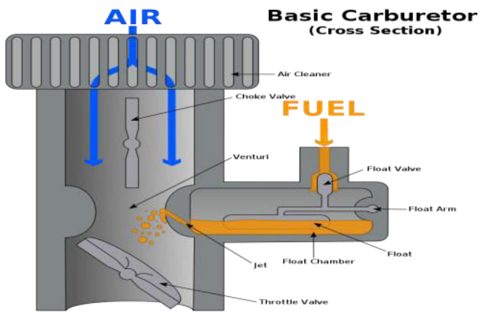

Fig3. Figure shows basic carburetor

As the throttle will specially works on the 2 circuits. Throttle is unfolded especially rely on the circuit which the principle rely upon that.Interferance allow plenty of similarity. As compares fundamental open throttle circuit.

Fuel is adjusted by way of the two primary strategies called off idle circuit and principal idle circuit. In off idle fuel interference foremost glide loads into the combustion chamber. Throttle is opened often because the air passes into carby extra within the primary idle off circuit. It may be anywhere paperwork a mechanical device. Attribute velocity will boom. Speed in which air skip in the centre and situate where it needs.

Generally challenge will impact durations to extend the air flow. Bernoulli's principle will carry out however it results huge effect on strength stroke. So that it's miles in particular used on in particular inventions. Equally large carburetors will blend rely on that standards only.

Power valve:

Valve will manufacture a whole lot of strength by means of this mechanism. Often we will use some self elastic tool command to conquer this mechanism. Because throttle will deliver numerous charge if you want to deliver a energy. Depend on revolutions per minute it offers a power so to vary it. Alternatively ought to use of have an impact on it can alternate to vary it. Nineteen fifties exchange of value degree the all time electricity in converting the strength valve. However some use them on every and circuit, as within the Quadra jet. Mainly this provides the strength based at the valve that materials the fee

Accelerator Pump:

The pump will gives you the excessive stress of price into the combustion chamber. The rate is blended not going and finely so that during right ratio by way of the throttle valve as a way to keep the unique deliver mixture. A mechanical device that's right away quicker than a gas rate of float increase. This will lessen the quantity of flow of hydrocarbon than the un burnt carbon particles. Further measures the additives into the waft device.

Choke:

In numerous carbureted cars, the choke is managed via using a cable related to a pull-knob at the dashboard operated via using the riding stress. In a few carbureted automobiles, it is mechanically managed with the aid of a thermostat the use of a bimetallic spring; that is exposed to engine heat, or to an electrical detail. This warmth also can be transferred to the choke thermostat via clean convection, via engine fluid, or via air heated by using using the exhaust. Extra present day styles use the engine heat completely in a roundabout way: A tool detects engine warmth and varies electric powered phenomenon to a tiny low detail that acts upon the bimetallic spring to modify its anxiety, thereby dominant the choke. A choke unloaded may be a linkage arrangement that forces the choke open against its spring as soon as the automobile's accelerator is emotional to the pinnacle of its excursion. This provision allows a "flooded" engine to be cleared out in order that it will begin.

Some carburetors do now not have a choke but as a substitute use a aggregate enrichment circuit, or enrichment. Generally used on little engines, notably motorcycles, enrichments paintings by using the usage of hole a secondary fuel circuit beneath the throttle valves. This circuit works exactly similar to the idle circuit, and as soon as engaged it actually gives extra fuel once the throttle is closed.

Oldern bikes, with aspect-draft slide-throttle carburetors, used any other fashion of "bloodless start device", referred to as a "tickler". This might be simply a elastic tool rod that, as quickly as depressed, manually pushes the float down and permits extra fuel to fill the waft bowl and flood the intake tract. If the "tickler" is command down too lengthy it moreover floods the floor of the mechanical device and therefore the housing underneath, and is therefore a fitness hazard.

Elements Of Others:

The circuit additionally can also may additionally moreover be affected by varied mechanical or fuel strain connections and additionally by way of heat touchy and electric elements.

3 RESULTS

Table 4.1 CFD ANALYSIS

Reynolds number (Re)	Nozzle dia. (mm)	Pressure (Pa)	Velocity (m/s)	Heat transfer coefficient (w/m2-k)	Mass flow rate (kg/s)	Heat transfer rate (W)
4000	15	8.80e-01	3.67e-02	8.645e+01	0.004434	68.007813
	20	5.98e-01	2.88e-02	8.41e+01	0.0001725	26.453125
	25	4.00e-01	2.35e-02	8.88e+01	0.0004085	62.71875
6000	15	1.71e+00	5.50e-2	8.645e+01	0.0015255	233.95313
	20	1.15e+00	4.29e-02	8.41e+01	2.52e-05	3.90625
	25	7.58e-01	3.47e-02	8.88e+01	0.0001152	17.609375

Table 4.2 THERMAL ANALYSIS

Material	Temperature (°C)		Heat flux(w/mm²)
	M ax	M in	
Brass	1 00	43 .646	14.142
Copper	1 00	55 .759	17.051
Aluminum	1 00	36 .03	12.016

3.1 GRAPHS

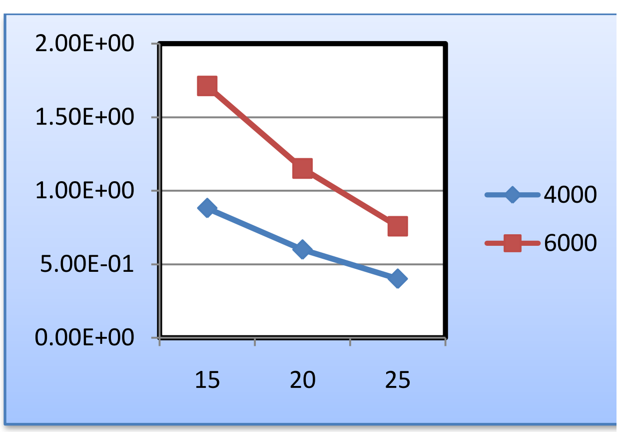

Fig.4 Pressure plot

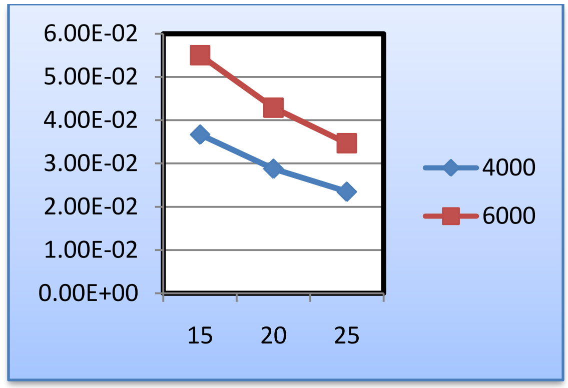

Fig.5 Velocity plot

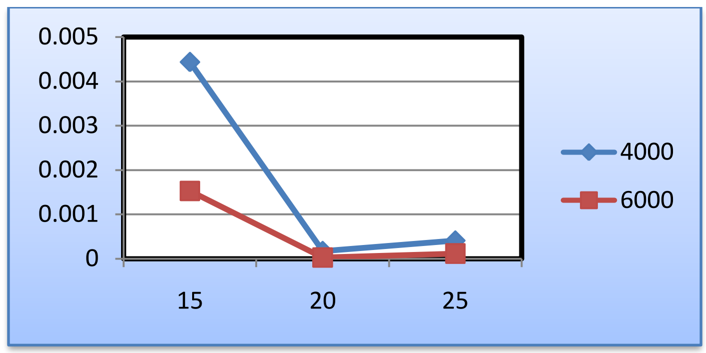

Fig.6 Mass flow rate plot

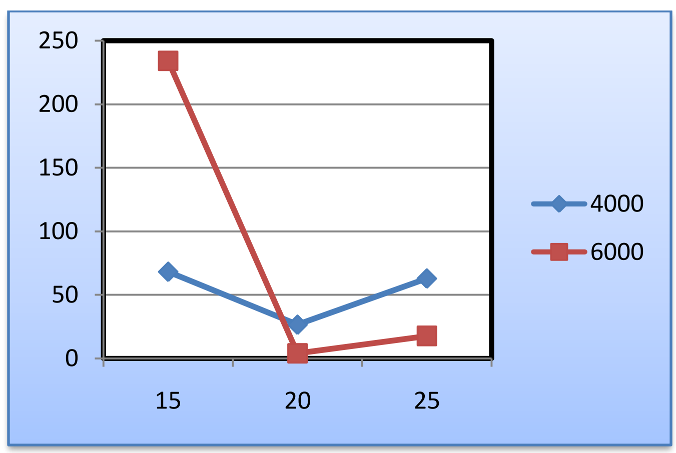

Fig.7 Heat transfer rate plot

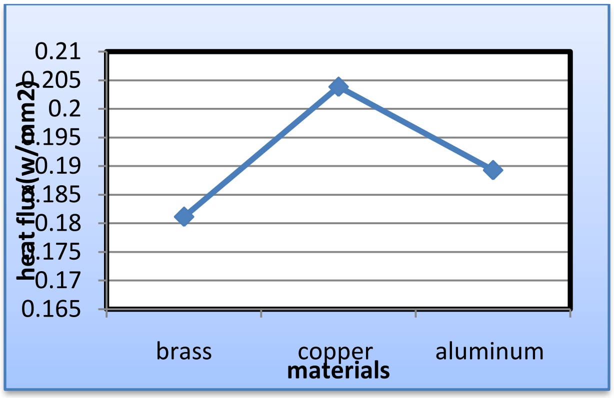

Fig.8 Heat Flux Plot

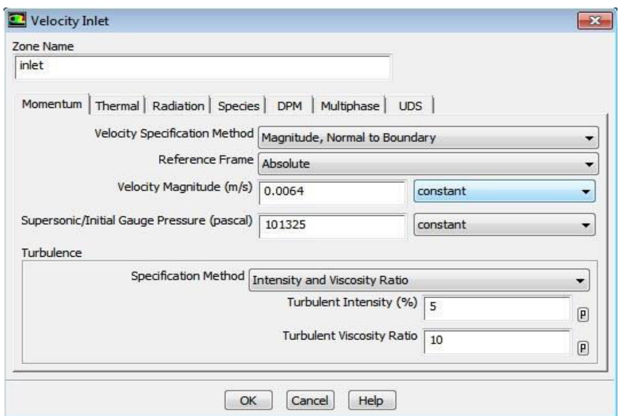

Fig.9 Pressure

4. Conclusion and Future Scope

In this project, a main jet of mechanical device is intended and sculptural in 3D modeling code CREO constant quantity code. Since the look of main jet of mechanical device is complicated, and potency is directly associated with material performance, material choice is of prime importance. during this project, totally {different completely different} materials and different nozzle diameters (15,20,25mm) by performed thermal analysis on the most jet of mechanical device for each the styles. By observant the CFD analysis the pressure drop, velocity, mass rate of flow and warmth transfer rate values square measure accumulated by increasing the Reynolds range. The heat transfer rate price is additional at 000 Reynolds range by the diameter of nozzle is 15mm.Thermal analysis the warmth flux price over brass compare with metallic element and copper material. So it are often conclude the 15mm nozzle DIA. of main jet in mechanical device is best model.

References

[1] G.Ciccarelli, Steve Reynolds, Phillip Oliver development of a unique passive top down uniflow scavenged stroke GDI engine, experimental thermal and fluid science 34(2010) 217-226

[2] R. Mikalsen , A.P. Roskilly, the layout and simulation of a stroke free piston compression ignition engine for electric electricity era applied thermal engineering 28(2008) 589-600

[3] Jesus Benajes, Ricardo Novella, Daniela De Lima, Pascal Tributte, Nicolas Quechon, Philippe Obernesser, Vincent Dugue, analysis of the combustion process, pollutant emission and performance of an innovative 2-stroke HSDI engine designed for car packages. Applied thermal engineering fifty eight(2013) 181-193

[4] J. Galindo, H. Climent, B.Pla, V. D. Jimenez correlation for wiebe feature parameters for combustion simulation in -stroke small engine. Applied thermal engineering 31(2011) 1190-1199

[5] Behrouz Chehroudi, David Schuh intake – port go with the flow behavior in a motored and fired two-stroke research engine. Experimental thermal and fluid technology 1995; 10:86-100

[6] Deepak Bharadwaj, Navprabhat Bhatt, Ashish Singh, PulkitBhargav, Bishakha, TarunKabadwal to take a look at overall performance of two-stroke engine with modified consumption gadget IJEST vol.Four no.08 August 2012 ISSN: 0975-5462

[7] S. Kumarappa, G.P. Prabhukumar improving the overall performance of -stroke spark ignition engine with the aid of direct digital CNG injection JJMIE vol.2 no.-four December 2008 ISSN 1995-6665 web page 169-174

[8] Dr.A.Srinivas, Dr.G. Venkatasubbaiah, P. Venkateswarrao, M.Penchal Reddy a few innovations in layout of low fee variable compression ratio stroke petrol engine IJME vol.2 issue five (may additionally 2012) ISSN 2277-7059

DESIGN AND CFD ANALYSIS OF HAIR PIN HEAT EXCHANGERS AT DIFFERENT NANO FLUIDS

Raghavan N[1]
Research scholar
Dept of Mechanical Engineering
Malla Reddy College of Engineering

Dr.P.velmurugan[2]
Professor
Dept of Mechanical Engineering
Malla Reddy College of engineering

ABSTRACT

Heat exchanger is equipment where the heat transfer takes place. In general the hedat flows from hot bodies to cold bodies. To mention a few commonly used applications

- Space heating
- Refrigeration
- Air conditioning
- Power stations
- Sewage treatment etc

Our Hairpin Exchangers are available in single tube (Double Pipe) or multiple tubes within a hairpin shell (Multitude), bare tubes, finned tubes, U-tubes, straight tubes (with rod-thru capability), fixed tube sheets and removable bundle.

In this thesis, Aluminium Oxide and Titanium carbide is mixed with base fluid water for two volume fractions 0.4, 0.5 and are analyzed for their performance in the hair pin heat exchanger. Calculations is done to find out the properties and obtained values is used as input for CFD analysis and Thermal analysis is done to find out suited material from Aluminum alloy and Copper.

Key words: Hair pin heat exchanger, CFD analysis, thermal analysis.

INTRODUCTION

Heat exchangers are one of the important devices in many industries. Heat Exchangers are used to transfer heat from hot streams to cold streams. Thermal process such as cooling, heating, condensation, boiling or evaporation of a fluid will require a heat exchanger for these purposes. The Heat exchanger is named different based on their application. For example, it is also called as boiler, condenser etc., Performance and efficiency parameters of heat exchanger which are of utmost importance are measured through the amount of heat transfer using least area of heat transfer and pressure drop. The measured values will provide an insight to calculate the capital cost and power requirements of a heat exchanger. Representation of its efficiency is done by calculating the overall heat transfer coefficient. Designer as to go through lots of literature and theories to design a H.E based on the requirements.

1.1 Classification of Heat Exchangers:-

1) Transfer Process
2) Number of fluids
3) Flow Arrangements
4) Heat Transfer Mechanism
5) Surface Compactness
6) Construction

Transfer Process: When heat is transmitted in-between fluids that are in direct contact with one other is direct or open contact heat exchanger, when the fluids are distinct by a wall through which heat is transmitted so that they never mix is indirect or closed contact heat exchanger.

Number of fluids: Process which involves cooling, heating, heat recovery and heat rejection, heat transfer takes place between fluids. It may be between two or more fluids with maximum up to 12 fluids in use.

Flow Arrangements: The choice of single pass exchanger or multi pass exchanger depends on the required H.E effectiveness, feasible pressure drops, minimum and maximum velocities possible, fluid flow direction and other design considerations.

Heat Transfer Mechanisms: The basic heat transfer mechanisms employed for transfer of heat energy from fluid on one side of the heat exchanger to the wall are single phase convection, two-phase convection and combined convection and radiation heat transfer.

Surface Compactness: In case of gas-to-fluid exchanger, it is referred as compact if it incorporates heat transfer surface having a surface space or area density larger than about 700m2/m3 and non compact if less than it. In case of liquid-to-liquid and phase-change, it is referred as compact for larger than about 400m2/m3 and non compact if less than it.

Construction:

Four main type construction types of heat exchangers are: tubular, plate-type, extended surfaces and regenerative heat exchangers. Other types of constructions such as scraped surface heat exchangers, tank heater, cooler cartridge heat exchangers, etc.., are also available. Some of these are also classified as tubular exchangers, but they have few unique features.

LITERATURE REVIEW

DESIGN AND ANALYSIS OF DOUBLEPIPEHEAT EXCHANGER USING COMPUTATIONAL METHOD

Research done on the double pipe heat exchanger gives an insight about heat transfer process. It describes about various applications. The running cost is directly related to the operating parameters. So, in this research the chosen exchanger is analyzed using computation method for the purpose of using it in refinery process which is highly efficient, compact and cost effective.

PROBLEM DESCRIPTION:

The objective of this project is to make a 3D model of the hair pin heat exchanger and study the CFD and thermal behavior of the heat exchanger by performing the finite element analysis. For this, CREO and ANSYS software is used for modeling and CFD, thermal analysis respectively.

CFD ANALYSIS OF HAIR PIN HEAT EXCHANGER

ALUMINUM OXIDE NANO FLUID VOLUME FRACTION - 0.4

STATIC PRESSURE

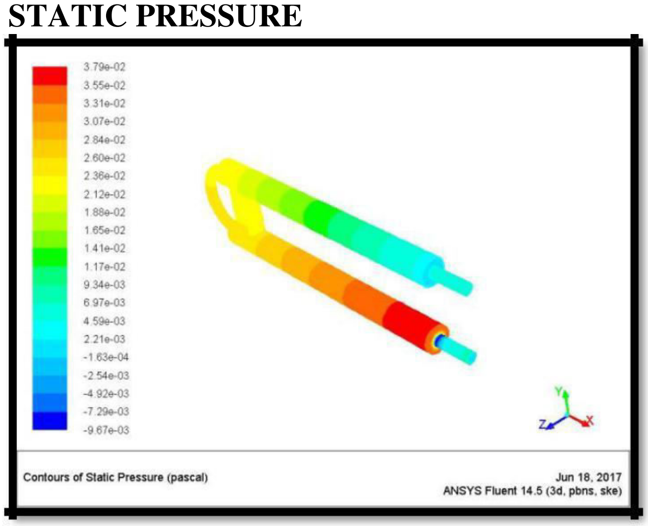

According to the above contour plot, the maximum static pressure inside of the heat exchanger tubes because the applied the boundary conditions at inlet of the heat exchanger tubes and minimum static pressure at the shell and tube heat exchanger casing.

According to the above contour plot, the maximum pressure is 3.79e-02Pa and minimum static pressure is -9.67e-03Pa.

VELOCITY MAGNITUDE

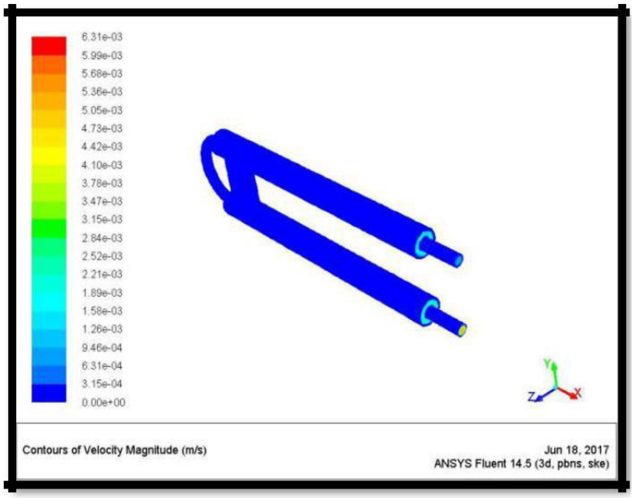

According to the above contour plot, the maximum velocity magnitude of the heat exchanger at hot fluid inlet and minimum velocity magnitude at cold fluid outlet.

According to the above contour plot, the maximum velocity is 6.31e-03m/s and minimum velocity is 3.15e-04m/s.

HEAT TRANSFER CO-EFFICIENT

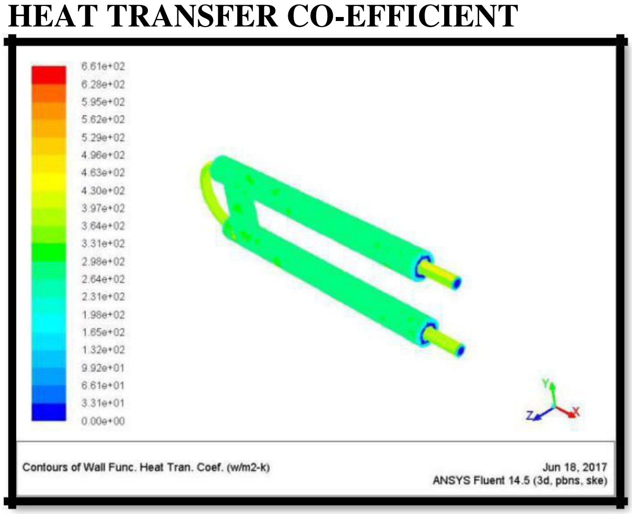

According to the above contour plot, the maximum heat transfer coefficient of the heat exchanger at inside the tubes and minimum heat transfer coefficient inside the heat exchanger casing. According to the above contour plot, the maximum heat transfer coefficient is 6.61e+02w/m^2-k and minimum heat transfer coefficient is 3.31e+01w/m^2-k.

MASS FLOW RATE

Mass Flow Rate	(kg/s)
cold_inlet	0.049999997
cold_outlet	-0.33894157
contact_region-contact_region_3-contact_region_2-contact_region_3-src	-
contact_region-contact_region_3-contact_region_2-contact_region_3-trg	
contact_region_4-src	0.017476412
contact_region_4-trg	-0.017476182
hot_inlet	0.69999987
hot_outlet	-0.46250656
interior-16	-0.55889207
interior-5	0.017476274
interior-____msbr	-15.532659
wall-14	0
wall-15	0
wall-17	0
wall-18	0
wall-____msbr	0
Net	-0.051450485

HEAT TRANSFER RATE

Total Heat Transfer Rate	(w)
cold_inlet	1343.1823
cold_outlet	-33630.828
contact_region-contact_region_3-contact_region_2-contact_region_3-src	
contact_region-contact_region_3-contact_region_2-contact_region_3-trg	
contact_region_4-src	0
contact_region_4-trg	0
hot_inlet	69456.445
hot_outlet	-41782.496
wall-14	0
wall-15	0
wall-17	0
wall-18	0
wall-____msbr	0
Net	-4613.6967

THERMAL ANALYSIS OF HAIR PIN HEAT EXCHANGER

MATERIAL-ALUMINUM ALLOY

IMPORTED MODEL

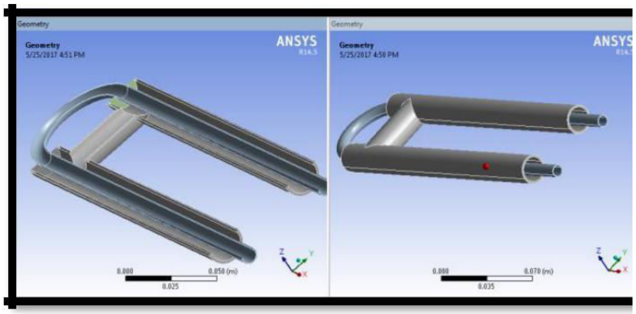

MESHED MODEL

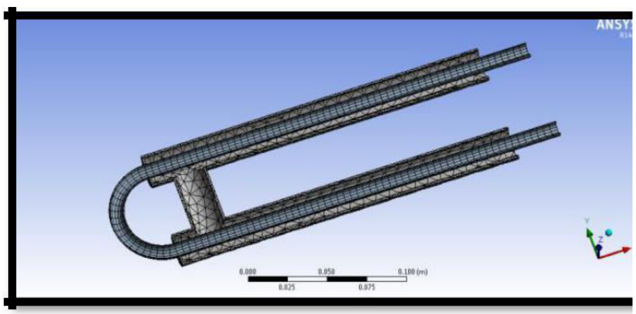

BOUNDARY CONDITIONS

T_1 =353K

APPLIED TEMPERATURE& CONVECTION

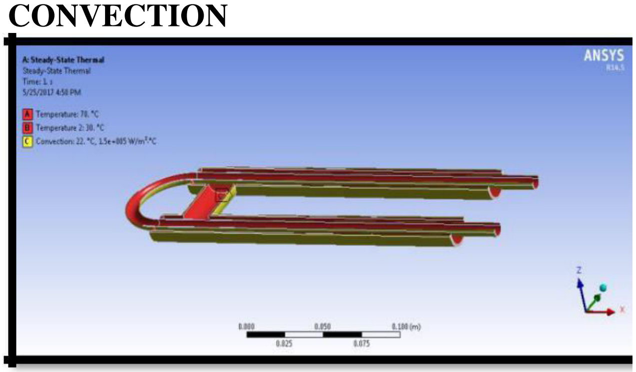

TEMPERATURE

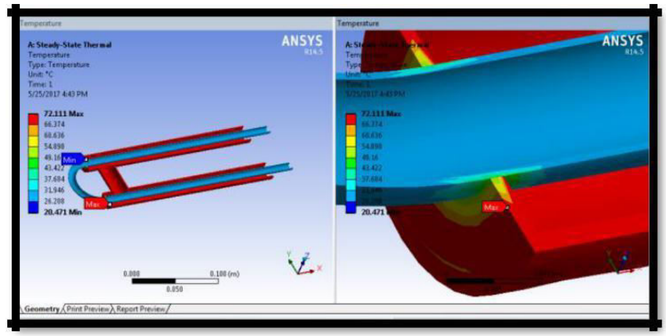

According to the contour plot, the temperature distribution maximum temperature at tubes because the nano fluid passing inside of the heat exchanger tubes. So we are applying the temperature inside of the tube and applying the convection except inside the tubes. Then the maximum temperature occurs at tubes and minimum temperature at steam boiler casing.

HEAT FLUX

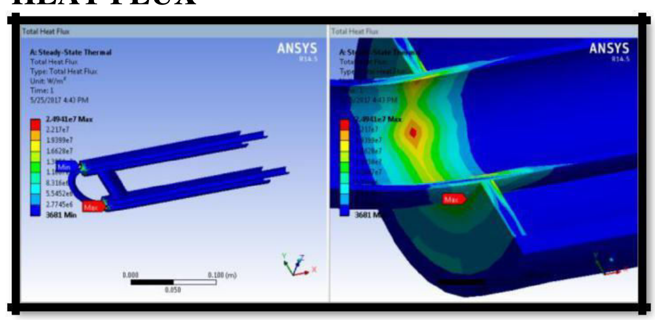

According to the contour plot, the maximum heat flux at inside the tubes because the nano fluid passing inside of the tube. So we are applying the temperature inside of the tube and applying the convection except inside the tubes. Then the maximum heat flux occurs at inside the tubes and minimum heat flux at heat exchanger casing and outside of the tubes.

According to the above contour plot, the maximum heat flux is $2.4947e^7$ w/m^2 and minimum heat flux is3681w/m^2

RESULTS

CFD analysis Graphs

PRESSURE PLOT

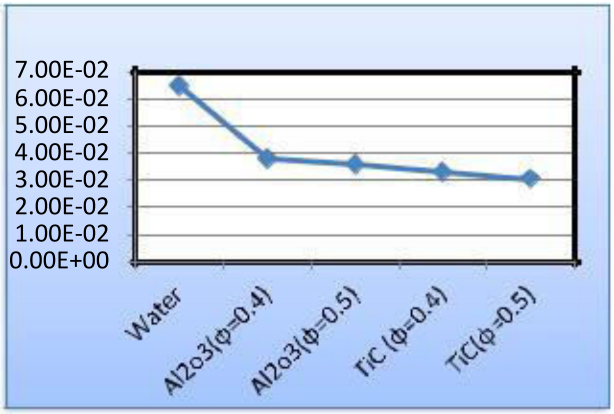

VELOCITY PLOT

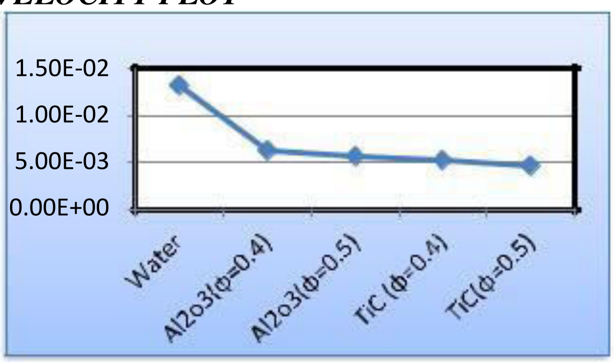

HEAT TRANSFER COEFFICIENT PLOT

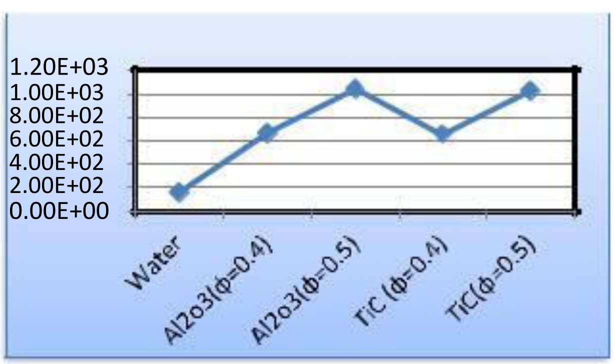

MASS FLOW RATE PLOT

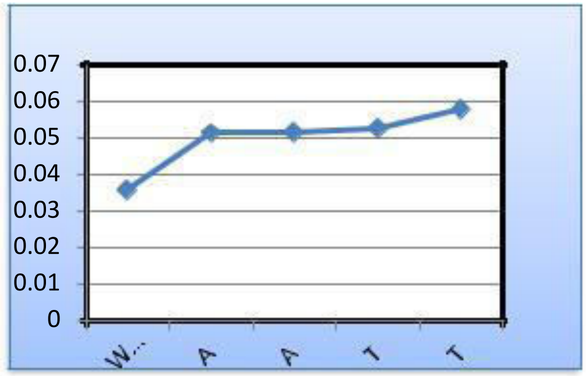

HEAT TRANSFER RATE PLOT

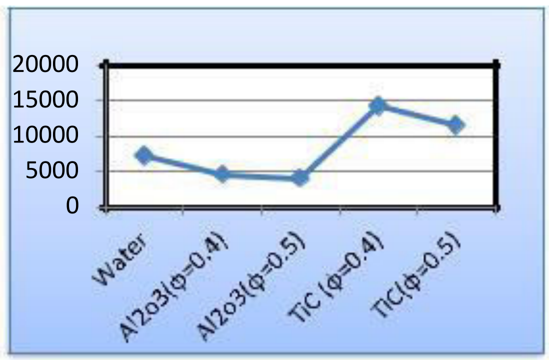

6.2 THERMAL ANALYSIS RESULTS TABLES

Material	Temperature (^{0}C)		Heat flux(w/m^2)
	Min.	Max.	
Aluminum alloy	20.471	72.111	2.4941e7
copper	19.28	72.316	2.7459e7

CONCLUSION

The results and graphs are tabulated above and it represents the variation of parameters, from which we can find out the desired results. In my report, it is found that the TiC (At 0.4) gives better 'h' value which is around 6.56e+02 by analyzing different volume fractions with different fluids.

The material best suited for fabricating the equipment is found to be Cu on comparison with AL alloy. So, we can conclude that the Cu is the material to be used for fabricating and the TiC is fluid suited to the above requirement.

REFERENCES

1.A.O. Adelaja, S. J. Ojolo and M. G. Sobamowo, "Computer Aided Analysis of Thermal and Mechanical Design of Shell and Tube Heat Exchangers", Advanced Materials Vol. 367 (2012) pp 731 -737 © (2012) Trans Tech Publications, Switzerland.

2. Yusuf Ali Kara, Ozbilen Guraras, "A computer program for designing of Shell and tube heat exchanger", Applied Thermal Engineering 24(2004) 1797–1805

3. Rajagapal THUNDIL KARUPPA RAJ and Srikanth GANNE, "Shell side numericalanalysis of a shell and tube heat exchanger considering the effects of baffle inclination angle on fluid flow", Thundil Karuppa Raj, R., et al: Shell Side Numerical Analysis of a Shell and Tube Heat Exchanger ,THERMAL SCIENCE: Year 2012, Vol. 16, No. 4, pp. 1165-1174.

4. S. Noie Baghban, M. Moghiman and E. Salehi, " Thermal analysis of shell-side flow of shell-and tube heat exchanger using experimental and theoretical methods" (Received: October 1, 1998 -Accepted in Revised Form: June 3, 1999).

5. A.GopiChand, Prof.A.V.N.L.Sharma , G.Vijay Kumar, A.Srividya, "Thermal analysis of shell and tube heat exchanger using mat lab and floefd software",Volume: 1 Issue: 3 276 –281,ISSN: 2319 –1163.

6. Hari Haran, Ravindra Reddy and Sreehari, "Thermal Analysis of Shell and Tube Heat ExChanger Using C and Ansys" ,International Journal of Computer Trends and Technology (IJCTT) –volume 4 Issue 7–July 2013.

7. Donald Q.Kern. 1965. Process Heat transfer (23rdprinting 1986). McGraw-Hill companies.ISBN 0 -07-Y85353-3.

8. Richard C. Byrne Secretary. 1968. Tubular Exchanger Manufacturers Association, INC. (8th Edition). 25 North Broadway Tarrytown, New York 10591.

9. R.H Perry. 1984. Perry's Chemical Engineer's Handbook (6th Edition ed.). McGraw-Hill. ISBN 0-07-049479-7.

10. Ender Ozden, Ilker Tari, Shell Side CFD Analysis of A Small Shell And Tube Heat Exchanger, Middle East Technical University,2010.

STUDIES ON FUEL CELLS

R.Vivek [a*], M.Muthukumar[a], A.P.Senthil Kumar[b]

[a*]*Department of Mechanical Engineering, Nandha Engineering College, Erode, India-638052*
[b] *Department of Mechanical Engineering, PSG College of Technology, Coimbatore, India-641004*

[a*]Vivekanu07@gmail.com

***Abstract*-- In PEM fuel cell, in addition to electricity, water and small amount of heat are generated as by-products. This generated water on cathode side is the flow paths and reducing electrochemical reactions. So water management is the main problem which is affecting on performance. The paper reviews ~~a~~ the various parameters (pressure, temperature and humidity) which affect the performance of fuel cell. Fuel cell performance is improved by proper water management on the membrane. From this studies, we observe that the fuel cell performance is developed by varying the temperature, pressure and using the proper flow field.**

***Keywords*—Proton Electrolyte membrane (PEM), Flow field design, Flow parameter, Water management.**

INTRODUCTION

Fuel cell is a device which is used to produce electrical energy from chemical energy. Fuel cell emitting zero pollution to the environment. It has more efficiency compare to other energy source.

TYPES OF FUEL CELL

- Alkaline fuel cell
- Phosphoric acid fuel cell
- Proton exchange membrane (PEM) fuel cell
- Molten carbonate fuel cell
- Solid oxide fuel cell

WORKING OF PEM FUEL CELL

Pure hydrogen gas passes through the anode and enters to the GDL (Gas Diffusion Layer) and diffused to the catalyst layer. Here the hydrogen atoms split into electrons and protons. Membrane allows only protons to the cathode side. At the same time the oxygen air produced to cathode side. In catalyst layer the oxygen atoms are split into electrons. Remaining O^- was reacting with protons and forms a water molecule with heat energy.

REACTIONS INVOLVED IN PEM FUEL CELL

- **AT ANODE :**

$$H_2 \rightarrow 2H^+ + 2e^-$$

- **AT CATHODE :**

$$\tfrac{1}{2} O_2 + 2\,H^+ + 2\,e^- \rightarrow H_2O$$

- **OVERALL REACTION :**

$$H_2 + \tfrac{1}{2} O_2 \rightarrow H_2O + \text{Heat} + \text{Electricity}$$

LITERATURE SURVEY

The following review has been used to identify the problems on the performance of the PEM fuel cell which help us to highlight and rectify the issue.

Nattawut Jaruwasupanta and Yottana Khunatorn [1] investigated the effects of channel configurations of flow field plates on the performance of a PEM fuel cell. Three-dimensional computational fluid dynamics (CFD) model was investigated the effects of serpentine flow channel designs on the performance of proton exchange membrane fuel cells. Flow field channel velocities of 1, 2, 3, 4, 5, 6 channels were analyzed.

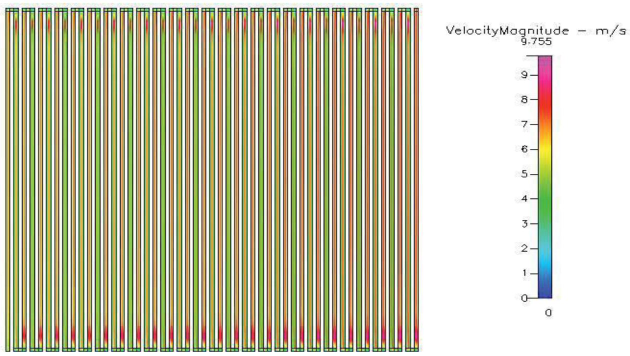

Fig.1 Velocity of flow field at 300 cm^3/min of sharp curve

From the Fig.1, the old fuel cell is 4 channels, smooth curve and depth 1 mm and the new choose is 6 channels, sharp curve and depth 1 mm. The new fuel cell has better performance than old fuel cell about 25%. At the outlet there is the distribution of gas regularly which releases the water from fuel cell. From the experiment results on 4 channels smooth curve and 6 channels sharp curve, there are found that the fuel cell has the density of electric power about 900 and 1200 mA/cm^2 at 0.6 V, respectively. Flow field has 6 channel is 25% better than 4 channels here we conclude in fuel cell water molecules are produced at cathode side.

Karthikeyan et al. [2] reported about the optimization of both operating and design parameters namely cell temperature, back pressure, anode and cathode inlet velocities, Gas Diffusion Layer (GDL) porosity and thickness, cathode water mass fraction, flow channel dimensions, rib width and porous electrode thickness. The Numerical model of single channel PEM fuel cell was introduced and analyzed by using COMSOL Multi physics 4.2 software package. At 1st stage analysis, it was inferred that back pressure had maximum effect and rib width had least effect on fuel cell performance. In 2nd stage of analysis, fine tuned optimization was performed on selected factors which caused for 3 % increase in power density and the results were also validated using COMSOL Multi physics 4.2. By optimization method maximum power density obtained P_{max}= 0.2214 W/cm².The full three-dimensional models of a proton exchange membrane fuel cell have been developed with a constant channel length of 20 mm and with different Landing to Channel width (LxC) in mm of 0.5x0.5, 1x1, 1.5x1.5, 2x2. While operating the fuel cell at different voltages, the current density values were obtained and the polarization and power density curves were drawn. From the results, it was found that the PEM fuel with landing to channel width of 0.5x0.5 mm has generated a high current density and high power density compared to other three designs. Also it was found that the smaller width of landing and channels are required for high current density and power density outputs of the PEM fuel cell due to the better water management.

The length of the channel was considered as 20 mm for all four designs. The Landing to Channel (L*C) width were taken as 0.5x0.5, 1x1, 1.5x1.5, 2x2 mm and the corresponding height of the channels were taken as 0.5, 1, 1.5, 2 mm respectively.

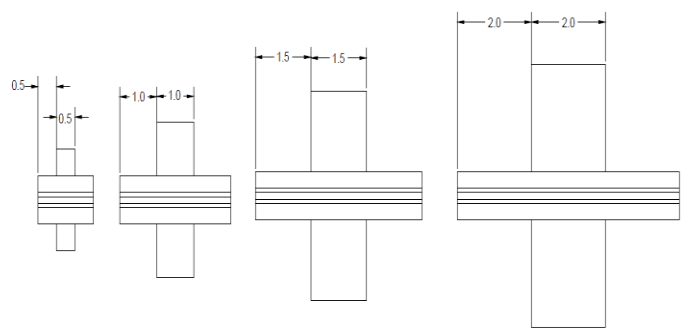

Fig. 2 Different L:C of channels [2]

The four models of PEM fuel cell with seven layers namely membrane, anode and cathode catalyst layers, anode and cathode GDL, anode and cathode flow channels were operated at the same operating conditions of 50°C temperature and 1.5 bar pressure. From the results, it can be concluded that the PEM fuel cell with landing to channel width of 0.5 x 0.5 mm has produced the better performance with peak power density of 0.4473 W/cm^2 and peak current density of 1.1183 A/cm^2 compared to other three designs.

Muthukumar et al. [3] investigated about the effects of serpentine flow field with different number of passes. The 2 pass, 3 pass and 4 pass serpentine flow field designs of same rib size and channel size were model and analyzed using commercially available software package. The channel dimensions are rib width of 0.7 mm, the channel width of 0.8 mm, plate width of 50 mm, GDL height of 0.5 mm, inner radius of channel corners of 0.25 mm, GDL porosity of 0.4, GDL permeability of 1.18*10^{11} m^2, inlet mass fraction of O_2 and H_2O of 0.228 and 0.023, water molar mass of 0.018 kg/mol, Oxygen molar mass of 0.032 kg/mol and reference pressure of 101000 Pa were taken for all the designs. The length of plate was kept as 50 mm to all the designs whereas the width were 6 mm, 9 mm and 12 mm for 2 pass, 3 pass and 4 pass designs respectively. The maximum power density were obtained as 0.46333, 0.46399 and 0.46336 W/cm^2 for 2 pass, 3 pass and 4 pass designs respectively, when the fuel cell models were operated at the cell voltage of 0.35 V. From the above results it is concluded that the number of pass in the serpentine flow field yields almost same power density as there is no much difference in the active area of the each design. While scaling-up the active area of the cell further, the influence of number of passes on the performance of fuel cell may be obtained due to proper water and thermal management.

Karthigeyan at el. [4] optimized the both operating and design parameters namely cell temperature, back pressure, anode and cathode inlet velocities, Gas Diffusion Layer (GDL) porosity and thickness, cathode water mass fraction, flow channel dimensions, rib width and porous electrode thickness. The Numerical model of single channel PEM fuel cell was developed and analyzed by using COMSOL Multi physics 4.2 software package. The maximum power found from polarization curve was 0.22143 W/cm². The deviation in result was 0.01% indicating that Taguchi results were in good agreement with software results. Hence, it is proved here that by increasing the number of levels through the usage of two-stage optimization, the error is getting reduced. Hence, it means that the model is determining the results to a more accurate level. Thus the refined optimized combination of input parameters was found to be back pressure of 1.5 bar, cell temperature of 298 K, GDL porosity of 65%, channels depth and width of 1mm x 1mm, rib width of 1.8 mm, porous electrode thickness of 60 microns, GDL thickness of 235 microns, anode inlet velocity of 0.5 m/s, cathode inlet velocity of 1.2 m/s and inlet water content in cathode of 5%. On refining the parameters to a more accurate level, the power density increased by 3% When cell temperature is higher than humidification temperature, the performance of the PEM fuel cell decreases. As the anode and cathode humidification temperatures in this analysis is low (293 K) corresponding to cell temperature, 298 K gives better performance.

Praveenkumar at el. [5] in this study, the effect of operating conditions such as pressure and temperature is investigated on the performance of outlet tapered single channel PEM fuel cell using ANSYS. The peak power density occurs in the temperature of 323K with the pressure of 2 bar because of the electrochemical reaction and tapered channel flow velocity which enhances the water removal. They create a 3D model of PEM fuel cell with outlet tapered flow channel by using the Volume of fluid method the model. The flow channel length is 20 mm, the inlet height is 1 mm and the outlet flow channel is 0.5 mm. The gas flow velocity increases by the decrement of flow outlet channel. So the flow channel outlet is reduced.

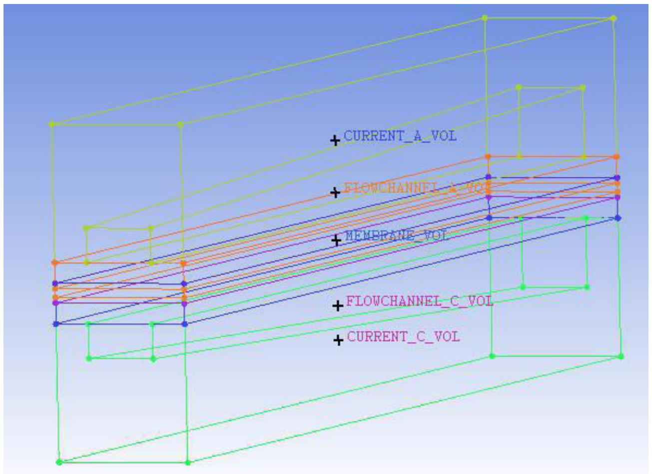

Fig.3 Isometric view of tapper channel [5]

A 3D mathematical model is analyzed at the operating conditions of 0.5 bar, 1 bar, 1.5 bar, 2 bar pressures and 313K, 318K, 323K, 328K, 333K temperatures. From that the variation in performance of tapered channel PEM fuel cell has en found. For each temperature and pressure value has changed and analyzed. The effect of pressure at different temperatures is explained by density curve. There is no significant differences were observed for these operating conditions, but the slight increment of power is obtained. The maximum power output was reached at the pressure of 2 bar and the intermediate temperature of 323K respectively. In 2 bar pressure iterations the peak power of 0.105220 W/cm^2 occurred at the voltage of 0.60V. Because of the electrochemical reaction and fluid flow at the outlet channel, the maximum power is produced.

Muthukumar at el. [6] investigated the 3D models of PEM fuel cell with multi-pass serpentine flow field designs having three, six and nine passes were analyzed using COMSOL Multi physics software package. The cross-section of the channel and the operating parameters were considered as same for all three designs.

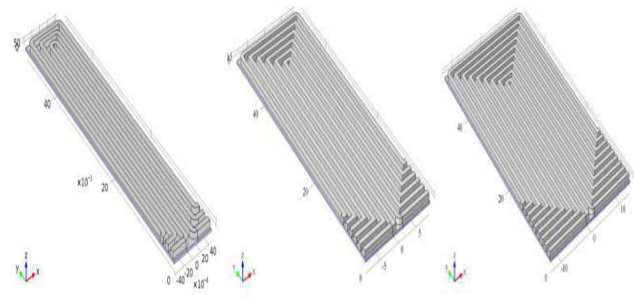

(a) (b) (c)

Fig.4 Serpentine flow field design with (a) 3 pass, (b) 6 pass, (c) 9 pass [6]

The PEM fuel cell models with three, six and nine passes serpentine flow field were analyzed numerically with the operating temperature of 323 K and the operating pressure of 1.5 bar. The open circuit voltage was kept as 1.23 V and the current density values were obtained for various cell potentials. PEM fuel cell with three pass serpentine flow channel has produced the current density of 1.1238 A/cm^2 and peak power density of 0.4495 W/cm^2 corresponding to the cell potential of 0.4 V. The PEM fuel cell with six pass serpentine flow channel has produced the current density of 1.1902 A/cm^2 and peak power density of 0.4761 W/cm^2 corresponding to the cell potential of 0.4 V. The PEM fuel cell with nine pass serpentine flow channel has produced the current density of 1.1798 A/cm^2 and peak corresponding to the cell potential of 0.4 V. The maximum power density were obtained as 0.4495, 0.4761 and 0.4719 W/cm2 for 3 pass, 6 pass and 9 pass designs respectively, when the fuel cell models were operated at the cell potential of 0.4V. The six pass serpentine flow channel yielded more power output compared to other two types. It is also concluded that while operating the fuel cell at the cell potential of 0.4 V, the maximum power outputs were obtained in all the designs. As the number passes were increased, the corresponding electrochemical reactions and the rate of water generation were also increased. The excess water generated in cathode side is to be removed properly; otherwise they stay on cathode side of fuel cell and block the flow of oxygen. This reduces the electrochemical reactions and overall power output of the fuel cell system in 9 pass serpentine flow channel design. Due to this, the performance of the 9 pass flow field design is low compared to 6 pass flow field.

Karthigeyan at el. [7] investigated a serpentine flow channel with Uniform and Zigzag positioned porous carbon inserts on cathode flow plate. The new cathode plate is experimentally analyzed with active area of 25 cm^2 with various flow channel designs on the cathode flow plate namely serpentine, uniform and zigzag pin type and flow channel with 2 mm cubical porous inserts on the uniform and zigzag pin type is experimentally investigated. The influence of porosity of carbon inserts on the cell performance is also studied by varying the porosity of carbon inserts in the range of 60-70%, 70-80%, 80 -90% respectively.

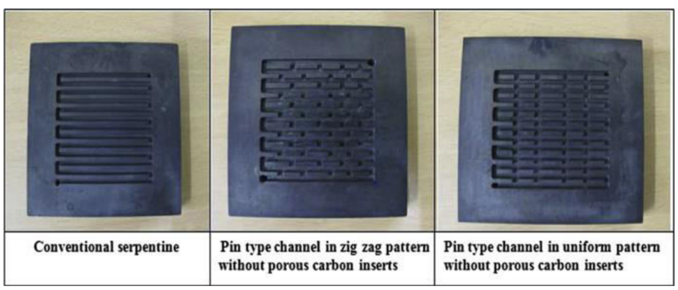

Fig.5 Flow field patterns [7]

The serpentine flow channel showed better performance of 7.5% and 4.3% increase in power densities when compared with uniform and zigzag patterned pin type flow channels. Both uniform and zigzag pin type flow channels, after the adoption of porous inserts showed a better performance, with 9.5% and 11.56% increase in power density, 10.65% and 7.1% increase on current density respectively when compared to conventional serpentine flow channel.

Nandhakumar et al. [8] investigated the Proton Exchange Membrane Fuel Cell for different gas flow parameters and serpentine model is chosen with the area of 25 cm^2 by varying the temperature and pressure. The optimum temperature and pressure are chosen from ANSYS 14.5 software .

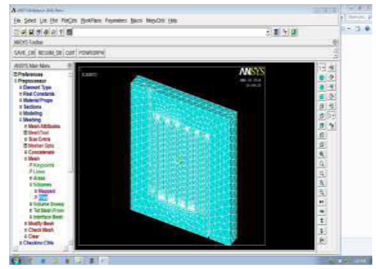

Fig.6 Model of 2x2 Serpentine Flow Channels [8]

Serpentine flow channels with varying temperature of 303 K, 313 K, 323K, 353K and Pressure of 0.5 bar, 1 bar, 1.5 bar, 2 bar ratio for analyzing to get numerical validation using ANSYS FLUENT software and the optimum design channels. At 323 K, 2 bar, with 1.3×10^{-6} kg/s for anode & 4.3×10^{-6} kg/s for cathode as mass flow inlet for serpentine flow channel (2x2) shows good performance improvement than other combinations.

Karthigeyan et al. [9] reported the water flooding problem with experimental studies have been carried out on 25 cm^2 and 70 cm^2 active area of PEM Fuel Cell with various flow channel designs on the cathode flow plate namely serpentine, uniform and zigzag pin type and flow channel with 2 mm cubical porous inserts on the uniform and zigzag pin flow channels.

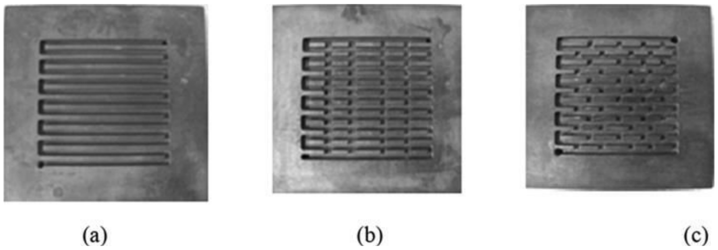

Fig.7 Flow Field Plate for 25 cm^2 PEM Fuel cell (A) Serpentine (B) Uniform Pin (C) Zigzag Pin [9]

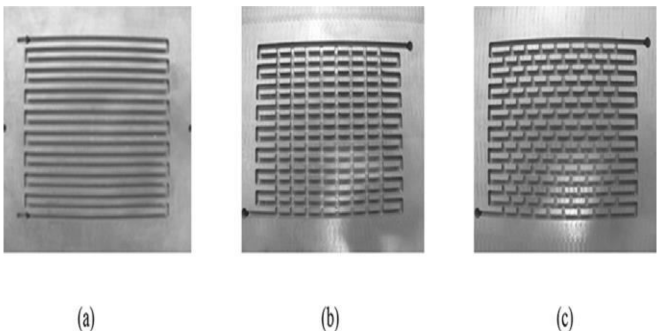

Fig.8 Flow field plate for 70 cm^2 PEM fuel cell (a) Serpentine (b) Uniform pin (c) Zigzag pin [9]

From the diagram on 25 cm^2 and 70 cm^2 PEM Fuel cell performance with various flow field designs, the serpentine flow field showed better performance with increased peak power densities of 7.5% and 4.3% on 25 cm^2 PEM Fuel cell, and 18.5% and 5.2% on 70 cm^2 PEM Fuel cell, when compared with uniform and zigzag patterned pin type flow field designs respectively. While adopting the porous carbon inserts with the porosity level of 80-90% on the uniform and zigzag pin type flow field designs, it showed a better performance with 9.5% and 11.6% increase in power densities respectively in 25 cm^2 PEM Fuel cell and 12.1% and 20.6% increase in power densities respectively in 70 cm^2 PEM Fuel cell, when compared to conventional serpentine flow field design.

Muthukumar et al. [10] investigated the power output of the PEM fuel cell by varying the operating pressure. The PEM fuel cell with serpentine flow field was modeled using Solid works software and analyzed using ANSYS software. The dimensions of the flow plate are 80 mm x 80 mm. The inlet and outlet diameter are 2 mm. The flow channel width and height are taken as 2 mm. The rib width is also taken as 2 mm. The active area of PEM fuel cell is 25 cm^2.

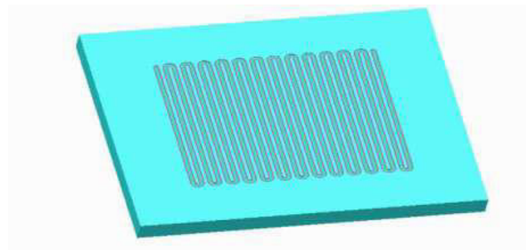

Fig.9 Model of serpentine channel flow field of PEM fuel cell [10]

The analysis was done with three different pressure (1 bar, 1.5 bar, 2 bar) and voltage (0.25 V - 0.85 V) at constant temperature of 323K using Ansys. From the results, 0.55 V with pressure of 2 bar gives high performance as compared to others. For 1 bar with 0.55 V, the current density was found to be 1.206385 A/cm^2 and the power density was found to be 0.66351175 W/cm^2 For 1.5 bar with 0.55 V, the current density was found to be 1.206648 A/cm^2 and the power density was found to be 0.6636564 W/cm^2. For 2 bar with 0.55 V, the current density was found to be 1.207008 A/cm^2 and the power density was found to be 0.6638544 W/cm^2. While comparing the performance of PEM fuel cell with three different pressures and at constant temperature, it was found that the pressure 2 bar is the optimum pressure at the cell potential of 0.55 V.

Tetsuro Kariya et al. [11] reported the several porous flow field structures in separators and discussed.

1) The maximum power density of the porous flow field type Separator-B-partition, aimed at improving uniform oxygen

supply to the entire flow field by placing partitions in the porous flow field, was approximately 25% higher compared to the base porous type Separator-A-base with densely packed alloy powders and 35% higher than the conventional groove type graphite separator. However, the pressure loss of this Separator-B-partition was approximately 1.5 times larger than Separator-A-base and the conventional groove type graphite separator.

2) Pressure loss was approximately 70% lowered by Separator-C-groove with evenly spaced linear grooves in its porous flow field, compared to Separator-A-base with densely packed alloy powders, furthermore, the power density property under 100% relative humidity in the cathode was remarkably stabilized due to the enhancement of water drainage. However, the maximum power densities of both separators were almost equivalent.

3)Developed porous flow field type Separator-D-network with finely dispersed space networks by utilizing the mixture of alloy powders and binders in its fabrication process demonstrated excellent performances for both lower pressure loss and higher power densities; i.e., 50% lower pressure loss and 40% higher maximum power density were obtained compared to Separator-A-base. In addition, further improvement in cell performance is highly expected as well, for instance, by combining the flow control partition technique employed in Separator-B partition, especially in the case that the practical separator size is larger than the tested samples in this study.

Abhishek Raj et al. [12] investigated multidimensional effect by developing two similar steady state 2D and 3D models in COMSOL. Both of these models have similar geometry and are simulated under similar operating conditions. The effect of multidimensionality on species concentration was investigated at various inlet stoichiometries, membrane conductivities and relative humidity values. The multidimensional effect as represented by difference in species distribution in the two models is found to be significant at lower operating voltages and more prominent at the cathode side. The inlet stoichiometry at the cathode and membrane conductivity values, are also found to influence the multidimensionality effects. The fuel cell performance is significantly influenced by the humidification levels of reactants. Appropriate amount of water is needed to sustain the proton conductivity of the polymer electrolyte membrane. An increase in relative humidity is expected to enhance the reaction rate and also the transport of H^+ ions by increasing the conductivity of the membrane. On the other hand, the excessive amount of water would result in the flooding of the electrode. Consequently, the access of oxygen to the cathode catalyst layer will be hindered and cause significant concentration polarization. The influence of relative humidity on the multidimensional effect was investigated by running the 2D and 3D model simulations with identical relative humidity values. In this study, the anode humidity was varied from 10% to 60% while the cathode humidity was kept at around 10%, and in the other case, the cathode humidity was varied from 10% to 75% sides while the anode humidity was kept at around 15%. The cell voltage and the membrane conductivity were kept at 0.6 V and 4.4 m/s respectively.

Tao Chan et al. [13] reported the numerical simulation of the PEM Fuel cell performance. It is impacted by the number and location of branches in bionic flow fields. The location of branches has a greater impact on the exit velocity; the more branches are more favorable to discharge of water. Finally different operating parameters like temperature, pressure, relative humidity, and stoichiometry in bionic flow fields are chosen. In order to calculate conveniently, the primary vein and secondary veins can be simplified and designed to be a main channel with a regular rectangular cross-section, while the net veins can be developed to be sub-flow channels that parallel the primary vein.

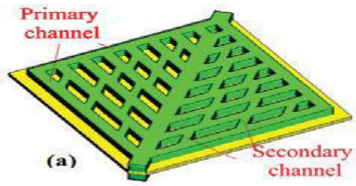

Fig.10 New Flow field patterns [13]

Increase in current density the voltage declines gradually because of a variety of polarization phenomena inside the fuel cells. Differences in structure play a minor role in the current density when the operating voltage is above 0.8 V, but it plays a bigger role when the operating voltage is lower than 0.7 V, which is particularly apparent when the current density is high. Under the same operating voltage, flow field (b) has a higher current density, about 2.6% higher than flow field (a). The maximum power density of (b) is 3.3% higher than (a). Therefore a reasonable flow pattern is conducive to the improvement in fuel cell performance. Show the water content distribution of the diffusion layer and catalyst layer interface (GDL/cat). It can be seen from the Figure that there is less water near the inlet, while a large amount of water gathers below the bipolar plates near the outlet, mainly due to the larger air current that brings the byproduct water to the outlet. It can also be seen there is less water in the flow channels, while a large amount of water gathers below the bipolar plates. The reason is that the rib is in close contact with the diffusion layer, making it difficult to get enough reaction gas; then byproduct water gathers under the rib. Consequently, the gas diffusivity has an effect on the fuel cell performance. The average water content of (a) is larger than that of (b) when inputting the same amount of gas.

Kap-Seung Choi et al. [14] reported the pressure drop, gas permeability of GDL, and the electrolyte membrane water content (λ) were compared for the FSI model. Which is a thermal fluid based PEM Fuel cell model (CFD model) that takes the GDL compression deformation into account. The GDL compression deformation, dependent on the fuel cell assembly pressure, affects the gas permeability caused by under-rib convection. A 25 cm^2 flow field with 5 passes 4 turns design were formed and tested by using the present numerical model of electrochemical reaction and transport phenomena. Therefore, the distributions of performance-related parameters are profiled and compared quantitatively at the same location. The performance-related parameters include the hydrogen and oxygen mass fraction, membrane water content (λ), net water flux per proton (α), liquid water mass fraction, total pressure, current density distributions, and polarization and power density curves. In the case of the FSI model, GDL compression deformation was generated due to the assembly pressure. Most of the GDL deformation, because the width of the channel and rib are within 1 mm, was in the form of expansion on the channel and there was compression in the rib and turn rib. Fig shows these results and how the GDL deformation affects the internal performance using the average current density (I_{avg}) 0.6 A/cm^2.

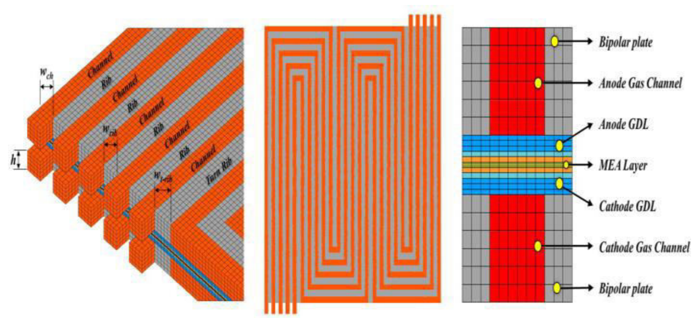

Fig.11 (a) Detail view (b) pattern

(c) Computational domain

The total pressure of the anode and cathode continuously decreases from the inlet until the outlet is reached, and it decreases dramatically in the turn-rib. This is caused by frictional and bending losses in the serpentine flow field pattern. Membrane water content (λ) is dependent on the total pressure; the liquid water of the fuel cell exists in liquid phase and vapor phase due to the partial pressure and total pressure of water vapor. For the membrane water content (λ), because the amount of water flowing in the direction of the flow channel increases to show a low membrane water content (λ), a larger amount of water is absorbed into the electrolyte membrane due to the high flow rate between the GDL and rib caused by the under-rib convection of the rib than the amount of water absorbed into the electrolyte membrane due to the high pressure at the inlet channel. Also the membrane water content (λ) of the electrolyte membrane increases due to the water that is not discharged out of the channel, due to the drop in pressure in the channel caused by the supplied gases moving from the inlet to the outlet.

When comparing the membrane water content (λ) of the FSI model and the net water flux per proton (α) with that of the CFD model, there was only a small difference, but the total pressure, O_2/H_2 mass fraction, anode/cathode liquid water mass fraction showed a big difference. This is due to the decrease in both the mobility of the reaction gases that move under the rib and also the mobility of the water produced, which is caused by the decrease in the channel cross sectional area and porosity being decreased by the GDL deformation. Also, although the liquid water mass fraction decreases significantly in the outlet, the membrane water content is not largely different from that of the CFD model, and therefore no membrane dehydration occurred, and it was confirmed that the uniformity of the current density increased.

Hideki Murakawa et al. [15] used neutron radiography for measuring the water distribution in a small fuel cell through-plane direction. The fuel cell had nine parallel channels for classifying the water-accumulation process in the gas diffusion layer (GDL) under the lands and channels. The experimental results were compared with numerical results. The PEM was Nafion NR-212 with a thickness of approximately 90 µm having a catalyst layer (CL) on both the anode and cathode sides. The electrode area was 10 × 19 mm^2. The GDL was carbon paper (Toray Ind.), with thicknesses of 190 µm at the cathode and anode. The porosity of the GDL was 78%. The experimental conditions included the following: current densities i = 158 mA/cm^2, hydrogen flow rate = 28 cc/min, and air flow rate = 66 cc/min without humidification. The hydrogen and oxygen utilization was 7.5%. The experiments were carried out at room temperature, and the temperature of the PEFC varied within the range of 30–35 °C. The exposure time was set to 60 s to obtain the water distribution in the through plane direction of the PEFC every 60 s during operation.

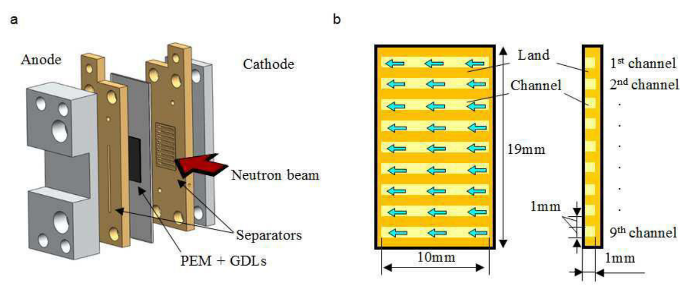

Fig.12 (a) Diagram of the PEFC; (b) geometry of the gas channel [15]

Water accumulation occurred as the operation time increased, as indicated by the blue color. The difference in the amount of water in the GDLs under the lands and under the channels apparently appears at 8 min. The water accumulation in the GDL under the land was larger than that under the channel during the period of early PEFC operation. Water accumulation started in the GDL, and a large amount of water existed in the GDL under the lands. The water-accumulation area extended to the GDL under the channels. Furthermore, with an increase in the operation time, the water evacuation from the GDL to the channels is confirmed to occur mainly around the land corners. Liquid droplets formed in the channels and these grew in the channels as the operation time increased. No water evacuation in the downstream channel direction was observed during the experiments. This is because the channels were parallel, and water evacuation to the outside of the channels was difficult. The water saturation and vapor mole fraction distributions in the cathode GDL at 2, 4 and 8 min. The horizontal and vertical scales are not identical for understanding the distributions easily. The liquid water accumulation is confirmed mainly at the boundary between the catalyst layer and the GDL. At the early time of the PEFC operation, the water accumulates almost uniformly along the catalyst layer. However, the difference of the water saturation appears with an increase of the operation time. The tendency of the water accumulation in the GDL is good agreement with the experimental results. Water saturation in the GDL near the channel is lower than that in the other region. The results are strongly affected by the boundary condition between the channel and GDL. It can be seen that the vapor mole fraction in the GDL under the land is also higher than that under the channel. The difference of the water accumulation in the GDL under the land and under the channel was related with the water vapor. Therefore, it can be thought that the higher vapor mole fraction causes the water accumulation in the GDL under the land.

Andreas Miege et al. [16] determined the fast humidity of fuel cell is required a stable fuel cell control. For laboratory fuel cell analyses the psychometric humidity detection has turned out as an appropriate method even at high humidity levels. Using no humidity sensors the electrochemical impedance spectroscopy is known appropriate method for humidity detection. Two specific adaptations (F-EIS and R-EIS) use the advantages of the EIS and yield a fast measurement of a simplified Nyquist plot which is defined by membrane resistant R_{mem} and the secant angle α. From α and R_{mem} the humidity-state indicator (HSI) is deduced representing the actual fuel cell condition. Due to degradation effects the set point of R_{mem} has to be regularly adjusted, which can be done much faster using the novel methods described. The angle α and membrane resistance creates the basis for the fuel cell humidity determination, independent which of the shown measurement methods is used. Aiming for an integration of the fuel cell humidity state into a fuel cell controller a significant parameter has to be created – the humidity state indicator (HSI). The HSI is deduced from the correlation of the angle (α) and the membrane resistant (R_{mem}). A HSI of 1 indicates a high humidification level near saturation which would lead to an accumulation of liquid water inside the fuel cell.

For the controlling process a state prediction or a tendency is favorable. The membrane resistance reacts slowly on changing conditions compared to the angle which is a fast indicator for drying or humidifying tendencies. Therefore the angle has to be considered in the HSI implementation for the fast response of the HSI. Drying and humidifying operation play the major role in short term controlling and managing the water content. The rather slow effect of drowning is difficult to detect but can be prevented by regular purging. Degradation as a long term influence requires a regular adjustment of the reference points for Rmem. After 60s the system measures the angle of the Nyquist-plot with the help of the F-EIS or R-EIS. If that angle is above 50°, the stack is well humidified and the measured Rmem can be used as reference value Rmem, the controlling of the following operation mode. This procedure is necessary because not only the humidification state but also aging effects influence the value of Rmem. Based on the HSI the controlling process of the fuel cell reacts immediately on a change of the fuel cell internal humidity conditions.

Mostafa Ghasemi et al. [17] report about the three types of PEM (Nafion 112, SPEEK and Nafion 117) , were applies to MFC and the amount of produced bio energy with the feed of waste water in 5000 ml chemical oxygen demand (COD). For the preparation of solfunated poly ether ether ketone (SPEEK), 20g of polyether ether ketone (PEEK) powder was dissolved slowly in 500mL of 95-98% concentrated sulphuric acid.

The maximum power generation of the MFC working with Nafion 117 as PEM is 179.7 mW/m^2 followed by SPEEK which generated the maximum power of 126.1 and the last one is Nafion 112 with 19.7 mW/m^2. As can be seen in all cases Nafion 117 has the highest power production among the studied membranes. It can be due to the great ion exchange properties of Nafion 117 and dense structure of that which block the passing of oxygen from cathode to anode which makes the reaction aerobic and disturb the microorganism's metabolism for electricity production. This obstacle can be seen once Nafion 112 is the separator. Because of thin thickness of the cross section of Nafion 112, most of the oxygen diffuses from cathode to anode and respiration of the substrate is aerobic. SPEEK also by having so many SO_3- groups produced acceptable amount of electricity however still the power production is lower than Nafion 117.

Suchart Kreesaeng et al. [18] simulated the cathode side in his study. The computational domain contains flow channel, gas diffusion layer and catalyst layer. Cathode channels are designed by varying channel aspect ratio (Width/Depth) and cross-sectional area (Width*Depth) with 6 different configurations. All configurations have the same reaction area of 100 mm^2 and the same gas diffusion layer and catalyst layer thickness of 0.41 mm and 0.01 mm respectively. a three-dimensional, single phase and isothermal model of an open-cathode PEM fuel cell. The model was focused on the cathode side. It was employed to investigate the design of cathode flow channels. The effects of cross-sectional area and aspect ratio on the cell performance of open-cathode PEM fuel cell were studied. Six configurations of cathode flow channels with a reaction area of 100 cm^2 were studied. The results showed that, designing of cathode flow channel by varying channel aspect ratio and cross-sectional area has a very small effect on performance of open-cathode PEM fuel cell. Increasing of channel aspect ratio and decreasing of cross-sectional area led to the reduction of rib area. Without under-rib convection, decreasing of rib area may lead to increasing of oxygen concentration between gas diffusion layer and catalyst layer which increases the rate of reaction and improves the cell performance.

Suangrat Kiattamrong et al. [19] fabricate the single-cell open-cathode PEM fuel cell as the test unit. The active area of the membrane electrolyte membrane (MEA) was 100 cm^2. This 5-layer MEA was for utilize with hydrogen and air. The membrane was Nafion 112 and coated with 410-µm thickness of carbon cloth gas diffusion layer (GDL). The platinum content and loading were 60 wt% and 0.5 mg/cm^2, respectively. The silicone seals were used as the gasket to prevent the reactant leakage. Six different sets of the aspect ratio (width/depth) and the flow area are tested. All test units were supplied by the predetermined amount of air flow rate calculated to meet the electrochemical and thermal requirements. The results from the transient operation confirmed the results from the steady operation. The flow area does not have the strong influence on the fuel cell performance when the precise air flow rate is supplied.

Owejan et al. [20] used the neutron radiography method to obtain two-dimensional distributions of liquid water in operating 50 cm^2 fuel cells. Variations were made of flow field channel and diffusion media properties to assess the effects on the overall volume and spatial distribution of accumulated water.

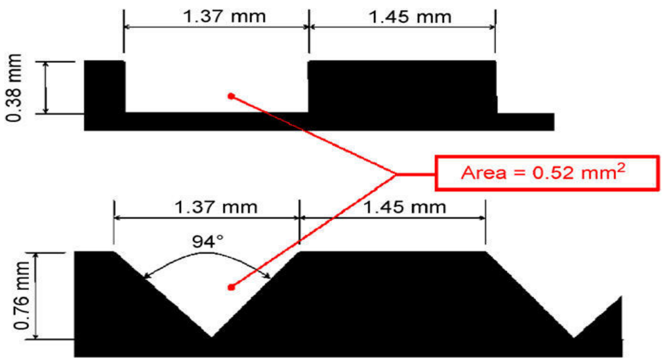

Fig.13 Cross-sectional view of flow channel geometries [20]

The performance of the two SGL GDM samples were similar as the average amount of liquid water accumulated at each test point was comparable and consistently lower than for Toray. The MPL on the SGL gas diffusion media samples likely plays a key role in optimizing the fuel cell water management. This is accomplished by facilitating transport of product water away from the MEA and distributing the water produced in the electrode layer more evenly over the active area.

The test apparatus featured anode and cathode flow fields, which were arranged orthogonally, to enable separate analysis of the water content on either side of the fuel cell. The GDLs manufactured by Toray and SGL varied most significantly in their in-plane gas permeability and through-plane thermal conductivity, which control the convective flow through the material and the effective temperature gradient between the membrane and the flow field plate. It was determined that the relatively low in-plane gas permeability of the Toray material accounts for the greater volume of retained water under the flow field lands. Despite the wide differences in thermal conductivity between the Toray and SGL samples, a simple two-dimensional thermal model indicated that the temperature gradient from the membrane to the flow field was within 0.5 ◦C over the entire range of current densities. It was observed that channel geometry and surface property both have appreciable effects on the volume of accumulated water and on the morphology of water droplets retained in the flow field channels. For both a rectangular and triangular channel with the same cross-sectional area, channel-level water accumulation was reduced by use of a PTFE coating, which provided a static contact angle of 95°. For a given flow field surface energy (either PTFE or "uncoated" gold-plated aluminum) the triangular channels retained less water. Moreover, the water morphology was generally characterized by pairs of droplets captured in the channel angles between the diffusion media and the flow field plate. It was also apparent that gravitational forces influenced the water accumulation profile, at least for the rectangular channels. These results provide strong evidence that channel geometry and surface properties must be accounted for in the design of fuel cell systems, due the affect on cell voltage performance, and water accumulation which would be expected to impact freeze operation and long-term material durability.

Dinesh & Sugumar [21] reviewed the water management in PEM fuel cell which affects the performance of the fuel cell. The water management is depends upon the relative humidity, flow field and wetting property of gas diffusion layer. Serpentine flow field with increase the cross flow as well as dropping the gathering of liquid because of this the trouble of flooding at cathode decrease. Relative humidity of anode and cathode side also result the performance of fuel cell for obtain the excellent performance of the fuel cell the reactant gases must be humid. By use of the serpentine flow channel and external humidifier the concert of the fuel cell get better. The performance of fuel cell also gets better by selecting the proper range of operating parameter (temperature, pressure and relative humidity).

CONCLUSION

Fuel cell performance depends on the several parameters like Design parameter, material properties, operating parameters and water management. Here water management was the main factor affecting performance of fuel cell. In PEM fuel cell addition to electricity, water and small amount of heat are generated as by-products. This generated water on cathode side is the flow paths and reducing electrochemical reactions. So water management is the main problem which is affecting on performance. In future work, new flow field will be designed to reduce the water management problems by adding porous carbon particles with extra active area. It will increase the performance of PEM fuel cell by decreasing the water molecule from the cathode side flow field.

REFERENCES

[1] Nattawut Jaruwasupanta and Yottana Khunatorn (2011) 'Effects of difference flow channel designs on Proton Exchange Membrane Fuel Cell using 3-D Model', Journal of energy and material science, Vol.6, pp. 326-337.

[2] Karthikeyan P, Muthukumar M, Vignesh Shanmugam S, Pravin Kumar P , Suryanarayanan Murali and Senthil Kumar A.P (2013) 'Optimization of Operating and Design Parameters on Proton Exchange Membrane Fuel Cell by using Taguchi method' – International Conference on Design and Manufacturing , Vol.64, pp.409 – 418.

[3] Muthukumar. M, Karthikeyan P, Vairavel M, Loganathan C, S.Praveenkumar and Senthil Kumar A.P (2014) 'Numerical Studies on PEM Fuel Cell with Different Landing to Channel Width of Flow Channel' - 12th Global Congress on Manufacturing and Management, Vol.96, pp.1534 – 1542.

[4] Muthukumar M ,Karthikeyan P, Lakshminarayanan V, Senthil Kumar A P, Vairavel M and Girimurugan R (2014) 'performance studies on PEM fuel cell with 2, 3 and 4 pass serpentine flow field designs' – journal of Applied Mechanics and Materials, Vol.592 – 594, pp.1728 – 1732.

[5] Praveenkumar S,Muruganantham S,Premkumar Muthukumar M and Vetrivel A (2015) 'Influence of Pressure and Temperature on the Performance of PEM Fuel Cell with Taper Flow Channel Design' - International Journal of Applied Chemistry, Vol.11, pp. 505 – 513.

[6] Muthukumar M, Saravanaperumal S, Lakshminarayanan V and Senthil Kumar A P (2015) 'Effect of Multi-pass Serpentine Flow Field Designs on the Performance of Proton Exchange Membrane Fuel Cell' - International Journal of Applied Engineering Research, Vol.10, pp.22429 – 22435.

[7] Karthikeyan P, Vasanth R J and Muthukumar M (2015) 'Experimental investigation on uniform and zigzag positioned porous inserts on the rib surface of cathode flow channel for performance enhancement in PEM Fuel Cell' – International Journal of Hydrogen Energy, Vol.40, pp.4642 – 4648.

[8] Nandhakumar V, Muthukumar M and Senthil Kumar A P (2016) 'Analysis of Parameters Influencing the Performance of PEM Fuel Cell by ANSYS' - International Journal of Advanced and Innovative Research, Vol.5, pp.2278 – 2291.

[9] Karthikeyan Palaniswamy, Muthukumar Marappan and Vasanth Rajendran Jothi (2016) 'Influence of porous carbon inserts on scaling up studies for performance enhancement on PEM FUEL CELL' – International Journal of Hydrogen Energy , Vol.41, pp.2867 – 2874.

[10] Muthukumar M, Karthikeyan P, Mathews Eldho, Nagarathinam P, Panneer Selvam E P and Prasanna R (2017) 'Impact Of Pressure On The Performance Of Proton Exchange Membrane Fuel Cell' – Journal of Advanced Chemistry Vol.13, pp.6462 – 6468.

[11] Tetsuro Kariya , Tomoki Hirono , Hiroshi Funakubo and Toshio Shudo (2014) 'Effects of the porous structures in the porous flow field type separators on fuel cell performances' – International Journal of Hydrogen Energy , Vol.6. pp.1 – 9.

[12] Abhishek Raj and Tariq Shamim (2014) 'Investigation of the effect of multidimensionality in PEM fuel cells' – journal of energy conversion and management, Vol.86, pp. 443 – 452.

[13] Tao Chen, Yong Xiao and Tiezhu Chen (2012) "The impact on PEM Fuel Cell of bionic flow field with a different branch" - Fuel cells 2012 Science and technology, Vol.28, pp. 134 – 139.

[14] Kap-Seung Choi (2015) "The flow-field pattern Optimization of the Bipolar Plate for PEM fuel cell considering the Nonlinear Material" - International Journal of Chemical science, Vol.10, pp.2564 – 2579.

[15] Hideki Murakawa, Katsumi Sugimotoa, Nobuki Kitamura, Masataka Sawada, Hitoshi Asano, Nobuyuki Takenaka and Yasushi Saito (2015) 'Visualization of water accumulation process in polymer electrolyte fuel cell using neutron radiography' - World Conference on Neutron Radiography, Vol.69, pp.607 – 611.

[16] Andreas Miege , Florian Steffen , Thomas Luschtinetz , Sven Jakubith and Maik Freitag (2012) 'Real time water detection for adaptive control strategy in PEM fuel cell systems' – World Hydrogen Energy Conference, Vol.29, pp.431 – 437.

[17] Mostafa Rahimnejad, Arash Adhami, Soheil Darvari, Alireza Zirepour and Sang-Eun Oh (2015) 'Microbial fuel cell as new technology for bioelectricity generation - A review' – journal of Alexandria Engineering, Vol. 54, pp.745–756.

[18] Suchart Kreesaeng, Benjapon Chalermsinsuwan and Pornpote Piumsomboon (2015) 'Effect of Channel Designs on Open-Cathode PEM Fuel Cell Performance - A Computational Study' – International Conference on Alternative Energy in Developing Countries and Emerging Economies, Vol.79, pp.733 – 745.

[19] Suangrat Kiattamrong and Angkee Sripakagorn (2015) 'Effects of the Geometry of the Air Flowfield on the Performance of an Open Cathode PEM FUEL CELL – Transient Load Operation' - International Conference on Alternative Energy in Developing Countries and Emerging Economies, Vol.79, pp.612 – 619.

[20] J.P. Owejana, T.A. Trabolda, D.L. Jacobsonb, M. Arifb and S.G. Kandlikar (2007) 'Effects of flow field and diffusion layer properties on Water accumulation in a PEM fuel cell '- International Journal of Hydrogen Energy, Vol.32, pp. 4489-4502.

[21] Dinesh J and Sugumar M (2015) 'Factors Influence Performance of PEM Fuel Cell – A Review' - International Journal of Advanced and Innovative Research, Vol. 5 Issue 4, pp.2278 – 7844.

Study on Design of solar buildings

Rajanikanth.k(1),Dr.P.Ramesh(2)
1.PG scholar Dept Mechanical Engineering Malla Reddy college of engineering
2.Professor, Dept Mechanical Engineering, crescent engineering college

***ABSTRACT*-Dynamic—Houses for the most part allude to an asylum or building that is implied as an abode or place for residence by people. "Houses" incorporate numerous sorts of abiding going from simple cottages or migrant clans to skyscraper flat structures. A noteworthy imperative in taking care of this demand is the spiraling expense of vitality and different changes in atmosphere. Detached sunlight based structures intend to keep up inside warm solace all through the sun's day by day and yearly cycles while diminishing the necessity for dynamic warming and cooling framework Passive sun powered building configuration is one a player in green building plan, The logical reason for latent sun oriented building configuration has been produced from a blend of climatology (especially warm exchange), and human warm solace (for structures to be occupied by people). Particular consideration is coordinated to the site and area of the home, the overarching atmosphere, outline and development, sun powered introduction, situation of coating and-shading components, and consolidation of warm mass. While these contemplations might be coordinated to any building, accomplishing a perfect arrangement requires watchful joining of these standards.**

KEYWORDS- Climatology, Skyscraper, Green Building Plan

INTRODUCTION

New construction offers the greatest opportunity for incorporating passive solar design, Passive solar system make use of natural energy flows as the primary means of harvesting solar energy, Passive solar system can provide space heating, cooling load avoidance, natural ventilation and day lighting. Passive solar design refers to the use of the sun's energy for the heating and cooling of living spaces. In this approach, the building itself or some element of it takes advantage of natural energy characteristics in materials and air created by exposure to the sun. Passive systems are simple, have few moving parts, and require minimal maintenance and require no mechanical systems Passive solar design refers to the use of the sun's energy for the heating and cooling of living spaces. In this approach, the building itself or some element of it takes advantage of natural energy characteristics in materials and air created by exposure to the sun. Passive systems are simple, have few moving parts, and require minimal maintenance and require no mechanical systems Sun light can provide ample heat, light, and shade and induce summertime ventilation into the well designed home. Passive solar design can reduce heating and cooling energy bills,increase spatial vitality, and improve comfort.Solar energy is a radiant heat source that causes natural processes upon which all life depends. Some of the natural processes can be managed through building design in a manner that helps heat and cool the building. The basic natural processes that are used in passive solar energy are the thermal energy flows associated with radiation, conduction, and natural convection. When sunlight strikes a building, the building materials can reflect, transmit, or absorb the solar radiation. Additionally, the heat produced by the sun causes air movement that can be predictable in designed spaces. These basic responses to solar heat lead to design elements, material choices and placements that can provide heating and cooling effects in a home.Passive solar energy means that mechanical means are not employed to utilize solar energy. To get the most from your home - think sun. That's right, the sun can heat and cool your home and reduce its energy use. More importantly, the energy from the sun can make your home comfortable year round.There are two types of solar design systems -passive and active.Homes constructed as passive solar design use the natural movement of heat and air to maintain comfortable temperatures, operating with little or no mechanical assistance. It's called passive solar because the design of the home maximizes the benefits it receives from the sun with standard construction features. Passive solar takes advantage of local breezes and landscape features such as shade trees and windbreaks, and uses a simple system to collect and store solar energy with no switches or controls.On the other hand, active solar systems use mechanical devices such as pumps and fans to move heat from collectors to storage or from storage to use. Photovoltaic panels that collect solar energy, turning it into electricity, are also considered an active solar system.

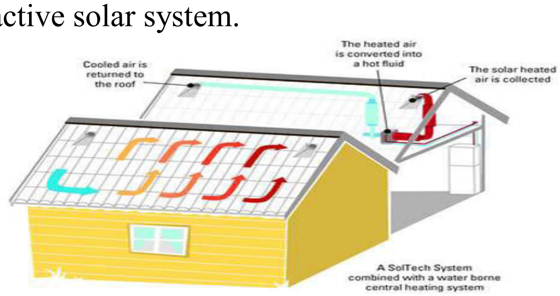

Passive Solar Building Design Concepts :

A total of eleven different passive concepts will be considered. Many other possible solar concepts were evaluated. The ones listed below are appropriate in a wide range of climates and building types.

- (H) Direct gain with storage
- (H) Indirect gain
- (H) Direct gain (without storage)
- (H) Sunspaces
- (C) Night Mechanical Ventilation
- (C) Natural Ventilation
- (L) Windows
- (L) Skylights
- (L) Sawtooth Apertures
- (L) Monitor Apertures
- (L) Atria

The letters (H), (C), and (L) stand for heating, cooling, and lighting, respectively, and are used to remind you of the purpose for each passive solar system concept.

Direct Gain

In this system, the actual living space is a solar collector, heat absorber and distribution system. South facing glass admits solar energy into the house where it strikes directly and indirectly thermal mass materials in the house such as masonry floors and walls. The direct gain system will utilize 60 - 75% of the sun's energy striking the windows.

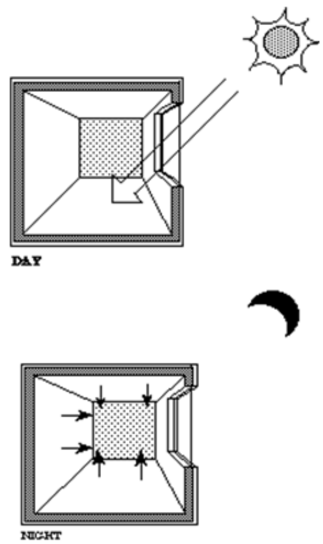

In a direct gain system, the thermal mass floors and walls are functional parts of the house. It is also possible to use water containers inside the house to store heat. However, it is more difficult to integrate water storage containers in the design of the house.

Direct gain system rules of thumb:

A heat load analysis of the house should be conducted.

- Do not exceed 6 inches of thickness in thermal mass materials.
- Do not cover thermal mass floors with wall to wall carpeting; keep as bare as functionally and aesthetically possible.
- Use a medium dark color for masonry floors; use light colors for other lightweight walls; thermal mass walls can be any color.
- For every square foot of south glass, use 150 pounds of masonry or 4 gallons of water for thermal mass.
- Fill the cavities of any concrete block used as thermal storage with concrete.
- Use thermal mass at less thickness throughout the living space rather than a concentrated area of thicker mass.
- The surface area of mass exposed to direct sunlight should be 9 times the area of the glazing.
- Sun tempering is the use of direct gain without added thermal mass. For most homes, multiply the house square footage by 0.08 to determine the amount of south facing glass for sun tempering.

THERMAL STORAGE WALLS:

- A thermal storage wall is a passive solar heating systemin which the primary thermal

storage medium is placed directly behind the glazing of the solar aperture.

Heat transfer to the living space is sometimes augmented by the addition of

circulation vents placed at the top and bottom of the mass wall.

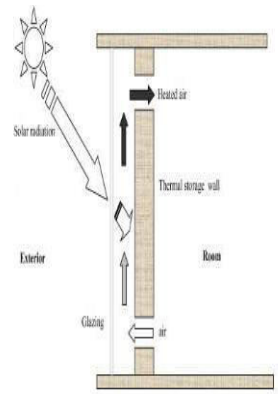

RADIENT PANELS:

Radiant panels are simple passive solar systems that are inexpensive and well suited as retrofits to metal buildings.

CONCRETE BLOCK WALLS:

- Concrete block buildings are very common they may offer opportunities for passive solar retrofits.
- Concrete floor slabs and massive partitions between zones help prevent overheating and otherwise improve the performance of concrete block thermal storage walls
- For new construction, superior performance of solid masonry walls by filling the cores of the block in the thermal storage wall with mortar as it is erected

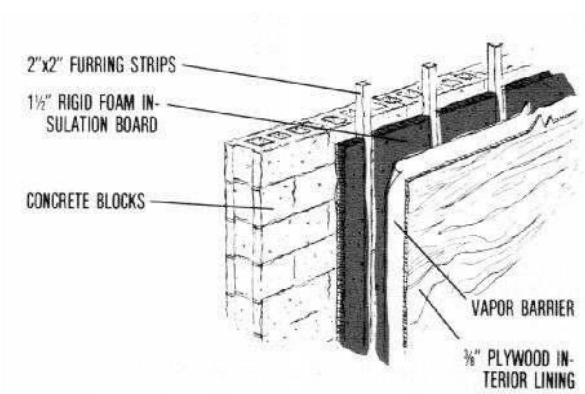

WATER WALLS:

Water walls are thermal storage walls that use containers of water placed directly behind the aperture glazing as the thermal storage medium.
It is more advantageous than a trombe wall by using half the space and being effective at much higher heat capacities.
The advantage over masonry walls is that water has a volumetric heat capacity about twice that of high density concrete; it is therefore possible to achieve the same heat capacity

SKY LIGHTS:

Skylights are a simple way of introducing light to rooms right below roof level. Both fixed and operable skylights are available.

Angled (splayed) walls broadcast the most light, and placing skylights near a wall creates a pleasant light-washing effect on the wall surface.Skylights also can produce unexpected glare and uncomfortably warm indoor temperatures unless they have shades. With this in mind, in most climates it is wise to limit skylights to north roof slopes

WINDOW GLAZING:

- In terms of energy efficiency, glazing is a very important element of the building envelope.
- Glazing transfers both radiant and conducted heat
- Daytime heat gain must be balanced against night time heat loss when selecting glazing areas.
- Window frames can conduct heat. Use timber or thermally separated metal window frames in cooler climates.

INSULATED GLAZING:

- when outside temperatures are significantly higher or lower than inside temperatures, heat pours through the weakest thermal link in the building envelop .

- Insulated glazing helps in keeping the heat from passing through.
- heat gain must be balanced against night time heat loss when selecting glazing areas.
- Lightweight prefabricated buildings have high levels of heat transmission; they are very influenced by outdoor conditions. Cooling in summer and heating in winter become less efficient and consume more energy. The use of insulation materials is especially beneficial in winter; they are not as efficient for summer

CONCLUSION:

- They can perform effortlessly and quietly without mechanical or electrical assistance.
- Reductions can be made to heating bills by as much as 40% annually, and also improve the comfort of living spaces.
- Simple techniques can make a huge difference in the comfort and energy consumption through the years.

- The economical solution to a warmer house in the winter and a cooler house in the summer is to insulate it well, while understanding the movement of heat. it is the better solution.

black lines and shapes. These figures should have no shades or half-tones of gray. Only black and white.

- *Author photos*
  Head and shoulders shots of authors which appear at the end of our papers.
- *Tables*

Data charts which are typically black and white, but sometimes include color.

- *Multipart figures*

Figures compiled of more than one sub-figure presented side-by-side, or stacked. If a multipart figure is made up of multiple figure types (one part is lineart, and another is grayscale or color) the figure should meet the stricter guidelines.

- *File Formats For Graphics*

Format and save your graphics using a suitable graphics processing program that will allow you to create the images as PostScript (PS), Encapsulated PostScript (.EPS), Tagged Image File Format (.TIFF), Portable Document Format (.PDF), or Portable Network Graphics (.PNG) sizes them, and adjusts the resolution settings. If you created your source files in one of the following programs you will be able to submit the graphics without converting to a PS, EPS, TIFF, PDF, or PNG file: Microsoft Word, Microsoft PowerPoint, or Microsoft Excel. Though it is not required, it is recommended that these files be saved in PDF format rather than DOC, XLS, or PPT. Doing so will protect your figures from common font and arrow stroke issues that occur when working on the files across multiple platforms. When submitting your final paper, your graphics should all be submitted individually in one of these formats along with the manuscript.

- *Sizing of Graphics*

Most charts, graphs, and tables are one column wide (3.5 inches / 88 millimeters / 21 picas) or page wide (7.16 inches / 181 millimeters / 43 picas). The maximum depth a graphic can be is 8.5 inches (216 millimeters / 54 picas). When choosing the depth of a graphic, please allow space for a caption. Figures can be sized between column and page widths if the author chooses, however it is recommended that figures are not sized less than column width unless when necessary.

- *Subfigure Labels in Multipart Figures and Tables*

Multipart figures should be combined and labeled before final submission. Labels should appear centered below each subfigure in 8 point Times New Roman font in the format of (a) (b) (c).

- *File Naming*

Figures (line artwork or photographs) should be named starting with the first 5 letters of the author's last name. The next characters in the filename should be the number that represents the sequential location of this image in your article. For example, in author "Anderson's" paper, the first three figures would be named ander1.tif, ander2.tif, and ander3.ps.

Tables should contain only the body of the table (not the caption) and should be named similarly to figures, except that '.t' is inserted in-between the author's name and the table number. For example, author Anderson's first three tables would be named ander.t1.tif, ander.t2.ps, ander.t3.eps.

Author photographs should be named using the first five characters of the pictured author's last name. For example, four author photographs for a paper may be named: oppen.ps, moshc.tif, chen.eps, and duran.pdf.

If two authors or more have the same last name, their first initial(s) can be substituted for the fifth, fourth, third... letters of their surname until the degree where there is differentiation. For example, two authors Michael and Monica Oppenheimer's photos would be named oppmi.tif, and oppmo.eps.

- *Referencing a Figure or Table Within Your Paper*

When referencing your figures and tables within your paper, use the abbreviation "Fig." even at the beginning of a sentence. Do not abbreviate "Table." Tables should be numbered with Roman Numerals.

- *Checking Your Figures: The IEEE Graphics Checker*

The IEEE Graphics Checker Tool enables authors to pre-screen their graphics for compliance with IEEE Transactions and Journals standards before submission. The online tool, located at http://graphicsqc.ieee.org/, allows authors to upload their graphics in order to check that each file is the correct file format, resolution, size and colorspace; that no fonts are missing or corrupt; that figures are not compiled in layers or have transparency, and that they are named according to the IEEE Transactions and Journals naming convention. At the end of this automated process, authors are provided with a detailed report on each graphic within the web applet, as well as by email.

For more information on using the Graphics Checker Tool or any other graphics related topic, contact the IEEE Graphics Help Desk by e-mail at graphics@ieee.org.

- *Submitting Your Graphics*

Because IEEE will do the final formatting of your paper, you do not need to position figures and tables at the top and bottom of each column. In fact, all figures, figure captions, and tables can be placed at the end of your paper. In addition to, or even in lieu of submitting figures within your final manuscript, figures should be submitted individually, separate from the manuscript in one of the file formats listed above in section VI-J. Place figure captions below the figures; place table titles above the tables. Please do not include captions as part of the figures, or put them in "text boxes" linked to the figures. Also, do not place borders around the outside of your figures.

- *Color Processing / Printing in IEEE Journals*

All IEEE Transactions, Journals, and Letters allow an author to publish color figures on IEEE *Xplore*® at no charge, and automatically convert them to grayscale for print versions. In most journals, figures and tables may alternatively be printed in color if an author chooses to do so. Please note that this service comes at an extra expense to the author. If you intend to have print color graphics, include a note with your final paper indicating which figures or tables you would like to be handled that way, and stating that you are willing to pay the additional fee.

- CONCLUSION

A conclusion section is not required. Although a conclusion may review the main points of the paper, do not replicate the abstract as the conclusion. A conclusion might elaborate on the importance of the work or suggest applications and extensions.

APPENDIX

Appendixes, if needed, appear before the acknowledgment.

ACKNOWLEDGMENT

The preferred spelling of the word "acknowledgment" in American English is without an "e" after the "g." Use the singular heading even if you have many acknowledgments. Avoid expressions such as "One of us (S.B.A.) would like to thank ... ." Instead, write "F. A. Author thanks ... ." In most cases, sponsor and financial support acknowledgments are placed in the unnumbered footnote on the first page, not here.

REFERENCES AND FOOTNOTES

- *References*

References need not be cited in text. When they are, number citations on the line, in square brackets inside the punctuation. Multiple references are each numbered with separate brackets. When citing a section in a book, please give the relevant page numbers. In text, refer simply to the reference number. Do not use "Ref." or "reference" except at the beginning of a sentence: "Reference [3] shows ... ." Please do not use automatic endnotes in *Word*, rather, type the reference list at the end of the paper using the "References" style.

Reference numbers are set flush left and form a column of their own, hanging out beyond the body of the reference. The reference numbers are on the line, enclosed in square brackets. In all references, the given name of the author or editor is abbreviated to the initial only and precedes the last name. Use them all; use *et al*. only if names are not given. Use commas around Jr., Sr., and III in names. Abbreviate conference titles. When citing IEEE transactions, provide the issue number, page range, volume number, year, and/or month if available. When referencing a patent, provide the day and the month of issue, or application. References may not include all information; please obtain and include relevant information. Do not combine references. There must be only one reference with each number. If there is a URL included with the print reference, it can be included at the end of the reference.

Other than books, capitalize only the first word in a paper title, except for proper nouns and element symbols. For papers published in translation journals, please give the English citation first, followed by the original foreign-language citation See the end of this document for formats and examples of common references. For a complete discussion of references and their formats, see "The IEEE Style Manual," available as a PDF link off the *Author Digital Toolbox* main page.

- *Footnotes*

Number footnotes separately in superscripts (Insert | Footnote). Place the actual footnote at the bottom of the column in which it is cited; do not put footnotes in the reference list (endnotes). Use letters for table footnotes (see Table I).

- SUBMITTING YOUR PAPER FOR REVIEW

- *Review Stage Using Word 6.0 or Higher*

If you want to submit your file with one column electronically, please do the following:

--First, click on the View menu and choose Print Layout.

--Second, place your cursor in the first paragraph. Go to the Format menu, choose Columns, choose one column Layout, and choose "apply to whole document" from the dropdown menu.

--Third, click and drag the right margin bar to just over 4 inches in width.

The graphics will stay in the "second" column, but you can drag them to the first column. Make the graphic wider to push out any text that may try to fill in next to the graphic.

- *Final Stage Using Word 6.0*

When you submit your final version (after your paper has been accepted), print it in two-column format, including figures and tables. You must also send your final manuscript on a disk, via e-mail, or through a Web manuscript submission system as directed by the society contact. You may use *Zip* for large files, or compress files using *Compress, Pkzip, Stuffit,* or *Gzip.*

Also, send a sheet of paper or PDF with complete contact information for all authors. Include full mailing addresses, telephone numbers, fax numbers, and e-mail addresses. This information will be used to send each author a complimentary copy of the journal in which the paper appears. In addition, designate one author as the "corresponding author." This is the author to whom proofs of the paper will be sent. Proofs are sent to the corresponding author only.

- *Review Stage Using ScholarOne® Manuscripts*

Contributions to the Transactions, Journals, and Letters may be submitted electronically on IEEE's on-line manuscript submission and peer-review system, ScholarOne® Manuscripts. You can get a listing of the publications that participate in ScholarOne at http://www.ieee.org/publications_standards/publications/authors/authors_submission.html First check if you have an existing account. If there is none, please create a new account. After logging in, go to your Author Center and click "Submit First Draft of a New Manuscript."

Along with other information, you will be asked to select the subject from a pull-down list. Depending on the journal, there are various steps to the submission process; you must complete all steps for a complete submission. At the end of each step you must click "Save and Continue"; just uploading the paper is not sufficient. After the last step, you should see a confirmation that the submission is complete. You should also receive an e-mail confirmation. For inquiries regarding the submission of your paper on ScholarOne Manuscripts, please contact oprs-support@ieee.org or call +1 732 465 5861.

ScholarOne Manuscripts will accept files for review in various formats. Please check the guidelines of the specific journal for which you plan to submit.

You will be asked to file an electronic copyright form immediately upon completing the submission process (authors are responsible for obtaining any security clearances). Failure to submit the electronic copyright could result in publishing delays later. You will also have the opportunity to designate your article as "open access" if you agree to pay the IEEE open access fee.

- *Final Stage Using ScholarOne Manuscripts*

Upon acceptance, you will receive an email with specific instructions regarding the submission of your final files. To avoid any delays in publication, please be sure to follow these instructions. Most journals require that final submissions be uploaded through ScholarOne Manuscripts, although some may still accept final submissions via email. Final submissions should include source files of your accepted manuscript, high quality graphic files, and a formatted pdf file. If you have any questions regarding the final submission process, please contact the administrative contact for the journal.

In addition to this, upload a file with complete contact information for all authors. Include full mailing addresses, telephone numbers, fax numbers, and e-mail addresses. Designate the author who submitted the manuscript on ScholarOne Manuscripts as the "corresponding author." This is the only author to whom proofs of the paper will be sent.

- *Copyright Form*

An IEEE copyright form should accompany your final submission. You can get a .pdf, .html, or .doc version at http://www.ieee.org/copyright. Authors are responsible for obtaining any security clearances.

- EDITORIAL POLICY

Submission of a manuscript is not required for participation in a conference. Do not submit a reworked version of a paper you have submitted or published elsewhere. Do not publish "preliminary" data or results. The submitting author is responsible for obtaining agreement of all coauthors and any consent required from sponsors before submitting a paper. The IEEE Transactions and Journals Department strongly discourages courtesy authorship. It is the obligation of the authors to cite relevant prior work.

The IEEE Transactions and Journals Department does not publish conference records or proceedings. The department does publish papers related to conferences that have been recommended for publication on the basis of peer review. As a matter of convenience and service to the technical community, these topical papers are typically collected and published in one special issue of most transactions publications.

At least two reviews are required for every paper submitted. For conference-related papers, the decision to accept or reject a paper is made by the conference editors and publications committee; the recommendations of the referees are advisory only. Indecipherable English is a valid reason for rejection. There is a service available that will help you improve your English for a fee, and the link to that service can be found at http://www.ieee.org/web/publications/authors/transjnl/index.html. Authors of rejected papers may revise and resubmit them as regular papers, whereupon they will be reviewed by two new referees.

- PUBLICATION PRINCIPLES

The two types of contents of that are published are; 1) peer-reviewed and 2) archival. The Transactions and Journals Department publishes scholarly articles of archival value as well as tutorial expositions and critical reviews of classical subjects and topics of current interest.

Authors should consider the following points:

- Technical papers submitted for publication must advance the state of knowledge and must cite relevant prior work.
- The length of a submitted paper should be commensurate with the importance, or appropriate to the complexity, of the work. For example, an obvious extension of previously published work might not be appropriate for publication or might be adequately treated in just a few pages.
- Authors must convince both peer reviewers and the editors of the scientific and technical merit of a paper; the standards of proof are higher when extraordinary or unexpected results are reported.
- Because replication is required for scientific progress, papers submitted for publication must provide sufficient information to allow readers to perform similar experiments or calculations and use the reported results. Although not everything need be disclosed, a paper must contain new, useable, and fully described information. For example, a specimen's chemical composition need not be reported if the main purpose of a paper is to introduce a new measurement technique. Authors should expect to be challenged by reviewers if the results are not supported by adequate data and critical details.
- Papers that describe ongoing work or announce the latest technical achievement, which are suitable for presentation at a professional conference, may not be appropriate for publication.

REFERENCES

Basic format for books:

- J. K. Author, "Title of chapter in the book," in *Title of His Published Book, x*th ed. City of Publisher, Country if not
- USA: Abbrev. of Publisher, year, ch. *x*, sec. *x*, pp. *xxx–xxx.*

Examples:

- G. O. Young, "Synthetic structure of industrial plastics," in *Plastics,* 2nd ed., vol. 3, J. Peters, Ed. New York: McGraw-Hill, 1964, pp. 15–64.
- W.-K. Chen, *Linear Networks and Systems.* Belmont, CA: Wadsworth, 1993, pp. 123–135.

Basic format for periodicals:

- J. K. Author, "Name of paper," *Abbrev. Title of Periodical*, vol. *x,* no. *x,* pp. *xxx-xxx,* Abbrev. Month, year.

Examples:

- J. U. Duncombe, "Infrared navigation—Part I: An assessment of feasibility," *IEEE Trans. Electron Devices*, vol. ED-11, no. 1, pp. 34–39, Jan. 1959.
- E. P. Wigner, "Theory of traveling-wave optical laser," *Phys. Rev*., vol. 134, pp. A635–A646, Dec. 1965.
- E. H. Miller, "A note on reflector arrays," *IEEE Trans. Antennas Propagat*., to be published.

Basic format for reports:

- J. K. Author, "Title of report," Abbrev. Name of Co., City of Co., Abbrev. State, Rep. *xxx*, year.

MODELING AND ANALYSIS OF MACHINE TOOL STRUCTURES

1. **G. LATHA SREE,** PG Scholar 2. **J. CHANDRA SEKHAR,** Assistant Professor,
DEPARTMENT OF MECHANICAL ENGINEERING
MALLA REDDY COLLEGE OF ENGINEERING
Maisammaguda, Dhulapally, Secunderabad,Hyderabad,India

ABSTRACT

The objective of this present work is to estimate the deflections and stresses that are induced in the machine tool structure. The emphasis in this project is on the application of computer aided analysis using finite element concept. A machine tool is a machine for shaping or machining metal or other rigid materials, usually by cutting, boring, grinding, shearing, or other forms of deformation. Machine tools employ some sort of tool that does the cutting or shaping. All machine tools have some means of constraining the work piece and provide a guided movement of the parts of the machine.

In analysis part the finite element of hollow machine member is created using solid tetrahedron elements, appropriate boundary conditions are applied, material properties are given and loads are applied as per its design, the resultant deformation and stresses obtained are reported and discussed.

1.INTRODUCTION

Beds, bases, columns and box type housings are called “structures” in machine tools. In machine tools, 70-90% of the total weight of the machine is due to the weight of the structure. In this chapter classification and functions of machine tool structure is described. Researchers have worked with different types of materials like cast iron, mild steel, granite and epoxy concrete for machine tool structure for different applications. Profile of the machine tool and selection of different stiffeners/ribs are suggested by researchers. Quality of the job produced on these machine tools depends directly on the quality and performance of machine tools. To develop good products, design engineers need to study how their designs will behave in real-world conditions.

The limitations of physical model techniques have led to the development of mathematical models representing a variety of mechanical structures. As in this approach, whole structure is divided into finite elements, it is known as ‘Finite Element Analysis’.

2. METHODOLGY

Generic Steps of Solving any Problem in ANSYS

Like solving any problem analytically, you need to define (1) your solution domain, (2) the physical model, (3) boundary conditions and (4) the physical properties. You then solve the problem and present the results. In numerical methods, the main difference is an extra step called mesh generation. This is the step that divides the complex model into small elements that become solvable in an otherwise too complex situation. Below describes the processes in terminology slightly more attune to the software.

A. Build Geometry

Construct a two or three dimensional representation of the object to be modeled and tested using the work plane coordinates system within ANSYS.

B. Define Material Properties

Now that the part exists, define a library of the necessary materials that compose the object (or project) being modeled. This includes thermal and mechanical properties.

C. Generate Mesh

At this point ANSYS understands the makeup of the part. Now define how the modeled system should be broken down into finite pieces.

D. Apply Loads

Once the system is fully designed, the last task is to burden the system with constraints, such as physical loadings or boundary conditions.

E. Obtain Solution

This is actually a step, because ANSYS needs to understand within what state (steady state, transient… etc.) the problem must be solved.

F. Present the Results

After the solution has been obtained, there are many ways to present ANSYS’ results, choose from many options such as tables, graphs, and contour plots.

3. EXPERIMENTATION

PREFERENCES – STRUCTURAL:

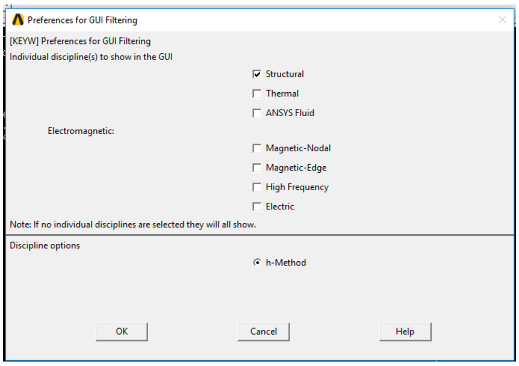

ELEMENT TYPE – ADD – 10NODE

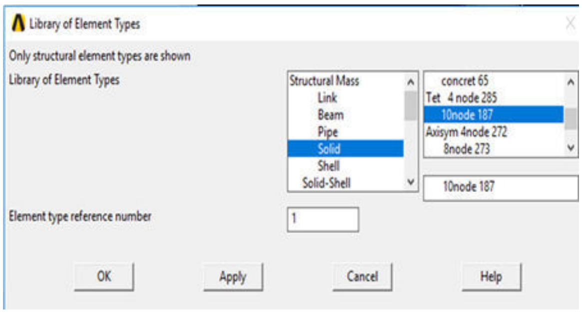

MATERIAL PROPERTIES – STRUCTURAL – LINEAR – ISOTROPIC

EX = 1.1 E5 PRXY = 0.23 DENSITY = 0.0075

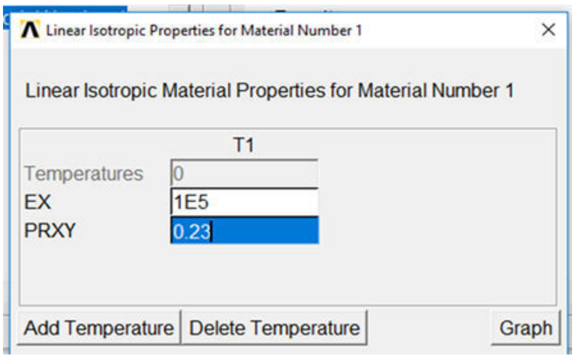

MODELING-CREATE – KEYPOINTS –LINES

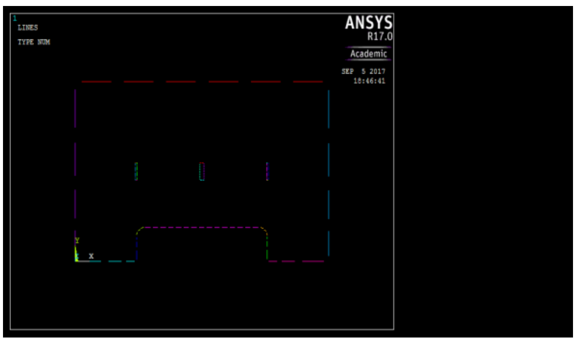

AREAS – ARBITRARY – BY LINES

EXTRUDE – VOLUMES

CASE-1 BED WITH RECTANGULAR HOLES

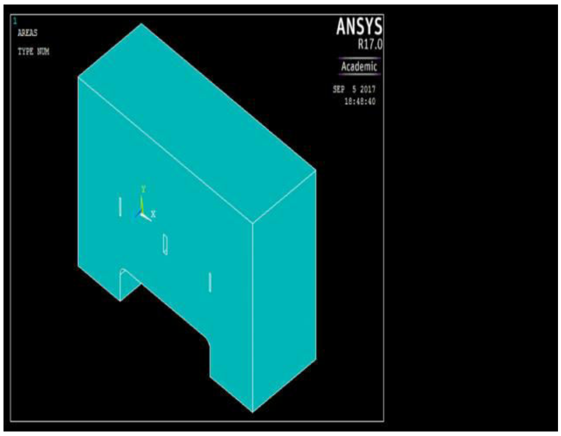

CASE-2 BED WITH CIRCULAR HOLES

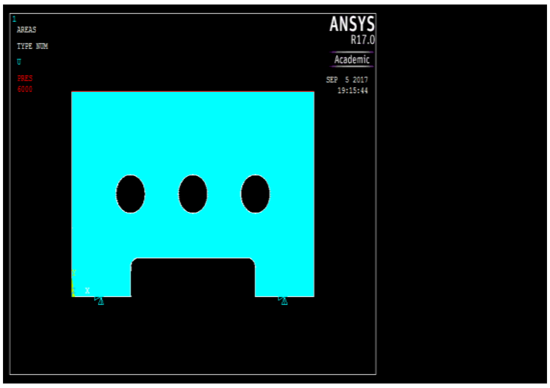

MESHING-VOLUMES

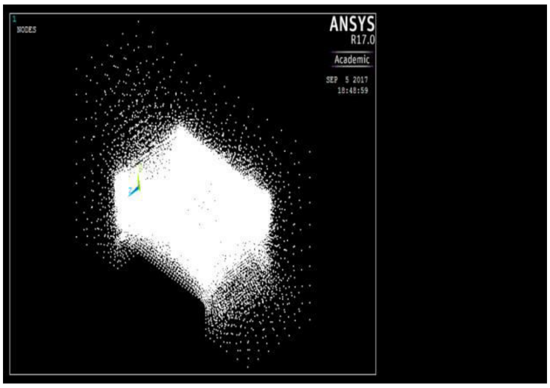

LOADS – PRESSURE – 6000N

4. RESULTS

CASE-1 BED WITH RECTANGULAR HOLES

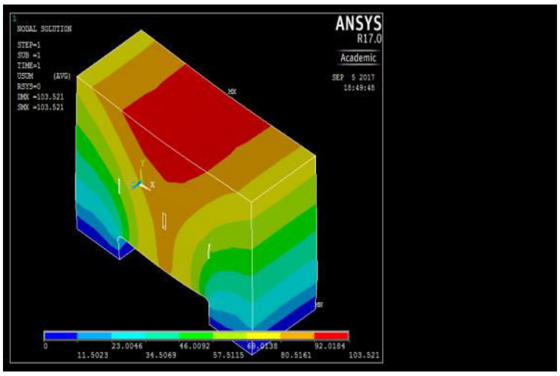

Displacement vector sum

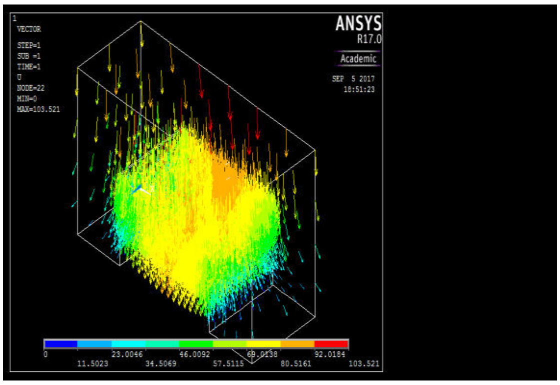

Vector plot

CASE-2 BED WITH CIRCULAR HOLES

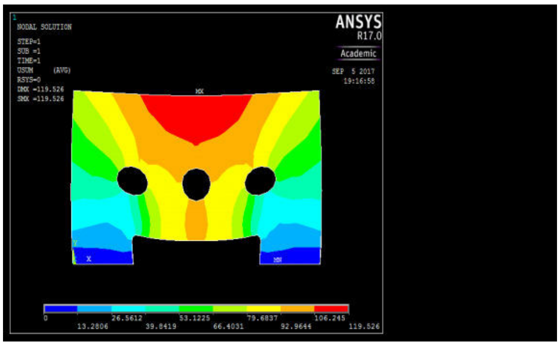

Displacement Vector sum

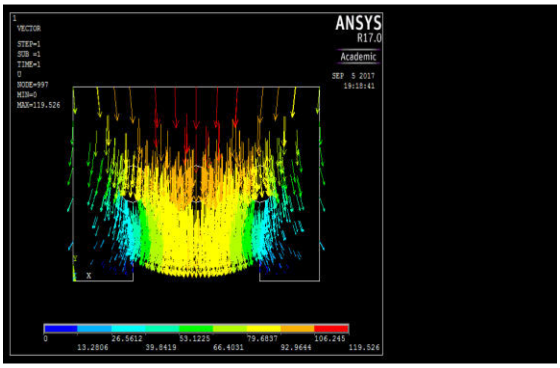

Vector plot

COMPARISION OF RESULTS:

MACHINE BED	VONMISES STRESS
CASE-1	103.521
CASE-2	119.526

CONCLUSION

Machine tools employ some sort of tool that does the cutting or shaping. All machine tools have some means of constraining the work piece and provide a guided movement of the parts of the machine. In analysis part the finite element of two profile machine members are alike rectangular hole and circular hole created using solid tetrahedron elements, appropriate boundary conditions are applied, material properties are given and loads are applied as per its design, the resultant deformation and stresses obtained are reported and discussed.

After comparing the two machine beds with rectangular and circular holes, on which i have analysed the stresses, its clear that the machine bed with rectangular holes can be preferred to mount the tool assembly.

REFERENCES

1. 1.Junior W K and Guanabara A S (2005), “Methodology for Product Design Based on the Study of Bionics”, Materials and Design, Vol. 26, pp. 149-155.
2. Kim D I, Jung S C, Lee J E and Chang S H (2006), “Parametric Study on Design of Composite-Foam-Resin Concrete Sandwich Structures for Precision Machine Tool Structures”, Composite Structures, Vol. 75, pp. 408-414.
3. Ma J F, Chen W Y, Zhao L and Zhao D H (2008), “Elastic Buckling of Bionic Cylindrical Shells Based on Bamboo”, Journal of Bionic Engineering, Vol. 5, pp. 231-238.
4. Ren L Q and Liang Y H (2010), “Biological Couplings: Function, Characteristics and Implementation Mode”, Science in China Series Es: Technological Sciences, Vol. 53, pp. 379-387.
5. Chen P Y, Lin A Y M, Lin Y S, Seki Y, Stokes A G, Peyras J, Olevsky E A, Meyers M A and McKittrick J (2008), “Structure and Mechanical Properties of Selected Biological Materials”, Journal of the Mechanical Behavior of Biomedical Materials, Vol. 1, pp. 208-226.
6. Rahman, M, Mansur, A, Karim, B. Non-conventional materials for machine tool

structures. JSME Int J C: Mech Sy 2001; 44: 1–11

7. Lee, DG, Suh, JD, Kim, HS. Design and manufacture of composite high speed machine tool structures. Compos Sci Technol 2004; 64: 1523–1530.
8. Möhring, HC, Brecher, C, Abele, E. Materials in machine tool structures. CIRP Ann: Manuf Techn 2015; 64: 725–748.
9. Huo, D, Cheng, K, Wardle, F. A holistic integrated dynamic design and modelling approach applied to the development of ultraprecision micro-milling machines. Int J Mach Tool Manu 2010; 50: 335–343.
10. Rahman, M., Mansur, M.A. and Chua, K.H. (1988), Evaluation advanced cementitious composites for machine tool structures. Annals of the CIRP, Vol. 37, pp. 373-376.

DESIGN AND STRUCTURAL ANALYSIS OF FORM TOOL

ASANABAD VENU
PG scholor,
Dept of mechanical,
Mallareddy college of engineering.
asanabadavenu@gmail.com

J. CHANDRA SEKHAR
Assistant. Professor
Dept of mechanical,
Mallareddy college of engineering.
chandu1439@gmail.com

ABSTRACT

A form tool is precision-ground into a pattern that resembles the part to be formed. The form tool can be used as a single operation and therefore eliminate many other operations from the slides (front, rear and/or vertical) and the turret, such as box tools. A form tool turns one or more diameters while feeding into the work. Before the use of form tools, diameters were turned by multiple slide and turret operations, and thus took more work to make the part. In this Project we model a form tool using ANSYS Modeller. The advantages of form tools are (a) cycle time, (b) it works as “POKA YOKA” (mistake proofing) (c) maintains relation between operation (d) cost optimization. This tool is modelled by using 3D modelling software. In this the design of form tool is analyzed using FEA software Ansys APDL.

INTRODUCTION

A form tool is precision-ground into a pattern that resembles the part to be formed. The form tool can be used as a single operation and therefore eliminate many other operations from the slides (front, rear and/or vertical) and the turret, such as box tools. A form tool is precision-ground into a pattern that resembles the part to be formed. A form tool has one or more cutting edges with well defined profile or contour that is to be reproduced as the desired shape on the work piece surface. Form tools are classified as flat form tools and circular form tools. Straight and flat form tools have square or rectangular cross-section with the form along its side or end.

The form tool can be used as a single operation and therefore eliminate many other operations from the slides (front, rear and/or vertical) and the turret, such as box tools. A form tool turns one or more diameters while feeding into the work. Before the use of form tools, diameters were turned by multiple slide and turret operations, and thus took more work to make the part. For example, a form tool can turn many diameters and

1) **Using a forming tool**

Various types of forming tools

1. **Flat Form Tool -**
2. **Circular Form Tool –**

Graphical method of determining profile of form tool

(i) Profile of Flat Form Tool

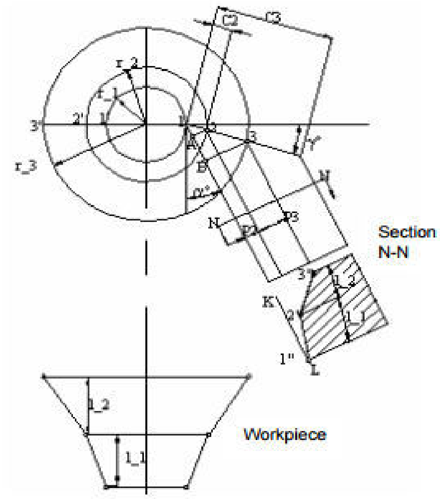

Figure shows Graphical Method of Determining the Profile of Flat Form Tool

ii) Profile of Circular Form Tool

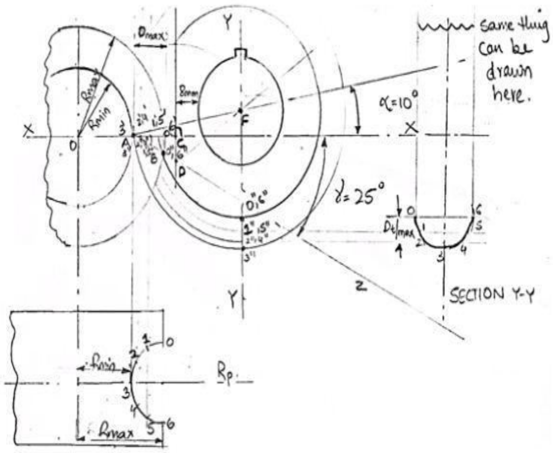

Figure shows Graphical Method of Determining the Profile of Circular Form Tool

FINITE ELEMENT METHOD

Explanation of fem by step by step procedure:.

1. Discretization of the domain

2. Basic Element Shapes

3. Size of Elements

4. Location of Nodes

Advantages of finite element method:

1. The use of separate sub regions or finite elements for the trail solutions permits a greater flexibility in considering continuation of complex shape.
2. Rather than requiring every trial solution to satisfy the boundary conditions, one prescribes the conditions after obtaining the algebraic equations for the assemblage.
3. As the boundary conditions do not enter into equations for the individual finite elements, one can use the same field variable for both internal and boundary elements.
4. The field variable models need not be changed when the boundary conditions change.
5. The introduction of boundary conditions in to assembled equations is a relatively easy process. No special techniques or artificial devices are necessary.
6. The finite element method not only accommodates complex geometry and boundary conditions, but also proven successful in representing various types of complicated material properties that are difficult to incorporate in other numerical methods.

Limitations of finite element method:

1. Cracking and Fracture behaviour.
2. Contact problems.
3. Bond failures of composite materials.
4. Non-Linear material behaviour with work softening.

Applications of FEM:

1. Mechanical Design
2. Civil Engineering Structures
3. Air Craft structures
4. Heat conduction
5. Nuclear Engineering

INTRODUCTION ABOUT ANSYS

Generic Steps to Solving any Problem in ANSYS

1. Build Geometry
2. Define Material Properties
3. Generate Mesh
4. Apply Loads
5. Obtain Solution
6. Present the Results

SPECIFIC CAPABILITIES OF ANSYS

1) **STRUCTURAL**
2) **THERMAL**

STRUCTURAL:

- Static Analysis
- Transient Dynamic Analysis
- Buckling Analysis
- Fracture mechanics,
- Composite material analysis,
- Fatigue.

PROCEDURE FOR ANALYSIS OF FORMTOOL

Case-1: procedure for static analysis of form tool using HSS steel material

Material properties of HSS steel

- **Modulus of elasticity, E=230E3** N/mm^2
- **Shear Modulus, G=E/[2(1+V)]** N/mm^2, **88461.5**N/mm^2
- **Poission's Ratio=0.3**
- **Density,= 7000** Kg/m^3

PREFERENCES – STRUCTURAL

ELEMENT TYPE – ADD – SOLID 187

MATERIAL PROPERTIES – STRUCTURAL – LINEAR – ELASTIC - ISOTROPIC

EX = 2.3E5

PRXY 0.3

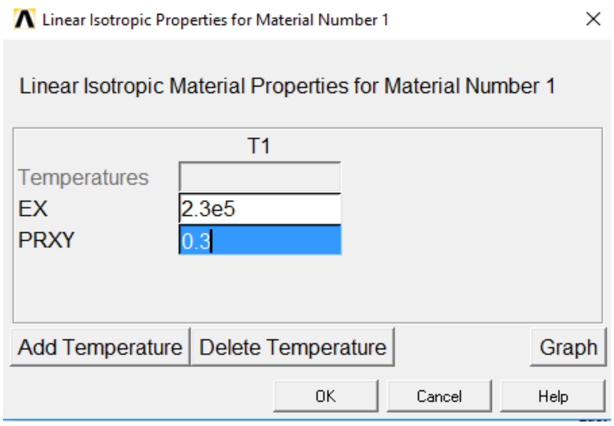

Fig shows Material model table

MODELING- CREATE- KEYPOINTS – LINES

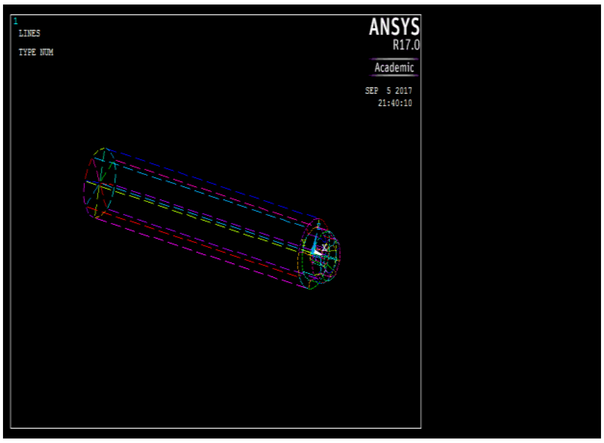

Figure shows Lines of the component

AREAS – VOLUMES – MESHING

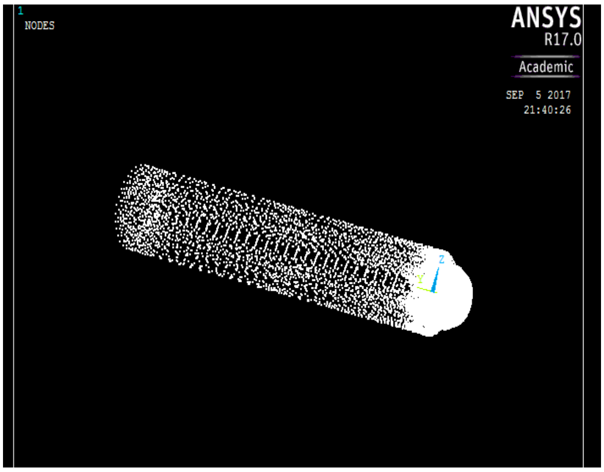

Figure shows Nodes of the component

LOADS – FORCES APPLIED

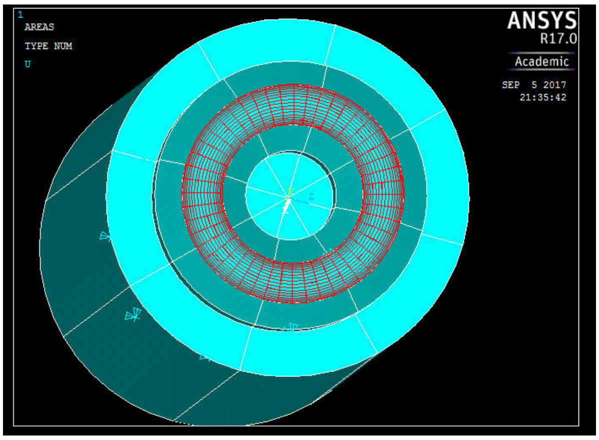

Figure shows Pressure applied

SOLUTION - SOLVE

CURRENT LS

POST PROCEDURE – PLOT RESULTS

Fig shows Deformed and UN deformed shape

PLOT RESULTS - CONTOURED PLOT

DEFORMATION

AT DISPLACEMENT VECTOR SUM

Fig shows Deformation vector sum

PLOT RESULTS - CONTOURED PLOT-VONMISES STRESS- AT X COMPONENT

Fig shows Stress values along X-axis

PLOT RESULTS - CONTOURED PLOT-VONMISES STRESS- AT Y COMPONENT

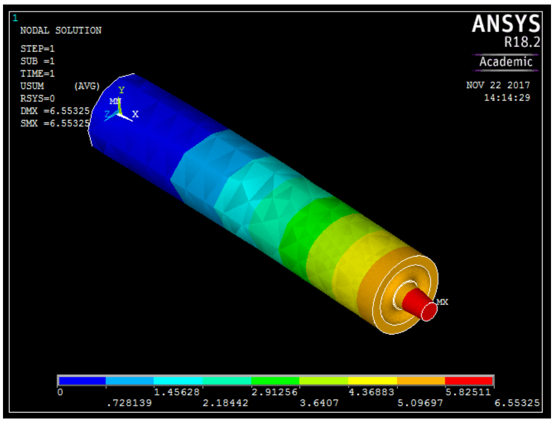

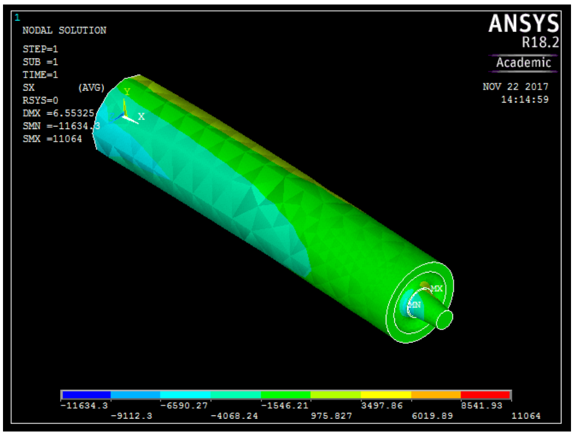

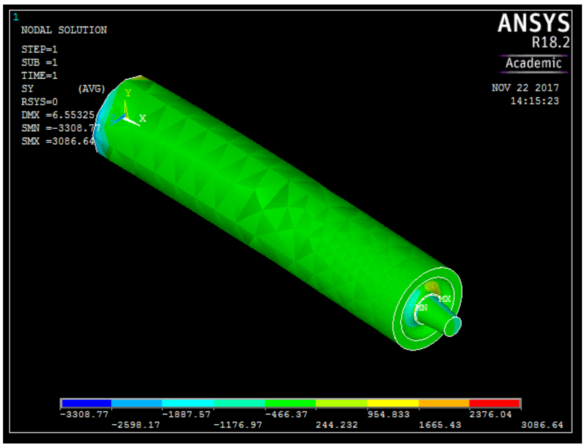

Fig shows Stress values along Y-axis

PLOT RESULTS - CONTOURED PLOT-VONMISES STRESS- AT Z COMPONENT

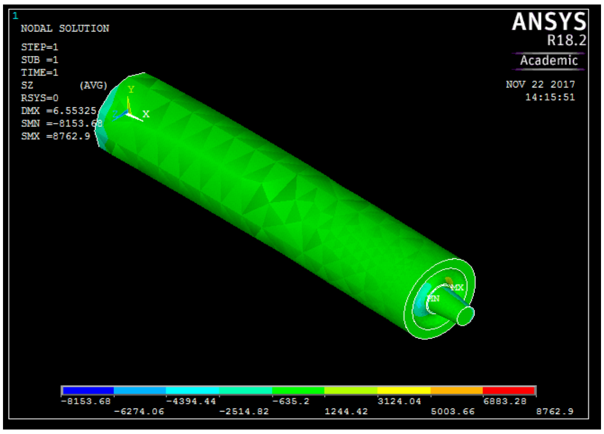

Fig shows Stress values along Z-axis

PLOT RESULTS - CONTOURED PLOT-VONMISES STRESS

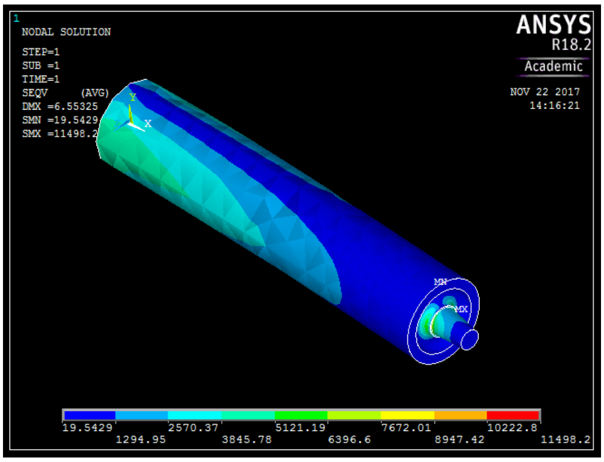

Fig shows Von misses Stress values along geometry

Procedure for modal analysis of form tool using HSS steel material

SOLUTION-ANALYSIS TYPE-NEW ANALYSIS-MODAL

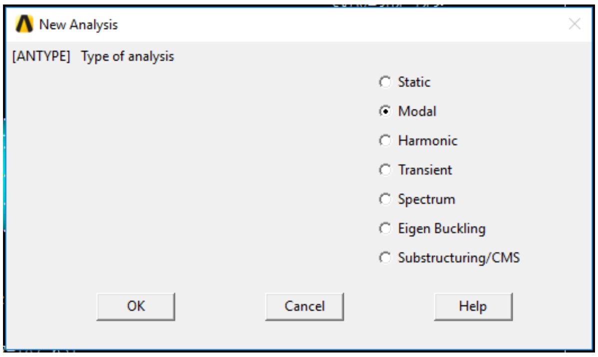

Fig shows Modal analysis selection

FREQUENCY RESULTS:

SET,LIST Command

File

***** INDEX OF DATA SETS ON RESULTS FILE *****

SET	TIME/FREQ	LOAD STEP	SUBSTEP	CUMULATIVE
1	0.20798	1	1	1
2	0.20800	1	2	2
3	1.1532	1	3	3

Fig shows Frequency results

Modal analysis results of HSS steel material

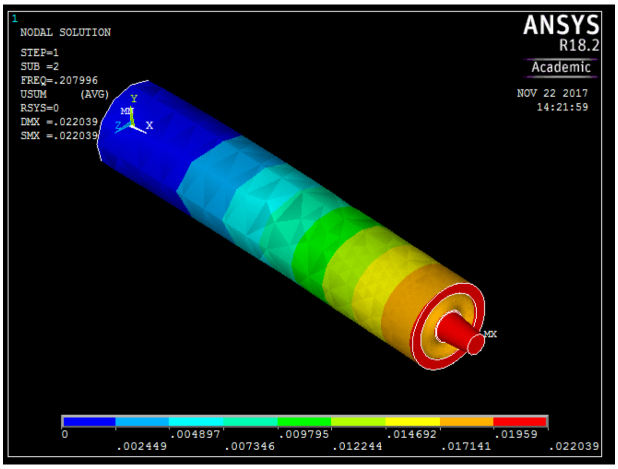

Fig shows Displacement vector sum of 2nd frequency

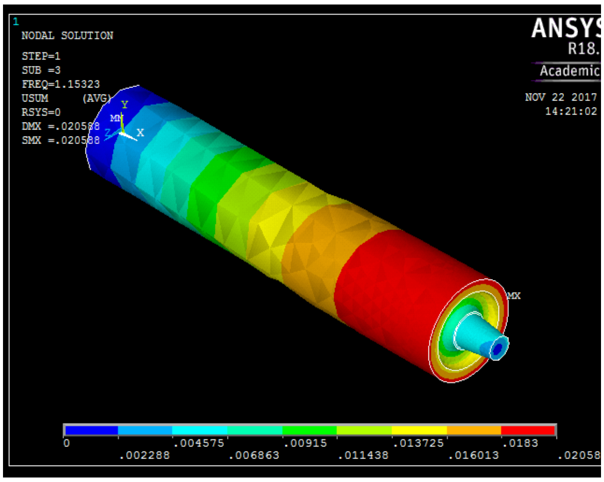

Fig shows Displacement vector sum of 3rd frequency

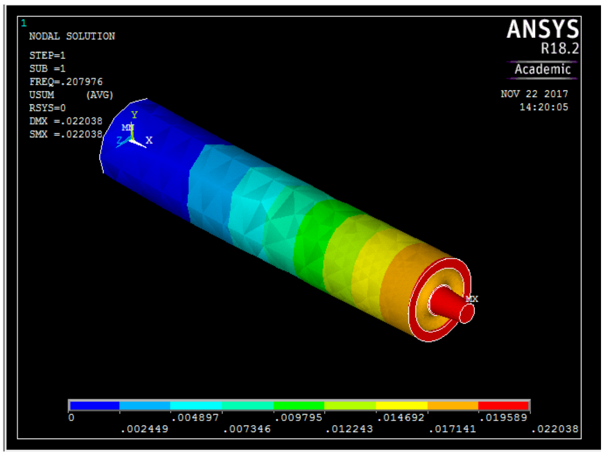

Fig shows Displacement vector sum of 1st

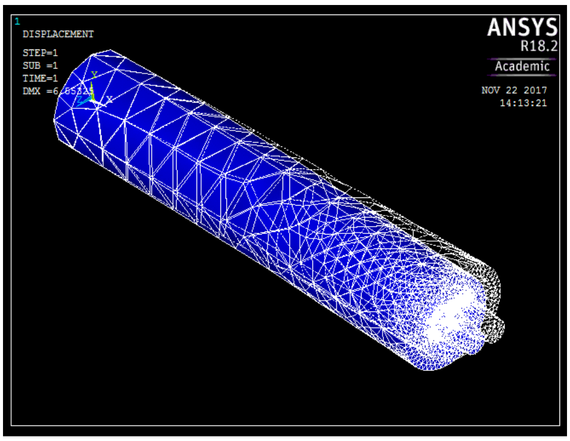

frequency

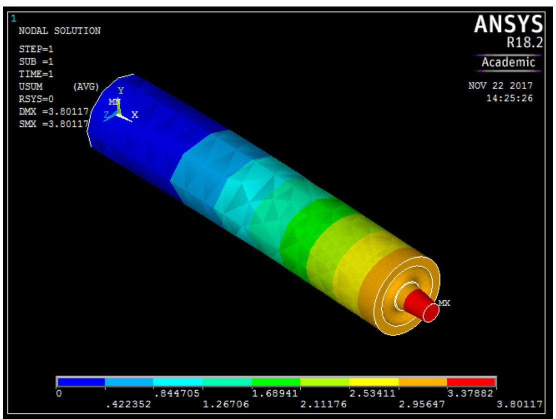

Static analysis of form tool using SISIC material

- **Material** = **Grey Cast Iron**
- **Modulus of Elasticity**, Ex= **26e6 Psi**
- **Poisson's Ratio**, Prxy = **0.29**
- **Density= 7500Kg/m^3**

PLOT RESULTS:

Fig shows displacement vector sum

PLOT RESULTS - CONTOURED PLOT-VONMISES STRESS

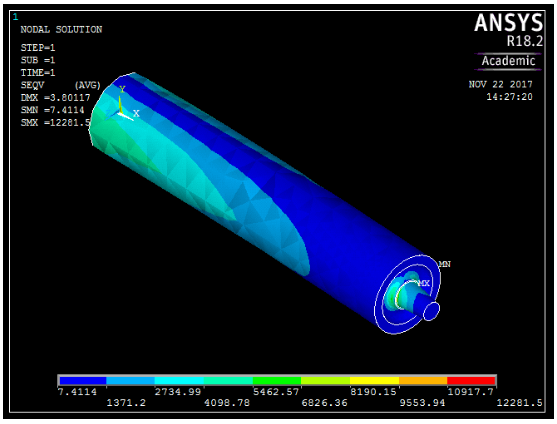

Fig shows Von misses Stress values along geometry

Modal analysis of form tool using SISIC material

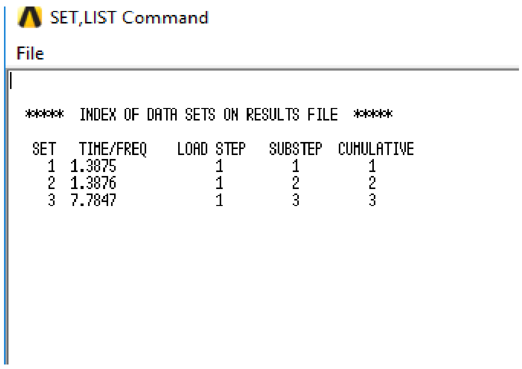
SET,LIST Command

File

***** INDEX OF DATA SETS ON RESULTS FILE *****

SET	TIME/FREQ	LOAD STEP	SUBSTEP	CUMULATIVE
1	1.3875	1	1	1
2	1.3876	1	2	2
3	7.7847	1	3	3

Fig shows Frequency values

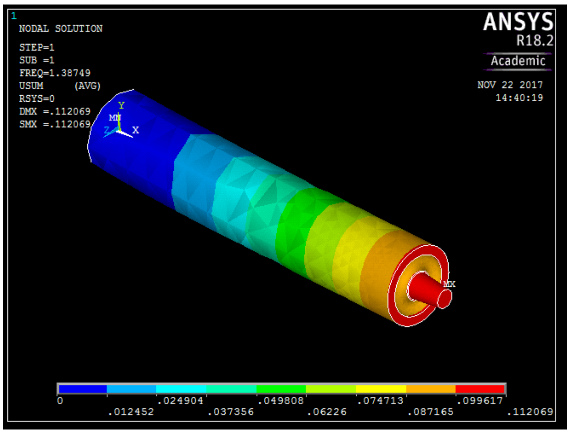

Fig shows Displacement values at 1st Frequency

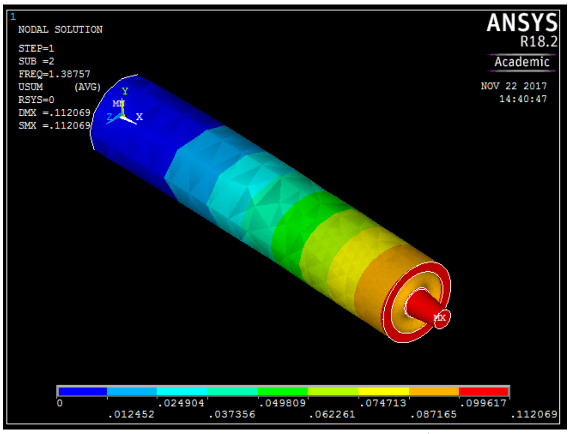

Fig shows Displacement values at 2nd Frequen

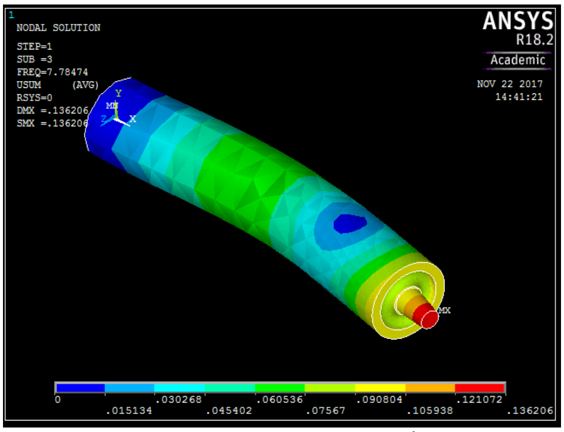

Fig shows Displacement values at 3rd Frequency

Static and modal analysis for ALUMINUM material

- **Material** = Aluminum
- **Modulus of Elasticity**, Ex= 72e3 psi
- **Poisson's Ratio**, Prxy = 0.29
- **Density=2700** g/m^3

PLOT RESULTS

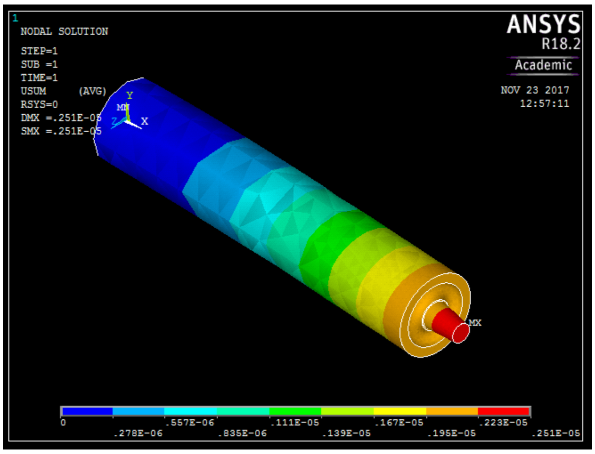

Fig. shows Deformation shape

PLOT RESULTS

PLOT RESULTS - CONTOURED PLOT-VONMISES STRESS

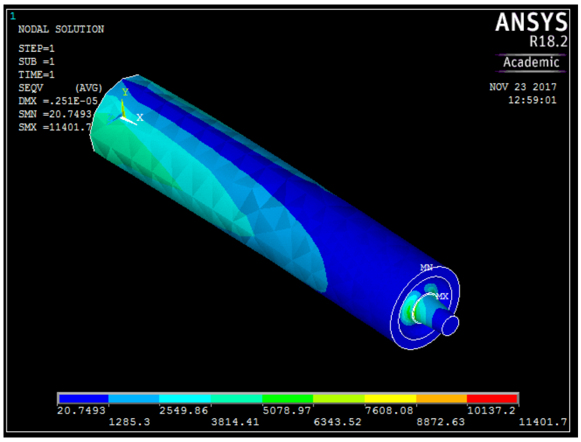

Fig shows Von misses Stress values along geometry

Modal analysis of FORM TOOL using ALUMINUM material

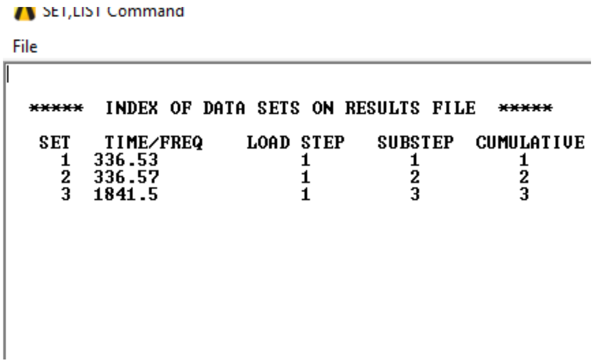
SET,LIST Command

File

***** INDEX OF DATA SETS ON RESULTS FILE *****

SET	TIME/FREQ	LOAD STEP	SUBSTEP	CUMULATIVE
1	336.53	1	1	1
2	336.57	1	2	2
3	1841.5	1	3	3

Fig shows Frequency values

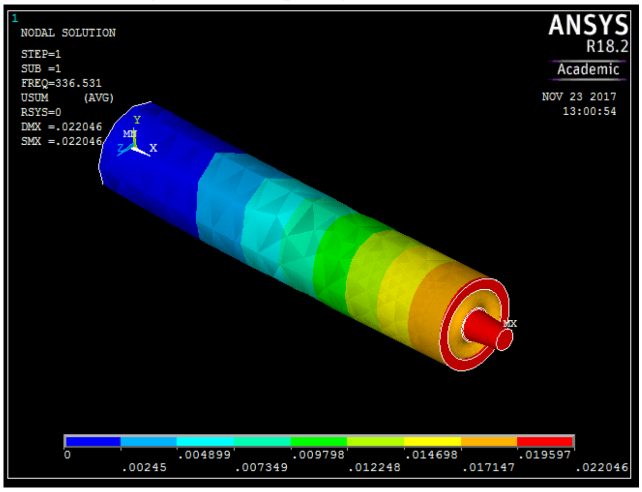

Fig shows Displacement values at 1st Frequency

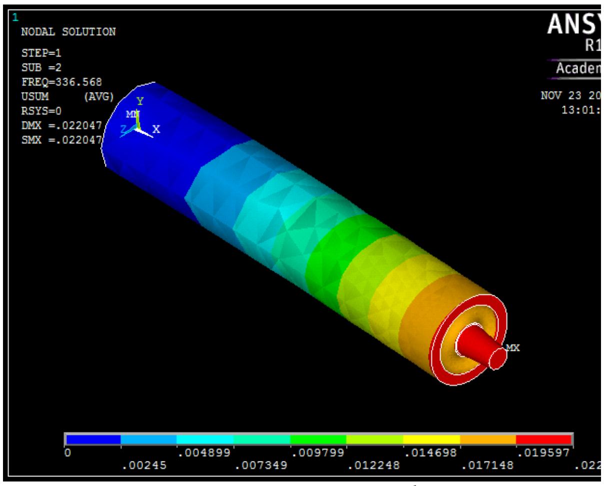

Fig shows Displacement values at 2nd Frequency

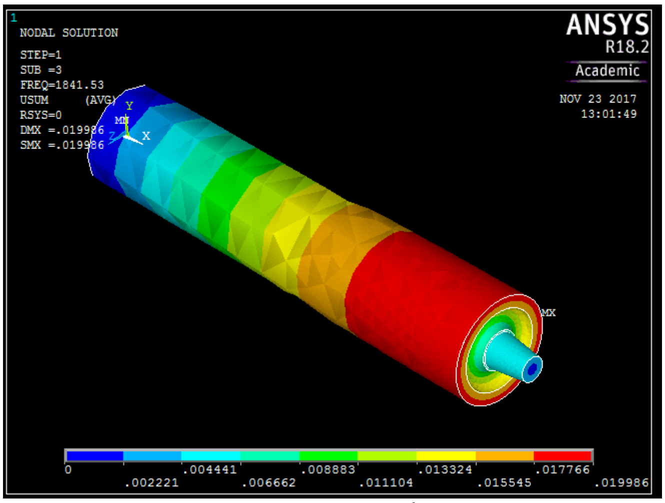

Fig shows Displacement values at 3rd Frequency

Results:

Comparison of results of three materials

HSS STEEL MATERIAL	SISIC MATERIAL	ALUMINIUM MATERIAL
DMX= 6.55	DMX= 3.801	DMX= 0.251e-5
Stress Values 1)X= 11064 2)Y= 3086.6 3)Z= 8762.9 Von misses =11498.5	Stress Values 1)X= 11203.8 2)Y= 1298.75 3)Z= 8740.02 Von misses = 12281.5	Stress Values 1)X= 11058.7 2)Y= 3487.24 3)Z= 8777.79 Von misses = 11401.7
Displacement Vector Sum 1ST Freq= 0.207 2nd Freq= 0.208 3rd Freq= 1.153	Displacement Vector Sum 1ST Freq= 1.3875 2nd Freq= 1.3876 3rd Freq= 7.7847	Displacement Vector Sum 1ST Freq= 336.53 2nd Freq= 336.57 3rd Freq= 1841.5

CONCLUSION

Forming a tool or die or designing a forming tool is one of vital factor of tool engineering. The part formed by forming operation is generally takes the shape of the dir or punch. In the forming operation, the metal flow is not uniform and localized to some extent, depending upon the shape of the work piece. Bending along a large radius in a straight line may also be referred to as a forming operation. From above stress, strain, total deformation we can observe that HSS steel, SISIC and Aluminium materials gave accurate results for form tool but according to cost HSS material is best.

REFERENCES

[1] S. Sundaram, P. Senthilkumar, A. Kumaravel and N. Manoharan, “Study Of Flank Wear In Single Point Cutting Tool Using Acoustic Emission Sensor Techniques”, ARPN Journal of Engineering and Applied Sciences, VOL. 3, NO. 4, AUGUST 2008.

[2] K. Kadirgama, K. A. Abou-El-Hossein, B. Mohammad, M. M. Noor and S. M. Sapuan, “Prediction of tool life by statistic method in end-milling operation”, Scientific Research and Essay, Vol. 3 (5), pp. 180-186, May, 2008.

[3] S. Dolinsek, J. Kopac, “Mechanism and types of tool wear; particularities in advanced cutting materials”, Journal of Achievements in Materials

ANALYSIS ON CRACK PROPAGATION FINDING ITS SIF BY USING FRACTURE MECHANICS THEORY

A. Happy
Mallareddy College of engineering
Hyderabad, India
Email: happy.angelika5@gmail.com

I. Prasanna
Mallareddy College of engineering
Hyderabad, India
Email: prasannabobba81@gmail.com

Abstract—The focus of this paper is to investigate how a crack propagates and grows in a rectangular plate with an elliptical crack through the centre. The finite Element Analysis tool Ansys is used to propagate the failure criteria and to compute stresses and Stress Intensity factor SIF (K). A specific object was created and central crack was investigated. This configuration was introduced since the engineers often detect Mode 1 Open type crack in object. The Stress Intensity Factor obtained theoretically is compared against same by Ansys 17.2 tool. Both of them obtained and also maximum stress zone is located at the crack tip in Ansys.

Keywords- Fracture Mechanics, ANSYS, Central Crack, Crack Propagation, Linear Elastic Fracture Mechanics (LEFM), Finite Element Method, Stress Intensity Factor, High Grade Steel C45. I.

I.INTRODUCTION

Failure of the engineering structures is caused by cracks, which is depending on the design and operating conditions that extend beyond a safe size. Cracks present to some extent in all structures, either as a result of manufacturing defects or localized damage in service [2]. The crack growth leads to a decrease in the structural strength. Fracture, the final catastrophic event takes place very rapidly and is preceded by crack growth. Damage Tolerance (DT) assessment is a procedure that defines whether a crack can be sustained safely during the projected service life of the structure. The fundamental assumption of linear elastic fracture mechanics is that the crack behavior is determined solely by the values of the stress intensity factors which area function of the applied load and the geometry of the cracked structure. Fracture mechanics deals with the study of how a crack in a structure propagates under applied loads propagation and failure with experimental results [5]. Calculating fracture parameters such as stress intensity factor in the crack region [1], which is used to estimate the crack growth, makes the analytical predictions. Some typical parameters are: Stress intensity factors (Open mode (a) KI, Shear mode (b) KII, Tear mode (c) KIII

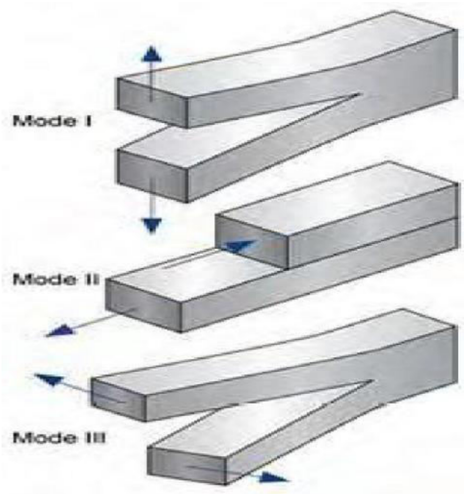

Figure 1: Three Types Of Loading On A Cracked Body; (A) Mode I; (B) Mode Ii And (C) Mode Iii

II.REVIEW

Dayal R. Parhi and Sasanka Choudhury a cantilever beam with a single crack has been taken into consideration. Finite element method is used to find out the natural frequencies of the faulty cantilever beam. A fuzzy controller has been designed using trapezoidal, Gaussian as well as triangular membership function to find out the crack depth and crack location [5,7]

D.K. Agarwalla concludes crack detection and localization is the main topic of discussion for various researchers across the globe. It is concluded that results obtained from experiment have a very good agreement with the results obtained from FEM and the structure vibrates with more frequency in the presence of a crack away from the fixed end.

An analytical and experimental approach by H. Nahvi and M. Jabbari et al. to the crack detection in cantilever beams by vibration analysis. Sensibility analysis of the inverse problem of the crack parameters (location and depth) determined by M. B. Rosales, C P Filipich and F S Buezas et al. An efficient numerical technique is necessary to obtain significant results.

III.PROBLEM STATEMENT

Cracks often develop in the corners of a structural member due to high stress concentration factor in those areas. If one can calculate the rate of crack growth, an engineer can schedule inspection accordingly and repair or replace the part before failure happens. Moreover, being able to predict the path of a crack helps a designer to incorporate adequate geometric tolerance in structural design to increase the part life [11]. While producing durable, reliable and safe structures are the goals of every aerospace component manufacturer, there are technical challenges that are not easy to be solved. Given limited engine design space, engineers strive to optimize using material geometry to produce high efficient and high performance engines that will operate at minimum weight and cost [6]. Engineers often look to shave materials from component and design the thinnest possible components. Benefits from this approach include reduced weight, and smaller probability of encountering brittleness inducing micro structural defects. The focus of this paper is to investigate the corner crack growth in a steel alloy plate. This paper will examine the stresses near the crack tip, compute the stress intensity factors and compare it against material toughness to determine the influence of the crack on the plate.

IV METHODOLOGY

Engineers strive to optimize part geometry by designing the thinnest possible components because this approach not only reduce engine weight but also reduce the risk of brittle structure often found in bulk materials [9]. Being able to determine the rate of crack growth, an engineer can schedule inspection accordingly and repair or replace the part before failure happens. Being able to predict the path of a crack helps a designer to incorporate adequate geometric tolerance in structural design to increase the part life [10]. The methodology used to investigate the mechanics of crack propagation consists of the following steps:

- Model creation
- Elastic stress analysis of the uncracked body
- Flaw implementation
- Crack propagation
- Elastic stress analysis of the cracked body
- Calculation of stress intensity factor
- Interpretation of results

V. EXPERIMENTS AND RESULTS

Model is having with the dimensions of 0.1m in height, 0.1m in width, and crack length is 0.02m. In addition, the symmetry boundary conditions of steel plate as shown in bellow fig 2.

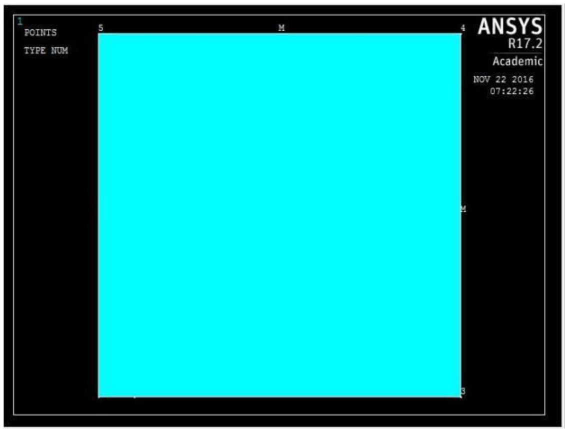

Figure 2: Basic model

Among all the steel based alloys, according to Immarigeon et al [3], high grade steel c45 is by far the most widely used, accounting for almost half of all steel used in aircraft because the material can increase the strength+to+weight ratio in structures and provide heat resistance with weight savings. However, the significant weight savings permitted by these steel application developments generate specific drawbacks that need particular technological developments. Among the most important concerns are brittle inclusions, which are difficult to detect by non-destructive testing, can initiate cracks and produce early failure of the structures [2]. Materials imperfections due to manufacturing process, for example, voids and impurities can develop flaws that may cause the material to become weak. For those reasons, the material chosen in this study is high grade steel C45 and the properties are summarized in Table 1

QUANTITY	MAX	MIN	UNITS
Density	7850	7850	Kg/m3
Youngs modulus	210000	210000	Mpa
Poisons ratio	0.27	0.3	
Tensile srength	600	800	Mpa
Yield strength	340	400	Mpa

THEORITICAL STRESS INTENSITY FACTOR (K1):

1. Stress intensity factor (K1) = $C\sigma\sqrt{\pi a}$
2. C = (1- 0.1 + 0.96)$\sqrt{1/COS(\pi\eta)}$

Where C is a constant.

3. $\eta = a/b$

Using the numerical package Ansys 17.2, we also determined the value of the stress intensity factor KI for the same geometry. This was computed using finite elements on a mesh with quadratic triangular elements on the vicinity of the crack tip, and quadratic rectangular elements everywhere else. Quarter point elements, formed by placing the mid-side node near the crack tip at the quarter point, were used to account for the crack singularity.

STRESS INTENSITY FACTOR K1	THEORITICAL	ANSYS
	27.785	23.433

ANALYSIS OF FAILURE CRITERIA A static fracture analysis was performed, where the goal was merely to compute the stress intensity factors.

Steps in Analysis Procedure:

- Pre-processing
- Give the job name
- Define Element Type
- 3Define Material Properties
- Define Key Points
- Define Line Segments
- Discretize Lines L3, L4&L5
- Create the Concentration Key point (Crack Tip)
- Create the Area
- Apply Boundary Conditions
- Apply Loads
- Mesh the Model
    - Processing (Solving the Solution)
    - Post Processing

- Zoom the Crack-Tip Region
- Define Crack-Face Path
- Define Local Crack-Tip Coordinate System
- Activate the Local Crack-Tip Coordinate System
- Define the Model-1 crack deformation Define the Model-1 Stress Intensity Factor using KCALC
    - Define the model-1 failure criteria From these figures it seems that there stress intensity factor & failure criteria of crack propagation to occur mainly in mode 1, during continued fracture.

VI.CONCLUSIONS

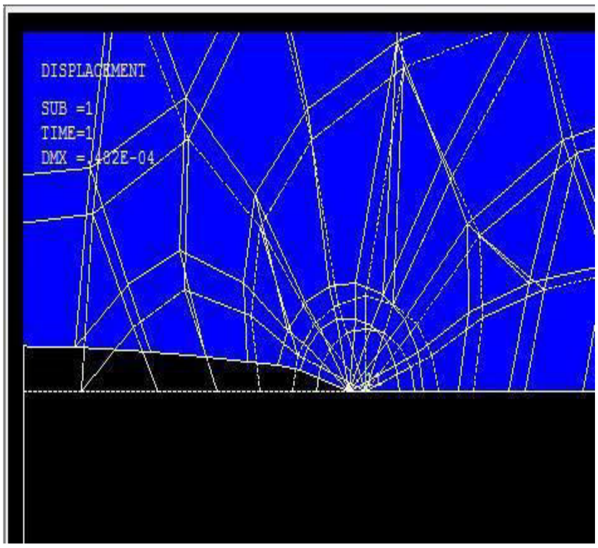

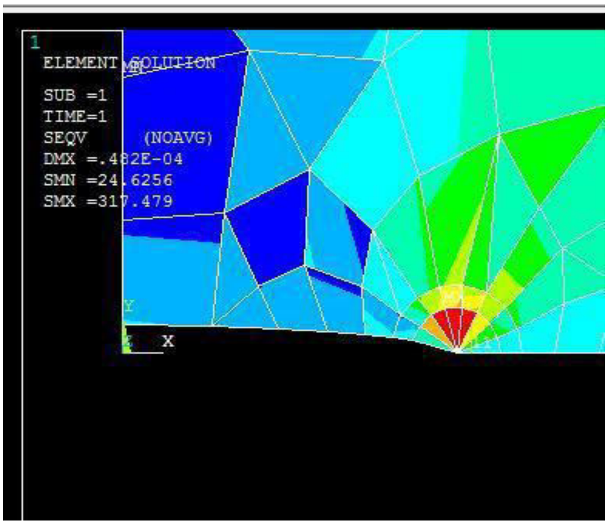

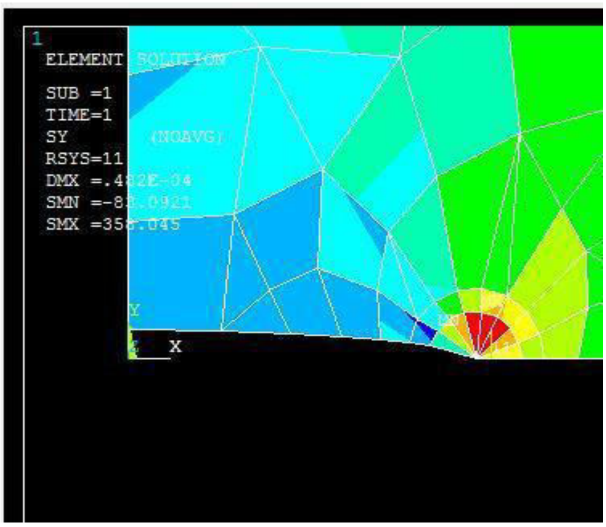

From the above figures the stress intensity factor & failure criteria of crack propagation to occur mainly in mode 1, during continued fracture.

V.REFERENCES

[1] M.H.Aliabadi and M.H.L'opez. Database of stress intensity factors. Computational mechanics Publications, 1996.

[2] S. N. Atluri. Path independent integrals in finite elasticity and inelas-ticity with body forces, inertia and arbitrary crack-face conditions .Eng.Fract. Mech, 16:341-364, 1982.

[3] M. F. Ashby and D. R. Jones .Engineering materials 1, an introduction to their properties and applications, Butterworth Heinemann, 1996.

[4] R. S. Barsoum. Triangular quarter-point elements as elastic and perfectly-plastic crack tip elements .Int. J. for Num. Meth.in Eng., 11:85-98, 1977.

[5] D.Broek. Elementary engineering fracture mechanics. Kluwer Academic Publishers, Dordrecht, 1986.

[6] G.P.Cherepanov .Mechanics of Brittle Fracture. MacDraw-Hill, New York 1979.

[7] L.B.Freund. Dynamic Fracture Mechanics. Cambridge University Press, 1990.

[8] A. A. Griffith. The phenomena of rupture and flows in solids. Phil. Trans.Roy. Soc. London, A221:163-197, 1921.

[9] D. Hegen.An Element-free Galerkin Method for Crack Propagation in Brittle Materials. PhD thesis, Eindhoven University of Technology, 1997.

[10] C. E. Inglis. Stresses in a plate due to the presence of cracks and sharp corners.Proc.Inst. Naval Architects, 60, 1913.

[11] G. R. Irwin. Analysis of stresses and strains near the end of a crack transversing a plate. Trans. A.S.M.E., J. Applied Mechanics, 361-364, 1957.

DESIGN AND ANALYSIS OF THERMOACOUSTIC REFRIGERATOR

Galeti Nikhilkumar

Regestration No.15Q91D2103

8th semester, Department of Thermal Engineering &Technology

Mallareddy College of Engg&Technology,HYDERABAD

gouthamnikhilkumar424@gmail.com

***Abstract*— The layout and functionality of thermo acoustic fridges has been the focus of massive interest from the studies since the 1980's.Domestic uses of fridge is present in almost all households so it lead to research in growth the performance of thermo acoustic systems, but they're normally complicated to fabricate, pricey, and barriers of H.E exist in phrases of performance and sturdiness. Reducing using H.E and the use of flow-thru designs dramatically reduces the price and complexity of thermo acoustic structures, doubtlessly with minimum performance loss. In this thesis, the outcomes are compared to get the best the wave pattern. The performace parameters such as acoustic strength, pressure drop, velocity, mass float fee and heat sharing rate at different velocities.3-D modeling of thermo acoustic refrigerator in CREO. Analysis is done ANSYS to find the best result.**

***Keywords*— Acoustic refrigeration, Sound wave, TAR, Stack, Conclusion.**

I. INTRODUCTION

ACOUSTIC REFRIGERATION

One commonly thinks of a sound wave as consisting handiest of coupled strain and role oscillations. In fact, temperature oscillations accompany the strain oscillations and whilst there are spatial gradients inside the temperature oscillations, oscillating warmth go with the flow happens. The aggregate of those oscillations produces a rich variety of "thermo acoustic" outcomes.

In normal life, the thermal results of sound are too small to be without difficulty observed; for example, the amplitude of the temperature oscillation in conversational stages of sound is handiest about zero.0001°C. However, in an exceptionally extreme sound wave in a pressurized gasoline, those thermo acoustic outcomes can be harnessed to create effective warmness engines and refrigerators. Whereas standard engines and refrigerators depend on crankshaft-coupled pistons or rotating mills, thermo acoustic engines and fridges have no shifting parts (or at maximum most effective flexing elements with out the want for sliding seals). This simplicity, coupled with reliability and relatively low fee, has highlighted the ability of thermo acoustic gadgets for realistic use. As a result, thermo acoustics is maturing quickly from a topic of basic medical studies via the stages of carried out research and directly to important sensible programs Recently, thermo acoustic phenomena had been hired inside the medical subject for imaging of tissues.

Thermo acoustic refrigeration uses advanced acoustic generation to improve cooling capability with out the want for environmentally unfavorable refrigerants. The mechanism of the TAR is straightforward, based at the growth and compression of a fuel via sound wave. When a sound wave from a vibrating diaphragm or loudspeaker is dispatched down a half of wave length tube, the stress pulsations from a standing wave, which purpose oscillatory movement of gasoline in the tube's axial direction.

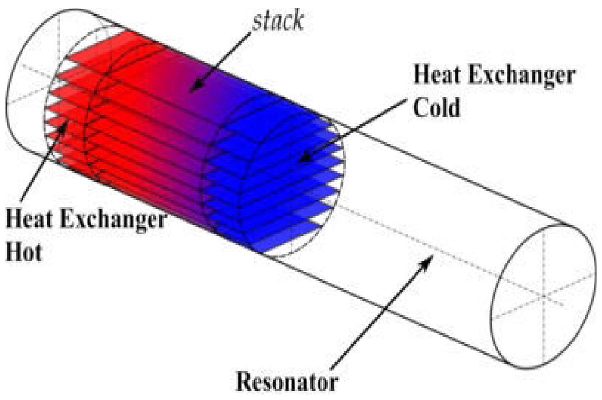

II. PRINCIPLE OF OPERATION:

When a sound wave is dispatched down a half of-wavelength tube with a vibrating diaphragm or a loudspeaker, the pressure pulsations make the fuel interior slosh back and forth. These paperwork areas wherein compression and heating take place,

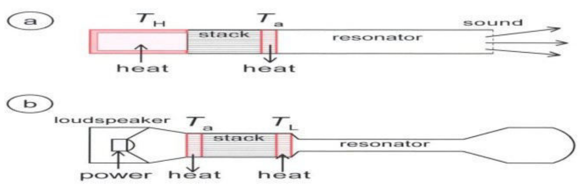

A thermo acoustic fridge is a resonator cavity that includes a stack of thermal garage elements (related to warm and cold heat exchangers) placed so the back-and-forth fuel movement occurs in the stack. The oscillating fuel parcels pick up heat from the stack and deposit it to the stack at a unique region. The device "acts like a bucket brigade" to cast off heat from the bloodless warmth exchanger and deposit it at the recent warmness exchanger, for that reason forming the idea of a refrigeration unit. The governing mathematical equations of the thermo acoustic phenomenon are given below.

III. STANDING-WAVE SYSTEMS:

The thermo acoustic engine (TAE) is a device that converts warmth electricity into work within the shape of acoustic power. A thermo acoustic engine is running the use of the effects that get up from the resonance of a status-wave in a gas. A standing-wave thermo acoustic engine usually has a thermo acoustic detail called the “stack”. A stack is a stable component with pores that permit the running gas fluid to oscillate while in touch with the strong partitions. The oscillation of the gasoline is followed with the trade of its temperature. Due to the creation of solid walls into the oscillating gasoline, the plate modifies the authentic, unperturbed temperature oscillations in both importance and segment for the gas approximately a thermal penetration intensity $\delta=\sqrt{(2k/\omega)}$ away from the plate, in which okay is the thermal diffusivity of the fuel and $\omega=2\pi f$ is the angular frequency of the wave.

Thermal penetration depth is described as the gap

that warmth can diffuse even though the gas throughout a time $1/\omega$. In air oscillating at one thousand Hz, the thermal penetration intensity is set 0.1 mm. Standing-wave TAE should be provided with the necessary warmth to hold the temperature gradient at the stack. This is done through H.E on both facets of the stack.

If we placed a skinny horizontal plate inside the sound discipline the thermal interaction between the oscillating fuel and the plate leads to thermo acoustic consequences. If the thermal conductivity of the plate fabric would be 0 the temperature in the plate would exactly fit the temperature profiles as in Fig. 1b. Consider the blue line in Fig. 1b because the temperature profile of a plate at that role. The temperature gradient inside the plate would be equal to the so- known as crucial temperature gradient. If we would fix the temperature on the left aspect of the plate at ambient temperature Ta (e.g. The usage of a heat exchanger) then the temperature at the right would be beneath Ta. In other phrases: we've got produced a cooler. This is the premise of thermo acoustic cooling as shown in Fig. 2b which represents a thermo acoustic refrigerator. It has a loudspeaker on the left. The device corresponds with the left 1/2 of Fig. 1b with the stack inside the role of the blue line. Cooling is produced at temperature TL.

Thermo acoustic engines nonetheless be afflicted by a few obstacles, which include that:

- The tool typically has low strength to quantity ratio.
- Very high densities of working fluids are required to gain high strength densities.
- The commercially-to be had linear alternators used to convert acoustic electricity into energy currently have low efficiencies compared to rotary electric powered mills
- Only high-priced particularly-made alternators can provide satisfactory overall performance.
- The first and second law efficiencies.
- The onset temperature distinction, defined as the minimum temperature difference throughout the perimeters of the stack at which the dynamic stress is generated.
- The variation of the resultant wave frequency with the TAE operating temperature

Travelling-wave structures

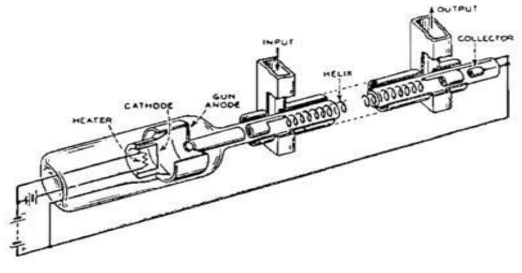

IV. ACOUSTIC DRIVER

Electrodynamics drivers are utilized in a class of electrically pushed thermo refrigeration structures. The mechanical and electric traits of the driver, together with the acoustic load impedance at the driver piston, determine the electro acoustic efficiency of the actuator. The electro acoustic efficiency is, of route, a key element inside the normal performance of the cooling device. For this cause, it's far beneficial to expand fashions that allow the performance of such a motive force to be expected for varying working conditions and hundreds. A special description of linear models of loudspeakers the usage of equivalent electrical circuits is readily to be had.

V. THERMOACOUSTIC REFREGERATORS:

Overview:

Thermo acoustic fridge (TAR) is a fridge that makes use of sound waves so as to provide the cooling. In a TAR, the operating fluid is a helium-argon combination, and the compressor is changed by using a loudspeaker. The benefits of this form of refrigeration cycle are -fold.

- The helium and argon are inert, environmentally friendly gases, unlike a few of the commonplace refrigerants.
- The loudspeaker is a simple tool this is extra long lasting than a compressor.

The drawback of the TAR is that as of but those sorts of refrigerators have did not reap efficiencies as excessive as those as standard refrigeration gadgets. Some researchers contend that the set-up of the TAR is such that it in no way can be able to reap efficiencies as excessive as well known refrigeration gadgets. Others trust that there's no reason that a TAR can't achieve efficiencies as high as preferred refrigeration units. They attribute the presently lower efficiencies to the ordinary sensitivity of the TAR to input parameters and the relative children of the field in general.

DIFFERENT TYPEAS OF TARs:

There are sorts of TARs. The first is known as a standing wave thermo acoustic refrigerator. The 2nd is a touring wave (or pulse tube) thermo acoustic fridge. The standing wave TAR makes use of a set number of oscillations with nodes that continue to be unchanged over time. In other phrases, the wave of as an entire does no longer pass over the years, closing desk bound. This is just like a state of affairs wherein you are taking a string and glued ends and then pluck it. Because of the constant ends the wave of the string remains fixed in vicinity.

The visiting wave TAR, as it sounds like, makes use of a wave of sound that travels throughout the TAR. This is similar to the state of affairs where you are taking the string and flick it forward like a whip. The disturbance of the whip creates a sound wave that sends the wave forward. Each kind of TAR has particular blessings in certain situations, and research is being achieved into cascading combinations of status wave and visiting wave TARS to try and take benefit of those various advantages.

VI. Standing Wave TAR:

The status wave TAR is much like a Sterling cycle, that's dependent on pressure oscillations that arise out of segment with each other. The status wave TAR consists of 5 predominant additives all incased in a tube of some kind. On one cease is the loudspeaker. This then results in a configuration of a stack with a hot warmth exchanger on one aspect and a chilly warmth exchanger on the other facet. The aggregate of those three additives is known as “the stack”. The stack consists of a huge wide variety of skinny, parallel plates with only small openings between them. Finally, on the other give up of the stack is a bulb known as the resonator.

The motive of the resonator is to keep a specific frequency as a status wave. Each of those components is critical to the TAR; but, resonators and loudspeakers are commonplace devices in acoustics in trendy. It is the stack this is specific to the TAR and is likewise in all likelihood the maximum complicated factor.

VII. STACK

Stack is the maximum touchy part of the fridge, as small changes in stack dimensions can result in huge modifications in overall performance. It consists of massive range of closely spaced surfaces aligned parallel to the duration of the resonating tube. The stack cloth and thickness are crucial layout considerations. A material that has a low thermal conductivity is favored because heat conducting across the stack works against the refrigerator. However, the material should also have a warmth potential a good deal large than the heat potential of the working fluid in order that sustained temperature gradient may be created.

Mylar and digital camera film are Few examples of materials used within the production of stack. Two crucial parameters for stack design are thermal penetration intensity and viscous penetration intensity. A constant factor will feel thermal effects from gasoline this is at the order of a thermal penetration intensity away, but will not feel the effect of gas that is much similarly away

VIII. ACOUSTICAL THEORY

The expertise of acoustic wave dynamics, i.e. The strain and speed fields created via an acoustic wave, is important to understand the running of a thermo acoustic device.

The expertise of acoustic wave dynamics, i.E. The strain and speed fields created via an acoustic wave, is important to understand the running of a thermo acoustic device. The acoustical concept deals with the observe of the longitudinal acoustic waves. The longitudinal acoustic waves are generated due to the compression, and expansion of the gasoline medium. The compression of a gasoline corresponds to the troughs of a sine wave.. The compression and enlargement of a longitudinal wave bring about the variation of strain alongside its longitudinal axis of oscillation. A longitudinal wave calls for a fabric medium which includes air or water to travel.

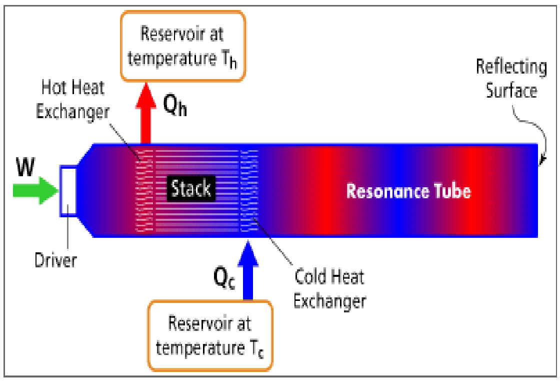

ADVANTAGES OF THERMOACOUSTIC REFRIGERATION: Advantages of thermo acoustic refrigeration easy production no need for lubricants makes use of cheap and readily to be had inert gases environment friendliness low life cycle price power saving via proportional manage greater monetary than domestic fridge.

IX. INTRODUCTION TO CREO

- PTC CREO, formerly known as Pro/ENGINEER, is 3D modeling software used in mechanical engineering, design, manufacturing, and in CAD drafting service firms. It was one of the first 3D CAD modeling applications that used a rule-based parametric system. Using parameters, dimensions and features to capture the behavior of the product, it can optimize the development product as well as the design itself.

X. INTRODUCTION TO FEA

- Finite element analysis is a method of solving, usually approximately, certain problems in engineering and science. It is used mainly for problems for which no exact solution, expressible in some mathematical form, is available. As such, it is a numerical rather than an analytical method. Methods of this type are needed because analytical methods cannot cope with the real, complicated problems that are met with in engineering. But neither will be very successful in finding out what is happening in part of a car suspension system during cornering.

XI. CFD ANALYSIS OF THERMO ACOUSTIC REFRIGERATOR

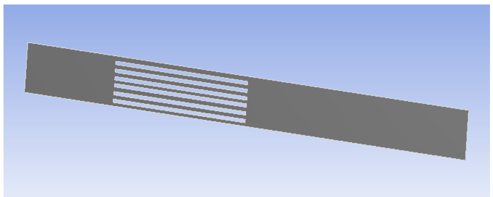

Meshed model

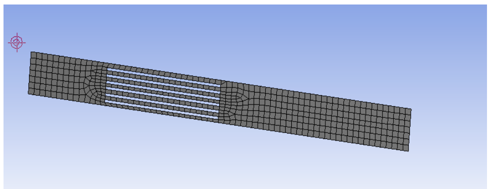

Inlet and outlet

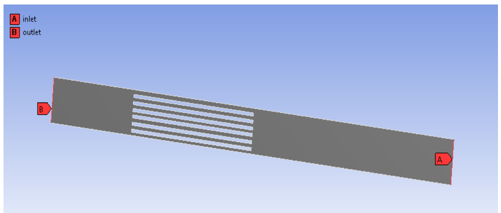

VELOCITY 340m/s PRESSURE

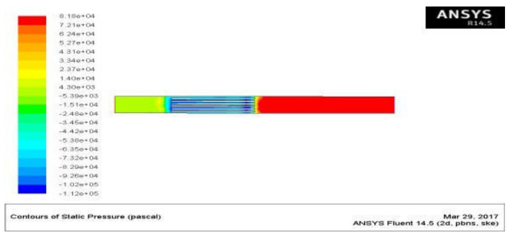

ACOUSTIC POWER

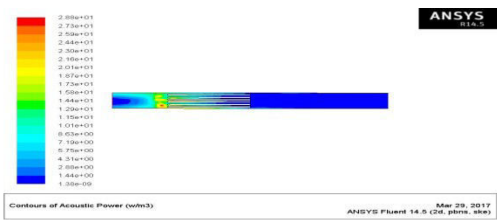

- **MASS FLOW RATE**

Mass Flow Rate	(kg/s)
inlet	20.825003
interior-_trm_srf	134.092
outlet	-20.758984
wall-_trm_srf	0
Net	0.066019058

- **HEAT TRANSFER RATE**

Total Heat Transfer Rate	(w)
inlet	311239.72
outlet	-310251.69
wall-_trm_srf	0
Net	988.03125

XII. CONCLUSION

- Reducing the use of heat-exchangers through the use of flow-through designs dramatically reduces the cost and complexity of thermo acoustic systems, potentially with minimal efficiency loss.

- In these thesis ,It was found that a sine wave pattern(frequencies) lead to superior cooling effects compared to other wave patterns tested. CFD analysis to determined the acoustic power, pressure drop, velocity, mass flow rate and heat transfer rate at different velocities.

- By observing the CFD analysis the acoustic power values are increased by increasing the velocity inputs. The heat transfer rate values are more at 340m/s input velocity.

- by comparing the fluids gas and air the heat transfer rate is more for gas fluid.

- So it can be conclude the velocity 340 m/s flow is better performance.

REFERENCES

- [1] Syeda HumairaTasnim and Roydon Andrew Fraser (2010), “Thermal Field Measurements of a Thermoacoustically Driven Thermoacoustic Refrigerator” ASME Journal of Thermal Science and Engineering Applications, vol. No.2,pp. 021010-1 to 021010-10.

- [2] R. C. Dhuley and M.D. Atrey (2011), "Cooldown Measurements in a Standing Wave Thermoacoustic Refrigerator", Indian Journal of Cryogenics, Vol.36, No.1-4, pp. 158-163.

- [3] B. V. Kamble, B. T. Kuzhiveli, S. Kasthurirengan, Upendra Behera, K.V. Dinesh, Geeta Sen, M. V. N. Prasad (2011) "Performance characterization by Optimized Design of Thermoacoustic Prime Mover", Indian Journal of Cryogenics, Vol.36, No.1-4, pp. 37-41.

- [4] Mehta S., Desai K., Naik H., Atrey M. (2013), " Investigations on performance improvement of standing wave type thermoacoustic prime mover using acoustic amplifier", Indian Journal of Cryogenics, Vol.38, No.1-4, pp.184-189.

- [5] Kartik M. Trivedi (2014), “Effect of Stack Positioning on a Temperature Difference of Thermoacoustic Refrigerator”, Indian Journal of Research, Vol.3, Issue 5, pp. 93-95.

Coupled Field Analysis of A Chimney Used in Cement Industry

Yelthuri Bhavitha[1] Sudhakar Jonnapalli[2] Dr. S S Gowda[3]

[1,2] PG Scohar, [3]Professor

Dept. of Mechanical Engineering, Malla Reddy College of Engineering, Maisammaguda, Hyderababad, Telangana, India.

Abstract

Chimney, which form the last component of a system using a flue gas such as boiler, play a vital role in maintaining efficiency, draft, etc, of a system and also in minimizing the atmospheric pollution. Steel chimneys are also known as steel stacks. The steel chimneys are made of steel plates and supported on foundation. The steel chimneys are used to escape and disperse the flue gases to such a height that the gases do not contaminate surrounding. In this thesis, chimney will be designed considering dead load and wind load. The Bureau of Indian Standards (BIS) design codes procedures will be used for the design of the chimney. The chimney was considered as a cantilever beam with annular cross section.

3D model of the chimney is done in Pro/Engineer and coupled field analysis is done on the chimney in ANSYS. A simplified model of chimneys with various thicknesses like 10mm, 12mm, 14mm and 16mm were modeled atmosphere.

Keywords

Chimney, Flue Gases, Coupled Field Analysis

I. Introduction

Chimneys or stacks are very important industrial structures for emission of poisonous gases to a higher elevation such that the gases do not contaminate surrounding atmosphere. These structures are tall, slender and generally withcircular cross-sections. Different construction materials, such as concrete, steel or masonry, are used to build chimneys. Steel chimneys are ideally suited for process work where a short heat-up period and low thermal capacity are required. also, steel chimneys are economical for height up to 45m. Fig. 1 shows a photograph of self-supporting steel chimneys located in an industrial plant.

Fig. 1: Shows a Photograph of Self-Supporting Steel Chimneys Located in an Industrial Plant

There are many standards available for designing self supporting industrial steel chimneys: Indian Standard IS 6533: 1989 (Part-1 and Part-2), Standards of International Committee on Industrial Chimneys CICIND 1999 (rev 1), etc. Geometryofa self supporting steel chimney plays an important role in its structural behavior under lateral dynamic loading. This is because geometry is primarily responsible for the stiffness parameters of the chimney. However, the basic geometrical parameters of the steel chimney (e.g., overall height, diameter at exit, etc.) are associated with the corresponding environmental Conditions.

II. Literature Review

1. Menon and Rao(1997) reviews the code measures to estimate the across wind response of reinforced concrete chimney.In this paper, the difficulties in the codal evaluation of across wind moments and load factor provisions are examinedthrough reliability approach. This paper mainly suggest that it is essential to design at certain conditions for the acrosswind loading [3].

2. K.R.C. Reddy, O.R.Jaiswal and P.N.Godbole (2011) discusses about wind and earthquake analysis of tall reinforced concrete chimney. In this paper two reinforced concrete chimneys are analysed for wind and earth quake loads. Earth quake analysis is done as per IS 1893 (part 4): 2005 and wind analysis is done as per IS 4998 (part 1): 1992. The combination of along & across wind loads of chimney is done as per ACI 307-98 code. Finally they computed the governing load for design of chimneys.

3. B. SivaKonda Reddy, C.Srikanth, V.RohiniPadmavathi (2012) discusses about wind load effects on tall reinforced concrete chimneys. In this paper they considered 275m reinforced concrete lined chimney. The study of this paper is along &across wind effects on this RCC Chimney for I and VI wind zones of India. Finally they concluded that, forWind zone –I across wind loads are governing and for wind zone-VI along wind loads are governing rather than the across wind loads .

III. Problem Description & Methodology

The objective of this project is to make a 3D model of the chimney and study the thermal and static behavior of the chimney by performing the finite element analysis. 3D modeling software (PRO-Engineer) was used for designing different geometries (10mm, 12mm, 14mm and 16mm thickness) and analysis software (ANSYS) was used for thermal and static analysis.

The methodology followed in the project is as follows:

- Create a 3D model of the steam chimney using parametric software pro-engineer.
- Perform thermal analysis and linear layer thermal analysis on the chimney for thermal loads, to find out the temperature distribution and heat flux
- Perform static analysis and linear layer static analysis on the chimney for thermal loads, to find out the deformation, stress and strain distribution.

IV. Introduction to CAD

Throughout the history of our industrial society, many inventions have been patented and whole new technologies have evolved. Perhaps the single development that has impacted manufacturing more quickly and significantly than any previous technology is the digital computer.

1. Introduction to PRO/Engineer

Pro/ENGINEER, PTC's parametric, integrated 3D CAD/CAM/CAE solution, is used by discrete manufacturers for mechanical engineering, design and manufacturing. Created by Dr. Samuel P. Geisberg in the mid-1980s, Pro/ENGINEER was the industry's first successful parametric, 3D CAD modeling system. The parametric modeling approach uses parameters, dimensions, features and relationships to capture intended product behavior and create a recipe which enables design automation and the optimization of design and product development processes.

B. Introduction to Finite Element Method

Finite Element Method (FEM) is also called as Finite Element Analysis (FEA). Finite Element Method is a basic analysis technique for resolving and substituting complicated problems by simpler ones, obtaining approximate solutions Finite element method being a flexible tool is used in various industries to solve several practical engineering problems. In finite element method it is feasible to generate the relative results. ANSYS is an Engineering Simulation Software (computer aided Engineering). Its tools cover Thermal, Static, Dynamic, and Fatigue finite element analysis along with other tools all designed to help with the development of the product. The company was founded in 1970 by Dr. John A. Swanson as Swanson Analysis Systems, Inc. SASI. Its primary purpose was to develop and market finite element analysis software for structural physics that could simulate static (stationary), dynamic (moving) and heat transfer (thermal) problems.

V. Modelling and Analysis

A. Models of Narrow Plate Using Pro-e Wildfire 5.0

The vertical narrow plate is modeled using the given specifications and design formula from data book. The isometric view of vertical narrow plate is shown in below figure. The vertical narrow plate profile is sketched in sketcher and then it is extruded vertical narrow plate using extrude option.

B. Original Chimney 3D and 2D Models

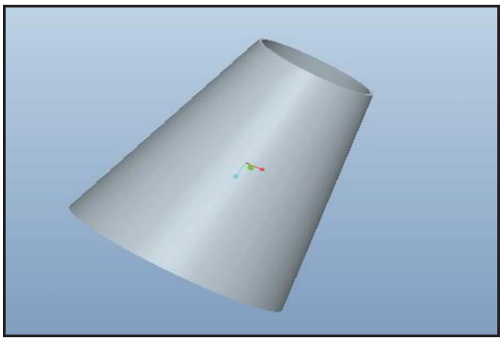
Fig. 2: 3D Chimney Model

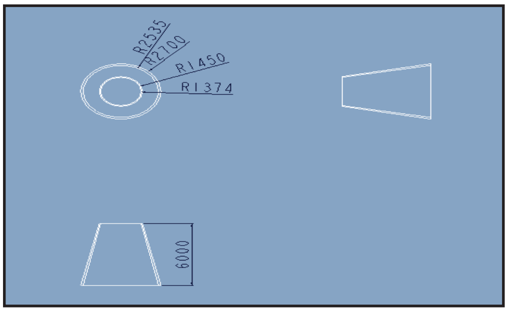

Fig. 3: 2D Chimney Model

C. Thermal Analysis

1. Material Concrete

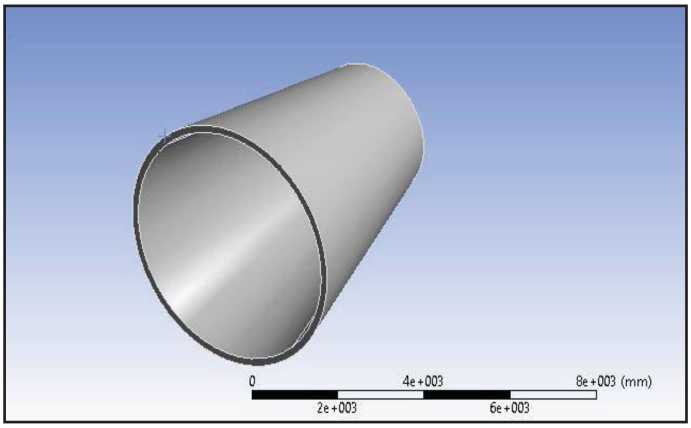

Fig. 4: Imported Model

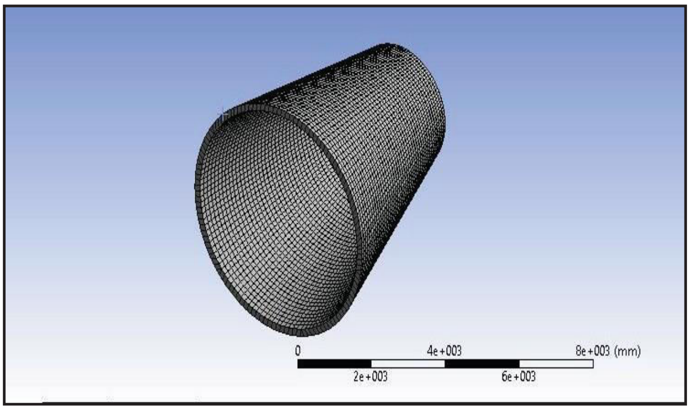

Fig. 5: Meshed Model

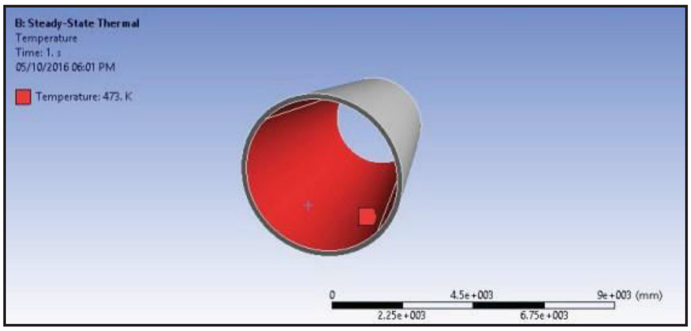

Fig 6 applied temperature

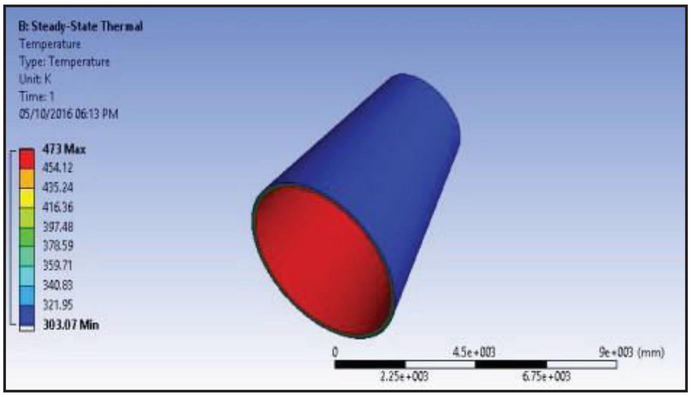

Fig. 7: Temperature Disturbtion

According to the contour plot, the temperature distribution maximum temperature at inside of the chimney because the temperature passing from the bottom inside of the chimney. So we are applying the temperature inside of the chimney and applying the convection except inside of the chimney.

D. Heat Flux

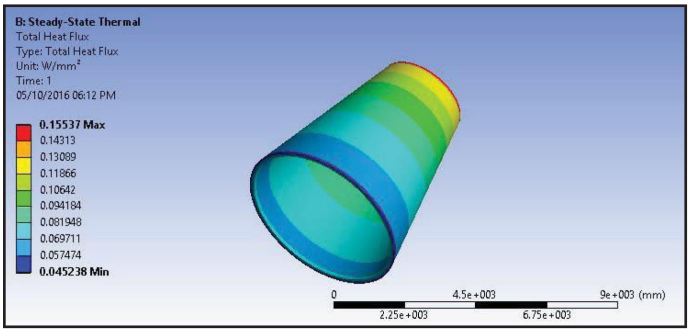

Fig. 8: Heat Flux

According to the contour plot, the maximum heat flux at inner side top portion of the chimney. Minimum heat flux bottom of the chimney.According to the above contour plot, the maximum heat flux is 0.15537w/mm^2 and minimum heat flux is 0.045238w/mm^2.

E. Static Analysis

1. Deformation

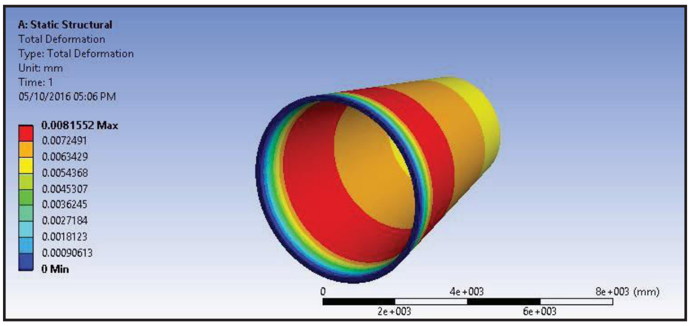

Fig. 9: Deformation

According To the Counter Plot, the maximum deformation at outer surface of the chimney and minimum deformation at bottom of chimney. The maximum deformation is 0.0081552 mm and minimum deformation is 0.0090613 mm.

2. Stress

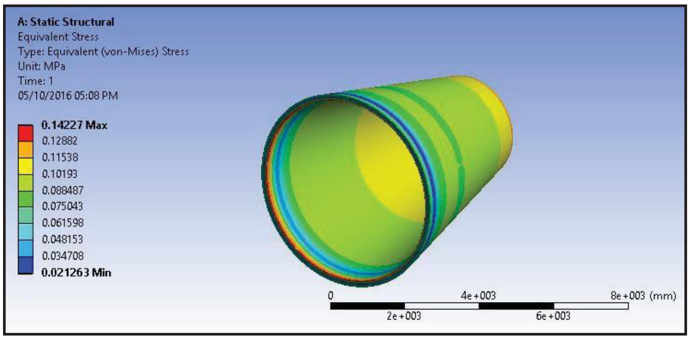

Fig. 10: Stress

According To the Counter Plot, the maximum stress at bottom end of the chimney and minimum stress at bottom surface of the chimney. The maximum stress is 0.1422 mm and minimum is 0.02126 mm.

3. Strain

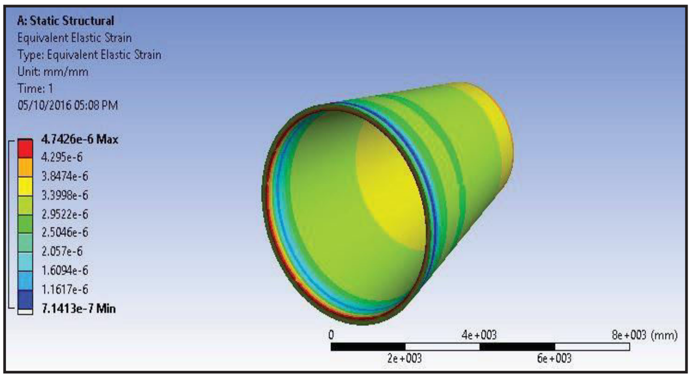

Fig. 11: Strain

According To the Counter Plot, the maximum strain at bottom end of the chimney and minimum strain at bottom outer surface of the chimney. The maximum strain is 4.7426e-6 mm and minimum deformation is 7.1416e-7 mm.

F. Linear Layer Thermal Analysis

1. Imported Model

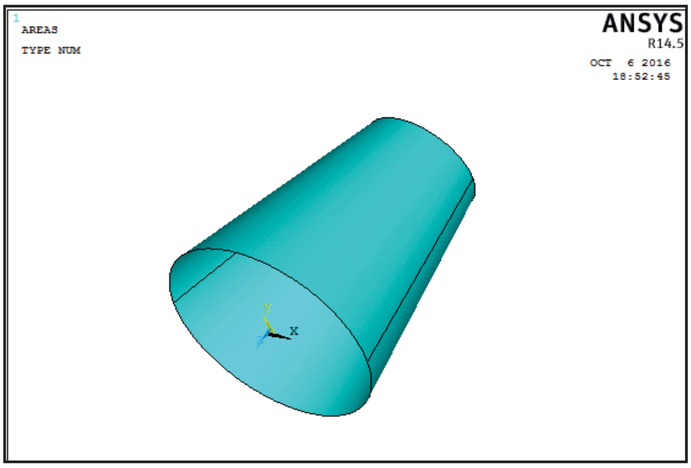

2. Meshed Model

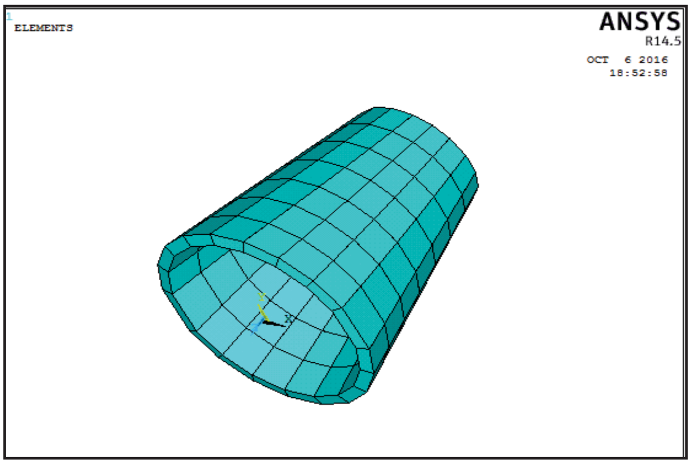

Finite element analysis or FEA representing a real project as a "mesh" a series of small, regularly shaped tetrahedron connected elements, as shown in the above fig. And then setting up and solving huge arrays of simultaneous equations. The finer the mesh, the more accurate the results but more computing power is required.

(I). Layer stacking

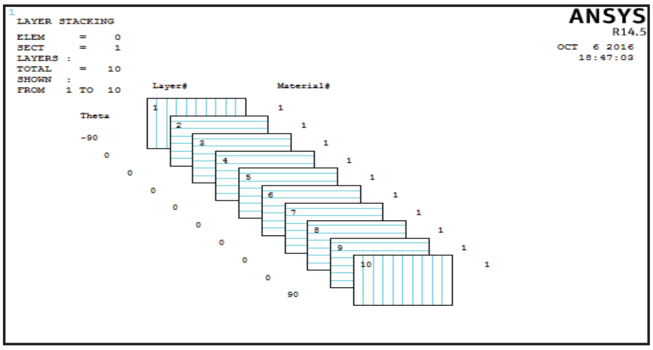

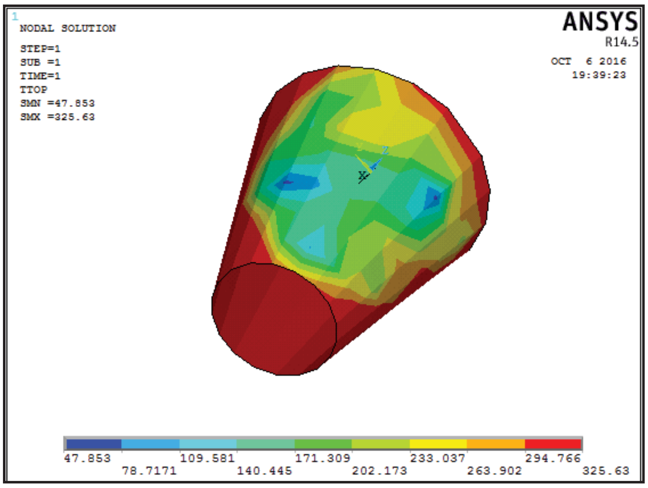

Fig. 12: Temperature

G. Heat Flux

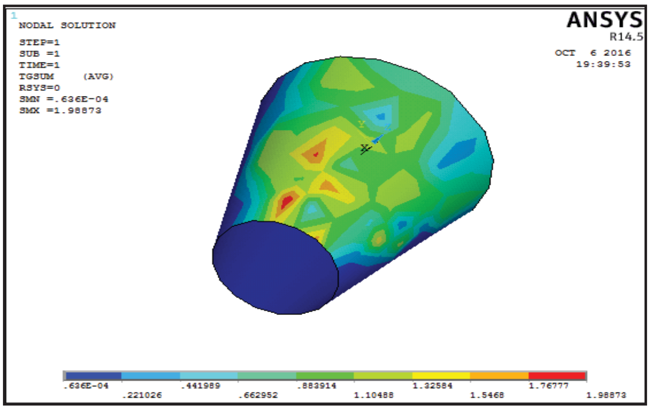

Fig. 13: Heat Flux

H. Linear Layer Static Analysis

1. Deformation

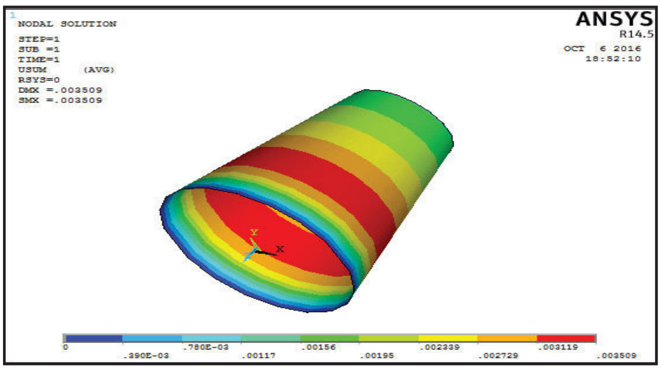

Fig. 14: Deformation

2. Stress

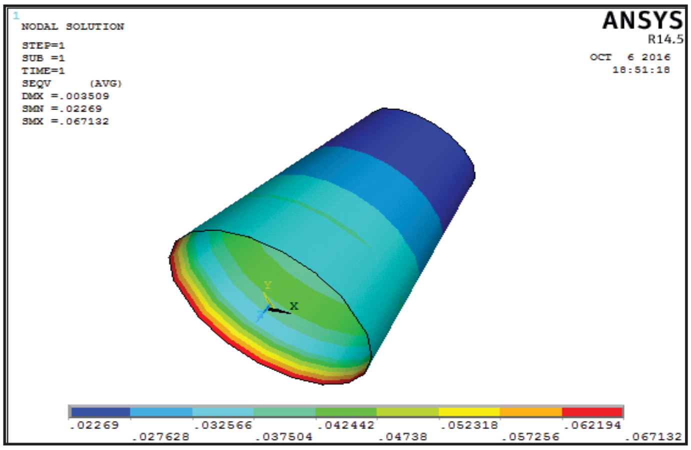

Fig. 15: Stress

3. Strain

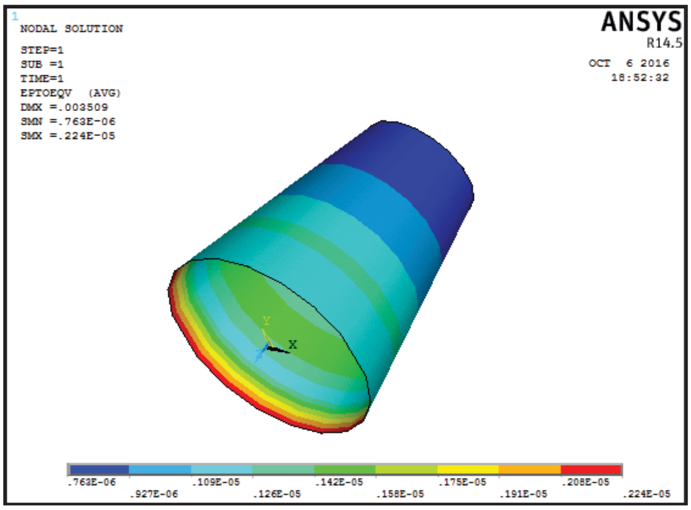

Fig. 16: Strain

VI. Results and Discussion

A. Thermal Analysis Results Table

Chimney thickness (mm)	Temperature (K)		Heat flux (W/mm^2)
	Min	max	
Original model	303.07	473	0.15537
10	303.02	473	0.14822
14	303.06	473	0.143
18	303.08	473	0.137
22	303.05	473	0.1290

B. Static Analysis Results Table

Thickness (mm)	Deformation (mm)	Stress (N/mm^2)	Strain
original	0.0081522	0.14227	4.7426 e-6
10	0.00785715	0.1537	5.126 e-6
14	0.0077429	0.13701	4.5672 e-6
18	0.0075227	0.13347	4.49 e-6
22	0.00721	0.12788	4.269 e-6

C. Linear Layer Thermal Analysis Results Tabels

Chimney thickness (mm)	Temperature (K)	Heat flux (W/mm^2)
Original model	325	1.980
10	324.319	3.574
14	323.818	3.564
18	323.33	3.562
22	322.865	1.971

D. Linear Layer Static Analysis Results Tabels

Thickness (mm)	Deformation (mm)	Stress (N/mm^2)	Strain
original	0.0025909	0.067132	0.224e-5
10	0.003404	0.065302	0.215e-5
14	0.00226	0.064556	0.214e-5
18	0.062317	0.063826	0.213e-5
22	0.002275	0.063111	0.210e-5

E. Graphs

1. Heat flux

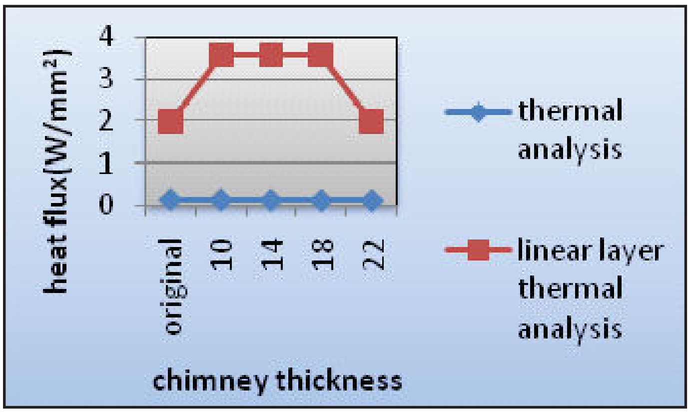

2. Stress

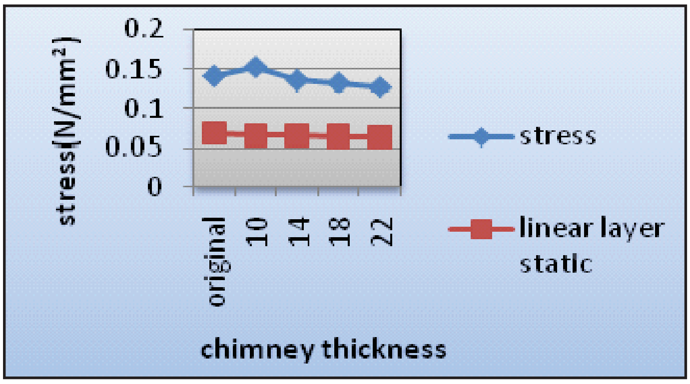

VII. Conclusion

3D model of the chimney is done in Pro/Engineer and coupled field analysis is done on the chimney in ANSYS. A simplified model of chimneys with various thicknesses like 10mm, 14mm, 18mm, and 22mm were modeled.

By Observing the thermal analysis the heat flux value is more for original model of chimney and linear layer thermal analysis the heat flux value is more for 10mm thickness of chimney model. When we compare the thermal analysis and linear layer thermal analysis the heat flux more for linear layer thermal analysis of chimney.

By observing the static analysis the deformation and stress values are less for 22mm thickness of the chimney and linear layer static analysis the deformation and stress values are less for 22mm thickness of chimney model. When we compare the static analysis and linear layer static analysis the stress values are less for linear layer static analysis of chimney.

So it can be conclude the 22 mm thickness of the chimney model is the best model when we do linear layer thermal and static analysis.

References

[1] S.N.Manohar,"Tall chimneys design and construction", TATA McGraw-Hill Publishing Company Limited-1985.

[2] Draft copy CED 38(7892): 2013 (third revision of IS 4998(part 1):1992), "Criteria for design of reinforced concrete chimneys", Bureau ofIndian standards, New Delhi, 2013.

[3] Menon.D, Srinivasrao.P,"Estimation of along wind moments in RC chimneys", Engineering Structures, Vol. 19, No. 1, pp. 71–78,1997

[4] K.R.C. Reddy, O.R.Jaiswal, P.N.Godbole,"Wind and earthquake analysis of tall RC Chimney", International journal of earth science and engineering, Vol. 4, pp. 508-511, 2011.

[5] B.Sivakondareddy,V.RohiniPadmavathi,Ch.Srikanth,"Study of wind load effects on tall RC Chimneys", International Journal of Advanced Engineering Technology, Vol. 3, Issue 2, pp. 92-97, 2012.

[6] K.R.C. Reddy, O.R. Jaiswal, P.N.Godbole,"Combined design moments of tall reinforced concrete chimneys", National conference on wind engineering, pp. 135-146, 2012.

[7] M.G. Shaikh, H.A.M.I. Khan,"Governing loads for design of a tall RCC chimney", Journal of mechanical and civil engineering (IOSRJMCE), pp. 12-19, 2009.

[8] IS 875(part 3): (1987),"Indian standard code of practice for criteria for design loads(other than earthquake) for buildings and structures", Bureau of Indian standards, New Delhi, Reaffirmed 1997.

[9] IS 1893(part 4):(2005),"Criteria for earthquake resistant design of structures",Bureau of Indian standards, New Delhi, 2005.

[10] K.Anil Pradeep, C.V.Sivaramaprasad,"Governing loads for design of a 100m RCC chimney", National conference on new trends in civil engineering, pp. 81-87, 2014.

Yelthuri Bhavitha
Thermal Engineering
Roll No. 15Q91D2111
E-mail: ybhavitha15@gmail.com
Under the guidance of T.Suresh

Design And Thermo Mechanical Analysis of Gas Turbine Blade Modification Using Cooling Passages

NUNNA MANIKANTA CHOWDARY
PG Schohar
Manikanta5894@gmail.com

Dr. P.VELMURUGAN
Professor
Velmurugan_mech@mrce.in

Dept. Of Mechanical Engineering
MallaReddy college of engineering, Hyderabad-500100

ABSTRACT:
The present research deals with the outcomes of major geometrical changes to the interior of a convection cooled gas turbine rotor blade.The primary focus is at the flow on the leading area channels and the impact on the heat transfer. Four cooling passage geometry configurations are investigated by the use of fluid structural analysis. Turbine blades considered have internal passages that offer cooling all through operation in a high temperature engine. The cooling passages design is very important to acquire close to uniform temperature of the blade for the duration of operation of blade. The temperature of the blade is depending on the fluid dynamics of the air circulating within the cooling passages as well as the thermal properties of the blade fabric. To layout lighter and more green systems Computational optimization techniques had been efficaciously carried out for lots aerospace structures. An further extension of these techniques is been carried out to guide the thermal layout of a turbine blade by designing the layout of optimal cooling passage. Different evaluation is done for determining the optimum pattern of the cooling passages after which optimizing the size of the individual cooling passages. The intention is to make a turbine blade design which goes to produce blades with better overall performance and longer lives.

***Index Terms*:** Gas Turbine, Computational optimization methods, Aerospace Structures, optimal cooling passage layout.

1.INTRODUCTION

Gas turbines play a vital role in the today's industrialized society, and as the demands for power increase, the power output and thermal efficiency of gas turbines must also increase. One method of increasing both the power output and thermal efficiency of the engine is to increase the temperature of the gas entering the turbine. In the advanced gas turbines of today, the turbine inlet temperature can be as high as 1500°C; however, this temperature exceeds the melting temperature of the metal airfoils. Therefore, it is imperative that the blades and vanes are cooled, so they can withstand these extreme temperatures. Cooling air around 650°C is extracted from the compressor and passes through the airfoils. With the hot gases and cooling air, the temperature of the blades can be lowered to approximately 1000°C, which is permissible for reliable operation of the engine. It is widely accepted that the life of a turbine blade can be reduced by half if the temperature prediction of the metal blade is off by only 30°C. By preventing local hot spots, the life of the turbine blades and vanes will increase. However, due to the complex flow around the airfoils it is difficult for designers to accurately predict the metal temperature. Figure 1 shows the heat fl ux distribution around an inlet guide vane and a rotor blade. At the leading edge of the vane, the heat transfer coefficients are very high, and as the flow splits and travels along the vane, the heat flux decreases. Along the suction side of the vane, the flow transitions from laminar to turbulent, and the heat transfer coefficients increase. As the flow accelerates along the pressure surface, the heat transfer coefficients also increase. The trends are similar for the turbine blade: the heat flux at the leading edge is very high and continues decrease as the flow travels along the blade; on the suction surface, the flow transitions from laminar to turbulent, and the heat flux sharply increases; the heat transfer on the pressure surface increases as the flow accelerates around the blade.

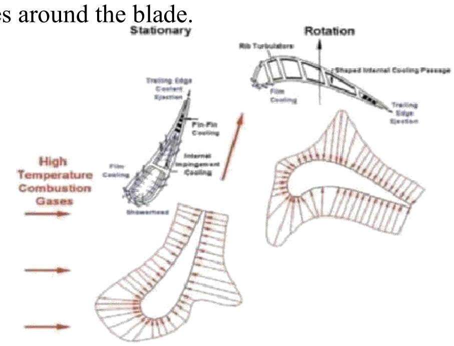

Fig. 1. Cross-Sectional View and Heat Flux Distribution of a Cooled vane and blade

They need detailed hot gas path heat transfer distributions. Heat transfer and film cooling data are also needed for the airfoils. The surface heat transfer on a stator vane is affected by the combustor-generated high turbulence, the laminar-to-turbulent transition, acceleration, film cooling flow, platform secondary flow, and surface roughness. These factors as well as the rotational, centrifugal forces and blade tip clearance and leakage must be considered for the rotating blades. After the potential hot spots on the airfoil surface are identified, the internal cooling schemes can be developed. Designers need new internal heat transfer data to improve current rotor blade cooling performance.

Enhanced Internal Cooling of Turbine Vanes

A typical cooled turbine vane is shown in figure 2. As shown in the figure, the vane is hollow, so cooling air can pass through the vane internally. The coolant is extracted from the internal channel for impingement and pin fin cooling. Jet impingement is a very aggressive cooling technique which very effectively removes heat from the vane wall. However, this technique is not readily applied to the narrow trailing edge. The vane trailing edge is cooled using pin-fins (an array of short cylinders). The pin-fins increase the heat transfer area while effectively mixing the coolant air to lower the wall temperature of the vanes. After impinging on the walls of the airfoil, the coolant exits the vane and provides a protective film on the vane's external surface. Similarly, the coolant traveling through the pin-fin array is ejected from the trailing edge of the airfoil.

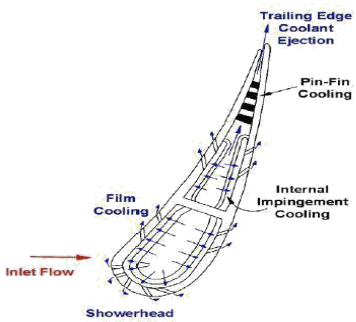

Fig. 2. Schematic of a Turbine Vane Cross-Section with Impingement and Trailing Edge Pin-Fin Cooling.

II. PARAMETERS OF GAS TURBINE BLADE

In a gas turbine engine, a single turbine section is made up of a disk or hub that holds many turbine blades. That turbine section is connected to a compressor section via a shaft (or "spool") , and that compressor section can either be axial or centrifugal. Air is compressed, raising the pressure and temperature, through the compressor stages of the engine. The temperature is then greatly increased by combustion of fuel inside the combustor, which sits between the compressor stages and the turbine stages. The high temperature and high pressure exhaust gases then pass through the turbine stages. The turbine stages extract energy from this flow, lowering the pressure and temperature of the air and transfer the kinetic energy to the compressor stages along the spool. This process is very similar to how an axial compressor works, only in reverse.

The number of turbine stages varies in different types of engines, with high bypass ratio engines tending to have the most turbine stages. The number of turbine stages can have a great effect on how the turbine blades are designed for each stage. Many gas turbine engines are twin spool designs, meaning that there is a high pressure spool and a low pressure spool. Other gas turbines use three spools, adding an intermediate pressure spool between the high and low pressure spool. The high pressure turbine is exposed to the hottest, highest pressure air, and the low pressure turbine is subjected to cooler, lower pressure air. The difference in conditions leads to the design of high pressure and low pressure turbine blades that are significantly different in material and cooling choices even though the aerodynamic and thermodynamic principles are the same. Under these severe operating conditions inside the gas and steam turbines, the blades face high temperature, high stresses, and potentially high vibrations. Steam turbine blades are critical components in power plants which convert the linear motion of high temperature and high pressure steam flowing down a pressure gradient into a rotary motion of the turbine shaft.

The open gas-turbine cycle can be modeled as a closed cycle as shown in Figure 2 by utilizing the air-standard assumptions. Here the compression and expansion process remain the same, but a constant-pressure heat-rejection process to the ambient air replaces the combustion process. The ideal cycle that the working fluid undergoes in this closed loop is the Brayton cycle, which is made up of four internally reversible processes:

1-2 Isentropic compression (in a compressor)

2-3 Constant pressure heat addition

3-4 Isentropic expansion (in a turbine)

4-1 Constant pressure heat rejection (2)

3.2 cross section gas turbine blade

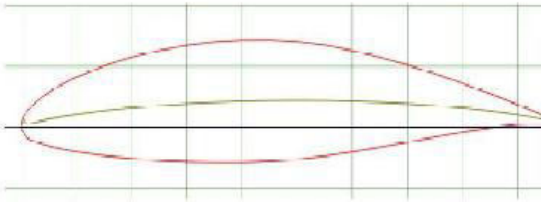

Fig 3: NACA 65-410 Aerofoil section.

The intricate cooling passages of the blade are modeled using CATIA software for estimation of cooling air mass flow distribution and temperature rise. Three sections are considered along the radial height for the network. Here first one is different diameter of holes provide along the longitudinal length of fin. second one is blade is designed as shell type through which more cooling fluid can send. And final model is rib support is providing on shell type of gas turbine blade.

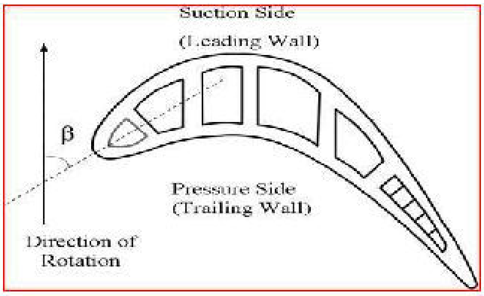

Fig 4: Shell And Rib Type Cooling Passage In Turbine Blade

The coolant pressure and temperature at the inlet and static pressure at the exit of each film cooling holes and tip cooling holes are given at the exit location. The heat loads in form of gas side heat transfer coefficient and gas temperature are given. The radial heights of all the geometrical sections and rotational speed are given as input. The values of Input are given in Table 1.

Inet gas temp	880 K
Inlet gas pressure	5 bar
Inlet cooling mediamum temp	300 K
Inlet cooling mediamum pressure	1.2 atm
Oulet	atm pressure

III. ANALYSIS ON GAS TURBINE BLADE

The purpose of a finite element analysis is to re-create mathematically the behavior of an actual engineering system. In other words, the analysis must be an accurate mathematical model of a physical prototype. In the broadest sense, this model comprises all the nodes, elements, material properties, real constants, boundary conditions and other features that are used to represent the physical system. ANSYS software is used to run the structural and couple field analysis for three type of model with six different materials.

Material properties

PROPERTIES	UNITS	Inconel 718	titanium	Ni-cr
Young's modulus	G.Pa	200	106	206
Poisson's ratio		0.31	0.3	0.3
Density	Kg/m3	8193	4420	8900
Thermal Conductivity	W/mK	11.2	90.7	14.3
Specific heat	J/KgK	556	527	441

Table: Material Properties

Structural Boundary Conditions To Be Applied On The Rotor Blade Model

Two structural boundary conditions namely displacement and fluid force were applied on the rotor blade model through fluid structural analysis. The solution part of ANSYS was opened and the displacement constraints (U) were imposed on the areas shaded and numbered in fig 5.

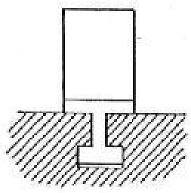

Fig 5 Structural boundary conditions on rotor blade

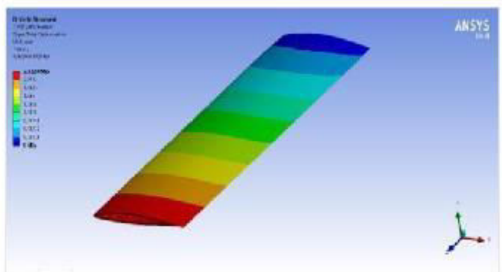

Fig 6: Thermal deformation of titanium shell with double rib type turbine blade.

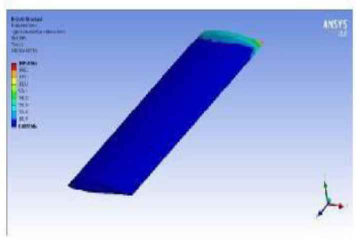

Fig 7: Thermal stresses of titanium shell with double rib type turbine blade.

SMODAL ANALYSIS

SHELL TYPE COOLING PASSAGE			
	Inconel 718	Titanium T6	NI-CR
DEFORMATION	3.5	2.5	3.9
STRESSES	7725	2735	8235
STRAIN	0.031	0.024	0.037

Table:Results Of Shell Type Cooling Passage

Any physical system can vibrate. The frequencies at which vibration naturally occurs, and the modal shapes which the vibrating system assumes are properties of the system, and can be determined analytically using Modal Analysis. Modal analysis is the procedure of determining a structure's dynamic characteristics; namely, resonant frequencies, damping values, and the associated pattern of structural deformation called mode shapes. It also can be a starting point for another, more detailed, dynamic analysis, such as a transient dynamic analysis, a harmonic response analysis, or a spectrum analysis. Modal analysis in the ANSYS family of products is a linear analysis. Any nonlinearities, such as plasticity and contact (gap) elements, are ignored even if they are defined. Modal analysis can be done through several mode extraction methods: subspace, Block Lanczos, Power Dynamics, Reduced, Unsymmetric and Damped. The damped method allows you to include damping in the structure.

IV. RESULTS AND DISCUSSION

3D model are created in CATIAV5 software and all models are saved as I.G.E.S format. And same files are imported in to ANSYS to run individual analysis. Here

initially fluent analysis is performed using fluent boundary conditions. And temperature and pressure distribution parameters are transferred to structural analysis. And fixed boundary condition is applied at one end of gas turbine blade. From fluid structural interface analysis deformation and thermal stresses are noted as shown below.

Modal analysis results:

SHELL TYPE COOLING PASSAGE			
MODE NO.	Inconel 718	Titanium T6	NI-CR
1	54.5	54	53.2
2	295	300	294
3	365	363	360
4	450	446	439
5	715	709	698

Table: Natural Frequencies of Shell Type Cooling Passage.

V. CONCLUSION

Whenever the material properties changes, deformation as thermal stresses may vary within the materials. From the structural analysis three model with titanium T6 materials having minimum deformation and stresses. Maximum temperatures are observed at the blade tip section and minimum temperature variations at the root of the blade. According to couple field (structural and thermal) analysis with titanium T6 materials having minimum deformation and stresses. Hence from this analysis titanium is the best suited material with holes placed on the surface for the rotor blade. Gas turbine blade with shell with single rib type model is having minimum thermal stresses and more heat transfer to cooling medium. And if we maintain the hole geometry configuration, life of turbine blade can improve. Finally conclude that gas turbine with water flow cooling passages are having minimum thermal stresses. and it increase the life of turbine blade.

REFERENCES

[1] Jaeyong Ahn, M.T. Schobeiri, Je-Chin Han, Hee-Koo Moon “Effect of rotation on leading edge region film cooling of a gas turbine blade with three rows of film cooling holes” International Journal of Heat and Mass Transfer, Volume 50, Issues 1-2, January 2007.

[2] Zhihong Gao, Diganta P. Narzary, Je-Chin Han, “Film cooling on a gas turbine blade pressure side or suction side with axial shaped holes” International Journal of Heat and Mass Transfer, Volume 51, Issues 9-10, May 2008.

[3] Cun-liang Liu, Hui-ren Zhu, Jiang-tao Bai, Du-chun Xu, “Film cooling performance of converging slot-hole rows on a gas turbine blade, International Journal of Heat and Mass Transfer, Volume 53, Issues 23-24, November 2010.

[4] J.P.E. Cleeton, R.M. Kavanagh, G.T. Parks, “Blade cooling optimisation in humid-air and steam-injected gas

turbines", Applied Thermal Engineering, Volume 29, Issue 16, November 2009.

[5] Jury Polezhaev, "The transpiration cooling for blades of high temperatures gas turbine", Energy Conversion and Management, Volume 38, Issues 10-13, July-September 1997.

[6] D. Lakehal, G. S. Theodoridis, W. Rodi, "Three- dimensional flow and heat transfer calculations of film cooling at the leading edge of a symmetrical turbine blade model", International Journal of Heat and Fluid Flow, Volume 22, Issue 2, April 2001.

[7] Mahfoud Kadja, George Bergeles, "Computational study of turbine blade cooling by slot-injection of a gas", Applied Thermal Engineering, Volume 17, Issue 12, December 1997.

[8] Bruno Facchini, Giovanni Ferrara, Luca Innocenti, "Blade cooling improvement for heavy duty gas turbine: the air coolant temperature reduction and the introduction of steam and mixed steam/air cooling", International Journal of Thermal Sciences, Volume 39, Issue 1, January 2000.

[9] Yiping Lu, David Allison, Srinath V. Ekkad, "Turbine Blade showerhead film cooling: Influence of hole angle and shaping" International Journal of Heat and Fluid Flow, Volume 28, Issue 5, October 2007.

[10] J.P.E. Cleeton, R.M. Kavangh, G.T. Parks, "Blade Cooling Optimisation in Humid-air and Steam Injected Gas Turbines", Applied Thermal Engineering 29 (2009).

DESIGN AND FLUID FLOW ANALYSIS OF HEAT EXCHANGER FIN WITH VARIOUS LOUVER FINS

Sudhakar Jonnapalli
Research Scholar
Dept. of Mechanical Engineering
Malla Reddy College of Engineering

L.Priyanka
Assistant Professor
Dept. of Mechanical Engineering
Malla Reddy College of Engineering

INTRODUCTION

A heat exchanger is a machine used to vary heat amongst an awesome object and a fluid, or between or additional fluids. The fluids could even be separated via using a perfect wall to preclude mixing or they are also in direct contact. They're largely utilized in residence heating, refrigeration, air conditioning, vigour stations, chemical plant life, petrochemical plant lifestyles, petroleum refineries, natural-gasoline processing, and sewage alleviation. The classic illustration of a heat exchanger is realized in an inside combustion engine the place a circulating fluid known as engine coolant flows by means of radiator coils and air flows prior the coils, which cools the coolant and heats the incoming air. One extraordinary illustration is the hot sink, that could be a passive heat exchanger that transfers the heat generated via digital or mechanical software to a fluid medium, as a rule air or a liquid coolant.

Flow arrangement

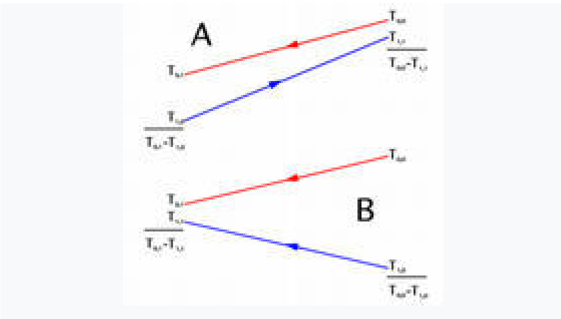

1. Counter current (A) and parallel (B) flows

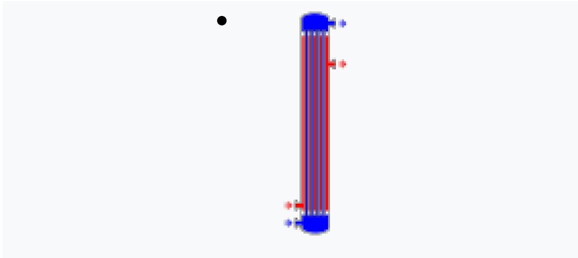

2. Shell and tube heat exchanger, single pass (1–1 parallel flow)

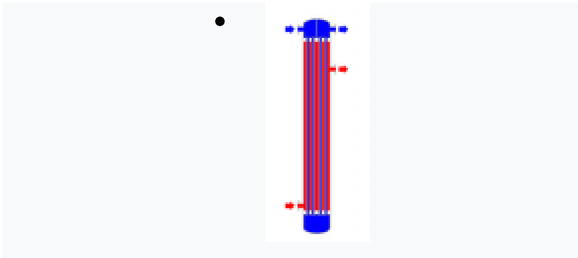

3. Shell and tube heat exchanger, 2-pass tube side (1–2 crossflow)

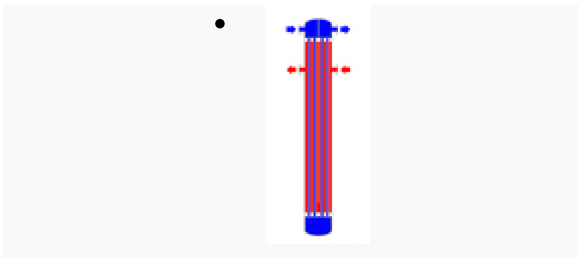

4. Shell and tube heat exchanger, 2-pass shell side, 2-pass tube side (2-2 countercurrent)

There are three quantities one classifications of heat exchangers in keeping with their go with the flow institution. In parallel-waft heat exchangers, the 2 fluids enter the exchanger on the equal quit, and tour in parallel to one more to the substitute side. In counter-flow heat exchangers, the fluids enter the exchanger from reverse ends. The counter reward-day design is by and large essentially the greenest, in that it's going to change the very best heat from the heat (swap) medium in maintaining with unit mass since the typical temperature difference alongside any unit interval is fit. See counter current exchange. In a go-flow heat exchanger, the fluids tour roughly perpendicular to 1 one other by way of the exchanger.

The utilising temperature during the heat trade floor varies with role; however, the suitable approach temperature could also be defined. In most useful approaches that's the "log advocate temperature difference" (LMTD). Repeatedly direct understanding of the LMTD is not available and the NTU system is used.

A PLATE-FIN HEAT EXCHANGER

A plate-fin heat exchanger is a variety of heat exchanger design that makes use of plates and finned chambers to switch heat among fluids. It is generally categorized as a compact heat exchanger to stress its significantly excessive heat switch surface area to extent ratio. The plate-fin heat exchanger is broadly utilized in lots of industries, together with the aerospace enterprise for its compact size and lightweight residences, as good as in cryogenics where its advantage to facilitate heat transfer with small temperature differences is utilized.

Design of plate-fin heat exchangers

Originally conceived through an Italian mechanic, Paolo Fruncillo. A plate-fin heat exchanger is fabricated from layers of corrugated sheets separated via flat metallic plates, customarily aluminium, to create a series of finned chambers. Separate warm and bloodless fluid streams go with the flow by means of alternating layers of the heat exchanger and are enclosed on the sides by means of aspect bars.

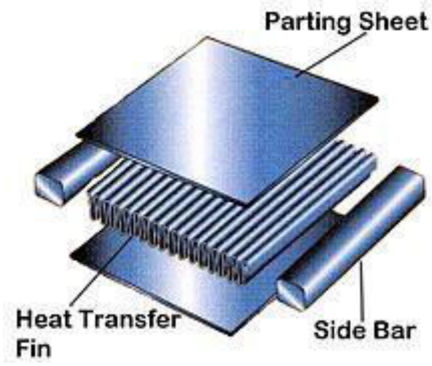

Major Parts of a Plate Fin Heat Exchanger (H.T)

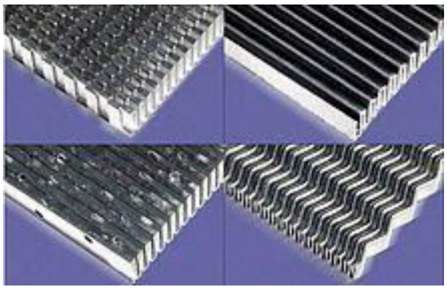

Varieties of Fin Structures for Plate Fin Heat Exchangers (H.T):

A crisis of plate-fin heat exchangers is that they're susceptible to fouling because of their small glide channels. Moreover, they are not capable to be robotically cleaned and require pleasant cleaning tactics and proper filtration for operation with doubtlessly-fouling streams.

counterblow, go-counterblow or parallel drift. If the fins are designed effectively, the plate-fin heat exchanger can artwork in fine counter current association.

The Price of plate-fin heat exchangers is quite often bigger than common heat exchangers thus of a higher measure of an aspect required all via manufacturer. However, those fees can most, as a rule, be outweighed through the fee saving produced via the introduced heat alternate.

Louvered Fin

A louver (American English) or louver is a window blind or shutter with horizontal slats which will also be angled to admit light and air, however, to preserve out rain and direct sunshine. The attitude of the slats could also be adjustable, often in blinds and residence house windows, or constant.

LITERATURE REVIEW

The Effect of Geometrical Parameters on Heat Transfer

The reward appears aimed to hold out the parametric evaluation of the thermo-hydraulic efficiency of a compact heat exchanger utilizing computational fluid dynamics (CFD). The analysis has been entirely at excessive-sufficient frontal air velocities through quite a lot of the geometrical parameters like fin pitch, transverse tube pitch, longitudinal tube pitch, louver pitch and louver factor of view. The airside effectivity of the heat exchanger has been evaluated by means of calculating Colburn section (j) and Fanning friction aspect (f). The analysis of CFD outcome with the experimental discovering out exhibited an superb contract and the effect of countless geometrical parameters for the chosen type of values on the stress drop, hot swap coefficient, and high-quality aspect grew to be analysed. The penalties bought from the analysis can be very indispensable to optimize the louvered fin and flat tube compact heat exchanger for bigger thermo-hydraulic effectivity evaluation without the necessity of time-eating and pricey experimentation.

3d-CFD simulation and neural workforce variant for the j and f explanations of the wavy fin-and-flat tube heat exchangers

A three-dimensional (3D) computational fluid dynamics (CFD) simulation and a neural group variant are supplied to estimate the behaviours of the Colburn facet (j) and the Fanning friction factor (f) for wavy fin-and-flat tube (WFFT) heat exchangers. The effect of the 5 geometrical reasons of fin pitch, fin top, fin dimension, fin thickness, and wave amplitude are investigated over a monstrous sort of Reynolds kind ($600 \leq Re \leq 7000$). The CFD simulation results that the geometrical parameters of wavy fins have a significant result on the j and f explanations as operate of Reynolds type. The computational results have a excellent plentiful accuracy when as in comparison with experimental advantage.

MODELS OF FINS

Case 1: fin angle 28^0 and fin pitch 1.0mm

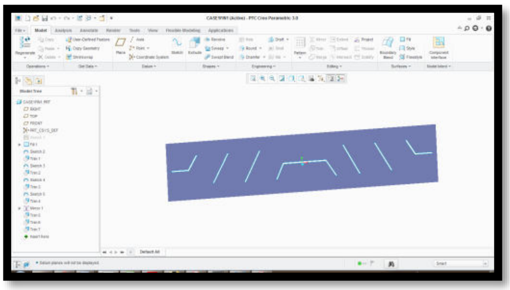

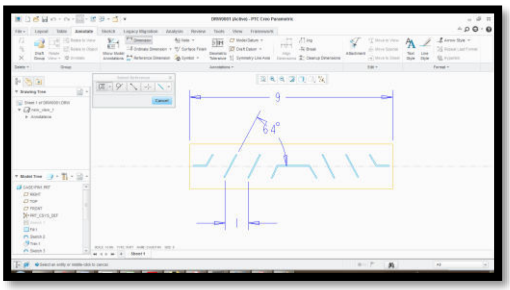

Case 1: fin angle 28^0 and fin pitch 2.0mm

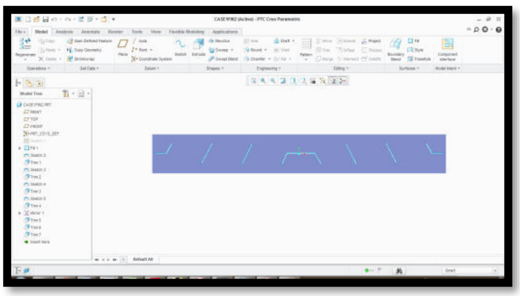

Case 1: fin angle 28^0 and fin pitch 4.0mm

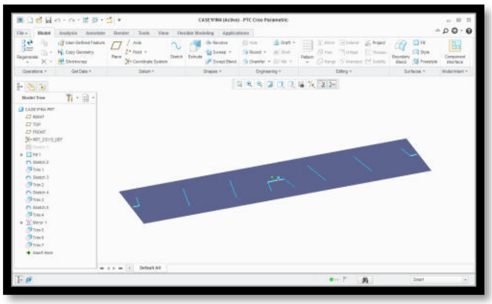

Case 2: fin angle 30^0 and fin pitch 1.0mm

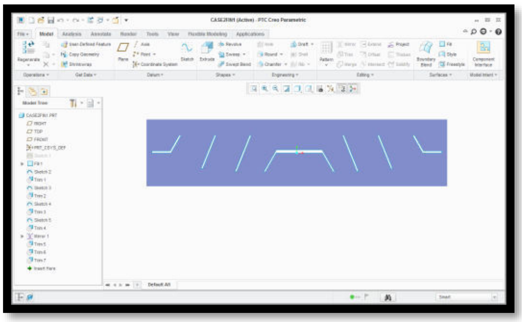

Case 2: fin angle 30^0 and fin pitch 2.0mm

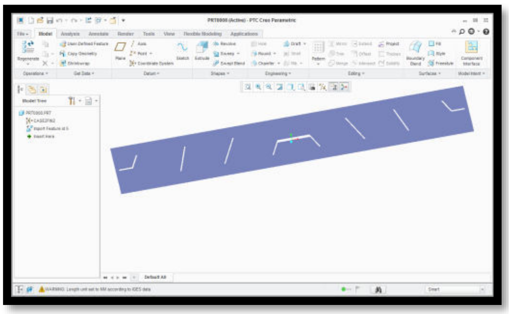

Case 2: fin angle 30^0 and fin pitch 4.0mm

3d Model

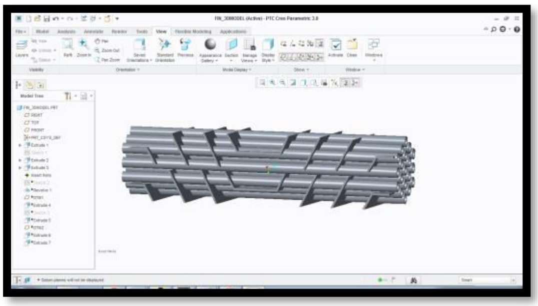

Inclined Fins on Tubes

IMPLEMENTAION

FEM:

FEM is developed to find out the solutions to the real-time problems. Engineering problems requires laborious process to find a solution, which is solved easily with FEM giving a result accurate. After the rapid development of computers, the use of FEM is used with almost in all industries. The analysis done in FEM is FEA.

The approach used in this FEM is variation type of approach. By doing so, it has contributed in formulating the technique. FEM can be used from comparing complicated structures to improving layout of systems.

In the initial usage of FEM, it had troubles for simple structural mechanics but over the time researchers have used it successfully for various types of engineering problems. It can also be used to normal and partial differential equations.

CFD ANALYSIS OF HEAT EXCHANGER FIN

Case 1: fin angle 28^0 and fin pitch 1.0mm

Save CREO Model as .IGES format.

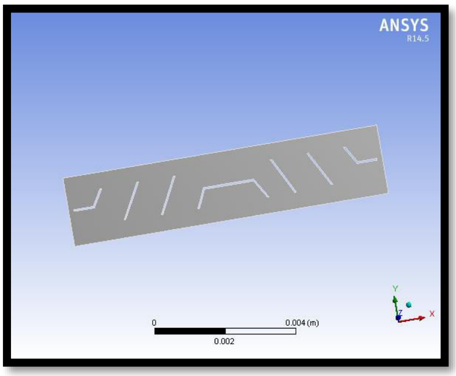

3D Model of Fin in ANSYS

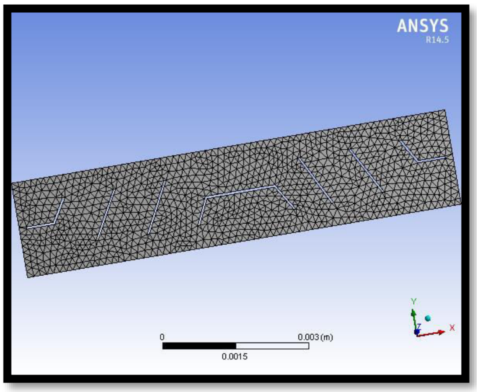

Meshed Model of Fin

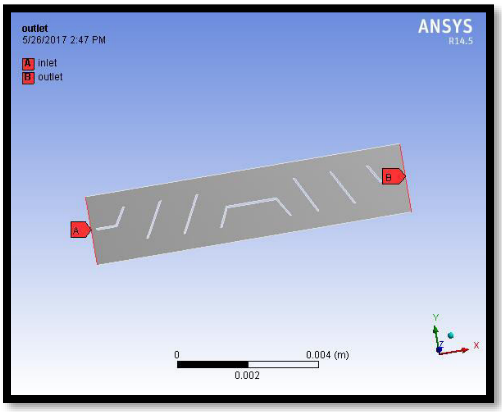

Specifying Boundaries for Inlet and Outlet of 3D Model Fin

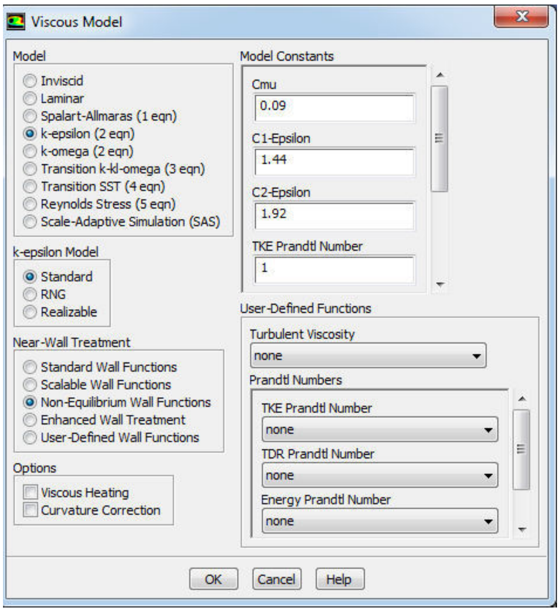

3D Model Viscous Details

Materials → new → create or edit → specify Fluid material → ethylene glycol coolant

Boundary conditions → Inlet → Edit

velocity 15 m/sec–pressure -101325 pa

Solution → Solution Initialization→ Hybrid Initialization →done

Run calculations → No of iterations = 100 → calculate → calculation complete

Case 1: fin length 0.009m

Angle 28^0

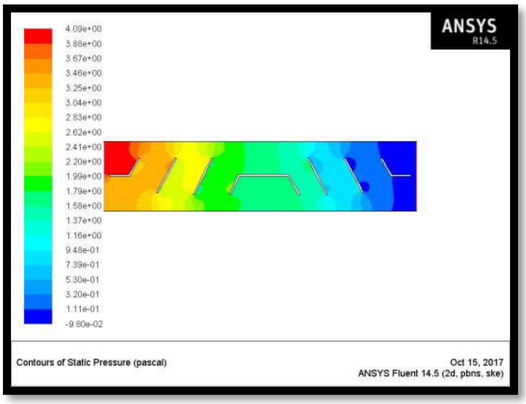

14.1. Pressure

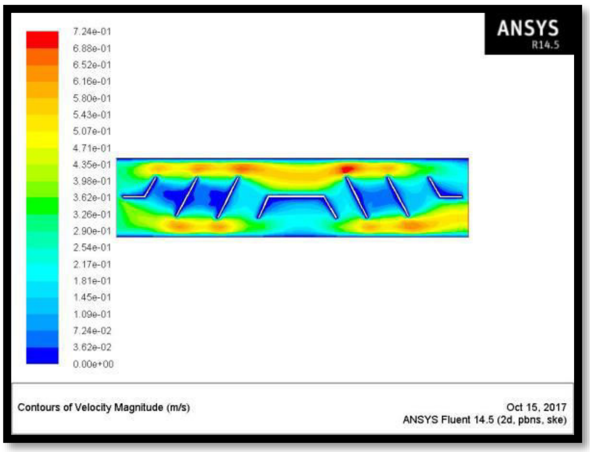

14.2. Velocity

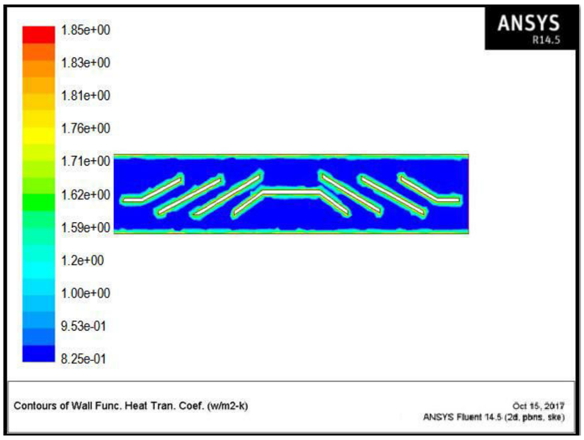

14.3. Heat transfer coefficient

Mass Flow Rate	(kg/s)
inlet	0.00070496299
interior-_trm_srf	-0.00099855475
outlet	-0.00070443825
wall-_trm_srf	0
Net	5.2474206e-07
Total Heat Transfer Rate	**(w)**
inlet	10.536011
outlet	-10.528211
wall-_trm_srf	0
Net	0.0078001022

14.4 Mass flow rate & H.T. rate

Case 2: fin length 0.016m

Angle 28^0

17.1. Pressure

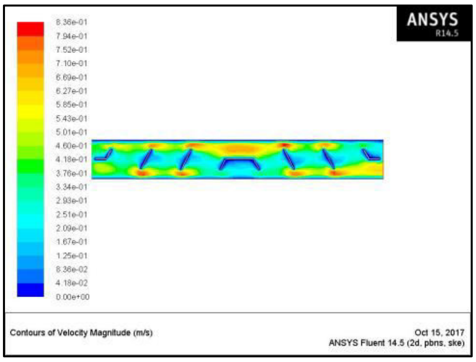

17.2. Velocity

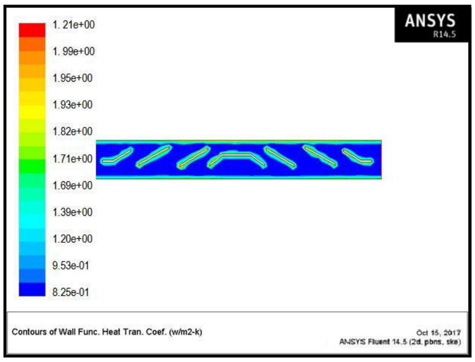

17.3. Heat transfer coefficient

Mass Flow Rate	(kg/s)
inlet	0.00094006513
interior-_trm_srf	-0.0015454747
outlet	-0.00093595358
wall-_trm_srf	0
Net	4.1115563e-06
Total Heat Transfer Rate	**(w)**
inlet	14.049713
outlet	-13.988391
wall-_trm_srf	0
Net	0.061322212

17.4. Mass flow rate & H.T. rate

Case 3: fin length 0.023m

Angle 28^0

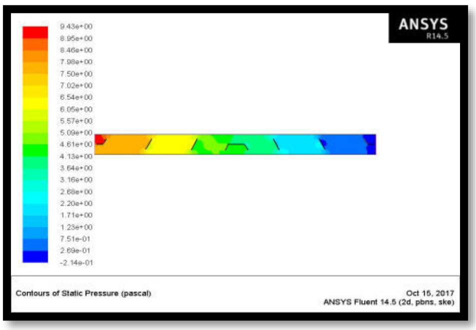

20.1 Pressure

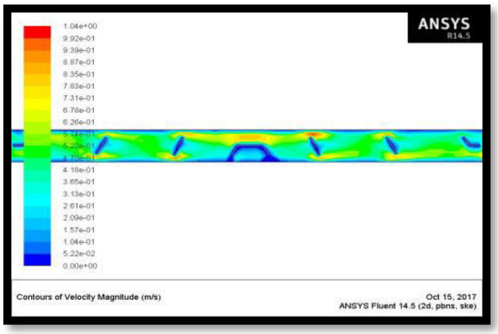

20.2 Velocity

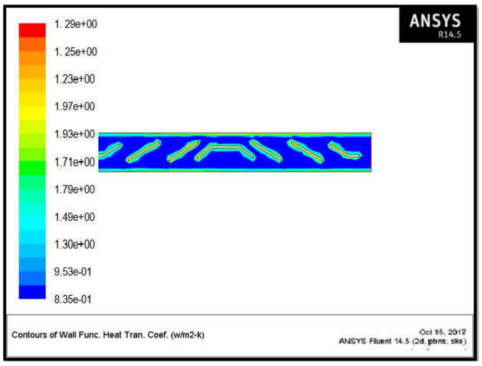

20.3 Heat transfer coefficient

```
                    Mass Flow Rate                (kg/s)
--------------------------- --------------------
                        inlet        0.0011270981
            interior-_trm_srf       -0.0019759021
                       outlet       -0.0011177879
                  wall-_trm_srf                   0
            ---------------- --------------------
                          Net       9.3101989e-06

         Total Heat Transfer Rate                 (w)
--------------------------- --------------------
                        inlet           16.845024
                       outlet          -16.705799
                  wall-_trm_srf                   0
            ---------------- --------------------
                          Net          0.13922501
```

20.4 Mass flow rate & H.T. rate

RESULT TABLE

Fin pitch (mm)	Angle (°)	Pressure (Pa)	Velocity (m/s)	H.T. coefficient (w/m2-k)	Mass flow rate(kg/s)	Heat transfer rate (W)
1mm	28	4.09e+00	7.24e-01	1.85 e+00	5.2474e-07	0.0078001022
	30	4.48e+00	7.65e-01	1.91 e+00	8.734e-07	0.0131282
	32	4.34e+00	7.06e-01	1.20 e+00	7.8580e-08	0.0013198
2mm	28	7.23e+00	8.36e-01	1.21 e+00	4.1111e-06	0.061322212
	30	7.42e+00	8.82e-01	1.219e+00	3.904e-06	0.058273315
	32	7.64e+00	8.48e-01	1.22 e+00	2.8242e-06	0.042238
4mm	28	9.43e+00	9.65e-01	1.29 e+00	9.3101e-06	0.13922
	30	1.02e+01	1.04e+00	2.03 e+00	5.459e-06	0.08139
	32	9.72e+00	1.00e+00	2.23e+00	6.2752e-06	0.09373

CONCLUSION

In this thesis by changing the geometrical parameter including louver pitch and louver altitude results are calculated at various frontal air velocities.

With help CFD analysis HT rate, mass flow rate, stress drop and velocity at 0.4481m/s inlet velocity are calculated.

From the thesis of calculations observed the 300+20-degree angle and 4mm pitch louver fins gives best performance compared to 300-20-degree angle and 4mm pitch louver fins

BIBLIOGRAPHY

- The Effect of Geometrical Parameters on Heat Transfer Characteristics of Compact Heat Exchanger with Louvered Fins.
- Experimental and parametric research of a louvered fin and flat tube compact warmness exchanger the usage of computational fluid dynamics.
- Experimental and numerical research of a louvered fin and elliptical tube compact warmness exchanger.
- Advanced numerical simulation of compact heat exchangers. Application to automobile, refrigeration and aircon industries.
- Comparative Study of Heat Transfer Enhancement in Rectangular and Interrupted Louvered Fins (Newly Designed) in Internal Combustion Engine Using Cfd Tool
- 3d-cfd simulation and neural network version for the j and f elements of the wavy fin-and-flat tube heat exchangers